SECTION A

JOURNAL OF RESEARCH

of the NATIONAL BUREAU OF STANDARDS

JNBAAR 79A (1) 1-128, Jan.-Feb. 1975

U.S. DEPARTMENT OF COMMERCE / National Bureau of Standards

Physics and Chemistry

Journal of Research

of the

National Bureau of Standards

A. Physics and Chemistry

Jan.–Feb. • 1975

VOLUME • 79A

NUMBER • 1

Editor: C. W. Beckett

Associate Editor: D. D. Wagman

Publication dates:
Feb. 1, Apr. 1, June 1, Aug. 1, Oct. 1, Dec. 1, 1975

J. Res. Nat. Bur. Stand. (U.S.), A

JOURNAL OF RESEARCH

The National Bureau of Standards Journal of Research reports research and development in the fields of activity shown at right. Also included from time to time are survey articles on topics closely related to the Bureau's scientific and technical program.

The Journal is published in two separate sections as follows:

A. Physics and Chemistry

Contains papers of interest primarily to scientists working in these fields. Issued six times a year. Annual subscription: domestic, $17.00; foreign, $21.25. Single copy, varies.

B. Mathematical Sciences

Presents studies and compilations designed mainly for the mathematician and the theoretical physicist. Issued quarterly. Annual subscription: domestic, $9.00; foreign, $11.25. Single copy, $2.25.

The National Bureau of Standards[1] was established by an act of Congress March 3, 1901. The Bureau's overall goal is to strengthen and advance the Nation's science and technology and facilitate their effective application for public benefit. To this end, the Bureau conducts research and provides: (1) a basis for the Nation's physical measurement system, (2) scientific and technological services for industry and government, (3) a technical basis for equity in trade, and (4) technical services to promote public safety. The Bureau consists of the Institute for Basic Standards, the Institute for Materials Research, the Institute for Applied Technology, the Institute for Computer Sciences and Technology, and the Office for Information Programs.

THE INSTITUTE FOR BASIC STANDARDS provides the central basis within the United States of a complete and consistent system of physical measurement; coordinates that system with measurement systems of other nations; and furnishes essential services leading to accurate and uniform physical measurements throughout the Nation's scientific community, industry, and commerce. The Institute consists of a Center for Radiation Research, an Office of Measurement Services and the following divisions:

Applied Mathematics — Electricity — Mechanics — Heat — Optical Physics — Nuclear Sciences[2] — Applied Radiation[2] — Quantum Electronics[3] — Electromagnetics[3] — Time and Frequency[3] — Laboratory Astrophysics[3] — Cryogenics[3].

THE INSTITUTE FOR MATERIALS RESEARCH conducts materials research leading to improved methods of measurement, standards, and data on the properties of well-characterized materials needed by industry, commerce, educational institutions, and Government; provides advisory and research services to other Government agencies; and develops, produces, and distributes standard reference materials. The Institute consists of the Office of Standard Reference Materials and the following divisions:

Analytical Chemistry — Polymers — Metallurgy — Inorganic Materials — Reactor Radiation — Physical Chemistry.

THE INSTITUTE FOR APPLIED TECHNOLOGY provides technical services to promote the use of available technology and to facilitate technological innovation in industry and Government; cooperates with public and private organizations leading to the development of technological standards (including mandatory safety standards), codes and methods of test; and provides technical advice and services to Government agencies upon request. The Institute consists of a Center for Building Technology and the following divisions and offices:

Engineering and Product Standards — Weights and Measures — Invention and Innovation — Product Evaluation Technology — Electronic Technology — Technical Analysis — Measurement Engineering — Structures, Materials, and Life Safety[4] — Building Environment[4] — Technical Evaluation and Application[4] — Fire Technology.

THE INSTITUTE FOR COMPUTER SCIENCES AND TECHNOLOGY conducts research and provides technical services designed to aid Government agencies in improving cost effectiveness in the conduct of their programs through the selection, acquisition, and effective utilization of automatic data processing equipment; and serves as the principal focus within the executive branch for the development of Federal standards for automatic data processing equipment, techniques, and computer languages. The Institute consists of the following divisions:

Computer Services — Systems and Software — Computer Systems Engineering — Information Technology.

THE OFFICE FOR INFORMATION PROGRAMS promotes optimum dissemination and accessibility of scientific information generated within NBS and other agencies of the Federal Government; promotes the development of the National Standard Reference Data System and a system of information analysis centers dealing with the broader aspects of the National Measurement System; provides appropriate services to ensure that the NBS staff has optimum accessibility to the scientific information of the world. The Office consists of the following organizational units:

Office of Standard Reference Data — Office of Information Activities — Office of Technical Publications — Library — Office of International Relations.

[1] Headquarters and Laboratories at Gaithersburg, Maryland, unless otherwise noted; mailing address Washington, D.C. 20234.
[2] Part of the Center for Radiation Research.
[3] Located at Boulder, Colorado 80302.
[4] Part of the Center for Building Technology.

U.S. DEPARTMENT OF COMMERCE
Frederick B. Dent, Secretary
NATIONAL BUREAU OF STANDARDS
Richard W. Roberts, Director

Order all publications from the Superintendent of Documents
U.S. Government Printing Office, Washington, D.C. 20402

The Secretary of Commerce has determined that the publication of this periodical is necessary in the transaction of the public business required by law of this Department. Use of funds for printing this periodical has been approved by the Director of the Office of Management and Budget through June 30, 1976.

JOURNAL OF RESEARCH of the National Bureau of Standards—A. Physics and Chemistry
Vol. 79A, No. 1, January–February 1975

Polarization Effects on Fluorescence Measurements

E. D. Cehelnik, K. D. Mielenz, and R. A. Velapoldi

Institute for Materials Research, National Bureau of Standards, Washington, D.C. 20234

(October 19, 1974)

Polarization effects on fluorescence measurements are a function of four independent variables. The first is F, the polarization ratio of the exciting light which reaches the sample. The second is r, the emission anisotropy of the sample, which is the polarization "response" of the sample to plane polarized exciting light. The third is G, the polarization ratio of the emission detection system, which is the ratio of the sensitivities of the detection system to vertically and horizontally polarized light. The fourth is α, the viewing angle, which is the angle between the direction of the propagation of the exciting light and the direction from which the emission is being detected.

The intensity and the degree of polarization of the fluorescence emission that the sample exhibits are functions of F, r, and α, while the actual readings obtained with a typical spectrofluorimeter are functions of all four variables, F, r, α, and G. A theoretical analysis is made taking all these factors into account, and proper mathematical models are developed for the different modes of operation in which a fluorimeter can be used. These are verified experimentally with data obtained for a sample which has a high degree of emission anisotropy (Nile Blue A Perchlorate in glycerol). A recently designed goniospectrofluorimeter was used. Calibration procedures are developed and recommendations are made for modes of operation and fluorescence standards.

Key words: Emission anisotropy; fluorescence; fluorescence quantum yield; fluorescence standards; fluorimetry; polarization; spectrofluorimetry; viewing angle.

1. Introduction

The measurement of fluorescence polarization is an important analytical technique in identifying molecular transitions and obtaining information on the structure of macromolecules. Polarization of fluorescence also constitutes a significant source of systematic errors in fluorescence intensity measurements, such as; measurements of excitation and emission spectra, relative quantum yield determinations, and fluorescence decay measurements. All of these measurements are fraught with experimental difficulties in that the intensity readings and the apparent degree of polarization of the fluorescence emission from a polarizing sample depend, not only on the emission anisotropy of the sample itself, but also on the state of polarization of the exciting radiation and on polarization effects introduced by the sample cell and the emission detection system. These instrumental artifacts have been considered by several authors. Weber and Teale [1][1] derived an equation for obtaining fluorescence quantum yields based on a solution scatterer as the standard. This equation is valid when the excitation is unpolarized and contains a correction factor that takes into account the polarizations of the sample and the standard. Azumi and McGlynn [2] developed a technique to obtain the correction factor required to eliminate the bias of the emission detection system with respect to the state of polarization of the fluorescence emission. This factor is obtained by successive measurements with a polarizer in the emission beam alined in the vertical and horizontal positions, and a polarizer alined horizontally in the excitation beam. For the spectral calibration of the emission detection system, Melhuish [3] used a magnesium-oxide scatterer to depolarize the incident radiation, and a polarizer at the entrance slit of the emission monochromator. True spectra are obtained by recording spectra with the polarizer in the vertical and horizontal positions, applying the appropriate correction factors, and adding. Whereas these authors use right-angle viewing, Almgren [4] and Shinitzky [5] pointed out that the fluorescence emission from a polarized sample displays a typical anisotropic distribution which may make it desirable to use a different viewing angle. Assuming unpolarized exciting radiation, they showed theoretically that the fluorescence intensity is unaffected by the emission anisotropy of the sample if a viewing angle of $\cos^{-1}\sqrt{1/3}$ is chosen.

In this paper we attempt to give a unified picture of the combined effects of sample emission anisotropy and spectrofluorimeter polarization properties on fluorescence intensity and polarization measurements. A theoretical analysis is made of the general case in which a sample having nonzero emission anisotropy is excited by partially polarized radiation, and is analyzed with a biased detection system at arbitrary

[1] Figures in brackets indicate the literature references at the end of this paper.

viewing angles. This analysis is reduced to proper mathematical models for the different modes of operation in which a fluorimeter can be used, and is verified experimentally. Calibration procedures are developed and recommendations are made for various modes of operation and uses of fluorescence standards.

2. Theory

Polarization of fluorescence indicates that the emission dipoles of the excited molecules are preferentially oriented with respect to the electric vector of the exciting radiation. This usually occurs when relatively large molecules with long molecular axes have short fluorescence lifetimes relative to their rotational relaxation times, so that after excitation these molecules emit before they can rotate sufficiently to lose all 'memory' of the exciting field.

The general expressions for this anisotropic distribution of emitting molecules are obtained as follows [6]. Referring to figure 1, we assume that the exciting

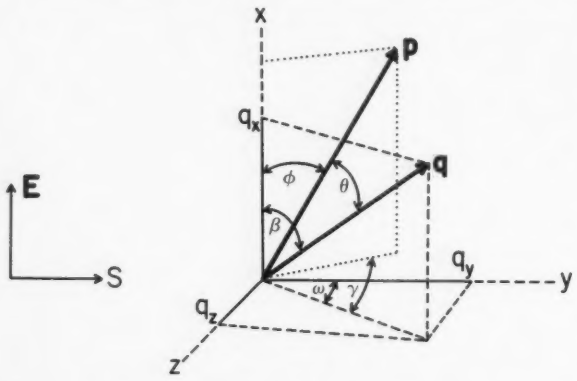

FIGURE 1. *Spatial orientation of the absorption and emission probability vectors,* **p** *and* **q**, *of a randomly oriented molecule relative to the electric vector,* **E**, *of the exciting radiation which propagates along the* y *axis with photon flux density,* S.

The emission probability vector has been resolved into the components q_x, q_y, and q_z along the x, y, and z axes. The coordinate system is the same as in ref. [5].

radiation is plane polarized with its electric vector **E** parallel to the x axis, and that it is propagating in the y direction with a photon flux density S ($h\nu$ cm^{-2} s^{-1}) [7]. This radiation field interacts with a randomly oriented collection of molecules with absorption and emission dipole oscillators that have fixed orientations relative to the molecular structure and enclose a given angle θ, as shown in figure 1. The probabilities for absorption and emission by one arbitrarily oriented molecule are given by the squared magnitudes of the probability vectors **p** and **q**, so that

$$|\mathbf{p}|^2 = S\sigma_0 \cos^2 \phi, \tag{1a}$$

$$|\mathbf{q}|^2 = Q|\mathbf{p}|^2, \tag{1b}$$

where ϕ is the angle between the absorption oscillator and the electric field, σ_0 is the absorption cross section for absorption oscillators which are parallel to the electric field of the exciting radiation, and Q is the quantum efficiency for fluorescence. The squared components of **q** in the directions of the three coordinate axes are:

$$q_x^2 = |\mathbf{q}|^2 \cos^2 \beta = S\sigma_0 Q \cos^2 \phi \cos^2 \beta, \tag{2a}$$

$$q_y^2 = |\mathbf{q}|^2 \sin^2 \beta \cos^2 \omega = S\sigma_0 Q \cos^2 \phi \sin^2 \beta \cos^2 \omega, \tag{2b}$$

$$q_z^2 = |\mathbf{q}|^2 \sin^2 \beta \sin^2 \omega = S\sigma_0 Q \cos^2 \phi \sin^2 \beta \sin^2 \omega, \tag{2c}$$

where β is given by

$$\cos \beta = \cos \theta \cos \phi + \sin \theta \sin \phi \cos \gamma, \tag{3}$$

γ being the angle between the planes **(E, p)** and **(E, q)**.

The corresponding expressions for a random collection of molecules are obtained by substituting the appropriate averages of the various trigonometric functions into these equations. Since the number of absorption oscillators in a solid angle element in the direction ϕ is proportional to $d(\cos \phi)$, we have

$$\overline{\cos^{2n} \phi} = \int_0^{\pi} \cos^{2n} \phi \, d(\cos \phi) \Big/ \int_0^{\pi} d(\cos \phi) = 1/(2n+1). \tag{4a}$$

On the other hand, the distribution of molecules is isotropic in γ and ω, so that

$$\overline{\cos \gamma} = \int_0^{2\pi} \cos \gamma d\gamma \Big/ \int_0^{2\pi} d\gamma = 0, \tag{4b}$$

$$\overline{\cos^2 \gamma} = \int_0^{2\pi} \cos^2 \gamma d\gamma \Big/ \int_0^{2\pi} d\gamma = 1/2, \tag{4c}$$

and similarly

$$\overline{\cos^2 \omega} = \overline{\sin^2 \omega} = 1/2. \tag{4d}$$

Therefore,

$$\begin{aligned}\overline{\cos^2 \phi \cos^2 \beta} &= \overline{\cos^2 \theta}\ \overline{\cos^4 \phi} \\ &\quad + \overline{\sin^2 \theta \cos^2 \phi \sin^2 \phi}\ \overline{\cos^2 \gamma} \\ &\quad + 2 \overline{\cos \theta \sin \theta \cos^3 \phi \sin \phi}\ \overline{\cos \gamma} \\ &= \overline{\cos^2 \theta}\ \overline{\cos^4 \phi} \\ &\quad + (1/2)\ \overline{\sin^2 \theta}\ (\overline{\cos^2 \phi} - \overline{\cos^4 \phi}) \\ &= (1/5)\ \overline{\cos^2 \theta} + (1/15)\ \overline{\sin^2 \theta} \\ &= (1/15)\ (\overline{2 \cos^2 \theta} + 1),\end{aligned} \tag{5a}$$

and

$$\overline{\cos^2 \phi \sin^2 \beta \cos^2 \omega} = \overline{\cos^2 \phi \sin^2 \beta \sin^2 \omega}$$

$$= (1/2)\,\overline{\cos^2\phi\,\sin^2\beta}$$

$$= (1/2)\,(\overline{\cos^2\phi}$$

$$-\overline{\cos^2\phi\,\cos^2\beta})$$

$$= (1/2)[(1/3)$$

$$-(1/15)(2\,\overline{\cos^2\theta}+1)]$$

$$= (1/15)(2-\overline{\cos^2\theta}). \tag{5b}$$

Hence, eqs (1a, b) and (2a, b, c) lead to

$$\overline{|\mathbf{p}|^2} = (1/3)S\sigma_0, \tag{6a}$$

$$\overline{|\mathbf{q}|^2} = (1/3)S\sigma_0 Q, \tag{6b}$$

$$\overline{q_x^2} = (1/15)S\sigma_0 Q(2\,\overline{\cos^2\theta}+1), \tag{6c}$$

$$\overline{q_y^2} = \overline{q_z^2} = (1/15)S\sigma_0 Q(2-\overline{\cos^2\theta}). \tag{6d}$$

In order to relate these results to the macroscopic properties of the sample, consider a volume element $dV = dxdydz$ containing dN molecules. The photon flux ($h\nu$ s^{-1}) into this volume element is

$$d\Phi_0 = S dx dz, \tag{7a}$$

and, according to eq (6a), the absorbed flux is

$$d\Phi_a = |p|^2 dN = (1/3)S\sigma_0 dN$$
$$= d\Phi_0 (1/3)\sigma_0 (dN/dV)\,dy. \tag{7b}$$

The analogous expression given by Beer's law is

$$d\Phi_a = d\Phi_0 (\ln 10)\,\epsilon c dy, \tag{7c}$$

where ϵ is the molar absorptivity (l mol^{-1} cm^{-1}) and c is the concentration (mol l^{-1}). If dV is measured in cm^3, we have $dN/dV = c\Re/1000$ (where $\Re$ is Avogadro's number) and therefore

$$\sigma = (1/3)\sigma_0 = \left[\frac{1000(\ln 10)}{\Re}\right]\epsilon. \tag{8a}$$

Here, σ represents the average absorption cross section (in cm^2) per molecule [8]. Similarly

$$\tau = \sigma Q = \left[\frac{1000(\ln 10)}{\Re}\right]\epsilon Q, \tag{8b}$$

is the corresponding cross section for fluorescence. Equations (6a, b) may then be expressed in the forms

$$\overline{|\mathbf{p}|^2} = S\sigma,\ \overline{|\mathbf{q}|^2} = S\tau, \tag{9a}$$

and by analogy eqs (6c, d) become

$$\overline{q_x^2} = S\tau_{\|},\ \overline{q_y^2} = \overline{q_z^2} = S\tau_{\perp}, \tag{9b}$$

where

$$\tau_{\|} = (1/5)\tau(\overline{2\cos^2\theta}+1), \tag{10a}$$

and

$$\tau_{\perp} = (1/5)\tau(2-\overline{\cos^2\theta}), \tag{10b}$$

are identified as the component cross sections for molecules with absorption dipole oscillators that are parallel and perpendicular, respectively, to the electric field vector of the exciting radiation. Alternative forms of eqs (10a, b) which are useful for mathematical convenience, are

$$\tau_{\|} = (1/3)\tau(1+2r), \tag{11a}$$

$$\tau_{\perp} = (1/3)\tau(1-r), \tag{11b}$$

where

$$r = \frac{\tau_{\|}-\tau_{\perp}}{\tau} = (1/5)\,(\overline{3\cos^2\theta}-1), \tag{12}$$

is the 'emission anisotropy' of the sample, as defined by Jablonski [9].

For a collection of randomly oriented molecules that do not rotate during the time interval between absorption and emission (a 'random but frozen' distribution), θ is constant and equal to the intramolecular angle of energy transfer between the absorption and emission dipoles, θ_0. In this case, eq (12) defines the intrinsic emission anisotropy of the molecule,

$$r_0 = (1/5)\ (3\cos^2\theta_0 - 1). \tag{13a}$$

The range of possible values for r_0 is

$$-0.2 \leqslant r_0 \leqslant 0.4, \tag{13b}$$

where the two limiting cases are those in which the absorption and emission dipoles are either parallel ($r_0 = 0.4$) or perpendicular ($r_0 = -0.2$) to each other. In a random aggregate of mobile emission oscillators, each molecule rotates over a certain angle θ' between absorption and emission. In this case the angle θ appearing in eq (12) is given by an expression similar to eq (3); that is,

$$\cos\theta = \cos\theta_0\cos\theta' + \sin\theta_0\sin\theta'\cos\gamma', \tag{14a}$$

where γ' is the angle between the two planes defined by the absorption and emission oscillators at the times of absorption and emission. As in the case of eqs (4b, c), we have

$$\overline{\cos\gamma'} = 0,\ \overline{\cos^2\gamma'} = 1/2,$$

and therefore

$$\overline{\cos^2\theta} = \cos^2\theta_0\,\overline{\cos^2\theta'} + (1/2)\,\sin^2\theta_0\,\overline{\sin^2\theta'}. \quad (14b)$$

This can be rearranged to give

$$(3\,\overline{\cos^2\theta} - 1) = (1/2)\,(3\cos^2\theta_0 - 1)\,(3\,\overline{\cos^2\theta'} - 1), \quad (14c)$$

so that

$$r = (1/2)\,r_0\,(3\,\overline{\cos^2\theta'} - 1). \quad (14d)$$

Thus, $r = 0$ for a completely relaxed system for which the fluorescence lifetime is significantly longer than the rotational relaxation time of the molecules, so that the distribution in θ' becomes random (i.e., $\overline{\cos^2\theta'} = 1/3$). The intermediate cases in which the randomization due to Brownian motion or intermolecular energy transfer is only partially effective ($\overline{\cos^2\theta'} > 1/3$) lead to values of $r \neq 0$ within a narrower range than that specified in (13b).

The fluorescence emission detected when a sample with given emission anisotropy r is analyzed with a typical spectrofluorimeter can now be calculated in the following manner, which is a generalization of the treatments given by Kalantar [10], Almgren [4], and Shinitzky [5]. As depicted in figure 2, the exciting radiation is assumed to be partially polarized and is regarded as the incoherent superposition of two plane-polarized components with photon flux densities, S^V and S^H, which are propagated in the y direction, and with electric vectors, $\mathbf{E}^V$ and $\mathbf{E}^H$, which are parallel to the x and z directions, respectively. The anisotropic distribution of emission dipoles is again described in terms of a probability vector $\mathbf{q}$, which is similarly regarded as the incoherent superposition of two vectors, $\mathbf{q}^V$ and $\mathbf{q}^H$. The components of the latter with respect to the three coordinate axes are obtained from eq (9b), once directly and once with interchanged x and z coordinates. Thus, the rms components of $\mathbf{q}$ are given by

$$\overline{q_x^2} = S^V\tau_{\parallel} + S^H\tau_{\perp}, \quad (15a)$$

$$\overline{q_y^2} = S^V\tau_{\perp} + S^H\tau_{\perp}, \quad (15b)$$

$$\overline{q_z^2} = S^V\tau_{\perp} + S^H\tau_{\parallel}. \quad (15c)$$

The fluorescence intensity $I(\alpha)$ ($h\nu\,s^{-1}\,sr^{-1}$) emitted into a given viewing direction α in the yz plane is proportional to the squared rms components of $\mathbf{q}$ in the plane perpendicular to this viewing direction and is polarized in the directions of these components. Thus it is seen that $I(\alpha)$ consists of vertically and horizontally polarized components which are proportional to q_x^2 and $(q_y^2\sin^2\alpha + q_z^2\cos^2\alpha)$, respectively. When eqs (15a, b, c) and (11a, b) are used to evaluate these expressions, it is seen that $I(\alpha)$ is the sum of the four components

$$I_V^V(\alpha) = kS^V\tau_{\parallel} = (1/3)kS^V\tau(1+2r), \quad (16a)$$

$$I_V^H(\alpha) = kS^H\tau_{\perp} = (1/3)kS^H\tau(1-r), \quad (16b)$$

$$I_H^V(\alpha) = kS^V\tau_{\perp} = (1/3)kS^V\tau(1-r), \quad (16c)$$

$$I_H^H(\alpha) = kS^H(\tau_{\perp}\sin^2\alpha + \tau_{\parallel}\cos^2\alpha) = (1/3)kS^H\tau[(1-r) + 3r(\cos^2\alpha)]. \quad (16d)$$

where k is an appropriate constant of proportionality. (Here, as in similar equations to be developed later on, superscripts refer to the state of polarization of the exciting radiation, and subscripts refer to the state of polarization of the emitted flux. The letters V and H denote vertically and horizontally polarized light, and similarly the letter U will be used to denote unpolarized light. No sub- or superscripts refer to the general case of partial polarization.)

The fluorescence intensities emitted along the three coordinate axes in figure 2 are

$$I_x = k\,(\overline{q_y^2} + \overline{q_z^2}),\ I_y = k\,(\overline{q_z^2} + \overline{q_x^2}),\ I_z = k\,(\overline{q_x^2} + \overline{q_y^2}). \quad (17a)$$

Therefore,

$$I_0 \equiv (1/3)(I_x + I_y + I_z) = (2/3)\,k\,(\overline{q_x^2} + \overline{q_y^2} + \overline{q_z^2}) = (2/3)k(S^V + S^H)\,(\tau_{\parallel} + 2\tau_{\perp}) = (2/3)k(S^V + S^H)\tau, \quad (17b)$$

represents the spatial average of the intensity emitted by the sample. This average intensity I_0 (which is equal to the intensity that would be emitted into any

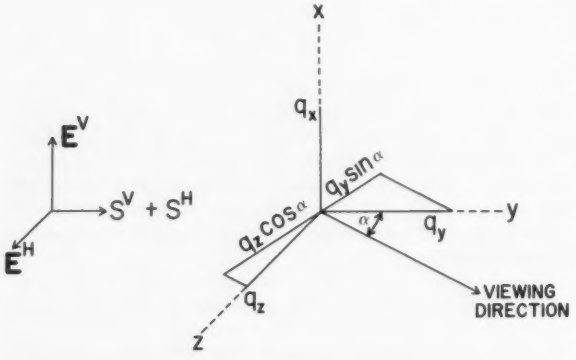

FIGURE 2. *Resolution of the emission probability vector,* $\mathbf{q}$, *into components:*

(a) q_x, q_y, q_z—*Components parallel and perpendicular to the electric field vectors,* $\mathbf{E}^V$ *and* $\mathbf{E}^H$ *of partially polarized exciting radiation with a photon flux density of* $S^V + S^H$, *and*

(b) ($q_z \cos\alpha$) *and* ($q_y \sin\alpha$)—*components perpendicular to the viewing angle,* α.

viewing direction if the sample had zero emission anisotropy) is proportional to the fluorescence quantum yield of the sample, and therefore constitutes a physically meaningful basis for fluorescence measurements. Thus, the bias introduced into fluorescence intensity measurements by the emission anisotropy r of a sample is revealed by combining eqs (16a–16d) and (17b) to give.

$$I(\alpha) = I_V^V(\alpha) + I_H^V(\alpha) + I_V^H(\alpha) + I_H^H(\alpha)$$

$$= I_0 \left\{ 1 + r \left[\frac{3\cos^2\alpha + (F-2)}{2(1+F)} \right] \right\}, \quad (18)$$

where

$$F \equiv S^V/S^H, \quad (19)$$

is the polarization ratio of the exciting radiation. In addition, eqs (16a–16d) show that the degree of polarization of the fluorescence emission,

$$P(\alpha) \equiv \frac{[I_V^V(\alpha) + I_V^H(\alpha)] - [I_H^V(\alpha) + I_H^H(\alpha)]}{[I_V^V(\alpha) + I_V^H(\alpha)] + [I_H^V(\alpha) + I_H^H(\alpha)]}$$

$$= \frac{3r(F - \cos^2\alpha)}{2(1+F) + r[3\cos^2\alpha + (F-2)]}, \quad (20)$$

is also a rather complicated function of emission anisotropy, polarization of the exciting radiation, and viewing geometry.

These results lead to several important conclusions for the particular cases in which the exciting radiation is either plane polarized or completely depolarized. These limiting cases will be discussed now.

(a) Vertically polarized excitation ($F = \infty$). In this case,

$$I^V = I_0^V(2+r)/2, \quad (21a)$$

$$P^V = 3r/(2+r), \quad (21b)$$

where the argument α is omitted since these expressions are independent of viewing angle. These two equations can be combined into

$$I^V = 3I_0^V/(3 - P^V), \quad (21c)$$

which is valid for arbitrary viewing angles α. Similarly eqs (21b) and (10a, b) show that the well-known relation

$$P^V = \frac{\tau_{\parallel} - \tau_{\perp}}{\tau_{\parallel} + \tau_{\perp}} = \frac{3\,\overline{\cos^2\theta} - 1}{3 + \overline{\cos^2\theta}}, \quad (21d)$$

is also valid for all values of α ($P_0^V = 1/2$ or $-1/3$ for $\theta_0 = 0$ and 90°, respectively). This independence of viewing angle and, thus, insensitivity to misalinement, as well as the simplicity of eqs (21c, d) make vertically polarized excitation a particularly desirable mode of operation of a fluorimeter.

(b) Horizontally polarized excitation ($F = 0$). Here, eqs (18) and (20) are reduced to

$$I^H(\alpha) = I_0^H[1 + (1/2)r(3\cos^2\alpha - 2)], \quad (22a)$$

$$P^H(\alpha) = \frac{-3r(\cos^2\alpha)}{2 + r(3\cos^2\alpha - 2)}, \quad (22b)$$

which shows that both quantities vary with viewing angle. A useful fact is that at the usual right angle viewing geometry of common fluorimeters $P^V(90°) = 0$, and thus the fluorescence emission is unpolarized. As pointed out by Azumi and McGlynn [2], this property of the horizontally polarized mode of excitation can be employed for the polarization calibration of emission monochromators.

(c) Unpolarized excitation ($F = 1$). In this case, one obtains

$$I^U(\alpha) = I_0^U[1 + (1/4)r(3\cos^2\alpha - 1)], \quad (23a)$$

$$P^U(\alpha) = \frac{3r(\sin^2\alpha)}{4 + r(3\cos^2\alpha - 1)}. \quad (23b)$$

Equation (23a) constitutes the basis for the previously mentioned proposal to use $\alpha_d = \cos^{-1}\sqrt{1/3}$ as the preferred viewing angle for which the fluorescence intensity, $I^U(\alpha_d) = I_0$, is unaffected by the emission anisotropy of the sample. Equation (23b) shows that $P^U(\alpha_d) = 1/2\ r$, which constitutes another interesting and not previously noted property of this particular viewing geometry. It should be noted, however, that

$$I^U(\alpha_d + \Delta\alpha) = I_0^U(1 - r\Delta\alpha/\sqrt{2} + \ldots), \quad (23c)$$

and

$$P^U(\alpha_d + \Delta\alpha) = (1/2)\ r\,[1 + (1+r)\,\Delta\alpha/\sqrt{2} + \ldots], \quad (23d)$$

which indicate that both conditions are sensitive to angular misalinements. For example, a 1° departure from α_d will produce a 0.5 percent error in $I^U(\alpha)$ and a 1.8 percent error in $P^U(\alpha)$ if $r = 0.4$. The common 90° geometry of ordinary fluorimeters is less sensitive to errors in angular alinement, since eqs (18) and (20) both have zero derivatives for $\alpha = 90°$.

For right-angle viewing, eqs (23a, b) are reduced to

$$I^U(90°) = I_0^U(4-r)/4, \quad (24a)$$

$$P^U(90°) = 3r/(4-r), \quad (24b)$$

which can be combined into the familiar form used in the Weber-Teale correction formula [1],

$$I^U(90°) = 3\,I_0^U/[3 + P^U(90°)]. \quad (24c)$$

Equations (24b) and (10a, b) also show that

$$P^U(90°) = \frac{\tau_{||} - \tau_\perp}{\tau_{||} + 3\tau_\perp} = \frac{3\,\overline{\cos^2\theta} - 1}{7 - \overline{\cos^2\theta}}, \qquad (24d)$$

which is another well-known expression ($P_0^U(90°) = 1/3$ and $-1/7$ for $\theta_0 = 0°$ and 90°, respectively). These equations are valid for right-angle viewing, only.

The preceding discussion is summarized in figures 3 and 4, which show plots of florescence intensity and degree of polarization versus viewing angle for the three modes of excitation assumed and for $r = 0.383$. In the Discussion Section, these graphs will be compared with experimental data.

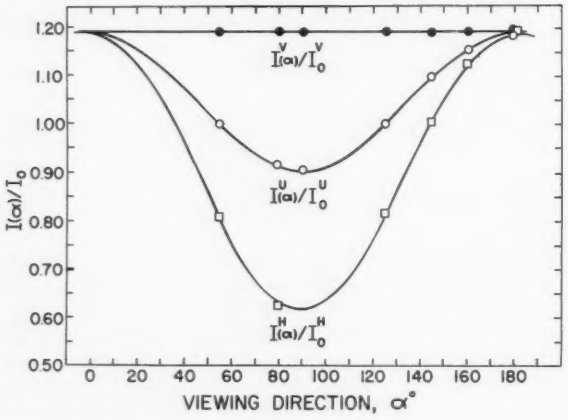

FIGURE 3. *Ratio of the fluorescence intensities for vertically* $\left(\frac{I^V(\alpha)}{I_0^V}\right)$, *horizontally* $\left(\frac{I^H(\alpha)}{I_0^H}\right)$, *and depolarized* $\left(\frac{I^U(\alpha)}{I_0^U}\right)$ *exciting radiation.*

The numerators are the intensities emitted by an anisotropic sample into the viewing angle, α and the denominators are the corresponding intensities of a sample having zero emission anisotropy. The solid lines represent theoretical curves and the symbols represent values obtained from experimental data.

In addition to providing partially polarized exciting radiation, most fluorimeters also have a detection system which is biased to the polarization of the fluorescence emission. Thus, the recorded signals corresponding to the four components of the fluorescence intensity given by eqs (16a–16d) are

$$R_V^V(\alpha) = T_V I_V^V(\alpha) = kS^V\tau_{||}T_V$$
$$= (1/3)kS^V\tau(1+2r)T_V, \qquad (25a)$$

$$R_V^H(\alpha) = T_V I_V^H(\alpha) = kS^H\tau_\perp T_V$$
$$= (1/3)kS^H\tau\,(1-r)\,T_V, \qquad (25b)$$

$$R_H^V(\alpha) = T_H I_H^V(\alpha) = kS^V\tau_\perp T_H$$
$$= (1/3)kS^V\tau\,(1-r)T_H, \qquad (25c)$$

$$R_H^H(\alpha) = T_H I_H^H(\alpha) = kS^H\,(\tau_\perp \sin^2\alpha + \tau_{||}\cos^2\alpha)\,T_H$$
$$= (1/3)\,kS^H\tau\,[(1-r) + 3r\,(\cos^2\alpha)]\,T_H, \qquad (25d)$$

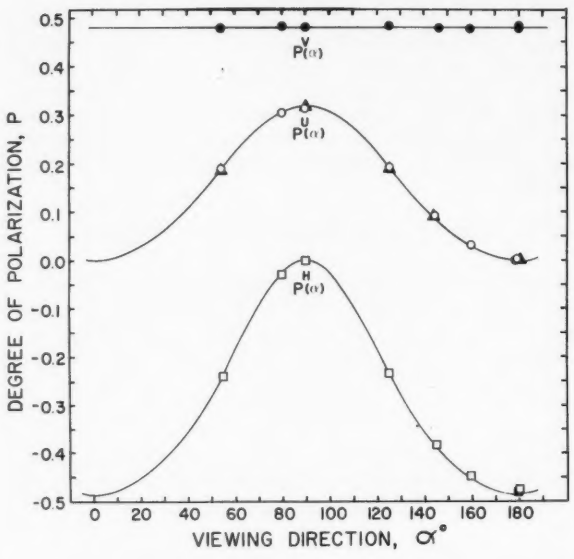

FIGURE 4. *The degree of polarization,* P, *for vertically* $[P^V(\alpha)]$, *horizontally* $[P^H(\alpha)]$, *and depolarized* $[P^U(\alpha)]$ *exciting radiation as a function of viewing angle.*

The solid lines represent theoretical curves and the symbols represent values obtained from experimental data.

where T_V and T_H are the sensitivities of the detection system for vertically and horizontally polarized radiation, respectively. Similarly, the signal corresponding to the (unpolarized) spatial average I_0 of the fluorescence intensity is

$$R_0 = (1/2)\,(T_V + T_H)I_0 = (1/3)k(S^V + S^H)\tau(T_V + T_H). \qquad (26)$$

Combining these equations gives

$$R(\alpha) = R_V^V(\alpha) + R_V^H(\alpha) + R_H^V(\alpha) + R_H^H(\alpha)$$
$$= R_0\left\{1 + r\left[\frac{3\cos^2\alpha - (1+F+G-2FG)}{(1+F)(1+G)}\right]\right\}, \qquad (27)$$

where $R(\alpha)$ is the total signal recorded, and where

$$G \equiv T_V/T_H, \qquad (28)$$

is the polarization ratio of the detection system.

Equation (27) is analogous to eq (18), and describes the combined polarization effects of sample, exciting radiation, viewing angle, and detection system. It reduces to eq. (23a) if $F = G = 1$, and shows that the general condition for which $R(\alpha) = R_0$ is given by

$$\cos^2\alpha = (1/3)\,(1+F+G-2FG). \qquad (29)$$

However, the angle so defined depends on the polarization ratios of the exciting radiation and the detection

system, and therefore is different for different fluorimeters, and for the same fluorimeter the angle varies with excitation and emission wavelengths. Furthermore, no real solution at all is obtained for α unless $0 \leq 1+F+G-2FG \leq 3$. Hence it is seen that, under typical laboratory conditions, there is no practicable viewing geometry for which the recorded signal is an unbiased measure of the quantum efficiency of a sample having a nonzero emission anisotropy r. In order to utilize the effect predicted by Almgren [4] and Shinitzky [5], it is necessary to depolarize the excitation and detection systems by using scrambler plates in both beams. However, most spectrofluorimeters cannot easily be adapted to provide the 54.75° or 125.25° viewing geometry required in this case. Furthermore, no information can be obtained about the emission anisotropy of the sample unless readings are also taken at other viewing angles, as will be shown.

A preferable approach is to use a fixed viewing geometry with polarizers in the excitation and emission beams. Taking the four readings defined by eqs (25a–25d) and forming the following ratios, one obtains

$$\frac{R_V^V(\alpha)}{R_H^V(\alpha)} = DG, \tag{30a}$$

$$\frac{R_H^V(\alpha)}{R_V^H(\alpha)} = F/G, \tag{30b}$$

$$\frac{R_H^H(\alpha)}{R_V^V(\alpha)} = [\cos^2\alpha + (1/D)\sin^2\alpha]/FG, \tag{30c}$$

where

$$D \equiv \tau_{\|}/\tau_{\perp}, \tag{31a}$$

is the 'dichroic ratio of emission' of the excited molecules. This quantity D is more convenient to work with than the emission anisotropy r, and is related to r by

$$D = \frac{1+2r}{1-r}, \qquad r = \frac{D-1}{D+2}. \tag{31b}$$

The possible range of values for D, as defined by eqs (13b) and (31b) is

$$1/2 \leq D \leq 3, \tag{31c}$$

with $D=1$ for an unpolarized sample. For arbitrary viewing angles α, G can be obtained by combining eqs (30a, 30b, 30c) to give

$$G^2\left[\frac{R_H^V(\alpha)}{R_V^H(\alpha)}\right]\left[\frac{R_H^H(\alpha)}{R_V^V(\alpha)}\right] - G\left[\frac{R_H^V(a)}{R_V^V(\alpha)}\right](\sin^2\alpha) - \cos^2\alpha = 0. \tag{32a}$$

Solving this quadratic gives

$$G = \left[\frac{R_V^H(\alpha)}{R_H^H(\alpha)}(\sin^2\alpha)/2\right] + \sqrt{\left[\frac{R_V^H(\alpha)}{R_H^H(\alpha)}(\sin^2\alpha)/2\right]^2 + \left[\frac{R_V^H(\alpha)}{R_H^H(\alpha)}\right]\left[\frac{R_V^V(\alpha)}{R_H^V(\alpha)}\right](\cos^2\alpha)}, \tag{32b}$$

where only the positive root has physical significance. With G determined, F and D are obtained from eqs (30a, 30b), so that the desired unbiased reading R_0 can now be found from the four individual readings in several different ways. A useful expression for R_0, which is independent of viewing angle, is obtained by combining eqs (25a, 25b, 25c) into

$$\frac{R_V^V(\alpha)}{S^V T_V} + \frac{R_V^H(\alpha)}{S^H T_V} + \frac{R_H^V(\alpha)}{S^V T_H} = k\tau. \tag{33a}$$

Upon substitution into eq (26), this leads to

$$R_0 = \frac{(1+F)(1+G)}{3FG}[R_V^V(\alpha) + FR_V^H(\alpha) + GR_H^V(\alpha)]. \tag{33b}$$

From this discussion, it is evident that the use of polarizers in the excitation and emission beams permits the complete characterization of sample and spectrofluorimeter, and yields more information than a system not using polarizers. Equations (30a) through (33b) are applicable for arbitrary viewing angles α but give the most accurate results for $\alpha = 90°$, where the angular variation of $R_H^H(\alpha)$ is smallest. For this preferred and most commonly used viewing geometry, eq (32b) is reduced to the correction formula used by Azumi and McGlynn [2] and one obtains

$$F = \frac{R_H^V(90°)}{R_H^H(90°)}, \tag{34a}$$

$$G = \frac{R_V^H(90°)}{R_H^H(90°)}, \tag{34b}$$

$$D = \frac{R_V^V(90°)R_H^H(90°)}{R_H^V(90°)R_V^H(90°)}, \tag{34c}$$

R_0 being the same as given by eq (33b).

3. Experimental Procedures [11]

Inherent in the derivation above are the assumptions that the sample is irradiated by a parallel beam of light and that the luminescence occurs from essentially a point source. The first condition is achieved experimentally by proper alinement of the optics and the second by working with small and dilute samples

so that the low light absorption approximation of Beer's law,

$$\Phi_a = \Phi_0(1 - e^{-2.303\epsilon bc}) \simeq \Phi_0 2.303\epsilon bc,$$

is valid. The system used to investigate the polarization effects consists of a fluorescent dye dissolved in the highly viscous solvent glycerol. Exciting light at 632.8 nm is absorbed by the dye and its fluorescence at 685.0 nm was measured as a function of angle relative to the direction of propagation of the exciting light. The measurements were made using a new goniospectroradiometer recently designed and built at NBS [12]. This versatile instrument can be operated in different modes, one of which is as a spectrofluorimeter. Basically, it consists of a xenon arc source, excitation monochromator, reference detector, sample compartment, emission monochromator, signal detector, and computer-interfaced electronics. The whole emission detection system is mounted on a rotary carriage which pivots about the center line of the sample, thus allowing for viewing the sample from arbitrary angles relative to the direction of the exciting radiation between 180° (straight through) and approximately 20°.

A scale diagram of the apparatus, as adapted for this experiment, is shown in figure 5. The xenon arc source, excitation monochromator, and reference detector were removed and replaced with a 15 milliwatt He-Ne laser (HNL), a light source of high intensity and monochromaticity. The 632.8 nm laser light is reflected from a flat mirror (FM) and impinges on a barium sulfate scatterer (B) at an angle 45° from normal. A certain solid angle of the diffusely reflected light is collected and focused by the biconvex lens (L) (45 mm diam., 148 mm f.l.) through a Glan-Taylor polarizing prism (P) to the sample cell (S). The position of the lens relative to the barium sulfate and sample cell was adjusted such that the beam cross section remained nearly constant in the neighborhood of the image, thus approximating a collimated beam through the sample. The laser|barium-sulfate|lens system approximates light as it would emerge from an excitation monochromator and is used to destroy the spatial coherence of the laser light while keeping the high intensity, monochromaticity and low scattered exciting light levels (of all other wavelengths) which a xenon lamp-monochromator system cannot supply. A cylindrical NMR tube with an internal diameter of 1.35 mm and an outside diameter of 5 mm was used as the sample cell. The tube was mounted in an air driven NMR sample spinner and was spun at 2,500 rpm to average out any irregularities in the glass. The beam diameter of the exciting light at the sample was 5 mm, thus giving a "glowing rod" of fluorescence 1.35 mm in diameter and 5 mm high. The absorbance of the dye was kept low ($A = 0.019$) to have a uniform emission intensity throughout the cell as the light propagated through it. A 14° cone of the fluorescence emission was focused at the monochromator entrance slit by the ellipsoidal mirror (EL). A second Glan-Taylor polarizer (P) was placed directly behind the sample (not behind the mirror, as shown inadvertently in figure 5), and a Schott RG 645 filter (F) was placed in front of the slit. The filter cut out most of the 632.8 nm exciting light but passed most of the fluo-

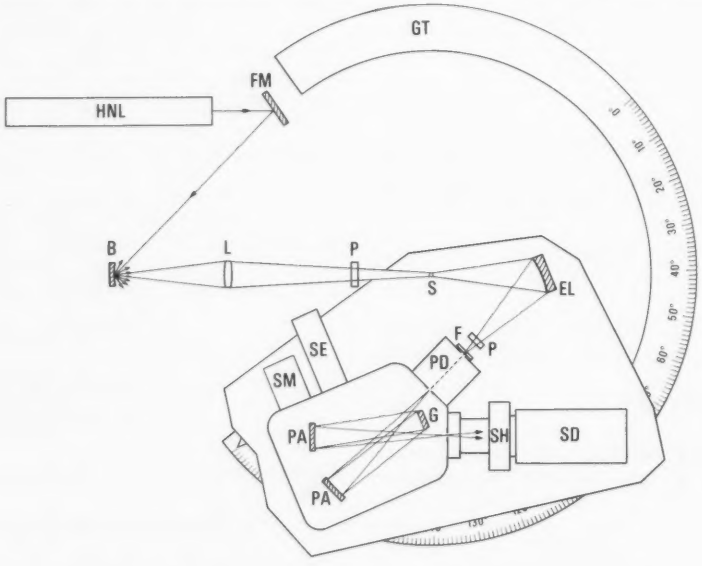

FIGURE 5. *The spectroradiometer as adapted for this experiment.*

HNL–helium neon laser; FM–flat mirror; B–barium sulfate scatterer; L–biconvex collecting lens; P–polarizer; S–spinning sample tube; EL–ellipsoidal mirror; F–Schott RG 645 filter; PD–prism predisperser; PA–G–PA–emission monochromator; SE–wavelength shaft encoder; SM–stepping motor; SH–shutter and SD–S20 photomultiplier tube. The emission detection system pivots around the sample tube on the track GT.

rescence at longer wavelengths. This made viewing at 180° (straight through) possible even though the solution absorbs only a very small percentage of the exciting light. The emission monochromator consists of a prism predisperser (PD) and a grating monochromator (PA, G, PA). The bandpass of the monochromator was 4.8 nm for the 2 mm slits which were used. The rotary table carrying the emission detection system is attached to the sample-holder support (S) by a large ball bearing, and is supported near its periphery by two rollers which move along a large circular track (GT). After the fluorescence passes through the monochromator, it was detected by an extended S–20 photomultiplier tube (SD). The signal from the PM tube was amplified and fed into a time shared computer which took a certain number of readings in a given time interval (usually 100 in 10 s). The average and the standard error were calculated and printed out on a teletype-writer. The readings were obtained in volts and the overall sensitivity of the system was adjusted by changing the dynode voltage applied to the PM tube.

Nile Blue A Perchlorate (Eastman Kodak, laser grade Lot #A3–X) was used without further purification. It was chosen because its maximum absorption band is near 632.8 nm, allowing extremely low concentrations to be used to minimize intermolecular energy transfer and self-absorption of the fluorescence which tend to depolarize the emission before it gets out of the cell. Glycerol (Fisher Certified ACS) was used as the solvent. The actual concentration of the dye used was 9.4×10^{-4} g/l (2.25×10^{-6} mol/l). No attempt was made to purge the solutions of dissolved oxygen. Blanks were run using a similar NMR tube filled with solvent only. The barium sulfate (Eastman White Reflectance Standard) was pressed into pellet form in a special holder. All measurements were carried out at room temperature, 22 °C.

4. Results

Data were taken with and without polarizers in the excitation and emission beams and at different viewing angles. With both polarizers in place, four readings were taken at each viewing angle, α, corresponding to the four different orthogonal positions the polarizers can have, $R_V^V(\alpha)$, $R_H^V(\alpha)$, $R_V^H(\alpha)$, and $R_H^H(\alpha)$ (see table 1). The superscript again refers to the mode of excitation and the subscript to the mode of the emission polarizer. The $R_H^H(\alpha)$ readings alone as a function of viewing angle α are listed in table 2. Typical standard errors of the readings of the sample and the blanks are given for the $R_H^H(\alpha)$ readings to show their magnitude and consistency as a function of the magnitude of the signal. The data are shown in the order in which they were taken and it was found that the system was stable over the time period it took to obtain a set of readings. Only a 2 or 3 percent drop in overall signal due to PM tube drift was apparent over the course of 2 hours. When the emission polarizer is removed it is only possible to take two readings at each α, $R^V(\alpha)$ and $R^H(\alpha)$. These data are shown in table 3. When the excitation polarizer is removed and the emission polarizer is left in place, again two readings are taken, $R_V(\alpha)$

TABLE 1. *Experimental readings obtained for the four orthogonal positions of the excitation and emission polarizers*

α	$R_V^V(\alpha)$	$R_H^V(\alpha)$	$R_V^H(\alpha)$	$R_H^H(\alpha)$
Degrees	*Volts*	*Volts*	*Volts*	*Volts*
180	[a] 0.2802	0.2786	0.09627	[a] 0.7795
144.75	.2814	.2798	.09772	.6092
125.25	.2817	.2781	.09739	.4436
90	.2797	.2766	.09698	.2761
54.75	.2782	.2754	.09607	.4440
180	[a] .2801	.2777	.09661	[a] .7797
160	.2821	.2796	.09688	.7163
80	.2803	.2773	.09708	.2931
Average	0.2805	0.2779	0.09688	
Std. error	0.0005	0.0005	0.0002	
% std. error	0.2	0.2	0.2	

[a] Nonzero blank subtracted from these readings.

TABLE 2. *Experimental readings for the excitation and emission polarizers in the horizontal mode as a function of viewing angle*

α	$R_H^H(\alpha)$	Std. error	Blank	Std. error blank
Degrees	*Volts*	*Volts*	*Volts*	*Volts*
180.5	0.7987	0.0038	0.0319	0.0007
175.5	.7959	.0040	.0327	.0006
170.5	.7734	.0044	.0217	.0006
165.5	.7478	.0042	.0116	.0003
160.5	.7186	.0039	.0035	.0002
155.5	.6862	.0031	.0007	.0000
150.5	.6526	.0036	.0000	.0000
145.5	.6137	.0031	.0000	.0000
140.5	.5734	.0025	.0000	.0000
135.5	.5316	.0026	.0000	.0000
130.5	.4892	.0033	.0000	.0000
125.5	.4469	.0023	.0000	.0000
120.5	.4075	.0024	.0000	.0000
115.5	.3711	.0022	.0000	.0000
110.5	.3401	.0022	.0000	.0000
105.5	.3147	.0017	.0000	.0000
100.5	.2953	.0028	.0000	.0000
95.5	.2821	.0024	.0000	.0000
90.5	.2774	.0017	.0000	.0000
85.5	.2811	.0023	.0000	.0000
80.5	.2906	.0021	.0000	.0000
75.5	.3077	.0021	.0000	.0000
70.5	.3308	.0020	.0000	.0000
65.5	.3612	.0020	.0000	.0000
60.5	.3986	.0027	.0000	.0000
55.5	.4363	.0024	.0000	.0000
50.5	.4799	.0026	.0000	.0000
45.5	.5229	.0028	.0000	.0000
180.5	.7932	.0048	.0319	.0007
125.75	.4485	.0024	.0000	.0000
55.25	.4420	.0026	.0000	.0000
54.75	.4449	.0023	.0000	.0000
125.25	.4441	.0028	.0000	.0000

TABLE 3. *Experimental readings for four different modes of spectrofluorimeter operation*

α	$R^V(\alpha)$	$R^H(\alpha)$[a]	$R_V(\alpha)$	$R_H(\alpha)$[b]	$R(\alpha)$[c]	$R_I^U(\alpha)$[d]
Degrees	*Volts*	*Volts*	*Volts*	*Volts*	*Volts*	*Volts*
180	[e]0.4955	[e]0.7977	[e]0.2829	[e]0.7981	[e]1.045	[e]0.8696
144.75	.5105	.6804	.2847	.6741	0.9043	.7826
125.25	.5207	.5295	.2855	.5495	.8029	.7096
90	.5345	.3622	.2877	.4254	.6863	.6407
54.75	.5513	.5452	.2868	.5554	.8495	.7107

[a]Polarizer in excitation beam.
[b]Polarizer in emission beam.
[c]No polarizers in excitation or emission beams.
[d]Both beams depolarized.
[e]Nonzero blanks subtracted.

and $R_H(\alpha)$ (see table 3). Also, both polarizers can be removed, as is common for most fluorimeters, and only one reading, $R(\alpha)$, can be taken at each α (see table 3). Finally, instead of placing polarizers in the excitation and emission beams, scrambler plates can be placed so as to depolarize both beams. In addition to giving unpolarized exciting light, this caused the emission detection system to see depolarized light and thus removed its bias. The scrambler plates are quartz wedges placed such that the polarized light beam is rotated different amounts depending on which part of the wedge the light is traversing. The plates therefore do not actually depolarize in the strict sense of the term, but supply to the grating strips of radiation polarized alternately parallel and perpendicular to the grating grooves [13]. Scrambler plates were placed only in the emission beam since it was found (as will be shown) that the laser|barium-sulfate|lens system supplied essentially depolarized exciting radiation. The readings taken with the scrambler plates in place, $R_I^U(\alpha)$ are also shown in table 3. It should be noted that when an optical component was removed or added, the overall sensitivity of the instrument was changed. The voltage on the PM tube was always adjusted to keep the maximum reading in a given set of readings at or below 1 volt. Therefore, only data with constant optics should be compared to each other.

5. Discussion

5.1. Excitation Polarizer In, Emission Polarizer In

The four readings $R_V^V(\alpha)$, $R_H^V(\alpha)$, $R_V^H(\alpha)$, and $R_H^H(\alpha)$ for each angle α (see table 1) are related to the intensity emitted by the sample by eqs (25a–25d). Equations (25a, 25b, 25c) predict that the $R_V^V(\alpha)$, $R_H^V(\alpha)$, and $R_V^H(\alpha)$ readings should be independent of viewing angle α. The data in table 1 show this to be true, and the average values of these readings and their standard errors are given. This shows that (a) the emission detection system collects the same solid angle at each α, (b) the rotating sample cell is uniform with respect to α, and (c) the sample is essentially a point source. The $R_H^H(\alpha)$ reading is the only one which has a dependence on α as predicted by eq (25d). Table 4 shows the values of G, F, and D calculated using eqs (32b), (30a), and (30b) and the data reported in table 1. As can be seen the values of G all agree and have an average value of 0.353. This value is what one might expect with a grating monochromator detection system viewing at 685.0 nm. The values of F agree and have an average value of 1.3 percent above unity which means that the barium sulfate scatterer is efficient in depolarizing the highly polarized He-Ne laser light, and that the sample cell transmits polarized light uniformly. The values of D are also nearly constant giving an average value of 2.86 ± 0.02. This value is close to the theoretical maximum of 3.0 (corresponding to $r_0 = 0.4$ or $P_0^V = 0.5$) for the case where the absorption and emission dipole oscillators are parallel to each other. The theoretical maximum of 3.0 is what one would expect in this case since the excitation occurs in the longest wavelength absorption band of the dye, the same state from which emission theoretically occurs. The small deviation from 3.0 is probably due to the fact that the solvent is not quite viscous enough at room temperature to completely prevent Brownian motion of the molecules during their excited state lifetime.

A value for D can also be obtained from the $R_H^H(\alpha)$ readings alone. Equation (25d) can be rearranged to give

$$R_H^H(\alpha) = k(\tau_{\parallel} - \tau_{\perp}) S^H T_H \cos^2\alpha + k\tau_{\perp} S^H T_H \,. \tag{35}$$

A plot of $R_H^H(\alpha)$ values (from table 2) versus $\cos^2\alpha$ is shown in figure 6. The slope to intercept ratio gives $D = 2.85 \pm 0.07$, which agrees well with the average value of 2.86 recorded in table 4. This shows that not only do eqs (25a–25*d*) accurately represent the data but also that the intensity effect predicted by Almgren [4], Shinitzky [5], and Kalantar [10] will be apparent once the correction factors F and G are applied. Equation (23a) can be written in terms of the experimentally obtainable readings as

$$\frac{I^U(\alpha)}{I_0^U} = (3/4)\left[1 + \frac{R_H^H(\alpha)}{\frac{R_V^V(\alpha)}{FG} + \frac{R_H^V(\alpha)}{F} + \frac{R_V^H(\alpha)}{G}}\right]. \tag{36}$$

A plot of $I^U(\alpha)/I_0^U$ versus α is shown in figure 3. The points, O, represent values obtained by taking the data reported in table 1 and applying eq (36) with the average values of F and G reported in table 4. The solid line represents the theoretical curve which is obtained using eq (23a) with a value of $r = 0.383$ corresponding to the experimentally determined value of $D = 2.86$. As can be seen, $I^U(\alpha)/I_0^U$ does have a value of unity at 125.25° and 54.75° as predicted by Almgren [4] and Shinitzky [5] and approaches 0.90 at 90° and 1.2 at 180°. Similarly, eqs (21a) and (22a) can be written as

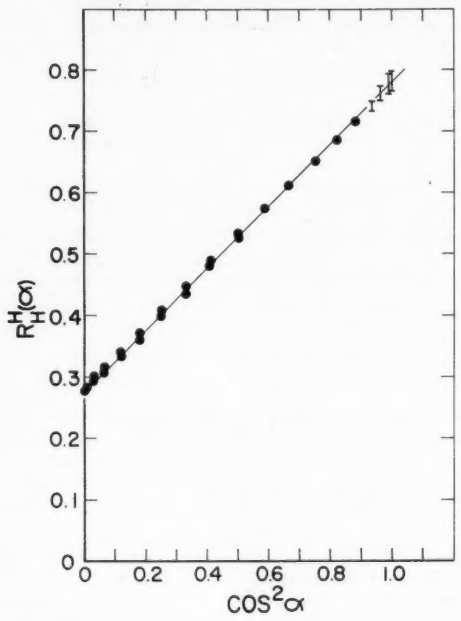

FIGURE 6. *Experimental readings,* $[R_H^H(\alpha)]$, *obtained with the excitation and emission polarizers in the horizontal position as a function of the* $\cos^2(\alpha)$ *where* α is the viewing angle.

The solid line refers to a least squares best fit of the data points.

$$\frac{I^V(\alpha)}{I_0^V} = (3/2)\left[\frac{R_V^V(\alpha)/G + R_H^V(\alpha)}{R_V^V(\alpha)/G + 2R_H^V(\alpha)}\right], \quad (37)$$

$$\frac{I^H(\alpha)}{I_0^H} = (3/2)\cos^2\alpha \left[\frac{R_H^H(\alpha) + R_V^H(\alpha)/G}{R_H^H(\alpha) + \frac{R_V^H(\alpha)}{G}(3\cos^2\alpha - 1)}\right]. \quad (38)$$

The data points on the $I^V(\alpha)/I_0^V$ and $I^H(\alpha)/I_0^H$ curves in figure 3 reflect the data recorded in tables 1 and 4 applied to eqs (37) and (38) while the solid lines are the theoretical curves given by eqs (21a) and (22a) for $r = 0.383$. The degree of polarization of the fluorescence emission can also be expressed in terms of the four readings and F and G. Equations (21b), (22b), and (23b) can be written in the forms

$$P^V(\alpha) = \left[\frac{R_V^V(\alpha)/G - R_H^V(\alpha)}{R_V^V(\alpha)/G + R_H^V(\alpha)}\right], \quad (39)$$

$$P^H(\alpha) = \left[\frac{R_V^H(\alpha)/G - R_H^H(\alpha)}{R_V^H(\alpha)/G + R_H^H(\alpha)}\right], \quad (40)$$

$$P^U(\alpha) = \frac{[R_V^V(\alpha)/FG + R_V^H(\alpha)/G] - [R_H^V(\alpha)/F + R_H^H(\alpha)]}{[R_V^V(\alpha)/FG + R_V^H(\alpha)/G] + [R_H^V(\alpha)/F + R_H^H(\alpha)]}. \quad (41)$$

Figure 4 shows plots of $P^V(\alpha)$, $P^H(\alpha)$, and $P^U(\alpha)$ as a function of α where the solid lines are calculated using $r = 0.383$ and eqs (21b), (22b), and (23b) respectively. The □, ○, and ● symbols refer to points obtained by applying the data in table 1 to eqs (39), (40), and (41) and again using the average values of F and G reported in table 4. As can be seen, the agreement with theory is good.

TABLE 4. *Calculated values of the polarization ratio for the detection system* (G), *the polarization ratio of the exciting radiation* (F), *and the dichroic ratio of emission* (D)

α Degrees	G	F	D
180	0.3524	1.023	2.845
144.75	.3558	1.019	2.827
125.25	.3551	1.014	2.853
90	.3512	1.002	2.879
54.75	.3515	1.008	2.874
180	.3535	1.016	2.853
160	.3551	1.025	2.841
80	.3501	1.000	2.887
Average	0.3531	1.013	2.857
Std. error	0.0007	0.003	0.007
% std. error	0.2	0.3	0.3

5.2. Excitation Polarizer Out, Emission Polarizer In

Since it was found that the exciting radiation is depolarized ($F = 1.013$), the $R_V(\alpha)$ and $R_H(\alpha)$ readings given in table 3 can be classified as $R_V^U(\alpha)$ and $R_H^U(\alpha)$, and expressed as

$$R_V^U(\alpha) = R_V^V(\alpha) + R_V^H(\alpha) = T_V[I_V^V(\alpha) + I_V^H(\alpha)] = kS^U T_V(\tau_{\parallel} + \tau_{\perp}), \quad (42a)$$

$$R_H^U(\alpha) = R_H^V(\alpha) + R_H^H(\alpha) = T_H[I_H^V(\alpha) + I_H^H(\alpha)] = kS^U T_H[\tau_{\parallel}\cos^2\alpha + \tau_{\perp}(2 - \cos^2\alpha)], \quad (42b)$$

where the superscript U denotes unpolarized excitation, and where $S^U = S^V = S^H$. Equation (42a) predicts that the $R_V(\alpha)$ readings in table 3 should be constant with respect to α and this was found to be true. The $R_H(\alpha)$ readings do change in accordance with eq (42b) as will be shown by obtaining expressions for $P^U(\alpha)$ and $I^U(\alpha)/I_0^U$. By combining eqs (42a) and (42b), $P^U(\alpha)$ can be expressed as

$$P^U(\alpha) = \left[\frac{R_V^U(\alpha)/G - R_H^U(\alpha)}{R_V^U(\alpha)/G + R_H^U(\alpha)}\right]. \quad (43)$$

TABLE 5. *Calculated and experimental values for the data obtained from four modes of spectrofluorimeter operation*

α Degrees	$\frac{I^U(\alpha)}{I_0^U}$	$\frac{I^U(\alpha)}{I^U(125.25°)}$ [a]	$\frac{R^V(\alpha)}{R^H(\alpha)}$ [b]		$\frac{I^U(\alpha)}{I_0^U}$	$\frac{R_U^U(\alpha)}{R_U^U(125.25°)}$ [c]	$\frac{R(\alpha)}{R(125.25°)}$ [d]	
	Eq (23a) Calc.	Eq (45) Expt.	Eq. (47) Calc.	Table 3 Expt.	Eq (23a) Calc.	Table 3 Expt.	Eq (50) Calc.	Table 3 Expt.
180	1.19	1.18	0.634	0.621	1.19	1.22	1.31	1.30
144.75	1.10	1.09	.785	.750	1.10	1.10	1.16	1.13
125.25	1.00	1.00	1.03	.983	1.00	1.00	1.00	1.00
90	0.905	0.913	1.50	1.48	0.905	0.903	0.846	0.855
54.75	1.00	1.01	1.03	1.01	1.00	1.00	1.00	1.06

[a] Polarizer in emission beam, no polarizer in the excitation beam.
[b] Polarizer in excitation beam, no polarizer in the emission beam.
[c] Both beams depolarized.
[d] No polarizers or depolarizers in either beam.

The points, ▲, on the $P^U(\alpha)$ curve in figure 4 reflect eq (43) applied to the $R_V(\alpha)$ and $R_H(\alpha)$ data in table 3 for a value of $G=0.353$ as in the previous section. At any viewing direction α, the total intensity received by the detection system is

$$I^U(\alpha) \propto R_V^U/G + R_H^U. \tag{44}$$

If the exciting light is unpolarized, then by eq (23b) $I^U(125.25°)$ or $I^U(54.75°)=I_0^U$. Therefore, the prediction is that

$$\frac{I^U(\alpha)}{I_0^U}=\frac{I^U(\alpha)}{I^U(125.25°)} = \left[\frac{R_V^U(\alpha)/G+R_H^U(\alpha)}{R_V^U(125.25°)/G+R_H^U(125.25°)}\right]. \tag{45}$$

A comparison of $I^U(\alpha)/I_0^U$ values as calculated using eq (23a) and a value of $r=0.383$ with $I^U(\alpha)/I^U(125.25°)$ values as calculated using eq (45) with the $R_V(\alpha)$ and $R_H(\alpha)$ data in table 3 and a value of $G=0.353$, is shown in table 5. In this comparison as well as the $P^U(\alpha)$ one, the agreement of the data with the theoretical values using eqs (23a) and (23b) is good, thus showing the validity of eqs (42a), (42b), (44), and (45) in describing the data. An even more rigorous test of eq (23a) would be when G as well as F has a value of unity. This will be shown in the section dealing with depolarized beams.

5.3. Excitation Polarizer In, Emission Polarizer Out

In this mode of operation the two readings $R^V(\alpha)$ and $R^H(\alpha)$ can be described as

$$R^V(\alpha) = R_V^V(\alpha) + R_H^V(\alpha) = kS^V(\tau_{\parallel}T_V + \tau_{\perp}T_H)$$

$$= T_V I_V^V(\alpha) + T_H I_H^V(\alpha), \tag{46a}$$

$$R^H(\alpha) = R_V^H(\alpha) + R_H^H(\alpha) = kS^H[\tau_{\perp}T_V + (\tau_{\parallel}\cos^2\alpha + \tau_{\perp}\sin^2\alpha)T_H]$$

$$= T_V I_V^H(\alpha) + T_H I_H^H(\alpha). \tag{46b}$$

Equation (46a) predicts that the $R^V(\alpha)$ readings should be constant with respect to α. Actually, the values increase slightly from 180° to 54.75° indicating that the beam was slightly displaced from the entrance slit of the emission monochromator when the emission polarizer was removed, so that the solid angle collected by the detection system changed slightly with α. However, the $R^H(\alpha)$ reading should also suffer the same effect and by taking the ratio of the two readings, the effects should cancel. No attempt was made to re-aline the optics for fear of changing F and G. This ratio is

$$\frac{R^V(\alpha)}{R^H(\alpha)}=F\left[\frac{(\tau_{\parallel}T_V+\tau_{\perp}T_H)}{(\tau_{\parallel}\cos^2\alpha+\tau_{\perp}\sin^2\alpha)T_H+\tau_{\perp}T_V}\right]$$

$$=\left[\frac{F(DG+1)}{(D-1)\cos^2\alpha+(G+1)}\right]. \tag{47}$$

Taking D, F, and G from table 4, the right side of eq (47) can be calculated and compared to the ratio $R^V(\alpha)/R^H(\alpha)$. This IS done in table 5 and the agreement is good. Equations (46a) and (46b) do not lend themselves to giving information on $P^U(\alpha)$ or $I^U(\alpha)/I_0^U$ easily and no attempt will be made to do so. Equation (47), however, proved very useful when alining the scrambler plates as will be shown in the next section.

5.4. Both Beams Depolarized

In order to remove the bias of the detection system, scrambler plates were placed in the emission beam. When this was done, it was found that the readings obtained were extremely sensitive to the alinement of the scrambler. This was also found by Rahn, Temple, and Hathaway [13] and Reed and Lendon [14]. To accomplish alinement it was necessary to put the excitation polarizer back in the system and place the

emission detection system at 180°. Under these conditions eq (47) becomes

$$\frac{R^V(180°)}{R^H(180°)}=\frac{F(DG+1)}{(G+D)} \tag{48}$$

The scrambler plates were then rotated and adjusted such that the $R^V(180°)$ reading equaled the $R^H(180°)$ reading. Since in this case F is essentially equal to unity, G must now also equal unity so as to satisfy eq (48). The excitation polarizer was then removed and readings, $R_U^U(\alpha)$, were taken at various angles α (see table 3). Since $F=G=1$, eq (23a) now applies and the experimentally obtained ratios of $R_U^U(\alpha)/R_U^U(125.25°)$ should agree with the calculated ratio $I^U(\alpha)/I_0^U$ as given by eq (23a) for the experimentally obtained value $r=0.383$. The comparison is shown in table 5 and shows the validity of Almgren [4] and Shinitzky's [5] predictions once the instrumental polarization artifacts (i.e., F and G) are eliminated.

Equation (23a) can be written as

$$r=\left[\frac{R_U^U(\alpha)}{R_U^U(125.25°)}-1\right]\left[\frac{4}{(3\cos^2\alpha-1)}\right], \tag{49}$$

and thus shows that r can be measured from $R_U^U(\alpha)$ readings at different viewing angles. For example at $\alpha=90°$, the value of $R_U^U(90°)/R(125.25°)$ is 0.903, giving a value of $r=0.388$ which is in fair agreement with a value of $r=0.383$ as given by the analysis with polarizers placed in the system. Thus we have the novel situation of being able to measure the anisotropy (or polarization) of a sample without using polarizers. It should be noted, however, that this type of measurement is extremely sensitive to small alinement errors as can be seen by eq (49). Thus, the best ratio to use is $R_U^U(180°)/R_U^U(125.25°)$. However, the $R_U^U(180°)$ measurement suffers from scattered exciting light problems and requires a fairly large blank subtraction. The next best set of angles to use is then $R_U^U(90°)$ and $R_U^U(125.25°)$.

5.5. No Polarizers or Scramblers

When there are no polarizers or depolarizers in the system, the reading, $R(\alpha)$, taken at each viewing angle α, can be described theoretically by eq (27). The reading R_0 that one would obtain if the emission anisotropy, r, were equal to zero cannot be measured independently. However, eq (27) can be tested by taking the ratio

$$\frac{R(\alpha_1)}{R(\alpha_2)}=\frac{(1+F)(1+G)+r[3\cos^2\alpha_1-(1+F+G-2FG)]}{(1+F)(1+G)+r[3\cos^2\alpha_2-(1+F+G-2FG)]} \tag{50}$$

of any two $R(\alpha)$ readings. Table 5 shows a comparison of the ratios $R(\alpha)/R(125.25°)$ obtained from the appropriate data in table 3 to that calculated using eq (50) with $r=0.383$, $F=1.013$ and $G=0.353$. As can be seen the agreement is good and this supports the validity of eq (27) in describing the error introduced into the system by polarization effects. The limiting values for the relative error, $R(\alpha)/R_0$, can be obtained by assuming the maximum and minimum values that F, G, and r can obtain. Some examples are given in table 6. For the cases where $F=G=1$, the

TABLE 6. *Theoretical estimates of errors, $R(\alpha)/R_0$, which can be introduced into fluorescence measurements by polarization effects*

α Degrees	r	F	G	$R(\alpha)/R_0$	Comments
90	0.4	1.0	1.0	0.90	absorption dipole || to
180	0.4	1.0	1.0	1.20	emission dipole.
125.25	0.4	1.0	1.0	1.00	
90	−0.2	1.0	1.0	1.05	absorption dipole ⊥ to
180	−0.2	1.0	1.0	0.90	emission dipole.
125.25	−0.2	1.0	1.0	1.00	
90	0.4	10^4	10^4	1.80	R_V^V absorption || to emission
90	0.4	10^4	10^{-4}	0.60	R_H^V
90	0.4	10^{-4}	10^4	0.60	R_V^H
90	0.4	10^{-4}	10^{-4}	0.60	R_H^H
180	0.4	10^4	10^4	1.80	R_V^V absorption || to emission
180	0.4	10^4	10^{-4}	0.60	R_H^V
180	0.4	10^{-4}	10^4	1.80	R_V^H
180	0.4	10^{-4}	10^{-4}	0.60	R_H^H
90	−0.2	10^4	10^4	0.60	R_V^V absorption ⊥ to emission
90	−0.2	10^4	10^{-4}	1.20	R_H^V
90	−0.2	10^{-4}	10^4	1.20	R_V^H
90	−0.2	10^{-4}	10^{-4}	1.20	R_H^H
180	−0.2	10^4	10^4	0.60	R_V^V absorption ⊥ to emission
180	−0.2	10^4	10^{-4}	1.20	R_H^V
180	−0.2	10^{-4}	10^4	0.60	R_V^H
180	−0.2	10^{-4}	10^{-4}	1.20	R_H^H
90	0.4	3.0	0.3	0.808	absorption || to emission;
180	0.4	3.0	0.3	1.04	excitation in U.V., emission
125.25	0.4	3.0	0.3	0.885	in red
90	−0.2	3.0	0.3	1.10	absorption ⊥ to emission;
180	−0.2	3.0	0.3	0.981	excitation in U.V., emission
125.25	−0.2	3.0	0.3	1.06	in red
90	0.4	3.0	2.8	1.26	absorption || to emission;
180	0.4	3.0	2.8	1.34	excitation in U.V., emission
125.25	0.4	3.0	2.8	1.29	in U.V.
90	−0.2	3.0	2.8	0.868	absorption ⊥ to emission;
180	−0.2	3.0	2.8	0.829	excitation in U.V., emission
125.25	−0.2	3.0	2.8	0.855	in U.V.
90	0.4	0.33	0.3	0.669	absorption || to emission;
180	0.4	0.33	0.3	1.36	excitation red, emission
125.25	0.4	0.33	0.3	0.90	in red
90	−0.2	0.33	0.3	1.16	absorption ⊥ to emission;
180	−0.2	0.33	0.3	0.819	excitation in red, emission
125.25	−0.2	0.33	0.3	1.05	in red

limits of Almgren [4], Shinitzky [5], and Kalantar [10] are obtained. The cases where F and G are very large or very small correspond to the cases where polarizers are placed in the emission and excitation beams. Finally, there are the cases where there are no polarizers (or scrambler plates) in the beams and the values of F and G run roughly from 2 to 3 in the UV to 0.2 to 0.3 in the red. In these cases, values of F and G are essentially determined by the polarization properties of the excitation and emission monochromators. Some of these cases are also given in table 6.

6. Conclusions

Errors introduced in fluorescence measurements by polarization effects can be quite large. In addition to the cases mentioned by Shinitzky [5], there are others in which polarization effects can introduce errors. Relative fluorescence quantum yield measurements where either or both the sample or reference have a degree of polarization will be susceptible to polarization errors [4, 5, 10]. Relative quantum yields measured as a function of temperature, especially at low temperatures where the viscosity of the solvent changes drastically, may have polarization errors since the emission anisotropy of the fluorescence is strongly dependent on the viscosity of the solvent. Also, quantum counters such as rhodamine B in ethylene glycol may exhibit a degree of polarization which is a function of α, r, F, and G, the most important being r which is a function of the dye and F which is a function of the excitation monochromator and beam splitter. These parameters will vary as the excitation wavelength changes. Another case where polarization effects can be large is in measuring relative fluorescence to phosphorescence ratios which are usually performed using low temperature glasses as solvents. Again the signal is a function of α, r, F, and G but in this case G will change drastically as one scans over the fluorescence and phosphorescence emission envelopes.

In general it can be said that in making fluorescence measurements, one should either polarize completely or depolarize completely since it is not known whether polarization effects are introducing errors until either the degree of polarization is determined or the effect is negated. If there is a nonzero degree of polarization, the readings will be a function of r, α, F, and G. The effects of these parameters can then be either (a) measured accurately by placing polarizers in both beams, thus completely describing the measuring system or (b) negated by placing depolarizing elements in both beams and measuring the signal at one of the 'depolarizing' angles 54.75° or 125.25°. With polarizers in both beams, more information is obtained; i.e., r, G, F, and R_0 can be calculated using the four readings at any viewing angle α. In this case, however, four scans must be made, which may be difficult if the sample is photochemically unstable. With depolarizers in both beams, 54.75° or 125.25° viewing must be used to measure R_0 and no information is obtained on r unless viewing is performed at another angle (e.g., 90°). Even so, the measurement of r in this way is more sensitive to small alinement errors than when r is determined using polarizers. One could use polarizers in addition to depolarizers to measure r at the 54.75° or 125.25° viewing angles, but this complicates the optics and, of course, is more expensive since a good set of depolarizers costs as much as a good set of polarizers. A distinct disadvantage in using depolarizers is the fact that 54.75° or 125.25° viewing must be used whereas most commercial fluorimeters are right angle viewing—a geometry preferred for use with polarizers. It should be mentioned that whichever one uses, polarizers or depolarizers, they must be efficient over a wide wavelength range. Also, since they are optical components their spectral sensitivity must be accounted for when calibrating the instrument to give corrected spectra. Considering all these factors, the recommended procedure is to use two polarizers (with right angle viewing as used by Azumi and McGlynn [2] for most applications), and obtain F, G, r, and R_0 directly from the four readings. This has the advantage that all four parameters are measured with the same solution and sample cell under conditions of constant optics and alinement. This is important since F is a function of the excitation optics up to and including the sample cell and G is a function of the total emission detection system which also includes the sample cell. Thus, r and I_0 are parameters of the solution only.

Finally, some recommendations for fluorescence standards can now be made. The recommendations made by Melhuish [3] and others that ideal fluorescence standards should be depolarized is confirmed here. If there are cases, however, in which a certain compound or solution has distinct advantages as a fluorescence standard even though it does exhibit a degree of polarization, the emission anisotropy, r, of the standard (a fundamental parameter of the system) should be measured as a function of wavelength and reported. The user can then refer to the appropriate equations listed in the theoretical section to determine I_0 or R_0 and the degree of polarization P that the standard will have under his experimental conditions.

7. References and Notes

[1] Weber, G., and Teale, F. W. J., Trans. Faraday Soc. **53**, 646 (1957).
[2] Azumi, T., and McGlynn, S. P., J. Chem. Phys. **37**, 2413 (1962).
[3] Melhuish, W. H., J. Res. Nat. Bur. Stand. (U.S.) **76A**, (Phys. and Chem.), No. 6, 547–560 (Nov.–Dec. 1972).
[4] Almgren, M., Photochem. and Photobiol. **8**, 231 (1968).
[5] Shinitzky, M., J. Chem. Phys. **56**, 5979 (1972).
[6] A summary of previous derivations of polarization equations is given by E. N. Hudson in Fluorescence Spectroscopy, Eds. A. J. Pesce, C.-G. Rosén and T. L. Pasby (M. Dekker, Inc., New York, 1971), pp. 111–130.
[7] The units for photon quantities used in this paper are those recommended by J. J. Muray, F. E. Nicodemus, and I. Wunderman, Appl. Opt. **10**, 1465 (1971).
[8] Berlman, I. B., in Handbook of Fluorescence Spectra of Aromatic Molecules (Academic Press, New York, 1971), 2d ed., pp. 18, 19.
[9] Jablonski, A., Acta. Phys. Polon. **16**, 471 (1957).
[10] Kalantar, A. H., J. Chem. Phys. **48**, 4992 (1968).

[11] In order to describe materials and experimental procedures adequately, it is occasionally necessary to identify commercial products by manufacturer's name or label. In no instances does such identification imply endorsement by the National Bureau of Standards, nor does it imply that the particular product or equipment is necessarily the best available for that purpose.

[12] Mielenz, K. D., to be published.
[13] Rahn, L., Temple, P., and Hathaway, C., Appl. Spectry. **25**, 675 (1971).
[14] Reed, P., and Lendon, D., Appl. Spectry. **26**, 489 (1972).

(Paper 79A1–842)

JOURNAL OF RESEARCH of the National Bureau of Standards—A. Physics and Chemistry
Vol. 79A, No. 1, January–February 1975

The Iron-Neon Hollow-Cathode Spectrum*

H. M. Crosswhite**

The Johns Hopkins University, Baltimore Md. 21218

(September 4, 1974)

Over 4000 wavelengths are listed between 1900 and 9000 Å for Fe I, Fe II, Ne I and Ne II lines measured in a hollow cathode discharge tube with iron electrodes and a neon gas filling. Photoelectric traces between 2400 and 5700 Å on a semiquantitative intensity scale are also included. For Fe I, energy values for 124 even and 240 odd levels have been computed. These have been used to calculate Ritz standards for most of the Fe I lines.

Key words: Hollow cathode; iron; neon; wavelength standards

For the past 20 years the Spectroscopy Laboratory at The Johns Hopkins University has been using an iron hollow-cathode discharge tube for spectroscopic wavelength standards and as a stable source for branching-ratio measurements. This paper is a progress report on the development of Ritz standards for Fe I, but also includes extensive data on Fe II, Ne I and Ne II which were obtained along the way.

The spectrum lines of neutral iron have long been used by spectroscopists as convenient laboratory wavelength standards. The Pfund atmospheric dc arc [Pfund, 1908] was for many years the best available source of Fe I lines, and was adopted by Commission 14 of the International Astronomical Union as a source of secondary standard wavelengths. A compilation of the atmospheric arc wavelengths was made by Russell and Moore [1944] from the best material available at that time.

It was known that line shifts and broadening from the effects of electric fields and atmospheric pressure were present and that many otherwise useful lines had to be avoided. As interest in problems requiring high resolution developed, coincident with availability of better gratings and more powerful spectrographs, the inadequacies of an atmospheric arc became more serious. Vacuum arcs [Burns and Walters, 1929 and 1931] and hollow-cathode discharge tubes [Williams and Middleton, 1939] were known to give much sharper lines but the required evacuating system was inconvenient.

A sealed-off discharge tube using a hollow iron cathode with a 3.5 torr filling of rare gas, preferably neon, becomes an excellent source of sharp spectral lines suitable for wavelength calibration of large grating spectrographs in a routine manner: a uranium metal getter in a side-arm may be used to reduce contamination from out-gassing [Crosswhite et al., 1955]. The Doppler broadening is not of serious consequence for grating instruments. The intensity of the spectrum is adequate and the lifetime (several hundred hours) long enough to give years of service in a normal installation. Tube currents from 90 to 400 mA were used in the experiments described here.

Wavelength measurements were carried out in several steps, the first being a series of interferometric ones with resolution limit of about 0.02 cm^{-1} [Stanley and Dieke, 1955; Crosswhite, 1958]. These were supplemented by measurements of a microwave-excited iron halide tube [Stanley and Meggers, 1957], which appear to be indistinguishable from those of the hollow-cathode lamp. These 367 lines were then used to determine 36 even and 69 odd energy level values with a precision of about 0.002 cm^{-1}. In tables I and II these levels are identified by an asterisk.

From these energy level values a set of average wavelengths was calculated. In addition to the original group of lines this set could be expanded to include additional lines of about twice this number, making up a set in sufficient quantity as to be useful for internal standards in further exposures with grating spectrographs.

Above about 2500 Å this could be done in a conventional way by interpolating new measurements between values of the above Ritz standards. Two spectrographs were used, the more useful being a five-meter plane-grating Jarrell-Ash spectrograph [Dieke and Heath, 1965], designed by W. G. Fastie [Fastie, 1963]. This instrument contains a 254 mm plane grating blazed near six microns (59°). Separation of orders is accomplished by using a small plane-grating predisperser. These measurements were all made with

*An invited paper.
** Present address: Chemistry Division, Argonne National Laboratory, Argonne, Ill. 60439.

562-903 O - 75 - 2

the spectrograph evacuated. The accuracy of the measurements is comparable to the previous interferometric ones, being limited by the Doppler broadening in the source.

Below 2500 Å the occurrence of suitable Ritz standards is irregular, and the following method was used [Crosswhite and Jones, 1974]. The predisperser was taken out of the beam and replaced by a specially-designed total-internal-reflection filter [Crosswhite, 1969] which could be adjusted so that only wavelengths below a set value would appear in the exposure. Longer wavelengths are attenuated by twelve reflections within a pair of high purity quartz prisms. Shorter wavelengths pass through unattenuated and undeviated. Exposures of several overlapping orders can thus be obtained free from interference from longer wavelengths (lower orders). Two sets of exposures were taken, one with the cutoff wavelength fixed at 2600 Å and the other at 2300 Å.

Tests of self-consistency of measurements made with overlapping orders, for Ritz standards between 2500 and 4500 Å, showed no discrepancies for this spectrograph. The lines are very symmetric and the dispersion is high enough that photographic plate imperfections are not a factor. The demonstrated resolving power of 1,000,000 at 2537 Å [Kielkopf, 1973] is more than adequate for this source. As this is near the theoretical resolving power, it is felt that the method of overlapping orders gives no problems over the limited range of orders used here.

TABLE 1. *Even energy levels of* Fe I

Designation	Level (cm^{-1})	Configuration	Designation	Level (cm^{-1})	Configuration	Designation	Level (cm^{-1})	Configuration
$a\,^5D_4$	0.000*	$3d^64s^2$	$a\,^3D_2$	26 623.730	$3d^74s$	$f\,^7D_2$	50 998.641	$3d^64s4d$
$a\,^5D_3$	415.932*	$3d^64s^2$	$b\,^3H_4$	26 627.604	$3d^74s$	$f\,^7D_1$	51 048.113	$3d^64s4d$
$a\,^5D_2$	704.004*	$3d^64s^2$	$a\,^1P_1$	27 543.004	$3d^74s$	$f\,^5F_5$	51 103.187	$3d^64s4d$
$a\,^5D_1$	888.179*	$3d^64s^2$	$a\,^1D_2$	28 604.606	$3d^74s$	$e\,^7F_3$	51 148.859	$3d^64s4d$
$a\,^5D_0$	978.072*	$3d^64s^2$	$a\,^1H_5$	28 819.946	$3d^74s$	$e\,^5S_2$	51 148.883	$3d^64s4d$
$a\,^5F_5$	6928.266*	$3d^74s$	$a\,^1I_6$	29 313.003	$3d^64s^2$	$e\,^7F_4$	51 192.270	$3d^64s4d$
$a\,^5F_4$	7376.760*	$3d^74s$	$b\,^3D_1$	29 320.028	$3d^64s^2$	$e\,^7F_1$	51 207.991	$3d^64s4d$
$a\,^5F_3$	7728.056*	$3d^74s$	$b\,^3D_2$	29 356.740	$3d^64s^2$	$e\,^5G_3$	51 219.017	$3d^64s4d$
$a\,^5F_2$	7985.780*	$3d^74s$	$b\,^3D_3$	29 371.811	$3d^64s^2$	$e\,^7G_5$	51 228.555	$3d^64s4d$
$a\,^5F_1$	8154.710*	$3d^74s$	$b\,^1G_4$	29 798.933	$3d^64s^2$	$e\,^3D_3$	51 294.222*	$3d^64s5s$
$a\,^3F_4$	11 976.234*	$3d^74s$	$c\,^3F_4$	32 873.619	$3d^8$	$e\,^7F_2$	51 331.044	$3d^64s4d$
$a\,^3F_3$	12 560.930*	$3d^74s$	$c\,^3F_3$	(33 412.706)	$3d^8$	$e\,^7G_4$	51 334.909	$3d^64s4d$
$a\,^3F_2$	12 968.549*	$3d^74s$	$c\,^3F_2$	(33 765.291)	$3d^8$	$g\,^5D_4$	51 350.491	$3d^64s5s$
$a\,^5P_3$	17 550.175*	$3d^74s$	$e\,^7D_5$	42 815.857*	$3d^64s5s$	$e\,^5G_2$	51 370.130	$3d^64s4d$
$a\,^5P_2$	17 726.981*	$3d^74s$	$e\,^7D_4$	43 163.327*	$3d^64s5s$	$e\,^7G_3$	51 460.516	$3d^64s4d$
$a\,^5P_1$	17 927.376*	$3d^74s$	e^7D_3	43 434.629*	$3d^64s5s$	$f\,^5F_4$	51 461.672	$3d^64s4d$
$a\,^3P_2$	18 378.181*	$3d^64s^2$	$e\,^7D_2$	43 633.534*	$3d^64s5s$	$e\,^7G_2$	51 539.712	$3d^64s4d$
$a\,^3H_6$	19 390.164	$3d^64s^2$	$e\,^7D_1$	43 763.980*	$3d^64s5s$	$e\,^7S_3$	51 570.084	$3d^64s4d$
$a\,^3P_1$	19 552.473	$3d^64s^2$	$e\,^5D_4$	44 677.004*	$3d^64s5s$	$f\,^5F_3$	51 604.102	$3d^64s4d$
$a\,^3H_5$	19 621.005	$3d^64s^2$	$e\,^5D_3$	45 061.327*	$3d^64s5s$	$f\,^5F_2$	51 705.007	$3d^64s4d$
$a\,^3H_4$	19 788.245	$3d^64s^2$	$e\,^5D_2$	45 333.875*	$3d^64s5s$	$e\,^3D_2$	51 739.920*	$3d^64s5s$
$a\,^3P_0$	20 037.813	$3d^64s^2$	$e\,^5D_1$	45 509.150*	$3d^64s5s$	$f\,^5F_1$	51 754.490	$3d^64s4d$
$b\,^3F_4$	20 641.109	$3d^64s^2$	$e\,^5F_5$	47 005.508*	$3d^75s$	$g\,^5D_3$	51 770.554*	$3d^64s5s$
$b\,^3F_3$	20 874.483	$3d^64s^2$	$e\,^5F_4$	47 377.962*	$3d^75s$	$e\,^3D_1$	52 039.886	$3d^64s5s$
$b\,^3F_2$	21 038.985	$3d^64s^2$	$e\,^5F_3$	47 755.539*	$3d^75s$	$g\,^5D_2$	52 049.814	$3d^64s5s$
$a\,^3G_5$	21 715.730*	$3d^74s$	$e\,^5F_2$	48 036.666	$3d^75s$	$e\,^5P_2$	52 067.459	$3d^64s4d$
$a\,^3G_4$	21 999.127*	$3d^74s$	$e\,^5F_1$	48 221.314	$3d^75s$	$g\,^5D_1$	52 214.336	$3d^64s5s$
$a\,^3G_3$	22 249.428	$3d^74s$	$f\,^7D_5$	50 377.913	$3d^64s4d$	$h\,^5D_3$	53 545.847	$3d^74d$
$b\,^3P_2$	22 838.318	$3d^74s$	$f\,^5D_4$	50 423.136*	$3d^64s4d$	$e\,^3G_5$	53 739.433	$3d^74d$
$b\,^3P_1$	22 946.808	$3d^74s$	$e\,^7P_4$	50 475.287	$3d^64s4d$	$f\,^5G_4$	53 768.969	$3d^74d$
$b\,^3P_0$	23 051.742	$3d^74s$	$e\,^5G_6$	50 522.946	$3d^64s4d$	$g\,^5F_3$	53 830.974	$3d^74d$
$b\,^3G_5$	23 783.614	$3d^84s^2$	$f\,^5D_3$	50 534.391	$3d^64s4d$	$f\,^3D_2$	54 066.758	$3d^74d$
$b\,^3G_4$	24 118.814	$3d^84s^2$	$e\,^7P_3$	50 611.260	$3d^64s4d$	$g\,^7D_4$	54 124.741	$3d^64s6s$
$c\,^3P_2$	24 335.759	$3d^74s$	$f\,^5D_2$	50 698.625	$3d^64s4d$	$h\,^5D_1$	54 132.550	$3d^74d$
$b\,^3G_3$	24 338.762	$3d^64s^2$	$e\,^5G_5$	50 703.866	$3d^64s4d$	$f\,^5G_3$	54 161.132	$3d^74d$
$a\,^1G_4$	24 574.650	$3d^74s$	$f\,^7D_4$	50 807.991	$3d^64s4d$	$g\,^5F_2$	54 257.505	$3d^74d$
$c\,^3P_1$	24 772.017	$3d^74s$	$e\,^7F_5$	50 833.428	$3d^64s4d$	$g\,^5F_1$	54 386.188	$3d^74d$
$c\,^3P_0$	25 091.597	$3d^74s$	e^7P_2	50 861.321	$3d^64s4d$	$g\,^7D_2$	54 611.703	$3d^64s6s$
$b\,^3H_6$	26 105.904	$3d^74s$	f^7D_3	50 861.816	$3d^64s4d$	$f\,^3F_4$	54 683.312	$3d^74d$
$a\,^3D_3$	26 224.966	$3d^74s$	$f\,^5D_1$	50 880.098	$3d^64s4d$	$i\,^5D_3$	57 813.940	$3d^64s4d$
$b\,^3H_5$	26 351.039	$3d^74s$	$e\,^7G_6$	50 967.826	$3d^64s4d$	$i\,^5D_2$	57 974.129	$3d^64s4d$
$a\,^3D_1$	26 406.470	$3d^74s$	$e\,^5G_4$	50 979.578*	$3d^64s4d$	4 $_2$	58 213.121	$3d^64s4d$

TABLE II. *Odd energy levels of* Fe I

Designation	Level (cm^{-1})	Configuration	Designation	Level (cm^{-1})	Configuration	Designation	Level (cm^{-1})	Configuration
$z\,^7D_5$	19 350.892*	$3d^64s4p$	$y\,^3D_1$	38 995.730	$3d^74p$	$z\,^3H_5$	47 008.366*	$3d^64s4p$
$z\,^7D_4$	19 562.440*	$3d^64s4p$	$x\,^5D_4$	39 625.799*	$3d^64s4p$	$w\,^3D_3$	47 017.188	$3d^74p$
$z\,^7D_3$	19 757.033*	$3d^64s4p$	$x\,^5D_3$	39 969.844*	$3d^64s4p$	$x\,^3F_3$	47 092.707	$3d^74p$
$z\,^7D_2$	19 912.494*	$3d^64s4p$	$y\,^7P_2$	40 052.030	$3d^54s^24p$	$z\,^3H_4$	47 106.477*	$3d^64s4p$
$z\,^7D_1$	20 019.635*	$3d^64s4p$	$y\,^7P_3$	40 207.086	$3d^54s^24p$	$w\,^3D_2$	47 136.072	$3d^74p$
$z\,^7F_6$	22 650.421	$3d^64s4p$	$x\,^5D_2$	40 231.333*	$3d^64s4p$	$u\,^5D_0$	47 171.517	$3d^74p$
$z\,^7F_5$	22 845.868*	$3d^64s4p$	$x\,^5F_5$	40 257.308*	$3d^64s4p$	$u\,^5D_1$	47 177.225	$3d^74p$
$z\,^7F_4$	22 996.677*	$3d^64s4p$	$x\,^5D_1$	40 404.506	$3d^64s4p$	$x\,^3F_2$	47 197.014	$3d^74p$
$z\,^7F_3$	23 110.937*	$3d^64s4p$	$x\,^5D_0$	40 491.274	$3d^64s4p$	$w\,^3D_1$	47 272.016	$3d^74p$
$z\,^7F_2$	23 192.497*	$3d^64s4p$	$x\,^5F_4$	40 594.429*	$3d^64s4p$	$w\,^5G_6$	47 363.369	$3d^64s4p$
$z\,^7F_1$	23 244.834*	$3d^64s4p$	$x\,^5F_3$	40 842.151*	$3d^64s4p$	$1\ \ ^2$	47 419.674	
$z\,^7F_0$	23 270.374	$3d^64s4p$	$z\,^5S_2$	40 894.986*	$3d^64s4p$	$w\,^5G_5$	47 420.229	$3d^64s4p$
$z\,^7P_4$	23 711.457*	$3d^64s4p$	$x\,^5F_2$	41 018.050*	$3d^64s4p$	$z\,^1G_4$	47 452.716	$3d^74p$
$z\,^7P_3$	24 180.864*	$3d^64s4p$	$x\,^5F_1$	41 130.627	$3d^64s4p$	$y\,^3S_1$	47 555.598	$3d^74p$
$z\,^7P_2$	24 506.919*	$3d^64s4p$	$x\,^5P_3$	42 532.736	$3d^64s4p$	$w\,^5G_4$	47 590.047	$3d^64s4p$
$z\,^5D_4$	25 899.987*	$3d^64s4p$	$x\,^5P_2$	42 859.771*	$3d^64s4p$	$v\,^5F_5$	47 606.095	$3d^64s4p$
$z\,^5D_3$	26 140.177*	$3d^64s4p$	$y\,^5G_5$	42 911.909*	$3d^64s4p$	$w\,^5G_3$	47 693.228	$3d^64s4p$
$z\,^5D_2$	26 339.691*	$3d^64s4p$	$z\,^5H_5$	(42 991.675)	$3d^64s4p$	$x\,^3G_4$	47 812.118	$3d^64s4p$
$z\,^5D_1$	26 479.376*	$3d^64s4p$	$y\,^5G_4$	43 022.975*	$3d^64s4p$	$w\,^5G_2$	47 831.150	$3d^64s4p$
$z\,^5D_0$	26 550.476*	$3d^64s4p$	$x\,^5P_1$	43 079.026	$3d^64s4p$	$x\,^3G_3$	47 834.218	$3d^64s4p$
$z\,^5F_5$	26 874.549*	$3d^64s4p$	$z\,^5H_4$	(43 108.914)	$3d^64s4p$	$x\,^3G_5$	47 834.542	$3d^64s4p$
$z\,^5F_4$	27 166.819*	$3d^64s4p$	$y\,^5G_3$	43 137.479	$3d^64s4p$	$v\,^5F_4$	47 929.999	$3d^64s4p$
$z\,^5F_3$	27 394.688*	$3d^64s4p$	$y\,^5G_2$	43 210.021	$3d^64s4p$	$v\,^5P_3$	47 966.572	$3d^74p$
$z\,^5F_2$	27 559.581*	$3d^64s4p$	$z\,^5H_3$	43 325.958	$3d^64s4p$	$v\,^5F_3$	48 122.928	$3d^64s4p$
$z\,^5F_1$	27 666.346*	$3d^64s4p$	$w\,^5D_4$	43 499.496	$3d^64s4p$	$v\,^5P_2$	48 163.438	$3d^74p$
$z\,^5P_3$	29 056.321*	$3d^64s4p$	$w\,^5D_3$	43 922.665	$3d^64s4p$	$w\,^3G_5$	48 231.271	
$z\,^5P_2$	29 469.020*	$3d^64s4p$	$w\,^5F_4$	44 022.535	$3d^64s4p$	$v\,^5F_2$	48 238.843	$3d^64s4p$
$z\,^5P_1$	29 732.733*	$3d^64s4p$	$w\,^5F_3$	44 166.203	$3d^64s4p$	$v\,^5P_1$	48 289.865	$3d^74p$
$z\,^3F_4$	31 307.243*	$3d^64s4p$	$w\,^5D_2$	44 183.620	$3d^64s4p$	$x\,^3P_2$	48 304.638	$3d^64s4p$
$z\,^3D_3$	31 322.611*	$3d^64s4p$	$w\,^5F_5$	44 243.673*	$3d^64s4p$	$v\,^5F_1$	48 350.601	$3d^64s4p$
$z\,^3D_2$	31 686.346*	$3d^64s4p$	$w\,^5F_2$	44 285.443	$3d^64s4p$	$w\,^3G_4$	48 361.878	
$z\,^3F_3$	31 805.067*	$3d^64s4p$	$w\,^5D_1$	44 411.151	$3d^64s4p$	$z\,^1H_5$	48 382.597	$3d^74p$
$z\,^3D_1$	31 937.316	$3d^64s4p$	$v\,^5D_4$	44 415.070	$3d^64s4p$	$x\,^3P_0$	48 460.099	$3d^64s4p$
$z\,^3F_2$	32 133.986*	$3d^64s4p$	$w\,^5D_0$	44 458.933	$3d^64s4p$	$w\,^3G_3$	48 475.668	
$y\,^5D_4$	33 095.937*	$3d^74p$	$y\,^5S_2$	44 511.806	$3d^74p$	$x\,^3P_1$	48 516.135	$3d^64s4p$
$y\,^5D_3$	33 507.120*	$3d^74p$	$v\,^5D_3$	44 551.331	$3d^64s4p$	$y\,^1G_4$	48 702.526	$3d^74p$
$y\,^5F_5$	33 695.394*	$3d^74p$	$v\,^5D_2$	44 664.068	$3d^64s4p$	$w\,^3F_4$	49 108.891	$3d^64s4p$
$y\,^5D_2$	33 801.567*	$3d^74p$	$v\,^5D_1$	44 760.739	$3d^64s4p$	$v\,^3D_3$	49 135.022	$3d^64s4p$
$z\,^3P_2$	33 946.929*	$3d^64s4p$	$v\,^5D_0$	44 826.894	$3d^64s4p$	$v\,^3D_2$	49 242.593	$3d^64s4p$
$y\,^5D_1$	34 017.098	$3d^74p$	$x\,^3D_3$	45 220.676	$3d^64s4p$	$w\,^3F_3$	49 242.880	$3d^64s4p$
$y\,^5F_4$	34 039.513*	$3d^74p$	$x\,^3D_2$	45 281.832	$3d^64s4p$	$v\,^3D_1$	49 297.620	$3d^64s4p$
$y\,^5D_0$	(34 121.596)	$3d^74p$	$y\,^3G_5$	45 294.846	$3d^64s4p$	$w\,^3F_2$	49 433.121	$3d^64s4p$
$y\,^5F_3$	34 328.749*	$3d^74p$	$y\,^3G_4$	45 428.396	$3d^64s4p$	$y\,^3H_6$	49 434.156	$3d^74p$
$z\,^3P_1$	34 362.871	$3d^64s4p$	$x\,^3D_1$	45 551.763	$3d^64s4p$	$v\,^3G_5$	49 460.890	$3d^74p$
$y\,^5F_2$	34 547.206*	$3d^74p$	$y\,^3G_3$	45 562.971	$3d^64s4p$	$z\,^1D_2$	(49 477.126)	$3d^74p$
$z\,^3P_0$	(34 555.597)	$3d^64s4p$	$x\,^5G_6$	(45 608.356)	$3d^64s4p$	$y\,^3H_5$	49 604.415	$3d^74p$
$y\,^5F_1$	34 692.144*	$3d^74p$	$x\,^5G_5$	45 726.117*	$3d^64s4p$	$v\,^3G_4$	49 627.877	$3d^74p$
$z\,^5G_5$	34 782.416*	$3d^74p$	$x\,^5G_3$	45 913.488	$3d^64s4p$	$v\,^3H_4$	49 726.977	$3d^74p$
$z\,^5G_4$	35 257.319*	$3d^74p$	$x\,^5G_2$	45 964.958	$3d^64s4p$	$v\,^3G_3$	49 850.582	$3d^74p$
$z\,^3G_5$	35 379.207*	$3d^74p$	$z\,^3I_6$	46 026.969	$3d^64s4p$	$w\,^3P_0$	49 951.341	$3d^74p$
$z\,^5G_3$	35 611.619*	$3d^74p$	$w\,^5P_3$	46 137.111	$3d^54s^24p$	$w\,^3P_1$	50 043.205	$3d^74p$
$z\,^3G_4$	35 767.561*	$3d^74p$	$w\,^5P_2$	46 313.535	$3d^54s^24p$	$w\,^3P_2$	50 186.831	$3d^74p$
$z\,^5G_2$	35 856.400*	$3d^74p$	$w\,^5P_1$	46 410.377	$3d^54s4p$	$z\,^1F_3$	50 586.874	$3d^74p$
$z\,^3G_3$	36 079.367*	$3d^74p$	$z\,^3S_1$	46 600.814	$3d^64s^24p$	$x\,^1G_4$	50 613.972	
$y\,^3F_4$	36 686.164*	$3d^74p$	$y\,^3P_0$	46 672.527	$3d^74p$	$u\,^5F_5$	51 016.658	$3d^64s5p$
$y\,^5P_3$	36 766.962	$3d^64s4p$	$u\,^5D_4$	46 720.836	$3d^74p$	$x\,^3H_6$	51 023.151	$3d^64s4p$
$y\,^5P_2$	37 157.557	$3d^64s4p$	$y\,^3P_2$	46 727.068	$3d^74p$	$x\,^3H_5$	51 068.710	$3d^64s4p$
$y\,^3F_3$	37 162.740*	$3d^74p$	$u\,^5D_3$	46 744.988	$3d^74p$	$t\,^5D_4$	51 076.626	$3d^64s5p$
$y\,^5P_1$	37 409.542*	$3d^64s4p$	$u\,^5D_2$	46 888.510	$3d^74p$	$v\,^3F_2$	51 201.284	$3d^64s4p$
$y\,^3F_2$	37 521.157*	$3d^74p$	$x\,^3F_4$	46 889.143	$3d^74p$	$v\,^3F_4$	51 304.603	$3d^64s4p$
$y\,^3D_3$	38 175.350*	$3d^74p$	$y\,^3P_1$	46 901.820	$3d^74p$	$t\,^5D_3$	51 361.394	$3d^64s5p$
$y\,^3D_2$	38 678.032*	$3d^74p$	$z\,^3H_6$	(46 982.317)	$3d^64s4p$	$v\,^3F_3$	51 365.308	$3d^64s4p$

TABLE II. *Odd energy levels of* Fe I.—Continued

Designation	Level (cm^{-1})	Configuration	Designation	Level (cm^{-1})	Configuration	Designation	Level (cm^{-1})	Configuration
$u\,^3G_5$	51 373.909	$3d^74p$	$y\,^3I_6$	52 513.549	$3d^74p$	$v\,^3H_5$	55 429.815	
$u\,^5F_4$	51 381.455	$3d^64s5p$	$w\,^3H_5$	52 613.084	$3d^74p$	$v\,^3H_4$	55 446.000	
4 4	51 409.117		$y\,^3I_7$	(52 654.986)	$3d^74p$	$v\,^3H_6$	(55 489.748)	
$u\,^5F_3$	51 619.069	$3d^64s5p$	$t\,^3D_2$	52 682.916	$3d^74p$	$w\,^3D_2$	55 754.239	$3d^74p$
6 5	51 630.172	$3d^64s5p$	$w\,^3H_4$	52 768.721	$3d^74p$	$w\,^1F_3$	55 790.673	
$u\,^3G_4$	51 668.189	$3d^74p$	8 1	52 857.790	$3d^74p$	$s\,^3G_4$	55 905.538	
$u\,^5P_3$	51 691.935	$3d^64s5p$	$y\,^3I_5$	52 898.971	$3d^74p$	$s\,^3G_5$	55 907.171	
$y\,^1D_2$	51 708.309	$3d^74p$	$v\,^3P_2$	52 916.292	$3d^74p$	$s\,^3G_3$	56 097.829	
$x\,^1D_2$	51 762.067		$z\,^1I_6$	53 093.521	$3d^74p$	$u\,^3H_6$	56 333.958	$3d^64s4p$
$u\,^3G_3$	51 825.773	$3d^74p$	$z\,^1P_1$	53 229.942	$3d^74p$	$u\,^3H_5$	56 382.662	$3d^64s4p$
$u\,^5F_2$	51 827.401	$3d^64s5p$	$x\,^1F_3$	53 763.271		$u\,^3H_4$	56 423.279	$3d^64s4p$
$t\,^5D_0$	51 941.786	$3d^64s5p$	$v\,^3P_1$	53 808.353	$3d^74p$	$u\,^3F_4$	56 592.699	$3d^74p$
$u\,^5P_2$	51 944.774	$3d^64s5p$	10 3	53 891.520	$3d^64s4p$	$u\,^3F_3$	56 783.317	$3d^74p$
$u\,^5F_1$	51 945.805	$3d^64s5p$	$t\,^3G_5$	53 983.284	$3d^64s4p$	$u\,^3F_2$	56 858.659	$3d^74p$
$u\,^3D_3$	51 969.079	$3d^74p$	12 5	54 013.748	$3d^64s4p$	$v\,^1G_4$	56 951.286	
$u\,^5P_1$	52 110.587	$3d^64s5p$	$t\,^5P_2$	54 112.218	$3d^64s4p$	$x\,^3I_6$	(57 070.186)	$3d^64s4p$
$t\,^3D_1$	52 180.804	$3d^74p$	$t\,^3G_4$	54 237.415	$3d^64s4p$	$x\,^3I_5$	(57 104.222)	$3d^64s4p$
$t\,^3D_3$	52 213.226	$3d^74p$	$t\,^5P_1$	54 271.057	$3d^64s4p$	$t\,^3F_2$	57 708.747	
$u\,^3D_2$	52 296.899	$3d^74p$	13 4	54 301.334		$r\,^3G_4$	60 172.058	$3d^64s4d$
$w\,^3H_6$	52 431.418	$3d^74p$	$t\,^3G_3$	54 600.346	$3d^64s4p$	$r\,^3G_3$	60 364.706	$3d^64s4d$
$u\,^3D_1$	52 512.445	$3d^74p$	$w\,^1G_4$	54 810.841		$q\,^3G_3$	60 806.653	

Below 2000 Å a few additional lines were measured in a more conventional way by comparison with external standards of longer wavelength (lower order).

In addition to these, earlier measurements taken on a 6.65 meter Paschen concave grating spectrograph are included. These values are generally several times less precise. The effective resolving power is about 250,000, and the line shape dissymmetries limit the accuracy attainable.

Approximately 4000 additional lines have been measured, including previously identified lines of Fe I, Fe II, Ne I and Ne II, as well as many for which no definite ion assignment has yet been made. The Fe I measurements were then used to construct the energy level scheme given in tables I and II. Using these, an expanded set of Ritz standards was computed. These replace the original measurements wherever possible in the line list given in table III.

A comparison of these energy level values for low-pressure sources shows systematic differences compared to those derived from the best averages available for the atmospheric arc [Edlén, 1955]. Edlén [1960] has suggested that for missing low odd levels, estimates for low pressure sources can be made by adding 0.015 cm^{-1} to the corresponding atmospheric arc value. The entries in table II given between parentheses were derived in this way.

The corresponding correction for low even levels appears to be negligible, and the parenthetical entries of table I are therefore taken directly from Edlén's 1957 atmospheric arc values.

An improved analysis of the Fe II spectrum in terms of Ritz standards also appears to be possible on the basis of these measurements, but this has been deferred pending the completion of more extensive five-meter measurements which eventually will replace the less precise Paschen ones. This work is now in progress.

Ne I and II lines show pronounced Doppler broadening in these sources. The Ne I measurements have been replaced wherever possible by more precise interferometric values given by Burns et al. [1950], and by Ritz standards derived by Kaufman and Edlén [1974] based on the energy level analysis of Kaufman and Minnhagen [1972].

A similar analysis of the Ne II spectrum has been made by Persson [1971]. The Ne II wavelength values given here are in all cases derived from his computed wave number values.

Some 4000 lines are set out in table III, and include 2377 Fe I, 596 Fe II, 189 Ne I and 92 Ne II (the ion designation is indicated in Column 4) as well as 744 for which no clear specification has been possible. Most of the latter are probably previously undetected lines of Fe I.

Column 1 gives typical intensities for a 90 mA discharge in a tube with an iron hollow cathode, filled with neon at 3.5 torr. The absolute scale is standardized in such a way that above 2900 Å the energy flux from 1 cm^2 of the light course per unit solid angle is in ergs per second. Below this the tungsten lamp reference source was not reliable because of scattered light problems, and an entirely different method based on absorption line strengths was devised [Crosswhite, 1958]. Recent experiments which extend the tungsten calibration to 2300 Å indicate that these short wavelength values are too high by some 40 percent. Because the relative intensities vary with pressure and are also very sensitive to the presence of small amounts of hydrogen, these values should be con-

sidered as only semiquantitative unless only relative values of lines having the same upper state are considered. For these reasons the intensities given in Column 1 have been put on a stylized scale 3, 4, 5, 6, 8, 10, 12, 15, 20, 25, 30 . . . etc. in multiples of 10. Lines with intensities less than one are given the value "0".

Columns 2 and 3 are air and vacuum wavelengths, respectively. For most of the Johns Hopkins measurements, the vacuum wavelengths are primary, as the interferometer and five-meter spectrograph both were evacuated. The air and vacuum wavelengths are related by Edlen's dispersion formula for standard air [Edlén, 1953 and 1966].

The fifth column (Ref) gives the source of the data, the key being given on the page preceding table III.

The last two columns give the energy level designations of the lower and upper levels of Fe I, respectively. Energy level values for most of these are given in tables I and II. A further discussion of these levels can be found in Reader and Sugar [1974].

A set of photoelectric traces similar to those originally given in the Spectroscopy Laboratory report on Fe I [Crosswhite, 1958] and in various editions of the AIP handbook [Crosswhite, 1972] follow table III. The intensities indicated in these traces are roughly those given in table III, although the latter contains results in addition to those from this specific run. The calibration of sensitivity variation with wavelength above 2900 Å was done with a standard tungsten lamp, but below this use was made of self-absorption measurements and thermodynamic considerations to get a rough extrapolation. Further details of these measurements will be reported at a later time.

Key to References in Table III, Column 5

BA	Burns, Adams and Longwell [1950]
BW	Burns and Walters [1931]
CA	Calculated from differences of energy levels given in tables I and II
CP	Calculated lines of Ne II given in Persson [1971]
ED	Calculated from differences of estimated energy levels [Edlén 1957, 1960]
FE	Interferometric measurements of Fe I [Crosswhite, 1958]
JA	JHU 5-meter Jarrell-Ash measurements
KE	Calculated lines of Ne I given in Kaufman and Edlén [1974]
P	JHU 6.65-meter Paschen measurements
SD	Stanley and Dieke [1955]
SM	Stanley and Meggers [1957]

This work was supported by a Grant from the National Science Foundation.

References

Burns, K., Adams, K. B., and Longwell, J., Interference measurements in the spectra of neon and natural mercury, J. Opt. Soc. Amer. **40,** 339 (1950).

Burns, K., and Walters, F. M. Jr., Wavelengths and atomic levels in the spectrum of the vacuum iron arc, Publ. Alleghany Observ. **6,** 159 (1929); **8,** 39 (1931).

Crosswhite, H. M., The Spectrum of Iron I, Johns Hopkins Spectroscopic Report No. 13 (1958).

Crosswhite, H. M., U. S. Patent No. 3,473,865 (1969).

Crosswhite, H. M., Section 7g of American Institute of Physics Handbook, D. E. Gray, editor (McGraw-Hill, New York, 1972).

Crosswhite, H. M., Dieke, G. H., and Legagneur, C. S., Hollow iron cathode discharge as source for wavelength and intensity standards, J. Opt. Soc. Amer. **45,** 270 (1955).

Crosswhite, H. M., and Jones, W. W., unpublished (1974).

Dieke, G. H., and Heath, D. F., High resolution vacuum spectrograph, Japan J. Appl. Phys. **4,** Suppl. 1, 455 (1965).

Edlén, B., The dispersion of standard air, J. Opt. Soc. Amer. **43,** 339 (1953).

Edlén, B., Report to the IAU Commission 14 (1955).

Edlén, B., Trans. Int. Astron. Union **IX,** 218 (1957).

Edlén, B., Trans. Int. Astron. Union **X,** 214 (1960).

Edlén, B., The refractive index of air, Metrologia (Germany) **2,** 71 (1966).

Fastie, W. G., U.S. Patent 3,011,391 (1963).

Kaufman, V., and Edlén, B., J. Chem. Phys. Ref. Data **3,** 825 (1974).

Reader, J., and Sugar, J., J. Phys. Chem. Ref. Data **5** (1975).

Kaufman, V., and Minnhagen, L., Accurate ground-term combinations in Ne I, J. Opt. Soc. Amer. **62,** 92 (1972).

Kielkopf, J. F., unpublished tests using self-reversed natural mercury lines (1973).

Persson, W., The spectrum of singly ionized neon, Ne II, Physica Scripta **3,** 133 (1971).

Pfund, A. H., Metallic arcs for spectroscopic investigations, Astrophys. Jour. **27,** 298 (1908).

Reader, J., and Sugar, J., J. Phys. Chem. Ref. Data **5** (1975).

Russel, H. N., and Moore, C. E., The arc spectrum of iron (Fe I), Trans. Am. Phil. Soc. **34,** Part 2, 113 (1944).

Stanley, R. W., and Dieke, G. H., Interferometric wavelengths of iron lines from a hollow cathode discharge, J. Opt. Soc. Amer. **45,** 280 (1955).

Stanley, R. W., and Meggers, W. F., Wavelengths from iron-halide lamps, J. Research N.B.S. **58,** 41 (1957) RP 2733.

Williams, W. E., and Middleton, A., Vacuum wavelength measurements in the iron spectrum by means of the reflection echelon grating, Proc. Roy. Soc. **A172,** 159 (1939).

(Paper 79A1–843)

TABLE III. *Spectrum of the Fe-Ne hollow cathode*

Intensity	Wavelength (Å) Air	Wavelength (Å) Vacuum	Ion	Ref	Classification
30		1934.5378	Fe I	CA	$a\,^5D_4 - u\,^5P_3$
25		1937.2686	Fe I	CA	$a\,^5D_4 - u\,^5F_3$
20		1940.6607	Fe I	CA	$a\,^5D_3 - u\,^5P_2$
8		1945.2762	Fe I	CA	$a\,^5D_2 - u\,^5P_1$
2		1946.2275	Fe I	CA	$a\,^5D_4 - u\,^5F_4$
50		1946.9877	Fe I	CA	$a\,^5D_4 - t\,^5D_3$
15		1950.2300	Fe I	CA	$a\,^5D_3 - u\,^5P_3$
25		1951.5710	Fe I	CA	$a\,^5D_2 - u\,^5P_2$
20		1952.2687	Fe I	CA	$a\,^5D_1 - u\,^5P_1$
30		1952.588	Fe I	JA	$a\,^5D_3 - t\,^5D_2$
30		1953.0053	Fe I	CA	$a\,^5D_3 - u\,^5F_3$
12		1955.7027	Fe I	CA	$a\,^5D_0 - u\,^5P_1$
15		1956.0516	Fe I	CA	$a\,^5D_2 - u\,^5F_2$
60		1957.8427	Fe I	CA	$a\,^5D_4 - t\,^5D_4$
10		1958.5694	Fe I	CA	$a\,^5D_1 - u\,^5F_1$
20		1958.6089	Fe I	CA	$a\,^5D_1 - u\,^5P_2$
60		1960.1441	Fe I	CA	$a\,^5D_4 - u\,^5F_5$
30		1961.246	Fe I	JA	$a\,^5D_2 - u\,^5P_3$
10		1962.0256	Fe I	CA	$a\,^5D_0 - u\,^5F_1$
50		1962.1107	Fe I	CA	$a\,^5D_3 - u\,^5F_2$
10		1962.8834	Fe I	CA	$a\,^5D_3 - t\,^5D_3$
15		1963.1219	Fe I	CA	$a\,^5D_1 - u\,^5F_2$
10		1964.0552	Fe I	CA	$a\,^5D_2 - u\,^5F_3$
10	2040.690	2041.345		JA	
5	2080.242	2080.905		JA	
2	2081.284	2081.947		JA	
100	2084.1217	2084.7852	Fe I	CA	$a\,^5D_4 - v\,^5P_3$
50	2085.424	2086.088		JA	
20	2085.463	2086.127	Ne II	CP	
4	2087.5109	2088.1750	Fe I	CA	$a\,^5D_3 - x\,^3P_2$
8	2087.542	2088.206		JA	
6	2090.3831	2091.0479	Fe I	CA	$a\,^5D_3 - v\,^5F_2$
6	2090.8545	2091.5194	Fe I	CA	$a\,^5D_2 - x\,^3P_1$
50	2093.711	2094.377		JA	
200	2096.106	2096.772	Ne II	CP	
15	2096.253	2096.920	Ne II	CP	
2	2098.163	2098.829		JA	
3	2098.9386	2099.6050	Fe I	CA	$a\,^5D_1 - x\,^3P_1$
10	2100.7976	2101.4646	Fe I	CA	$a\,^5D_2 - v\,^5P_1$
20	2102.3541	2103.0211	Fe I	CA	$a\,^5D_3 - v\,^5P_3$
6	2103.0530	2103.7202	Fe I	CA	$a\,^5D_2 - v\,^5F_2$
2	2106.2600	2106.9278	Fe I	CA	$a\,^5D_1 - v\,^5F_1$
10	2106.3946	2107.0626	Fe I	CA	$a\,^5D_2 - v\,^5P_2$
10	2108.9591	2109.6274	Fe I	CA	$a\,^5D_1 - v\,^5P_1$
8	2110.2354	2110.9040	Fe I	CA	$a\,^5F_5 - 13\ \ 4$
2	2110.732	2111.401		JA	
4	2130.964	2131.637		JA	
10	2132.0167	2132.6899	Fe I	CA	$a\,^5D_4 - x\,^3F_4$
2	2135.948	2136.622		JA	
4	2138.5924	2139.2668	Fe I	CA	$a\,^5D_4 - u\,^5D_3$
15	2139.6980	2140.3727	Fe I	CA	$a\,^5D_4 - u\,^5D_4$
3	2139.738	2140.413		JA	
2	2139.9349	2140.6094	Fe I	CA	$a\,^5D_2 - 1\ \ 2$
6	2141.7180	2142.3931	Fe I	CA	$a\,^5D_3 - x\,^3F_3$
12	2145.1891	2145.8649	Fe I	CA	$a\,^5D_3 - w\,^3D_3$
2	2147.045	2147.721		JA	
2	2147.702	2148.379		JA	
5	2150.1844	2150.8610	Fe I	CA	$a\,^5D_2 - x\,^3F_2$
5	2150.621	2151.298	Fe II	JA	
10	2151.695	2152.372		JA	
2	2152.480	2153.157		JA	
15	2153.0065	2153.6839	Fe I	CA	$a\,^5D_2 - w\,^3D_2$
4	2155.0197	2155.6972	Fe I	CA	$a\,^5D_2 - x\,^3F_3$
50	2157.7943	2158.4727	Fe I	CA	$a\,^5D_3 - u\,^5D_3$
3	2158.474	2159.153		JA	
15	2158.5341	2159.2123	Fe I	CA	$a\,^5D_2 - w\,^3D_3$
5	2158.6296	2159.3079	Fe I	CA	$a\,^5D_3 - y\,^3P_2$
2	2158.7345	2159.4128	Fe I	CA	$a\,^5D_1 - x\,^3F_2$
5	2158.9202	2159.5985	Fe I	CA	$a\,^5D_3 - u\,^5D_4$
3	2159.4313	2160.1097	Fe I	CA	$a\,^5D_0 - w\,^3D_1$
3	2159.638	2160.317		JA	
5	2159.6575	2160.3360	Fe I	CA	$a\,^5D_1 - u\,^5D_1$
5	2159.8357	2160.5142	Fe I	CA	$a\,^5F_2 - t\,^5P_1$
3	2159.881	2160.590		JA	
6	2159.9239	2160.6024	Fe I	CA	$a\,^5D_1 - u\,^5D_0$
3	2161.159	2161.838	Fe II	JA	
15	2161.5792	2162.2583	Fe I	CA	$a\,^5D_1 - w\,^3D_2$
15	2162.021	2162.701	Fe II	JA	
8	2162.248	2162.927		JA	
30	2164.5486	2165.2283	Fe I	CA	$a\,^5D_2 - u\,^5D_2$
30	2165.752	2166.432		JA	
15	2166.587	2167.267		JA	
40	2166.7727	2167.4526	Fe I	CA	$a\,^5D_4 - w\,^5P_3$
30	2171.2968	2171.9779	Fe I	CA	$a\,^5D_2 - u\,^5D_3$
2	2172.1443	2172.8236	Fe I	CA	$a\,^5D_2 - y\,^3P_2$
15	2172.5851	2173.2662	Fe I	CA	$a\,^5D_1 - y\,^3P_1$
25	2173.2136	2173.8951	Fe I	CA	$a\,^5D_1 - u\,^5D_2$
10	2175.454	2176.136		JA	
20	2176.8404	2177.5226	Fe I	CA	$a\,^5D_0 - y\,^3P_1$
5	2177.6946	2178.3768	Fe I	CA	$a\,^5F_2 - 10\ \ 3$
300	2178.1182	2178.8007	Fe I	CA	$a\,^5D_2 - z\,^3S_1$
15	2180.8686	2181.5514	Fe I	CA	$a\,^5D_1 - y\,^3P_2$
8	2183.7963	2184.4797	Fe I	CA	$a\,^5F_2 - x\,^1F_3$
6	2186.2500	2186.9340	Fe I	CA	$a\,^5D_4 - x\,^5G_5$
250	2186.4862	2187.1702	Fe I	CA	$a\,^5D_3 - w\,^5P_3$
60	2186.8922	2187.5766	Fe I	CA	$a\,^5D_1 - z\,^3S_1$
120	2187.1946	2187.8787	Fe I	CA	$a\,^5D_2 - w\,^5P_1$
25	2191.2043	2191.8893	Fe I	CA	$a\,^5D_0 - z\,^3S_1$
250	2191.8391	2192.5242	Fe I	CA	$a\,^5D_2 - w\,^5P_2$
150	2196.0429	2196.7281	Fe I	CA	$a\,^5D_1 - w\,^5P_1$
80	2200.3900	2201.0769	Fe I	CA	$a\,^5D_0 - w\,^5P_1$
80	2200.7243	2201.4113	Fe I	CA	$a\,^5D_1 - w\,^5P_2$
5	2201.590	2202.277		JA	
5	2206.083	2206.771		JA	
8	2206.150	2206.838		JA	
4	2207.0684	2207.7567	Fe I	CA	$a\,^5D_4 - y\,^3G_5$
15	2208.407	2209.096	Fe II	JA	
8	2209.034	2209.723	Fe II	JA	
8	2210.6887	2211.3778	Fe I	CA	$a\,^5D_4 - x\,^3D_3$
20	2213.655	2214.345	Fe II	JA	
8	2214.039	2214.729	Fe II	JA	
8	2215.077	2215.767	Fe II	JA	
4	2215.702	2216.393	Fe II	JA	
12	2218.262	2218.952	Fe II	JA	
10	2219.896	2220.587	Fe II	JA	
20	2220.381	2221.072	Fe II	JA	
8	2221.167	2221.858	Fe II	JA	
8	2223.487	2224.179	Fe II	JA	
12	2228.1715	2228.8643	Fe I	CA	$a\,^5D_3 - x\,^3D_2$
2	2229.0728	2229.7658	Fe I	CA	$a\,^5D_2 - x\,^3D_1$
15	2231.2128	2231.9065	Fe I	CA	$a\,^5D_3 - x\,^3D_3$
60	2244.244	2244.940		JA	
25	2245.578	2246.275		JA	
10	2245.6527	2246.3494	Fe I	CA	$a\,^5D_2 - x\,^3D_3$
20	2248.8602	2249.5574	Fe I	CA	$a\,^5F_5 - u\,^5F_4$
50	2250.437	2251.134		JA	
50	2250.7904	2251.4880	Fe I	CA	$a\,^5D_4 - v\,^5D_4$
60	2251.8739	2252.5717	Fe I	CA	$a\,^5D_1 - x\,^3D_2$

TABLE III. *Spectrum of the Fe-Ne hollow cathode*—Continued

Intensity	Wavelength (Å) Air	Wavelength (Å) Vacuum	Ion	Ref	Classification
25	2255.766	2256.465	Fe II	JA	
20	2255.8647	2256.5634	Fe I	CA	$a\ ^5F_4 - u\ ^5P_3$
300	2259.5106	2260.2101	Fe I	CA	$a\ ^5D_4 - w\ ^5F_5$
60	2264.3893	2265.0898	Fe I	CA	$a\ ^5F_5 - t\ ^5D_4$
40	2265.0543	2265.7550	Fe I	CA	$a\ ^5D_3 - v\ ^5D_3$
15	2266.9063	2267.6074	Fe I	CA	$a\ ^5F_3 - u\ ^5F_2$
80	2267.0847	2267.7859	Fe I	CA	$a\ ^5D_3 - y\ ^5S_2$
80	2267.4695	2268.1707	Fe I	CA	$a\ ^5F_5 - u\ ^5F_5$
15	2269.1000	2269.8016	Fe I	CA	$a\ ^5D_2 - v\ ^5D_1$
50	2270.8619	2271.5638	Fe I	CA	$a\ ^5D_4 - w\ ^5F_4$
30	2271.7827	2272.4848	Fe I	CA	$a\ ^5F_4 - u\ ^5F_4$
150	2272.0696	2272.7718	Fe I	CA	$a\ ^5D_3 - v\ ^5D_4$
30	2272.8188	2273.5212	Fe I	CA	$a\ ^5F_4 - t\ ^5D_3$
30	2274.0893	2274.7919	Fe I	CA	$a\ ^5D_2 - v\ ^5D_2$
12	2275.1917	2275.8946	Fe I	CA	$a\ ^5D_1 - v\ ^5D_0$
10	2275.5972	2276.3002	Fe I	CA	$a\ ^3F_4 - s\ ^3G_5$
150	2276.0258	2276.7289	Fe I	CA	$a\ ^5D_4 - w\ ^5D_3$
15	2277.1054	2277.8087	Fe I	CA	$a\ ^5F_3 - t\ ^5D_2$
20	2277.6673	2278.3707	Fe I	CA	$a\ ^5F_3 - u\ ^5F_3$
80	2279.9368	2280.6407	Fe I	CA	$a\ ^5D_2 - v\ ^5D_3$
12	2280.2158	2280.9198	Fe I	CA	$a\ ^5F_2 - u\ ^5F_2$
5	2282.8647	2283.5693	Fe I	CA	$a\ ^5F_1 - u\ ^5F_1$
8	2283.0743	2283.7789	Fe I	CA	$a\ ^5F_1 - t\ ^5D_0$
20	2283.3053	2284.0099	Fe I	CA	$a\ ^5D_0 - v\ ^5D_1$
30	2283.6551	2284.3599	Fe I	CA	$a\ ^5D_1 - v\ ^5D_2$
150	2284.0857	2284.7905	Fe I	CA	$a\ ^5D_3 - w\ ^5D_2$
150	2287.2498	2287.9553	Fe I	CA	$a\ ^5D_2 - w\ ^5D_1$
40	2287.6309	2288.3365	Fe I	CA	$a\ ^5F_4 - t\ ^5D_4$
20	2289.0366	2289.7425	Fe I	CA	$a\ ^5F_1 - u\ ^5F_2$
10	2290.0663	2290.7724	Fe I	CA	$a\ ^5F_3 - u\ ^5F_4$
25	2290.5533	2291.2595	Fe I	CA	$a\ ^5F_2 - t\ ^5D_2$
10	2290.7748	2291.4811	Fe I	CA	$a\ ^5F_4 - u\ ^5F_5$
40	2291.1193	2291.8256	Fe I	CA	$a\ ^5F_2 - u\ ^5F_3$
8	2291.6267	2292.3331	Fe I	CA	$a\ ^5D_1 - y\ ^5S_2$
20	2291.999	2292.706		JA	
300	2292.5240	2293.2306	Fe I	CA	$a\ ^5D_3 - w\ ^5F_4$
30	2292.828	2293.535		JA	
25	2293.8478	2294.5548	Fe I	CA	$a\ ^5D_2 - w\ ^5F_2$
80	2294.4078	2295.1149	Fe I	JA	$a\ ^5D_1 - w\ ^5D_0$
15	2296.890	2297.598		JA	
25	2296.9269	2297.6345	Fe I	CA	$a\ ^5D_1 - w\ ^5D_1$
8	2297.463	2298.171		JA	
200	2297.7870	2298.4948	Fe I	CA	$a\ ^5D_3 - w\ ^5D_3$
600	2298.1693	2298.8772	Fe I	CA	$a\ ^5D_4 - w\ ^5D_4$
10	2298.221	2298.929	Fe II	JA	
15	2298.446	2299.154		JA	
20	2298.6602	2299.3682	Fe I	CA	$a\ ^5D_1 - w\ ^5F_1$
80	2299.2201	2299.9283	Fe I	CA	$a\ ^5D_2 - w\ ^5D_2$
4	2299.751	2300.459		JA	
300	2300.1416	2300.8499	Fe I	CA	$a\ ^5D_2 - w\ ^5F_3$
4	2300.524	2301.232		JA	
100	2301.175	2301.884		JA	
4	2301.567	2302.276		JA	
4	2301.601	2302.310		JA	
50	2301.6839	2302.3925	Fe I	CA	$a\ ^5D_0 - w\ ^5D_1$
4	2301.965	2302.674		JA	
8	2303.353	2304.062	Fe II	JA	
100	2303.4244	2304.1334	Fe I	CA	$a\ ^5D_0 - w\ ^5F_1$
150	2303.5810	2304.2900	Fe I	CA	$a\ ^5D_1 - w\ ^5F_2$
4	2304.207	2304.916		JA	
12	2304.7336	2305.4429	Fe I	CA	$a\ ^5F_2 - t\ ^5D_3$
4	2304.906	2305.615	Fe II	JA	
6	2306.1716	2306.8812	Fe I	CA	$a\ ^5F_3 - t\ ^5D_4$
15	2306.3823	2307.0920	Fe I	CA	$a\ ^3F_3 - s\ ^3G_4$
6	2306.667	2307.377		JA	
5	2306.856	2307.566		JA	
6	2307.077	2307.787		JA	
6	2307.314	2308.024	Fe II	JA	
6	2308.377	2309.087		JA	
5	2308.767	2309.477	Fe II	JA	
120	2308.9990	2309.7093	Fe I	CA	$a\ ^5D_1 - w\ ^5D_2$
8	2309.442	2310.153		JA	
4	2310.090	2310.801	Fe II	JA	
6	2310.166	2310.877		JA	
6	2310.260	2310.971		JA	
4	2311.224	2311.935	Fe II	JA	
5	2311.291	2312.002	Fe II	JA	
6	2312.024	2312.736	Fe II	JA	
5	2312.315	2313.026		JA	
6	2312.611	2313.322		JA	
150	2313.1041	2313.8153	Fe I	CA	$a\ ^5D_2 - w\ ^5D_3$
10	2313.190	2313.901		JA	
5	2313.262	2313.973		JA	
6	2313.564	2314.276		JA	
6	2313.941	2314.652		JA	
10	2314.701	2315.413		JA	
8	2315.729	2316.441		JA	
6	2316.512	2317.224		JA	
10	2316.911	2317.623		JA	
20	2317.352	2318.064		JA	
8	2317.380	2318.092	Fe II	JA	
8	2317.596	2318.308		JA	
8	2317.8983	2318.6105	Fe I	CA	$a\ ^3F_2 - s\ ^3G_3$
8	2318.151	2318.863		JA	
6	2318.187	2318.899		JA	
6	2318.318	2319.030		JA	
15	2320.035	2320.748		JA	
200	2320.3579	2321.0707	Fe I	CA	$a\ ^5D_3 - w\ ^5D_4$
10	2320.405	2321.118		JA	
6	2321.243	2321.956		JA	
8	2321.50	2322.21		JA	
10	2321.690	2322.403	Fe II	JA	
15	2321.755	2322.468		JA	
6	2322.331	2323.044	Fe II	JA	
10	2322.941	2323.654		JA	
8	2323.014	2323.727		JA	
8	2323.187	2323.900		JA	
6	2323.372	2324.085		JA	
6	2323.422	2324.135		JA	
6	2324.128	2324.841		JA	
8	2324.202	2324.915		JA	
6	2324.414	2325.127		JA	
12	2324.473	2325.187		JA	
8	2324.580	2325.293		JA	
8	2324.816	2325.529		JA	
10	2325.035	2325.748		JA	
10	2325.296	2326.009		JA	
8	2325.587	2326.300		JA	
6	2325.638	2326.351		JA	
10	2325.715	2326.429		JA	
6	2325.764	2326.477		JA	
6	2326.157	2326.870		JA	
6	2326.221	2326.935		JA	
6	2326.362	2327.075		JA	
6	2326.770	2327.484		JA	
6	2326.810	2327.524		JA	
100	2327.3962	2328.1105	Fe II	JA	
15	2327.875	2328.590	Fe II	JA	

TABLE III. *Spectrum of the Fe-Ne hollow cathode*—Continued

Intensity	Wavelength (Å) Air	Wavelength (Å) Vacuum	Ion	Ref	Classification
8	2327.962	2328.675		JA	
10	2328.749	2329.463		JA	
5	2329.6406	2330.3554	Fe I	CA	$a\ ^5D_4 - y\ ^5G_5$
15	2329.992	2330.707		JA	
5	2331.057	2331.772		JA	
6	2331.112	2331.827		JA	
8	2331.172	2331.888		JA	
100	2331.3082	2332.0234	Fe II	JA	
15	2331.975	2332.691	Fe II	JA	
5	2332.241	2332.957		JA	
300	2332.7994	2333.5149	Fe II	JA	
15	2333.232	2333.948		JA	
10	2333.708	2334.424	Fe II	JA	
8	2334.321	2335.037		JA	
12	2334.726	2335.442		JA	
6	2334.896	2335.612	Fe II	JA	
6	2335.024	2335.741		JA	
8	2335.702	2336.418		JA	
6	2336.824	2337.540	Fe II	JA	
4	2337.762	2338.479		JA	
200	2338.0070	2338.7237	Fe II	JA	
6	2338.147	2338.864		JA	
8	2339.408	2340.125	Fe II	JA	
4	2339.508	2340.226		JA	
40	2339.645	2340.362		JA	
10	2339.882	2340.600		JA	
10	2340.462	2341.180	Fe II	JA	
12	2341.174	2341.892	Fe II	JA	
25	2341.452	2342.170		JA	
15	2341.648	2342.366		JA	
5	2342.309	2343.026		JA	
10	2342.888	2343.606		JA	
25	2343.307	2344.025		JA	
600	2343.4941	2344.2121	Fe II	JA	
80	2343.9600	2344.6780	Fe II	JA	
25	2344.154	2344.872		JA	
150	2344.2809	2344.9990	Fe II	JA	
30	2344.602	2345.320		JA	
25	2344.984	2345.702	Fe II	JA	
50	2345.339	2346.057	Fe II	JA	
15	2345.568	2346.287		JA	
25	2346.354	2347.072		JA	
30	2346.615	2347.334		JA	
12	2346.681	2347.400		JA	
10	2347.778	2348.497		JA	
200	2348.113	2348.832	Fe II	JA	
250	2348.299	2349.019	Fe II	JA	
30	2349.268	2349.988		JA	
12	2350.178	2350.897	Fe II	JA	
15	2350.247	2350.967		JA	
8	2350.4107	2351.1302	Fe I	CA	$a\ ^5D_4 - x\ ^5P_3$
8	2350.523	2351.243	Fe II	JA	
50	2351.201	2351.920	Fe II	JA	
6	2351.607	2352.327		JA	
15	2351.666	2352.386	Fe II	JA	
25	2352.309	2353.029	Fe II	JA	
30	2353.469	2354.190	Fe II	JA	
40	2353.607	2354.328		JA	
15	2353.678	2354.399	Fe II	JA	
50	2354.477	2355.198	Fe II	JA	
40	2354.889	2355.610	Fe II	JA	
12	2355.216	2355.936	Fe II	JA	
40	2355.3340	2356.0545	Fe I	CA	$a\ ^5D_3 - x\ ^5P_2$
10	2357.048	2357.769		JA	
6	2358.767	2359.488		JA	
20	2358.884	2359.605		JA	
50	2358.951	2359.673		JA	
200	2359.118	2359.840	Fe II	JA	
15	2359.595	2360.317	Fe II	JA	
150	2359.997	2360.719	Fe II	JA	
120	2360.293	2361.014	Fe II	JA	
30	2360.411	2361.133		JA	
30	2360.511	2361.233	Fe II	JA	
12	2361.009	2361.731		JA	
40	2362.020	2362.742	Fe II	JA	
60	2363.860	2364.582	Fe II	JA	
12	2364.710	2365.433		JA	
200	2364.826	2365.549	Fe II	JA	
10	2364.908	2365.631		JA	
10	2365.294	2366.017		JA	
80	2365.764	2366.487	Fe II	JA	
25	2366.591	2367.315	Fe II	JA	
80	2368.595	2369.319	Fe II	JA	
10	2368.929	2369.653		JA	
80	2369.455	2370.179	Fe II	JA	
80	2369.4558	2370.1795	Fe I	CA	$a\ ^5D_1 - x\ ^5P_1$
60	2369.7272	2370.4510		JA	
20	2369.777	2370.501		JA	
10	2369.915	2370.639		JA	
80	2369.9536	2370.6774	Fe II	JA	
25	2370.4993	2371.2232	Fe II	JA	
12	2370.774	2371.498		JA	
4	2370.909	2371.634		JA	
120	2371.4305	2372.1547	Fe I	CA	$a\ ^5D_2 - x\ ^5P_2$
10	2372.633	2373.357	Fe II	JA	
300	2373.6245	2374.3492	Fe I	CA	$a\ ^5D_3 - x\ ^5P_3$
150	2373.7351	2374.4598	Fe II	JA	
8	2373.806	2374.531		JA	
6	2374.085	2374.810		JA	
8	2374.247	2374.972		JA	
10	2374.389	2375.114	Fe II	JA	
120	2374.5182	2375.2430	Fe I	CA	$a\ ^5D_0 - x\ ^5P_1$
20	2374.995	2375.720		JA	
60	2375.1935	2375.9185	Fe II	JA	
120	2376.4297	2377.1550	Fe II	JA	
6	2377.891	2378.617		JA	
20	2378.125	2378.851	Fe II	JA	
10	2378.820	2379.546		JA	
80	2379.273	2379.999	Fe II	JA	
20	2379.407	2380.133	Fe II	JA	
40	2380.205	2380.931	Fe II	JA	
120	2380.7615	2381.4877	Fe II	JA	
15	2380.875	2381.601		JA	
150	2381.8346	2382.5611	Fe I	CA	$a\ ^5D_1 - x\ ^5P_2$
1000	2382.0355	2382.7620	Fe II	JA	
20	2382.897	2383.624	Fe II	JA	
20	2383.060	2383.787	Fe II	JA	
60	2383.2452	2383.9720	Fe II	JA	
50	2384.3883	2385.1154	Fe II	JA	
100	2384.4225	2385.1496		JA	
20	2384.548	2385.275		JA	
10	2385.005	2385.732	Fe II	JA	
5	2387.216	2387.944		JA	
8	2387.508	2388.236		JA	
12	2388.235	2388.963	Fe II	JA	
40	2388.3725	2389.1004	Fe II	JA	
300	2388.6283	2389.3563	Fe II	JA	
200	2389.9728	2390.7012	Fe I	CA	$a\ ^5D_2 - x\ ^5P_3$

TABLE III. *Spectrum of the Fe-Ne hollow cathode*—Continued

Intensity	Wavelength (Å) Air	Wavelength (Å) Vacuum	Ion	Ref	Classification
30	2390.0975	2390.8259	Fe II	JA	
20	2390.766	2391.494	Fe II	JA	
15	2391.478	2392.207	Fe II	JA	
10	2392.089	2392.818	Fe II	JA	
25	2392.1499	2392.8787		JA	
20	2392.578	2393.308	Fe II	JA	
8	2394.832	2395.562		JA	
40	2395.4196	2396.1492	Fe II	JA	
1000	2395.624	2396.354	Fe II	JA	
20	2396.1014	2396.8311		JA	
15	2396.719	2397.449	Fe II	JA	
300	2399.2413	2399.9717	Fe II	JA	
20	2400.049	2400.780	Fe II	JA	
15	2401.2917	2402.0226	Fe II	JA	
50	2404.4307	2405.1623	Fe II	JA	
15	2404.515	2405.247		JA	
800	2404.885	2405.617	Fe II	JA	
10	2405.6826	2406.4145	Fe II	JA	
250	2406.660	2407.393	Fe II	JA	
80	2406.9750	2407.7072	Fe II	JA	
8	2407.188	2407.920		JA	
4	2407.527	2408.259		JA	
4	2408.0456	2408.7780	Fe I	CA	$a\ ^5F_3 - w\ ^3F_3$
4	2408.0623	2408.7947	Fe I	CA	$a\ ^5F_3 - v\ ^3D_2$
300	2410.518	2411.251	Fe II	JA	
200	2411.0678	2411.8009	Fe II	JA	
50	2411.8082	2412.5415	Fe II	JA	
150	2413.3102	2414.0438	Fe II	JA	
5	2416.080	2416.814		JA	
20	2416.4456	2417.1799	Fe II	JA	
10	2416.791	2417.525		JA	
5	2417.490	2418.225	Fe I	BW	$a\ ^3F_4 - 9\ _4$
10	2417.821	2418.556		JA	
80	2417.8707	2418.6054	Fe II	JA	
5	2418.029	2418.763		JA	
15	2418.4369	2419.1717	Fe II	JA	
4	2419.004	2419.739		JA	
5	2419.0629	2419.7978	Fe I	CA	$a\ ^5F_4 - y\ ^1G_4$
5	2419.8784	2420.6135	Fe I	CA	$a\ ^5F_2 - v\ ^3D_1$
8	2419.989	2420.724		JA	
5	2420.178	2420.913		JA	
60	2420.3961	2421.1313	Fe I	CA	$a\ ^5F_5 - w\ ^3G_5$
60	2422.688	2423.424	Fe II	JA	
8	2422.785	2423.521		JA	
60	2423.0893	2423.8251	Fe I	CA	$a\ ^5F_2 - w\ ^3F_3$
8	2423.1062	2423.8420	Fe I	CA	$a\ ^5F_2 - v\ ^3D_2$
40	2423.210	2423.946	Fe II	JA	
10	2423.499	2424.235	Fe II	JA	
150	2424.144	2424.880	Fe II	JA	
15	2424.390	2425.126	Fe II	JA	
30	2424.592	2425.329	Fe II	JA	
5	2425.363	2426.100		JA	
20	2425.638	2426.374		JA	
10	2425.685	2426.422	Fe II	JA	
12	2426.077	2426.814		JA	
12	2427.199	2427.936	Fe II	JA	
12	2427.281	2428.018	Fe II	JA	
30	2428.292	2429.029	Fe II	JA	
120	2428.364	2429.101	Fe II	JA	
8	2428.455	2429.192		JA	
5	2428.641	2429.378		JA	
25	2428.800	2429.538	Fe II	JA	
25	2429.035	2429.773	Fe II	JA	
10	2429.152	2429.889	Fe II	JA	
20	2429.386	2430.124	Fe II	JA	
10	2429.8150	2430.5524	Fe I	CA	$a\ ^5F_1 - v\ ^3D_1$
30	2429.860	2430.598	Fe II	JA	
120	2430.078	2430.815	Fe II	JA	
6	2430.433	2431.170		JA	
5	2430.838	2431.576		JA	
6	2430.881	2431.619		JA	
25	2431.025	2431.763	Fe II	JA	
8	2432.030	2432.768		JA	
80	2432.2616	2432.9995	Fe II	JA	
60	2432.873	2433.611	Fe II	JA	
6	2433.500	2434.238		JA	
25	2434.059	2434.797	Fe II	JA	
20	2434.237	2434.975	Fe II	JA	
20	2434.648	2435.387	Fe II	JA	
50	2434.729	2435.468	Fe II	JA	
50	2434.951	2435.690	Fe II	JA	
25	2435.002	2435.741		JA	
15	2435.870	2436.609		JA	
4	2436.219	2436.958		JA	
20	2436.346	2437.085		JA	
25	2436.622	2437.361	Fe II	JA	
10	2436.995	2437.735	Fe II	JA	
15	2437.203	2437.942		JA	
5	2437.650	2438.390		JA	
60	2438.1819	2438.9212	Fe I	CA	$a\ ^5F_5 - v\ ^5F_4$
10	2439.170	2439.910		JA	
150	2439.3015	2440.0411	Fe II	JA	
15	2439.630	2440.370	Fe I	JA	$a\ ^3F_4 - s\ ^3D_3$
150	2439.744	2440.484	Fe I	JA	$a\ ^3H_6 - t\ ^3H_6$
80	2440.109	2440.849	Fe I	JA	$a\ ^3H_4 - t\ ^3H_4$
40	2440.423	2441.163	Fe II	JA	
12	2440.585	2441.325		JA	
15	2440.748	2441.487		P	
10	2441.128	2441.868	Fe II	JA	
20	2442.130	2442.871		JA	
30	2442.374	2443.115	Fe II	JA	
100	2442.567	2443.307	Fe I	JA	$a\ ^3H_5 - t\ ^3H_5$
60	2443.709	2444.450	Fe II	P	
250	2443.8721	2444.6127	Fe I	CA	$a\ ^5F_5 - x\ ^3G_5$
100	2444.515	2445.256	Fe II	JA	
50	2445.106	2445.847	Fe II	JA	
50	2445.2125	2445.9534	Fe I	CA	$a\ ^5F_5 - x\ ^3G_4$
100	2445.573	2446.314	Fe II	JA	
40	2445.797	2446.538	Fe II	P	
50	2446.111	2446.852	Fe II	P	
10	2446.321	2447.062		P	
15	2446.407	2447.148		P	
30	2446.471	2447.212	Fe II	P	
40	2447.204	2447.945	Fe II	P	
25	2447.327	2448.068	Fe II	P	
60	2447.7093	2448.4508	Fe I	CA	$a\ ^5D_4 - x\ ^5F_3$
30	2447.755	2448.497	Fe II	P	
8	2449.590	2450.332		P	
25	2449.965	2450.707	Fe II	P	
12	2450.032	2450.774	Fe II	P	
25	2450.205	2450.947	Fe II	P	
12	2450.444	2451.186	Fe I	P	$a\ ^3F_3 - a\ X_3$
20	2451.675	2452.418	Fe I	P	
12	2452.139	2452.882		P	
6	2452.590	2453.333	Fe I	BW	$a\ ^3H_4 - t\ ^3H_5$
12	2453.153	2453.896	Fe II	P	
100	2453.4756	2454.2185	Fe I	CA	$a\ ^5F_4 - v\ ^5F_3$
10	2453.797	2454.540	Fe II	P	

TABLE III. *Spectrum of the Fe-Ne hollow cathode*—Continued

Intensity	Wavelength (Å) Air	Wavelength (Å) Vacuum	Ion	Ref	Classification
20	2453.976	2454.719	Fe II	P	
30	2454.578	2455.321	Fe II	P	
20	2455.567	2456.311		P	
15	2455.692	2456.435		P	
15	2455.708	2456.452	Fe II	P	
15	2455.898	2456.641	Fe II	P	
40	2456.189	2456.932		P	
15	2457.095	2457.839	Fe II	P	
10	2457.340	2458.083		P	
1500	2457.5978	2458.3416	Fe I	CA	$a\ ^5F_5 - v\ ^5F_5$
25	2458.5678	2459.3118	Fe I	CA	$a\ ^5F_5 - w\ ^5G_4$
150	2458.784	2459.528	Fe II	P	
40	2458.973	2459.717	Fe II	P	
6	2460.154	2460.898	Fe II	P	
10	2460.299	2461.043	Fe I	P	
60	2460.440	2461.185	Fe II	P	
25	2461.059	2461.803		P	
80	2461.283	2462.028	Fe II	P	
10	2461.668	2462.413	Fe II	P	
100	2461.860	2462.605	Fe II	JA	
10	2462.134	2462.879		P	
100	2462.1808	2462.9257	Fe I	CA	$a\ ^5D_3 - x\ ^5F_2$
1500	2462.6472	2463.3921	Fe I	CA	$a\ ^5D_4 - x\ ^5F_4$
40	2462.967	2463.712	Fe I	P	
15	2463.159	2463.904		P	
50	2463.292	2464.037	Fe II	P	
50	2463.7304	2464.4756	Fe I	CA	$a\ ^5F_3 - x\ ^3P_2$
40	2464.009	2464.754	Fe II	P	
40	2464.904	2465.650	Fe II	P	
800	2465.1487	2465.8942	Fe I	CA	$a\ ^5F_4 - v\ ^5F_4$
10	2465.199	2465.945	Fe II	P	
15	2465.666	2466.411		P	
15	2465.876	2466.621		P	
50	2465.912	2466.658	Fe II	P	
15	2466.496	2467.242	Fe II	P	
60	2466.671	2467.417	Fe II	P	
30	2466.695	2467.441		P	
20	2466.766	2467.512		P	
60	2466.819	2467.564	Fe II	P	
30	2467.567	2468.313	Fe I	P	
60	2467.7321	2468.4782	Fe I	CA	$a\ ^5F_3 - v\ ^5F_2$
25	2467.99	2468.74	Bl	P	
15	2468.295	2469.042	Fe II	P	
600	2468.8795	2469.6258	Fe I	CA	$a\ ^5F_5 - w\ ^5G_5$
60	2469.514	2470.260	Fe II	P	
25	2470.408	2471.154	Fe II	P	
80	2470.670	2471.417	Fe II	JA	
10	2470.764	2471.511	Fe II	P	
20	2470.879	2471.625		P	
80	2470.9655	2471.7123	Fe I	CA	$a\ ^5F_4 - x\ ^3G_5$
6	2472.072	2472.819	Fe II	P	
800	2472.3359	2473.0830	Fe I	CA	$a\ ^5F_4 - x\ ^3G_4$
800	2472.3515	2473.0987	Fe I	CA	$a\ ^5F_5 - w\ ^5G_6$
40	2472.428	2473.175	Fe II	P	
40	2472.605	2473.352	Fe II	P	
20	2472.643	2473.390		P	
1000	2472.8948	2473.6421	Fe I	CA	$a\ ^5D_3 - x\ ^5F_3$
2000	2473.156	2473.904	Fe I	JA	$a\ ^5D_4 - y\ ^7P_4$
50	2473.321	2474.069	Fe II	P	
30	2473.386	2474.134		P	
15	2473.671	2474.419		P	
30	2474.054	2474.801	Fe II	P	
60	2474.442	2475.190		P	
10	2474.766	2475.514	Fe II	P	
600	2474.8139	2475.5617	Fe I	CA	$a\ ^5F_3 - v\ ^5F_3$
10	2475.019	2475.767	Fe I	P	
50	2475.117	2475.865	Fe II	P	
40	2475.541	2476.289	Fe II	P	
0	2476.031	2476.779		P	
15	2476.262	2477.010	Fe II	P	
40	2476.471	2477.219	Fe I	P	
60	2476.6566	2477.4047	Fe I	CA	$a\ ^5F_2 - v\ ^5F_1$
15	2476.8650	2477.6132	Fe I	CA	$a\ ^5F_1 - x\ ^3P_1$
25	2477.342	2478.091	Fe II	P	
10	2477.498	2478.247	Fe II	P	
20	2477.907	2478.655		P	
10	2478.057	2478.806		P	
10	2478.112	2478.861	Fe II	P	
60	2478.571	2479.320	Fe II	JA	
10	2479.259	2480.008	Fe II	P	
120	2479.4801	2480.2289	Fe I	CA	$a\ ^5F_2 - x\ ^3P_2$
25	2479.630	2480.379		P	
1200	2479.7761	2480.5250	Fe I	CA	$a\ ^5D_2 - x\ ^5F_2$
100	2480.157	2480.906	Fe II	P	
25	2480.187	2480.936		P	
10	2480.951	2481.700		P	
15	2481.048	2481.797	Fe II	P	
80	2482.117	2482.866	Fe II	P	
25	2482.325	2483.075	Fe II	P	
100	2482.657	2483.406	Fe II	P	
20	2482.752	2483.502		P	
15	2482.866	2483.615	Fe II	P	
15	2483.021	2483.771		P	
10000	2483.2713	2484.0210	Fe I	CA	$a\ ^5D_4 - x\ ^5F_5$
15	2483.369	2484.119		P	
300	2483.5332	2484.2829	Fe I	CA	$a\ ^5F_2 - v\ ^5F_2$
10	2483.663	2484.413		P	
15	2483.721	2484.471	Fe II	P	
20	2483.786	2484.536		P	
1000	2484.1853	2484.9352	Fe I	CA	$a\ ^5D_1 - x\ ^5F_1$
60	2484.241	2484.991	Fe II	JA	
30	2484.441	2485.191	Fe II	P	
20	2484.707	2485.457		P	
15	2485.139	2485.889		P	
10	2485.264	2486.014		P	
50	2485.9899	2486.7402	Fe I	CA	$a\ ^5F_4 - w\ ^5G_4$
800	2486.3733	2487.1237	Fe I	CA	$a\ ^5D_4 - y\ ^7P_3$
100	2486.6914	2487.4419	Fe I	CA	$a\ ^5F_3 - v\ ^5F_4$
100	2487.0659	2487.8165	Fe I	CA	$a\ ^5F_1 - v\ ^5F_1$
120	2487.3696	2488.1203	Fe I	CA	$a\ ^5D_2 - z\ ^5S_2$
4000	2488.1426	2488.8934	Fe I	CA	$a\ ^5D_3 - x\ ^5F_4$
100	2488.9450	2489.6961	Fe I	CA	$b\ ^3F_4 - q\ ^3G_3$
20	2489.009	2489.761		P	
10	2489.074	2489.825	Fe II	P	
80	2489.482	2490.234	Fe II	P	
20	2489.517	2490.268		P	
1000	2489.7503	2490.5015	Fe I	CA	$a\ ^5D_0 - x\ ^5F_1$
50	2489.829	2490.580	Fe II	P	
50	2489.9132	2490.6644	Fe I	CA	$a\ ^5F_1 - x\ ^3P_2$
15	2490.124	2490.875		P	
3000	2490.6441	2491.3955	Fe I	CA	$a\ ^5D_2 - x\ ^5F_3$
100	2490.706	2491.457	Fe II	P	
60	2490.858	2491.610	Fe II	P	
2000	2491.1547	2491.9062	Fe I	CA	$a\ ^5D_1 - x\ ^5F_2$
30	2491.193	2491.945		P	
100	2491.396	2492.148	Fe II	P	
40	2491.466	2492.218		P	
20	2491.673	2492.425		P	

TABLE III. *Spectrum of the Fe-Ne hollow cathode*—Continued

Intensity	Wavelength (Å) Air	Wavelength (Å) Vacuum	Ion	Ref	Classification
30	2491.982	2492.734	Fe I	P	$b\,^3F_4 - t\,^3H_4$
30	2492.229	2492.980	Fe I	P	$b\,^3F_4 - q\,^3G_4$
25	2492.344	2493.095	Fe II	P	
30	2492.377	2493.129		P	
30	2492.6305	2493.3824	Fe I	CA	$a\,^5F_3 - x\,^3G_3$
15	2492.680	2493.432	Fe I	P	
10	2492.890	2493.641		P	
100	2493.184	2493.936	Fe II	P	
500	2493.262	2494.014	Fe II	JA	
15	2493.751	2494.503		P	
20	2493.876	2494.628	Fe II	P	
60	2494.0005	2494.7526	Fe I	CA	$a\,^5F_1 - v\,^5F_2$
50	2494.2515	2495.0037	Fe I	CA	$a\,^5F_5 - z\,^3H_5$
10	2494.5094	2495.2617	Fe I	CA	$a\,^5F_4 - z\,^1G_4$
6	2494.781	2495.533	Fe I	P	
100	2495.871	2496.623	Fe I	P	$a\,^5F_5 - z\,^3H_6$
8	2496.337	2497.089		P	
15	2496.396	2497.149		P	
600	2496.5333	2497.2861	Fe I	CA	$a\,^5F_4 - w\,^5G_5$
40	2496.792	2497.544		P	
20	2496.991	2497.744	Fe I	P	$b\,^3F_4 - q\,^3G_5$
5	2497.714	2498.467	Fe II	P	
50	2497.819	2498.572	Fe II	P	
8	2498.082	2498.835	Fe II	P	
8	2498.203	2498.957		P	
5	2498.343	2499.096	Fe II	P	
8	2498.819	2499.572		P	
150	2498.8975	2499.6508	Fe I	JA	$a\,^5D_3 - y\,^7P_4$
40	2500.924	2501.678	Fe II	JA	
1000	2501.1323	2501.8861	Fe I	CA	$a\,^5D_4 - x\,^5D_3$
40	2501.312	2502.066	Fe II	JA	
25	2501.652	2502.406		P	
50	2501.6935	2502.4475	Fe I	CA	$a\,^5F_5 - x\,^3F_4$
12	2501.725	2502.479		P	
60	2502.3930	2503.1471	Fe II	JA	
25	2502.4907	2503.2449	Fe I	JA	
40	2503.3265	2504.0809	Fe II	JA	
25	2503.4921	2504.2465	Fe I	CA	$b\,^3F_3 - q\,^3G_3$
20	2503.566	2504.320	Fe II	P	
60	2503.8742	2504.6287	Fe II	JA	
12	2505.011	2505.766	Fe I	P	$b\,^3F_4 - t\,^3H_5$
20	2505.4397	2506.1945		JA	
40	2505.4849	2506.2398	Fe I	JA	
25	2505.653	2506.408		P	
80	2506.0934	2506.8484	Fe II	JA	
12	2506.434	2507.189	Fe II	P	
15	2506.574	2507.329	Fe I	P	$b\,^3F_3 - t\,^3H_4$
40	2506.7963	2507.5515	Fe II	JA	
25	2506.908	2507.663		JA	
8	2507.026	2507.781	Fe II	P	
15	2507.688	2508.443	Fe II	P	
15	2507.739	2508.494		P	
500	2507.8999	2508.6553	Fe I	CA	$a\,^5F_3 - w\,^5G_4$
30	2508.3411	2509.0966	Fe II	JA	
50	2508.7530	2509.5086	Fe I	CA	$a\,^5F_2 - x\,^3G_3$
15	2509.123	2509.879	Fe II	P	
12	2509.866	2510.621	Fe II	P	
1000	2510.8348	2511.5909	Fe I	CA	$a\,^5D_3 - x\,^5D_2$
12	2511.382	2512.138	Fe II	P	
120	2511.7606	2512.5169	Fe II	JA	
80	2512.2754	2513.0319	Fe I	CA	$a\,^5F_5 - u\,^5D_4$
400	2512.3649	2513.1213	Fe I	CA	$a\,^5D_3 - y\,^7P_3$
15	2512.521	2513.278	Fe II	P	
15	2513.498	2514.255		P	
20	2513.785	2514.542		P	
8	2513.8487	2514.6055	Fe I	CA	$b\,^3F_2 - q\,^3G_3$
30	2514.2794	2515.0363		JA	
20	2514.3059	2515.0628		JA	
50	2514.3831	2515.1400	Fe II	JA	
8	2514.520	2515.277		P	
15	2514.569	2515.326		P	
20	2514.7091	2515.4661		JA	
12	2515.119	2515.876	Fe II	P	
0	2515.8543	2516.6115	Fe I	CA	$a\,^3F_3 - u\,^3D_2$
50	2516.112	2516.869		JA	
15	2516.2502	2517.0076	Fe I	CA	$a\,^5F_4 - z\,^3H_4$
80	2516.5705	2517.3279	Fe I	CA	$a\,^5F_3 - z\,^1G_4$
50	2517.131	2517.889	Fe II	JA	
300	2517.6615	2518.4192	Fe I	CA	$a\,^5F_2 - w\,^5G_3$
800	2518.1020	2518.8597	Fe I	CA	$a\,^5D_2 - x\,^5D_1$
8	2518.533	2519.291		P	
15	2518.826	2519.584	Fe I	P	$b\,^3F_3 - g\ X_3$
60	2519.0460	2519.8052	Fe II	JA	
15	2519.201	2519.960		P	
150	2519.6292	2520.3874	Fe I	CA	$a\,^5F_1 - w\,^5G_2$
8	2520.262	2521.020	Fe II	P	
8	2520.868	2521.627		P	
25	2520.9713	2521.7298	Fe I	JA	
40	2521.0920	2521.8505	Fe II	JA	
8	2521.218	2521.977	Fe II	JA	
30	2521.8155	2522.5742	Fe II	JA	
40	2521.9183	2522.6770	Fe I	CA	$a\,^5F_4 - w\,^3D_3$
15	2522.197	2522.956	Fe II	JA	
50	2522.4798	2523.2386	Fe I	CA	$a\,^5F_4 - z\,^3H_5$
30	2522.511	2523.270		P	
4000	2522.8494	2523.6083	Fe I	CA	$a\,^5D_4 - x\,^5D_4$
50	2522.892	2523.651		JA	
40	2523.137	2523.897		JA	
12	2523.323	2524.082		P	
15	2523.374	2524.133		P	
15	2523.441	2524.200	Fe II	P	
200	2523.6618	2524.4209	Fe I	JA	
20	2523.998	2524.758		JA	
20	2524.108	2524.867		P	
500	2524.2927	2525.0519	Fe I	CA	$a\,^5D_1 - x\,^5D_0$
12	2524.602	2525.361	Fe I	P	
100	2525.0239	2525.7833	Fe I	JA	
15	2525.109	2525.868	Fe II	P	
200	2525.3881	2526.1476	Fe II	JA	
12	2525.862	2526.622	Fe II	P	
8	2525.919	2526.679	Fe II	JA	
25	2526.075	2526.835	Fe II	JA	
25	2526.198	2526.957		P	
300	2526.2941	2527.0538	Fe II	JA	
8	2526.836	2527.596	Fe II	JA	
15	2526.909	2527.668		P	
20	2527.105	2527.865	Fe II	JA	
20	2527.267	2528.027	Fe I	P	
2000	2527.4349	2528.1949	Fe I	CA	$a\,^5D_3 - x\,^5D_3$
30	2527.705	2528.465	Fe II	JA	
15	2528.172	2528.932		JA	
15	2528.508	2529.268		P	
20	2528.877	2529.638	Fe II	JA	
20	2529.077	2529.838	Fe II	JA	
800	2529.1348	2529.8952	Fe I	CA	$a\,^5D_2 - x\,^5D_2$
25	2529.229	2529.989	Fe II	P	
80	2529.308	2530.069	Fe I	JA	$b\,^3F_2 - g\ X_3$
250	2529.549	2530.310	Fe II	JA	

TABLE III. *Spectrum of the Fe-Ne hollow cathode*—Continued

Intensity	Wavelength (Å) Air	Wavelength (Å) Vacuum	Ion	Ref	Classification
150	2529.8357	2530.5963	Fe I	CA	$a\ ^5D_1 - x\ ^5D_1$
40	2530.108	2530.869	Fe II	JA	
200	2530.6872	2531.4480	Fe I	CA	$a\ ^5D_2 - y\ ^7P_3$
15	2530.969	2531.730		P	
8	2531.429	2532.190	Fe I	P	$b\ ^3F_3 - r\ ^3G_3$
20	2531.871	2532.632	Fe II	JA	
12	2532.373	2533.134		P	
25	2532.8754	2533.6366	Fe I	CA	$a\ ^5F_3 - x\ ^3F_2$
15	2533.140	2533.902		P	
120	2533.627	2534.388	Fe II	JA	
12	2533.737	2534.498		P	
60	2533.804	2534.565	Fe I	JA	
100	2534.416	2535.178	Fe II	JA	
25	2535.1277	2535.8895	Fe I	CA	$a\ ^5F_2 - 1\ \ 2$
10	2535.362	2536.124	Fe II	P	
40	2535.449	2536.211		JA	
120	2535.486	2536.248	Fe II	JA	
400	2535.6074	2536.3693	Fe I	CA	$a\ ^5D_0 - x\ ^5D_1$
60	2536.673	2537.435	Fe II	P	
10	2536.697	2537.459		P	
200	2536.7925	2537.5547	Fe I	CA	$a\ ^5F_3 - w\ ^3D_2$
200	2536.803	2537.565	Fe II	P	
50	2536.845	2537.608	Fe II	JA	
50	2537.138	2537.900	Fe II	JA	
50	2537.170	2537.932		P	
40	2537.4585	2538.2208	Fe I	CA	$a\ ^3F_4 - u\ ^3G_5$
50	2538.204	2538.967	Fe II	JA	
40	2538.501	2539.264	Fe II	JA	
20	2538.680	2539.443	Fe II	P	
40	2538.6992	2539.4618	Fe I	CA	$a\ ^5F_3 - z\ ^3H_4$
100	2538.799	2539.562	Fe II	JA	
25	2538.829	2539.592		P	
100	2538.909	2539.672	Fe II	JA	
150	2538.993	2539.756	Fe II	JA	
25	2539.328	2540.091		P	
50	2539.3566	2540.1194	Fe I	CA	$a\ ^5F_4 - u\ ^5D_3$
6	2539.5873	2540.3501	Fe I	CA	$a\ ^5F_3 - x\ ^3F_3$
6	2539.854	2540.617		P	
10	2540.441	2541.204		P	
20	2540.523	2541.286	Fe II	JA	
200	2540.661	2541.425	Fe II	JA	
40	2540.730	2541.493		JA	
600	2540.9719	2541.7350	Fe I	CA	$a\ ^5D_1 - x\ ^5D_2$
80	2541.101	2541.865	Fe II	JA	
60	2541.836	2542.600	Fe II	JA	
300	2542.101	2542.865	Fe I	JA	$b\ ^3F_2 - r\ ^3G_3$
20	2542.736	2543.500		JA	
25	2542.785	2543.548	Fe II	P	
15	2543.079	2543.843	Fe II	P	
60	2543.377	2544.141	Fe II	JA	
60	2543.430	2544.194	Fe II	P	
250	2543.923	2544.687	Fe I	JA	$b\ ^3F_3 - r\ ^3G_4$
20	2544.658	2545.422		P	
150	2544.705	2545.469	Fe I	P	$b\ ^3F_4 - r\ ^3G_5$
40	2544.972	2545.737	Fe II	P	
40	2545.220	2545.985	Fe II	JA	
20	2545.444	2546.208	Fe II	P	
800	2545.9785	2546.7429	Fe I	CA	$a\ ^5D_2 - x\ ^5D_3$
12	2546.104	2546.869		P	
40	2546.1745	2546.9389	Fe I	CA	$a\ ^3P_2 - t\ ^3F_3$
40	2546.442	2547.206	Fe II	P	
10	2546.508	2547.272		P	
80	2546.670	2547.434	Fe II	P	
80	2546.866	2547.631	Fe I	P	
15	2547.338	2548.102	Fe II	P	
15	2548.084	2548.849		P	
15	2548.325	2549.090	Fe II	P	
20	2548.589	2549.353	Fe II	P	
100	2548.743	2549.508	Fe II	P	
20	2548.912	2549.677		JA	
15	2548.922	2549.688	Fe II	P	
80	2549.083	2549.848	Fe II	P	
80	2549.395	2550.160	Fe II	P	
60	2549.461	2550.226	Fe II	P	
600	2549.6132	2550.3784	Fe I	CA	$a\ ^5D_3 - x\ ^5D_4$
40	2549.767	2550.532	Fe II	P	
60	2550.027	2550.793	Fe II	P	
25	2550.149	2550.914	Fe II	P	
12	2550.506	2551.271		P	
50	2550.683	2551.448	Fe II	P	
40	2551.092	2551.858	Fe I	P	
12	2551.205	2551.970	Fe II	P	
40	2552.6059	2553.3717	Fe I	CA	$a\ ^5D_1 - y\ ^7P_2$
15	2552.8306	2553.5965	Fe I	CA	$a\ ^5F_3 - u\ ^5D_2$
15	2555.067	2555.834	Fe II	P	
15	2555.219	2555.985		P	
15	2555.453	2556.219	Fe II	P	
0	2555.6466	2556.4132	Fe I	CA	$a\ ^5F_1 - w\ ^3D_1$
15	2556.3032	2557.0700	Fe I	CA	$a\ ^3F_3 - u\ ^3G_4$
40	2556.863	2557.630	Fe I	P	$a\ ^5F_5 - z\ ^3I_6$
12	2557.2700	2558.0370	Fe I	CA	$a\ ^3F_4 - x\ ^3H_5$
10	2557.505	2558.272	Fe II	P	
5	2558.478	2559.245		P	
5	2558.822	2559.589		P	
15	2559.270	2560.038	Fe II	P	
12	2559.924	2560.692	Fe II	P	
40	2560.281	2561.049	Fe II	P	
20	2560.5565	2561.3242	Fe I	CA	$a\ ^5F_1 - x\ ^3F_2$
8	2561.2713	2562.0392	Fe I	CA	$a\ ^5F_2 - w\ ^3D_3$
10	2561.700	2562.468		P	
12	2561.8551	2562.6231	Fe I	CA	$a\ ^5F_1 - u\ ^5D_1$
25	2562.092	2562.860	Fe II	P	
20	2562.2216	2562.9898	Fe I	CA	$a\ ^5F_3 - u\ ^5D_3$
20	2562.225	2562.993	Fe I	P	$a\ ^5F_1 - u\ ^5D_0$
400	2562.535	2563.304	Fe II	P	
15	2563.399	2564.168		P	
200	2563.477	2564.245	Fe II	P	
8	2563.8087	2564.5773	Fe I	CA	$a\ ^5F_3 - u\ ^5D_4$
12	2564.5598	2565.3285	Fe I	CA	$a\ ^5F_1 - w\ ^3D_2$
20	2566.220	2566.989	Fe II	P	
10	2566.401	2567.171	Fe II	P	
60	2566.912	2567.682	Fe II	P	
10	2567.631	2568.401	Fe II	P	
8	2567.8589	2568.6284	Fe I	CA	$a\ ^5P_1 - u\ ^3F_2$
12	2568.409	2569.178	Fe II	P	
12	2568.865	2569.634	Fe I	P	$a\ ^5F_2 - y\ ^3P_1$
25	2569.596	2570.366	Fe I	P	$a\ ^5F_5 - x\ ^5G_4$
15	2569.7437	2570.5137	Fe I	CA	$a\ ^5F_2 - u\ ^5D_2$
8	2569.779	2570.549	Fe II	P	
25	2570.525	2571.296	Fe II	P	
30	2570.848	2571.618	Fe II	P	
15	2572.7533	2573.5240	Fe I	CA	$a\ ^3F_2 - u\ ^3G_3$
12	2572.967	2573.738	Fe II	P	
10	2573.211	2573.981	Fe II	P	
150	2574.362	2575.133	Fe II	P	
50	2575.742	2576.514	Fe I	P	
300	2576.6907	2577.4623	Fe I	CA	$a\ ^5F_5 - x\ ^5G_5$
25	2576.861	2577.633	Fe II	P	

TABLE III. *Spectrum of the Fe-Ne hollow cathode*—Continued

Intensity	Wavelength (Å)		Ion	Ref	Classification
	Air	Vacuum			
60	2577.919	2578.691	Fe II	P	
15	2578.003	2578.774		P	
10	2578.209	2578.981		P	
15	2579.115	2579.887	Fe II	P	
40	2579.2599	2580.0320	Fe I	CA	$a\ ^5F_2 - u\ ^5D_3$
8	2579.413	2580.185	Fe II	P	
12	2579.844	2580.616		P	
8	2580.0652	2580.8376	Fe I	CA	$a\ ^5F_1 - y\ ^3P_1$
8	2580.2941	2581.0665	Fe I	CA	$a\ ^3F_3 - v\ ^3F_4$
12	2580.4530	2581.2254	Fe I	CA	$a\ ^5F_2 - y\ ^3P_2$
8	2581.110	2581.882	Fe II	P	
8	2581.464	2582.237		P	
50	2581.796	2582.569		P	
8	2582.413	2583.186	Fe II	P	
100	2582.580	2583.353	Fe II	P	
1500	2584.5363	2585.3098	Fe I	ED	$a\ ^5F_5 - x\ ^5G_6$
60	2593.510	2594.285	Fe I	BW	$z\ ^7D_5 - h\ ^7D_5$
0	2594.1514	2594.9271	Fe I	CA	$a\ ^5F_4 - x\ ^5G_3$
0	2595.4251	2596.2011	Fe I	CA	$a\ ^5F_1 - y\ ^3P_0$
10	2603.554	2604.332	Fe I	P	
3	2604.003	2604.781		P	
15	2604.754	2605.532	Fe I	P	
12	2604.864	2605.642	Fe I	P	
15	2605.037	2605.815	Fe II	P	
20	2605.339	2606.117	Fe II	P	
20	2605.424	2606.202	Fe II	P	
60	2605.6566	2606.4351	Fe I	CA	$a\ ^5F_5 - y\ ^3G_5$
8	2605.902	2606.680	Fe II	P	
10	2606.303	2607.081		P	
300	2606.512	2607.291	Fe II	P	
800	2606.8269	2607.6056	Fe I	CA	$a\ ^5F_4 - x\ ^5G_5$
10	2607.529	2608.307	Fe II	P	
6	2607.628	2608.407	Fe II	P	
20	2608.577	2609.356	Fe I	P	
4	2608.852	2609.631	Fe II	P	
6	2609.036	2609.815		P	
12	2609.125	2609.904	Fe II	P	
10	2609.221	2610.000	Fe I	P	$a\ ^3G_3 - g\ X_3$
4	2609.440	2610.219	Fe II	P	
8	2609.579	2610.359		P	
10	2609.866	2610.646	Fe II	P	
15	2610.006	2610.785		P	
4	2610.442	2611.222		P	
10	2610.7505	2611.5302	Fe I	CA	$a\ ^5D_2 - y\ ^3D_1$
3	2611.002	2611.782		P	
20	2611.073	2611.853	Fe II	P	
600	2611.873	2612.653	Fe II	P	
20	2612.7722	2613.5523	Fe I	CA	$a\ ^5D_3 - y\ ^3D_2$
8	2613.265	2614.045		P	
12	2613.416	2614.196	Fe II	P	
8	2613.925	2614.705	Ne I	P	
4	2614.370	2615.151		P	
25	2614.4940	2615.2745	Fe I	CA	$a\ ^5F_3 - x\ ^5G_2$
20	2615.422	2616.202	Fe I	P	
10	2615.849	2616.630		P	
12	2616.739	2617.520		P	
8	2617.132	2617.914		P	
250	2618.0183	2618.7997	Fe I	CA	$a\ ^5F_3 - x\ ^5G_3$
25	2618.7098	2619.4913	Fe I	CA	$a\ ^5D_4 - y\ ^3D_3$
20	2619.074	2619.855	Fe II	P	
10	2620.172	2620.953	Fe II	P	
12	2620.408	2621.190	Fe II	P	
20	2620.695	2621.477	Fe II	P	
12	2621.623	2622.405		P	
40	2621.669	2622.451	Fe II	P	
3	2621.942	2622.724		P	
3	2621.965	2622.747		P	
4	2623.107	2623.890	Fe II	P	
20	2623.3657	2624.1484	Fe I	CA	$a\ ^5D_1 - y\ ^3D_1$
400	2623.533	2624.316	Fe I	P	$a\ ^5F_3 - x\ ^5G_4$
6	2623.626	2624.409		P	
15	2623.726	2624.508	Fe II	P	
5	2624.661	2625.444		P	
50	2625.490	2626.273	Fe II	P	
200	2625.667	2626.450	Fe II	P	
15	2626.501	2627.284	Fe II	P	
3	2627.1272	2627.9108	Fe I	CA	$a\ ^3F_3 - x\ ^1G_4$
3	2627.160	2627.944		P	
5	2627.2243	2628.0078	Fe I	CA	$a\ ^5F_4 - y\ ^3G_4$
150	2628.293	2629.076	Fe II	P	
15	2629.5725	2630.3566	Fe I	CA	$a\ ^5D_0 - y\ ^3D_1$
5	2629.721	2630.505		P	
5	2629.885	2630.669		P	
20	2630.071	2630.855	Fe II	P	
3	2630.498	2631.282		P	
30	2631.012	2631.796		P	
250	2631.047	2631.831	Fe II	P	
250	2631.322	2632.106	Fe II	P	
50	2631.608	2632.393	Fe II	P	
100	2632.2369	2633.0216	Fe I	CA	$a\ ^5F_2 - x\ ^5G_2$
20	2632.5939	2633.3788	Fe I	CA	$a\ ^5D_2 - y\ ^3D_2$
5	2632.988	2633.773		P	
20	2633.122	2633.907		P	
8	2633.203	2633.989	Fe II	P	
2	2633.621	2634.406		P	
3	2634.740	2635.525		P	
3	2635.304	2636.089	Fe II	P	
5	2635.402	2636.188	Fe II	P	
10	2635.723	2636.508		P	
300	2635.8092	2636.5948	Fe I	CA	$a\ ^5F_2 - x\ ^5G_3$
5	2635.932	2636.717		P	
6	2635.971	2636.757	Ne I	P	
6	2636.075	2636.860		P	
30	2636.4781	2637.2639	Fe I	CA	$a\ ^5F_4 - y\ ^3G_5$
2	2637.054	2637.840		P	
5	2637.497	2638.284	Fe II	P	
15	2637.644	2638.430	Fe II	P	
12	2638.560	2639.346		P	
10	2638.655	2639.441		P	
5	2638.711	2639.497		P	
15	2638.747	2639.533		P	
12	2639.564	2640.351	Fe II	P	
6	2641.029	2641.815	Fe I	P	
8	2641.084	2641.870		P	
5	2641.123	2641.910	Fe II	P	
50	2641.6456	2642.4326	Fe I	CA	$a\ ^5F_4 - x\ ^3D_3$
8	2642.013	2642.800	Fe II	P	
3	2643.647	2644.434	Fe II	P	
200	2643.9980	2644.7855	Fe I	CA	$a\ ^5F_1 - x\ ^5G_2$
2	2644.097	2644.885	Ne I	P	
6	2644.628	2645.416		P	
5	2645.083	2645.871	Fe II	P	
3	2645.334	2646.122	Fe II	P	
10	2645.4216	2646.2095	Fe I	CA	$a\ ^5D_1 - y\ ^3D_2$
2	2645.645	2646.433	Ne I	P	
10	2646.032	2646.820		P	
5	2646.098	2646.886		P	
20	2647.5575	2648.3459	Fe I	CA	$a\ ^5D_3 - y\ ^3D_3$

TABLE III. *Spectrum of the Fe-Ne hollow cathode*—Continued

Intensity	Wavelength (Å) Air	Wavelength (Å) Vacuum	Ion	Ref	Classification
12	2647.918	2648.707		P	
2	2648.446	2649.235		P	
2	2649.222	2650.010		P	
6	2649.469	2650.258	Fe II	P	
2	2650.481	2651.270	Fe II	P	
3	2651.270	2652.059	Fe II	P	
25	2651.7063	2652.4959	Fe I	CA	$a\ ^5F_3 - y\ ^3G_4$
25	2651.71	2652.50	Fe II	P	
2	2652.566	2653.356	Fe II	P	
2	2653.557	2654.347	Fe II	P	
2	2653.667	2654.457	Fe II	P	
5	2654.629	2655.419	Fe II	P	
8	2655.692	2656.483	Fe II	P	
40	2656.147	2656.938	Fe I	P	$a\ ^3H_6 - x\ ^3I_7$
12	2656.7920	2657.5826	Fe I	CA	$a\ ^3F_4 - y\ ^3H_5$
3	2657.171	2657.961	Fe II	P	
12	2657.554	2658.345	Ne I	P	
6	2657.588	2658.378	Fe II	P	
3	2657.621	2658.411		P	
3	2657.921	2658.712	Fe II	P	
10	2658.252	2659.043	Fe II	P	
8	2658.478	2659.269		P	
3	2658.946	2659.737		P	
4	2659.249	2660.041		P	
5	2660.236	2661.027	Fe II	P	
15	2660.3973	2661.1888	Fe I	CA	$a\ ^5F_2 - y\ ^3G_3$
8	2661.1911	2661.9828	Fe I	CA	$a\ ^5F_2 - x\ ^3D_1$
12	2661.305	2662.096		P	
8	2661.416	2662.207		P	
6	2661.771	2662.563	Fe II	P	
30	2662.0562	2662.8480	Fe I	CA	$a\ ^5F_3 - x\ ^3D_2$
20	2662.304	2663.096		P	
5	2662.558	2663.350	Fe II	P	
3	2662.901	2663.693		P	
2	2663.165	2663.957	Fe I	P	
3	2663.260	2664.050	Bl	P	
10	2663.343	2664.135		P	
3	2663.779	2664.572		P	
5	2663.945	2664.737	Fe II	P	
15	2664.043	2664.835	Fe I	P	
12	2664.168	2664.960		P	
6	2664.260	2665.052	Fe II	P	
60	2664.663	2665.456	Fe II	P	
15	2665.541	2666.333	Fe II	P	
25	2666.3986	2667.1915	Fe I	CA	$a\ ^5F_3 - x\ ^3D_3$
8	2666.455	2667.248		P	
30	2666.636	2667.429	Fe II	P	
60	2666.751	2667.544		P	
300	2666.8123	2667.6054	Fe I	CA	$a\ ^5F_5 - v\ ^5D_4$
60	2666.9652	2667.7583	Fe I	CA	$a\ ^3F_4 - v\ ^3G_5$
10	2667.220	2668.010	Bl	P	
12	2667.9125	2668.7058	Fe I	CA	$a\ ^5D_2 - y\ ^3D_3$
2	2668.711	2669.505		P	
15	2668.910	2669.700	Bl	P	
5	2668.963	2669.756		P	
12	2669.008	2669.801	Fe II	P	
25	2669.493	2670.286	Fe I	P	$a\ ^3H_5 - x\ ^3I_6$
8	2669.722	2670.516		P	
2	2669.933	2670.726	Fe II	P	
8	2670.786	2671.580		P	
5	2670.992	2671.786		P	
10	2671.922	2672.716	Fe II	P	
10	2672.139	2672.933	Fe II	P	
12	2672.480	2673.275		P	
6	2672.548	2673.342	Fe II	P	
3	2672.784	2673.579		P	
5	2673.086	2673.881		P	
15	2673.2129	2674.0075	Fe I	CA	$a\ ^5F_1 - x\ ^3D_1$
2	2674.7146	2675.5095	Fe I	CA	$a\ ^3P_2 - w\ ^1D_2$
2	2674.983	2675.778		P	
15	2675.275	2676.070	Ne I	P	
1	2675.440	2676.235	Fe II	P	
6	2676.078	2676.874		P	
1	2676.159	2676.955	Fe I	P	
2	2676.423	2677.219		P	
6	2676.883	2677.678	Fe II	P	
1	2677.389	2678.185	Ne I	P	
15	2677.905	2678.701	Ne I	P	
8	2677.971	2678.766		P	
6	2678.030	2678.826		P	
1	2678.142	2678.938		P	
1	2678.270	2679.066	Fe II	P	
12	2678.691	2679.487		P	
600	2679.0622	2679.8582	Fe I	CA	$a\ ^5F_5 - w\ ^5F_5$
3	2679.208	2680.004	Ne I	P	
2	2679.714	2680.510		P	
5	2679.775	2680.571	Fe II	P	
10	2680.117	2680.914		P	
8	2680.160	2680.957	Fe II	P	
3	2680.233	2681.029	Fe II	P	
2	2680.273	2681.069		P	
25	2680.4526	2681.2489	Fe I	CA	$a\ ^5F_2 - x\ ^3D_2$
15	2680.702	2681.499	Fe II	P	
15	2680.818	2681.615	Fe II	P	
4	2680.9127	2681.7091	Fe I	CA	$a\ ^3F_3 - v\ ^3G_3$
3	2680.991	2681.788		P	
2	2681.023	2681.820		P	
2	2681.042	2681.839	Fe II	P	
12	2681.203	2681.999		P	
10	2681.461	2682.257		P	
20	2681.586	2682.383	Fe I	P	$z\ ^7D_4 - 3\ \ 4$
1	2681.885	2682.681		P	
20	2682.211	2683.008		P	
6	2682.511	2683.308	Fe II	P	
5	2682.576	2683.373		P	
6	2682.998	2683.795	Fe II	P	
2	2683.033	2683.830		P	
8	2683.082	2683.879		P	
4	2683.710	2684.507		P	
4	2683.776	2684.573	Fe II	P	
6	2683.830	2684.627		P	
15	2683.936	2684.733		P	
20	2684.068	2684.865		P	
1	2684.517	2685.314		P	
3	2684.584	2685.381		P	
500	2684.754	2685.551	Fe II	P	
1	2684.900	2685.698		P	
1	2684.963	2685.760	Fe II	P	
5	2685.099	2685.897		P	
4	2685.140	2685.940	Bl	P	
3	2685.253	2686.050	Ne I	P	
6	2685.436	2686.233	Fe II	P	
2	2685.863	2686.661		P	
1	2686.107	2686.905	Fe II	P	
15	2686.218	2687.015	Fe II	P	
1	2686.436	2687.234	Fe II	P	
1	2686.604	2687.402		P	
12	2686.742	2687.540	Ne I	P	

TABLE III. *Spectrum of the Fe-Ne hollow cathode*—Continued

Intensity	Wavelength (Å) Air	Wavelength (Å) Vacuum	Ion	Ref	Classification
1	2686.952	2687.750	Fe II	P	
20	2687.054	2687.852		P	
10	2687.415	2688.213		P	
1	2687.534	2688.332		P	
15	2687.801	2688.599		P	
3	2688.191	2688.990	Fe II	P	
400	2689.2125	2690.0109	Fe I	CA	$a\ ^5F_4 - v\ ^5D_3$
20	2689.415	2690.213		P	
25	2689.8292	2690.6278	Fe I	CA	$a\ ^3F_3 - y\ ^3H_4$
12	2689.881	2690.680		P	
12	2690.0686	2690.8672	Fe I	CA	$a\ ^5D_4 - y\ ^3F_3$
5	2690.178	2690.977		P	
2	2690.422	2691.220		P	
8	2691.490	2692.289		P	
6	2691.737	2692.536	Fe II	P	
10	2692.2482	2693.0473	Fe I	CA	$a\ ^3F_4 - w\ ^3F_4$
3	2692.449	2693.249		P	
5	2692.520	2693.320		P	
60	2692.602	2693.402	Fe II	P	
6	2692.6495	2693.4487	Fe I	CA	$a\ ^5F_1 - x\ ^3D_2$
3	2692.806	2693.605		P	
6	2692.834	2693.633	Fe II	P	
3	2693.005	2693.805		P	
5	2693.355	2694.155		P	
3	2693.402	2694.202		P	
2	2693.479	2694.279		P	
3	2693.539	2694.339		P	
2	2693.857	2694.656	Fe II	P	
3	2694.047	2694.847		P	
5	2694.184	2694.983		P	
5	2694.2386	2695.0382	Fe I	CA	$a\ ^5D_3 - y\ ^3F_2$
15	2694.536	2695.336	Fe I	P	$z\ ^7D_5 - 2\ \ 4$
30	2695.0344	2695.8342	Fe I	CA	$a\ ^5F_5 - w\ ^5F_4$
2	2695.149	2695.949		P	
1	2695.180	2695.980		P	
4	2695.209	2696.009		P	
1	2695.308	2696.108		P	
3	2695.362	2696.161		P	
20	2695.530	2696.330		P	
3	2695.590	2696.390		P	
12	2695.651	2696.451	Fe I	P	$z\ ^7D_3 - 3\ \ 4$
5	2695.681	2696.481		P	
25	2695.989	2696.789		P	
6	2696.123	2696.923		P	
50	2696.283	2697.083	Fe I	P	$z\ ^7D_5 - 1\ \ 5$
8	2696.592	2697.392	Fe II	P	
2	2696.786	2697.586		P	
2	2696.895	2697.695		P	
1	2696.953	2697.753		P	
20	2697.0210	2697.8213	Fe I	CA	$a\ ^3F_3 - v\ ^3G_4$
6	2697.331	2698.132	Fe II	P	
12	2697.461	2698.261	Fe II	P	
6	2697.721	2698.521	Fe II	P	
10	2697.797	2698.598	Fe II	P	
5	2697.982	2698.782		P	
20	2698.165	2698.965	Fe I	P	
5	2698.285	2699.085		P	
1	2698.377	2699.178		P	
200	2699.1064	2699.9072	Fe I	CA	$a\ ^5F_4 - v\ ^5D_4$
3	2699.199	2700.000	Fe II	P	
6	2699.452	2700.253		P	
1	2699.542	2700.342		P	
6	2699.622	2700.423	Fe II	P	
4	2699.775	2700.576		P	
10	2700.356	2701.157	Fe II	P	
3	2701.104	2701.905		P	
8	2701.145	2701.946		P	
4	2701.198	2701.999		P	
8	2701.541	2702.343	Fe II	P	
6	2701.639	2702.440	Ne I	P	
8	2701.9092	2702.7106	Fe I	CA	$b\ ^3F_4 - t\ ^3F_3$
2	2702.297	2703.099		P	
2	2702.407	2703.208		P	
8	2702.4492	2703.2508	Fe I	CA	$a\ ^3H_6 - u\ ^3H_5$
6	2702.560	2703.362	Ne I	P	
1	2702.762	2703.564		P	
60	2703.988	2704.790	Fe II	P	
8	2704.748	2705.551		P	
2	2704.866	2705.668		P	
1	2705.081	2705.883		P	
80	2706.0121	2706.8146	Fe I	CA	$a\ ^3H_6 - u\ ^3H_6$
20	2706.067	2706.870		P	
400	2706.5822	2707.3848	Fe I	CA	$a\ ^5F_3 - v\ ^5D_2$
3	2706.821	2707.623		P	
2	2706.879	2707.682		P	
6	2706.913	2707.716	Fe II	P	
2	2707.000	2707.803		P	
5	2707.034	2707.837		P	
10	2707.448	2708.251	Fe I	P	$b\ ^3F_4 - f\ X_3$
1	2707.709	2708.512		P	
3	2708.003	2708.806		P	
2	2708.040	2708.843		P	
5	2708.417	2709.220	Fe II	P	
60	2708.5712	2709.3742	Fe I	CA	$b\ ^3F_4 - t\ ^3F_4$
5	2708.653	2709.456		P	
3	2708.890	2709.693		P	
20	2709.054	2709.858	Fe II	P	
4	2709.691	2710.495	Fe I	P	$b\ ^3G_5 - q\ ^3G_5$
20	2709.989	2710.793	Fe I	P	$z\ ^7D_4 - 2\ \ 4$
8	2710.037	2710.840	Fe II	P	
3	2710.417	2711.221		P	
3	2710.440	2711.244		P	
20	2710.5437	2711.3473	Fe I	CA	$a\ ^3F_2 - v\ ^3G_3$
4	2710.938	2711.741		P	
1	2711.011	2711.815		P	
2	2711.051	2711.855		P	
2	2711.195	2711.999		P	
10	2711.460	2712.263		P	
200	2711.6554	2712.4592	Fe I	CA	$a\ ^5F_4 - w\ ^5F_5$
10	2711.842	2712.646	Fe II	P	
15	2712.296	2713.100	Fe II	P	
10	2712.391	2713.195	Fe II	P	
2	2712.685	2713.489		P	
5	2713.445	2714.249		P	
6	2713.483	2714.287		P	
10	2713.640	2714.444		P	
20	2714.0591	2714.8635	Fe I	CA	$b\ ^3F_3 - t\ ^3F_2$
80	2714.413	2715.218	Fe II	P	
40	2714.8691	2715.6737	Fe I	CA	$a\ ^5F_3 - v\ ^5D_3$
8	2714.938	2715.742		P	
5	2715.120	2715.925		P	
3	2715.171	2715.976		P	
5	2715.3205	2716.1252	Fe I	CA	$a\ ^5D_2 - y\ ^3F_2$
6	2715.405	2716.209		P	
3	2715.500	2716.300	Bl	P	
6	2715.685	2716.490	Fe II	P	
3	2716.002	2716.807		P	
50	2716.217	2717.022	Fe II	P	

TABLE III. *Spectrum of the Fe-Ne hollow cathode*—Continued

Intensity	Wavelength (Å) Air	Wavelength (Å) Vacuum	Ion	Ref	Classification
50	2716.2575	2717.0624	Fe I	CA	$a\ ^3H_4 - u\ ^3F_4$
6	2716.4184	2717.2234	Fe I	CA	$a\ ^3H_5 - u\ ^3H_4$
15	2716.564	2717.369	Fe II	P	
3	2716.701	2717.506	Fe II	P	
15	2717.3658	2718.1710	Fe I	CA	$a\ ^5F_4 - w\ ^5F_3$
50	2717.7865	2718.5917	Fe I	CA	$a\ ^5F_3 - y\ ^5S_2$
50	2717.873	2718.679	Fe II	P	
12	2717.929	2718.734		P	
250	2718.4362	2719.2416	Fe I	CA	$a\ ^5F_2 - v\ ^5D_1$
8	2718.640	2719.446	Fe II	P	
4000	2719.0275	2719.8331	Fe I	CA	$a\ ^5D_4 - y\ ^5P_3$
40	2719.0604	2719.8660	Fe I	CA	$b\ ^3F_3 - t\ ^3F_3$
12	2719.301	2720.107	Fe II	P	
100	2719.4199	2720.2256	Fe I	CA	$a\ ^3H_5 - u\ ^3H_5$
15	2719.592	2720.398		P	
50	2720.1967	2721.0026	Fe I	CA	$a\ ^5P_3 - 13\ _4$
0	2720.5188	2721.3247	Fe I	CA	$a\ ^5D_3 - y\ ^3F_3$
1500	2720.9026	2721.7087	Fe I	CA	$a\ ^5D_3 - y\ ^5P_2$
8	2721.108	2721.914		P	
12	2722.0387	2722.8450	Fe I	CA	$a\ ^3F_4 - y\ ^1G_4$
10	2722.062	2722.869	Fe II	P	
5	2722.740	2723.547	Fe II	P	
400	2723.5778	2724.3845	Fe I	CA	$a\ ^5D_2 - y\ ^5P_1$
8	2723.787	2724.594	Ne I	P	
12	2724.339	2725.146	Fe I	P	$z\ ^7D_3 - 2\ _4$
10	2724.670	2725.477		P	
30	2724.884	2725.691	Fe II	P	
150	2724.9531	2725.7601	Fe I	CA	$a\ ^5F_3 - v\ ^5D_4$
8	2725.285	2726.092		P	
5	2725.3292	2726.1363	Fe I	CA	$a\ ^3F_3 - w\ ^3F_3$
12	2725.6014	2726.4085	Fe I	CA	$a\ ^5F_2 - v\ ^5D_2$
80	2726.055	2726.862	Fe I	P	$a\ ^5F_1 - v\ ^5D_0$
50	2726.2351	2727.0425	Fe I	CA	$b\ ^3F_2 - t\ ^3F_2$
25	2727.383	2728.191	Fe II	P	
80	2727.538	2728.346	Fe II	P	
200	2728.0197	2728.8275	Fe I	CA	$a\ ^5F_4 - w\ ^5F_4$
50	2728.8196	2729.6275	Fe I	CA	$a\ ^3H_4 - u\ ^3H_4$
80	2728.905	2729.713	Fe II	P	
8	2728.9690	2729.7770	Fe I	CA	$a\ ^5D_1 - y\ ^3F_2$
5	2729.329	2730.137	Fe II	P	
10	2730.700	2731.508		P	
40	2730.734	2731.542	Fe II	P	
40	2730.9819	2731.7904	Fe I	CA	$a\ ^5F_1 - v\ ^5D_1$
8	2731.243	2732.052	Fe II	P	
5	2731.2814	2732.0900	Fe I	CA	$b\ ^3F_2 - t\ ^3F_3$
5	2732.008	2732.817	Fe II	P	
1000	2733.5807	2734.3898	Fe I	CA	$a\ ^5F_5 - w\ ^5D_4$
60	2734.0053	2734.8145	Fe I	CA	$a\ ^5F_2 - v\ ^5D_3$
50	2734.2676	2735.0769	Fe I	CA	$a\ ^5P_3 - t\ ^5P_2$
30	2734.6159	2735.4252	Fe I	CA	$a\ ^5F_3 - w\ ^5F_2$
500	2735.4751	2736.2847	Fe I	CA	$a\ ^5F_4 - w\ ^5D_3$
50	2735.6120	2736.4216	Fe I	CA	$a\ ^5P_2 - t\ ^5P_1$
8	2736.9639	2737.7739	Fe I	CA	$a\ ^5F_2 - y\ ^5S_2$
500	2737.3096	2738.1196	Fe I	CA	$a\ ^5D_1 - y\ ^5P_1$
0	2737.6399	2738.4500	Fe I	CA	$a\ ^3H_6 - s\ ^3G_5$
120	2737.832	2738.643	Fe I	P	
5	2738.2135	2739.0237	Fe I	CA	$a\ ^5F_1 - v\ ^5D_2$
400	2739.546	2740.357	Fe II	P	
8	2741.1015	2741.9124	Fe I	CA	$c\ ^3P_2 - q\ ^3G_3$
1	2741.5767	2742.3878	Fe I	CA	$a\ ^3F_2 - w\ ^3F_2$
10	2742.0156	2742.8268	Fe I	CA	$a\ ^5D_2 - y\ ^3F_3$
250	2742.2542	2743.0654	Fe I	CA	$a\ ^5F_3 - w\ ^5D_2$
800	2742.4055	2743.2168	Fe I	CA	$a\ ^5D_2 - y\ ^5P_2$
200	2743.196	2744.008	Fe II	P	
150	2743.5651	2744.3766	Fe I	CA	$a\ ^5F_3 - w\ ^5F_3$
200	2744.0679	2744.8795	Fe I	CA	$a\ ^5D_0 - y\ ^5P_1$
80	2744.5274	2745.3392	Fe I	CA	$a\ ^5F_2 - w\ ^5D_1$
300	2746.483	2747.295	Fe II	P	
40	2746.982	2747.795	Fe I	P	$a\ ^5F_5 - z\ ^5H_6$
1	2747.5549	2748.3674	Fe I	CA	$a\ ^5P_2 - t\ ^5P_2$
100	2749.320	2750.133	Fe II	P	
500	2749.485	2750.298	Fe II	P	
1200	2750.1405	2750.9537	Fe I	CA	$a\ ^5D_3 - y\ ^5P_3$
5	2750.6967	2751.5099	Fe I	CA	$a\ ^5P_1 - t\ ^5P_1$
30	2750.8735	2751.6868	Fe I	CA	$a\ ^5P_3 - 10\ _3$
20	2751.125	2751.938	Fe II	P	
4	2751.8029	2752.6164	Fe I	CA	$a\ ^3F_2 - v\ ^3D_1$
20	2752.150	2752.964	Fe II	P	
12	2753.098	2753.911		P	
80	2753.287	2754.101	Fe II	P	
50	2753.686	2754.500	Fe I	P	$a\ ^5F_1 - w\ ^5D_0$
150	2754.0324	2754.8465	Fe I	CA	$a\ ^5F_2 - w\ ^5F_2$
100	2754.4258	2755.2399	Fe I	CA	$a\ ^5F_3 - w\ ^5F_4$
30	2754.888	2755.703	Fe II	P	
12	2754.942	2755.757		P	
15	2755.1809	2755.9953	Fe I	CA	$a\ ^3H_5 - s\ ^3G_4$
800	2755.734	2756.549	Fe II	P	
4	2756.086	2756.901		P	
4	2756.2672	2757.0818	Fe I	CA	$a\ ^5D_3 - y\ ^3F_4$
250	2756.3284	2757.1430	Fe I	CA	$a\ ^5D_1 - y\ ^5P_2$
6	2756.509	2757.324	Fe II	P	
80	2756.62	2757.43	Bl	P	
8	2757.030	2757.845	Fe II	P	
100	2757.3157	2758.1306	Fe I	CA	$a\ ^5F_1 - w\ ^5D_1$
30	2757.422	2758.237		P	
8	2757.535	2758.350		P	
5	2757.836	2758.651	Fe II	P	
5	2757.858	2758.673	Fe I	P	
4	2758.749	2759.564		P	
6	2759.479	2760.294		P	
50	2759.813	2760.628	Fe I	P	$a\ ^5F_1 - w\ ^5F_1$
25	2760.891	2761.707		P	
8	2761.183	2761.998	Fe II	P	
8	2761.449	2762.265		P	
4	2761.4802	2762.2961	Fe I	CA	$a\ ^3P_1 - w\ ^1D_2$
120	2761.7798	2762.5957	Fe I	CA	$a\ ^5F_2 - w\ ^5D_2$
150	2761.812	2762.628	Fe II	P	
150	2762.0264	2762.8424	Fe I	CA	$a\ ^5F_3 - w\ ^5D_3$
20	2762.33	2763.15	Bl	P	
12	2762.681	2763.497		P	
120	2762.7719	2763.5881	Fe I	CA	$a\ ^5P_1 - t\ ^5P_2$
25	2762.922	2763.738	Ne II	CP	
120	2763.1093	2763.9256	Fe I	CA	$a\ ^5F_2 - w\ ^5F_3$
20	2763.656	2764.472	Fe II	P	
20	2764.118	2764.935	Fe I	P	
30	2764.3230	2765.1396	Fe I	CA	$a\ ^5P_2 - 10\ _3$
25	2765.128	2765.945	Fe II	P	
8	2765.224	2766.040	Fe II	P	
4	2765.991	2766.808		P	
6	2766.372	2767.189	Ne I	P	
12	2766.659	2767.476		P	
80	2766.9096	2767.7268	Fe I	CA	$a\ ^5F_1 - w\ ^5F_2$
250	2767.5222	2768.3396	Fe I	CA	$a\ ^5F_4 - w\ ^5D_4$
20	2768.105	2768.922		P	
15	2768.432	2769.249	Fe I	P	$a\ ^5P_3 - y\ ^1F_3$
10	2768.580	2769.397		P	
12	2768.934	2769.752	Fe II	P	
8	2769.153	2769.970	Fe II	P	

TABLE III. *Spectrum of the Fe-Ne hollow cathode*—Continued

Intensity	Wavelength (Å) Air	Wavelength (Å) Vacuum	Ion	Ref	Classification
50	2769.2970	2770.1148	Fe I	ED	$a\ ^3H_6 - v\ ^3H_6$
25	2769.355	2770.173	Fe II	P	
40	2769.6713	2770.4891	Fe I	CA	$a\ ^5F_5 - y\ ^5G_4$
10	2769.835	2770.652	Fe II	P	
4	2770.505	2771.323	Fe II	P	
8	2770.575	2771.393		P	
10	2770.6951	2771.5132	Fe I	CA	$a\ ^5P_2 - v\ ^3P_1$
40	2771.880	2772.698		P	
300	2772.0736	2772.8921	Fe I	ED	$a\ ^5F_5 - z\ ^5H_5$
8	2772.1099	2772.9284	Fe I	CA	$a\ ^5D_2 - y\ ^5P_3$
20	2772.318	2773.137	Fe I	P	$a\ ^5P_3 - b\ X_4$
25	2772.508	2773.327	Fe I	P	$a\ ^5P_2 - c\ X_3$
8	2772.826	2773.644	Fe I	P	$b\ ^3G_4 - r\ ^3G_4$
50	2773.232	2774.050	Fe I	P	
8	2773.659	2774.478	Fe II	P	
6	2773.9027	2774.7216	Fe I	CA	$a\ ^3H_6 - v\ ^3H_5$
6	2774.1614	2774.9804	Fe I	CA	$a\ ^5P_2 - x\ ^1F_3$
20	2774.686	2775.505	Fe II	P	
20	2774.7297	2775.5488	Fe I	CA	$a\ ^5F_1 - w\ ^5D_2$
10	2774.938	2775.757		P	
10	2775.844	2776.663		P	
15	2776.397	2777.217		P	
3	2776.448	2777.267		P	
15	2776.907	2777.727	Fe II	P	
15	2777.631	2778.450		P	
5	2777.889	2778.709	Fe II	P	
60	2778.067	2778.887	Fe I	P	
600	2778.2205	2779.0405	Fe I	CA	$a\ ^5F_5 - y\ ^5G_5$
40	2778.841	2779.662	Fe I	P	
40	2779.299	2780.119	Fe II	P	
5	2779.907	2780.728	Fe II	P	
15	2780.03	2780.85	Bl	P	
15	2780.6975	2781.5181	Fe I	CA	$b\ ^3F_4 - u\ ^3F_4$
12	2780.8826	2781.7032	Fe I	CA	$a\ ^5F_4 - z\ ^5H_3$
20	2781.8355	2782.6563	Fe I	CA	$a\ ^5F_2 - w\ ^5D_3$
6	2782.053	2782.874	Fe I	P	$a\ ^5P_2 - y\ ^1F_3$
3	2783.5509	2784.3722	Fe I	CA	$a\ ^3F_3 - w\ ^3G_3$
50	2783.691	2784.512	Fe II	P	
5	2784.0087	2784.8300	Fe I	CA	$b\ ^3F_3 - u\ ^3F_3$
8	2784.343	2785.164	Fe I	P	$a\ ^3H_5 - x\ ^1H_5$
3	2785.127	2785.949		P	
30	2785.193	2786.015	Fe II	P	
8	2785.275	2786.097		P	
6	2786.781	2787.603	Fe I	P	
5	2786.944	2787.767		P	
5	2787.241	2788.064	Fe II	P	
20	2787.9317	2788.7540	Fe I	CA	$a\ ^3F_4 - x\ ^3G_5$
3000	2788.104	2788.926	Fe I	P	$a\ ^5F_5 - y\ ^5G_6$
15	2789.477	2790.300	Fe I	P	$a\ ^5P_3 - t\ ^5P_3$
5	2789.678	2790.500	Fe II	P	
20	2789.8019	2790.6247	Fe I	CA	$a\ ^3G_5 - t\ ^3F_4$
6	2789.847	2790.670		P	
12	2791.454	2792.278		P	
20	2791.7856	2792.6088	Fe I	CA	$a\ ^3H_5 - v\ ^3H_5$
100	2792.017	2792.840	Ne II	CP	
30	2792.319	2793.142	Ne I	P	
25	2792.3987	2793.2221	Fe I	CA	$a\ ^3F_3 - w\ ^3G_4$
3	2793.368	2794.192		P	
5	2793.787	2794.611		P	
20	2793.888	2794.712	Fe II	P	
30	2793.928	2794.752		P	
60	2794.219	2795.043	Ne II	CP	
20	2794.7022	2795.5262	Fe I	CA	$a\ ^5F_3 - w\ ^5D_4$
12	2795.0054	2795.8294	Fe I	CA	$a\ ^5D_4 - z\ ^3G_4$
30	2795.5401	2796.3643	Fe I	CA	$a\ ^5F_4 - y\ ^5G_3$
15	2795.857	2796.681		P	
10	2796.627	2797.452	Fe II	P	
2	2796.8706	2797.6951	Fe I	CA	$a\ ^3F_3 - x\ ^3P_2$
10	2797.195	2798.019	Fe II	P	
200	2797.7752	2798.5999	Fe I	ED	$a\ ^5F_4 - z\ ^5H_4$
30	2799.146	2799.971	Fe I	P	
30	2799.294	2800.119	Fe II	P	
10	2800.467	2801.292		P	
6	2800.537	2801.362	Fe II	P	
6	2803.1663	2803.9924	Fe I	CA	$a\ ^5D_3 - z\ ^3G_3$
8	2803.430	2804.256	Fe II	P	
10	2803.6129	2804.4390	Fe I	CA	$a\ ^3H_4 - y\ ^3H_4$
5	2803.936	2804.762	Fe II	P	
400	2804.5206	2805.3469	Fe I	CA	$a\ ^5F_4 - y\ ^5G_4$
10	2804.8622	2805.6886	Fe I	CA	$a\ ^3G_4 - t\ ^3F_3$
5	2804.999	2805.826	Fe II	P	
5	2805.104	2805.930		P	
6	2805.8079	2806.6346	Fe I	CA	$a\ ^3F_4 - v\ ^5F_5$
5	2806.070	2806.897	Fe I	P	$a\ ^3P_2 - 11\ 3$
1500	2806.9843	2807.8115	Fe I	ED	$a\ ^5F_4 - z\ ^5H_5$
3	2807.179	2808.006	Fe II	P	
3	2807.2452	2808.0722	Fe I	CA	$a\ ^5D_4 - z\ ^5G_3$
40	2808.3269	2809.1542	Fe I	CA	$a\ ^5F_3 - z\ ^5H_3$
5	2808.398	2809.225	Fe II	P	
60	2809.484	2810.312	Ne II	CP	
10	2809.783	2810.611	Fe II	P	
5	2810.262	2811.090		P	
1	2811.1624	2811.9904	Fe I	CA	$a\ ^3F_3 - v\ ^5F_3$
12	2812.0422	2812.8704	Fe I	CA	$a\ ^3G_4 - t\ ^3F_4$
3	2812.114	2812.943		P	
2500	2813.2866	2814.1151	Fe I	CA	$a\ ^5F_4 - y\ ^5G_5$
3	2814.691	2815.520	Ne I	P	
3	2815.0144	2815.8434	Fe I	CA	$a\ ^3P_2 - 10\ 3$
20	2815.5075	2816.3365	Fe I	CA	$a\ ^3F_2 - w\ ^3G_3$
6	2817.088	2817.917	Fe II	P	
20	2817.5036	2818.3331	Fe I	CA	$a\ ^5F_3 - y\ ^5G_2$
5	2817.940	2818.770		P	
12	2819.3031	2820.1331	Fe I	CA	$a\ ^3G_3 - t\ ^3F_2$
3	2820.690	2821.521	Fe II	P	
2	2820.8028	2821.6331	Fe I	CA	$a\ ^5D_3 - z\ ^5G_2$
3	2822.058	2822.889	Fe II	P	
300	2823.2760	2824.1069	Fe I	CA	$a\ ^5F_3 - y\ ^5G_3$
3	2824.7001	2825.5314	Fe I	CA	$a\ ^3G_3 - t\ ^3F_3$
600	2825.5557	2826.3874	Fe I	ED	$a\ ^5F_3 - z\ ^5H_4$
50	2825.6874	2826.5190	Fe I	CA	$a\ ^5D_4 - z\ ^3G_5$
1	2825.9945	2826.8261	Fe I	CA	$a\ ^5D_2 - z\ ^3G_3$
8	2826.4973	2827.3291	Fe I	CA	$a\ ^3F_3 - v\ ^5F_4$
10	2827.589	2828.421	Ne I	P	
12	2827.8919	2828.7240	Fe I	CA	$a\ ^5D_3 - z\ ^3G_4$
6	2828.627	2829.459	Fe II	P	
5	2828.678	2829.510	Fe II	P	
120	2828.8082	2829.6405	Fe I	CA	$a\ ^5F_2 - z\ ^5H_3$
6	2830.960	2831.793	Fe II	P	
6	2831.255	2832.088	Fe II	P	
25	2831.561	2832.394	Fe II	P	
1500	2832.4358	2833.2690	Fe I	CA	$a\ ^5F_3 - y\ ^5G_4$
10	2833.085	2833.918	Fe II	P	
30	2833.401	2834.235	Fe I	P	$a\ ^3P_2 - y\ ^1F_3$
3	2833.408	2834.241		P	
3	2833.817	2834.650		P	
6	2834.1728	2835.0064	Fe I	CA	$a\ ^3F_3 - x\ ^3G_3$
1	2834.4133	2835.2470	Fe I	CA	$a\ ^3F_2 - v\ ^5F_2$
1	2834.4194	2835.2530	Fe I	CA	$a\ ^3F_3 - w\ ^5G_2$

562-903 O - 75 - 3

TABLE III. *Spectrum of the Fe-Ne hollow cathode*—Continued

Intensity	Wavelength (Å) Air	Wavelength (Å) Vacuum	Ion	Ref	Classification
10	2834.7535	2835.5873	Fe I	CA	$b\ ^3F_4 - s\ ^3G_5$
15	2835.4565	2836.2905	Fe I	CA	$a\ ^5D_4 - z\ ^5G_4$
5	2835.661	2836.495		P	
12	2835.711	2836.545	Fe II	P	
120	2835.9497	2836.7838	Fe I	CA	$a\ ^3F_3 - x\ ^3G_4$
5	2836.315	2837.149	Fe I	P	$z\ ^7F_6 - h\ ^7D_5$
200	2838.1193	2838.9539	Fe I	CA	$a\ ^5F_2 - y\ ^5G_2$
6	2838.215	2839.050	Fe II	P	
8	2838.448	2839.282		P	
30	2839.513	2840.348	Fe II	P	
20	2839.799	2840.634	Fe II	P	
6	2840.344	2841.179	Fe II	P	
12	2840.4220	2841.2572	Fe I	CA	$a\ ^5D_3 - z\ ^5G_3$
15	2840.649	2841.484	Fe II	P	
12	2840.758	2841.594	Fe II	P	
4	2840.9367	2841.7720	Fe I	CA	$a\ ^5P_2 - v\ ^3P_2$
2	2842.911	2843.747		P	
4	2843.213	2844.049		P	
200	2843.6307	2844.4666	Fe I	CA	$a\ ^5F_4 - x\ ^5P_3$
0	2843.9202	2844.7563	Fe I	CA	$a\ ^5D_2 - z\ ^5G_2$
1000	2843.9766	2844.8126	Fe I	CA	$a\ ^5F_2 - y\ ^5G_3$
5	2844.957	2845.793	Fe II	P	
8	2845.425	2846.261	Fe II	P	
3	2845.488	2846.325	Fe II	P	
12	2845.5473	2846.3837	Fe I	CA	$a\ ^3F_3 - w\ ^5G_3$
100	2845.5945	2846.4309	Fe I	CA	$a\ ^5F_3 - x\ ^5P_2$
12	2845.7137	2846.5502	Fe I	CA	$a\ ^3F_4 - z\ ^3H_4$
6	2846.8296	2847.6664	Fe I	CA	$a\ ^3F_4 - x\ ^3F_3$
8	2847.773	2848.610	Fe II	P	
4	2847.883	2848.720		P	
8	2848.052	2848.889	Fe II	P	
15	2848.106	2848.943	Fe II	P	
15	2848.320	2849.157	Fe II	P	
40	2848.7139	2849.5511	Fe I	CA	$a\ ^5F_2 - x\ ^5P_1$
4	2849.605	2850.443	Fe II	P	
5	2851.5094	2852.3473	Fe I	CA	$b\ ^3F_2 - s\ ^3G_3$
12	2851.722	2852.560	Fe II	P	
800	2851.7968	2852.6347	Fe I	CA	$a\ ^5F_1 - y\ ^5G_2$
3	2852.127	2852.965		P	
10	2852.606	2853.444		P	
1	2852.9653	2853.8035	Fe I	CA	$a\ ^3F_4 - w\ ^3D_3$
8	2853.6838	2854.5223	Fe I	CA	$a\ ^3F_4 - z\ ^3H_5$
6	2853.7716	2854.6100	Fe I	CA	$b\ ^3F_3 - s\ ^3G_4$
8	2855.689	2856.528	Fe II	P	
4	2856.147	2856.986	Fe II	P	
12	2856.377	2857.216	Fe II	P	
30	2856.908	2857.747	Fe II	P	
5	2857.174	2858.014	Fe II	P	
4	2857.810	2858.650		P	
6	2857.99	2858.83	Bl	P	
25	2858.340	2859.180	Fe II	P	
5	2858.629	2859.469	Fe II	P	
12	2858.8956	2859.7353	Fe I	CA	$a\ ^5D_1 - z\ ^5G_2$
15	2862.4939	2863.3345	Fe I	CA	$a\ ^5F_1 - x\ ^5P_1$
25	2863.4292	2864.2700	Fe I	CA	$a\ ^3F_4 - x\ ^3F_4$
15	2863.8635	2864.7044	Fe I	CA	$a\ ^5D_2 - z\ ^5G_3$
5	2866.201	2867.043	Fe II	P	
30	2866.6249	2867.4665	Fe I	CA	$a\ ^5F_2 - x\ ^5P_2$
12	2866.719	2867.561		P	
15	2867.3091	2868.1508	Fe I	CA	$a\ ^3F_2 - x\ ^3G_3$
10	2867.5614	2868.4032	Fe I	CA	$a\ ^3F_2 - w\ ^5G_2$
4	2867.8788	2868.7207	Fe I	CA	$a\ ^3F_3 - 1\ _2$
8	2868.2140	2869.0559	Fe I	CA	$z\ ^7D_3 - g\ ^7D_2$
6	2868.4534	2869.2955	Fe I	CA	$a\ ^3P_2 - z\ ^1P_1$
10	2869.230	2870.072		P	
50	2869.3075	2870.1497	Fe I	CA	$a\ ^5D_3 - z\ ^5G_4$
5	2869.826	2870.668	Fe I	P	$z\ ^7D_2 - g\ ^7D_1$
1	2871.273	2872.115		P	
50	2872.3338	2873.1768	Fe I	CA	$a\ ^5F_3 - x\ ^5P_3$
10	2872.385	2873.228	Fe II	P	
0	2872.4987	2873.3417	Fe I	CA	$b\ ^3P_2 - t\ ^3F_3$
25	2872.666	2873.510	Ne I	P	
8	2873.6527	2874.4960	Fe I	CA	$b\ ^3F_4 - v\ ^3H_5$
80	2874.1725	2875.0159	Fe I	CA	$a\ ^5D_4 - z\ ^5G_5$
8	2874.8806	2875.7242	Fe I	CA	$z\ ^7D_5 - g\ ^7D_4$
4	2875.246	2876.090		P	
10	2875.3019	2876.1456	Fe I	CA	$a\ ^3F_4 - u\ ^5D_3$
8	2875.348	2876.192	Fe II	P	
4	2876.804	2877.648	Fe II	P	
40	2877.3007	2878.1449	Fe I	CA	$a\ ^3F_4 - u\ ^5D_4$
4	2878.9516	2879.7962	Fe I	CA	$a\ ^3F_2 - w\ ^5G_3$
0	2879.4570	2880.3018	Fe I	CA	$a\ ^3P_1 - t\ ^5P_1$
5	2880.5791	2881.4241	Fe I	CA	$a\ ^5F_1 - x\ ^5P_2$
5	2880.757	2881.602	Fe II	P	
4	2880.831	2881.676	Fe II	P	
12	2881.578	2882.423		P	
6	2882.506	2883.351	Fe II	P	
8	2883.711	2884.556	Fe II	P	
8	2883.7475	2884.5933	Fe I	CA	$a\ ^3G_5 - u\ ^3H_5$
5	2884.269	2885.115	Fe II	P	
5	2884.765	2885.611	Fe II	P	
2	2885.933	2886.779	Fe II	P	
6	2886.3159	2887.1624	Fe I	CA	$a\ ^3F_3 - x\ ^3F_2$
2	2887.3580	2888.2048	Fe I	CA	$a\ ^3H_6 - 12\ _5$
15	2887.8048	2888.6516	Fe I	CA	$a\ ^3G_5 - u\ ^3H_6$
1	2887.9565	2888.8033	Fe I	CA	$a\ ^3H_5 - t\ ^3G_4$
4	2888.095	2888.942	Fe II	P	
2	2889.864	2890.711		P	
4	2889.9008	2890.7482	Fe I	CA	$a\ ^3H_6 - t\ ^3G_5$
5	2889.9887	2890.8361	Fe I	CA	$z\ ^7D_1 - g\ ^7D_2$
1	2890.8562	2891.7038	Fe I	CA	$a\ ^3D_3 - q\ ^3G_3$
1	2891.4035	2892.2512	Fe I	CA	$a\ ^3F_3 - w\ ^3D_2$
3	2891.688	2892.535		P	
3	2891.7068	2892.5546	Fe I	CA	$b\ ^3F_3 - v\ ^3H_4$
4	2891.905	2892.753	Fe I	P	$a\ ^3H_4 - e\ X_3$
6	2892.4779	2893.3259	Fe I	CA	$z\ ^7D_4 - g\ ^7D_4$
8	2893.7627	2894.6110	Fe I	CA	$a\ ^5F_2 - x\ ^5P_3$
8	2893.8807	2894.7290	Fe I	CA	$a\ ^3F_3 - z\ ^3H_4$
50	2894.5038	2895.3523	Fe I	CA	$a\ ^3P_2 - v\ ^3P_2$
3	2894.779	2895.627	Fe II	P	
40	2895.0347	2895.8833	Fe I	CA	$a\ ^3F_3 - x\ ^3F_3$
4	2895.220	2896.069	Fe II	P	
5	2897.266	2898.115	Fe II	P	
2	2897.637	2898.486	Fe I	P	$z\ ^7D_2 - g\ ^7D_3$
8	2898.351	2899.200		P	
1	2898.8573	2899.7068	Fe I	CA	$a\ ^5P_2 - t\ ^3D_3$
2	2899.258	2900.107		P	
25	2899.4152	2900.2649	Fe I	CA	$a\ ^3P_2 - 8\ _1$
15	2901.3802	2902.2303	Fe I	CA	$a\ ^3F_3 - w\ ^3D_3$
25	2901.910	2902.761	Fe I	P	$z\ ^7D_5 - g\ ^7D_5$
2	2904.087	2904.938		P	
5	2904.160	2905.011		P	
2	2905.744	2906.595	Fe II	P	
5	2906.416	2907.267		P	
20	2907.5170	2908.3687	Fe I	CA	$a\ ^3G_4 - u\ ^3H_5$
8	2908.8561	2909.7081	Fe I	CA	$z\ ^7D_3 - g\ ^7D_4$
2	2909.3157	2910.1678	Fe I	CA	$a\ ^3H_5 - t\ ^3G_5$
5	2909.499	2910.351		P	

TABLE III. *Spectrum of the Fe-Ne hollow cathode*—Continued

Intensity	Wavelength (Å) Air	Wavelength (Å) Vacuum	Ion	Ref	Classification
6	2910.061	2910.913	Ne II	CP	
6	2910.408	2911.260		P	
3	2910.9260	2911.7785	Fe I	CA	$a\,^3G_3 - u\,^3F_4$
120	2912.1574	2913.0103	Fe I	CA	$a\,^5D_4 - y\,^5F_3$
1	2912.2566	2913.1095	Fe I	CA	$a\,^3F_3 - u\,^5D_2$
60	2913.174	2914.027	Ne I	P	
3	2914.197	2915.050		P	
6	2914.3038	2915.1572	Fe I	CA	$a\,^3F_2 - w\,^3D_1$
40	2918.024	2918.878	Fe I	P	$b\,^3H_6 - t\,^3H_6$
10	2918.3525	2919.2068	Fe I	CA	$a\,^3P_1 - v\,^3P_1$
3	2918.528	2919.383	Fe II	P	
4	2918.816	2919.671		P	
4	2919.214	2920.069		P	
8	2919.840	2920.695	Fe I	P	$z\,^7D_4 - g\,^7D_5$
4	2920.6900	2921.5449	Fe I	CA	$a\,^3F_2 - x\,^3F_2$
4	2920.981	2921.837		P	
2	2922.211	2923.067		P	
6	2922.623	2923.479	Fe I	P	$a\,^5P_3 - 7\ _2$
5	2923.164	2924.020		P	
20	2923.286	2924.142	Fe I	P	$b\,^3H_5 - t\,^3H_5$
12	2923.430	2924.286		P	
30	2923.8528	2924.7085	Fe I	CA	$a\,^3G_5 - s\,^3G_5$
12	2925.3578	2926.2139	Fe I	CA	$a\,^3G_3 - u\,^3H_4$
3	2925.618	2926.474	Ne II	CP	
10	2925.785	2926.641		P	
10	2925.8996	2926.7558	Fe I	CA	$a\,^3F_2 - w\,^3D_2$
2	2926.553	2927.410		P	
10	2926.586	2927.443	Fe II	P	
4	2926.614	2927.471		P	
3	2928.103	2928.960	Fe I	P	$a\,^5P_3 - u\,^5P_3$
3	2928.7507	2929.6076	Fe I	CA	$a\,^3P_2 - u\,^3D_1$
120	2929.0072	2929.8642	Fe I	CA	$a\,^5D_3 - y\,^5F_2$
15	2929.109	2929.966	Fe I	P	$b\,^3H_4 - t\,^3H_4$
4	2929.239	2930.096		P	
6	2929.6180	2930.4751	Fe I	CA	$a\,^3F_2 - x\,^3F_3$
2	2931.4121	2932.2697	Fe I	CA	$a\,^3H_4 - 10\ _3$
3	2931.8052	2932.6629	Fe I	CA	$a\,^3G_4 - s\,^3G_3$
10	2932.727	2933.584	Ne I	P	
2	2934.371	2935.229	Fe I	P	$a\,^5P_3 - u\,^5F_3$
2	2935.883	2936.742	Fe II	P	
5	2936.068	2936.927	Fe II	P	
8	2936.1161	2936.9748	Fe I	CA	$a\,^3F_2 - w\,^3D_3$
4	2936.438	2937.297		P	
1200	2936.9034	2937.7623	Fe I	CA	$a\,^5D_4 - y\,^5F_4$
40	2937.807	2938.666	Fe I	P	$a\,^5P_2 - 7\ _2$
4	2939.071	2939.931	Fe I	P	$a\,^5P_1 - t\,^5D_0$
3	2940.114	2940.974	Fe II	P	
10	2940.589	2941.449	Fe I	P	$z\,^7F_5 - 3\ _4$
60	2941.3426	2942.2027	Fe I	CA	$a\,^5D_2 - y\,^5F_1$
2	2943.574	2944.434		P	
12	2944.397	2945.257	Fe II	P	
10	2945.052	2945.913	Fe I	P	$a\,^3H_4 - b\ X_3$
60	2947.303	2948.164	Ne I	P	
6	2947.3631	2948.2246	Fe I	CA	$a\,^3P_2 - u\,^3D_2$
1000	2947.8759	2948.7376	Fe I	CA	$a\,^5D_3 - y\,^5F_3$
40	2948.4329	2949.2947	Fe I	CA	$a\,^3G_4 - s\,^3G_4$
3	2948.727	2949.589	Fe I	P	$a\,^5P_2 - t\,^5D_2$
3	2948.952	2949.813		P	
60	2950.243	2951.105	Fe I	P	$a\,^5P_3 - 5\ _3$
25	2953.4862	2954.3493	Fe I	CA	$a\,^3G_3 - s\,^3G_3$
2	2953.539	2954.402		P	
600	2953.9399	2954.8031	Fe I	CA	$a\,^5D_2 - y\,^5F_2$
12	2954.6522	2955.5155	Fe I	CA	$a\,^3P_2 - t\,^3D_3$
100	2955.725	2956.589	Ne II	CP	
6	2956.704	2957.568	Fe I	P	$a\,^5P_3 - t\,^5D_3$
3	2956.858	2957.722	Fe I	P	$a\,^3G_5 - x\,^1H_5$
250	2957.3644	2958.2284	Fe I	CA	$a\,^5D_1 - y\,^5F_1$
6	2957.4863	2958.3503	Fe I	CA	$a\,^3P_2 - t\,^3D_1$
5	2959.329	2960.193		P	
3	2959.602	2960.467	Fe II	P	
15	2959.683	2960.547	Fe I	P	$z\,^7F_6 - 1\ _5$
4	2959.838	2960.702	Fe II	P	
80	2959.9912	2960.8559	Fe I	ED	$a\,^3G_5 - v\,^3H_6$
6	2960.2961	2961.1608	Fe I	CA	$a\,^3P_0 - v\,^3P_1$
3	2960.554	2961.419		P	
3	2960.6602	2961.5251	Fe I	CA	$b\,^3G_5 - t\,^3F_4$
1	2962.1080	2962.9732	Fe I	CA	$a\,^3F_4 - x\,^5G_5$
15	2963.237	2964.103	Ne II	CP	
6	2963.868	2964.733	Fe II	P	
1	2964.140	2965.000	Bl	P	
8	2965.035	2965.901	Fe II	P	
150	2965.2544	2966.1204	Fe I	CA	$a\,^5D_0 - y\,^5F_1$
15	2965.806	2966.672	Fe I	P	$a\,^3H_5 - 9\ _4$
25	2966.264	2967.131	Fe I	P	$a\,^5P_1 - t\,^5D_2$
1500	2966.8982	2967.7646	Fe I	CA	$a\,^5D_4 - y\,^5F_5$
3	2968.4774	2969.3442	Fe I	CA	$a\,^3P_1 - z\,^1P_1$
120	2969.360	2970.227	Fe I	P	$a\,^5D_1 - z\,^3P_0$
50	2969.4743	2970.3414	Fe I	CA	$a\,^5F_5 - x\,^5F_4$
800	2970.0995	2970.9667	Fe I	CA	$a\,^5D_1 - y\,^5F_2$
800	2970.1181	2970.9853	Fe I	CA	$a\,^5D_2 - z\,^3P_1$
15	2970.517	2971.384	Fe II	P	
50	2972.280	2973.147	Fe I	P	$a\,^5P_2 - t\,^5D_3$
1200	2973.1322	2974.0002	Fe I	CA	$a\,^5D_2 - y\,^5F_3$
500	2973.2352	2974.1032	Fe I	CA	$a\,^5D_3 - y\,^5F_4$
150	2974.722	2975.590	Ne I	P	
0	2974.780	2975.649	Fe I	P	$z\,^7F_5 - 2\ _4$
12	2976.1282	2976.9969	Fe I	CA	$a\,^3P_2 - u\,^3D_3$
3	2976.4970	2977.3658	Fe I	CA	$a\,^3F_4 - y\,^3G_3$
2	2976.909	2977.778	Fe I	P	$z\,^7F_5 - 1\ _5$
6	2979.355	2980.225	Fe II	P	
3	2979.812	2980.681	Ne I	P	
12	2980.5341	2981.4039	Fe I	CA	$a\,^3G_3 - w\,^1F_3$
20	2980.649	2981.518	Ne I	P	
25	2980.93	2981.80	Bl	P	
600	2981.4451	2982.3151	Fe I	CA	$a\,^5D_3 - z\,^3P_2$
25	2981.852	2982.722	Fe I	P	$a\,^5P_3 - t\,^5D_4$
2	2982.2288	2983.0990	Fe I	CA	$b\,^3G_4 - t\,^3F_3$
120	2982.672	2983.542	Ne I	P	
1000	2983.5698	2984.4403	Fe I	CA	$a\,^5D_4 - y\,^5D_3$
5	2984.559	2985.430		P	
60	2984.767	2985.638	Fe I	P	$a\,^5F_5 - y\,^7P_4$
50	2984.824	2985.695	Fe II	P	
3	2984.960	2985.831		P	
15	2986.4557	2987.3270	Fe I	CA	$a\,^5D_1 - z\,^3P_1$
4	2986.650	2987.530	Bl	P	
30	2987.2902	2988.1617	Fe I	CA	$a\,^5F_4 - x\,^5F_3$
3	2988.113	2988.985		P	
8	2988.4716	2989.3434	Fe I	CA	$a\,^3F_4 - y\,^3G_4$
4	2988.882	2989.754		P	
40	2990.3913	2991.2635	Fe I	CA	$a\,^3G_4 - v\,^3H_5$
3	2991.632	2992.504	Fe I	P	
15	2991.762	2992.635		P	
60	2992.432	2993.304	Ne I	P	
5	2993.181	2994.054		P	
6	2993.793	2994.666		P	
1000	2994.4269	2995.3002	Fe I	CA	$a\,^5D_3 - y\,^5D_2$
250	2994.5019	2995.3751	Fe I	CA	$a\,^5D_0 - z\,^3P_1$
5	2995.676	2996.549		P	

TABLE III. *Spectrum of the Fe-Ne hollow cathode*—Continued

Intensity	Wavelength (Å) Air	Wavelength (Å) Vacuum	Ion	Ref	Classification
10	2996.3850	2997.2587	Fe I	CA	$a\ ^3P_1 - v\ ^3P_2$
3	2997.216	2998.089	Fe II	P	
4	2997.302	2998.176		P	
5	2998.265	2999.139		P	
8	2999.191	3000.066		P	
500	2999.5118	3000.3863	Fe I	CA	$a\ ^5F_5 - x\ ^5F_5$
10	2999.699	3000.573		P	
120	3000.4508	3001.3255	Fe I	CA	$a\ ^3F_4 - y\ ^3G_5$
800	3000.9477	3001.8226	Fe I	CA	$a\ ^5D_2 - y\ ^5D_1$
60	3001.6554	3002.5304	Fe I	CA	$c\ ^3P_2 - t\ ^3F_3$
6	3002.199	3003.074	Fe II	P	
15	3002.645	3003.521	Fe II	P	
25	3003.0302	3003.9055	Fe I	CA	$a\ ^5F_3 - x\ ^5F_2$
4	3003.863	3004.739		P	
6	3004.1157	3004.9913	Fe I	CA	$a\ ^3H_5 - y\ ^3I_5$
3	3004.630	3005.505	Fe I	P	$a\ ^3F_3 - x\ ^5G_4$
8	3005.305	3006.181	Fe I	P	$a\ ^3H_6 - y\ ^3I_7$
4	3006.448	3007.324		P	
5	3006.543	3007.419		P	
40	3007.1452	3008.0216	Fe I	CA	$a\ ^3F_4 - x\ ^3D_3$
200	3007.2823	3008.1588	Fe I	CA	$a\ ^5D_2 - z\ ^3P_2$
500	3008.1390	3009.0157	Fe I	SM	$a\ ^5D_1 - y\ ^5D_0$
10	3009.0933	3009.9702	Fe I	CA	$a\ ^3H_6 - w\ ^3H_5$
120	3009.5689	3010.4460	Fe I	CA	$a\ ^5F_4 - x\ ^5F_4$
4	3010.174	3011.051	Fe II	P	
50	3011.4817	3012.3592	Fe I	CA	$a\ ^3G_3 - v\ ^3H_4$
25	3012.137	3013.015	Ne I	P	
5	3012.443	3013.320		P	
30	3012.959	3013.837	Ne I	P	
3	3014.1057	3014.9839	Fe I	CA	$b\ ^3G_5 - v\ ^1G_4$
4	3014.1732	3015.0514	Fe I	CA	$a\ ^5F_3 - z\ ^5S_2$
6	3015.9205	3016.7991	Fe I	CA	$a\ ^3H_5 - w\ ^3H_4$
12	3016.1815	3017.0602	Fe I	CA	$a\ ^5F_2 - x\ ^5F_1$
3	3017.259	3018.138		P	
40	3017.310	3018.189	Ne II	CP	
80	3017.356	3018.235	Ne I	P	
4	3017.418	3018.297		P	
60	3017.6272	3018.5062	Fe I	CA	$a\ ^5D_1 - y\ ^5D_1$
5	3017.856	3018.735		P	
4	3018.047	3018.926		P	
5	3018.1359	3019.0151	Fe I	CA	$a\ ^3H_6 - y\ ^3I_6$
60	3018.9826	3019.8620	Fe I	CA	$c\ ^5F_3 - x\ ^5F_3$
25	3019.234	3020.113		P	
4	3019.2898	3020.1693	Fe I	CA	$a\ ^3H_4 - y\ ^3I_5$
20	3019.381	3020.261		P	
5	3019.652	3020.532		P	
30	3019.804	3020.684		P	
60	3020.009	3020.889	Fe II	P	
500	3020.4907	3021.3704	Fe I	CA	$a\ ^5D_2 - y\ ^5D_2$
1500	3020.6391	3021.5189	Fe I	CA	$a\ ^5D_4 - y\ ^5D_4$
600	3021.0727	3021.9526	Fe I	CA	$a\ ^5D_3 - y\ ^5D_3$
50	3021.331	3022.211		P	
25	3021.749	3022.629		P	
6	3022.330	3023.211		P	
4	3022.773	3023.654		P	
5	3023.192	3024.072		P	
500	3024.0325	3024.9131	Fe I	CA	$a\ ^5D_1 - z\ ^3P_2$
10	3024.283	3025.164		P	
3	3024.582	3025.463		P	
5	3024.798	3025.679		P	
5	3024.871	3025.752		P	
15	3025.280	3026.161	Fe I	P	$a\ ^5F_4 - y\ ^7P_4$
150	3025.6384	3026.5194	Fe I	CA	$a\ ^3H_6 - w\ ^3H_6$
500	3025.8425	3026.7235	Fe I	CA	$a\ ^5D_0 - y\ ^5D_1$
30	3026.4614	3027.3426	Fe I	CA	$a\ ^5F_2 - x\ ^5F_2$
30	3027.016	3027.897	Ne II	CP	
6	3028.700	3029.582		P	
30	3028.863	3029.745	Ne II	CP	
8	3029.2337	3030.1156	Fe I	CA	$a\ ^3F_3 - y\ ^3G_3$
80	3030.1484	3031.0306	Fe I	CA	$a\ ^3H_5 - w\ ^3H_5$
4	3030.322	3031.204	Ne I	P	
4	3030.6033	3031.4856	Fe I	CA	$a\ ^3P_2 - v\ ^3F_3$
10	3030.787	3031.669	Fe I	P	$b\ ^3G_4 - x\ ^3I_5$
60	3031.2144	3032.0969	Fe I	CA	$a\ ^3H_4 - w\ ^3H_4$
5	3031.324	3032.206		P	
25	3031.6336	3032.5161	Fe I	CA	$a\ ^5F_1 - x\ ^5F_1$
3	3031.718	3032.600		P	
5	3033.1002	3033.9831	Fe I	CA	$a\ ^3P_1 - u\ ^3D_1$
5	3033.395	3034.278		P	
60	3034.462	3035.345	Ne II	CP	
60	3034.4842	3035.3675	Fe I	CA	$a\ ^3F_2 - x\ ^5G_3$
5	3035.737	3036.621		P	
30	3035.922	3036.805	Ne II	CP	
5	3036.123	3037.007		P	
40	3036.964	3037.848	Fe II	P	
800	3037.3887	3038.2726	Fe I	CA	$a\ ^5D_1 - y\ ^5D_2$
50	3037.7793	3038.6633	Fe I	CA	$a\ ^5F_2 - z\ ^5S_2$
5	3038.314	3039.198	Fe I	P	
4	3038.653	3039.537		P	
4	3039.3182	3040.2027	Fe I	CA	$a\ ^3H_5 - y\ ^3I_6$
10	3039.585	3040.470	Ne II	CP	
50	3040.4271	3041.3119	Fe I	CA	$a\ ^5F_4 - x\ ^5F_5$
4	3040.962	3041.847		P	
80	3041.6372	3042.5222	Fe I	CA	$a\ ^3F_3 - y\ ^3G_4$
50	3041.7384	3042.6234	Fe I	CA	$a\ ^5F_3 - x\ ^5F_4$
15	3042.0192	3042.9043	Fe I	CA	$a\ ^5F_1 - x\ ^5F_2$
25	3042.6644	3043.5497	Fe I	CA	$a\ ^5F_2 - x\ ^5F_3$
4	3042.843	3043.728		P	
3	3044.088	3044.974	Ne II	CP	
3	3044.323	3045.208		P	
40	3045.0783	3045.9642	Fe I	CA	$a\ ^5F_4 - y\ ^7P_3$
3	3045.503	3046.389		P	
4	3045.556	3046.442	Ne II	CP	
12	3045.5874	3046.4734	Fe I	CA	$a\ ^3H_4 - w\ ^3H_5$
5	3046.337	3047.223		P	
8	3046.9265	3047.8129	Fe I	CA	$a\ ^3H_5 - w\ ^3H_6$
15	3047.0498	3047.9362	Fe I	CA	$b\ ^3G_5 - u\ ^3F_4$
800	3047.6043	3048.4909	Fe I	CA	$a\ ^5D_2 - y\ ^5D_3$
6	3048.452	3049.339		P	
5	3048.876	3049.763		P	
4	3048.994	3049.881	Fe II	P	
3	3049.354	3050.241	Fe I	P	
4	3050.473	3051.360	Ne II	CP	
10	3053.0670	3053.9549	Fe I	CA	$a\ ^3P_1 - u\ ^3D_2$
8	3053.429	3054.317	Fe I	P	
6	3053.455	3054.343		P	
3	3053.538	3054.426		P	
3	3053.878	3054.766		P	
5	3054.346	3055.234		P	
10	3054.675	3055.564	Ne II	CP	
50	3055.2620	3056.1505	Fe I	CA	$a\ ^3F_3 - x\ ^3D_2$
4	3055.294	3056.182		P	
5	3055.351	3056.240	Fe II	P	
4	3055.710	3056.599		P	
4	3056.173	3057.061		P	
8	3056.242	3057.130	Fe I	P	$b\ ^3F_2 - a\ X_2$
600	3057.4456	3058.3346	Fe I	CA	$a\ ^5F_5 - x\ ^5D_4$
6	3057.789	3058.678		P	

TABLE III. *Spectrum of the Fe-Ne hollow cathode*—Continued

Intensity	Wavelength (Å) Air	Wavelength (Å) Vacuum	Ion	Ref	Classification
5	3057.812	3058.701		P	
8	3058.034	3058.924		P	
5	3058.364	3059.253		P	
20	3058.493	3059.383		P	
1000	3059.0856	3059.9750	Fe I	CA	$a\ ^5D_3 - y\ ^5D_4$
5	3060.359	3061.249		P	
5	3060.5375	3061.4272	Fe I	CA	$b\ ^3G_4 - u\ ^3F_3$
4	3060.621	3061.511		P	
4	3060.777	3061.667		P	
5	3060.9832	3061.8731	Fe I	CA	$a\ ^3F_3 - x\ ^3D_3$
3	3062.491	3063.382		P	
5	3063.301	3064.192		P	
5	3063.696	3064.587	Ne I	P	
5	3063.9306	3064.8212	Fe I	CA	$a\ ^3P_1 - t\ ^3D_1$
4	3064.018	3064.909		P	
4	3065.316	3066.207	Fe II	P	
6	3066.4786	3067.3699	Fe I	CA	$a\ ^3G_4 - t\ ^3G_3$
4	3066.999	3067.891		P	
30	3067.1182	3068.0096	Fe I	CA	$a\ ^3F_2 - y\ ^3G_3$
250	3067.2441	3068.1355	Fe I	CA	$a\ ^5F_4 - x\ ^5D_3$
5	3067.9482	3068.8398	Fe I	CA	$a\ ^3G_5 - 13\ _4$
25	3068.1732	3069.0649	Fe I	CA	$a\ ^3F_2 - x\ ^3D_1$
3	3068.724	3069.616	Fe II	P	
4	3069.330	3070.222		P	
3	3069.443	3070.335		P	
3	3070.884	3071.776		P	
6	3071.087	3071.980	Ne II	CP	
5	3071.124	3072.017	Fe II	P	
5	3071.530	3072.422		P	
3	3072.045	3072.938		P	
4	3072.290	3073.182		P	
3	3072.651	3073.544	Ne II	P	
3	3073.233	3074.126	Fe I	P	$a\ ^1G_4 - x\ ^3I_5$
4	3073.9783	3074.8714	Fe I	CA	$a\ ^3G_5 - t\ ^3G_4$
5	3074.1473	3075.0404	Fe I	CA	$b\ ^3G_3 - u\ ^3F_2$
5	3074.437	3075.330		P	
120	3075.7193	3076.6128	Fe I	CA	$a\ ^5F_3 - x\ ^5D_2$
4	3075.950	3076.843		P	
5	3076.357	3077.250		P	
3	3076.435	3077.329	Fe II	P	
20	3076.976	3077.870	Ne I	P	
4	3077.170	3078.064	Fe II	P	
4	3077.636	3078.530		P	
15	3078.0155	3078.9096	Fe I	CA	$a\ ^5F_3 - y\ ^7P_3$
3	3078.259	3079.153		P	
6	3078.4324	3079.3267	Fe I	CA	$a\ ^3P_0 - u\ ^3D_1$
3	3078.588	3079.482		P	
5	3078.681	3079.575	Fe II	P	
4	3078.878	3079.772	Ne I	P	
4	3079.181	3080.075	Ne I	P	
1	3079.990	3080.885		P	
4	3080.110	3081.005		P	
4	3081.002	3081.897		P	
3	3081.342	3082.237		P	
3	3081.734	3082.629		P	
3	3082.153	3083.048		P	
50	3083.7413	3084.6368	Fe I	CA	$a\ ^5F_2 - x\ ^5D_1$
4	3084.461	3085.357		P	
3	3085.573	3086.469		P	
20	3088.665	3089.562		P	
2	3090.2051	3091.1023	Fe I	CA	$a\ ^3G_3 - t\ ^3G_3$
120	3091.5769	3092.4745	Fe I	CA	$a\ ^5F_1 - x\ ^5D_0$
10	3092.710	3093.608		P	
10	3092.7811	3093.6789	Fe I	CA	$a\ ^5F_3 - y\ ^7P_2$
10	3092.901	3093.799	Ne II	CP	
6	3093.355	3094.253		P	
8	3093.8044	3094.7025	Fe I	CA	$a\ ^3F_2 - x\ ^3D_2$
30	3093.878	3094.776	Fe I	P	$b\ ^3F_4 - s\ ^3D_3$
5	3094.006	3094.904	Ne II	CP	
10	3094.900	3095.798		P	
6	3095.2668	3096.1652	Fe I	CA	$a\ ^3G_5 - 12\ _5$
12	3097.133	3098.032	Ne II	CP	
6	3097.775	3098.674		P	
5	3097.884	3098.783		P	
80	3098.1891	3099.0883	Fe I	CA	$a\ ^3G_5 - t\ ^3G_5$
100	3099.8951	3100.7947	Fe I	CA	$a\ ^5F_1 - x\ ^5D_1$
100	3099.9679	3100.8675	Fe I	CA	$a\ ^5F_4 - x\ ^5D_4$
60	3100.3031	3101.2028	Fe I	CA	$a\ ^5F_2 - x\ ^5D_2$
100	3100.6651	3101.5649	Fe I	CA	$a\ ^5F_3 - x\ ^5D_3$
10	3100.8363	3101.7361	Fe I	CA	$a\ ^3H_6 - 6\ _5$
0	3101.0017	3101.9016	Fe I	CA	$a\ ^3G_4 - t\ ^3G_4$
5	3102.637	3103.537	Fe I	P	
4	3106.5383	3107.4396	Fe I	CA	$a\ ^3H_4 - u\ ^3D_3$
5	3109.0376	3109.9395	Fe I	CA	$z\ ^7D_2 - e\ ^5P_2$
6	3111.6847	3112.5873	Fe I	CA	$b\ ^3F_4 - w\ ^3H_4$
4	3112.0775	3112.9802	Fe I	CA	$b\ ^3G_5 - s\ ^3G_5$
4	3116.251	3117.155	Fe I	P	$z\ ^7D_3 - e\ ^5P_3$
5	3116.510	3117.410	Bl	P	
8	3116.6313	3117.5352	Fe I	CA	$a\ ^5F_1 - x\ ^5D_2$
5	3117.6395	3118.5436	Fe I	CA	$a\ ^5F_2 - y\ ^7P_2$
20	3119.4944	3120.3989	Fe I	CA	$a\ ^3H_5 - u\ ^3G_4$
15	3120.4346	3121.3394	Fe I	CA	$a\ ^3H_4 - u\ ^3G_3$
5	3121.7563	3122.6614	Fe I	CA	$a\ ^5P_1 - w\ ^3P_0$
3	3122.6674	3123.5728	Fe I	CA	$a\ ^3G_4 - 12\ _5$
4	3123.3481	3124.2536	Fe I	CA	$z\ ^7D_4 - e\ ^7S_3$
3	3124.096	3125.002	Fe I	P	$z\ ^7D_1 - e\ ^5P_1$
40	3125.6509	3126.5570	Fe I	CA	$a\ ^5F_2 - x\ ^5D_3$
40	3125.6555	3126.5616	Fe I	CA	$z\ ^7D_5 - e\ ^7G_4$
40	3126.18	3127.09	Bl	P	
100	3126.1986	3127.1051	Ne I	BA	
5	3128.8977	3129.8046	Fe I	CA	$a\ ^3F_3 - y\ ^5S_2$
4	3129.3331	3130.2402	Fe I	CA	$a\ ^3F_4 - w\ ^5D_3$
5	3132.5178	3133.4256	Fe I	CA	$z\ ^5D_4 - i\ ^5D_3$
10	3134.1097	3135.0179	Fe I	CA	$a\ ^5F_3 - x\ ^5D_4$
5	3135.8596	3136.7683	Fe I	CA	$a\ ^3H_4 - u\ ^3G_4$
5	3139.6579	3140.5675	Fe I	CA	$z\ ^7D_5 - e\ ^7F_4$
6	3140.3903	3141.3001	Fe I	CA	$z\ ^5D_3 - i\ ^5D_2$
30	3141.331	3142.242	Ne II	CP	
8	3142.4536	3143.3639	Fe I	CA	$z\ ^7D_3 - e\ ^7S_3$
10	3142.8885	3143.7990	Fe I	CA	$a\ ^3P_2 - w\ ^3P_2$
10	3143.2425	3144.1531	Fe I	CA	$a\ ^5D_4 - z\ ^3F_3$
6	3143.720	3144.631	Ne II	CP	
15	3143.990	3144.901	Fe I	P	$z\ ^5D_4 - i\ ^5D_4$
6	3144.4837	3145.3946	Fe I	CA	$z\ ^7D_2 - f\ ^5F_2$
5	3145.0565	3145.9675	Fe I	CA	$b\ ^3G_4 - s\ ^3G_4$
0	3146.4676	3147.3790	Fe I	CA	$z\ ^7D_4 - e\ ^7G_4$
4	3147.291	3148.202		P	
5	3147.603	3148.515		P	
4	3147.7954	3148.7070	Fe I	CA	$b\ ^3G_3 - s\ ^3G_3$
4	3148.4064	3149.3182	Fe I	CA	$a\ ^3H_5 - u\ ^3G_5$
6	3148.6107	3149.5229	Ne I	BA	
4	3150.3073	3151.2196	Fe I	CA	$z\ ^5D_1 - 4\ _2$
20	3151.352	3152.264	Fe I	P	$a\ ^3G_4 - y\ ^1H_5$
6	3151.8658	3152.7786	Fe I	CA	$a\ ^5D_3 - z\ ^3F_2$
4	3153.0502	3153.9632	Fe I	CA	$a\ ^5P_2 - w\ ^3F_2$
10	3153.1994	3154.1125	Fe I	CA	$z\ ^7D_3 - f\ ^5F_4$
4	3153.3144	3154.2275	Fe I	CA	$z\ ^7D_3 - e\ ^7G_3$
6	3153.4107	3154.3241	Ne I	BA	

TABLE III. *Spectrum of the Fe-Ne hollow cathode*—Continued

Intensity	Wavelength (Å) Air	Wavelength (Å) Vacuum	Ion	Ref	Classification
4	3153.751	3154.665		P	
6	3154.201	3155.115	Fe II	P	
6	3154.4155	3155.3288	Fe I	CA	$a\ ^5P_3 - v\ ^3D_2$
3	3154.4960	3155.4094	Fe I	CA	$z\ ^7D_2 - f\ ^5F_3$
3	3154.993	3155.906	Ne II	P	
3	3155.1169	3156.0304	Fe I	CA	$z\ ^7D_1 - f\ ^5F_2$
6	3155.2936	3156.2072	Fe I	CA	$a\ ^3H_5 - v\ ^3F_4$
4	3155.796	3156.710		P	
10	3156.2734	3157.1872	Fe I	CA	$z\ ^5D_3 - i\ ^5D_3$
4	3156.4631	3157.3770	Fe I	CA	$b\ ^3G_4 - w\ ^1F_3$
20	3157.0358	3157.9498	Fe I	CA	$z\ ^7D_4 - e\ ^7G_5$
4	3157.143	3158.057		P	
12	3157.8858	3158.8000	Fe I	CA	$z\ ^7D_2 - e\ ^7S_3$
3	3157.9869	3158.9012	Fe I	CA	$z\ ^7D_4 - e\ ^5G_3$
4	3158.183	3159.097	Fe I	P	
6	3160.1971	3161.1119	Fe I	CA	$z\ ^5D_2 - i\ ^5D_2$
20	3160.3420	3161.2568	Fe I	CA	$a\ ^3H_6 - x\ ^3H_6$
25	3160.6575	3161.5725	Fe I	CA	$z\ ^7D_4 - e\ ^7F_4$
5	3161.3712	3162.2863	Fe I	CA	$a\ ^3F_3 - w\ ^5D_2$
12	3161.9467	3162.8620	Fe I	CA	$z\ ^7D_5 - e\ ^7G_6$
5	3162.3305	3163.2458	Fe I	CA	$z\ ^7D_3 - e\ ^5G_2$
6	3163.871	3164.787		P	
5	3164.275	3165.191		P	
4	3164.2963	3165.2122	Fe I	CA	$z\ ^7D_3 - g\ ^5D_4$
5	3164.429	3165.345	Ne II	CP	
15	3164.6628	3165.5787		P	
5	3164.9992	3165.9152	Fe I	CA	$z\ ^7D_4 - e\ ^5S_2$
5	3165.0016	3165.9176	Fe I	CA	$z\ ^7D_4 - e\ ^7F_3$
5	3165.649	3166.566	Ne II	CP	
6	3165.8578	3166.7740	Fe I	CA	$z\ ^7D_3 - e\ ^7G_4$
3	3165.936	3166.853	Fe II	P	
15	3166.4353	3167.3517	Fe I	CA	$b\ ^3F_4 - t\ ^3D_3$
4	3167.5762	3168.4931	Ne I	BA	
6	3167.857	3168.774	Fe II	P	
6	3167.923	3168.840	Fe I	P	$z\ ^5D_3 - i\ ^5D_4$
3	3168.462	3169.379		P	
3	3168.600	3169.517		P	
3	3168.8538	3169.7708	Fe I	CA	$z\ ^7D_2 - e\ ^7G_3$
10	3171.3429	3172.2606	Fe I	CA	$a\ ^3F_4 - w\ ^5D_4$
10	3171.3513	3172.2689	Fe I	CA	$a\ ^1G_4 - s\ ^3G_3$
3	3171.6633	3172.5810	Fe I	CA	$z\ ^7D_1 - e\ ^7G_2$
5	3172.0838	3173.0016	Fe I	CA	$a\ ^5P_2 - w\ ^3F_3$
4	3173.410	3174.329	Fe I	P	$z\ ^7F_1 - g\ ^7D_1$
6	3173.6078	3174.5260	Fe I	CA	$z\ ^7F_3 - g\ ^7D_2$
8	3173.690	3174.608	Fe I	P	$a\ ^5P_2 - 3\ _3$
5	3175.314	3176.233	Fe I	P	$a\ ^3G_3 - c\ X_3$
80	3175.4454	3176.3641	Fe I	CA	$z\ ^7D_5 - e\ ^7F_5$
4	3176.3612	3177.2801	Fe I	CA	$b\ ^3F_2 - u\ ^3D_1$
5	3177.536	3178.455	Fe II	P	
20	3177.9590	3178.8783	Fe I	CA	$z\ ^7D_2 - e\ ^5G_2$
20	3178.0133	3178.9326	Fe I	CA	$z\ ^7D_5 - f\ ^7D_4$
3	3178.312	3179.231		P	
4	3178.5375	3179.4569	Fe I	CA	$b\ ^3G_3 - w\ ^1F_3$
15	3178.9627	3179.8823	Fe I	CA	$a\ ^3H_5 - x\ ^3H_5$
6	3179.53	3180.45	Bl	P	
50	3180.2236	3181.1434	Fe I	CA	$z\ ^7D_3 - e\ ^7F_4$
50	3180.2236	3181.1434	Fe I	CA	$z\ ^7D_3 - e\ ^7F_4$
50	3180.7554	3181.6754	Fe I	CA	$a\ ^5D_2 - z\ ^3F_2$
8	3181.5213	3182.4415	Fe I	CA	$b\ ^3F_3 - u\ ^3D_2$
5	3181.8463	3182.7666	Fe I	CA	$z\ ^7F_2 - g\ ^7D_2$
5	3181.9126	3182.8329	Fe I	CA	$z\ ^7D_2 - e\ ^7F_2$
6	3181.974	3182.894		P	
6	3182.0558	3182.9762	Fe I	CA	$z\ ^7D_4 - e\ ^5G_4$
10	3182.9774	3183.8980	Fe I	CA	$a\ ^5P_2 - v\ ^3D_3$
5	3183.450	3184.371		P	
3	3183.578	3184.499		P	
5	3184.6216	3185.5426	Fe I	CA	$z\ ^7D_3 - e\ ^7F_3$
150	3184.8947	3185.8157	Fe I	CA	$a\ ^5D_3 - z\ ^3F_3$
4	3186.741	3187.662	Fe II	P	
10	3188.5681	3189.4901	Fe I	CA	$z\ ^7D_5 - e\ ^5G_5$
10	3188.741	3189.663	Ne II	CP	
15	3188.820	3189.742	Fe I	P	
1	3190.0162	3190.9385	Fe I	CA	$b\ ^3F_3 - t\ ^3D_3$
3	3190.6496	3191.5721	Fe I	CA	$a\ ^1G_4 - s\ ^3G_5$
5	3190.8159	3191.7385	Fe I	CA	$a\ ^1G_4 - s\ ^3G_4$
6	3190.865	3191.787	Ne II	CP	
1	3191.1131	3192.0357	Fe I	CA	$b\ ^3F_4 - u\ ^3D_3$
250	3191.6591	3192.5819	Fe I	CA	$a\ ^5D_4 - z\ ^3D_3$
5	3192.4127	3193.3356	Fe I	CA	$a\ ^5P_1 - v\ ^3D_2$
6	3192.507	3193.430	Fe I	P	
5	3192.563	3193.486		P	
6	3192.8009	3193.7239	Fe I	CA	$z\ ^7D_1 - e\ ^7F_2$
6	3192.8426	3193.7656	Fe I	CA	$b\ ^3G_4 - v\ ^3H_5$
500	3193.2258	3194.1490	Fe I	CA	$a\ ^5D_4 - z\ ^3F_4$
800	3193.2992	3194.2224	Fe I	CA	$z\ ^7D_2 - e\ ^5G_3$
4	3193.893	3194.817	Fe II	P	
6	3194.4244	3195.3478	Fe I	CA	$z\ ^7D_2 - e\ ^7F_1$
12	3194.577	3195.501	Ne II	CP	
12	3196.076	3196.999	Fe II	P	
5	3196.1223	3197.0461	Fe I	CA	$z\ ^7F_5 - g\ ^7D_4$
200	3196.9281	3197.8522	Fe I	CA	$z\ ^7D_4 - e\ ^7F_5$
50	3196.9869	3197.9110	Fe I	CA	$a\ ^5D_3 - z\ ^3D_2$
5	3197.520	3198.444	Fe I	P	$z\ ^5F_2 - g\ ^5G_2$
50	3198.587	3199.511	Ne II	CP	
80	3199.4996	3200.4243	Fe I	CA	$a\ ^5D_1 - z\ ^3F_2$
80	3199.5309	3200.4556	Fe I	CA	$z\ ^7D_4 - f\ ^7D_4$
4	3200.317	3201.242		P	
60	3200.471	3201.396	Fe I	P	
12	3200.7847	3201.7097	Fe I	CA	$a\ ^5D_2 - z\ ^3D_1$
6	3202.5575	3203.4830	Fe I	CA	$a\ ^1G_4 - w\ ^1F_3$
3	3202.862	3203.787		P	
50	3205.3985	3206.3248	Fe I	CA	$z\ ^7D_1 - e\ ^7F_1$
5	3207.0749	3208.0016	Fe I	CA	$z\ ^7D_5 - e\ ^5G_6$
8	3208.470	3209.397	Fe I	P	$z\ ^5F_1 - g\ ^5G_2$
6	3208.965	3209.892	Ne II	CP	
40	3209.298	3210.225	Fe I	P	$z\ ^7F_6 - g\ ^7D_5$
10	3209.356	3210.283	Ne II	CP	
30	3210.2293	3211.1568	Fe I	CA	$z\ ^7D_4 - e\ ^5G_5$
40	3210.8280	3211.7556	Fe I	CA	$z\ ^7D_2 - f\ ^7D_1$
12	3211.4851	3212.4129	Fe I	CA	$z\ ^7D_1 - e\ ^5S_2$
5	3211.608	3212.536		P	
50	3211.675	3212.603	Fe I	P	$z\ ^5F_5 - g\ ^5G_6$
100	3211.876	3212.804	Fe I	P	$a\ ^5P_1 - 2\ _2$
6	3211.9859	3212.9138	Fe I	CA	$z\ ^7D_5 - e\ ^7P_4$
4	3212.161	3213.089		P	
6	3213.310	3214.239	Fe II	P	
40	3213.735	3214.664	Fe I	P	$b\ ^3G_3 - v\ ^3H_4$
200	3214.0111	3214.9395	Fe I	CA	$z\ ^7D_3 - f\ ^7D_3$
30	3214.328	3215.256	Ne II	CP	
200	3214.3956	3215.3241	Fe I	CA	$a\ ^5D_2 - z\ ^3F_3$
5	3215.411	3216.340		P	
60	3215.9380	3216.8669	Fe I	CA	$z\ ^7D_2 - f\ ^7D_2$
50	3217.3770	3218.3063	Fe I	CA	$z\ ^7D_5 - f\ ^5D_4$
80	3219.5827	3220.5125	Fe I	CA	$z\ ^7D_3 - f\ ^7D_4$
60	3219.7664	3220.6962	Fe I	CA	$a\ ^5D_1 - z\ ^3D_1$
60	3219.8044	3220.7343	Fe I	CA	$z\ ^7D_4 - e\ ^7P_3$
6	3221.9153	3222.8457	Fe I	CA	$z\ ^7D_1 - f\ ^7D_1$
300	3222.0452	3222.9757	Fe I	CA	$b\ ^3G_5 - w\ ^1G_4$

TABLE III. *Spectrum of the Fe-Ne hollow cathode*—Continued

Intensity	Wavelength (Å) Air	Wavelength (Å) Vacuum	Ion	Ref	Classification
300	3222.0666	3222.9971	Fe I	CA	$z\,^7D_5 - f\,^7D_5$
8	3222.924	3223.855	Fe II	P	
4	3223.272	3224.203	Fe I	P	$a\,^3F_4 - z\,^5H_5$
3	3223.8405	3224.7714	Fe I	CA	$a\,^5F_2 - y\,^3D_1$
40	3224.818	3225.749	Ne II	CP	
6	3225.6071	3226.5385	Fe I	CA	$a\,^3H_5 - x\,^1G_4$
600	3225.785	3226.716	Fe I	P	$z\,^7D_5 - e\,^7F_6$
6	3226.7133	3227.6449	Fe I	CA	$a\,^5D_2 - z\,^3D_2$
80	3227.7959	3228.7278	Fe I	CA	$z\,^7D_4 - f\,^5D_3$
5	3227.9956	3228.9276	Fe I	CA	$b\,^3P_2 - v\,^3P_1$
20	3228.2490	3229.1810	Fe I	CA	$z\,^7D_2 - f\,^5D_1$
6	3228.901	3229.833	Fe I	P	$z\,^7D_1 - f\,^5D_0$
40	3229.1207	3230.0530	Fe I	CA	$a\,^5D_0 - z\,^3D_1$
60	3229.57	3230.51	Bl	P	
10	3229.797	3230.729	Fe I	P	$b\,^3F_3 - u\,^5F_2$
0	3229.994	3230.927	Fe I	P	$a\,^1G_4 - x\,^1H_5$
200	3230.070	3231.001	Ne II	CP	
20	3230.2076	3231.1401	Fe I	CA	$z\,^7D_2 - e\,^7P_2$
20	3230.420	3231.352	Fe II	P	
40	3230.9631	3231.8958	Fe I	CA	$z\,^7D_3 - f\,^5D_2$
4	3232.023	3232.956	Fe II	P	
80	3233.051	3233.984	Fe I	P	$b\,^3H_6 - x\,^3I_7$
50	3233.9675	3234.9010	Fe I	CA	$z\,^7D_4 - e\,^7P_4$
120	3234.6130	3235.5466	Fe I	CA	$a\,^5D_3 - z\,^3D_3$
300	3236.2222	3237.1562	Fe I	CA	$a\,^5D_3 - z\,^3F_4$
4	3237.227	3238.161	Fe I	P	$b\,^3F_3 - 7\ _2$
5	3239.0125	3239.9473	Fe I	CA	$a\,^3P_2 - w\,^3F_3$
5	3239.0427	3239.9775	Fe I	CA	$a\,^3P_2 - v\,^3D_2$
100	3239.4328	3240.3676	Fe I	CA	$z\,^7D_4 - f\,^5D_4$
100	3239.4572	3240.3920	Fe I	CA	$z\,^7D_1 - f\,^5D_1$
4	3243.1077	3244.0435	Fe I	CA	$a\,^3H_4 - x\,^1G_4$
8	3243.404	3244.340	Fe I	P	$z\,^5F_5 - i\,^5D_4$
80	3244.1869	3245.1230	Fe I	CA	$z\,^7D_4 - f\,^7D_5$
4	3245.9653	3246.9018	Fe I	CA	$a\,^5F_4 - y\,^3D_3$
80	3246.0047	3246.9412	Fe I	CA	$a\,^5D_1 - z\,^3D_2$
6	3246.4802	3247.4168	Fe I	CA	$b\,^3F_3 - u\,^3G_4$
12	3246.9602	3247.8970	Fe I	CA	$a\,^5P_2 - x\,^3P_1$
4	3247.177	3248.113	Fe II	P	
5	3247.210	3248.146		P	
10	3247.2790	3248.2159	Fe I	CA	$z\,^7D_2 - f\,^5D_2$
8	3248.2047	3249.1417	Fe I	CA	$z\,^7D_3 - f\,^5D_3$
3	3248.345	3249.282		P	
6	3249.1918	3250.1291	Fe I	CA	$b\,^3F_4 - 4\ _4$
15	3250.3716	3251.3092	Fe I	CA	$a\,^3P_2 - v\,^3D_3$
15	3250.3959	3251.3335	Fe I	CA	$b\,^3P_0 - v\,^3P_1$
12	3250.6229	3251.5605	Fe I	CA	$a\,^5P_3 - x\,^3P_2$
5	3250.760	3251.698		P	
15	3251.2335	3252.1713	Fe I	CA	$a\,^5P_2 - w\,^3G_3$
6	3252.430	3253.368		P	
8	3252.9142	3253.8525	Fe I	CA	$b\,^3F_4 - u\,^3G_5$
10	3253.6003	3254.5387	Fe I	CA	$a\,^3D_3 - v\,^1G_4$
8	3253.8249	3254.7634	Fe I	CA	$b\,^3F_4 - v\,^3F_3$
3	3253.9431	3254.8817	Fe I	CA	$b\,^3F_2 - x\,^1D_2$
60	3254.3608	3255.2994	Fe I	ED	$b\,^3H_5 - x\,^3I_6$
5	3254.7265	3255.6653	Fe I	CA	$a\,^3G_5 - w\,^3H_6$
5	3257.2119	3258.1513	Fe I	CA	$a\,^5F_2 - y\,^3D_2$
5	3257.2358	3258.1752	Fe I	CA	$b\,^3G_4 - w\,^1G_4$
12	3257.5923	3258.5317	Fe I	CA	$a\,^5P_3 - v\,^5F_2$
5	3258.774	3259.714	Fe II	P	
3	3259.052	3259.992	Fe II	P	
8	3259.9894	3260.9294	Fe I	CA	$z\,^7D_3 - f\,^5D_4$
6	3260.2668	3261.2069	Fe I	CA	$b\,^3F_4 - v\,^3F_4$
4	3261.3255	3262.2659	Fe I	CA	$z\,^5F_2 - 4\ _2$
5	3262.0086	3262.9492	Fe I	CA	$z\,^5F_4 - i\,^5D_3$
3	3262.274	3263.214	Fe I	P	
6	3263.3678	3264.3087	Fe I	CA	$a\,^3P_1 - w\,^3P_2$
6	3263.411	3264.352	Ne II	CP	
8	3264.5121	3265.4533	Fe I	CA	$a\,^5P_2 - v\,^5F_1$
4	3264.6957	3265.6369	Fe I	CA	$z\,^7D_2 - f\,^5D_3$
80	3265.0465	3265.9879	Fe I	CA	$a\,^5D_2 - z\,^3D_3$
50	3265.6166	3266.5580	Fe I	CA	$a\,^5P_3 - v\,^5P_2$
4	3265.923	3266.865		P	
8	3268.2326	3269.1748	Fe I	CA	$a\,^5P_1 - x\,^3P_1$
3	3269.2285	3270.1709	Fe I	CA	$z\,^5F_3 - i\,^5D_2$
6	3269.872	3270.814	Ne II	CP	
3	3269.9437	3270.8863	Fe I	CA	$a\,^5P_3 - v\,^5F_3$
6	3270.800	3271.743	Ne II	CP	
50	3270.9997	3271.9425	Fe I	CA	$a\,^5P_2 - v\,^5P_1$
5	3271.4848	3272.4278	Fe I	CA	$a\,^3D_3 - u\,^3F_3$
5	3271.6829	3272.6260	Fe I	CA	$a\,^3F_4 - x\,^5P_3$
5	3274.450	3275.394	Fe I	P	$z\,^5F_4 - i\,^5D_4$
4	3275.180	3276.124	Ne II	CP	
3	3275.6718	3276.6158	Fe I	CA	$a\,^3G_3 - w\,^3H_4$
3	3275.8406	3276.7846	Fe I	CA	$b\,^3G_5 - 13\ _4$
5	3276.4696	3277.4138	Fe I	CA	$a\,^5P_2 - v\,^5F_2$
8	3278.7303	3279.6751	Fe I	CA	$b\,^3F_3 - v\,^3F_3$
8	3278.7403	3279.6851	Fe I	CA	$a\,^3P_1 - w\,^3P_1$
4	3279.7299	3280.6750	Fe I	CA	$b\,^3G_4 - t\,^3G_3$
50	3280.2593	3281.2045	Fe I	ED	$b\,^3H_4 - x\,^3I_5$
4	3280.7473	3281.6927	Fe I	CA	$b\,^3G_3 - w\,^1G_4$
3	3282.7165	3283.6623	Fe I	CA	$b\,^3G_5 - t\,^3G_4$
10	3282.8903	3283.8361	Fe I	CA	$a\,^3D_1 - u\,^3F_2$
4	3283.4180	3284.3640	Fe I	CA	$a\,^5F_3 - y\,^3D_3$
4	3283.543	3284.489		P	
8	3284.5872	3285.5335	Fe I	CA	$a\,^5P_2 - v\,^5P_2$
5	3285.1936	3286.1401	Fe I	CA	$z\,^7P_3 - g\,^7D_2$
8	3285.417	3286.363		P	
5	3286.0158	3286.9625	Fe I	CA	$a\,^5P_1 - v\,^5F_1$
4	3286.4450	3287.3918	Fe I	CA	$z\,^5F_3 - i\,^5D_3$
150	3286.7508	3287.6977	Fe I	SM	$a\,^5P_3 - v\,^5P_3$
8	3287.0900	3288.0369	Fe I	CA	$z\,^7P_4 - g\,^7D_4$
4	3288.6488	3289.5962	Fe I	CA	$a\,^3P_1 - w\,^3P_0$
3	3288.690	3289.637		P	
5	3288.9648	3289.9122	Fe I	CA	$a\,^5P_2 - v\,^5F_3$
2	3289.4327	3290.3802	Fe I	CA	$b\,^3P_2 - z\,^1P_1$
4	3290.7104	3291.6583	Fe I	CA	$a\,^5P_3 - v\,^5F_4$
12	3290.9879	3291.9358	Fe I	CA	$a\,^5P_1 - x\,^3P_2$
40	3292.0207	3292.9688	Fe I	CA	$a\,^3D_3 - u\,^3F_4$
20	3292.5893	3293.5376	Fe I	CA	$a\,^5P_1 - v\,^5P_1$
6	3293.1402	3294.0887	Fe I	CA	$a\,^3F_2 - z\,^5H_3$
4	3296.4640	3297.4134	Fe I	CA	$b\,^3F_3 - v\,^3F_2$
3	3296.8031	3297.7525	Fe I	CA	$b\,^3H_4 - v\,^1G_4$
15	3298.1316	3299.0814	Fe I	CA	$a\,^5P_1 - v\,^5F_2$
3	3299.076	3300.026	Fe I	P	$z\,^5F_3 - i\,^5D_4$
3	3299.5062	3300.4563	Fe I	CA	$a\,^3F_3 - x\,^5P_2$
4	3301.2176	3302.1681	Fe I	CA	$b\,^3P_1 - z\,^1P_1$
4	3301.441	3302.392		P	
4	3301.9128	3302.8635	Fe I	CA	$b\,^3H_6 - u\,^3H_5$
4	3303.529	3304.481		P	
5	3303.5684	3304.5196	Fe I	CA	$b\,^3G_3 - t\,^3G_3$
4	3303.774	3304.725		P	
120	3305.9700	3306.9217	Fe I	ED	$a\,^5P_2 - v\,^5P_3$
200	3306.3430	3307.2949	Fe I	CA	$a\,^1G_4 - w\,^1G_4$
200	3306.3571	3307.3090	Fe I	CA	$a\,^5P_1 - v\,^5P_2$
6	3306.4810	3307.4329	Fe I	CA	$a\,^3D_2 - u\,^3F_2$
5	3307.0055	3307.9575	Fe I	CA	$b\,^3G_5 - 12\ _5$
5	3307.144	3308.096		P	
25	3307.2331	3308.1852	Fe I	CA	$b\,^3H_6 - u\,^3H_6$

TABLE III. *Spectrum of the Fe-Ne hollow cathode*—Continued

Intensity	Wavelength (Å) Air	Wavelength (Å) Vacuum	Ion	Ref	Classification
5	3307.685	3308.638		P	
150	3309.737	3310.690	Ne II	CP	
10	3310.3415	3311.2944	Fe I	CA	$b\,^3G_5 - t\,^3G_5$
4	3310.4903	3311.4432	Fe I	CA	$a\,^3D_3 - u\,^3H_4$
20	3311.272	3312.225	Ne II	CP	
3	3311.4491	3312.4022	Fe I	CA	$a\,^5F_2 - y\,^3D_3$
3	3312.2226	3313.1759	Fe I	CA	$b\,^3G_4 - 13_4$
3	3313.7146	3314.6683	Fe I	CA	$a\,^3F_2 - y\,^5G_3$
3	3314.0647	3315.0185	Fe I	CA	$a\,^1P_1 - t\,^3F_2$
3	3314.4431	3315.3970	Fe I	CA	$b\,^3F_2 - v\,^3F_2$
5	3314.674	3315.628	Ne II	CP	
40	3314.7412	3315.6952	Fe I	CA	$a\,^3D_2 - u\,^3F_3$
4	3316.704	3317.659		P	
5	3317.1207	3318.0753	Fe I	CA	$a\,^3P_2 - x\,^3P_1$
5	3319.031	3319.986		P	
8	3319.2522	3320.2074	Fe I	CA	$b\,^3G_4 - t\,^3G_4$
500	3319.723	3320.678	Ne II	CP	
5	3320.197	3321.152	Ne II	CP	
3	3320.415	3321.370		P	
5	3320.6447	3321.6001	Fe I	CA	$a\,^3H_5 - y\,^3H_4$
5	3320.7756	3321.7312	Fe I	CA	$z\,^7P_2 - g\,^7D_2$
10	3322.471	3323.427	Fe I	P	$z\,^7P_4 - g\,^7D_5$
1000	3323.734	3324.690	Ne II	CP	
5	3324.184	3325.140		P	
15	3324.3695	3325.3259	Fe I	CA	$b\,^3H_5 - u\,^3H_4$
4	3324.485	3325.441		P	
12	3324.5369	3325.4934	Fe I	CA	$a\,^3H_6 - v\,^3G_5$
6	3325.4647	3326.4214	Fe I	CA	$a\,^3H_4 - v\,^3G_3$
4	3326.582	3327.539		P	
100	3327.152	3328.109	Ne II	CP	
5	3327.4953	3328.4525	Fe I	CA	$a\,^3H_6 - y\,^3H_6$
4	3327.667	3328.625		P	
5	3327.9516	3328.9089	Fe I	CA	$a\,^5P_3 - w\,^5G_4$
4	3328.287	3329.245		P	
5	3328.696	3329.653		P	
25	3328.8658	3329.8233	Fe I	CA	$b\,^3H_5 - u\,^3H_5$
4	3329.045	3330.002	Fe II	P	
30	3329.157	3330.115	Ne II	CP	
5	3329.5229	3330.4806	Fe I	CA	$a\,^1G_4 - t\,^3G_3$
5	3330.735	3331.693	Ne II	CP	
6	3331.6117	3332.5700	Fe I	CA	$a\,^3H_5 - v\,^3G_4$
5	3331.7760	3332.7343	Fe I	CA	$a\,^3P_0 - w\,^3P_1$
6	3334.141	3335.100		P	
8	3334.2188	3335.1777	Fe I	CA	$a\,^3H_5 - y\,^3H_5$
5	3334.2734	3335.2323	Fe I	CA	$b\,^3H_5 - u\,^3H_6$
600	3334.836	3335.795	Ne II	CP	
4	3335.3920	3336.3512	Fe I	CA	$b\,^3F_4 - x\,^1G_4$
12	3335.5097	3336.4689	Fe I	CA	$a\,^3F_3 - x\,^5P_3$
5	3335.714	3336.674		P	
6	3335.7680	3336.7274	Fe I	CA	$b\,^3P_1 - v\,^3P_2$
6	3336.092	3337.051	Ne II	CP	
5	3336.2567	3337.2162	Fe I	CA	$b\,^3H_4 - u\,^3F_4$
12	3337.6642	3338.6240	Fe I	CA	$a\,^3G_5 - u\,^3G_4$
5	3338.6208	3339.5809	Fe I	CA	$z\,^7P_3 - g\,^7D_4$
5	3339.1946	3340.1548	Fe I	CA	$a\,^3H_4 - y\,^3H_4$
4	3339.5777	3340.5380	Fe I	CA	$c\,^3P_2 - t\,^5P_1$
8	3340.5643	3341.5248	Fe I	CA	$a\,^3P_2 - x\,^3P_2$
15	3341.9060	3342.8669	Fe I	CA	$a\,^3G_5 - 6_5$
4	3342.140	3343.101		P	
6	3342.2142	3343.1752	Fe I	CA	$a\,^3P_2 - v\,^5P_1$
6	3342.2926	3343.2536	Fe I	CA	$b\,^3P_1 - 8_1$
4	3343.2361	3344.1974	Fe I	CA	$a\,^5P_3 - z\,^1G_4$
4	3343.508	3344.469		P	
4	3343.760	3344.721		P	
6	3344.938	3345.900		P	
800	3345.454	3346.415	Ne II	CP	
150	3345.829	3346.791	Ne II	CP	
8	3346.9346	3347.8968	Fe I	CA	$a\,^5P_3 - 1_2$
4	3347.4982	3348.4605	Fe I	CA	$b\,^3G_4 - t\,^3G_5$
8	3347.9251	3348.8875	Fe I	CA	$a\,^3P_2 - v\,^5F_2$
4	3349.7273	3350.6901	Fe I	CA	$b\,^3P_2 - t\,^3D_2$
4	3350.2564	3351.2194	Fe I	CA	$a\,^3H_5 - v\,^3G_5$
6	3351.5219	3352.4852	Fe I	CA	$a\,^5P_2 - y\,^3S_1$
8	3351.7433	3352.7067	Fe I	CA	$a\,^3G_4 - u\,^3G_3$
8	3351.7492	3352.7126	Ne I	KE	
4	3352.9211	3353.8848	Fe I	CA	$a\,^3H_4 - y\,^3H_5$
3	3353.2607	3354.2245	Fe I	CA	$a\,^3H_5 - y\,^3H_6$
4	3353.567	3354.531	Ne II	CP	
6	3354.0598	3355.0238	Fe I	CA	$b\,^3P_0 - 8_1$
4	3355.018	3355.982	Ne II	CP	
400	3355.2275	3356.1918	Fe I	CA	$b\,^3H_4 - u\,^3H_4$
80	3355.5173	3356.4817	Fe I	CA	$a\,^5F_3 - y\,^3F_2$
5	3356.3196	3357.2841	Fe I	CA	$a\,^5F_4 - y\,^3F_3$
5	3356.4011	3357.3657	Fe I	CA	$a\,^3P_2 - v\,^5P_2$
4	3356.685	3357.649	Fe I	P	$a\,^1G_4 - e\,X_3$
15	3357.82	3358.78	Bl	P	
4	3359.4870	3360.4523	Fe I	CA	$a\,^5F_5 - y\,^3F_4$
4	3359.8077	3360.7731	Fe I	CA	$b\,^3H_4 - u\,^3H_5$
4	3360.272	3361.237	Fe II	P	
5	3360.461	3361.426		P	
100	3360.595	3361.561	Ne II	CP	
4	3360.9272	3361.8929	Fe I	CA	$a\,^3P_1 - v\,^3D_1$
10	3361.9489	3362.9149	Fe I	CA	$b\,^3P_1 - t\,^3D_2$
4	3362.161	3363.127		P	
4	3362.267	3363.233		P	
5	3362.708	3363.674		P	
8	3362.938	3363.904	Ne II	CP	
4	3363.405	3364.371		P	
4	3363.8105	3364.7770	Fe I	CA	$a\,^3G_3 - u\,^3D_3$
4	3364.264	3365.231		P	
4	3364.6326	3365.5993	Fe I	CA	$b\,^3F_3 - z\,^1F_3$
30	3366.7860	3367.7532	Fe I	CA	$a\,^3G_5 - 4_4$
30	3366.8647	3367.8320	Fe I	CA	$a\,^5P_2 - 1_2$
5	3366.981	3367.949	Fe II	P	
5	3367.1564	3368.1238	Fe I	CA	$a\,^3P_1 - v\,^3D_2$
80	3367.216	3368.184	Ne II	CP	
5	3368.172	3369.140		P	
5	3368.9712	3369.9390	Fe I	CA	$b\,^3P_2 - u\,^3D_1$
5	3369.1395	3370.1074	Fe I	CA	$a\,^3H_4 - v\,^3G_5$
60	3369.5463	3370.5142	Fe I	CA	$a\,^3G_4 - u\,^3G_4$
120	3369.8080	3370.7760	Ne I	KE	
400	3369.9078	3370.8758	Ne I	KE	
5	3370.081	3371.049		P	
3	3370.560	3371.528		P	
3	3370.613	3371.581		P	
120	3370.7829	3371.7512	Fe I	CA	$a\,^3G_5 - u\,^3G_5$
4	3371.485	3372.454		P	
20	3371.797	3372.765	Ne II	CP	
6	3372.0723	3373.0409	Fe I	CA	$a\,^5P_3 - x\,^3F_2$
4	3372.3432	3373.3118	Fe I	CA	$b\,^3G_4 - x\,^1F_3$
4	3372.856	3373.825		P	
4	3373.8696	3374.8387	Fe I	CA	$a\,^3G_4 - 6_5$
5	3374.062	3375.031	Ne II	CP	
3	3374.191	3375.160		P	
3	3374.443	3375.412		P	
15	3375.6490	3376.6185	Ne I	KE	
6	3376.489	3377.459		P	
6	3377.155	3378.125	Ne II	CP	

TABLE III. *Spectrum of the Fe-Ne hollow cathode*—Continued

Intensity	Wavelength (Å)		Ion	Ref	Classification
	Air	Vacuum			
15	3377.977	3378.947	Fe I	P	
800	3378.217	3379.187	Ne II	CP	
50	3378.6785	3379.6488	Fe I	CA	$a\ ^3G_5 - v\ ^3F_4$
3	3378.732	3379.702		P	
25	3379.0184	3379.9887	Fe I	CA	$a\ ^5P_3 - w\ ^3D_2$
8	3379.319	3380.290	Ne II	CP	
50	3380.1097	3381.0803	Fe I	CA	$a\ ^3G_3 - u\ ^3G_3$
3	3380.748	3381.719	Fe I	P	
3	3381.12	3382.09	Bl	P	
3	3381.3259	3382.2968	Fe I	CA	$a\ ^3D_3 - w\ ^1F_3$
10	3382.4019	3383.3732	Fe I	CA	$a\ ^5P_3 - z\ ^3H_4$
4	3382.463	3383.434		P	
4	3382.716	3383.687		P	
20	3383.6919	3384.6634	Fe I	CA	$a\ ^5P_2 - w\ ^3D_1$
60	3383.9785	3384.9502	Fe I	CA	$a\ ^5P_3 - x\ ^3F_3$
5	3385.436	3386.408		P	
4	3385.545	3386.517		P	
4	3386.202	3387.175	Ne II	CP	
12	3387.4062	3388.3787	Fe I	CA	$a\ ^3G_3 - x\ ^1D_2$
4	3387.618	3388.590		P	
50	3388.419	3389.392	Ne II	CP	
3	3388.618	3389.591		P	
8	3388.9678	3389.9408	Fe I	CA	$c\ ^3P_1 - t\ ^5P_1$
12	3389.7426	3390.7158	Fe I	CA	$a\ ^5P_1 - 1\ _2$
5	3390.551	3391.525	Ne II	CP	
4	3390.627	3391.601		P	
10	3392.0090	3392.9827	Fe I	CA	$c\ ^3P_2 - v\ ^3P_1$
50	3392.3037	3393.2775	Fe I	CA	$a\ ^5P_2 - x\ ^3F_2$
150	3392.6514	3393.6252	Fe I	CA	$a\ ^5P_3 - w\ ^3D_3$
600	3392.799	3393.773	Ne II	CP	
6	3392.986	3393.960		P	
12	3393.182	3394.156		P	
5	3393.3781	3394.3521	Fe I	CA	$b\ ^3P_0 - u\ ^3D_1$
4	3393.9156	3394.8898	Fe I	CA	$a\ ^3P_2 - x\ ^3G_3$
4	3394.0771	3395.0513	Fe I	CA	$a\ ^3H_4 - w\ ^3F_3$
20	3394.5833	3395.5576	Fe I	CA	$a\ ^5P_2 - u\ ^5D_1$
4	3396.3777	3397.3525	Fe I	CA	$a\ ^5F_3 - y\ ^3F_3$
5	3396.9759	3397.9509	Fe I	CA	$a\ ^5F_3 - y\ ^5P_2$
5	3397.2055	3398.1805	Fe I	CA	$c\ ^3P_2 - x\ ^1F_3$
5	3397.5521	3398.5272	Fe I	CA	$b\ ^3G_3 - x\ ^1F_3$
5	3397.6385	3398.6136	Fe I	CA	$a\ ^5F_2 - y\ ^5P_1$
4	3397.866	3398.841	Ne II	CP	
5	3398.2161	3399.1913	Fe I	CA	$a\ ^3G_3 - u\ ^3G_4$
5	3398.625	3399.601	Fe I	P	
5	3398.824	3399.799		P	
4	3399.156	3400.132		P	
5	3399.2296	3400.2051	Fe I	CA	$a\ ^3G_4 - 4\ _4$
150	3399.3335	3400.3090	Fe I	CA	$a\ ^5P_2 - w\ ^3D_2$
4	3400.042	3401.018		P	
10	3401.5184	3402.4945	Fe I	CA	$a\ ^5F_4 - y\ ^5P_3$
20	3402.255	3403.231	Fe I	P	$b\ ^3H_6 - v\ ^3H_6$
5	3403.3039	3404.2805	Fe I	CA	$a\ ^3G_4 - u\ ^3G_5$
5	3404.2699	3405.2467	Fe I	CA	$a\ ^5F_1 - y\ ^3F_2$
5	3404.3007	3405.2775	Fe I	CA	$a\ ^3G_4 - v\ ^3F_3$
80	3404.3535	3405.3304	Fe I	CA	$a\ ^5P_2 - x\ ^3F_3$
15	3404.759	3405.736	Fe I	P	$a\ ^3G_4 - t\ ^5D_3$
5	3404.821	3405.798		P	
5	3404.890	3405.867	Fe I	P	
5	3405.572	3406.550		P	
10	3405.8319	3406.8091	Fe I	CA	$a\ ^3G_5 - x\ ^3H_5$
8	3406.4365	3407.4139	Fe I	CA	$a\ ^3D_1 - w\ ^1D_2$
25	3406.7999	3407.7773	Fe I	CA	$a\ ^5P_1 - w\ ^3D_1$
20	3406.946	3407.924	Ne II	CP	
500	3407.4585	3408.4361	Fe I	CA	$a\ ^5P_3 - x\ ^3F_4$
4	3407.530	3408.508		P	
4	3409.2082	3410.1863	Fe I	CA	$b\ ^3H_6 - v\ ^3H_5$
4	3410.0270	3411.0053	Fe I	CA	$a\ ^1G_4 - 10\ _3$
12	3410.1683	3411.1466	Fe I	CA	$a\ ^1P_1 - u\ ^3F_2$
5	3410.8957	3411.8742	Fe I	CA	$a\ ^5F_4 - y\ ^3F_4$
6	3411.1264	3412.1050	Fe I	CA	$a\ ^3G_5 - x\ ^3H_6$
15	3411.3528	3412.3314	Fe I	CA	$a\ ^3G_4 - v\ ^3F_4$
250	3413.1312	3414.1103	Fe I	CA	$a\ ^5P_2 - w\ ^3D_3$
12	3414.501	3415.481		P	
5	3414.764	3415.743		P	
5	3414.888	3415.868	Ne II	CP	
12	3415.5299	3416.5096	Fe I	CA	$a\ ^5P_1 - x\ ^3F_2$
6	3416.047	3417.027	Fe II	P	
5	3416.283	3417.263		P	
4	3416.6775	3417.6575	Fe I	CA	$a\ ^3P_0 - v\ ^3D_1$
10	3416.912	3417.893	Ne II	CP	
5	3417.131	3418.111		P	
6	3417.689	3418.669	Ne II	CP	
40	3417.8408	3418.8211	Fe I	CA	$a\ ^5P_1 - u\ ^5D_1$
500	3417.9035	3418.8839	Ne I	KE	
150	3418.0062	3418.9865	Ne I	KE	
10	3418.164	3419.145	Fe I	P	$z\ ^5D_1 - e\ ^3P_0$
40	3418.508	3419.489	Fe I	P	$a\ ^5P_1 - u\ ^5D_0$
5	3418.867	3419.847		P	
5	3419.146	3420.127	Fe I	P	$z\ ^5D_3 - f\ ^3F_2$
4	3419.6943	3420.6750	Fe I	CA	$b\ ^3P_1 - t\ ^3D_1$
4	3422.118	3423.100	Fe I	P	
15	3422.493	3423.474	Fe I	P	$b\ ^3G_4 - 9\ _4$
30	3422.6563	3423.6378	Fe I	CA	$a\ ^5P_1 - w\ ^3D_2$
4	3423.571	3424.553	Fe I	P	
50	3423.9126	3424.8944	Ne I	KE	
60	3424.2840	3425.2660	Fe I	CA	$a\ ^5P_3 - u\ ^5D_3$
20	3425.0104	3425.9925	Fe I	CA	$a\ ^1G_4 - x\ ^1F_3$
4	3425.672	3426.655		P	
12	3426.3257	3427.3081	Fe I	CA	$a\ ^3P_2 - y\ ^3S_1$
20	3426.3793	3427.3618	Fe I	CA	$a\ ^5F_2 - y\ ^3F_3$
20	3426.3872	3427.3697	Fe I	CA	$a\ ^5P_3 - y\ ^3P_2$
25	3426.6285	3427.6110	Fe I	CA	$a\ ^5P_2 - y\ ^3P_1$
6	3426.666	3427.649		P	
5	3426.9882	3427.9708	Fe I	CA	$a\ ^5F_2 - y\ ^5P_2$
500	3427.1192	3428.1019	Fe I	CA	$a\ ^5P_3 - u\ ^5D_4$
10	3427.193	3428.176		P	
4	3427.834	3428.817		P	
5	3428.011	3428.994		P	
4	3428.1925	3429.1755	Fe I	CA	$a\ ^5P_2 - u\ ^5D_2$
5	3428.228	3429.211		P	
5	3428.409	3429.391		P	
5	3428.452	3429.435		P	
6	3428.498	3429.481		P	
10	3428.686	3429.669		P	
60	3428.7485	3429.7316	Fe I	CA	$z\ ^5P_3 - 4\ _2$
20	3429.491	3430.474		P	
8	3431.8135	3432.7973	Fe I	CA	$b\ ^3P_2 - u\ ^3D_3$
8	3431.8431	3432.8270	Fe I	CA	$a\ ^3D_2 - w\ ^1D_2$
8	3433.568	3434.552		P	
6	3436.0363	3437.0213	Fe I	CA	$b\ ^3H_5 - v\ ^3H_4$
5	3436.467	3437.452		P	
12	3437.045	3438.030	Fe I	P	$a\ ^1G_4 - y\ ^1F_3$
5	3437.6243	3438.6097	Fe I	CA	$a\ ^3H_5 - y\ ^1G_4$
6	3437.9488	3438.9342	Fe I	CA	$b\ ^3H_5 - v\ ^3H_5$
12	3438.308	3439.293	Fe I	P	
8	3438.933	3439.919	Ne II	CP	
6	3439.0360	3440.0217	Fe I	CA	$a\ ^3G_4 - x\ ^3H_5$
12	3439.887	3440.873		P	

TABLE III. *Spectrum of the Fe-Ne hollow cathode*—Continued

Intensity	Wavelength (Å) Air	Wavelength (Å) Vacuum	Ion	Ref	Classification
6000	3440.6058	3441.5919	Fe I	CA	$a\,^5D_4 - z\,^5P_3$
2500	3440.9887	3441.9749	Fe I	CA	$a\,^5D_3 - z\,^5P_2$
6	3441.223	3442.210		P	
6	3441.905	3442.892	Fe II	P	
6	3442.141	3443.127		P	
20	3442.3626	3443.3492	Fe I	CA	$a\,^3P_2 - 1\ _2$
6	3442.6692	3443.6559	Fe I	CA	$a\,^5F_3 - y\,^5P_3$
3	3442.9671	3443.9538	Fe I	CA	$a\,^1D_2 - t\,^3F_3$
3	3442.9739	3443.9606	Fe I	CA	$c\,^3P_1 - v\,^3P_1$
5	3443.706	3444.693	Ne II	CP	
1000	3443.8762	3444.8632	Fe I	CA	$a\,^5D_2 - z\,^5P_1$
5	3444.166	3445.153		P	
6	3444.431	3445.418		P	
200	3445.1487	3446.1360	Fe I	CA	$a\,^5P_2 - u\,^5D_3$
8	3445.763	3446.750		P	
8	3445.867	3446.855		P	
5	3446.027	3447.014		P	
4	3446.261	3447.249		P	
5	3446.7864	3447.7741	Fe I	CA	$b\,^3F_2 - w\,^3P_1$
4	3446.9496	3447.9374	Fe I	CA	$a\,^5F_1 - y\,^5P_2$
25	3447.2776	3448.2655	Fe I	CA	$a\,^5P_2 - y\,^3P_2$
600	3447.7028	3448.6908	Ne I	KE	
6	3447.999	3448.987		P	
4	3448.421	3449.409	Fe II	P	
4	3449.074	3450.063		P	
4	3449.409	3450.398		P	
5	3449.469	3450.457		P	
5	3449.650	3450.638		P	
25	3450.3286	3451.3173	Fe I	CA	$a\,^5P_1 - y\,^3P_1$
80	3450.7650	3451.7537	Ne I	KE	
5	3451.345	3452.333	Fe II	P	
6	3451.61	3452.60	Bl	P	
25	3451.9144	3452.9035	Fe I	CA	$a\,^5P_1 - u\,^5D_2$
20	3452.2751	3453.2642	Fe I	CA	$a\,^5F_3 - y\,^3F_4$
15	3453.0206	3454.0099	Fe I	CA	$a\,^3G_3 - v\,^3F_2$
5	3453.066	3454.057	Ne II	CP	
15	3453.615	3454.604	Fe II	P	
500	3454.1949	3455.1845	Ne I	KE	
10	3454.772	3455.762		P	
5	3456.245	3457.235		P	
10	3456.608	3457.598	Ne II	CP	
5	3457.004	3457.995	Fe II	P	
8	3457.0863	3458.0767	Fe I	CA	$z\,^5P_3 - i\,^5D_2$
5	3457.5081	3458.4985	Fe I	CA	$a\,^3H_4 - y\,^1G_4$
10	3458.3041	3459.2948	Fe I	CA	$a\,^3P_1 - x\,^3P_0$
12	3459.321	3460.312	Ne II	CP	
8	3459.4272	3460.4181	Fe I	CA	$a\,^3G_5 - x\,^1G_4$
6	3459.742	3460.733		P	
10	3459.9131	3460.9042	Fe I	CA	$c\,^3P_2 - z\,^1P_1$
5	3460.438	3461.429		P	
250	3460.5243	3461.5156	Ne I	KE	
6	3461.652	3462.644		P	
5	3462.3517	3463.3434	Fe I	CA	$a\,^5P_2 - z\,^3S_1$
6	3462.8125	3463.8043	Fe I	CA	$b\,^3P_2 - y\,^1D_2$
5	3463.3013	3464.2932	Fe I	CA	$a\,^3F_4 - x\,^5F_3$
300	3464.3387	3465.3309	Ne I	KE	
2	3464.9126	3465.9049	Fe I	CA	$b\,^3F_3 - y\,^3H_4$
1200	3465.8603	3466.8529	Fe I	CA	$a\,^5D_1 - z\,^5P_1$
4	3466.2806	3467.2733	Fe I	CA	$a\,^3H_6 - w\,^3G_5$
0	3466.4984	3467.4911	Fe I	CA	$a\,^5F_5 - z\,^3G_4$
300	3466.5787	3467.5715	Ne I	KE	
10	3468.8456	3469.8390	Fe I	CA	$b\,^3F_4 - v\,^3G_5$
8	3469.0124	3470.0058	Fe I	CA	$b\,^3H_4 - v\,^3H_4$
25	3469.3899	3470.3834	Fe I	CA	$b\,^3P_1 - x\,^1D_2$
12	3469.8310	3470.8246	Fe I	CA	$b\,^3F_2 - v\,^3G_3$
15	3471.2653	3472.2593	Fe I	CA	$a\,^5P_1 - y\,^3P_2$
15	3471.3435	3472.3375	Fe I	CA	$a\,^3P_2 - u\,^5D_1$
600	3472.5711	3473.5654	Ne I	KE	
2000	3475.4500	3476.4451	Fe I	CA	$a\,^5D_2 - z\,^5P_2$
20	3475.650	3476.645	Fe I	P	$a\,^5P_3 - w\,^5P_2$
25	3475.8638	3476.8590	Fe I	CA	$a\,^3H_5 - z\,^1H_5$
25	3475.8748	3476.8700	Fe I	CA	$b\,^3P_1 - y\,^1D_2$
10	3476.345	3477.340	Fe I	P	
500	3476.7016	3477.6970	Fe I	CA	$a\,^5D_0 - z\,^5P_1$
15	3476.8549	3477.8503	Fe I	CA	$b\,^3F_3 - v\,^3G_4$
6	3477.0034	3477.9989	Fe I	CA	$a\,^3P_1 - x\,^3P_2$
8	3477.647	3478.643	Ne II	CP	
6	3477.8518	3478.8475	Fe I	CA	$a\,^5P_1 - y\,^3P_0$
6	3478.3697	3479.3655	Fe I	CA	$a\,^3H_5 - w\,^3G_4$
200	3481.934	3482.930	Ne II	CP	
6	3483.0071	3484.0041	Fe I	CA	$a\,^5F_4 - z\,^3G_3$
6	3484.8506	3485.8480	Fe I	CA	$a\,^3H_4 - w\,^3G_3$
6	3484.9785	3485.9760	Fe I	CA	$a\,^3P_1 - v\,^5F_2$
12	3485.3397	3486.3373	Fe I	ED	$a\,^5P_2 - w\,^5P_1$
3	3486.5503	3487.5482	Fe I	CA	$a\,^5P_1 - z\,^3S_1$
12	3489.6701	3490.6688	Fe I	CA	$b\,^3G_5 - w\,^3H_6$
2500	3490.5737	3491.5727	Fe I	CA	$a\,^5D_3 - z\,^5P_3$
2	3493.2808	3494.2804	Fe I	CA	$a\,^3F_4 - x\,^5F_4$
6	3493.6897	3494.6895	Fe I	CA	$a\,^3G_4 - x\,^1G_4$
6	3494.1636	3495.1635	Fe I	CA	$a\,^3P_1 - v\,^5P_2$
25	3495.2867	3496.2868	Fe I	CA	$b\,^3F_4 - w\,^3F_3$
4	3496.1936	3497.1940	Fe I	CA	$a\,^3H_4 - z\,^1H_5$
30	3497.1008	3498.1014	Fe I	CA	$a\,^5P_3 - w\,^5P_3$
500	3497.8404	3498.8412	Fe I	CA	$a\,^5D_1 - z\,^5P_2$
250	3498.0640	3499.0649	Ne I	KE	
5	3500.5661	3501.5676	Fe I	CA	$b\,^3F_3 - w\,^3F_2$
300	3501.2163	3502.2180	Ne I	KE	
4	3504.8614	3505.8640	Fe I	CA	$a\,^3P_2 - y\,^3P_1$
15	3506.4977	3507.5008	Fe I	CA	$a\,^3P_2 - u\,^5D_2$
10	3508.5179	3509.5214	Fe I	CA	$b\,^3F_4 - v\,^3D_3$
5	3510.4388	3511.4429	Fe I	CA	$a\,^3P_0 - x\,^3P_1$
80	3510.7212	3511.7253	Ne I	KE	
20	3511.580	3512.584	Ne II	CP	
3	3511.7385	3512.7429	Fe I	CA	$b\,^3F_4 - w\,^3F_4$
2	3512.0823	3513.0867	Fe I	CA	$z\,^7F_4 - f\,^5F_4$
3	3512.2249	3513.2294	Fe I	CA	$z\,^7F_4 - e\,^7G_3$
3	3512.9548	3513.9595	Fe I	CA	$c\,^3P_1 - z\,^1P_1$
0	3513.0543	3514.0590	Fe I	CA	$a\,^3F_3 - x\,^5F_2$
250	3513.8173	3514.8222	Fe I	CA	$a\,^5F_5 - z\,^3G_5$
3	3514.6280	3515.6332	Fe I	CA	$a\,^3H_6 - x\,^3G_5$
250	3515.1907	3516.1960	Ne I	KE	
10	3516.4106	3517.4162	Fe I	CA	$b\,^3G_3 - w\,^3H_4$
6	3516.5571	3517.5627	Fe I	CA	$z\,^7F_3 - e\,^7G_2$
8	3518.6823	3519.6885	Fe I	CA	$z\,^7F_2 - f\,^5F_3$
5	3518.818	3519.824	Fe I	P	$a\,^5P_2 - w\,^5P_3$
1500	3520.4717	3521.4783	Ne I	KE	
6	3520.8472	3521.8539	Fe I	CA	$b\,^3F_2 - w\,^3F_2$
300	3521.2608	3522.2677	Fe I	CA	$a\,^5F_4 - z\,^3G_4$
5	3521.837	3522.844	Fe I	P	$a\,^5P_1 - w\,^5P_2$
10	3522.2675	3523.2746	Fe I	CA	$z\,^7F_5 - e\,^7G_5$
4	3522.9005	3523.9077	Fe I	CA	$z\,^7F_2 - e\,^7S_3$
4	3523.312	3524.319	Fe I	P	$z\,^7F_2 - e\,^7G_1$
20	3524.0775	3525.0850	Fe I	CA	$b\,^3F_3 - v\,^3D_2$
15	3524.2394	3525.2470	Fe I	CA	$a\,^3P_2 - u\,^5D_3$
400	3526.0405	3527.0485	Fe I	CA	$a\,^5D_2 - z\,^5P_3$
100	3526.1656	3527.1737	Fe I	CA	$a\,^5F_3 - z\,^3G_3$
60	3526.2373	3527.2454	Fe I	CA	$z\,^7F_3 - f\,^5F_4$
60	3526.3811	3527.3892	Fe I	CA	$z\,^7F_3 - e\,^7G_3$

TABLE III. *Spectrum of the Fe-Ne hollow cathode*—Continued

Intensity	Wavelength (Å) Air	Wavelength (Å) Vacuum	Ion	Ref	Classification
60	3526.4671	3527.4753	Fe I	CA	$a\ ^3P_2 - y\ ^3P_2$
30	3526.6751	3527.6833	Fe I	CA	$z\ ^7F_2 - e\ ^7G_2$
25	3527.7930	3528.8016	Fe I	CA	$z\ ^7F_4 - e\ ^7G_4$
6	3529.5258	3530.5347	Fe I	CA	$a\ ^1G_4 - y\ ^3I_5$
20	3529.820	3530.829	Fe I	P	$z\ ^7F_1 - e\ ^7G_1$
12	3530.3878	3531.3970	Fe I	CA	$z\ ^7F_6 - e\ ^7G_6$
4	3531.4368	3532.4462	Fe I	CA	$a\ ^3H_5 - v\ ^5F_4$
25	3533.007	3534.017	Fe I	P	$z\ ^7F_0 - e\ ^7G_1$
100	3533.1986	3534.2085	Fe I	CA	$z\ ^7F_1 - e\ ^7G_2$
5	3534.527	3535.537	Fe I	P	$a\ ^1H_5 - x\ ^3I_5$
200	3536.5558	3537.5666	Fe I	CA	$z\ ^7F_2 - e\ ^7G_3$
5	3537.4919	3538.5029	Fe I	CA	$b\ ^3F_3 - v\ ^3D_3$
15	3537.7302	3538.7413	Fe I	CA	$b\ ^3F_2 - v\ ^3D_1$
25	3537.8951	3538.9062	Fe I	CA	$z\ ^7F_5 - f\ ^5F_5$
4	3538.3040	3539.3152	Fe I	CA	$a\ ^1D_2 - u\ ^3F_2$
0	3538.5546	3539.5659	Fe I	CA	$a\ ^3P_0 - v\ ^5P_1$
6	3538.781	3539.792	Fe I	P	$a\ ^1H_5 - x\ ^3I_6$
20	3540.1207	3541.1324	Fe I	CA	$z\ ^7F_3 - g\ ^5D_4$
10	3540.7094	3541.7212	Fe I	CA	$a\ ^5F_4 - z\ ^5G_3$
300	3541.0832	3542.0951	Fe I	CA	$z\ ^7F_4 - e\ ^7G_5$
250	3542.0752	3543.0874	Fe I	CA	$z\ ^7F_3 - e\ ^7G_4$
15	3542.2433	3543.2555	Fe I	CA	$a\ ^3P_2 - z\ ^3S_1$
4	3543.3853	3544.3979	Fe I	CA	$a\ ^3H_5 - x\ ^3G_5$
6	3543.6743	3544.6869	Fe I	CA	$a\ ^1P_1 - w\ ^1D_2$
5	3544.6327	3545.6456	Fe I	CA	$b\ ^3F_2 - v\ ^3D_2$
20	3545.6403	3546.6534	Fe I	CA	$z\ ^7F_4 - e\ ^7F_4$
4	3545.8318	3546.8450	Fe I	CA	$a\ ^1G_4 - w\ ^3H_4$
3	3546.2040	3547.2172	Fe I	CA	$a\ ^3H_5 - x\ ^3G_4$
5	3547.1950	3548.2085	Fe I	CA	$b\ ^3H_4 - w\ ^1G_4$
5	3547.2238	3548.2373	Fe I	CA	$z\ ^7F_6 - e\ ^7F_5$
5	3548.0197	3549.0334	Fe I	CA	$c\ ^3P_2 - u\ ^3D_1$
2	3549.8601	3550.8743	Fe I	CA	$a\ ^3F_2 - x\ ^5F_1$
8	3552.1056	3553.1203	Fe I	CA	$c\ ^3P_1 - v\ ^3P_2$
12	3552.8287	3553.8437	Fe I	CA	$z\ ^7F_2 - e\ ^7F_2$
80	3553.7390	3554.7541	Fe I	CA	$a\ ^1H_5 - v\ ^1G_4$
5	3554.1175	3555.1328	Fe I	CA	$a\ ^5F_3 - z\ ^5G_2$
8	3554.5027	3555.5181	Fe I	CA	$z\ ^7F_1 - e\ ^5G_2$
400	3554.9247	3555.9402	Fe I	CA	$z\ ^7F_5 - e\ ^7G_6$
6	3556.6799	3557.6958	Fe I	CA	$z\ ^7F_3 - e\ ^5G_3$
200	3556.8785	3557.8945	Fe I	CA	$z\ ^7F_4 - f\ ^5F_5$
400	3558.5148	3559.5312	Fe I	CA	$a\ ^5F_2 - z\ ^3G_3$
5	3559.5048	3560.5215	Fe I	CA	$c\ ^3P_1 - 8\ 1$
10	3560.6972	3561.7141	Fe I	CA	$a\ ^3D_3 - 13\ 4$
2	3564.1078	3565.1257	Fe I	CA	$a\ ^3F_2 - x\ ^5F_2$
1000	3565.3786	3566.3967	Fe I	CA	$a\ ^5F_3 - z\ ^3G_4$
50	3565.5800	3566.5982	Fe I	CA	$z\ ^7F_3 - e\ ^7F_3$
4	3566.5793	3567.5978	Fe I	CA	$a\ ^3H_6 - w\ ^5G_5$
10	3567.0304	3568.0491	Fe I	CA	$z\ ^7F_2 - e\ ^5G_3$
10	3567.3673	3568.3860	Fe I	CA	$a\ ^3H_4 - x\ ^3G_4$
15	3568.8223	3569.8413	Fe I	CA	$a\ ^3D_3 - t\ ^3G_4$
10	3568.9755	3569.9946	Fe I	CA	$a\ ^3G_5 - y\ ^3H_4$
0	3570.0106	3571.0299	Fe I	CA	$a\ ^3P_1 - y\ ^3S_1$
1200	3570.0971	3571.1165	Fe I	CA	$a\ ^5F_4 - z\ ^3G_5$
800	3570.255	3571.274	Fe I	P	$z\ ^7F_6 - e\ ^7G_7$
12	3571.2241	3572.2438	Fe I	CA	$a\ ^3F_4 - x\ ^5D_3$
120	3571.9961	3573.0160	Fe I	CA	$z\ ^7F_5 - e\ ^7F_5$
8	3572.5908	3573.6108	Fe I	CA	$z\ ^7F_4 - e\ ^5G_4$
100	3573.3934	3574.4137	Fe I	CA	$a\ ^3D_2 - t\ ^3G_3$
60	3573.8292	3574.8496	Fe I	CA	$a\ ^3H_6 - w\ ^5G_6$
60	3573.8883	3574.9087	Fe I	CA	$b\ ^3H_4 - t\ ^3G_3$
250	3574.62	3575.64	Bl	P	
5	3575.1135	3576.1342	Fe I	CA	$z\ ^7F_1 - e\ ^7F_1$
12	3575.2456	3576.2664	Fe I	CA	$z\ ^7F_5 - f\ ^7D_4$
15	3575.3713	3576.3921	Fe I	CA	$c\ ^3P_2 - u\ ^3D_2$
10	3575.9794	3577.0003	Fe I	CA	$z\ ^7F_2 - e\ ^5S_2$
10	3575.9824	3577.0033	Fe I	CA	$z\ ^7F_2 - e\ ^7F_3$
30	3576.7586	3577.7797	Fe I	CA	$b\ ^3H_5 - 13\ 4$
2	3578.3818	3579.4033	Fe I	CA	$z\ ^7F_0 - e\ ^7F_1$
4000	3581.1925	3582.2148	Fe I	SD	$a\ ^5F_5 - z\ ^5G_6$
15	3581.6472	3582.6696	Fe I	CA	$a\ ^3G_5 - v\ ^3G_4$
10	3581.8073	3582.8298	Fe I	CA	$c\ ^3P_1 - t\ ^3D_2$
150	3582.1995	3583.2220	Fe I	CA	$b\ ^3H_6 - 12\ 5$
2	3582.5668	3583.5894	Fe I	CA	$a\ ^3H_4 - w\ ^5G_3$
4	3582.6867	3583.7094	Fe I	CA	$z\ ^7F_1 - e\ ^5S_2$
12	3583.326	3584.349	Fe I	P	$z\ ^5D_0 - f\ ^3D_1$
150	3584.6604	3585.6836	Fe I	CA	$a\ ^3G_5 - y\ ^3H_5$
2	3584.7865	3585.8097	Fe I	CA	$z\ ^7F_3 - f\ ^7D_2$
120	3584.9290	3585.9522	Fe I	CA	$z\ ^7P_3 - e\ ^5P_2$
120	3584.9572	3585.9805	Fe I	CA	$b\ ^3H_5 - t\ ^3G_4$
1	3585.1887	3586.2120	Fe I	CA	$b\ ^3G_5 - u\ ^3G_4$
300	3585.3189	3586.3422	Fe I	CA	$a\ ^5F_3 - z\ ^5G_3$
150	3585.7052	3586.7286	Fe I	CA	$a\ ^5F_4 - z\ ^5G_4$
200	3586.1030	3587.1265	Fe I	CA	$c\ ^3P_2 - t\ ^3D_3$
200	3586.1141	3587.1376	Fe I	CA	$b\ ^3H_6 - t\ ^3G_5$
15	3586.7387	3587.7624	Fe I	CA	$z\ ^7F_6 - e\ ^5G_6$
400	3586.9840	3588.0077	Fe I	CA	$a\ ^5F_2 - z\ ^5G_2$
15	3587.2387	3588.2626	Fe I	CA	$z\ ^7F_3 - e\ ^5G_4$
15	3587.4241	3588.4479	Fe I	CA	$a\ ^3P_1 - 1\ 2$
40	3587.7606	3588.7845	Fe I	CA	$a\ ^3D_1 - t\ ^5P_1$
50	3588.6093	3589.6335	Fe I	CA	$z\ ^7F_5 - e\ ^5G_5$
12	3588.9161	3589.9403	Fe I	CA	$z\ ^7F_2 - f\ ^7D_1$
20	3589.1050	3590.1293	Fe I	CA	$a\ ^5F_5 - z\ ^5G_5$
15	3589.4523	3590.4767	Fe I	CA	$a\ ^3G_4 - v\ ^3G_3$
6	3590.0834	3591.1080	Fe I	CA	$b\ ^3G_5 - 6\ 5$
4	3591.0006	3592.0254	Fe I	CA	$z\ ^5D_4 - e\ ^3G_5$
10	3591.3482	3592.3731	Fe I	CA	$z\ ^7F_4 - e\ ^7F_5$
3	3591.4823	3592.5073	Fe I	CA	$z\ ^5D_0 - g\ ^5F_1$
3	3592.4723	3593.4974	Fe I	CA	$b\ ^3F_3 - y\ ^1G_4$
4	3592.672	3593.697	Fe I	P	$z\ ^5D_3 - h\ ^5D_2$
2	3592.8933	3593.9186	Fe I	CA	$a\ ^5P_2 - x\ ^3D_1$
6	3593.3247	3594.3501	Fe I	CA	$z\ ^5D_2 - f\ ^5G_3$
500	3593.5262	3594.5516	Ne I	KE	
300	3593.6396	3594.6651	Ne I	KE	
100	3594.6331	3595.6588	Fe I	CA	$z\ ^7F_4 - f\ ^7D_4$
5	3595.3016	3596.3275	Fe I	CA	$z\ ^7F_2 - f\ ^7D_2$
3	3595.8630	3596.8890	Fe I	CA	$a\ ^3H_4 - w\ ^5G_4$
12	3596.1966	3597.2227	Fe I	CA	$a\ ^3H_5 - w\ ^5G_5$
6	3597.0201	3598.0465	Fe I	CA	$z\ ^5D_2 - h\ ^5D_1$
12	3598.715	3599.742	Fe I	P	$a\ ^3D_3 - 11\ 3$
2	3598.9277	3599.9545	Fe I	CA	$z\ ^5D_1 - g\ ^5F_2$
3	3598.9781	3600.0049	Fe I	CA	$z\ ^7F_0 - f\ ^7D_1$
12	3599.6243	3600.6513	Fe I	CA	$a\ ^1H_5 - u\ ^3F_4$
150	3600.1691	3601.1963	Ne I	KE	
3	3602.0817	3603.1093	Fe I	CA	$z\ ^7F_1 - f\ ^7D_2$
15	3602.4617	3603.4894	Fe I	CA	$z\ ^7F_3 - f\ ^7D_3$
20	3602.5259	3603.5537	Fe I	CA	$z\ ^7F_3 - e\ ^7P_2$
20	3602.5479	3603.5757	Fe I	CA	$z\ ^7P_4 - f\ ^5F_4$
150	3603.2043	3604.2323	Fe I	CA	$a\ ^3G_5 - v\ ^3G_5$
5	3603.5675	3604.5955	Fe I	CA	$a\ ^3H_5 - w\ ^5G_6$
6	3603.8189	3604.8470	Fe I	CA	$c\ ^3P_1 - u\ ^3D_1$
2	3604.367	3605.395	Fe I	P	$z\ ^7F_1 - f\ ^5D_0$
200	3605.4537	3606.4822	Fe I	CA	$a\ ^3G_4 - y\ ^3H_4$
200	3605.5003	3606.5288	Fe I	CA	$z\ ^7F_6 - f\ ^7D_5$
500	3606.6797	3607.7085	Fe I	CA	$a\ ^3G_5 - y\ ^3H_6$
15	3608.1424	3609.1716	Fe I	CA	$z\ ^7F_4 - e\ ^5G_5$
1500	3608.8587	3609.8881	Fe I	CA	$a\ ^5F_1 - z\ ^5G_2$
20	3609.1790	3610.2085	Ne I	KE	
250	3610.158	3611.188	Fe I	P	$z\ ^7F_6 - e\ ^7F_6$

TABLE III. *Spectrum of the Fe-Ne hollow cathode*—Continued

Intensity	Wavelength (Å) Air	Wavelength (Å) Vacuum	Ion	Ref	Classification
5	3610.6951	3611.7250	Fe I	CA	$z\,^7F_2 - f\,^5D_1$
60	3612.0679	3613.0982	Fe I	CA	$z\,^7F_5 - e\,^5G_6$
3	3612.9265	3613.9569	Fe I	CA	$a\,^5P_3 - x\,^3D_3$
3	3612.9393	3613.9698	Fe I	CA	$a\,^3F_3 - x\,^5D_2$
3	3613.1455	3614.1760	Fe I	CA	$z\,^7F_2 - e\,^7P_2$
6	3614.550	3615.581	Fe I	P	
2	3615.1904	3616.2214	Fe I	CA	$z\,^5D_1 - h\,^5D_1$
2	3615.6622	3616.6934	Fe I	CA	$a\,^3F_4 - x\,^5D_4$
3	3616.1468	3617.1781	Fe I	CA	$z\,^5D_4 - h\,^5D_3$
4	3616.3194	3617.3507	Fe I	CA	$a\,^3P_1 - x\,^3F_2$
8	3616.562	3617.593	Fe I	P	
2	3617.0999	3618.1314	Fe I	CA	$a\,^1G_4 - t\,^3D_3$
8	3617.318	3618.350	Fe I	P	
150	3617.7879	3618.8196	Fe I	CA	$c\,^3P_2 - u\,^3D_3$
25	3618.3808	3619.4126	Fe I	CA	$z\,^5D_3 - f\,^5G_4$
25	3618.3862	3619.4181	Fe I	CA	$a\,^3G_4 - v\,^3G_4$
1500	3618.7676	3619.7995	Fe I	CA	$a\,^5F_2 - z\,^5G_3$
3	3619.7683	3620.8005	Fe I	CA	$a\,^3H_6 - z\,^3H_5$
5	3620.2425	3621.2749	Fe I	CA	$z\,^7F_4 - e\,^7P_3$
200	3621.4616	3622.4943	Fe I	CA	$a\,^3G_4 - y\,^3H_5$
6	3621.7181	3622.7508	Fe I	CA	$a\,^1H_5 - u\,^3H_4$
150	3622.0042	3623.0370	Fe I	CA	$a\,^3G_3 - v\,^3G_3$
150	3623.1856	3624.2187	Fe I	ED	$a\,^3H_6 - z\,^3H_6$
25	3623.4296	3624.4628	Fe I	CA	$b\,^3G_5 - u\,^3G_5$
25	3623.4472	3624.4803	Fe I	CA	$b\,^3F_4 - w\,^3G_5$
10	3623.7722	3624.8055	Fe I	CA	$z\,^7F_3 - f\,^5D_2$
3	3624.3092	3625.3426	Fe I	CA	$a\,^3P_1 - w\,^3D_2$
25	3625.1414	3626.1750	Fe I	CA	$z\,^7F_5 - f\,^5D_4$
15	3630.3484	3631.3834	Fe I	CA	$z\,^7F_4 - f\,^5D_3$
100	3631.0961	3632.1312	Fe I	CA	$z\,^7F_5 - f\,^7D_5$
1200	3631.4629	3632.4981	Fe I	CA	$a\,^5F_3 - z\,^5G_4$
60	3632.0410	3633.0763	Fe I	CA	$c\,^3P_1 - u\,^3D_2$
15	3632.5547	3633.5902	Fe I	CA	$b\,^3G_5 - v\,^3F_4$
12	3632.9777	3634.0134	Fe I	CA	$a\,^3P_0 - y\,^3S_1$
200	3633.6646	3634.7004	Ne I	KE	
25	3634.3282	3635.3642	Fe I	CA	$z\,^7P_4 - e\,^5G_3$
30	3634.698	3635.734	Fe I	P	
3	3636.2235	3637.2600	Fe I	CA	$a\,^1D_2 - s\,^3G_3$
25	3636.9946	3638.0312	Fe I	CA	$b\,^3F_3 - w\,^3G_4$
100	3638.2978	3639.3348	Fe I	CA	$a\,^3G_3 - y\,^3H_4$
200	3640.3892	3641.4268	Fe I	CA	$a\,^3G_4 - v\,^3G_5$
30	3643.6216	3644.6600	Fe I	CA	$z\,^7P_4 - e\,^7F_3$
80	3643.7170	3644.7554	Fe I	CA	$b\,^3F_2 - w\,^3G_3$
12	3645.4748	3646.5137	Fe I	CA	$z\,^7F_3 - f\,^5D_3$
12	3645.4945	3646.5333	Fe I	CA	$b\,^3G_3 - x\,^1D_2$
12	3645.5035	3646.5423	Fe I	CA	$z\,^7P_3 - f\,^5F_3$
15	3645.8212	3646.8602	Fe I	CA	$c\,^3P_0 - u\,^3D_1$
12	3647.4087	3648.4480	Fe I	CA	$a\,^3F_3 - x\,^5D_3$
1500	3647.8424	3648.8819	Fe I	CA	$a\,^5F_4 - z\,^5G_5$
20	3649.3029	3650.3427	Fe I	CA	$a\,^5D_4 - z\,^5F_3$
250	3649.5064	3650.5463	Fe I	CA	$a\,^3G_5 - w\,^3F_4$
20	3650.0313	3651.0714	Fe I	CA	$z\,^7P_3 - e\,^7S_3$
80	3650.2793	3651.3194	Fe I	CA	$a\,^3H_5 - z\,^3H_5$
200	3651.4674	3652.5078	Fe I	CA	$a\,^3G_3 - v\,^3G_4$
15	3655.4645	3656.5059	Fe I	CA	$b\,^3P_2 - w\,^3P_2$
50	3659.5164	3660.5589	Fe I	CA	$a\,^3H_4 - z\,^3H_4$
150	3664.073	3665.117	Ne II	CP	
6	3664.5367	3665.5805	Fe I	CA	$z\,^7P_3 - f\,^5F_4$
10	3667.252	3668.297	Fe I	BW	$z\,^5D_4 - f\,^5P_3$
15	3669.1520	3670.1970	Fe I	CA	$b\,^3G_4 - v\,^3F_3$
15	3669.5210	3670.5661	Fe I	CA	$a\,^3G_4 - w\,^3F_3$
120	3670.0237	3671.0689	Fe I	CA	$b\,^3P_1 - w\,^3P_2$
150	3670.0890	3671.1342	Fe I	CA	$b\,^3G_5 - x\,^3H_6$
0	3671.519	3672.565	Fe I	BW	$z\,^5D_2 - f\,^5P_2$
100	3676.3115	3677.3584	Fe I	CA	$b\,^3F_4 - x\,^3G_5$
2	3677.3076	3678.3547	Fe I	CA	$a\,^1D_2 - w\,^1F_3$
150	3677.6288	3678.6760	Fe I	CA	$a\,^3G_3 - w\,^3F_2$
12	3678.8601	3679.9076	Fe I	CA	$a\,^3P_1 - y\,^3P_2$
1500	3679.9132	3680.9610	Fe I	CA	$a\,^5D_4 - z\,^5F_4$
10	3680.669	3681.717	Fe I	P	$z\,^5D_4 - g\,^5F_5$
200	3682.2425	3683.2909	Fe I	CA	$a\,^1D_2 - w\,^1D_2$
200	3682.2426	3683.2909	Ne I	KE	
120	3683.0545	3684.1030	Fe I	CA	$a\,^5D_3 - z\,^5F_2$
150	3684.1068	3685.1557	Fe I	CA	$a\,^3G_4 - v\,^3D_3$
120	3685.7357	3686.7850	Ne I	KE	
120	3685.9983	3687.0476	Fe I	CA	$z\,^7P_4 - e\,^7F_5$
8	3686.2588	3687.3082	Fe I	CA	$a\,^3P_1 - y\,^3P_0$
8	3687.0965	3688.1461	Fe I	CA	$a\,^5P_3 - v\,^5D_2$
500	3687.4564	3688.5061	Fe I	CA	$a\,^5F_5 - y\,^5F_4$
30	3687.6581	3688.7079	Fe I	CA	$a\,^3G_4 - w\,^3F_4$
120	3689.4773	3690.5276	Fe I	CA	$b\,^3P_1 - w\,^3P_1$
20	3690.7266	3691.7772	Fe I	CA	$a\,^1H_5 - s\,^3G_5$
150	3694.0078	3695.0592	Fe I	CA	$z\,^7P_2 - e\,^7S_3$
250	3694.214	3695.265	Ne II	CP	
120	3695.0514	3696.1031	Fe I	CA	$a\,^1G_4 - 6\,^5$
120	3695.0523	3696.1040	Fe I	CA	$b\,^3F_3 - v\,^5F_4$
2	3695.5159	3696.5677	Fe I	CA	$z\,^5F_2 - g\,^7D_2$
2	3695.5163	3696.5681	Fe I	CA	$b\,^3F_4 - w\,^5G_3$
30	3697.4251	3698.4774	Fe I	CA	$z\,^7P_3 - e\,^5G_3$
10	3698.6021	3699.6547	Fe I	CA	$c\,^3P_2 - v\,^3F_3$
150	3701.0865	3702.1397	Fe I	CA	$z\,^7P_3 - e\,^7F_4$
100	3701.2250	3702.2783	Ne I	KE	
8	3702.0285	3703.0820	Fe I	CA	$b\,^3P_1 - w\,^3P_0$
4	3703.547	3704.601	Fe I	P	
3	3703.6914	3704.7453	Fe I	CA	$z\,^7P_4 - e\,^5G_5$
15	3703.8212	3704.8751	Fe I	CA	$b\,^3P_0 - w\,^3P_1$
80	3704.4617	3705.5158	Fe I	CA	$a\,^3G_5 - y\,^1G_4$
1200	3705.5657	3706.6201	Fe I	CA	$a\,^5D_3 - z\,^5F_3$
60	3707.0411	3708.0959	Fe I	CA	$z\,^7P_3 - e\,^5S_2$
60	3707.0444	3708.0992	Fe I	CA	$z\,^7P_3 - e\,^7F_3$
150	3707.8215	3708.8765	Fe I	CA	$a\,^5D_2 - z\,^5F_1$
300	3707.9195	3708.9745	Fe I	CA	$a\,^5P_3 - y\,^5S_2$
600	3709.2459	3710.3013	Fe I	CA	$a\,^5F_4 - y\,^5F_3$
0	3709.5341	3710.5895	Fe I	CA	$b\,^3G_4 - x\,^3H_5$
150	3709.621	3710.676	Ne II	CP	
50	3711.2225	3712.2784	Fe I	CA	$b\,^3F_3 - x\,^3G_4$
30	3711.4075	3712.4634	Fe I	CA	$c\,^3P_1 - y\,^1D_2$
400	3713.080	3714.136	Ne II	CP	
15	3715.9106	3716.9677	Fe I	CA	$a\,^3P_2 - x\,^3D_2$
120	3716.4421	3717.4993	Fe I	CA	$z\,^7P_4 - e\,^7P_3$
15	3718.4063	3719.4640	Fe I	CA	$a\,^3G_3 - v\,^3D_3$
8000	3719.9346	3720.9927	Fe I	CA	$a\,^5D_4 - z\,^5F_5$
8	3721.1840	3722.2425	Fe I	CA	$c\,^3P_2 - v\,^3F_2$
12	3721.2714	3722.3299	Fe I	CA	$a\,^5P_3 - v\,^5D_4$
12	3721.2728	3722.3312	Fe I	CA	$z\,^5F_5 - e\,^3G_5$
10	3721.3944	3722.4529	Fe I	CA	$a\,^3P_0 - y\,^3P_1$
25	3721.5046	3722.5631	Fe I	CA	$z\,^7P_2 - e\,^5G_2$
25	3721.5999	3722.6585	Fe I	CA	$b\,^3G_3 - v\,^3F_2$
20	3722.0240	3723.0827	Fe I	CA	$a\,^3G_3 - w\,^3F_4$
1500	3722.5625	3723.6213	Fe I	CA	$a\,^5D_2 - z\,^5F_2$
120	3724.3768	3725.4361	Fe I	CA	$a\,^3P_2 - x\,^3D_3$
60	3725.4911	3726.5507	Fe I	CA	$a\,^1G_4 - 4\,^4$
15	3726.8963	3727.9562	Fe I	CA	$a\,^5P_2 - v\,^5D_3$
15	3726.9273	3727.9873	Fe I	CA	$z\,^7P_2 - e\,^7F_2$
60	3727.0930	3728.1530	Fe I	CA	$z\,^7P_4 - f\,^5D_3$
200	3727.105	3728.165	Ne II	CP	
500	3727.6187	3728.6788	Fe I	CA	$a\,^5F_3 - y\,^5F_2$
8	3727.670	3728.730		P	

TABLE III. *Spectrum of the Fe-Ne hollow cathode*—Continued

Intensity	Wavelength (Å) Air	Wavelength (Å) Vacuum	Ion	Ref	Classification
30	3727.8097	3728.8698	Fe I	CA	$z\,^7P_3 - f\,^7D_2$
15	3728.6674	3729.7278	Fe I	CA	$b\,^3F_4 - z\,^1G_4$
50	3730.3856	3731.4464	Fe I	CA	$a\,^1G_4 - u\,^3G_5$
50	3730.9461	3732.0070	Fe I	CA	$b\,^3F_2 - x\,^3G_3$
10	3731.3733	3732.4344	Fe I	CA	$b\,^3F_2 - w\,^5G_2$
150	3732.3960	3733.4573	Fe I	CA	$a\,^5P_2 - y\,^5S_2$
1200	3733.3169	3734.3785	Fe I	CA	$a\,^5D_1 - z\,^5F_1$
5000	3734.8636	3735.9256	Fe I	CA	$a\,^5F_5 - y\,^5F_5$
120	3735.3239	3736.3860	Fe I	CA	$z\,^7P_4 - e\,^7P_4$
6000	3737.1313	3738.1938	Fe I	CA	$a\,^5D_3 - z\,^5F_4$
100	3738.3058	3739.3687	Fe I	CA	$b\,^3H_5 - z\,^1I_6$
25	3739.522	3740.585	Fe I	P	$a\,^3D_3 - a\,X_3$
8	3740.0440	3741.1074	Fe I	CA	$z\,^5F_3 - g\,^7D_4$
8	3740.0581	3741.1214	Fe I	CA	$a\,^1G_4 - v\,^3F_4$
15	3740.239	3741.302	Fe I	P	$a\,^3D_3 - s\,^3D_3$
25	3742.6168	3743.6808	Fe I	CA	$z\,^7P_4 - f\,^5D_4$
2	3742.946	3744.010	Fe I	BW	$z\,^5F_1 - f\,^5G_2$
400	3743.3616	3744.4258	Fe I	CA	$a\,^5F_2 - y\,^5F_1$
80	3743.466	3744.530	Fe I	P	$a\,^1H_5 - x\,^1H_5$
5	3743.7772	3744.8415	Fe I	CA	$a\,^3G_4 - y\,^1G_4$
12	3744.1036	3745.1680	Fe I	CA	$z\,^7P_2 - e\,^7F_1$
6000	3745.5608	3746.6256	Fe I	CA	$a\,^5D_2 - z\,^5F_3$
1200	3745.8989	3746.9638	Fe I	CA	$a\,^5D_0 - z\,^5F_1$
50	3746.9270	3747.9921	Fe I	CA	$z\,^7P_3 - f\,^7D_3$
3000	3748.2617	3749.3272	Fe I	CA	$a\,^5D_1 - z\,^5F_2$
80	3748.9640	3750.0296	Fe I	CA	$z\,^7P_4 - f\,^7D_5$
3000	3749.4847	3750.5504	Fe I	CA	$a\,^5F_4 - y\,^5F_4$
5	3750.6818	3751.7479	Fe I	CA	$b\,^3F_2 - w\,^5G_3$
6	3751.8213	3752.8877	Fe I	CA	$a\,^3G_5 - w\,^3G_4$
40	3753.6108	3754.6776	Fe I	CA	$a\,^5P_3 - w\,^5D_2$
25	3754.2156	3755.2826	Ne I	KE	
6	3756.0671	3757.1346	Fe I	CA	$a\,^5P_3 - w\,^5F_3$
15	3756.9364	3758.0041	Fe I	CA	$a\,^1H_5 - v\,^3H_5$
5	3757.4529	3758.5207	Fe I	CA	$a\,^3D_2 - z\,^1P_1$
1500	3758.2324	3759.3005	Fe I	CA	$a\,^5F_3 - y\,^5F_3$
400	3760.0491	3761.1176	Fe I	SD	$a\,^3H_6 - z\,^3I_7$
25	3760.5317	3761.6003	Fe I	CA	$a\,^5P_1 - y\,^5S_2$
8	3761.4085	3762.4773	Fe I	CA	$b\,^3F_3 - z\,^1G_4$
1500	3763.7885	3764.8580	Fe I	CA	$a\,^5F_2 - y\,^5F_2$
400	3765.5385	3766.6084	Fe I	SD	$b\,^3H_6 - y\,^3I_7$
80	3766.260	3767.330	Ne II	CP	
600	3767.1914	3768.2618	Fe I	CA	$a\,^5F_1 - y\,^5F_1$
6	3768.027	3769.098	Fe I	BW	$a\,^5P_1 - w\,^5D_0$
10	3769.9864	3771.0575	Fe I	CA	$z\,^7P_3 - f\,^5D_2$
40	3770.3020	3771.3732	Fe I	CA	$a\,^3G_5 - w\,^3G_5$
4	3770.410	3771.481	Fe I	P	$a\,^3H_5 - z\,^3I_5$
6	3774.8243	3775.8967	Fe I	CA	$a\,^5P_1 - w\,^5D_1$
4	3775.8557	3776.9283	Fe I	CA	$a\,^3G_4 - w\,^3G_3$
60	3776.4522	3777.5249	Fe I	CA	$a\,^5P_3 - w\,^5F_4$
100	3777.134	3778.207	Ne II	CP	
6	3777.4498	3778.5228	Fe I	CA	$b\,^3F_4 - z\,^3H_4$
8	3778.5090	3779.5823	Fe I	CA	$a\,^3D_3 - t\,^3D_2$
3	3778.6962	3779.7696	Fe I	CA	$a\,^5P_2 - w\,^5D_2$
10	3781.1855	3782.2595	Fe I	CA	$a\,^5P_2 - w\,^5F_3$
5	3785.7070	3786.7822	Fe I	CA	$b\,^3H_6 - y\,^3I_6$
250	3785.946	3787.021	Fe I	P	$a\,^3H_5 - z\,^3I_6$
30	3786.1901	3787.2654	Fe I	CA	$b\,^3P_2 - v\,^3D_2$
100	3786.6764	3787.7518	Fe I	ED	$a\,^5F_1 - z\,^3P_0$
250	3787.8800	3788.9557	Fe I	CA	$a\,^5F_1 - y\,^5F_2$
10	3789.1758	3790.2518	Fe I	CA	$a\,^3G_4 - z\,^1H_5$
250	3790.0923	3791.1686	Fe I	CA	$a\,^5F_2 - z\,^3P_1$
50	3792.1539	3793.2308	Fe I	CA	$a\,^3G_4 - w\,^3G_4$
10	3793.4813	3794.5585	Fe I	CA	$z\,^7P_3 - f\,^5D_3$
8	3793.8722	3794.9495	Fe I	CA	$b\,^3P_1 - v\,^3D_1$
150	3794.337	3795.415	Fe I	P	$a\,^3H_4 - z\,^3I_5$
400	3795.0017	3796.0793	Fe I	CA	$a\,^5F_2 - y\,^5F_3$
8	3796.0127	3797.0905	Fe I	CA	$a\,^3H_6 - x\,^5G_5$
120	3797.5180	3798.5962	Fe I	CA	$b\,^3H_6 - w\,^3H_6$
6	3797.9485	3799.0268	Fe I	CA	$b\,^3F_3 - x\,^3F_2$
250	3798.5107	3799.5892	Fe I	CA	$a\,^5F_4 - y\,^5F_5$
400	3799.5469	3800.6256	Fe I	CA	$a\,^5F_3 - y\,^5F_4$
30	3801.6786	3802.7579	Fe I	CA	$b\,^3P_2 - v\,^3D_3$
15	3801.8114	3802.8908	Fe I	CA	$b\,^3P_1 - v\,^3D_2$
5	3801.997	3803.077	Fe I	P	$z\,^5F_5 - f\,^5G_6$
200	3805.3452	3806.4254	Fe I	CA	$b\,^3H_4 - y\,^3I_5$
12	3806.2170	3807.2975	Fe I	CA	$a\,^1P_1 - v\,^3P_1$
80	3806.6959	3807.7765	Fe I	CA	$b\,^3H_5 - w\,^3H_5$
40	3807.5370	3808.6178	Fe I	CA	$a\,^5P_1 - w\,^5D_2$
25	3808.7279	3809.8090	Fe I	CA	$b\,^3F_4 - x\,^3F_4$
4	3809.0409	3810.1221	Fe I	CA	$b\,^3P_0 - v\,^3D_1$
10	3810.7568	3811.8385	Fe I	CA	$a\,^3D_2 - 8_1$
30	3811.8931	3812.9750	Fe I	CA	$a\,^3G_3 - w\,^3G_3$
600	3812.9641	3814.0463	Fe I	CA	$a\,^5F_3 - z\,^3P_2$
60	3813.0586	3814.1409	Fe I	CA	$b\,^3F_3 - x\,^3F_3$
10	3813.6338	3814.7163	Fe I	CA	$a\,^3G_5 - v\,^5F_4$
10	3813.882	3814.965	Fe I	P	$a\,^1I_6 - x\,^1H_5$
50	3814.5227	3815.6054	Fe I	CA	$a\,^5F_1 - z\,^3P_1$
1500	3815.8397	3816.9227	Fe I	CA	$a\,^3F_4 - y\,^3D_3$
15	3816.3397	3817.4228	Fe I	CA	$a\,^5P_2 - w\,^5D_3$
15	3817.640	3818.723	Fe I	P	$z\,^5F_5 - g\,^5F_5$
2500	3820.4251	3821.5093	Fe I	CA	$a\,^5F_5 - y\,^5D_4$
150	3821.1788	3822.2632	Fe I	CA	$b\,^3H_5 - y\,^3I_6$
30	3821.8334	3822.9180	Fe I	CA	$b\,^3F_2 - x\,^3F_2$
50	3824.0737	3825.1588	Fe I	CA	$b\,^3F_3 - w\,^3D_3$
80	3824.3060	3825.3912	Fe I	CA	$b\,^3H_4 - w\,^3H_4$
2500	3824.4436	3825.5288	Fe I	CA	$a\,^5D_4 - z\,^5D_3$
1500	3825.8805	3826.9661	Fe I	CA	$a\,^5F_4 - y\,^5D_3$
6	3826.8408	3827.9267	Fe I	CA	$a\,^3G_4 - v\,^5F_3$
25	3827.5720	3828.6581	Fe I	CA	$a\,^3G_5 - x\,^3G_5$
1200	3827.8226	3828.9087	Fe I	CA	$a\,^3F_3 - y\,^3D_2$
40	3829.4541	3830.5407	Fe I	CA	$a\,^3D_1 - u\,^3D_1$
25	3830.7583	3831.8452	Fe I	CA	$b\,^3F_2 - w\,^3D_2$
12	3830.8610	3831.9479	Fe I	CA	$a\,^3G_5 - x\,^3G_4$
40	3833.3083	3834.3958	Fe I	CA	$b\,^3F_4 - u\,^5D_4$
1000	3834.2222	3835.3100	Fe I	CA	$a\,^5F_3 - y\,^5D_2$
40	3836.3301	3837.4185	Fe I	CA	$a\,^3D_2 - t\,^3D_2$
10	3837.1345	3838.2231	Fe I	CA	$b\,^3F_2 - x\,^3F_3$
120	3839.2567	3840.3458	Fe I	CA	$a\,^1G_4 - x\,^1G_4$
500	3840.4372	3841.5266	Fe I	CA	$a\,^5F_2 - y\,^5D_1$
800	3841.0475	3842.1371	Fe I	CA	$a\,^3F_2 - y\,^3D_1$
120	3843.2563	3844.3465	Fe I	CA	$a\,^1G_4 - z\,^1F_3$
20	3845.1683	3846.2589	Fe I	CA	$a\,^3P_1 - x\,^3D_1$
20	3846.4102	3847.5012	Fe I	CA	$a\,^1H_5 - w\,^1G_4$
80	3846.8002	3847.8913	Fe I	CA	$a\,^3D_3 - t\,^3D_3$
200	3849.9591	3851.0510	Fe I	SD	$a\,^5F_1 - y\,^5D_0$
120	3850.8174	3851.9095	Fe I	CA	$a\,^5F_2 - z\,^3P_2$
25	3852.5729	3853.6654	Fe I	CA	$a\,^5P_3 - w\,^5D_4$
10	3854.366	3855.459	Fe I	P	$z\,^5D_4 - e\,^5P_3$
2500	3856.3717	3857.4652	Fe I	CA	$a\,^5D_3 - z\,^5D_2$
150	3859.2117	3860.3060	Fe I	CA	$a\,^3H_6 - y\,^3G_5$
10000	3859.9114	3861.0058	Fe I	CA	$a\,^5D_4 - z\,^5D_4$
15	3861.3363	3862.4311	Fe I	CA	$a\,^3D_1 - u\,^3D_2$
15	3861.3459	3862.4408	Fe I	CA	$a\,^3G_5 - v\,^5F_5$
3	3861.5920	3862.6869	Fe I	CA	$a\,^3D_2 - u\,^3D_1$
15	3863.7408	3864.8362	Fe I	CA	$a\,^3G_5 - w\,^5G_4$
150	3865.5230	3866.6190	Fe I	CA	$a\,^5F_1 - y\,^5D_1$
60	3867.2152	3868.3116	Fe I	CA	$c\,^3P_2 - w\,^3P_2$
25	3869.5588	3870.6557	Fe I	CA	$a\,^3G_4 - x\,^3G_5$

TABLE III. *Spectrum of the Fe-Ne hollow cathode*—Continued

Intensity	Wavelength (Å)		Ion	Ref	Classification
	Air	Vacuum			
0	3869.6073	3870.7043	Fe I	CA	$a\,^3G_4 - x\,^3G_3$
20	3871.7489	3872.8465	Fe I	CA	$b\,^3G_5 - y\,^3H_5$
250	3872.5009	3873.5987	Fe I	CA	$a\,^5F_2 - y\,^5D_2$
10	3872.9203	3874.0182	Fe I	CA	$a\,^3G_4 - x\,^3G_4$
150	3873.7608	3874.8589	Fe I	CA	$a\,^3H_5 - y\,^3G_4$
10	3876.0395	3877.1382	Fe I	CA	$a\,^5F_1 - z\,^3P_2$
250	3878.0176	3879.1168	Fe I	CA	$a\,^5F_3 - y\,^5D_3$
2000	3878.5730	3879.6723	Fe I	CA	$a\,^5D_2 - z\,^5D_1$
5	3878.6703	3879.7697	Fe I	CA	$a\,^3H_4 - y\,^3G_3$
4	3878.7293	3879.8287	Fe I	CA	$a\,^3D_1 - t\,^3D_1$
20	3883.2826	3884.3831	Fe I	CA	$a\,^3D_3 - u\,^3D_3$
40	3884.3580	3885.4588	Fe I	CA	$a\,^3G_5 - z\,^1G_4$
40	3885.5095	3886.6107	Fe I	CA	$a\,^3P_1 - x\,^3D_2$
4000	3886.2820	3887.3833	Fe I	CA	$a\,^5D_3 - z\,^5D_3$
200	3887.0477	3888.1492	Fe I	CA	$a\,^5F_4 - y\,^5D_4$
0	3888.4166	3889.5185	Fe I	CA	$z\,^5D_2 - g\,^5D_2$
300	3888.5134	3889.6153	Fe I	CA	$a\,^3F_2 - y\,^3D_2$
25	3888.8216	3889.9236	Fe I	CA	$c\,^3P_2 - w\,^3P_1$
20	3890.8414	3891.9439	Fe I	CA	$a\,^3G_4 - w\,^5G_3$
15	3891.9263	3893.0291	Fe I	CA	$a\,^1P_1 - z\,^1P_1$
10	3893.3089	3894.4120	Fe I	CA	$b\,^3P_2 - x\,^3P_1$
50	3893.3909	3894.4941	Fe I	CA	$b\,^3G_5 - v\,^3G_5$
15	3893.9119	3895.0152	Fe I	CA	$a\,^3H_5 - y\,^3G_5$
10	3894.0137	3895.1171	Fe I	CA	$a\,^3D_2 - u\,^3D_2$
800	3895.6558	3896.7596	Fe I	CA	$a\,^5D_1 - z\,^5D_0$
8	3897.4488	3898.5530	Fe I	CA	$b\,^3G_5 - y\,^3H_6$
50	3897.8900	3898.9944	Fe I	CA	$a\,^3G_5 - w\,^5G_6$
40	3898.0088	3899.1132	Fe I	CA	$a\,^5F_1 - y\,^5D_2$
15	3899.0282	3900.1329	Fe I	CA	$a\,^3H_4 - y\,^3G_4$
1200	3899.7073	3900.8121	Fe I	CA	$a\,^5D_2 - z\,^5D_2$
400	3902.9452	3904.0509	Fe I	CA	$a\,^3F_3 - y\,^3D_3$
15	3903.8990	3905.0049	Fe I	CA	$b\,^3G_4 - y\,^3H_4$
250	3906.4794	3907.5859	Fe I	CA	$a\,^5D_1 - z\,^5D_1$
10	3906.7468	3907.8535	Fe I	CA	$a\,^3D_2 - t\,^3D_3$
10	3907.4654	3908.5722	Fe I	CA	$a\,^3G_3 - x\,^3G_3$
30	3907.9340	3909.0410	Fe I	CA	$a\,^3G_3 - w\,^5G_2$
12	3909.8285	3910.9359	Fe I	CA	$b\,^3P_1 - x\,^3P_1$
15	3910.8435	3911.9513	Fe I	CA	$a\,^3G_3 - x\,^3G_4$
8	3913.6311	3914.7396	Fe I	CA	$a\,^3P_2 - w\,^5D_3$
80	3916.7308	3917.8400	Fe I	CA	$b\,^3H_6 - 6\,^5$
15	3917.1802	3918.2896	Fe I	CA	$a\,^5F_2 - y\,^5D_3$
20	3918.3148	3919.4245	Fe I	CA	$a\,^3P_0 - x\,^3D_1$
25	3918.4161	3919.5258	Fe I	CA	$b\,^3P_1 - x\,^3P_0$
30	3918.6419	3919.7517	Fe I	CA	$b\,^3G_3 - v\,^3G_3$
12	3919.0655	3920.1754	Fe I	CA	$b\,^3G_4 - v\,^3G_4$
600	3920.2577	3921.3679	Fe I	CA	$a\,^5D_0 - z\,^5D_1$
1200	3922.9115	3924.0223	Fe I	CA	$a\,^5D_3 - z\,^5D_4$
20	3925.6433	3926.7549	Fe I	CA	$b\,^3P_2 - x\,^3P_2$
25	3925.9405	3927.0522	Fe I	CA	$b\,^3P_0 - x\,^3P_1$
10	3926.0126	3927.1242	Fe I	CA	$z\,^5D_3 - f\,^5F_3$
1200	3927.9197	3929.0319	Fe I	CA	$a\,^5D_1 - z\,^5D_2$
0	3928.0829	3929.1952	Fe I	CA	$z\,^5D_4 - g\,^5D_4$
6	3929.1181	3930.2306	Fe I	CA	$a\,^3G_3 - w\,^5G_3$
6	3929.2070	3930.3195	Fe I	CA	$a\,^3D_3 - u\,^3G_4$
2000	3930.2962	3931.4090	Fe I	CA	$a\,^5D_2 - z\,^5D_3$
6	3931.1168	3932.2299	Fe I	CA	$z\,^5D_2 - g\,^5D_3$
25	3932.626	3933.740	Fe I	P	$a\,^5G_4 - w\,^5G_5$
25	3932.626	3933.740	Fe I	P	$a\,^3D_1 - u\,^5F_2$
12	3933.5994	3934.7130	Fe I	CA	$c\,^3P_1 - w\,^3P_2$
12	3933.6017	3934.7154	Fe I	CA	$z\,^5D_2 - f\,^5F_1$
25	3935.8121	3936.9264	Fe I	CA	$b\,^3P_2 - v\,^5F_2$
25	3935.8581	3936.9724	Fe I	CA	$z\,^5D_2 - e\,^3D_2$
20	3937.3279	3938.4426	Fe I	CA	$a\,^3G_5 - z\,^3H_4$
8	3940.8770	3941.9925	Fe I	CA	$a\,^5F_3 - y\,^5D_4$
10	3941.2756	3942.3913	Fe I	CA	$z\,^5D_2 - f\,^5F_2$
12	3942.4390	3943.5550	Fe I	CA	$b\,^3P_1 - x\,^3P_2$
10	3943.3388	3944.4550	Fe I	CA	$a\,^5P_2 - x\,^5P_1$
8	3944.8901	3946.0067	Fe I	CA	$b\,^3G_4 - v\,^3G_5$
15	3945.1167	3946.2334	Fe I	CA	$a\,^3G_3 - w\,^5G_4$
10	3946.9939	3948.1110	Fe I	CA	$z\,^5D_4 - e\,^7G_5$
10	3947.5068	3948.6241	Fe I	CA	$b\,^3G_5 - w\,^3F_4$
10	3947.5313	3948.6486	Fe I	CA	$b\,^3P_2 - v\,^5P_2$
25	3948.0964	3949.2138	Fe I	CA	$z\,^5D_3 - f\,^5F_4$
60	3948.7740	3949.8916	Fe I	CA	$b\,^3H_5 - u\,^3G_4$
60	3949.9527	3951.0707	Fe I	CA	$a\,^5P_3 - x\,^5P_2$
50	3951.1636	3952.2819	Fe I	CA	$a\,^3D_1 - y\,^1D_2$
50	3952.6014	3953.7200	Fe I	CA	$a\,^3G_5 - z\,^3H_5$
12	3953.1516	3954.2704	Fe I	CA	$b\,^3G_3 - v\,^3G_4$
10	3955.3416	3956.4609	Fe I	CA	$z\,^5D_1 - f\,^5F_1$
6	3955.9560	3957.0755	Fe I	CA	$c\,^3P_1 - w\,^3P_1$
60	3956.4544	3957.5740	Fe I	CA	$b\,^3H_6 - u\,^3G_5$
250	3956.6769	3957.7966	Fe I	SD	$a\,^3G_5 - z\,^3H_6$
25	3957.0172	3958.1369	Fe I	CA	$z\,^5D_2 - f\,^5F_3$
20	3963.1006	3964.2220	Fe I	CA	$z\,^5D_1 - f\,^5F_2$
5	3964.5152	3965.6370	Fe I	CA	$b\,^3P_1 - v\,^5P_2$
25	3966.0610	3967.1832	Fe I	CA	$a\,^3F_2 - y\,^3D_3$
10	3966.4998	3967.6220	Fe I	CA	$z\,^5D_0 - f\,^5F_1$
60	3966.6139	3967.7362	Fe I	CA	$a\,^3G_3 - z\,^1G_4$
60	3966.6278	3967.7501	Fe I	CA	$z\,^5D_4 - f\,^5F_5$
12	3967.4198	3968.5423	Fe I	CA	$b\,^3H_4 - u\,^3G_3$
2	3967.9610	3969.0836	Fe I	CA	$z\,^5D_3 - e\,^7G_4$
100	3969.2570	3970.3800	Fe I	CA	$a\,^3F_4 - y\,^3F_3$
15	3969.6282	3970.7513	Fe I	CA	$a\,^3D_3 - 4\,^4$
15	3970.3892	3971.5124	Fe I	CA	$c\,^3P_1 - w\,^3P_0$
30	3971.3215	3972.4450	Fe I	CA	$a\,^3G_5 - x\,^3F_4$
10	3973.6494	3974.7735	Fe I	CA	$a\,^1D_2 - x\,^1F_3$
15	3976.6138	3977.7387	Fe I	CA	$a\,^1P_1 - t\,^3D_2$
12	3976.8628	3977.9878	Fe I	CA	$a\,^3D_2 - x\,^1D_2$
80	3977.7407	3978.8659	Fe I	CA	$a\,^5P_2 - x\,^5P_2$
40	3981.7711	3982.8973	Fe I	CA	$a\,^3G_4 - z\,^3H_4$
50	3983.9561	3985.0829	Fe I	CA	$a\,^3G_4 - x\,^3F_3$
10	3985.3858	3986.5130	Fe I	CA	$a\,^3D_2 - y\,^1D_2$
25	3986.1711	3987.2985	Fe I	CA	$a\,^3D_3 - v\,^3F_4$
25	3986.1784	3987.3058	Fe I	CA	$z\,^5D_4 - e\,^5G_4$
6	3990.3733	3991.5018	Fe I	CA	$a\,^1G_4 - v\,^3G_4$
60	3994.1138	3995.2433	Fe I	CA	$a\,^1G_4 - y\,^3H_5$
12	3995.9822	3997.1121	Fe I	CA	$a\,^3G_4 - w\,^3D_3$
8	3996.9654	3998.0956	Fe I	CA	$b\,^1G_4 - w\,^1G_4$
200	3997.3919	3998.5222	Fe I	CA	$a\,^3G_4 - z\,^3H_5$
40	3998.0527	3999.1831	Fe I	CA	$a\,^3G_5 - u\,^5D_4$
6	4000.4573	4001.5884	Fe I	CA	$b\,^3G_4 - w\,^3F_4$
15	4001.6608	4002.7923	Fe I	CA	$a\,^5P_3 - x\,^5P_3$
25	4004.8276	4005.9599	Fe I	CA	$b\,^3H_6 - x\,^3H_5$
6	4004.9793	4006.1116	Fe I	CA	$c\,^3P_2 - v\,^3D_1$
6	4004.9842	4006.1165	Fe I	CA	$z\,^5D_4 - f\,^7D_3$
400	4005.2414	4006.3737	Fe I	CA	$a\,^3F_3 - y\,^3F_2$
20	4006.3109	4007.4436	Fe I	CA	$b\,^3H_5 - v\,^3F_4$
10	4006.6249	4007.7577	Fe I	CA	$c\,^3P_0 - w\,^3P_1$
20	4007.2710	4008.4039	Fe I	CA	$a\,^3G_3 - x\,^3F_2$
60	4009.7126	4010.8462	Fe I	CA	$a\,^5P_1 - x\,^5P_2$
10	4013.8277	4014.9623	Fe I	CA	$c\,^3P_2 - v\,^3D_2$
80	4014.5308	4015.6656	Fe I	SD	$a\,^1H_5 - y\,^1H_5$
20	4017.1494	4018.2848	Fe I	CA	$a\,^1G_4 - v\,^3G_5$
100	4021.8669	4023.0036	Fe I	CA	$a\,^3G_3 - z\,^3H_4$
20	4024.7245	4025.8620	Fe I	CA	$z\,^5D_3 - e\,^5G_4$
6	4029.6254	4030.7641	Fe I	CA	$z\,^5D_2 - e\,^5S_2$
6	4029.6293	4030.7680	Fe I	CA	$z\,^5D_2 - e\,^7F_3$
5	4030.1837	4031.3226	Fe I	CA	$a\,^5P_2 - x\,^5P_3$

TABLE III. *Spectrum of the Fe-Ne hollow cathode*—Continued

Intensity	Wavelength (Å) Air	Wavelength (Å) Vacuum	Ion	Ref	Classification
30	4030.4885	4031.6274	Fe I	CA	$z\,^5D_4 - e\,^5G_5$
20	4031.9620	4033.1013	Fe I	CA	$a\,^3D_1 - v\,^3F_2$
5	4032.6267	4033.7663	Fe I	CA	$a\,^3F_4 - y\,^5P_3$
50	4040.6377	4041.7793	Fe I	CA	$a\,^3D_2 - v\,^3F_3$
8	4043.8852	4045.0276	Fe I	CA	$a\,^3G_4 - u\,^5D_4$
8	4043.8966	4045.0391	Fe I	CA	$z\,^5D_3 - f\,^7D_3$
25	4044.6098	4045.7525	Fe I	CA	$b\,^3P_2 - y\,^3S_1$
4000	4045.8130	4046.9560	Fe I	CA	$a\,^3F_4 - y\,^3F_4$
5	4046.653	4047.796	Fe I	P	$c\,^3P_1 - z\,^1D_2$
6	4054.807	4055.952	Fe I	P	
5	4054.8674	4056.0127	Fe I	CA	$z\,^5F_2 - g\,^5D_1$
30	4055.0348	4056.1802	Fe I	CA	$b\,^3F_4 - y\,^3G_5$
25	4057.3424	4058.4884	Fe I	CA	$a\,^3G_3 - x\,^3F_4$
25	4058.2172	4059.3634	Fe I	CA	$z\,^5D_4 - f\,^5D_3$
3	4058.7539	4059.9002	Fe I	CA	$a\,^3P_1 - w\,^5D_2$
15	4062.4413	4063.5886	Fe I	CA	$b\,^3P_1 - y\,^3S_1$
15	4063.2759	4064.4234	Fe I	CA	$z\,^5F_4 - g\,^5D_3$
1500	4063.5939	4064.7415	Fe I	CA	$a\,^3F_3 - y\,^3F_3$
1	4064.4503	4065.5981	Fe I	CA	$a\,^3F_3 - y\,^5P_2$
8	4066.5856	4067.7340	Fe I	CA	$b\,^3G_4 - y\,^1G_4$
50	4066.9753	4068.1238	Fe I	CA	$b\,^3P_2 - 1\ _2$
25	4067.2712	4068.4198	Fe I	CA	$b\,^3F_4 - x\,^3D_3$
50	4067.9774	4069.1262	Fe I	CA	$z\,^5D_4 - e\,^7P_4$
25	4070.7691	4071.9186	Fe I	CA	$z\,^5D_3 - f\,^5D_2$
0	4071.5209	4072.6706	Fe I	CA	$b\,^3F_3 - y\,^3G_4$
1200	4071.7372	4072.8869	Fe I	CA	$a\,^3F_2 - y\,^3F_2$
25	4073.7617	4074.9120	Fe I	CA	$z\,^5D_2 - f\,^5D_1$
20	4074.7857	4075.9362	Fe I	CA	$a\,^1G_4 - w\,^3F_4$
8	4076.4896	4077.6406	Fe I	CA	$b\,^3F_2 - y\,^3G_3$
40	4076.6286	4077.7796	Fe I	CA	$z\,^5D_4 - f\,^5D_4$
5	4076.7989	4077.9499	Fe I	CA	$z\,^5D_2 - f\,^7D_3$
15	4078.3535	4079.5050	Fe I	CA	$b\,^3F_2 - x\,^3D_1$
20	4079.8384	4080.9903	Fe I	CA	$b\,^3P_0 - y\,^3S_1$
6	4080.211	4081.363	Fe I	P	$z\,^5D_1 - f\,^5D_0$
25	4084.4914	4085.6445	Fe I	CA	$z\,^5F_5 - g\,^5D_4$
30	4085.0049	4086.1581	Fe I	CA	$b\,^3P_1 - 1\ _2$
20	4085.3024	4086.4557	Fe I	CA	$z\,^5D_3 - e\,^7P_3$
4	4087.0934	4088.2472	Fe I	CA	$z\,^5F_5 - e\,^7G_4$
15	4089.2172	4090.3715	Fe I	CA	$b\,^3G_5 - w\,^3G_5$
25	4091.5534	4092.7083	Fe I	CA	$b\,^3P_2 - w\,^3D_1$
30	4092.4564	4093.6116	Fe I	CA	$a\,^5F_4 - z\,^3F_3$
15	4095.9707	4097.1268	Fe I	CA	$b\,^3F_3 - x\,^3D_2$
15	4098.1760	4099.3327	Fe I	CA	$z\,^5D_3 - f\,^5D_3$
40	4100.7374	4101.8948	Fe I	CA	$a\,^5F_5 - z\,^3F_4$
8	4104.1118	4105.2700	Fe I	CA	$z\,^5D_2 - f\,^5D_2$
40	4107.4888	4108.6479	Fe I	CA	$b\,^3P_2 - u\,^5D_1$
30	4109.8020	4110.9618	Fe I	CA	$b\,^3P_1 - w\,^3D_1$
10	4112.0878	4113.2481	Fe I	CA	$a\,^1D_2 - v\,^3P_2$
6	4112.955	4114.116	Fe I	P	$y\,^5F_5 - g\,^5G_6$
20	4114.4457	4115.6066	Fe I	CA	$b\,^3P_2 - w\,^3D_2$
150	4118.5442	4119.7062	Fe I	CA	$a\,^1H_5 - z\,^1I_6$
20	4120.2064	4121.3688	Fe I	CA	$b\,^3G_4 - z\,^1H_5$
20	4121.8022	4122.9650	Fe I	CA	$b\,^3P_2 - x\,^3F_3$
15	4122.5133	4123.6763	Fe I	CA	$b\,^3P_1 - x\,^3F_2$
15	4123.728	4124.892	Fe I	P	
2	4125.8802	4127.0441	Fe I	CA	$b\,^3P_1 - u\,^5D_1$
10	4126.1831	4127.3471	Fe I	CA	$z\,^5F_5 - f\,^5F_5$
40	4127.6081	4128.7725	Fe I	CA	$b\,^3P_0 - w\,^3D_1$
12	4127.813	4128.978	Fe I	P	
400	4132.0578	4133.2234	Fe I	CA	$a\,^3F_2 - y\,^3F_3$
30	4132.8996	4134.0654	Fe I	CA	$b\,^3P_1 - w\,^3D_2$
6	4133.8552	4135.0212	Fe I	CA	$z\,^5F_4 - g\,^5D_4$
20	4134.3353	4135.5015	Fe I	CA	$a\,^5D_4 - z\,^7P_3$
80	4134.6762	4135.8424	Fe I	CA	$b\,^3P_2 - w\,^3D_3$
40	4136.9973	4138.1641	Fe I	CA	$a\,^1P_1 - y\,^1D_2$
12	4139.9268	4141.0944	Fe I	CA	$a\,^5F_2 - z\,^3F_2$
12	4141.8648	4143.0329	Fe I	CA	$b\,^3G_3 - w\,^3G_3$
200	4143.4151	4144.5836	Fe I	CA	$a\,^1G_4 - y\,^1G_4$
800	4143.8688	4145.0374	Fe I	CA	$a\,^3F_3 - y\,^3F_4$
15	4146.0648	4147.2340	Fe I	CA	$b\,^3G_4 - w\,^3G_5$
25	4147.6687	4148.8384	Fe I	CA	$a\,^3F_4 - z\,^3G_3$
15	4149.3653	4150.5354	Fe I	CA	$z\,^5F_5 - e\,^7G_6$
2	4149.7598	4150.9300	Fe I	CA	$a\,^5D_3 - z\,^7P_2$
5	4150.2496	4151.4199	Fe I	CA	$z\,^5F_1 - f\,^5F_1$
30	4152.1686	4153.3394	Fe I	CA	$a\,^5F_3 - z\,^3F_3$
40	4153.8985	4155.0697	Fe I	CA	$z\,^5F_3 - f\,^5F_4$
50	4154.4996	4155.6710	Fe I	CA	$b\,^3P_2 - y\,^3P_1$
30	4154.8045	4155.9760	Fe I	CA	$z\,^5F_4 - e\,^7G_5$
1	4156.6716	4157.8436	Fe I	CA	$b\,^3G_5 - x\,^3G_5$
60	4156.7989	4157.9709	Fe I	CA	$b\,^3P_2 - u\,^5D_2$
25	4157.7792	4158.9515	Fe I	CA	$z\,^5F_2 - f\,^5F_3$
15	4158.7930	4159.9655	Fe I	CA	$z\,^5F_1 - f\,^5F_2$
4	4161.4840	4162.6573	Fe I	CA	$b\,^3G_3 - w\,^3G_4$
20	4170.9008	4172.0765	Fe I	CA	$c\,^3P_2 - x\,^3P_2$
4	4171.6910	4172.8670	Fe I	CA	$b\,^1G_4 - x\,^1F_3$
5	4171.8992	4173.0752	Fe I	CA	$a\,^3D_2 - z\,^1F_3$
20	4172.1218	4173.2979	Fe I	CA	$a\,^3D_3 - w\,^3P_2$
0	4172.6416	4173.8178	Fe I	CA	$z\,^5F_5 - e\,^7F_5$
50	4172.7443	4173.9205	Fe I	CA	$a\,^5F_3 - z\,^3D_2$
5	4173.3153	4174.4917	Fe I	CA	$b\,^3P_1 - y\,^3P_1$
20	4173.9211	4175.0976	Fe I	CA	$a\,^5F_2 - z\,^3D_1$
60	4174.9121	4176.0888	Fe I	CA	$a\,^5F_4 - z\,^3D_3$
50	4175.6355	4176.8125	Fe I	CA	$b\,^3P_1 - u\,^5D_2$
25	4176.5679	4177.7452	Fe I	CA	$z\,^5F_3 - e\,^7F_2$
50	4177.5931	4178.7706	Fe I	CA	$a\,^5F_4 - z\,^3F_4$
120	4181.7544	4182.9330	Fe I	CA	$b\,^3P_2 - u\,^5D_3$
20	4182.3817	4183.5605	Fe I	CA	$c\,^3P_2 - v\,^5F_2$
50	4184.8913	4186.0707	Fe I	CA	$b\,^3P_2 - y\,^3P_2$
120	4187.0384	4188.2184	Fe I	CA	$z\,^7D_3 - e\,^7D_2$
120	4187.7947	4188.9749	Fe I	CA	$z\,^7D_4 - e\,^7D_3$
80	4191.4296	4192.6107	Fe I	CA	$z\,^7D_2 - e\,^7D_1$
8	4191.6772	4192.8584	Fe I	CA	$b\,^3P_0 - y\,^3P_1$
40	4195.3292	4196.5113	Fe I	CA	$z\,^5F_5 - e\,^5G_5$
3	4195.6177	4196.7999	Fe I	CA	$c\,^3P_2 - v\,^5P_2$
20	4196.2075	4197.3898	Fe I	CA	$z\,^5F_3 - e\,^5G_3$
0	4198.2464	4199.4294	Fe I	CA	$z\,^5F_4 - e\,^5G_4$
150	4198.3036	4199.4865	Fe I	CA	$z\,^7D_5 - e\,^7D_4$
12	4198.6360	4199.8191	Fe I	CA	$z\,^5F_2 - e\,^5G_2$
40	4199.0949	4200.2781	Fe I	CA	$a\,^1G_4 - z\,^1H_5$
12	4199.9827	4201.1661	Fe I	CA	$a\,^5D_2 - z\,^7P_2$
20	4200.9239	4202.1075	Fe I	CA	$z\,^5F_3 - e\,^7F_4$
300	4202.0286	4203.2125	Fe I	CA	$a\,^3F_4 - z\,^3G_4$
8	4202.7526	4203.9367	Fe I	CA	$a\,^1G_4 - w\,^3G_4$
8	4202.7629	4203.9470	Fe I	CA	$c\,^3P_2 - v\,^5F_3$
4	4203.5694	4204.7537	Fe I	CA	$a\,^5F_1 - z\,^3D_1$
0	4203.9385	4205.1229	Fe I	CA	$a\,^1I_6 - z\,^1I_6$
40	4203.9840	4205.1684	Fe I	CA	$b\,^3P_1 - y\,^3P_2$
4	4205.5397	4206.7245	Fe I	CA	$z\,^5F_2 - e\,^7F_2$
80	4206.6956	4207.8807	Fe I	CA	$a\,^5D_3 - z\,^7P_3$
10	4207.1268	4208.3120	Fe I	CA	$b\,^3P_2 - z\,^3S_1$
10	4208.5971	4209.7827	Fe I	CA	$z\,^5F_3 - e\,^5S_2$
10	4208.6013	4209.7869	Fe I	CA	$z\,^5F_3 - e\,^7F_3$
80	4210.3428	4211.5289	Fe I	CA	$z\,^7D_1 - e\,^7D_1$
20	4213.6483	4214.8353	Fe I	CA	$b\,^3P_1 - y\,^3P_0$
12	4215.4236	4216.6111	Fe I	CA	$b\,^3G_4 - x\,^3G_5$
12	4215.4587	4216.6461	Fe I	CA	$a\,^3G_3 - x\,^5G_2$
0	4215.9678	4217.1554	Fe I	CA	$a\,^3G_5 - y\,^3G_4$
400	4216.1828	4217.3704	Fe I	CA	$a\,^5D_4 - z\,^7P_4$

TABLE III. *Spectrum of the Fe-Ne hollow cathode*—Continued

Intensity	Wavelength (Å) Air	Wavelength (Å) Vacuum	Ion	Ref	Classification
15	4217.5477	4218.7357	Fe I	CA	$z\,^5F_1 - e\,^5G_2$
100	4219.3600	4220.5484	Fe I	CA	$a\,^1H_5 - y\,^3I_6$
12	4220.3434	4221.5321	Fe I	CA	$c\,^3P_1 - x\,^3P_0$
50	4222.2124	4223.4016	Fe I	CA	$z\,^7D_3 - e\,^7D_3$
25	4224.1725	4225.3622	Fe I	CA	$z\,^5F_4 - e\,^7F_5$
8	4224.5137	4225.7036	Fe I	CA	$z\,^5F_1 - e\,^7F_2$
20	4225.4533	4226.6433	Fe I	CA	$z\,^5F_2 - e\,^5G_3$
50	4225.9563	4227.1464	Fe I	CA	$a\,^1G_4 - w\,^3G_5$
10	4226.4233	4227.6137	Fe I	CA	$b\,^3P_1 - z\,^3S_1$
200	4227.4235	4228.6141	Fe I	CA	$z\,^5F_2 - e\,^7F_1$
3	4229.5116	4230.7027	Fe I	CA	$a\,^3D_1 - w\,^3P_1$
3	4229.5330	4230.7241	Fe I	CA	$b\,^3G_5 - w\,^5G_5$
1	4229.7533	4230.9445	Fe I	CA	$a\,^3F_4 - z\,^5G_3$
6	4231.637	4232.829	Ne II	CP	
10	4232.7252	4233.9171	Fe I	CA	$a\,^5D_1 - z\,^7P_2$
100	4233.6019	4234.7941	Fe I	CA	$z\,^7D_1 - e\,^7D_2$
250	4235.9362	4237.1290	Fe I	CA	$z\,^7D_4 - e\,^7D_4$
10	4237.0729	4238.2660	Fe I	CA	$a\,^5F_3 - z\,^3D_3$
12	4238.0164	4239.2098	Fe I	CA	$z\,^5F_2 - e\,^5S_2$
12	4238.0207	4239.2141	Fe I	CA	$z\,^5F_2 - e\,^7F_3$
50	4238.8092	4240.0028	Fe I	CA	$z\,^5F_3 - e\,^5G_4$
25	4239.7323	4240.9261	Fe I	CA	$b\,^3G_5 - w\,^5G_6$
5	4239.8344	4241.0282	Fe I	CA	$a\,^5F_3 - z\,^3F_4$
5	4239.8473	4241.0412	Fe I	CA	$a\,^3G_5 - y\,^3G_5$
4	4240.3720	4241.5660	Fe I	CA	$a\,^1D_2 - t\,^3D_1$
4	4242.7291	4243.9237	Fe I	CA	$a\,^3D_2 - w\,^3P_2$
15	4245.2565	4246.4518	Fe I	CA	$b\,^3P_0 - z\,^3S_1$
0	4245.3439	4246.5392	Fe I	CA	$z\,^5F_5 - f\,^5D_4$
5	4246.0842	4247.2797	Fe I	CA	$b\,^3D_3 - v\,^3P_2$
50	4247.4255	4248.6213	Fe I	CA	$z\,^5F_4 - e\,^5G_5$
10	4248.2242	4249.4202	Fe I	CA	$c\,^3P_1 - x\,^3P_2$
200	4250.1181	4251.3146	Fe I	CA	$z\,^7D_2 - e\,^7D_3$
300	4250.7866	4251.9833	Fe I	CA	$a\,^3F_3 - z\,^3G_3$
2	4255.4999	4256.6979	Fe I	CA	$b\,^3G_3 - w\,^5G_2$
40	4258.3147	4259.5133	Fe I	CA	$a\,^5D_2 - z\,^7P_3$
3	4258.9502	4260.1491	Fe I	CA	$b\,^3G_3 - x\,^3G_4$
6	4259.999	4261.198	Fe I	P	
6	4260.1353	4261.3345	Fe I	CA	$c\,^3P_1 - v\,^5F_2$
800	4260.4733	4261.6725	Fe I	CA	$z\,^7D_5 - e\,^7D_5$
4	4264.2031	4265.4033	Fe I	CA	$z\,^5F_4 - e\,^7P_3$
15	4266.9644	4268.1654	Fe I	CA	$a\,^3G_4 - y\,^3G_4$
12	4267.8264	4269.0276	Fe I	CA	$c\,^3P_0 - x\,^3P_1$
5	4268.7491	4269.9505	Fe I	CA	$a\,^3D_2 - w\,^3P_1$
3	4270.2674	4271.4696	Ne I	BA	
250	4271.1530	4272.3551	Fe I	CA	$z\,^7D_3 - e\,^7D_4$
1200	4271.7593	4272.9615	Fe I	CA	$a\,^3F_4 - z\,^3G_5$
1200	4282.4021	4283.6072	Fe I	CA	$a\,^5P_3 - z\,^5S_2$
12	4285.4420	4286.6478	Fe I	CA	$b\,^3H_6 - y\,^3H_6$
10	4288.1459	4289.3524	Fe I	CA	$a\,^3G_3 - y\,^3G_3$
10	4290.3778	4291.5849	Fe I	CA	$b\,^3G_4 - w\,^5G_5$
80	4291.4625	4292.6699	Fe I	CA	$a\,^5D_3 - z\,^7P_4$
12	4294.1243	4295.3324	Fe I	CA	$a\,^3F_4 - z\,^5G_4$
20	4298.0370	4299.2461	Fe I	CA	$a\,^1G_4 - x\,^3G_5$
250	4299.2337	4300.4432	Fe I	CA	$z\,^7D_4 - e\,^7D_5$
250	4299.2414	4300.4508	Fe I	CA	$b\,^3H_5 - y\,^3H_5$
10	4302.1845	4303.3948	Fe I	CA	$a\,^1G_4 - x\,^3G_4$
4	4304.5401	4305.7510	Fe I	CA	$b\,^3G_5 - z\,^3H_5$
15	4305.4509	4306.6620	Fe I	CA	$c\,^3P_2 - y\,^3S_1$
1200	4307.9015	4309.1132	Fe I	CA	$a\,^3F_3 - z\,^3G_4$
10	4309.0314	4310.2434	Fe I	CA	$a\,^1I_6 - y\,^3I_6$
30	4309.3739	4310.5860	Fe I	ED	$b\,^3G_5 - z\,^3H_6$
150	4315.0837	4316.2974	Fe I	CA	$a\,^5P_2 - z\,^5S_2$
2	4324.9471	4326.1633	Fe I	CA	$a\,^5P_2 - x\,^5F_3$
1500	4325.7615	4326.9779	Fe I	CA	$a\,^3F_2 - z\,^3G_3$
3	4326.7516	4327.9682	Fe I	CA	$b\,^3G_5 - x\,^3F_4$
20	4327.0937	4328.3105	Fe I	CA	$a\,^1D_2 - y\,^1D_2$
30	4337.0457	4338.2651	Fe I	CA	$a\,^3F_3 - z\,^5G_3$
5	4343.2754	4344.4964	Fe I	CA	$a\,^3D_3 - v\,^3D_2$
5	4343.6962	4344.9173	Fe I	CA	$a\,^1G_4 - w\,^3G_4$
4	4346.5526	4347.7745	Fe I	CA	$b\,^3H_4 - v\,^3G_4$
2	4348.9370	4350.1595	Fe I	CA	$b\,^3G_4 - z\,^3H_4$
8	4351.5436	4352.7668	Fe I	CA	$b\,^3G_4 - x\,^3F_3$
80	4352.7340	4353.9575	Fe I	CA	$a\,^5P_1 - z\,^5S_2$
6	4358.5006	4359.7257	Fe I	CA	$b\,^3G_5 - u\,^5D_4$
25	4367.5781	4368.8056	Fe I	CA	$b\,^3G_4 - z\,^3H_5$
2	4367.9026	4369.1301	Fe I	CA	$a\,^3F_2 - z\,^5G_2$
80	4369.7707	4370.9988	Fe I	CA	$a\,^1G_4 - z\,^1G_4$
5	4373.5328	4374.7618	Fe I	CA	$b\,^3F_4 - w\,^5D_4$
5	4373.5586	4374.7876	Fe I	CA	$b\,^3G_3 - x\,^3F_2$
800	4375.9294	4377.1590	Fe I	CA	$a\,^5D_4 - z\,^7F_5$
2	4376.838	4378.068	Fe I	P	
10	4382.7671	4383.9985	Fe I	CA	$a\,^1H_5 - 6\,_5$
3000	4383.5445	4384.7761	Fe I	CA	$a\,^3F_4 - z\,^5G_5$
12	4387.8927	4389.1255	Fe I	CA	$c\,^3P_1 - y\,^3S_1$
15	4388.406	4389.639	Fe I	P	$z\,^5P_3 - e\,^5P_3$
15	4389.2445	4390.4776	Fe I	CA	$a\,^5D_3 - z\,^7F_2$
15	4390.9506	4392.1841	Fe I	CA	$b\,^3G_3 - z\,^3H_4$
8	4401.2896	4402.5259	Fe I	CA	$z\,^5P_3 - g\,^5D_3$
3	4401.4423	4402.6787	Fe I	CA	$b\,^3P_2 - x\,^3D_1$
1200	4404.7499	4405.9871	Fe I	CA	$a\,^3F_3 - z\,^5G_4$
3	4407.7081	4408.9461	Fe I	CA	$a\,^5P_3 - x\,^5D_2$
4	4408.4140	4409.6522	Fe I	CA	$a\,^5P_2 - x\,^5D_1$
3	4409.1209	4410.3592	Fe I	CA	$a\,^3D_2 - v\,^3D_1$
0	4414.471	4415.711	Fe I	P	$a\,^3D_1 - 2\,_2$
300	4415.1222	4416.3622	Fe I	CA	$a\,^3F_2 - z\,^5G_3$
0	4418.4194	4419.6602	Fe I	CA	$b\,^3G_4 - u\,^5D_3$
25	4422.5670	4423.8089	Fe I	CA	$b\,^3P_1 - x\,^3D_1$
1	4423.1408	4424.3829	Fe I	CA	$b\,^3G_4 - u\,^5D_4$
1	4423.8420	4425.0843	Fe I	CA	$z\,^5P_2 - e\,^5P_2$
1	4424.1867	4425.4291	Fe I	CA	$a\,^1D_2 - v\,^3F_2$
1	4425.6572	4426.8999	Fe I	CA	$a\,^1H_5 - 4\,_4$
0	4525.8628	4527.1320	Fe I	CA	$z\,^7F_1 - e\,^5D_2$
600	4427.2990	4428.5421	Fe I	CA	$z\,^5P_2 - g\,^5D_2$
600	4427.3088	4428.5520	Fe I	CA	$a\,^5D_3 - z\,^7F_4$
2	4430.1896	4431.4335	Fe I	CA	$c\,^3P_2 - y\,^3P_1$
5	4430.6142	4431.8583	Fe I	CA	$a\,^5P_1 - x\,^5D_0$
3	4432.5659	4433.8105	Fe I	CA	$a\,^1H_5 - u\,^3G_5$
12	4433.216	4434.460	Fe I	P	$z\,^5P_2 - e\,^5P_1$
4	4433.7813	4435.0261	Fe I	CA	$z\,^5P_3 - f\,^5F_3$
30	4435.1485	4436.3937	Fe I	CA	$a\,^5D_2 - z\,^7F_1$
2	4436.9208	4438.1665	Fe I	CA	$a\,^1G_4 - z\,^3H_4$
1	4438.344	4439.590	Fe I	P	$z\,^5P_1 - g\,^5D_0$
1	4439.6340	4440.8804	Fe I	CA	$a\,^1G_4 - x\,^3F_3$
2	4439.8809	4441.1274	Fe I	CA	$a\,^3P_2 - z\,^5S_2$
0	4440.4807	4441.7274	Fe I	CA	$z\,^5P_3 - e\,^7S_3$
1	4440.822	4442.068	Fe I	P	$z\,^3D_1 - f\,^3D_1$
1	4440.9682	4442.2150	Fe I	CA	$a\,^3D_2 - v\,^3D_3$
2	4442.3379	4443.5851	Fe I	CA	$a\,^5P_2 - x\,^5D_2$
10	4442.8308	4444.0781	Fe I	CA	$a\,^5P_3 - y\,^7P_2$
30	4443.1930	4444.4404	Fe I	CA	$b\,^3P_0 - x\,^3D_1$
2	4445.4705	4446.7185	Fe I	CA	$a\,^5D_2 - z\,^7F_2$
2	4446.8330	4448.0813	Fe I	CA	$z\,^5P_1 - g\,^5D_1$
6	4447.1294	4448.3778	Fe I	CA	$a\,^5P_2 - y\,^7P_3$
10	4447.7179	4448.9664	Fe I	CA	$a\,^5P_1 - x\,^5D_1$
10	4450.3174	4451.5666	Fe I	CA	$c\,^3P_0 - y\,^3S_1$
0	4542.6964	4543.9700	Fe I	CA	$z\,^5P_1 - e\,^3D_2$
8	4454.3800	4455.6303	Fe I	CA	$b\,^3P_2 - x\,^3D_2$
25	4454.3800	4455.6303	Fe I	CA	$b\,^3P_2 - x\,^3D_2$

TABLE III. *Spectrum of the Fe-Ne hollow cathode*—Continued

Intensity	Wavelength (Å) Air	Wavelength (Å) Vacuum	Ion	Ref	Classification
0	4554.4510	4555.7277	Fe I	CA	$z\,^7F_3 - e\,^5D_3$
1	4454.6725	4455.9229	Fe I	CA	$b\,^3D_1 - x\,^1D_2$
2	4455.029	4456.280	Fe I	P	$z\,^3F_4 - f\,^3D_3$
8	4456.3255	4457.5763	Fe I	CA	$a\,^1G_4 - z\,^3H_5$
3	4458.086	4459.337	Fe I	P	$z\,^3D_3 - f\,^3D_3$
15	4459.1176	4460.3692	Fe I	CA	$a\,^5P_3 - x\,^5D_3$
400	4461.6521	4462.9043	Fe I	CA	$a\,^5D_2 - z\,^7F_3$
2	4464.7654	4466.0184	Fe I	CA	$c\,^3P_2 - y\,^3P_2$
0	4465.370	4466.623	Fe I	P	$y\,^5F_4 - 1\ _5$
120	4466.5508	4467.8044	Fe I	CA	$b\,^3P_2 - x\,^3D_3$
1	4466.9392	4468.1928	Fe I	CA	$z\,^3D_2 - f\,^3D_2$
25	4469.3742	4470.6285	Fe I	SD	$z\,^5P_2 - e\,^5P_3$
1	4471.6761	4472.9309	Fe I	CA	$a\,^5D_1 - z\,^7F_1$
80	4476.0171	4477.2731	Fe I	CA	$b\,^3P_1 - x\,^3D_2$
0	4476.0765	4477.3325	Fe I	CA	$z\,^5P_1 - e\,^5P_2$
5	4490.0833	4491.3430	Fe I	CA	$c\,^3P_2 - z\,^3S_1$
1	4478.0169	4479.2735	Fe I	CA	$a\,^5P_2 - y\,^7P_2$
4	4479.5981	4480.8550	Fe I	CA	$a\,^1I_6 - 6\ _5$
4	4479.6156	4480.8726	Fe I	CA	$z\,^5P_1 - g\,^5D_2$
2	4480.1352	4481.3923	Fe I	CA	$a\,^1G_4 - x\,^3F_4$
1	4481.6093	4482.8668	Fe I	CA	$z\,^5P_1 - e\,^3D_1$
80	4482.1690	4483.4267	Fe I	CA	$a\,^5D_1 - z\,^7F_2$
200	4482.2518	4483.5094	Fe I	CA	$a\,^5P_1 - x\,^5D_2$
2	4482.7386	4483.9964	Fe I	CA	$z\,^5P_2 - g\,^5D_3$
12	4484.2194	4485.4776	Fe I	CA	$z\,^5P_3 - g\,^5D_4$
5	4485.671	4486.930	Fe I	P	$z\,^5P_1 - e\,^5P_1$
4	4488.1343	4489.3935	Fe I	CA	$z\,^5P_3 - e\,^7F_2$
1	4488.9049	4490.1643	Fe I	CA	$z\,^5P_2 - e\,^3D_2$
50	4489.7389	4490.9985	Fe I	CA	$a\,^5D_0 - z\,^7F_1$
0	4492.6766	4493.9370	Fe I	CA	$z\,^3F_2 - g\,^5F_1$
0	4493.368	4494.629		P	
25	4494.5632	4495.8241	Fe I	CA	$a\,^5P_2 - x\,^5D_3$
0	4495.3891	4496.6503	Fe I	CA	$z\,^7F_0 - e\,^5D_1$
0	4495.4241	4496.6852	Fe I	CA	$z\,^3F_4 - h\,^5D_3$
0	4495.5661	4496.8273	Fe I	CA	$z\,^5P_3 - e\,^3D_3$
1	4495.9531	4497.2143	Fe I	CA	$z\,^5P_2 - f\,^5F_2$
2	4502.5911	4503.8541	Fe I	CA	$a\,^1H_5 - x\,^3H_6$
1	4504.829	4506.092	Fe I	P	$z\,^5D_2 - e\,^3F_3$
5	4514.1840	4515.4501	Fe I	CA	$a\,^1G_4 - u\,^5D_4$
0	4515.1645	4516.4308	Fe I	CA	$z\,^7F_2 - e\,^5D_2$
2	4517.5259	4518.7929	Fe I	CA	$c\,^3P_1 - y\,^3P_1$
1	4518.4319	4519.6991	Fe I	CA	$b\,^3H_6 - w\,^3G_5$
1	4523.4004	4524.6689	Fe I	CA	$z\,^5P_2 - e\,^7S_3$
15	4525.1413	4526.4103	Fe I	CA	$z\,^5P_3 - e\,^5S_2$
15	4525.1462	4526.4152	Fe I	CA	$z\,^5P_3 - e\,^7F_3$
1	4526.5620	4527.8314	Fe I	CA	$c\,^3P_0 - u\,^5D_1$
0	4527.7829	4529.0526	Fe I	CA	$a\,^3D_3 - x\,^3P_2$
50	4528.6133	4529.8832	Fe I	CA	$a\,^5P_3 - x\,^5D_4$
6	4529.556	4530.826	Fe I	P	$z\,^3D_3 - g\,^5F_4$
12	4531.1474	4532.4179	Fe I	CA	$a\,^3F_4 - y\,^5F_4$
1	4533.1301	4534.4012	Fe I	CA	$a\,^3D_1 - x\,^3P_0$
1	4536.4632	4537.7352	Fe I	CA	$b\,^3F_3 - y\,^5G_5$
12	4537.6712	4538.9435	Fe I	CA	$b\,^3H_5 - z\,^1H_5$
0	4538.7494	4540.0219	Fe I	CA	$a\,^3P_2 - x\,^5D_1$
0	4541.9428	4543.2162	Fe I	CA	$b\,^3H_5 - w\,^3G_4$
1	4542.4114	4543.6849	Fe I	CA	$b\,^3D_2 - v\,^3F_3$
0	4547.0170	4548.2918	Fe I	CA	$a\,^3F_3 - y\,^5F_2$
25	4547.8462	4549.1211	Fe I	CA	$a\,^1D_2 - z\,^1F_3$
0	4551.6491	4552.9250	Fe I	CA	$z\,^3F_3 - f\,^5G_4$
5	4552.548	4553.824	Fe I	P	
10	4556.1261	4557.4032	Fe I	CA	$z\,^3F_3 - f\,^3D_3$
0	4556.9252	4558.2025	Fe I	CA	$a\,^3D_3 - v\,^5P_2$
1	4558.111	4559.389	Fe I	P	
1	4560.0879	4561.3661	Fe I	CA	$z\,^5P_3 - e\,^5G_4$
1	4564.6991	4565.9785	Fe I	CA	$z\,^5P_2 - e\,^5G_2$
1	4564.8240	4566.1035	Fe I	CA	$c\,^3P_1 - y\,^3P_0$
1	4565.3123	4566.5919	Fe I	CA	$a\,^3D_1 - x\,^3P_2$
1	4565.6625	4566.9421	Fe I	CA	$z\,^5D_3 - e\,^5F_2$
1	4566.5143	4567.7942	Fe I	CA	$a\,^3D_2 - x\,^3P_1$
1	4566.9915	4568.2715	Fe I	CA	$a\,^1P_1 - w\,^3F_2$
5	4568.7643	4570.0448	Fe I	CA	$z\,^5D_2 - e\,^5F_1$
1	4572.8602	4574.1417	Fe I	CA	$z\,^5P_2 - e\,^7F_2$
1	4574.2143	4575.4962	Fe I	CA	$z\,^5D_4 - e\,^5F_3$
4	4574.7170	4575.9991	Fe I	CA	$a\,^3P_2 - x\,^5D_2$
1	4575.7822	4577.0646	Fe I	CA	$b\,^3H_4 - w\,^3G_3$
0	4579.329	4580.612	Fe I	P	
0	4579.8209	4581.1043	Fe I	CA	$c\,^3P_1 - z\,^3S_1$
2	4580.5755	4581.8591	Fe I	CA	$z\,^5P_2 - e\,^3D_3$
5	4581.507	4582.791	Fe I	P	$z\,^5D_3 - e\,^3F_4$
1	4584.7152	4585.9999	Fe I	CA	$z\,^5P_3 - f\,^7D_3$
1	4584.8193	4586.1040	Fe I	CA	$z\,^5P_3 - e\,^7P_2$
1	4587.1280	4588.4133	Fe I	CA	$a\,^1H_5 - x\,^1G_4$
6	4592.6506	4593.9374	Fe I	CA	$a\,^3F_3 - y\,^5F_3$
0	4593.525	4594.812	Fe I	P	$z\,^3F_3 - f\,^5P_2$
5	4595.3583	4596.6459	Fe I	CA	$b\,^3H_4 - z\,^1H_5$
2	4596.0604	4597.3481	Fe I	CA	$z\,^5P_3 - f\,^7D_4$
0	4596.4139	4597.7017	Fe I	CA	$z\,^5P_2 - e\,^5G_3$
4	4598.1177	4599.4060	Fe I	CA	$z\,^5D_1 - e\,^5F_1$
3	4600.9323	4602.2213	Fe I	CA	$b\,^3H_6 - x\,^3G_5$
1	4602.0002	4603.2895	Fe I	CA	$a\,^3F_2 - y\,^5F_1$
12	4602.9401	4604.2296	Fe I	CA	$a\,^3F_4 - y\,^5F_5$
0	4603.951	4605.240	Fe I	P	$b\,^3G_4 - x\,^5G_4$
6	4607.6439	4608.9347	Fe I	CA	$z\,^3F_2 - g\,^5F_3$
10	4611.2835	4612.5753	Fe I	CA	$z\,^5P_2 - e\,^5S_2$
10	4611.2887	4612.5804	Fe I	CA	$z\,^5P_2 - e\,^7F_3$
4	4613.2039	4614.4962	Fe I	CA	$z\,^5D_0 - e\,^5F_1$
2	4614.2054	4615.4979	Fe I	CA	$a\,^3D_2 - v\,^5P_1$
4	4618.7572	4620.0509	Fe I	CA	$b\,^3G_5 - y\,^3G_4$
8	4619.2864	4620.5802	Fe I	CA	$z\,^5P_3 - f\,^5D_2$
8	4625.0438	4626.3392	Fe I	CA	$z\,^5D_3 - e\,^5F_3$
1	4630.1205	4631.4172	Fe I	CA	$a\,^3P_2 - x\,^5D_3$
0	4631.482	4632.779	Fe I	P	$z\,^5G_4 - 3\ _4$
2	4632.9111	4634.2085	Fe I	CA	$a\,^3F_2 - y\,^5F_2$
0	4633.7552	4635.0529	Fe I	CA	$b\,^3G_3 - x\,^5G_3$
1	4635.8458	4637.1440	Fe I	CA	$b\,^3P_1 - y\,^5S_2$
8	4637.5034	4638.8021	Fe I	CA	$z\,^5D_1 - e\,^5F_2$
8	4638.0091	4639.3079	Fe I	CA	$z\,^5P_3 - e\,^7P_3$
4	4643.4633	4644.7636	Fe I	CA	$z\,^5P_2 - f\,^7D_2$
30	4647.4329	4648.7342	Fe I	CA	$b\,^3G_5 - y\,^3G_5$
1	4649.8196	4651.1216	Fe I	CA	$b\,^3H_6 - v\,^5F_5$
15	4654.4974	4655.8006	Fe I	CA	$a\,^3F_3 - y\,^5F_4$
15	4654.6086	4655.9118	Fe I	CA	$z\,^5P_3 - f\,^5D_3$
15	4654.6290	4655.9322	Fe I	CA	$z\,^5D_4 - e\,^5F_4$
6	4656.3936	4657.6973	Ne I	BA	
0	4657.5853	4658.8893	Fe I	CA	$b\,^3P_1 - w\,^5D_1$
0	4658.2937	4659.5979	Fe I	CA	$b\,^3H_5 - x\,^3G_4$
1	4661.5345	4662.8395	Fe I	CA	$y\,^5P_3 - 4\ _2$
3	4661.9699	4663.2751	Fe I	CA	$b\,^3G_4 - y\,^3G_3$
1	4663.1784	4664.4839	Fe I	CA	$a\,^1D_2 - w\,^3P_1$
15	4667.4528	4668.7594	Fe I	CA	$z\,^5P_3 - e\,^7P_4$
12	4668.1323	4669.4391	Fe I	CA	$z\,^5D_2 - e\,^5F_3$
4	4669.1724	4670.4794	Fe I	CA	$z\,^5P_2 - f\,^5D_1$
4	4673.1626	4674.4707	Fe I	CA	$z\,^5P_2 - f\,^7D_3$
15	4678.8451	4680.1547	Fe I	CA	$z\,^5P_3 - f\,^5D_4$
2	4679.222	4680.532	Fe I	P	$z\,^5F_4 - e\,^3F_3$
1	4680.2939	4681.6039	Fe I	CA	$a\,^3F_2 - y\,^5F_3$
1	4680.4674	4681.7774	Fe I	CA	$b\,^3P_0 - w\,^5D_1$
0	4682.5587	4683.8693	Fe I	CA	$z\,^7P_4 - e\,^5D_3$

562-903 O - 75 - 4

TABLE III. *Spectrum of the Fe-Ne hollow cathode*—Continued

Intensity	Wavelength (Å) Air	Wavelength (Å) Vacuum	Ion	Ref	Classification
1	4683.5607	4684.8716	Fe I	CA	$b\ ^3P_2 - w\ ^5D_2$
1	4687.3855	4688.6974	Fe I	CA	$b\ ^3P_2 - w\ ^5F_3$
1	4690.1354	4691.4480	Fe I	CA	$z\ ^5P_1 - f\ ^7D_1$
20	4691.4116	4692.7245	Fe I	CA	$b\ ^3G_4 - y\ ^3G_4$
1	4700.1914	4701.5066	Fe I	CA	$b\ ^1G_4 - x\ ^3H_5$
1	4701.0465	4702.3620	Fe I	CA	$z\ ^5P_1 - f\ ^7D_2$
25	4704.3949	4705.7113	Ne I	BA	
3	4704.947	4706.263	Fe I	P	$z\ ^5P_1 - f\ ^5D_0$
1	4705.4571	4706.7737	Fe I	CA	$a\ ^1D_2 - v\ ^3G_3$
20	4707.2717	4708.5888	Fe I	CA	$z\ ^5D_3 - e\ ^5F_4$
1	4707.4875	4708.8047	Fe I	CA	$b\ ^3P_1 - w\ ^5D_2$
30	4708.8619	4710.1795	Ne I	BA	
0	4708.9683	4710.2859	Fe I	CA	$b\ ^3D_2 - z\ ^1F_3$
5	4709.0857	4710.4033	Fe I	CA	$z\ ^5P_2 - f\ ^5D_2$
20	4710.0669	4711.3848	Ne I	BA	
20	4710.2828	4711.6008	Fe I	CA	$b\ ^3G_3 - y\ ^3G_3$
4	4712.0661	4713.3845	Ne I	BA	
2	4714.0679	4715.3869	Fe I	CA	$y\ ^5P_3 - i\ ^5D_2$
2	4714.1910	4715.5100	Fe I	CA	$b\ ^3H_4 - x\ ^3G_3$
15	4715.3466	4716.6659	Ne I	BA	
1	4720.9994	4722.3202	Fe I	CA	$b\ ^3G_4 - y\ ^3G_5$
0	4726.1373	4727.4595	Fe I	CA	$z\ ^7P_3 - e\ ^5D_2$
8	4727.3989	4728.7214	Fe I	CA	$z\ ^5P_1 - f\ ^5D_1$
6	4728.5449	4729.8677	Fe I	CA	$z\ ^5P_2 - e\ ^7P_3$
3	4729.0173	4730.3402	Fe I	CA	$c\ ^3F_4 - 12\ _5$
1	4729.675	4730.998	Fe I	P	$z\ ^5F_3 - e\ ^3F_3$
2	4733.5910	4734.9151	Fe I	CA	$a\ ^3F_4 - y\ ^5D_4$
1	4734.096	4735.420	Fe I	P	$b\ ^1D_2 - w\ ^1D_2$
6	4735.8418	4737.1665	Fe I	CA	$c\ ^3F_4 - t\ ^3G_5$
30	4736.7715	4738.0965	Fe I	CA	$z\ ^5D_4 - e\ ^5F_5$
1	4737.6346	4738.9598	Fe I	CA	$b\ ^3H_5 - z\ ^1G_4$
1	4740.3398	4741.6657	Fe I	CA	$b\ ^3G_3 - y\ ^3G_4$
1	4741.064	4742.390	Fe I	P	$z\ ^5F_5 - e\ ^3F_4$
2	4741.5288	4742.8550	Fe I	CA	$b\ ^3P_2 - w\ ^5D_3$
4	4745.8001	4747.1274	Fe I	CA	$z\ ^5P_2 - f\ ^5D_3$
4	4745.8398	4747.1671	Fe I	CA	$y\ ^5D_4 - f\ ^5G_3$
4	4749.9474	4751.2759	Fe I	CA	$y\ ^5P_3 - i\ ^5D_3$
10	4752.7320	4754.0612	Ne I	BA	
4	4757.5821	4758.9126	Fe I	CA	$a\ ^3D_1 - 1\ _2$
4	4757.595	4758.925	Fe I	P	$z\ ^3P_1 - e\ ^3P_1$
1	4765.4795	4766.8121	Fe I	CA	$a\ ^3F_2 - z\ ^3P_2$
0	4768.3183	4769.6516	Fe I	CA	$z\ ^5P_1 - f\ ^5D_2$
4	4768.3967	4769.7300	Fe I	CA	$z\ ^7P_4 - e\ ^5D_4$
0	4771.6961	4773.0303	Fe I	CA	$a\ ^5P_2 - y\ ^3D_2$
4	4772.8303	4774.6487	Fe I	CA	$c\ ^3P_2 - x\ ^3D_2$
1	4776.0690	4777.4044	Fe I	CA	$a\ ^3D_2 - y\ ^3S_1$
1	4776.385	4777.720	Fe I	P	$y\ ^5P_3 - i\ ^5D_4$
1	4779.4423	4780.7786	Fe I	CA	$a\ ^1P_1 - x\ ^3P_0$
1	4785.959	4787.297	Fe I	P	$c\ ^3F_3 - 13\ _4$
8	4786.8062	4788.1444	Fe I	CA	$c\ ^3P_2 - x\ ^3D_3$
1	4787.8273	4789.1658	Fe I	CA	$z\ ^7P_3 - e\ ^5D_3$
12	4788.7567	4790.0954	Fe I	ED	$b\ ^3H_6 - z\ ^3H_6$
25	4789.6499	4790.9889	Fe I	FE	$a\ ^1D_2 - z\ ^1D_2$
1	4791.2502	4792.5896	Fe I	CA	$a\ ^3D_1 - w\ ^3D_1$
3	4798.264	4799.605	Fe I	P	$c\ ^3F_2 - t\ ^3G_3$
0	4798.7311	4800.0725	Fe I	CA	$a\ ^3F_2 - y\ ^5D_2$
1	4799.4057	4800.7472	Fe I	CA	$b\ ^3D_2 - w\ ^3P_2$
1	4800.1281	4801.4699	Fe I	CA	$z\ ^7P_2 - e\ ^5D_2$
4	4800.648	4801.990	Fe I	P	$c\ ^3F_3 - t\ ^3G_4$
4	4802.8762	4804.2187	Fe I	CA	$b\ ^1G_4 - x\ ^1G_4$
4	4802.8807	4804.2231	Fe I	CA	$b\ ^3D_3 - w\ ^3P_2$
3	4804.5169	4805.8598	Fe I	CA	$a\ ^1H_5 - v\ ^3G_4$
6	4807.708	4809.052	Fe I	P	$z\ ^5F_4 - e\ ^3F_4$
1	4808.1467	4809.4906	Fe I	CA	$a\ ^3D_3 - w\ ^3D_3$
0	4809.1371	4810.4812	Fe I	CA	$b\ ^1G_4 - z\ ^1F_3$
0	4809.9404	4811.2848	Fe I	CA	$a\ ^1H_5 - y\ ^3H_5$
5	4810.0640	4811.4084	Ne I	BA	
4	4817.6386	4818.9850	Ne I	BA	
2	4818.788	4820.134	Ne I	P	
5	4821.9236	4823.2711	Ne I	BA	
1	4824.1667	4825.5148	Fe I	CA	$b\ ^3D_1 - w\ ^3P_1$
2	4832.7283	4834.0787	Fe I	CA	$b\ ^3D_2 - w\ ^3P_1$
2	4835.8686	4837.2199	Fe I	CA	$y\ ^5D_4 - f\ ^5G_4$
15	4837.3139	4838.6655	Ne I	BA	
2	4838.5130	4839.8649	Fe I	CA	$z\ ^5F_2 - e\ ^5F_1$
6	4839.5452	4840.8974	Fe I	CA	$b\ ^3H_5 - z\ ^3H_5$
1	4840.3218	4841.6742	Fe I	CA	$y\ ^5D_3 - f\ ^5G_3$
0	4841.782	4843.135	Fe I	P	$y\ ^5D_2 - f\ ^3D_1$
1	4842.7876	4844.1407	Fe I	CA	$y\ ^5D_4 - e\ ^3G_5$
4	4843.1437	4844.4969	Fe I	CA	$z\ ^5F_3 - e\ ^5F_2$
2	4844.0128	4845.3662	Fe I	CA	$a\ ^1D_2 - w\ ^3F_3$
1	4845.6474	4847.0012	Fe I	CA	$b\ ^3D_1 - w\ ^3P_0$
3	4855.6718	4857.0283	Fe I	CA	$z\ ^5F_4 - e\ ^5F_3$
0	4859.125	4860.483	Fe I	P	$y\ ^5D_2 - f\ ^5G_2$
50	4859.7406	4861.0982	Fe I	CA	$z\ ^7F_2 - e\ ^7D_1$
1	4860.983	4862.341	Fe I	P	$z\ ^5F_3 - e\ ^3F_4$
4	4863.6453	4865.0039	Fe I	CA	$z\ ^5F_1 - e\ ^5F_1$
120	4871.3172	4872.6778	Fe I	CA	$z\ ^7F_3 - e\ ^7D_2$
0	4871.9283	4873.2891	Fe I	CA	$a\ ^3D_3 - u\ ^5D_3$
60	4872.1363	4873.4971	Fe I	CA	$z\ ^7F_1 - e\ ^7D_1$
3	4875.8748	4877.2366	Fe I	CA	$z\ ^5F_5 - e\ ^5F_4$
30	4878.2081	4879.5705	Fe I	CA	$z\ ^7F_0 - e\ ^7D_1$
6	4881.7178	4883.0812	Fe I	CA	$b\ ^3H_4 - z\ ^3H_4$
5	4882.1440	4883.5075	Fe I	CA	$z\ ^5F_2 - e\ ^5F_2$
10	4884.9170	4886.2812	Ne I	BA	
6	4885.4303	4886.7947	Fe I	CA	$z\ ^3F_4 - g\ ^5D_3$
4	4886.336	4887.701	Fe I	P	$y\ ^5D_3 - h\ ^5D_2$
3	4887.1913	4888.5561	Fe I	CA	$y\ ^5D_2 - g\ ^5F_2$
5	4888.6319	4889.9971	Fe I	CA	$y\ ^5D_4 - h\ ^5D_3$
0	4889.0002	4890.3656	Fe I	CA	$a\ ^5P_2 - y\ ^3D_3$
4	4889.1020	4890.4673	Fe I	CA	$z\ ^3D_3 - g\ ^5D_3$
100	4890.7540	4892.1198	Fe I	CA	$z\ ^7F_2 - e\ ^7D_2$
250	4891.4919	4892.8579	Fe I	CA	$z\ ^7F_4 - e\ ^7D_3$
3	4892.866	4894.232	Fe I	P	$y\ ^5D_1 - f\ ^3D_1$
1	4896.4377	4897.8050	Fe I	CA	$z\ ^3D_3 - e\ ^3D_2$
30	4903.3087	4904.6778	Fe I	CA	$z\ ^7F_1 - e\ ^7D_2$
1	4905.1336	4906.5032	Fe I	CA	$z\ ^3D_2 - e\ ^5P_2$
3	4907.7328	4909.1031	Fe I	CA	$z\ ^5F_1 - e\ ^5F_2$
3	4909.3840	4910.7548	Fe I	CA	$z\ ^3D_2 - g\ ^5D_2$
8	4910.0150	4911.3859	Fe I	CA	$z\ ^5F_3 - e\ ^5F_3$
5	4910.3254	4911.6964	Fe I	CA	$y\ ^5D_2 - f\ ^5G_3$
5	4910.565	4911.936	Fe I	P	$y\ ^5D_1 - f\ ^5G_2$
1	4911.7788	4913.1501	Fe I	CA	$z\ ^3D_2 - e\ ^3D_1$
3	4917.2285	4918.6013	Fe I	CA	$y\ ^5D_2 - h\ ^5D_1$
2	4918.011	4919.384	Fe I	P	$y\ ^5D_0 - f\ ^3D_1$
150	4918.9925	4920.3658	Fe I	CA	$z\ ^7F_3 - e\ ^7D_3$
500	4920.5018	4921.8754	Fe I	CA	$z\ ^7F_5 - e\ ^7D_4$
6	4924.7699	4926.1447	Fe I	CA	$a\ ^3P_2 - y\ ^3D_2$
3	4927.4170	4928.7925	Fe I	CA	$a\ ^1H_5 - w\ ^3F_4$
3	4930.3148	4931.6910	Fe I	CA	$z\ ^3D_1 - g\ ^5D_1$
0	4933.1927	4934.5698	Fe I	CA	$y\ ^5D_2 - f\ ^3D_2$
5	4933.346	4934.723	Fe I	P	$y\ ^5D_0 - g\ ^5F_1$
6	4933.8740	4935.2513	Fe I	CA	$z\ ^3F_3 - e\ ^5P_2$
5	4934.0063	4935.3836	Fe I	CA	$y\ ^5D_3 - f\ ^5G_4$
6	4938.1745	4939.5528	Fe I	CA	$z\ ^3F_3 - g\ ^5D_2$
25	4938.8125	4940.1910	Fe I	CA	$z\ ^7F_2 - e\ ^7D_3$
10	4939.2334	4940.6120	Fe I	CA	$y\ ^5D_1 - g\ ^5F_2$
10	4939.6860	4941.0648	Fe I	CA	$a\ ^5F_5 - z\ ^5F_4$

TABLE III. *Spectrum of the Fe-Ne hollow cathode*—Continued

Intensity	Wavelength (Å) Air	Wavelength (Å) Vacuum	Ion	Ref	Classification
1	4945.6365	4947.0168	Fe I	CA	$z\,^3P_2 - f\,^5G_3$
12	4946.3849	4947.7655	Fe I	CA	$z\,^5F_4 - e\,^5F_4$
5	4950.1041	4951.4857	Fe I	CA	$z\,^5F_2 - e\,^5F_3$
2	4952.6393	4954.0215	Fe I	CA	$z\,^3P_2 - h\,^5D_1$
12	4957.2982	4958.6817	Fe I	CA	$z\,^7F_4 - e\,^7D_4$
1500	4957.5966	4958.9801	Fe I	CA	$z\,^7F_6 - e\,^7D_5$
2	4962.555	4963.940	Fe I	P	$y\,^5F_5 - e\,^3H_6$
25	4966.0872	4967.4730	Fe I	CA	$z\,^5F_5 - e\,^5F_5$
10	4967.896	4969.282	Fe I	P	$y\,^5D_2 - f\,^5P_1$
4	4968.689	4970.076	Fe I	P	$b\,^3D_2 - z\,^1D_2$
6	4969.9157	4971.3025	Fe I	CA	$y\,^5D_1 - h\,^5D_1$
3	4970.4986	4971.8856	Fe I	CA	$b\,^3D_1 - w\,^3F_2$
10	4973.1005	4974.4881	Fe I	CA	$z\,^3D_1 - e\,^3D_1$
6	4978.6037	4979.9928	Fe I	CA	$z\,^3F_2 - g\,^5D_1$
25	4982.4977	4983.8878	Fe I	FE	$y\,^5D_4 - f\,^5P_3$
15	4983.248	4984.638	Fe I	P	$y\,^5D_3 - f\,^5P_2$
20	4983.8517	4985.2422	Fe I	FE	$y\,^5D_4 - h\,^5D_4$
15	4985.2514	4986.6422	Fe I	CA	$z\,^3D_2 - e\,^3D_2$
12	4985.5458	4986.9368	Fe I	CA	$z\,^7F_3 - e\,^7D_4$
1	4986.2244	4987.6155	Fe I	CA	$y\,^5D_1 - f\,^3D_2$
10	4988.9450	4990.3369	Fe I	CA	$y\,^5D_3 - h\,^5D_3$
3	4991.2667	4992.6592	Fe I	CA	$y\,^5D_2 - g\,^5F_3$
1	4993.676	4995.069	Fe I	P	$z\,^3P_2 - h\,^5D_2$
15	4994.1288	4995.5221	Fe I	CA	$a\,^5F_4 - z\,^5F_3$
1	4999.114	5000.509	Fe I	P	$c\,^3F_2 - x\,^1F_3$
80	5001.8622	5003.2575	Fe I	CA	$z\,^3F_4 - e\,^3D_3$
6	5002.7893	5004.1848	Fe I	CA	$z\,^5F_3 - e\,^5F_4$
4	5004.036	5005.432	Fe I	P	$z\,^3P_2 - f\,^5P_1$
40	5005.1587	5006.5553	Ne I	BA	
30	5005.7110	5007.1073	Fe I	CA	$z\,^3D_3 - e\,^3D_3$
100	5006.1175	5007.5140	Fe I	CA	$z\,^7F_5 - e\,^7D_5$
10	5007.2463	5008.6431	Fe I	CA	$z\,^3F_3 - g\,^5D_3$
60	5012.0674	5013.4654	Fe I	CA	$a\,^5F_5 - z\,^5F_5$
30	5014.9412	5016.3399	Fe I	CA	$z\,^3F_3 - e\,^3D_2$
15	5022.2353	5023.6360	Fe I	CA	$z\,^3F_2 - e\,^3D_1$
3	5023.4984	5024.8994	Fe I	CA	$z\,^5G_5 - f\,^3F_4$
12	5027.122	5028.524	Fe I	BW	$y\,^5D_3 - g\,^5F_4$
0	5027.2257	5028.6278	Fe I	CA	$b\,^3D_2 - w\,^3F_3$
1	5027.7558	5029.1580	Fe I	CA	$z\,^3P_2 - g\,^5F_3$
12	5028.1260	5029.5283	Fe I	CA	$a\,^1H_5 - y\,^1G_4$
2	5029.6211	5031.0237	Fe I	CA	$a\,^1P_1 - 1\ _2$
25	5030.772	5032.175	Fe I	P	$b\,^3H_6 - z\,^3I_7$
25	5031.3504	5032.7539	Ne I	BA	
100	5037.7512	5039.1560	Ne I	BA	
4	5039.2501	5040.6554	Fe I	CA	$z\,^5F_4 - e\,^5F_5$
8	5040.8528	5042.2585	Fe I	CA	$y\,^5F_3 - f\,^5G_3$
8	5040.898	5042.304	Fe I	P	$y\,^5F_2 - e\,^3G_3$
15	5041.0708	5042.4765	Fe I	CA	$a\,^5F_3 - z\,^5F_2$
150	5041.7553	5043.1612	Fe I	CA	$a\,^3F_4 - z\,^3F_3$
4	5044.2105	5045.6171	Fe I	CA	$z\,^7F_4 - e\,^7D_5$
4	5048.4331	5049.8408	Fe I	CA	$z\,^3D_1 - e\,^3D_2$
30	5049.8193	5051.2273	Fe I	CA	$a\,^3P_2 - y\,^3D_3$
30	5051.6336	5053.0421	Fe I	CA	$a\,^5F_4 - z\,^5F_4$
1	5054.6415	5056.0508	Fe I	CA	$b\,^3D_2 - v\,^3D_3$
1	5060.0780	5061.4888	Fe I	CA	$a\,^5D_4 - z\,^7D_3$
20	5065.016	5066.428	Fe I	P	$y\,^5F_3 - e\,^3G_4$
4	5065.1935	5066.6056	Fe I	CA	$b\,^3D_3 - w\,^3F_4$
3	5067.1508	5068.5634	Fe I	CA	$y\,^5F_4 - f\,^5G_4$
20	5068.7653	5070.1783	Fe I	CA	$z\,^7P_4 - e\,^7D_3$
0	5072.0758	5073.4898	Fe I	CA	$y\,^5F_2 - g\,^5F_2$
2	5072.665	5074.079	Fe I	P	$y\,^5F_4 - f\,^3D_3$
20	5074.2007	5075.6156	Ne I	BA	
25	5074.7479	5076.1626	Fe I	CA	$y\,^5F_4 - e\,^3G_5$
2	5076.2620	5077.6771	Fe I	CA	$y\,^5F_1 - g\,^5F_1$
0	5078.971	5080.387	Fe I	FE	$y\,^5F_1 - f\,^5G_2$
12	5079.2238	5080.6396	Fe I	CA	$a\,^5P_2 - y\,^5P_1$
10	5079.7385	5081.1545	Fe I	CA	$a\,^5F_2 - z\,^5F_1$
60	5080.3852	5081.8014	Ne I	BA	
20	5083.3377	5084.7547	Fe I	CA	$a\,^5F_3 - z\,^5F_3$
4	5090.775	5092.194	Fe I	BW	$y\,^5F_3 - h\,^5D_2$
5	5096.9978	5098.4184	Fe I	CA	$y\,^5F_2 - f\,^5G_3$
4	5098.5705	5099.9915	Fe I	CA	$z\,^3D_2 - e\,^3D_3$
8	5098.6990	5100.1201	Fe I	CA	$a\,^5P_3 - y\,^5P_2$
0	5104.4362	5105.8587	Fe I	CA	$y\,^5F_2 - h\,^5D_1$
15	5107.4464	5108.8697	Fe I	CA	$a\,^5F_2 - z\,^5F_2$
5	5107.6408	5109.0643	Fe I	CA	$a\,^3F_3 - z\,^3F_2$
5	5109.6497	5111.0736	Fe I	CA	$y\,^5F_1 - g\,^5F_2$
150	5110.3573	5111.7814	Fe I	CA	$a\,^1H_5 - z\,^1H_5$
150	5110.4125	5111.8366	Fe I	CA	$a\,^5D_4 - z\,^7D_4$
20	5113.6724	5115.0978	Ne I	BA	
1	5115.7757	5117.2013	Fe I	CA	$a\,^1H_5 - w\,^3G_4$
80	5116.503	5117.929	Ne I	P	
3	5121.6411	5123.0683	Fe I	CA	$y\,^5F_2 - f\,^3D_2$
20	5123.7190	5125.1467	Fe I	CA	$a\,^5F_1 - z\,^5F_1$
15	5125.1119	5126.5399	Fe I	CA	$y\,^5F_4 - h\,^5D_3$
1	5126.1918	5127.6202	Fe I	CA	$y\,^5F_3 - g\,^5F_3$
10	5127.3581	5128.7867	Fe I	CA	$a\,^5F_4 - z\,^5F_5$
1	5129.6295	5131.0588	Fe I	CA	$z\,^3F_3 - e\,^3D_3$
1	5131.4697	5132.8994	Fe I	CA	$a\,^5P_1 - y\,^5P_1$
40	5133.6885	5135.1189	Fe I	FE	$y\,^5F_5 - f\,^5G_6$
12	5137.380	5138.812	Fe I	P	$y\,^5F_5 - h\,^5D_4$
40	5139.2507	5140.6826	Fe I	CA	$z\,^7P_3 - e\,^7D_2$
100	5139.4621	5140.8940	Fe I	CA	$z\,^7P_4 - e\,^7D_4$
2	5141.7387	5143.1712	Fe I	CA	$a\,^3P_1 - y\,^3D_1$
10	5142.4928	5143.9255	Fe I	CA	$y\,^5F_1 - h\,^5D_1$
10	5142.9275	5144.3603	Fe I	CA	$a\,^5F_3 - z\,^5F_4$
0	5145.0945	5146.5279	Fe I	CA	$a\,^5P_2 - y\,^5P_2$
4	5148.048	5149.482	Fe I	P	$y\,^5F_2 - h\,^5D_2$
6	5148.220	5149.654	Fe I	P	$y\,^5F_3 - f\,^3D_3$
3	5150.8385	5152.2734	Fe I	CA	$a\,^5F_2 - z\,^5F_3$
25	5151.9101	5153.3453	Fe I	CA	$a\,^5F_1 - z\,^5F_2$
25	5151.9610	5153.3976	Ne I	BA	
4	5159.058	5160.495	Fe I	P	$y\,^5F_2 - f\,^5P_1$
30	5162.2710	5163.7090	Fe I	FE	$y\,^5F_5 - g\,^5F_5$
1	5164.552	5165.991	Fe I	P	$z\,^3G_4 - f\,^3F_3$
6	5165.411	5166.850	Fe I	BW	$y\,^5F_4 - g\,^5F_4$
80	5166.2814	5167.7204	Fe I	CA	$a\,^5D_4 - z\,^7D_5$
2500	5167.4873	5168.9267	Fe I	CA	$a\,^3F_4 - z\,^3D_3$
80	5168.8968	5170.3366	Fe I	CA	$a\,^5D_3 - z\,^7D_3$
500	5171.5953	5173.0357	Fe I	CA	$a\,^3F_4 - z\,^3F_4$
1	5178.8028	5180.2452	Fe I	CA	$z\,^3G_5 - z\,^3F_4$
2	5184.2649	5185.7087	Fe I	CA	$y\,^5F_2 - g\,^5F_3$
2	5187.908	5189.353	Fe I	P	$c\,^3F_3 - t\,^3D_2$
30	5188.6122	5190.0572	Ne I	BA	
50	5191.4545	5192.9002	Fe I	CA	$z\,^7P_2 - e\,^7D_1$
80	5192.3433	5193.7893	Fe I	CA	$z\,^7P_3 - e\,^7D_3$
200	5194.9412	5196.3878	Fe I	CA	$a\,^3F_3 - z\,^3F_3$
10	5195.4732	5196.9200	Fe I	FE	$y\,^5F_4 - f\,^5G_5$
4	5196.1020	5197.5490	Fe I	FE	$y\,^5F_3 - f\,^5P_2$
2	5198.7114	5200.1591	Fe I	CA	$a\,^5P_1 - y\,^5P_2$
8	5202.3351	5203.7837	Fe I	CA	$a\,^5P_3 - y\,^5P_3$
30	5203.8962	5205.3453	Ne I	BA	
30	5204.5821	5206.0313	Fe I	CA	$a\,^5D_2 - z\,^7D_2$
15	5208.5932	5210.0435	Fe I	CA	$z\,^5D_3 - e\,^5D_2$
8	5210.5672	5212.0184	Ne I	BA	
25	5215.1793	5216.6313	Fe I	CA	$z\,^5D_2 - e\,^5D_1$
150	5216.2737	5217.7260	Fe I	CA	$a\,^3F_2 - z\,^3F_2$
15	5217.3889	5218.8415	Fe I	CA	$z\,^5D_4 - e\,^5D_3$

TABLE III. *Spectrum of the Fe-Ne hollow cathode*—Continued

Intensity	Wavelength (Å) Air	Wavelength (Å) Vacuum	Ion	Ref	Classification
40	5222.3517	5223.8061	Ne I	BA	
8	5225.5253	5226.9801	Fe I	CA	$a\,^5F_1 - z\,^7D_1$
60	5226.8616	5228.3167	Fe I	CA	$z\,^7P_2 - e\,^7D_2$
1000	5227.1502	5228.6054	Fe I	CA	$a\,^3P_1 - y\,^3D_2$
1000	5227.1892	5228.6444	Fe I	CA	$a\,^3F_3 - z\,^3D_2$
15	5229.8474	5231.3031	Fe I	FE	$z\,^5D_1 - e\,^5D_0$
250	5232.9394	5234.3962	Fe I	CA	$z\,^7P_4 - e\,^7D_5$
5	5235.4166	5236.8741	Fe I	CA	$b\,^3F_3 - x\,^5D_3$
15	5242.4907	5243.9500	Fe I	CA	$a\,^1I_6 - z\,^1H_5$
2	5243.783	5245.243	Fe I	P	$y\,^5F_3 - g\,^5F_4$
10	5247.0488	5248.5093	Fe I	CA	$a\,^5D_2 - z\,^7D_3$
2	5250.2083	5251.6697	Fe I	CA	$a\,^5D_0 - z\,^7D_1$
6	5250.6447	5252.1062	Fe I	CA	$a\,^5P_2 - y\,^5P_3$
12	5253.4610	5254.9233	Fe I	CA	$z\,^5D_1 - e\,^5D_1$
15	5263.3047	5264.7696	Fe I	CA	$z\,^5D_2 - e\,^5D_2$
100	5266.5546	5268.0203	Fe I	CA	$z\,^7P_3 - e\,^7D_4$
1200	5269.5366	5271.0032	Fe I	CA	$a\,^5F_5 - z\,^5D_4$
800	5270.3571	5271.8239	Fe I	CA	$a\,^3F_2 - z\,^3D_1$
15	5273.1631	5274.6306	Fe I	CA	$z\,^5D_0 - e\,^5D_1$
4	5273.3736	5274.8412	Fe I	CA	$a\,^3P_0 - y\,^3D_1$
5	5280.0853	5281.5551	Ne I	BA	
30	5281.7894	5283.2592	Fe I	CA	$z\,^7P_2 - e\,^7D_3$
60	5283.6206	5285.0909	Fe I	CA	$z\,^5D_3 - e\,^5D_3$
3	5288.5279	5289.9995	Fe I	CA	$b\,^1G_4 - y\,^1G_4$
20	5298.1891	5299.6637	Ne I	BA	
25	5302.2989	5303.7742	Fe I	CA	$z\,^5D_1 - e\,^5D_2$
12	5304.7580	5306.2353	Ne I	BA	
20	5307.3600	5308.8367	Fe I	CA	$a\,^3F_2 - z\,^3F_3$
1	5322.0407	5323.5213	Fe I	CA	$a\,^3P_2 - y\,^3F_3$
150	5324.1782	5325.6593	Fe I	CA	$z\,^5D_4 - e\,^5D_4$
800	5328.0376	5329.5197	Fe I	CA	$a\,^5F_4 - z\,^5D_3$
300	5328.5306	5330.0129	Fe I	CA	$a\,^3F_3 - z\,^3D_3$
5	5329.9873	5331.4699	Fe I	CA	$c\,^3F_4 - 6\ s$
250	5330.7775	5332.2608	Ne I	BA	
100	5332.8987	5334.3822	Fe I	CA	$a\,^3F_3 - z\,^3F_4$
80	5339.9282	5341.4135	Fe I	CA	$z\,^5D_2 - e\,^5D_3$
500	5341.0233	5342.5089	Fe I	CA	$a\,^3F_2 - z\,^3D_2$
80	5343.2834	5344.7700	Ne I	BA	
6	5349.2038	5350.6910	Ne I	BA	
12	5360.0121	5361.5032	Ne I	BA	
25	5364.8717	5366.3637	Fe I	FE	$z\,^5G_2 - e\,^5H_3$
20	5365.3963	5366.8884	Fe I	CA	$a\,^1H_5 - z\,^1G_4$
40	5367.4671	5368.9598	Fe I	SD	$z\,^5G_3 - e\,^5H_4$
50	5369.9621	5371.4554	Fe I	SD	$z\,^5G_4 - e\,^5H_5$
400	5371.4892	5372.9829	Fe I	CA	$a\,^5F_3 - z\,^5D_2$
4	5373.7096	5375.2039	Fe I	CA	$z\,^3G_3 - f\,^3F_4$
4	5379.5740	5381.0699	Fe I	CA	$b\,^1G_4 - z\,^1H_5$
60	5383.3689	5384.8658	Fe I	SD	$z\,^5G_5 - e\,^5H_6$
6	5389.4786	5390.9771	Fe I	CA	$z\,^5G_3 - f\,^5G_3$
40	5393.1668	5394.6663	Fe I	CA	$z\,^5D_3 - e\,^5D_4$
300	5397.1269	5398.6275	Fe I	CA	$a\,^5F_4 - z\,^5D_4$
1	5397.6187	5399.1194	Fe I	CA	$a\,^1I_6 - x\,^3G_5$
0	5400.5022	5402.0037	Fe I	CA	$z\,^5G_4 - f\,^5G_4$
600	5400.5617	5402.0632	Ne I	KE	
5	5403.8182	5405.3206	Fe I	CA	$c\,^3F_4 - u\,^3G_5$
60	5404.1185	5405.6209	Fe I	FE	$z\,^5G_5 - f\,^5G_5$
0	5404.1510	5405.6534	Fe I	FE	$z\,^3G_4 - e\,^3H_5$
250	5405.7741	5407.2770	Fe I	CA	$a\,^5F_2 - z\,^5D_1$
30	5410.9101	5412.4143	Fe I	SD	$z\,^3G_3 - e\,^3H_4$
60	5415.1997	5416.7051	Fe I	SD	$z\,^3G_5 - e\,^3H_6$
60	5424.0686	5425.5764	Fe I	SD	$z\,^5G_6 - e\,^5H_7$
250	5429.6955	5431.2048	Fe I	CA	$a\,^5F_3 - z\,^5D_3$
2	5432.9460	5434.4562	Fe I	CA	$z\,^5G_2 - g\,^5F_2$
15	5433.6513	5435.1620	Ne I	BA	
100	5434.5228	5436.0333	Fe I	CA	$a\,^5F_1 - z\,^5D_0$
20	5445.0424	5446.5558	Fe I	CA	$z\,^3G_5 - e\,^3G_5$
200	5446.8713	5448.3852	Fe I	CA	$a\,^3F_2 - z\,^3D_3$
200	5446.9161	5448.4300	Fe I	CA	$a\,^5F_2 - z\,^5D_2$
25	5455.453	5456.969	Fe I	BW	$z\,^5G_6 - f\,^5G_6$
120	5455.6090	5457.1252	Fe I	CA	$a\,^5F_1 - z\,^5D_1$
8	5462.9601	5464.4782	Fe I	FE	$z\,^3G_3 - e\,^3G_3$
15	5463.2749	5464.7931	Fe I	FE	$z\,^3G_4 - e\,^3G_4$
4	5466.3897	5467.9088	Fe I	CA	$z\,^5G_4 - h\,^5D_3$
6	5473.9003	5475.4213	Fe I	CA	$y\,^5D_3 - g\,^5D_3$
12	5476.5634	5478.0851	Fe I	CA	$y\,^5D_4 - g\,^5D_4$
6	5487.7433	5489.2681	Fe I	FE	$c\,^3F_3 - t\,^5D_2$
6	5494.4613	5495.9879	Fe I	CA	$c\,^3F_4 - x\,^3H_5$
25	5497.5160	5499.0434	Fe I	CA	$a\,^5F_1 - z\,^5D_2$
20	5501.4641	5502.9925	Fe I	CA	$a\,^5F_3 - z\,^5D_4$
3	5505.8820	5507.4116	Fe I	CA	$z\,^5G_3 - f\,^5G_4$
30	5506.7776	5508.3074	Fe I	CA	$a\,^5F_2 - z\,^5D_3$
4	5535.4148	5536.9523	Fe I	CA	$a\,^3D_3 - w\,^5F_2$
4	5543.1468	5544.6863	Fe I	CA	$b\,^1G_4 - x\,^3G_3$
2	5543.9364	5545.4761	Fe I	CA	$y\,^5D_1 - g\,^5D_2$
6	5554.8932	5556.4359	Fe I	CA	$y\,^3F_4 - f\,^3F_4$
50	5562.7662	5564.3114	Ne I	BA	
4	5563.5990	5565.1440	Fe I	CA	$y\,^5D_2 - g\,^5D_3$
6	5565.7040	5567.2496	Fe I	FE	$y\,^3F_3 - f\,^3F_3$
30	5569.6177	5571.1644	Fe I	CA	$z\,^5F_2 - e\,^5D_1$
60	5572.8412	5574.3887	Fe I	CA	$z\,^5F_3 - e\,^5D_2$
15	5576.0874	5577.6358	Fe I	SD	$z\,^5F_1 - e\,^5D_0$
120	5586.7553	5588.3066	Fe I	CA	$z\,^5F_4 - e\,^5D_3$
1	5594.6586	5596.2119	Fe I	FE	$y\,^3F_4 - e\,^3H_4$
6	5598.2973	5599.8516	Fe I	FE	$y\,^3F_2 - f\,^3F_2$
15	5602.9449	5604.5004	Fe I	CA	$z\,^5F_1 - e\,^5D_1$
1	5615.2990	5616.8579	Fe I	CA	$b\,^3F_3 - y\,^3D_2$
200	5615.6436	5617.2026	Fe I	CA	$z\,^5F_5 - e\,^5D_4$
20	5624.5413	5626.1026	Fe I	CA	$z\,^5F_2 - e\,^5D_2$
15	5652.5664	5654.1352	Ne I	BA	
100	5656.6588	5558.2024	Ne I	BA	
15	5658.8156	5660.3860	Fe I	CA	$z\,^5F_3 - e\,^5D_3$
50	5662.5153	5664.0867	Fe I	CA	$y\,^5F_5 - g\,^5D_4$
80	5689.8163	5691.3955	Ne I	BA	
0	5701.5448	5703.1267	Fe I	CA	$b\,^3F_4 - y\,^3D_3$
0	5709.3777	5710.9617	Fe I	CA	$z\,^5F_4 - e\,^5D_4$
50	5719.2248	5720.8119	Ne I	BA	
120	5748.2985	5749.8933	Ne I	BA	
0	5753.1213	5754.7170	Fe I	CA	$z\,^3P_1 - e\,^3D_2$
20	5762.9901	5764.5884	Fe I	CA	$z\,^3P_2 - e\,^3D_3$
800	5764.4188	5766.0170	Ne I	BA	
0	5775.0795	5776.6811	Fe I	CA	$y\,^5F_4 - g\,^5D_4$
120	5804.4496	5806.0595	Ne I	BA	
400	5820.1558	5821.7699	Ne I	BA	
25000	5852.4878	5854.1101	Ne I	KE	
30	5862.3534	5863.9783	Fe I	CA	$y\,^3F_4 - e\,^3G_5$
200	5872.8275	5874.4557	Ne I	BA	
10000	5881.8952	5883.5254	Ne I	KE	
400	5902.4623	5904.0984	Ne I	BA	
150	5906.4294	5908.0666	Ne I	BA	
80	5913.6327	5915.2718	Ne I	BA	
30	5914.1145	5915.7532	Fe I	CA	$y\,^3F_3 - f\,^3D_2$
80	5918.9068	5920.5473	Ne I	BA	
12000	5944.8342	5946.4812	Ne I	KE	
50	5961.6228	5963.2748	Ne I	BA	
200	5965.4710	5967.1250	Ne I	BA	
3000	5975.5340	5977.1892	Ne I	KE	
30	5986.9560	5988.6143	Fe I	CA	$y\,^3D_2 - e\,^3P_1$
120	5987.9074	5989.5664	Ne I	BA	

TABLE III. *Spectrum of the Fe-Ne hollow cathode*—Continued

Intensity	Wavelength (Å) Air	Wavelength (Å) Vacuum	Ion	Ref	Classification
50	5991.6532	5993.3132	Ne I	BA	
5000	6029.9969	6031.6667	Ne I	KE	
40	6065.4820	6067.1614	Fe I	CA	$b\,^3F_2 - y\,^3F_2$
12000	6074.3377	6076.0194	Ne I	KE	
15000	6096.1631	6097.8507	Ne I	KE	
30	6102.1593	6103.8485	Fe I	CA	$y\,^3D_1 - f\,^3F_2$
1000	6128.4499	6130.1462	Ne I	KE	
40	6136.6144	6138.3128	Fe I	CA	$a\,^3H_4 - z\,^3G_3$
40	6137.6937	6139.3924	Fe I	CA	$b\,^3F_3 - y\,^3F_3$
15000	6143.0626	6144.7628	Ne I	KE	
10000	6163.5939	6165.2996	Ne I	KE	
200	6182.1460	6183.8581	Ne I	BA	
40	6191.5583	6193.2715	Fe I	CA	$a\,^3H_5 - z\,^3G_4$
30	6213.4289	6215.1479	Fe I	CA	$a\,^5P_1 - y\,^5D_1$
10000	6217.2812	6219.0013	Ne I	KE	
30	6219.2794	6221.0000	Fe I	CA	$a\,^5P_2 - y\,^5D_2$
40	6230.7260	6232.4497	Fe I	CA	$b\,^3F_4 - y\,^3F_4$
20	6246.3172	6248.0451	Fe I	CA	$z\,^5P_3 - e\,^5D_3$
30	6252.5537	6254.2832	Fe I	CA	$a\,^3H_6 - z\,^3G_5$
10	6265.1312	6266.8641	Fe I	CA	$a\,^5P_3 - y\,^5D_3$
15000	6266.4950	6268.2283	Ne I	KE	
15	6301.4983	6303.2410	Fe I	CA	$z\,^5P_2 - e\,^5D_2$
10000	6304.7890	6306.5325	Ne I	KE	
10	6318.0176	6319.7647	Fe I	CA	$a\,^3H_4 - z\,^5G_3$
20000	6334.4278	6336.1794	Ne I	KE	
15000	6382.9917	6384.7562	Ne I	KE	
20	6393.6018	6395.3692	Fe I	CA	$a\,^3H_5 - z\,^5G_4$
30	6399.9995	6401.7686	Fe I	CA	$z\,^5P_3 - e\,^5D_4$
25000	6402.2460	6404.0157	Ne I	KE	
20	6411.6468	6413.4191	Fe I	CA	$z\,^5P_2 - e\,^5D_3$
15	6421.3487	6423.1241	Fe I	CA	$a\,^3P_2 - z\,^3P_2$
60	6444.7118	6446.4929	Ne I	BA	
60	6494.9807	6496.7753	Fe I	CA	$a\,^3H_6 - z\,^5G_5$
20000	6506.5281	6508.3259	Ne I	KE	
12000	6532.8822	6534.6870	Ne I	KE	
12	6546.2385	6548.0470	Fe I	CA	$a\,^3G_3 - y\,^3F_2$
20	6592.9131	6594.7341	Fe I	CA	$a\,^3G_4 - y\,^3F_3$
15000	6598.9529	6600.7755	Ne I	KE	
150	6652.0927	6653.9295	Ne I	KE	
40	6677.9892	6679.8331	Fe I	CA	$a\,^3G_5 - y\,^3F_4$
25000	6678.2762	6680.1202	Ne I	KE	
20000	6717.0430	6718.8974	Ne I	KE	
25000	6929.4673	6931.3788	Ne I	KE	
10	6945.2031	6947.1189	Fe I	CA	$a\,^3P_1 - z\,^3P_2$
6	6978.8499	6980.7747	Fe I	CA	$a\,^3P_0 - z\,^3P_1$
4000	7024.0504	7025.9874	Ne I	KE	
25000	7032.4131	7034.3524	Ne I	KE	
200	7051.2923	7053.2366	Ne I	KE	
800	7059.1074	7061.0538	Ne I	KE	
10000	7173.9381	7175.9155	Ne I	KE	
30	7207.3809	7209.3673	Fe I	CA	$y\,^5D_3 - e\,^5F_4$
20000	7245.1666	7247.1631	Ne I	KE	
12	7389.4009	7391.4363	Fe I	CA	$y\,^5F_1 - e\,^5F_1$
15	7411.1539	7413.1958	Fe I	CA	$y\,^5F_2 - e\,^5F_2$
30	7445.7458	7447.7964	Fe I	CA	$y\,^5F_3 - e\,^5F_3$
250	7472.4386	7474.4964	Ne I	KE	
2500	7488.8712	7490.9335	Ne I	KE	
40	7495.0593	7497.1233	Fe I	CA	$y\,^5F_4 - e\,^5F_4$
60	7511.0452	7513.1135	Fe I	CA	$y\,^5F_5 - e\,^5F_5$
2500	7535.7741	7537.8490	Ne I	BA	
1000	7544.0443	7546.1215	Ne I	BA	
12	7748.2733	7750.4056	Fe I	CA	$b\,^3G_5 - y\,^3F_4$
15	7839.0546	7841.2114	Ne I	KE	
30	7927.1177	7929.2983	Ne I	KE	
100	7936.9961	7939.1793	Ne I	KE	
80	7937.1307	7939.3140	Fe I	CA	$z\,^5G_5 - e\,^5F_4$
500	7943.1814	7945.3663	Ne I	KE	
60	7945.9842	7948.1699	Fe I	CA	$a\,^3P_1 - z\,^3F_2$
80	7998.9395	8001.1394	Fe I	CA	$z\,^5G_4 - e\,^5F_3$
60	8046.0466	8048.2593	Fe I	CA	$z\,^5G_3 - e\,^5F_2$
400	8082.4581	8084.6806	Ne I	KE	
50	8085.1760	8087.3992	Fe I	CA	$z\,^5G_2 - e\,^5F_1$
250	8118.5492	8120.7815	Ne I	KE	
80	8128.9108	8131.1459	Ne I	KE	
1000	8136.4057	8138.6428	Ne I	KE	
20	8248.6824	8250.9498	Ne I	KE	
200	8259.3790	8261.6493	Ne I	KE	
500	8266.0772	8268.3493	Ne I	KE	
2000	8300.3263	8302.6077	Ne I	KE	
120	8327.0526	8329.3412	Fe I	CA	$a\,^5P_2 - z\,^5P_1$
20	8331.9076	8334.1975	Fe I	CA	$z\,^3G_5 - e\,^5F_4$
250	8365.7486	8368.0476	Ne I	KE	
10000	8377.6065	8379.9088	Ne I	KE	
120	8387.7700	8390.0750	Fe I	CA	$a\,^5P_3 - z\,^5P_2$
1500	8418.4274	8420.7408	Ne I	KE	
300	8463.3575	8465.6830	Ne I	KE	
30	8468.4042	8470.7310	Fe I	CA	$a\,^5P_1 - z\,^5P_1$
80	8484.4435	8486.7746	Ne I	KE	
6000	8495.3598	8497.6940	Ne I	KE	
15	8514.0694	8516.4086	Fe I	CA	$a\,^5P_2 - z\,^5P_2$
100	8544.6959	8547.0433	Ne I	KE	
200	8571.3524	8573.7071	Ne I	KE	
3000	8591.2587	8593.6188	Ne I	KE	
2500	8634.6470	8637.0188	Ne I	KE	
5000	8654.3831	8656.7602	Ne I	KE	
60	8661.8978	8664.2769	Fe I	CA	$a\,^5P_1 - z\,^5P_2$
1000	8679.4925	8681.8765	Ne I	KE	
1200	8681.9211	8684.3057	Ne I	KE	
150	8688.6213	8691.0077	Fe I	CA	$a\,^5P_3 - z\,^5P_3$
150	8704.1116	8706.5022	Ne I	KE	
800	8771.6563	8774.0652	Ne I	KE	
4000	8780.6210	8783.0323	Ne I	KE	
3000	8783.7533	8786.1654	Ne I	KE	
20	8824.2166	8826.6397	Fe I	CA	$a\,^5P_2 - z\,^5P_3$
40	8830.9072	8833.3321	Ne I	KE	
1500	8853.8669	8856.2979	Ne I	KE	
1000	8865.3063	8867.7405	Ne I	KE	
1000	8865.7552	8868.1895	Ne I	KE	
400	8919.5007	8921.9495	Ne I	BA	
10	8999.5546	9002.0251	Fe I	CA	$^3P_2 - z\,^3P_2$

90mA Iron-Neon
Hollow Cathode

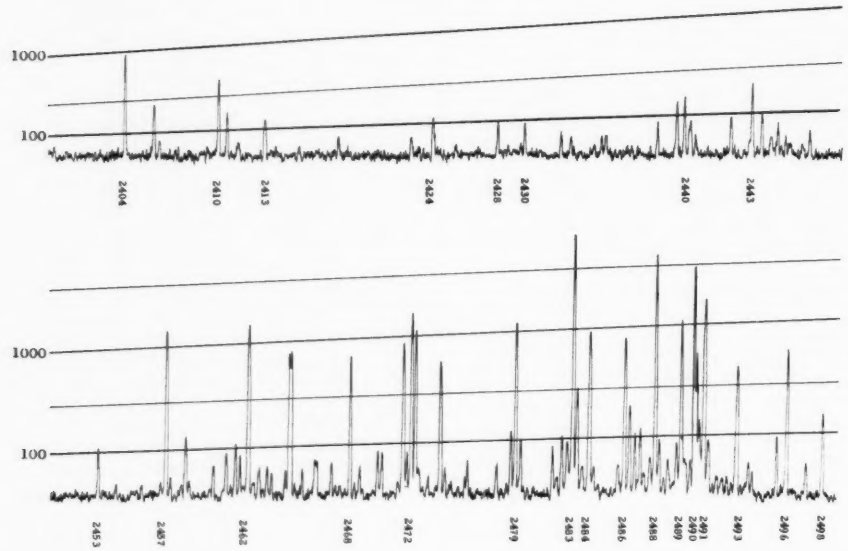

90mA Iron-Neon
Hollow Cathode

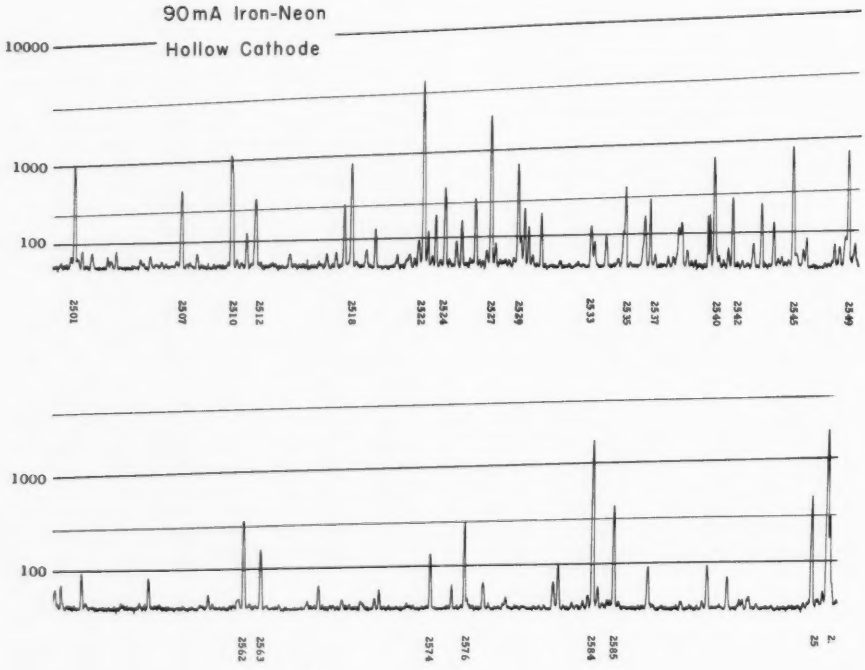

90mA Iron-Neon
Hollow Cathode

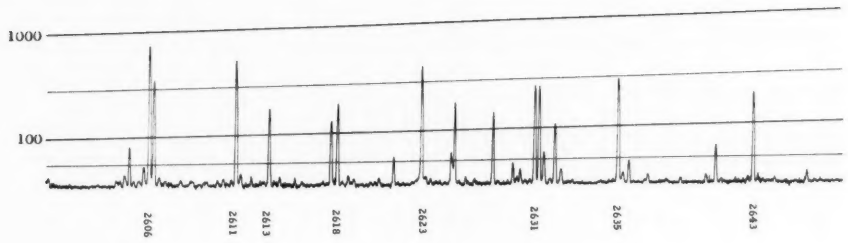

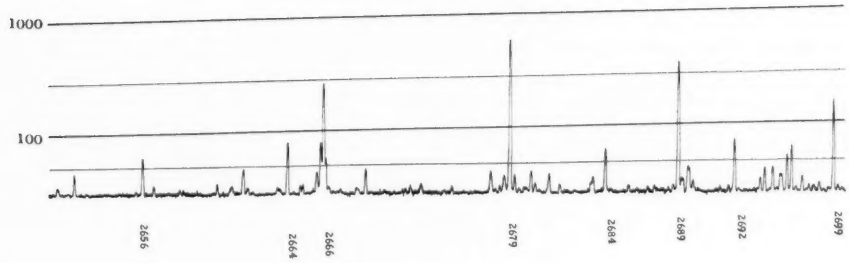

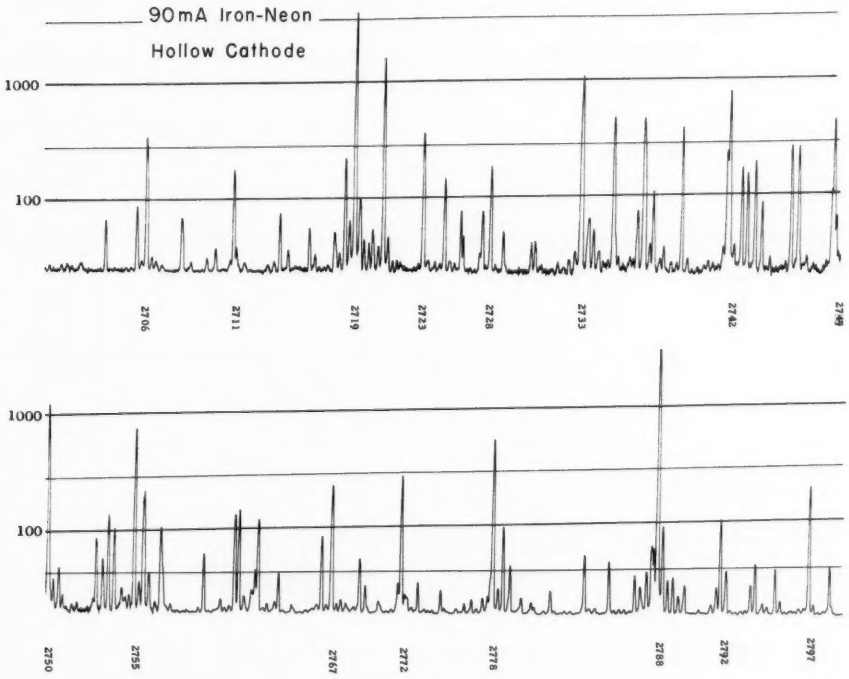

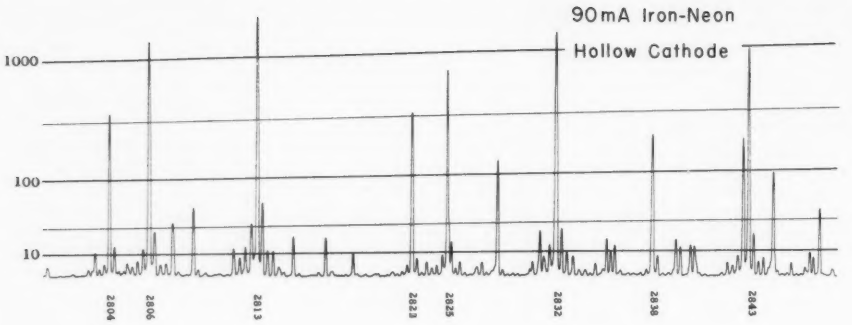
90mA Iron-Neon
Hollow Cathode
1000
100
10
2804
2806
2813
2823
2825
2832
2838
2843

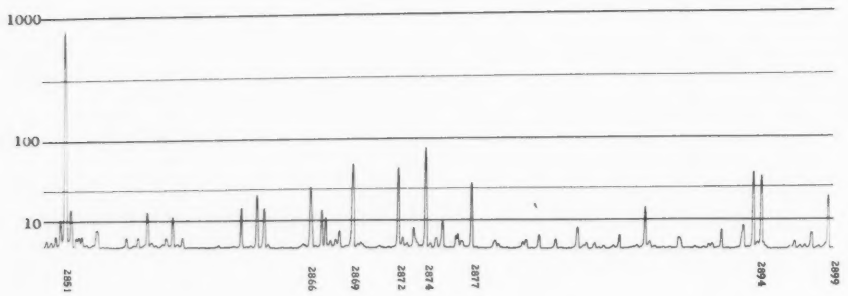
1000
100
10
2851
2866
2869
2872
2874
2877
2894
2899

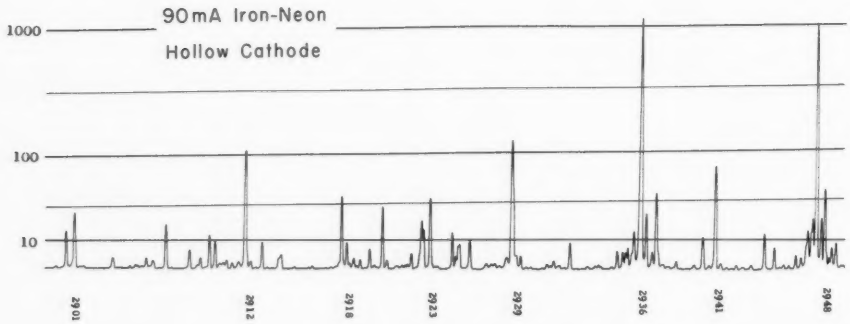
90mA Iron-Neon
Hollow Cathode
1000
100
10
2901
2912
2918
2923
2929
2936
2941
2948

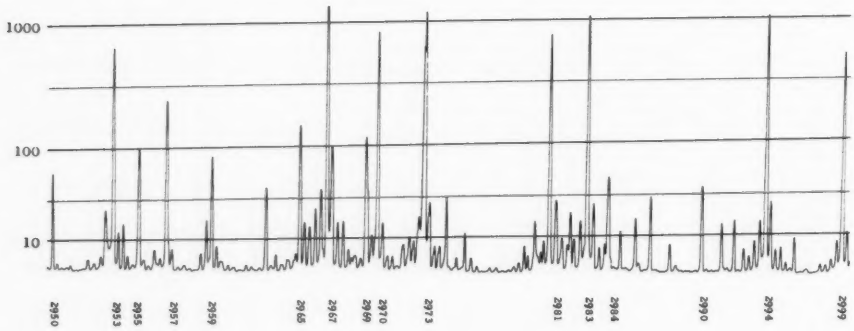
1000
100
10
2950
2953
2955
2957
2959
2965
2967
2969
2970
2973
2981
2983
2984
2990
2994
2999

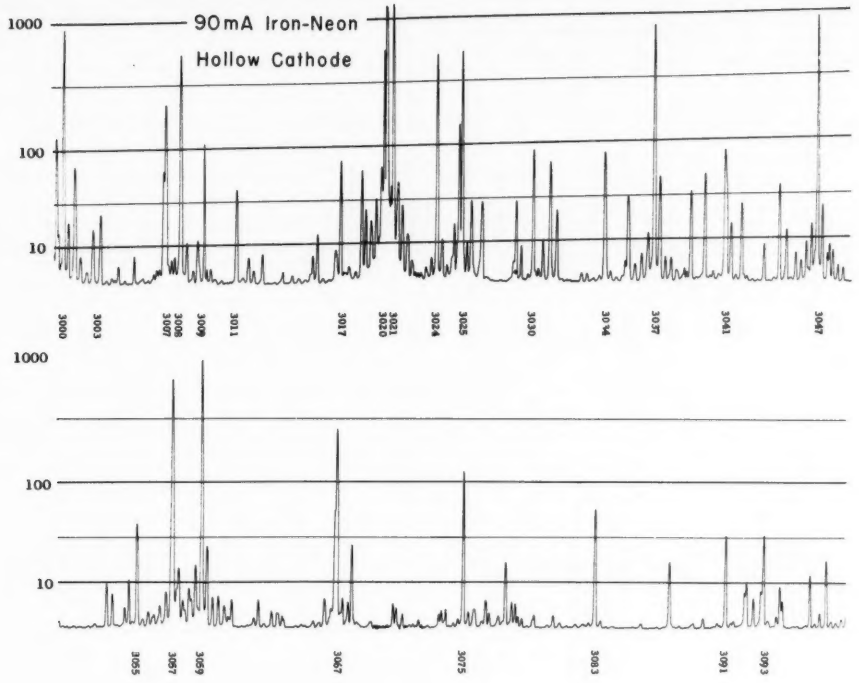
90mA Iron-Neon
Hollow Cathode
1000
100
10
3000
3003
3007
3008
3009
3011
3017
3020
3021
3024
3025
3030
3034
3037
3041
3047
1000
100
10
3065
3067
3069
3087
3075
3083
3091
3093

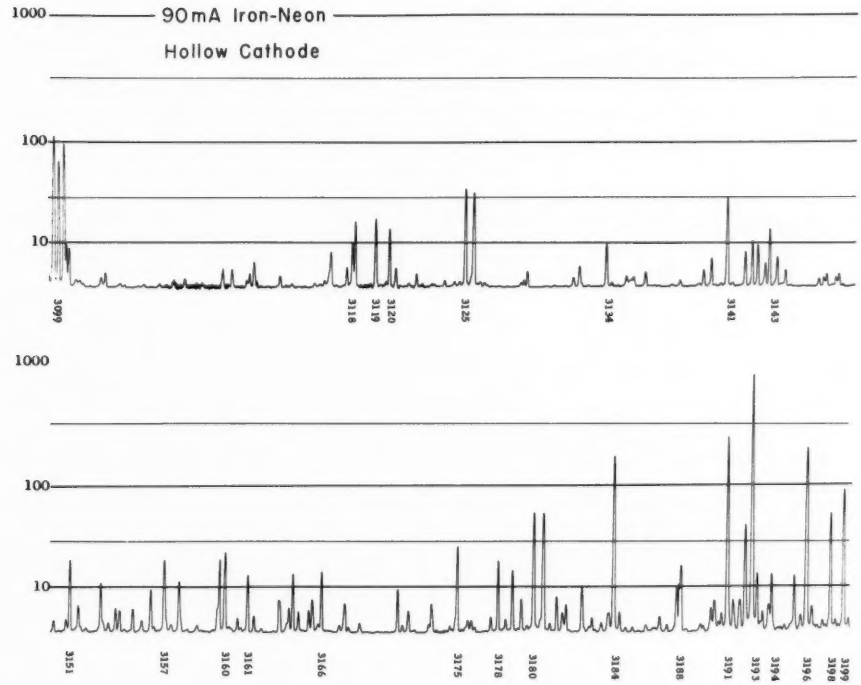
90mA Iron-Neon
Hollow Cathode
1000
100
10
3099
3116
3119
3120
3125
3134
3141
3143
1000
100
10
3151
3157
3160
3161
3166
3175
3178
3180
3184
3188
3191
3193
3194
3196
3198
3199

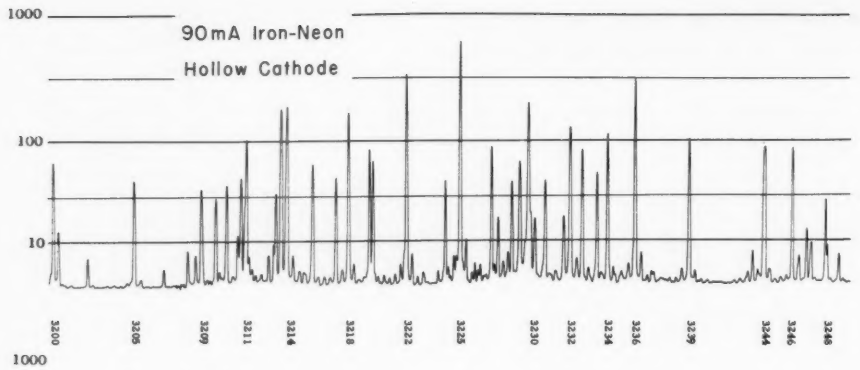
90mA Iron-Neon
Hollow Cathode
1000
100
10
3200
3205
3209
3211
3214
3218
3222
3225
3230
3232
3234
3236
3239
3244
3246
3248

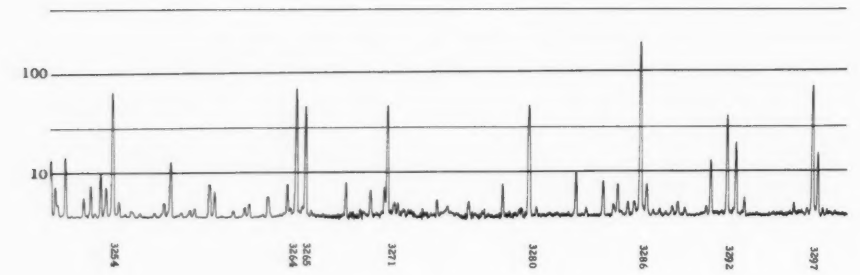
1000
100
10
3254
3264
3266
3271
3280
3286
3292
3297

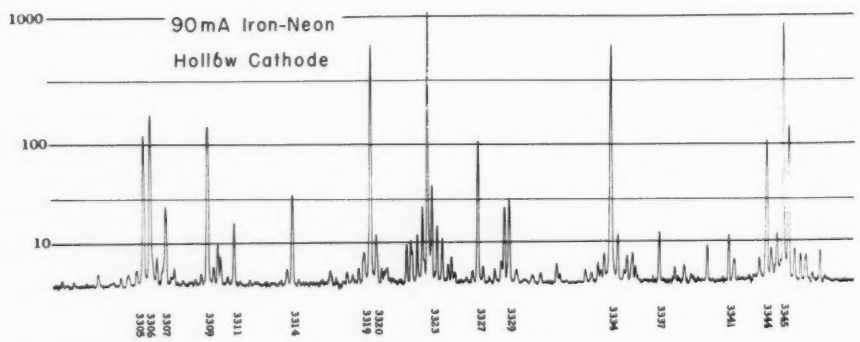
90mA Iron-Neon
Hollow Cathode
1000
100
10
3305
3306
3307
3309
3311
3314
3319
3320
3323
3327
3329
3334
3337
3341
3344
3345

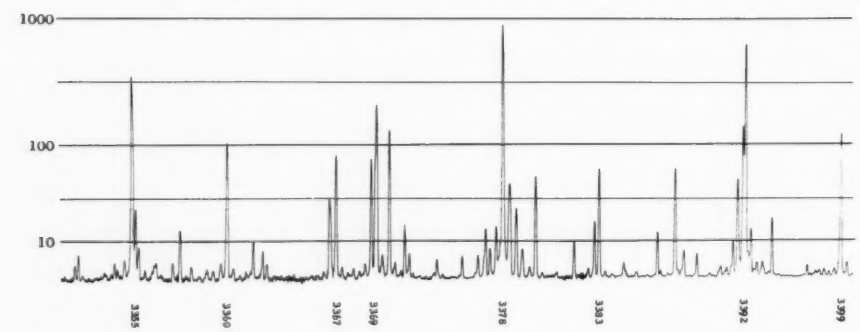
1000
100
10
3355
3360
3367
3369
3378
3383
3392
3399

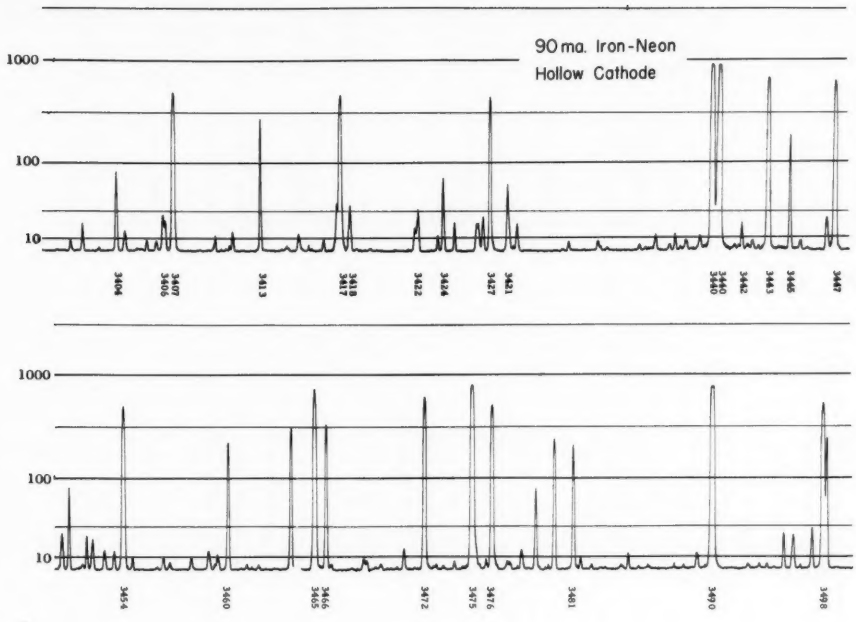
90 ma. Iron-Neon
Hollow Cathode
1000
100
10
3404
3406
3407
3413
3417
3418
3422
3424
3427
3431
3440
3440
3442
3443
3446
3447
1000
100
10
3454
3460
3465
3466
3472
3475
3476
3481
3490
3498

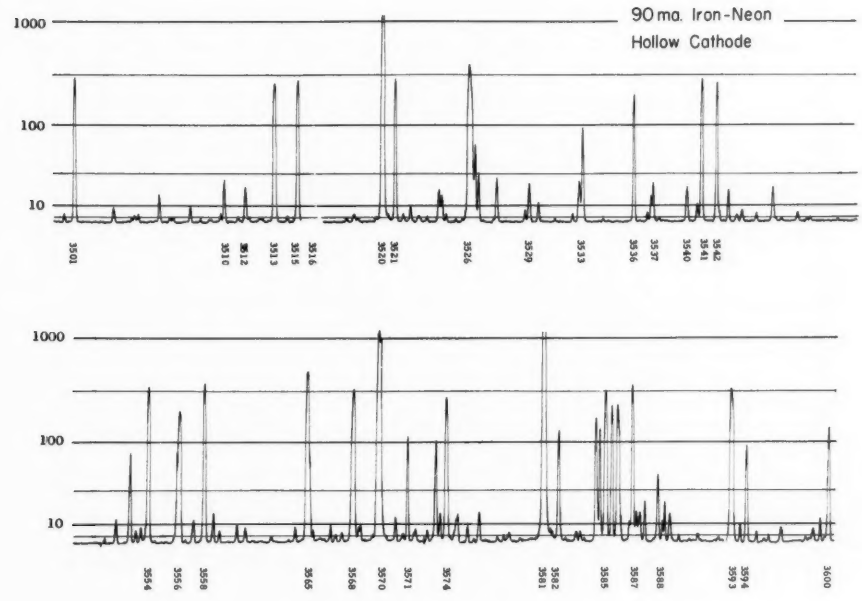
90 ma. Iron-Neon
Hollow Cathode
1000
100
10
3501
3510
3512
3513
3515
3516
3521
3520
3526
3529
3533
3536
3537
3540
3541
3542
1000
100
10
3554
3556
3558
3565
3568
3570
3571
3574
3581
3582
3585
3587
3588
3593
3594
3600

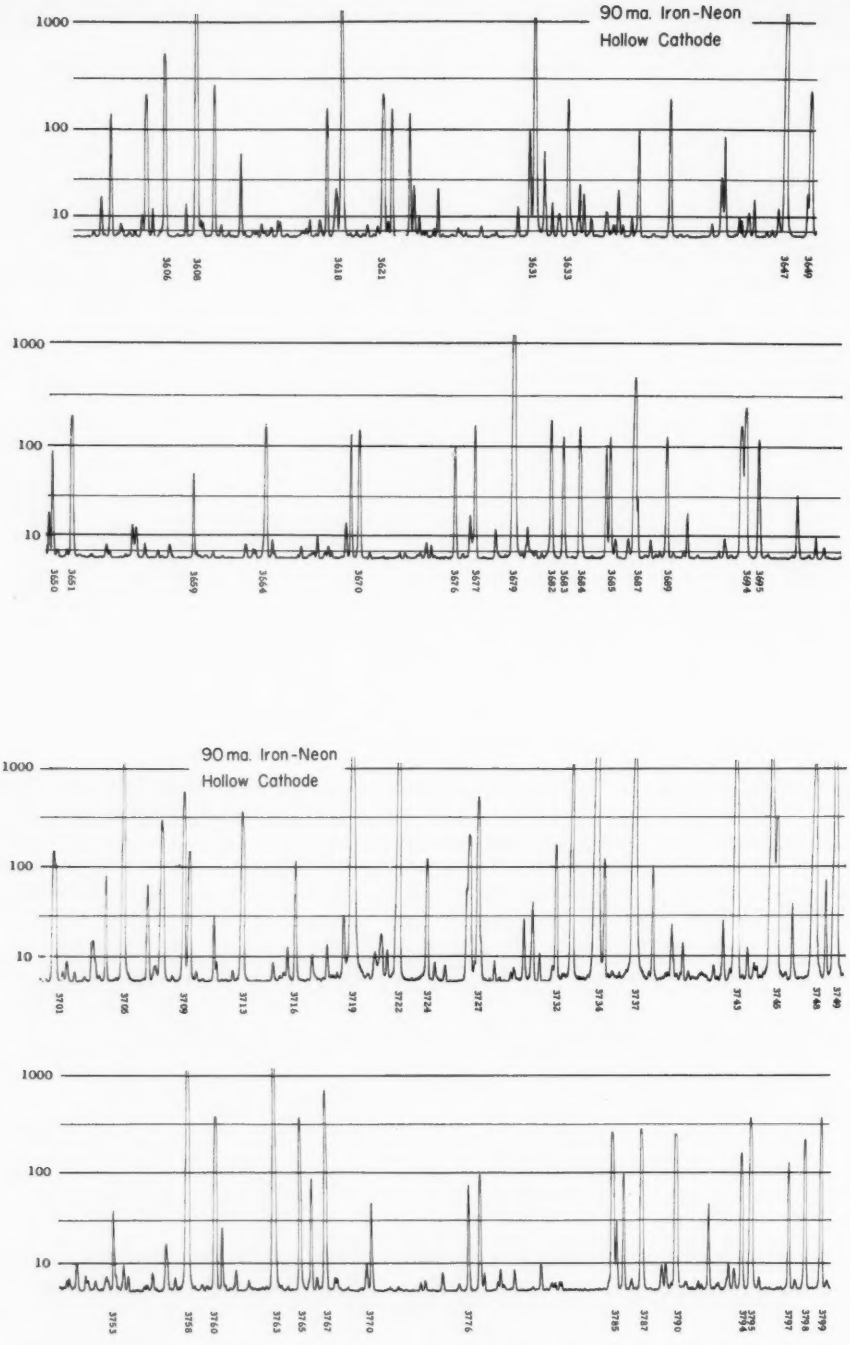
90 ma. Iron-Neon
Hollow Cathode
1000
100
10
3606
3608
3618
3621
3631
3633
3647
3649
1000
100
10
3650
3651
3659
3664
3670
3676
3677
3679
3682
3683
3684
3685
3687
3689
3694
3695
90 ma. Iron-Neon
Hollow Cathode
1000
100
10
3701
3706
3709
3713
3716
3719
3722
3724
3727
3732
3734
3737
3745
3746
3748
3749
1000
100
10
3753
3758
3760
3763
3765
3767
3770
3776
3785
3787
3790
3795
3794
3797
3798
3799

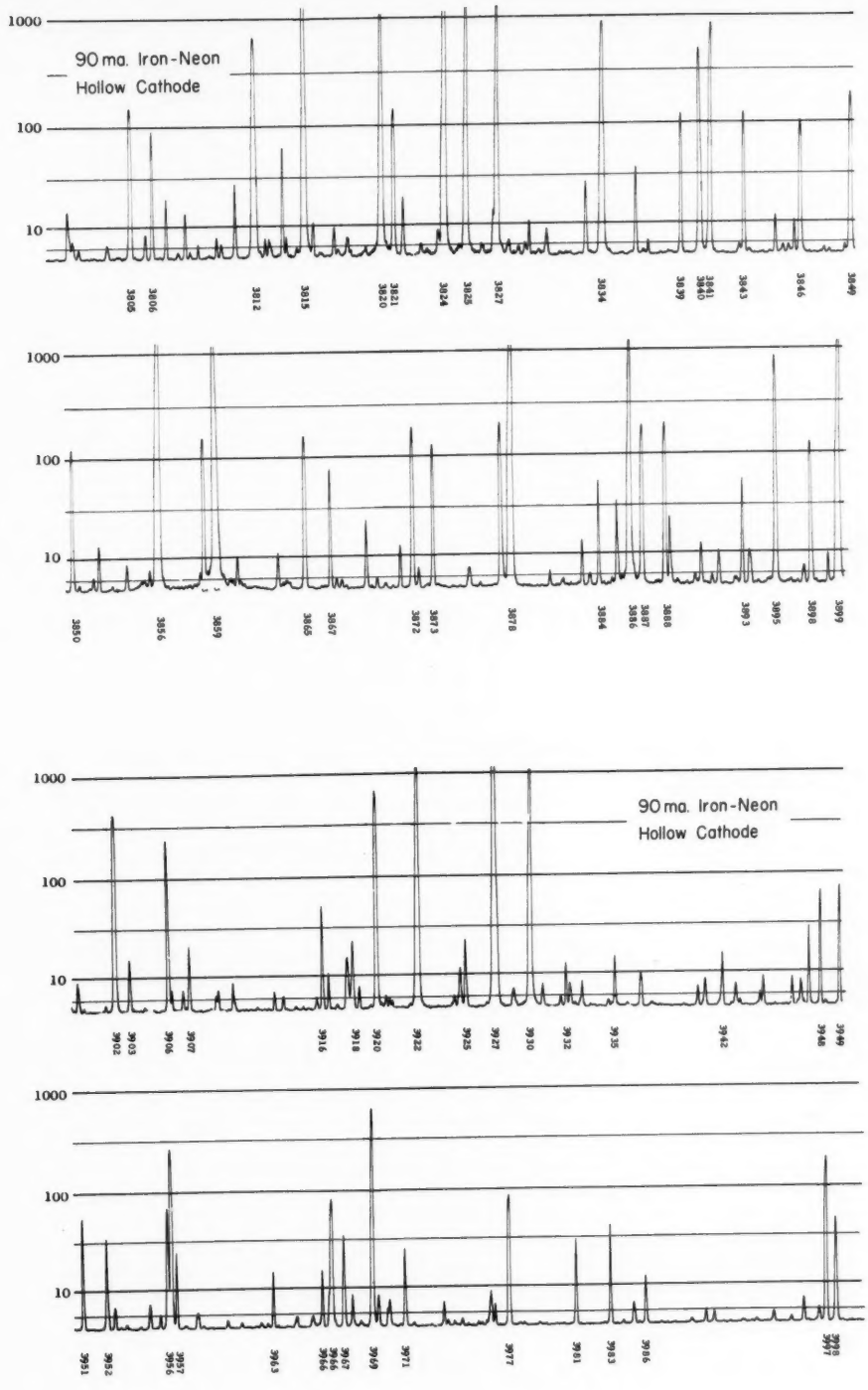
90 ma. Iron-Neon
Hollow Cathode
1000
100
10
3805
3806
3812
3815
3820
3821
3824
3825
3827
3834
3839
3840
3841
3843
3846
3849
3850
3856
3859
3865
3867
3872
3873
3878
3884
3886
3887
3888
3893
3895
3898
3899
90 ma. Iron-Neon
Hollow Cathode
3902
3903
3906
3907
3916
3918
3920
3922
3925
3927
3930
3932
3935
3942
3948
3949
3951
3952
3956
3957
3963
3966
3967
3969
3971
3977
3981
3983
3986
3997

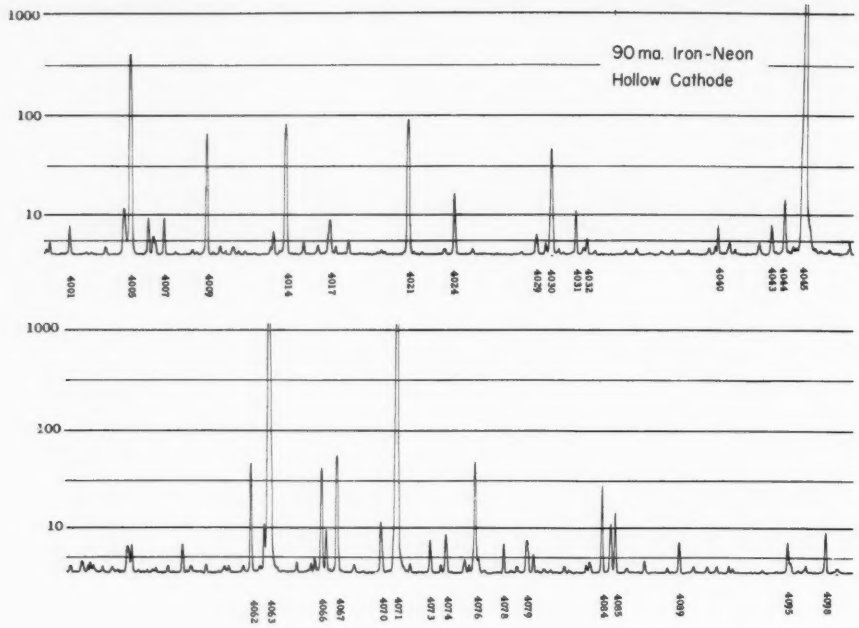
90 ma. Iron-Neon
Hollow Cathode
1000
100
10
4001 4005 4007 4009 4014 4017 4021 4024 4029 4030 4031 4032 4040 4043 4044 4045
1000
100
10
4062 4063 4066 4067 4070 4071 4073 4074 4076 4078 4079 4084 4085 4089 4095 4098

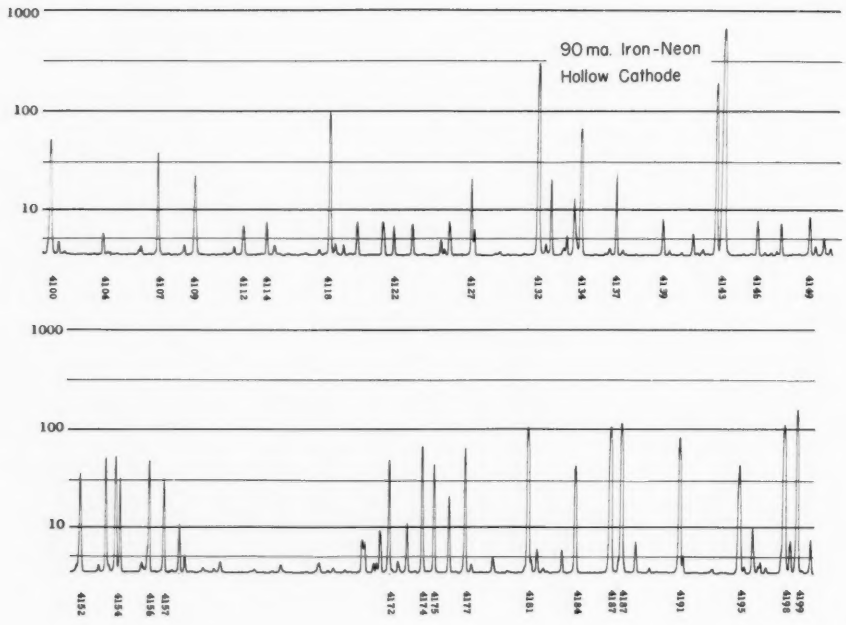
90 ma. Iron-Neon
Hollow Cathode
1000
100
10
4100 4104 4107 4109 4112 4114 4118 4122 4127 4132 4134 4137 4139 4143 4146 4149
1000
100
10
4152 4154 4156 4157 4172 4174 4175 4177 4181 4184 4187 4187 4191 4195 4198 4199

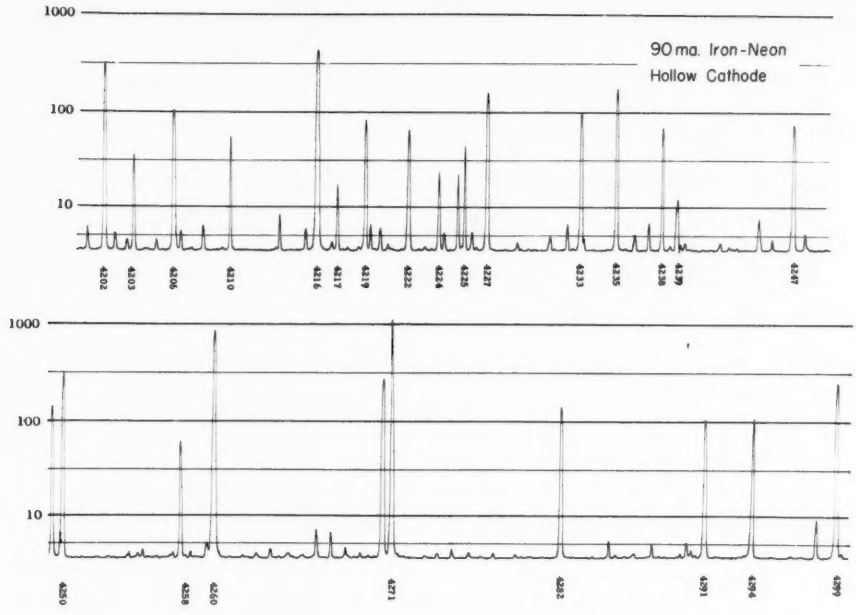
1000
100
10
90 ma. Iron-Neon
Hollow Cathode
4202
4203
4206
4210
4216
4217
4219
4222
4224
4225
4227
4233
4235
4238
4239
4247
1000
100
10
4250
4258
4260
4271
4282
4291
4294
4299

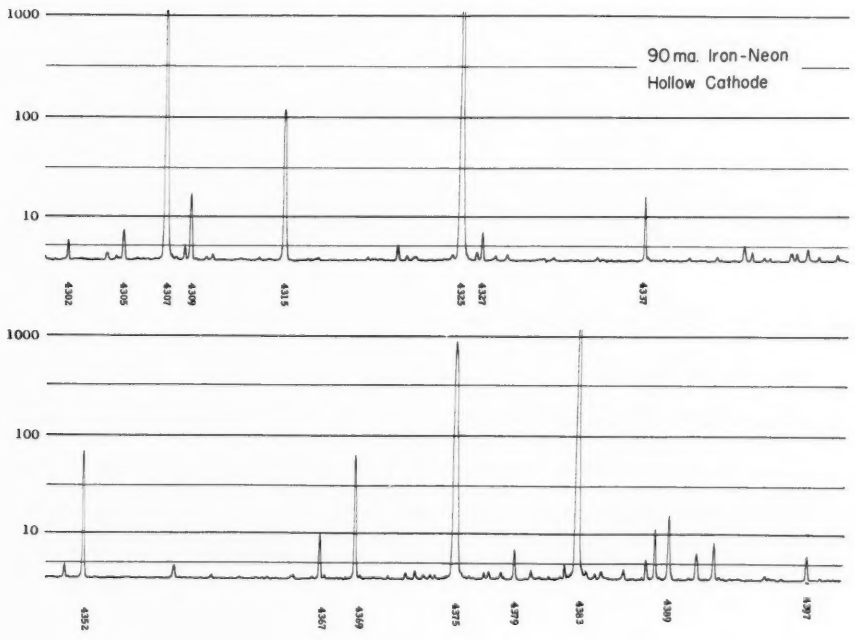
1000
100
10
90 ma. Iron-Neon
Hollow Cathode
4302
4305
4307
4309
4315
4325
4327
4337
1000
100
10
4352
4367
4369
4375
4379
4383
4389
4397

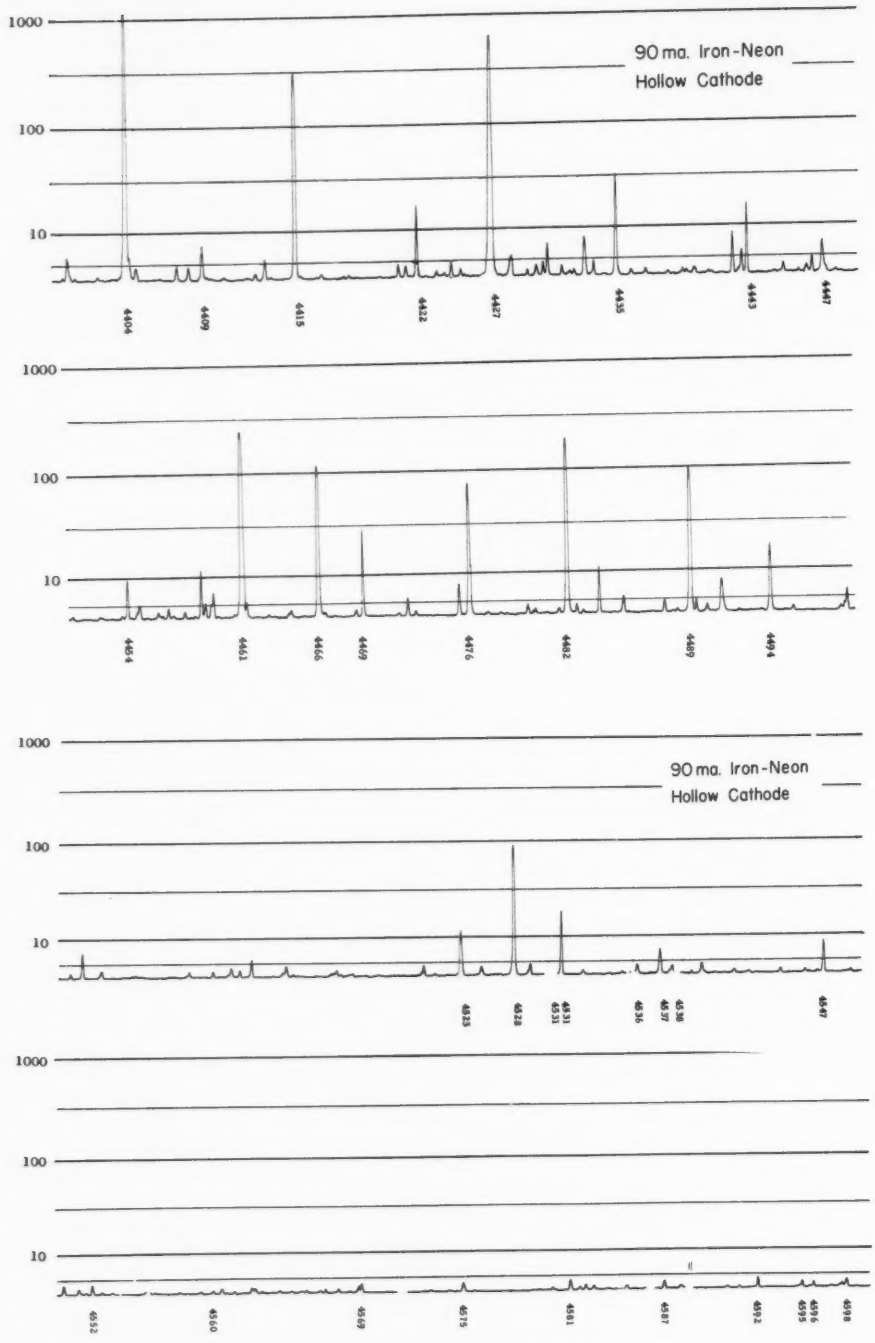
90 ma. Iron-Neon
Hollow Cathode
1000
100
10
4404
4409
4415
4422
4427
4435
4443
4447
1000
100
10
4454
4461
4466
4469
4476
4482
4489
4494
1000
90 ma. Iron-Neon
Hollow Cathode
100
10
4623
4628
4631
4631
4636
4637
4638
4647
1000
100
10
4552
4560
4569
4575
4581
4587
4592
4595
4596
4598

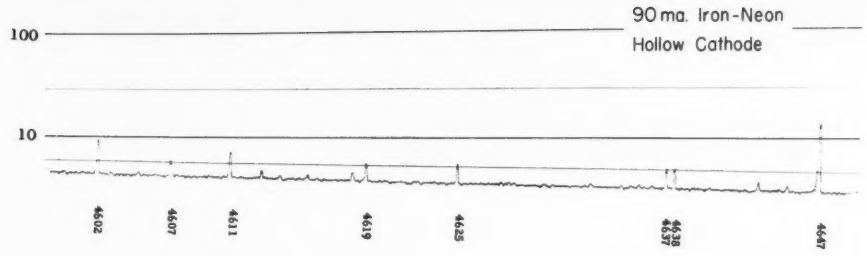
90 ma. Iron-Neon
Hollow Cathode
100
10
4602
4607
4611
4619
4625
4638
4637
4647

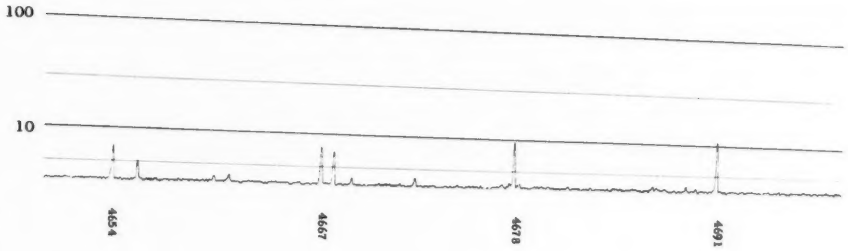
100
10
4654
4667
4678
4691

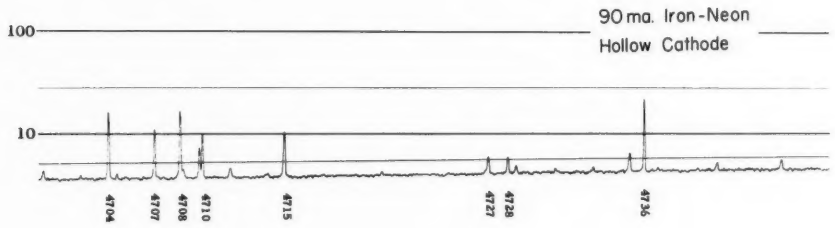
90 ma. Iron-Neon
Hollow Cathode
100
10
4704
4707
4708
4710
4715
4727
4728
4736

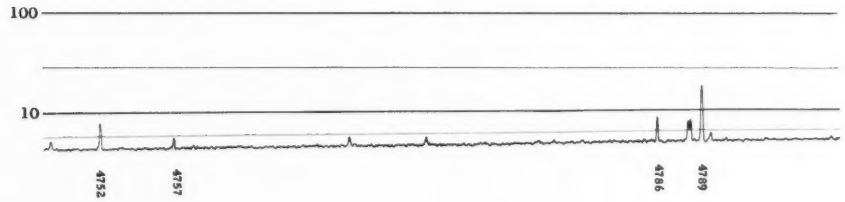
100
10
4752
4757
4786
4789

562-903 O - 75 - 5

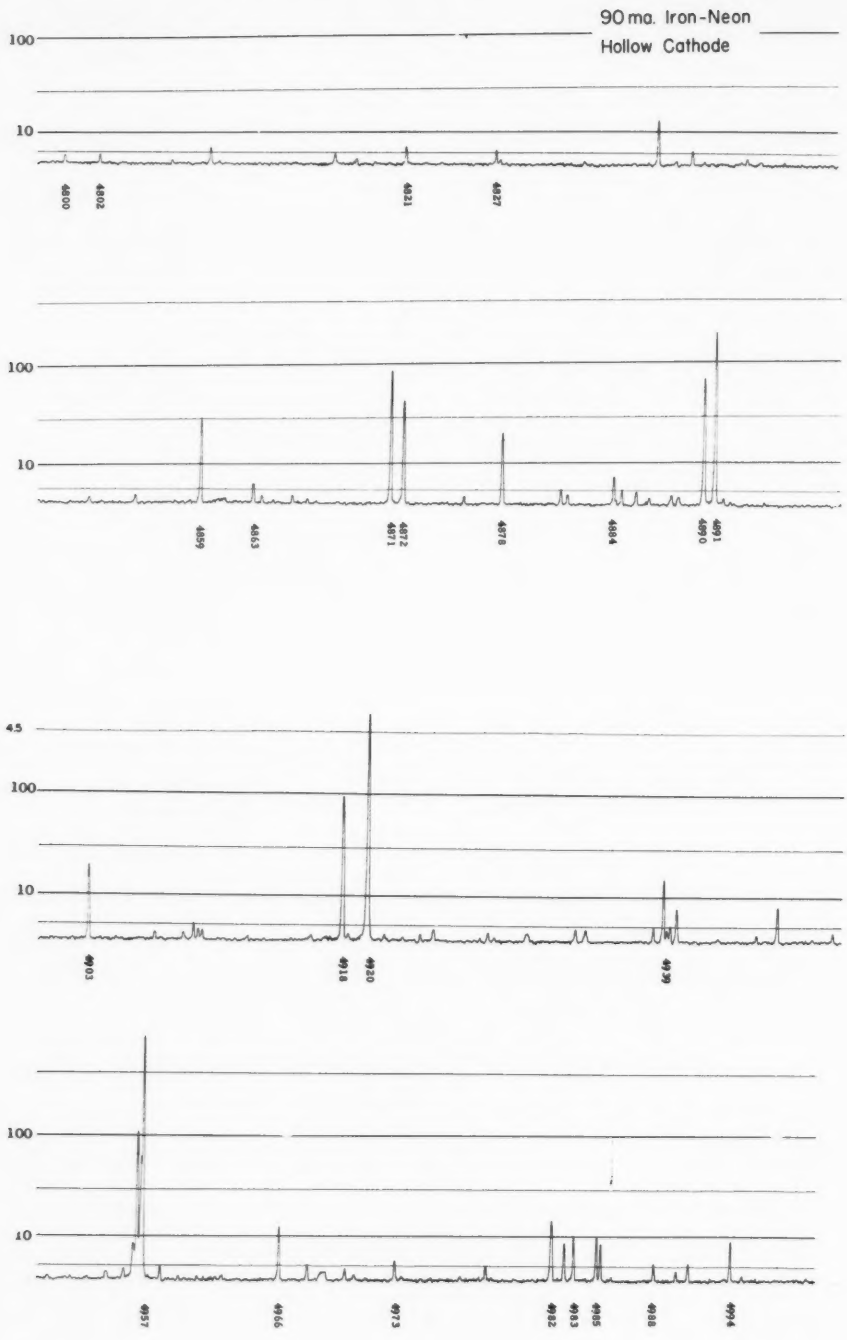
90 ma. Iron-Neon
Hollow Cathode
100
10
4800
4802
4821
4827
100
10
4859
4863
4871
4872
4878
4884
4890
4891
45
100
10
4903
4918
4920
4936
100
10
4957
4966
4973
4982
4983
4985
4988
4994

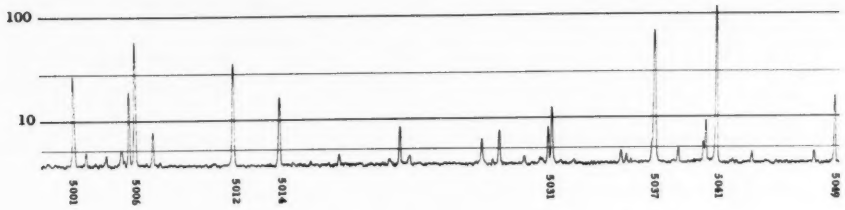
100
10
5001
5006
5012
5014
5031
5037
5041
5049

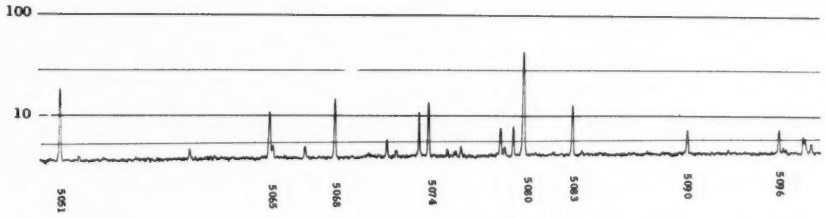
100
10
5051
5065
5068
5074
5080
5083
5090
5096

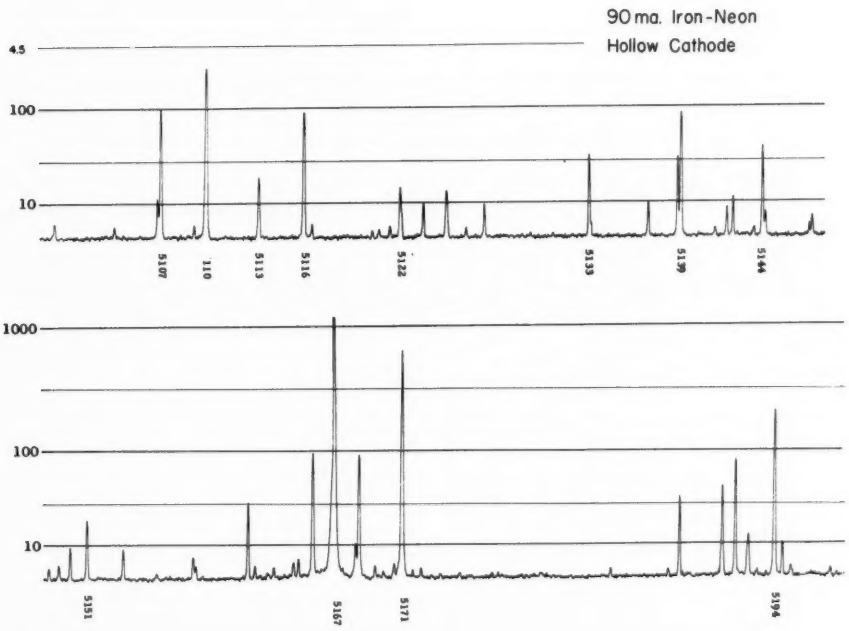
90 ma. Iron-Neon
Hollow Cathode
4.5
100
10
5107
110
5113
5116
5122
5133
5139
5144
1000
100
10
5151
5167
5171
5194

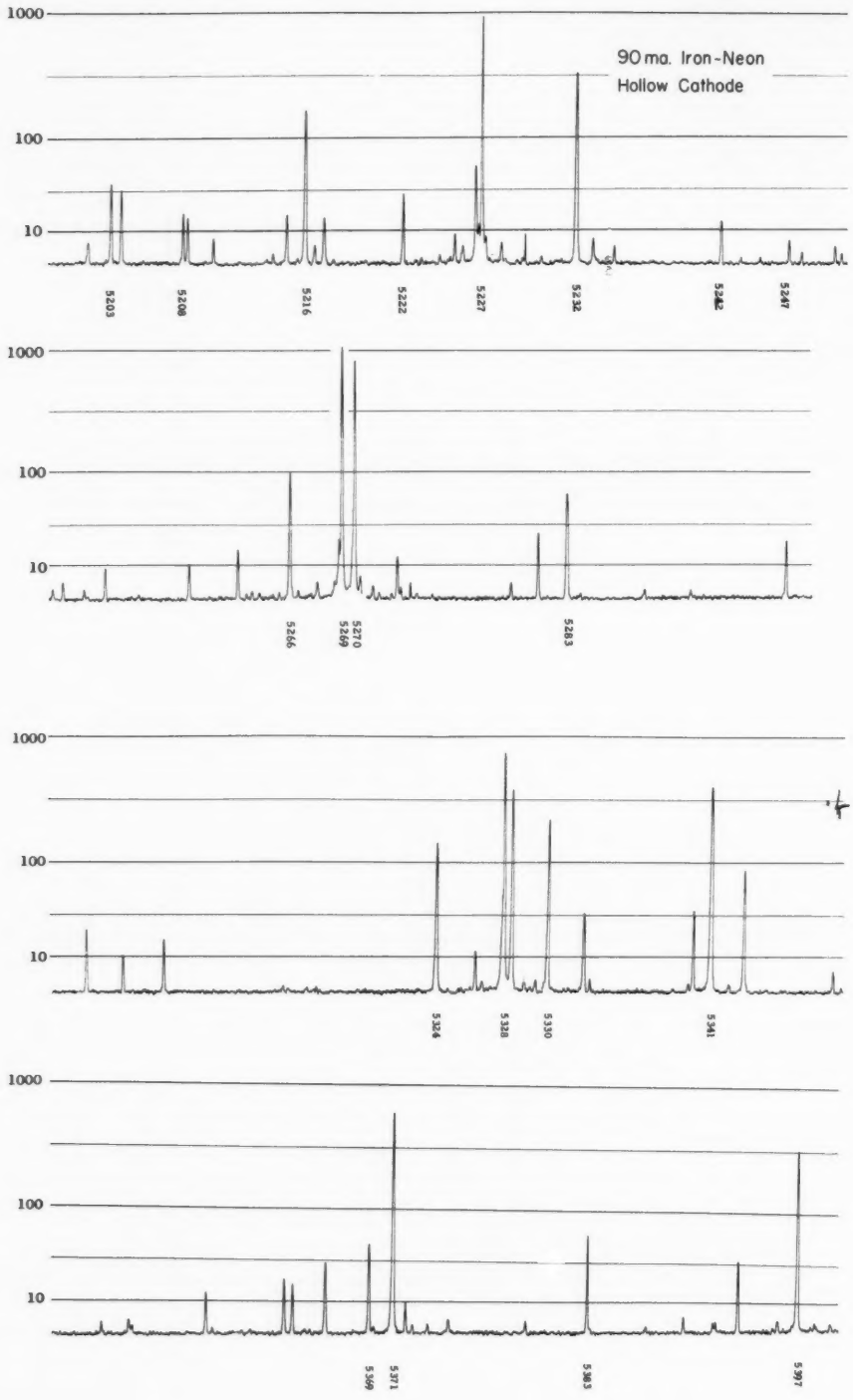
90 ma. Iron-Neon
Hollow Cathode
1000
100
10
5203
5208
5216
5222
5227
5232
5242
5247
1000
100
10
5266
5269
5270
5283
1000
100
10
5324
5328
5330
5341
1000
100
10
5369
5371
5383
5397

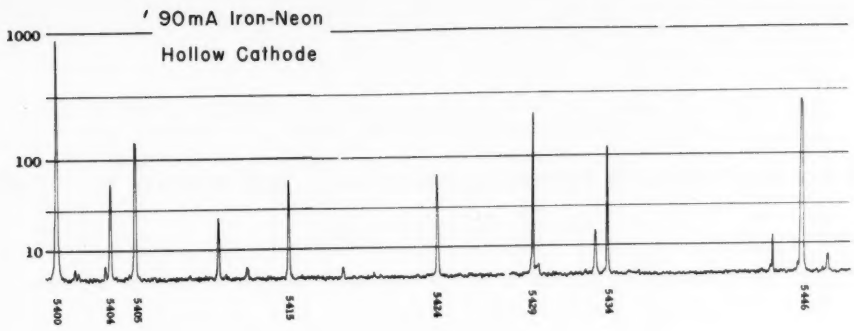
90mA Iron-Neon
Hollow Cathode
1000
100
10
5400
5404
5405
5415
5424
5429
5434
5446

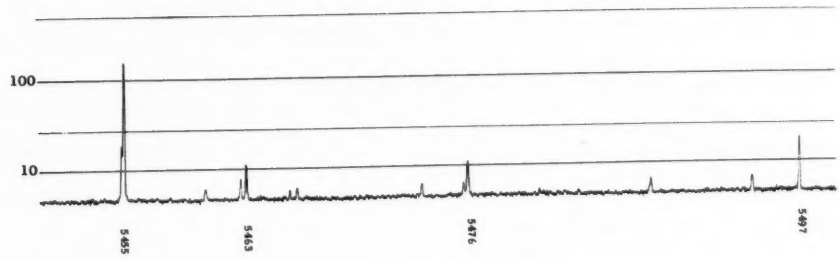
100
10
5455
5463
5476
5497

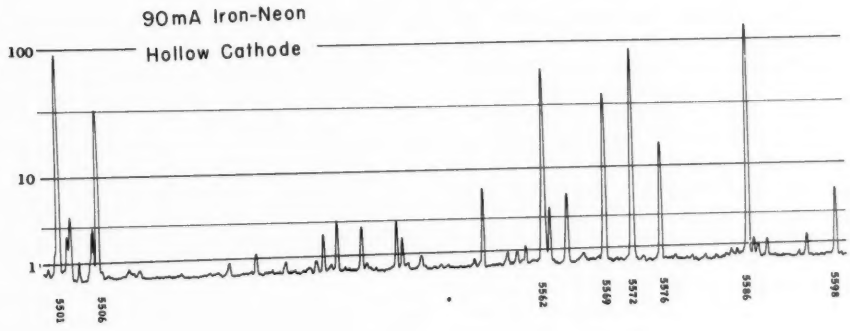
90mA Iron-Neon
Hollow Cathode
100
10
1
5501
5506
5562
5569
5572
5576
5586
5598

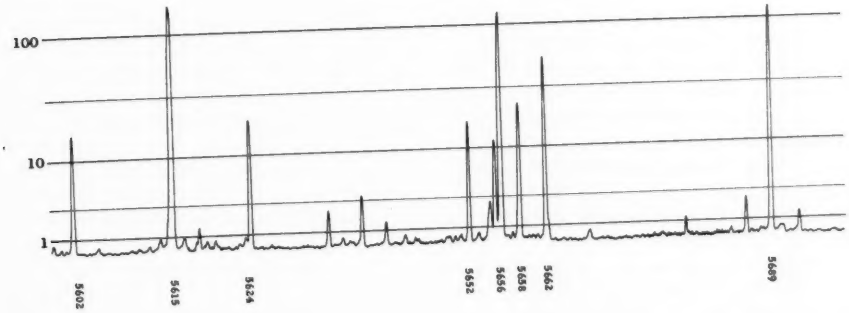
100
10
1
5602
5615
5624
5652
5656
5658
5662
5669

JOURNAL OF RESEARCH of the National Bureau of Standards—A. Physics and Chemistry
Vol. 79A, No. 1, January–February 1975

Equation of State for Thermodynamic Properties of Fluids*

Robert D. Goodwin**

Institute for Basic Standards, National Bureau of Standards, Boulder, Colo. 80302

September 6, 1974

This equation of state was developed from *PVT* compressibility data on methane and ethane. The highly-constrained form originates on a given liquid-vapor coexistence boundary (described by equations for the vapor pressures and the orthobaric densities). It then requires only five least-squares coefficients, and ensures a qualitatively correct behavior of the $P(\rho, T)$ surface and of its derivatives, especially about the critical point. This nonanalytic equation yields a maximum in the specific heats $C_v(\rho, T)$ at the critical point.

Key words: Coexistence boundary; critical point; ethane; equation of state; fluids; methane; orthobaric densities; specific heats; vapor pressures.

Symbols and Units

Subscripts c and t refer to critical and liquid triple points
Subscript σ refers to liquid-vapor coexistence

α, b, δ	nonlinear constants in the equation of state
$B(\rho)$, $C(\rho)$	density-dependent coefficients in the equation of state
$C\sigma(T)$,	molal heat capacity for saturated liquid
$C_v^\circ(T)$,	molal heat capacity for ideal gas states
$C_v(\rho,T)$,	molal heat capacity at constant density
$C_p(\rho,T)$,	molal heat capacity at constant pressure
d,	density, mol/l
J,	the Joule, 1 N-m
l,	the liter, 10^{-3}m^3
mol,	16.043 g of CH_4; 30.070 g of C_2H_6, (C^{12} scale)
P,	pressure in bars, 1 bar = 10^5 N/m^2, (1 atm = 1.01325 bar)
$P\sigma(\rho)$,	the vapor pressure, bar
R,	the gas constant, 8.31434 (J/mol)/K
ρ,	d/d_t, density reduced at the liquid triple point
σ,	d/d_c, density reduced at the critical point
T,	temperautre, K, (IPTS–1968)
$T\sigma(\rho)$,	temperature at liquid-vapor coexistence
$\theta(\rho)$,	defined locus of temperatures, figure 3
$u(\rho,T)$,	$T/T_\sigma(\rho)$, temperature reduced at coexistence
v,	$1/d$, molal volume, l/mol
$W(\rho,T)$,	the speed of sound
$x(T)$,	T/T_c, temperature reduced at the critical point
$x_\sigma(\rho)$,	$T_\sigma(\rho)/T_c$, reduced temperature at coexistence
$Z(P,\rho,T)$	Pv/RT, the "compressibility factor"

*This work at the National Bureau of Standards was supported by The American Gas Association, 1515 Wilson Boulevard, Arlington, Va. 22209.
**Cryogenics Division, National Bureau of Standards, Boulder, Colo. 80302.

1. Introduction

A problem of importance for the natural gas industry is the prediction of thermodynamic properties of liquefied, multicomponent mixtures. For the wide range of compositions encountered, it may be necessary to utilize accurate properties of the pure components. We therefore believe that it will be helpful to have a relatively simple and rational equation of state of identical form for each component, such as the equation of state described below.

This equation originates on a given, liquid-vapor coexistence boundary, thus eliminating the long-standing problem of consistency between equations of state and this independently-derived envelope [26]. It ensures a maximum in the specific heats $C_v(\rho,T)$ approaching the critical point, qualitatively consistent with experimental behavior near, but not necessarily exactly at this pole [16], and it has only five arbitrary, least-squares coefficients. Experimental compressibility data for methane and ethane have been used at densities to the triple-point liquid density, temperatures to twice the critical, and pressures to 350 bar or greater.

Our objective in the present report is to give a concise description of this new type of equation of state which, with full documentation, has been presented in previous publications [14, 15].

For methane we have shown in [14] that an equation similar to that described below yields calculated specific heats, $C_\sigma(T)$, $C_v(\rho,T)$, $C_p(\rho,T)$, and speeds of sound in acceptable agreement with experimental data, without any weighting of the equation of state to those data. In a current report on ethane [15] we compute provisional thermodynamic and related properties by means of the simpler equation of state (1) described herein.

Symbols and units used here are given in a List. Fixed-point values from [14, 15] are given in table 1.

For equation of state (1) the gas constant is $R \equiv (0.0831434) \cdot (d_t)$ bar/K, consistent with use of the dimensionless density, $\rho \equiv d/d_t$.

TABLE 1. *Fixed-point values from [14, 15]*

Triple point	Methane	Ethane
Density.....mol/l...		
Vapor.....	1.567 865·10⁻²	1.35114·10⁻⁶
Liquid.....	28.147	21.68
Temperature.....K...	90.680	89.899
Pressure.....bar [a]...	0.1174 35675	1.009 906·10⁻⁵
Critical point		
Density.....mol/l...	10.0	6.74
Temperature.....K...	190.555	305.37
Pressure.....bar...	45.988	48.755

[a] Precision required for vapor-pressure equation.

Various methods for utilizing the equations of state of pure components to derive properties of mixtures are described in a number of recent publications, e.g., [1, 4a, 17, 18, 19, 20, 21, 21a, 22, 23, 24, 27].

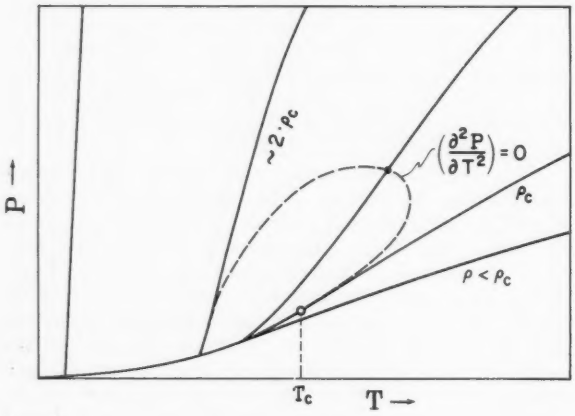

FIGURE 1. *The locus of isochore inflection points.*

2. The Equation of State

The $P(\rho, T)$ surface and equations of state are described in several reports, e.g., [6, 7, 10, 12, 14, 15, 20, 24, 28]. Figure 1 shows the qualitative behavior of isochores as indicated by Rowlinson [20], needed to give a calculated maximum in $C_v(\rho, T)$ at the critical point via the isothermal computation—

$$\Delta C_v = -T \cdot \int_0^\rho (\partial^2 P/\partial T^2) \cdot d\rho/\rho^2. \qquad \text{(a)}$$

Figure 2 shows the well-known zero slope and curvature of the critical isotherm at the critical point. This monotonic behavior (nonnegative slopes) is difficult to achieve from equations of state, yet is very important for such computations as—

$$C_p(\rho, T) = C_v(\rho, T) + T \cdot (\partial P/\partial T)^2/(\partial P/\partial \rho)/\rho^2, \qquad \text{(b)}$$

$$W(\rho, T) = [C_p \cdot (\partial P/\partial \rho)/C_v]^{1/2}. \qquad \text{(c)}$$

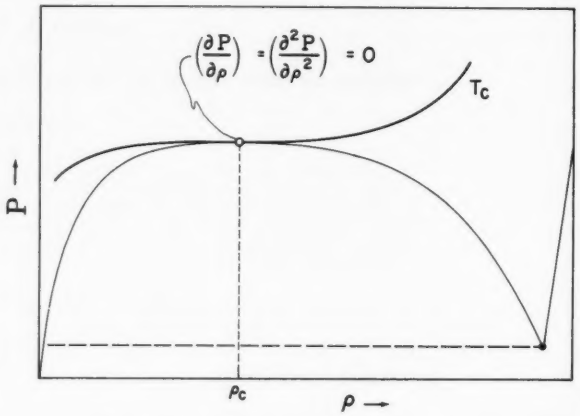

FIGURE 2. *Behavior of the critical isotherm.*

The liquid-vapor envelope, $T_\sigma(\rho)$, figure 3, is an important boundary of the $P(\rho, T)$ surface for the equation of state. We constrain the equation to this bound-

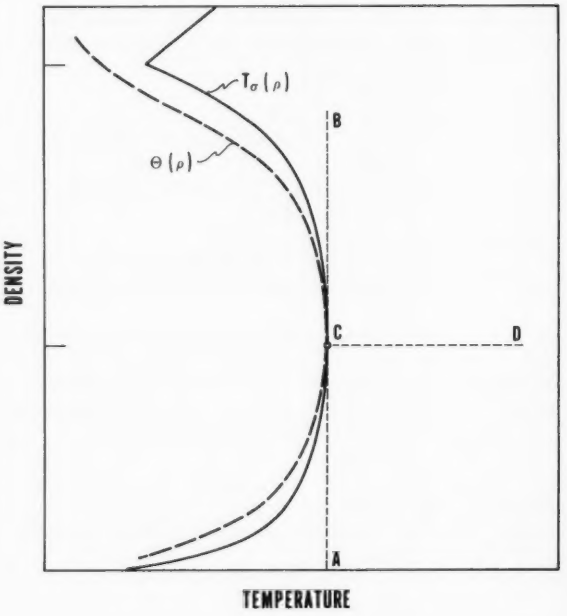

FIGURE 3. *Behavior of the locus $\theta(\rho)$.*

Point C is the critical point, and $T_\sigma(\rho)$ is the liquid-vapor coexistence envelope.

ary as follows, by use of the vapor pressures and the coexistence temperatures $T_\sigma(\rho)$ formulated in the appendix.

For any density (isochore), obtain the coexistence temperature from the function $T_\sigma(\rho)$. Use this to obtain the vapor pressure $P_\sigma[T_\sigma(\rho)]$ as a function of density, thus defining the equation of state at coexistence. By subtraction one then obtains an equation of the type of eq (1). The melting line is not a part of this equation of state

$$P-P_\sigma(\rho)=\rho R\cdot[T-T_\sigma(\rho)]+\rho^2RT_c\cdot F(\rho, T),$$

where,

$$F(\rho, T)\equiv B(\rho)\cdot\Phi(\rho, T)+C(\rho)\cdot\Psi(\rho, T). \quad (1)$$

The functions $B(\rho)$ and $C)\rho)$ are polynomial coefficients to be found by least squares. The temperature-dependent functions $\Phi(\rho, T)$ and $\Psi(\rho, T)$ must be defined to be zero on the coexistence boundary at $T=T_\sigma(\rho)$, as shown by figures 4 and 5.

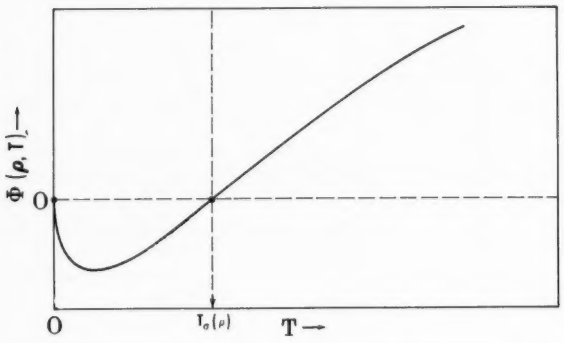

FIGURE 4. *Behavior of the function* $\Phi(\rho, T)$.

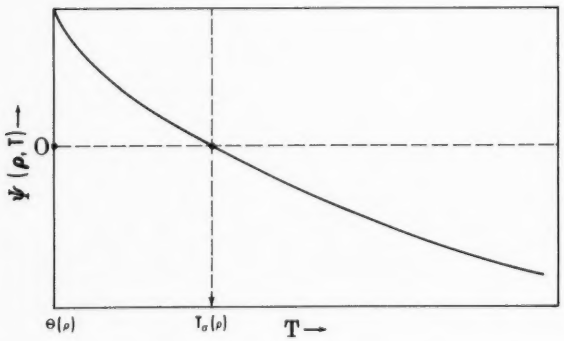

FIGURE 5. *Behavior of the function* $\Psi(\rho, T)$.

Equation (1) has, in addition to ρRT, only two temperature-dependent functions, which is the minimum number of functions (monotonic in T) needed to describe the sigmoid shape of isochores in the density range $\rho_c<\rho<2\cdot\rho_c$, figure 1.

The first of these functions is –

$$\Phi(\rho, T)\equiv x^{1/2}\cdot\ln[u(\rho, T)], \quad (2)$$

where $u(\rho, T)\equiv T/T_\sigma(\rho)$. It is linear ($\partial^2\Phi/\partial T^2=0$) everywhere on the coexistence boundary at $u=1$, figure 4. It therefore gives a critical isochore which is linear at the critical point because $C(\rho)=0$ by definition along this isochore, eq (6).

The second of these functions, $\Psi(\rho,T)$, is defined such that eq (1) will yield a maximum in the specific heats $C_v(\rho,T)$ at the critical point via eq (a). We first define the arguments –

$$\omega(\rho,T)\equiv\delta\cdot[T/\theta(\rho)-1].$$

$$\omega_\sigma(\rho)\equiv\delta\cdot[T_\sigma(\rho)/\theta(\rho)-1],$$

where δ is an arbitrary constant, and $\theta(\rho)$ is our locus of temperatures inside the coexistence envelope, figure 3,

$$\theta(\rho)\equiv T_\sigma(\rho)\cdot\exp[-\alpha\cdot f(\sigma)]. \quad (3)$$

The function $f(\sigma)$ here is normalized to unity at the liquid triple-point density –

$$f(\sigma)\equiv|\sigma-1|^3/(\sigma_t-1)^3,$$

where $\sigma_t\equiv d_t/d_c$ is a constant.

Function $\Psi(\rho, T)$ now is defined as the difference,

$$\Psi(\rho,T)\equiv\psi(\rho,T)-\psi_\sigma(\rho), \quad (4)$$

such that $\Psi=0$ at coexistence, $T=T_\sigma(\rho)$. Component functions, $\psi(\rho, T)$, are designed to give infinite curvature ($\partial^2\psi/\partial T^2$) at the origin, $\omega=0$,

$$\psi_1(\rho,T)\equiv[1-\omega\cdot\ln(1+1/\omega)]/x, \quad (4\text{–a})$$

$$\psi_\sigma(\rho)\equiv[1-\omega_\sigma\cdot\ln(1+1/\omega_\sigma)]/x_\sigma. \quad (4\text{–b})$$

Figure 5 shows behavior of $\Psi(\rho,T)$. Sufficiently far away from the critical point it behaves roughly like $1/T^2$, found in the well-known, Beattie-Bridgeman equation of state.

Behavior of the coefficients $B(\rho)$ and $C(\rho)$ in eq (1) is shown by figure 6 for methane. The following polynomial representations have been developed tediously by trial,

$$B(\rho)\equiv B_0+B_1\cdot\rho+B_2\cdot\rho^2/(1+b\cdot\rho^2), \quad (5)$$

$$C(\rho)\equiv(\sigma-1)\cdot(\sigma-C_0)\cdot(C_1+C_2\cdot\rho). \quad (6)$$

The sign of the curvature of isochores ($\partial^2P/\partial T^2$) at the coexistence boundary is determined *uniquely* by the sign of $C(\rho)$, figure 6, because $\Phi(\rho,T)$ is linear

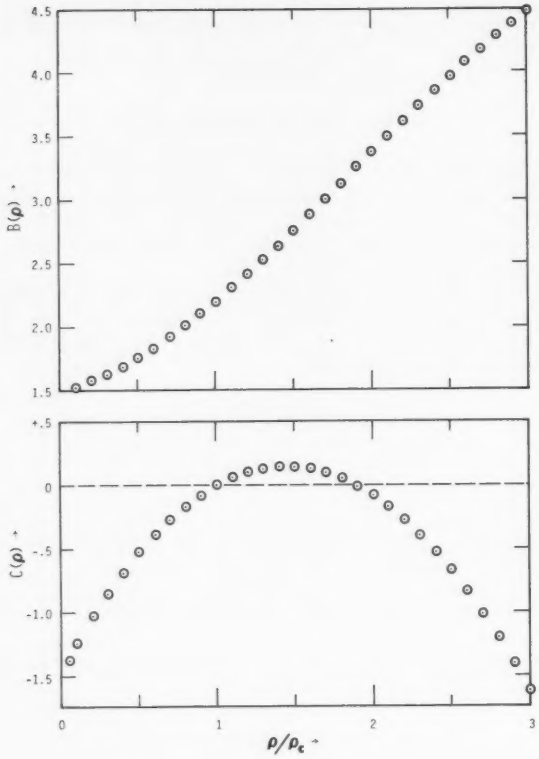

FIGURE 6. *Behavior of the coefficients* B(ρ), C(ρ) *for methane.*

on this boundary. The root in $C(\rho)$ at $\sigma = 1.9$ was found by least squares for methane and for ethane. It then was introduced as the constant C_0 in eq (6). This constraint is valuable because, under various conditions, we often have failed to obtain any such root from *PVT* data by least squares.

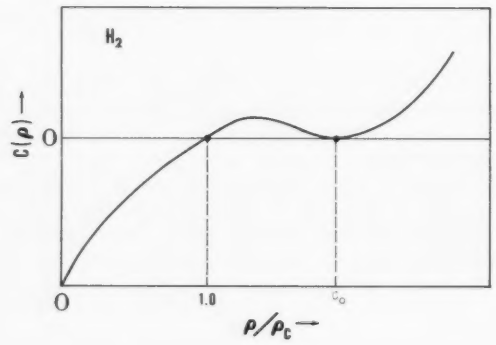

FIGURE 7. *Presumed behavior of* C(ρ) *for hydrogen, reflecting observed positive isochore curvatures in compressed liquid states at the lowest temperatures* [7].

Figure 7 shows the presumed behavior of $C(\rho)$ for hydrogen, needed to give the observed positive curvature of isochores in compressed liquid states at the lowest temperatures [3, 7]. The behavior of figure 7 is described by a double root at C_0, e.g.,

$$C(\rho) = C_1 \cdot (\sigma - 1) \cdot (\sigma - C_0)^2,$$

or without a root by—

$$C(\rho) = (\sigma - 1) \cdot (C_1 + C_2 \cdot \rho + C_3 \cdot \rho^2).$$

Table 2 presents constants of eq (1) for methane and ethane. Individual deviations of experimental *PVT* data from eq (1) are given for ethane in [15]. For methane with eq (1) they are comparable with those obtained in [14] using nine least-squares coefficients. Complete computer programs are reported in [15] for adjusting the vapor-pressure equation, the orthobaric-densities equations, the coexistence-temperatures equations, and the equation of state (1).

TABLE 2. *Constants for equation of state (1)*

	Methane	Ethane
α	2	2
b	1	1
δ	1/2	1/2
C_0	1.9	1.9
B_0	1.5082 12989	1.8481 67996
B_1	0.6544 90304	1.5697 04511
B_2	4.1320 82291	5.5601 86452
C_1	−0.7654 09076	−1.0428 42462
C_2	−0.0590 88717	+0.2249 78299
N	756	562
$\Delta P/P$, %	0.42	0.57

3. Comments on the Equation

Behavior of the critical isotherm from eq (1) at the critical point is deduced as follows. The functions $P_\sigma[T\sigma(\rho)]$ and $\Phi(\rho, T)$ depend directly upon $T_\sigma(\rho)$, which gives the overpowering factor $\exp[-\gamma/|\sigma - 1|]$ for derivatives with respect to density at the critical point, $\sigma = 1$. The function $\Psi(\rho, T)$ has a finite third derivative because it depends also on $\theta(\rho)$, eq (3). Its coefficient, $C(\rho)$, however, is zero at the critical density, eq (6). The first, second, and third derivatives of eq (1) therefore are zero at the critical point.

Detailed examinations of this isotherm from eq (1) show, however, that small variations in the assigned (ρ_c, T_c) critical point give small irregularities (negative slopes) nearby at $\sigma \lesssim 1$. We find that, given an accurate value of T_c, eq (1) serves to find the critical density which yields a well-behaved critical isotherm [15]. For methane and ethane the value of the critical density obtained by this method is roughly 1 percent lower than estimated by the conventional procedure of extrapolating the rectilinear diameter to the critical

temperature [14, 15, 20], but in each case falls within bounds of uncertainty in published works.

Isochore inflection points figure 1, calculated from eq (1), are obtained as the difference of second derivatives (versus T) from the functions composing $F(\rho, T)$. We therefore expect high sensitivity to the analytical forms of $\Phi(\rho, T)$ and $\Psi(\rho, T)$. Variations of these forms might improve accuracy in representing *PVT* data. In the following we describe two alternative functions for $\Psi(\rho, T)$ from among many different functions investigated both for $\Phi(\rho, T)$ and for $\Psi(\rho, T)$. We then compare computed specific heats obtained via these two forms in the modified equation of state described below. Each of the following component functions must be differenced, as indicated by eq (4), to obtain $\Psi(\rho, T)$ for the equation of state. The argument for each of the following functions is changed to—

$$\omega(\rho, T) \equiv [1-\theta(\rho)/T].$$

In (7) the adjustable exponent is $1<\epsilon<2$, and the adjustable coefficient was selected by trial to be $\delta=1/\epsilon$,

$$\psi_2(\rho, T) \equiv 1-(\omega-\delta\cdot\omega^{\epsilon})/(1-\delta). \qquad (7)$$

This function approaches zero at high temperatures in proportion to $1/T^2$, as seen by expanding ω^{ϵ}. By trial with methane and ethane *PVT* data, we found $\epsilon=3/2$, and hence $\partial^2\psi_2/\partial T^2$ behaves like $(1/\omega)^{1/2}$ on approach to the origin, $\omega=0$.

In (8) we use the arbitrary constant $0\leq\delta\leq 1$ to give relative weighting to two terms behaving, respectively, like $1/T$ and $1/T^2$ at high temperatures,

$$\psi_3(\rho, T) \equiv \delta\cdot(\theta/T)+(1-\delta)\cdot[1-\omega+\omega\cdot\ln(\omega)]. \qquad (8)$$

The last term in (8) was explored for hydrogen [10]. Equation (8) can be simplified for computations. This function gives $\partial^2\psi_3/\partial T^2 \sim (1/\omega)$ on approach to the origin, $\omega=0$, similar to definition (4–a) above.

With above functions, we find that coefficients B_1 and C_2 of eq (1) become nonsignificant for methane, leaving an equation of state with only three arbitrary, least-squares coefficients.

For computations on mixtures, the simplest possible equation of state is desirable. We have modified (1) such that it is suitable for corresponding-states adaptations, by specifying that densities shall be reduced at the critical point (hence $R=0.0831434\cdot d_c$, bar/K), and by introducing the critical pressure. The functions $\Phi(\rho, T)$ and $\Psi(\rho, T)$ remain unchanged—

$$P-P_{\sigma}(\rho)=\sigma R\cdot[T-T_{\sigma}(\rho)]+P_c\cdot\sigma^2\cdot F(\rho, T), \qquad (1\text{–A})$$

$$B(\sigma)\equiv B_0+B_2\cdot\sigma^2/(1+b\cdot\sigma^2), \qquad (5\text{–A})$$

$$C(\sigma)\equiv C_1\cdot(\sigma-1)\cdot(\sigma-C_0). \qquad (6\text{–A})$$

Table 3 for methane gives the rms of relative density deviations for authors in [14], corresponding to each function $\psi(\rho, T)$ described above and, on the bottom line, the mean of combined pressure deviations. Tables 4 and 5 give the constants for eq (1–A), so that it will be possible to compute specific heats.

TABLE 3. *Methane density deviations, rms percent*

Equation of state.....		eq (1)	eq (1–A)	
Function $\psi(\rho, T)$.....		ψ_1, eq (4–a)	ψ_2, eq (7)	ψ_3, eq (8)
Authors	N			
Virial eq, [14].....	46	0.06	0.12	0.16
Douslin et al. [4].....	171	.06	.13	.10
NBS [14].....	539	.51	.60	.50
Mean $\Delta P/P$, %...	756	.42	.46	.45

TABLE 4. *Constants for equation of state (1–A), using $\psi_2(\rho,T)$, eq (7)*

	Methane	Ethane
b	1/8	1/8
α	1/2	1/2
δ	2/3	2/3
ϵ	3/2	3/2
B_0	1.9894 21671	2.2373 56347
B_2	0.7924 35706	0.9304 97491
C_0	1.9	1.9
C_1	−0.8309 40825	−1.0494 11810
N	756	562
$\Delta P/P$, %	0.46	0.79

TABLE 5. *Constants for equation of state (1–A), using $\psi_3(\rho,T)$, eq (8)*

	Methane	Ethane
b	1/8	1/8
α	1/2	2/3
δ	1/3	1/2
B_0	1.9794 55787	2.1805 54662
B_2	0.8017 24817	0.9814 53571
C_0	1.9	1.9
C_1	−0.9465 70360	−1.3543 33999
N	756	562
$\Delta P/P$, %	0.45	0.75

The interaction specific heats $(C_v-C_v^0)$ for methane have been compared along the critical isochore, as computed by equations (a) and (1–A), using the functions $\psi_2(\rho, T)$ and $\psi_3(\rho, T)$. Experimental behavior of specific heats suggests that these data should be described very near the critical temperature by—

$$(C_v-C_v^0)\sim(T/T_c-1)^{-n}, \qquad (9)$$

where exponent $0 < n < 1$, and usually, $0.05 \leq n \leq 0.15$, [16].

Figure 8 shows the computed results via $\psi_2(\rho, T)$, eq (7). Their qualitative behavior is correct, but they cannot be represented by (9). Instead, they are described accurately to 210 K by—

$$(C_v - C_v^0) = 15.1 - 18.0 \cdot (T/T_c - 1)^{1/3}, \quad J/\text{mol}/K,$$

suggesting that they might become finite at the critical temperature.

Using $\psi_3(\rho, T)$, eq (8), on the other hand, yields results on the logarithmic plot of figure 9. The slope, $n \approx 1/3$, is close to that observed for our experimental oxygen specific heats [8].

We conclude that $\psi_2(\rho, T)$ gives too weak a curvature to isochores from (1–A) approaching coexistence, and that the forms $\psi_1(\rho, T)$ and $\psi_3(\rho, T)$ may be preferable, despite the logarithmic infinity in their first derivatives versus T at the origin, $\omega = 0$.

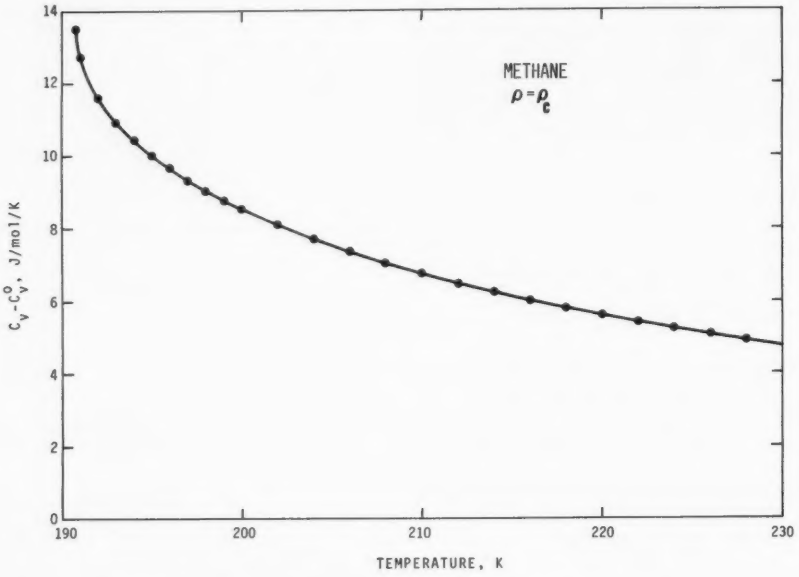

FIGURE 8. *Computed interaction specific heats* $(C_v - C_v^0)$ *of methane along the critical isochore, via eq* (1–A) *and* ψ_2 (ρ, T).

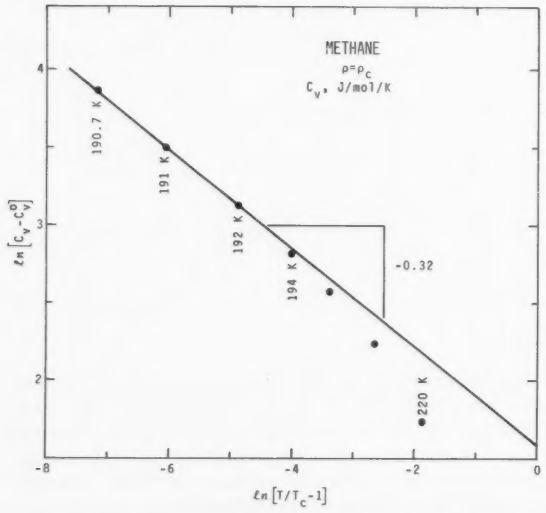

FIGURE 9. *Computed interaction specific heats* $(C_v - C_v^0)$ *of methane along the critical isochore, via eq* (1–A) *and* ψ_3 (ρ, T).

4. Conclusions

As argued above, the present equation of state (1) is rational because we understand the purpose of most of its component parts. Inclusion of the vapor pressures and orthobaric densities in this equation merely incorporates these physical properties which almost invariably must be used for a consistent network of thermodynamic functions, and eliminates the long-standing problem of continuity at the coexistence boundary [26].

We believe eq (1) to be valuable for thermal computations because it ensures an inherently correct behavior of the $P(\rho, T)$ surface, giving a maximum in the specific heats $C_v(\rho, T)$ at the critical point. The very small number of arbitrary least-squares coefficients (five, and possibly only three) facilitates comparisons of the equation of state for different substances, and may be attractive for work on mixtures.

We cannot expect eq (1) to represent some high-precision *PVT* data as well as equations with a much greater number of arbitrary constants. As the precision of "good" *PVT* data probably is often much bet-

ter than absolute accuracy, especially in the critical region, it would appear to be a self-defeating exercise to strive for the ultimate "representation" while ignoring essential features of the $P(\rho,T)$ surface. Any inaccuracies in the given, liquid-vapor, P—ρ—T boundary for eq (1), however, will be propagated along calculated isochores because eq (1) originates on this boundary.

Equation (1) almost certainly cannot be integrated analytically to express derived properties in closed form. It therefore would not be convenient for multiproperty analysis [2]. Equations amenable to integration, however, probably are not accurate in the critical region, which influences a large fraction of the $P(\rho,T)$ surface. To some extent, this must create a need for multiproperty analysis.

For methane with an equation of state similar to eq (1), on the other hand, we have used a minimum of specific heat data only to compute around the critical point for high densities near the critical temperature (fig. 3). In all other regions we computed specific heats and speeds of sound "a priori" via ideal gas specific heats and the equation of state, finding acceptable agreement with experimental data. We concluded that if such data do not exist experimentally, they could be estimated via the present type of equation of state for many but probably not all regions of the $P(\rho,T)$ surface [14].

5. Appendices

5.1. The Vapor Pressure Equation

The original form of our vapor pressure function [9] is satisfactory for methane [14], but for ethane it has been necessary to add the term $d\cdot x^4$ [15]. Define the argument—

$$x(T) \equiv (1-T_t/T)/(1-T_t/T_c),$$

when the function is—

$$\ln(P/P_t) = a\cdot x + b\cdot x^2 + c\cdot x^3 + d\cdot x^4 + e\cdot x\cdot(1-x)^{3/2}. \tag{5.1}$$

Table 6 presents the coefficients.

TABLE 6. *Constants for vapor-pressure equation (5.1)*

	Methane	Ethane
a	4.7774 8580	10.7954 9166
b	1.7606 5363	8.3589 9001
c	−0.5678 8894	−3.1149 0770
d	0.0	−0.6496 9799
e	1.3278 6231	6.0734 9549

5.2. The Orthobaric Densities

The following expressions are constrained to the boundaries, the triple- and critical points [15]. In each case the basic behavior is described by—

$$Y(\rho, T) = \text{const.},$$

and polynomials are selected to represent small deviations. For the saturated liquid, define the variables,

$$x(T) \equiv (T_c-T)/(T_c-T_t),$$

$$y(\rho) \equiv (\rho-\rho_c)/(\rho_t-\rho_c),$$

$$Y(\rho, T) \equiv (y-x)/(x^\epsilon-x),$$

when the function is—

$$Y = a + b\cdot x^{2/3} + c\cdot x. \tag{5.2}$$

For the saturated vapor, define the variables,

$$x(T) \equiv (T_c/T-1)/(T_c/T_t-1),$$

$$y(\rho) \equiv \ln(\rho_c/\rho)/\ln(\rho_c/\rho_t)$$

$$Y(\rho,T) \equiv (y-x)/(x^\epsilon-x),$$

when the function is—

$$Y = A_1 + \sum_{i=2}^{5} A_i \cdot x^{i/3}. \tag{5.3}$$

Table 7 presents constants for (5.2) and (5.3).

TABLE 7. *Constants for orthobaric densities equations*

	Methane	Ethane
Saturated liquid densities, eq (5.2)		
ϵ	0.36	0.33
a	.8595 3758	.7219 0944
b	.0243 6448	.2965 7790
c	−.0268 5285	−.3003 6548
Saturated vapor densities, eq (5.3)		
ϵ	0.41	0.39
A_1	.4171 4211	.2158 7515
A_2	−.5194 9762	−.0852 2342
A_3	1.2077 7553	−.6152 3457
A_4	−1.4613 0509	.2545 2490
A_5	0.5765 8540	.1517 7230

5.3. The Coexistence Envelope, $T_\sigma(\rho)$

This envelope is shown by figure 3. For the equation of state (1) we obtain the coexistence temperature for any density from the following analytical descriptions. If the coexistence density must be found at a given temperature, it is obtained (for consistency in the equation of state) from the following expressions by iteration, using eqs (5.2) and (5.3) only to estimate an initial density.

An important feature of the present formulations [15] is that derivatives—

$$d^n T\sigma/dp^n$$

of all orders, n, are zero at $\sigma=1$, the critical point. We describe $T_\sigma(\rho)$ in two parts, according as $\sigma \lesseqgtr 1$.

This simplifies constraint to the boundaries (liquid and vapor triple points). For each range the dependent variable is—

$$Y[T_\sigma(\rho)] \equiv (T_c/T_\sigma - 1)/(T_c/T_t - 1)\,,$$

and we use the following function, infinite at the critical density

$$U(\sigma) \equiv -\gamma \cdot [1/|\sigma - 1| - 1/|\sigma_t - 1|]$$

where $\sigma_t = d_t/d_c$ is a constant, and d_t refers to vapor or liquid at the triple point according as $\sigma \lesseqgtr 1$.

For the liquid range at $\sigma \geqslant 1$ the equation is—

$$\ln(Y) = U(\sigma) + \sum_{i=1}^{5} A_i \cdot (\sigma^i - \sigma_t^i)\,. \qquad (5.4)$$

For extremely low densities in the vapor range at $\sigma \leqslant 1$ we modify the above expression as follows. Define the variable

$$W(\sigma) \equiv \ln(1 + s/\sigma)/\ln(1 + s/\sigma_t)\,,$$

where s is an arbitrary constant. Our equation for the vapor range now is—

$$\ln(Y) = U(\sigma) + B_0 \cdot \ln(W) + B_1 \cdot (\sigma^{1/3} - \sigma_t^{1/3}) + B_2 \cdot (\sigma^{2/3} - \sigma_t^{2/3}) + \sum_{i=3}^{7} B_i \cdot (\sigma^{i-2} - \sigma_t^{i-2})\,. \qquad (5.5)$$

Table 8 presents constants for (5.4) and (5.5)

TABLE 8. *Constants for the* $T_\sigma(\rho)$ *equations*

	Methane	Ethane
Saturated liquid, eq (5.4)		
γ	1/2	1/2
A_1	11.4317 7230	23.7245 1840
A_2	−3.8765 9480	−14.8860 5161
A_3	0.5378 8326	5.4317 7443
A_4	.0	−1.0715 0566
A_5	.0	0.0913 5183
Saturated vapor, eq (5.5)		
s	1/4	1/4
B_0	0.9034 9557	0.8681 0517
B_1	.0	.0151 6978
B_2	.0	−.7296 0432
B_3	−.3834 4338	1.0096 5493
B_4	−3.9210 8638	−8.7340 2710
B_5	6.2600 3837	21.1071 2823
B_6	−9.3296 0083	−31.4499 4087
B_7	5.6060 2816	17.8637 0397

Anneke L. Sengers emphasized to us some time ago the importance of the critical region for the entire equation of state, thus motivating present developments. In this laboratory, R. D. McCarty provided the essential least-squares program, and we are indebted to D. E. Diller and L. A. Weber for discussions and valuable suggestions. The American Gas Association very kindly has supported this work.

6. References

[1] Bazúa, E. R., and Prausnitz, J. M., Vapor-liquid equilibria for cryogenic mixtures, Cryogenics **11**, No. 2, 114 (April, 1971).
[2] Cox, K. W., Bono, J. L., Kwok, Y. C., and Starling, K. E., Multiproperty analysis. Modified BWR equation for methane from *PVT* and enthalpy data, Ind. Eng. Chem. Fundam. **10**, No. 5, 245 (1971).
[3] Diller, D. E., The specific heats (C_v) of dense simple fluids, Cryogenics **11**, No. 3, 186 (June, 1971).
[4] Douslin, D. R., Harrison, R. H., Moore, R. T., and McCullough, J. P., *P-V-T* relations for methane, J. Chem. Eng. Data **9**, No. 3, 358 (1964).
[4a] Fisher, G. D. and Leland, T. W., Jr., Corresponding states principle using shape factors, Ind. Eng. Chem. Fundam. **9**, No. 4, 537 (1970).
[5] Furtado, André W., The measurement and prediction of thermal properties of selected mixtures of methane, ethane, and propane, (Ph. D. Thesis, Dept. of Chemical Engineering, Univ. of Michigan, Ann Arbor, Mich., Dec. 1973.)
[6] Goodwin, R. D., Approximate Wide-Range Equation of State for Parahydrogen, Advances in Cryogenic Engineering **6**, 450 (Plenum Press, New York, 1961).
[7] Goodwin, R. D., An equation of state for fluid parahydrogen from the triple point to 100 °K at pressures to 350 atmospheres, J. Res. Nat. Bur. Stand. (U.S.) **71A** (Phys. and Chem.), No. 3, 203–212 (May–June 1967).
[8] Goodwin, R. D. and Weber, L. A., Specific heats C_r of fluid oxygen from the triple point to 300 K at pressures to 350 atmospheres, J. Res. Nat. Bur. Stand. (U.S.), **73A** (Phys. and Chem.), No. 1, 15–24 (Jan.–Feb. 1969).
[9] Goodwin, R. D., Nonanalytic vapor pressure equation with data for nitrogen and oxygen, J. Res. Nat. Bur. Stand. (U.S.) **73A** (Phys. and Chem.), No. 5, 487–491 (Sept.–Oct. 1969).
[10] Goodwin, R. D., Formulation of a nonanalytic equation of state for parahydrogen, J. Res. Nat. Bur. Stand. (U.S.) **73A** (Phys. and Chem.), No. 6, 585–591 (Sept.–Oct. 1969).
[11] Goodwin, R. D., Estimation of critical constants T_c, ρ_c, from the $\rho(T)$ and $T(\rho)$ relations at coexistence, J. Res. Nat. Bur. Stand. (U.S.) **74A** (Phys. and Chem.), No. 2, 221–227 (Mar.–Apr. 1970).
[12] Goodwin, R. D. and Prydz, R., Densities of compressed liquid methane, and the equation of state, J. Res. Nat. Bur. Stand. (U.S.), (Phys. and Chem.), No. 2, 81–101 (Mar.–Apr. 1972).
[13] Goodwin, R. D., Nonanalytic equation of state for methane, constrained to the vapor-liquid P–ρ–T boundary, unpublished NBS IR.
[14] Goodwin, R. D., The thermophysical properties of methane from 90 to 500 K at pressures to 700 bar, Nat. Bur. Stand. (U.S.), Tech. Note 653, 280 pages (Apr. 1974).
[15] Goodwin, R. D., Provisional values for the thermodynamic functions of ethane, unpublished manuscript, June, 1974.
[16] Green, M. S., and Sengers, J. V., Editors, Critical phenomena, Nat. Bur. Stand. (U.S.), Misc. Publ. 273, 256 pages (Dec. 1966).
[17] Kirk, B. S., Ziegler, W. T., and Mullins, J. C., A comparison of methods of predicting equilibrium gas phase compositions in pressurized binary systems containing an essentially pure condensed phase, Advances in Cryogenic Engineering **6**, 413 (1961).
[18] Mollerup, J., and Rowlinson, J. S., The prediction of the densities of liquefied natural gas and of lower molecular weight hydrocarbons, Chem. Eng. Sci. **29**, 1373 (1974).

[19] Rowlinson, J. S., Molecular theories of liquids and mixtures, Ind. Eng. Chem. **59,** No. 12, 28 (1967).
[20] Rowlinson, J. S., Liquids and Liquid Mixtures, p. 98, (Butterworths Scientific Publications, London, 1959). See also second edition (1969).
[21] Smith, G. E., Sonntag, R. E., and Van Wylen, G. J., Analysis of the solid-vapor equilibrium system carbon dioxide-nitrogen, Advances in Cryogenic Engineering **8,** 162 (1963).
[21a] Smith, W. R., Perturbation theory and one-fluid corresponding states theories for fluid mixtures, The Can. J. Chem. Eng. **50,** 271 (1972).
[22] Sood, S. K. and Haselden, G. G., Prediction methods for vapor-liquid equilibria in multicomponent cryogenic mixtures, Cryogenics **10,** No. 3, 199 (June, 1970).
[23] Starling, K. E., Fluid Thermodynamic Properties for Light Hydrocarbon Systems (Gulf Publishing Co., Houston, Texas, 1973).
[24] Tsonopoulos, C. and Prausnitz, J. M., Equations of state: a review for engineering applications, Cryogenics **9,** No. 5, 315 (Oct., 1969).
[25] Verbeke, O.B., Representation of *P–V–T* data by means of a "universal" state equation for simple fluids, Paper F–6, Advances in Cryogenic Engineering **18,** 256 (1972).
[26] Wagner, W., A method to establish equations of state exactly representing all saturated state variables applied to nitrogen, Cryogenics **12,** No. 3, 214 (June, 1972).
[27] Zellner, M. G., Claitor, L. C., and Prausnitz, J. M., Prediction of vapor-liquid equilibria and enthalpies of mixtures at low temperatures, Ind. Eng. Chem. Fundam. **9,** No. 4, 549 (1970).
[28] Zemansky, M. W., Heat and Thermodynamics (McGraw-Hill Book Co., Inc., New York, 1957).

(Paper 79A1–844)

JOURNAL OF RESEARCH of the National Bureau of Standards—A. Physics and Chemistry
Vol. 79A, No. 1, January–February 1974

Thermodynamic Studies of the $\alpha \rightarrow \beta$ Phase Transformation in Zirconium Using a Subsecond Pulse Heating Technique*

A. Cezairliyan and F. Righini**

Institute for Materials Research, National Bureau of Standards, Washington, D.C. 20234

(September 5, 1974)

Measurements of the temperature and energy of the $\alpha \rightarrow \beta$ phase transformation, and the electrical resistivity near and at the transformation point of zirconium using a subsecond duration pulse heating technique are described. The results yield 1147 K for the transformation temperature and 3980 J · mol^{-1} for the transformation energy. Electrical resistivity is found to decrease by 17 percent during the transformation. Estimated inaccuracies of the measured properties are: 10 K for the transformation temperature, 5 percent for the transformation energy, and 2 percent for the electrical resistivity.

Key words: Electrical resistivity; high-speed measurements; high temperature; solid-solid phase transformation; thermodynamics; zirconium.

1. Introduction

In another publication [1],[1] the applicability of a rapid pulse heating technique to studies of solid-solid phase transformations at high temperatures was demonstrated by measurements on iron at the $\gamma \rightarrow \delta$ transformation point.

The objective of the work described in this paper has been to apply the same technique to studies of the $\alpha \rightarrow \beta$ phase transformation in zirconium. Measurements of the temperature and energy of the phase transformation, and electrical resistivity near and at the transformation point are reported.

The method is based on rapid resistive self-heating of the specimen from room temperature to high temperatures in less than one second by the passage of an electrical current pulse through it; and on measuring, such experimental quantities as current through the specimen, potential drop across the specimen, and specimen temperature. Recordings of the experimental quantities are made digitally every 0.4 ms with a full-scale signal resolution of approximately one part in 8000. Specimen temperature is measured with a high-speed photoelectric pyrometer [2]. The details regarding the construction and operation of the measurement system are given in earlier publications [3, 4].

2. Measurements

The measurements were made on three zirconium specimens of 99.98% purity. The specimens were tubes fabricated from rods by removing the center portion using an electro-erosion technique. The nominal dimensions of the specimens were: length, 76.2 mm; outside diameter, 6.3 mm; and wall thickness, 0.5 mm. The outer surfaces of the specimens were polished to reduce heat loss due to thermal radiation. According to the manufacturer's analysis, the specimens contained the following impurities, in ppm by weight: O, 125; Hf, 40; Fe, 30; C, 6; H, 3.3; Al, 3; N, 2.1; Ni and Si, 1.5 each; and Ti, 1. The total amount of all other detected elements was less than 6 ppm, each element being below 1 ppm limit.

Duration of the current pulses ranged from 220 to 620 ms. Specimen heating rates varied from 1800 K·s^{-1} to 4000 K·s^{-1}. All the experiments were conducted with the specimens in a vacuum environment of approximately 1.3×10^{-3} N·m^{-2} ($\sim 10^{-5}$ torr).

The $\alpha \rightarrow \beta$ transformation (from hexagonal close-packed form to body-centered cubic) was manifested by a plateau in the temperature versus time relation for the specimen during heating. The transformation temperature for each specimen was obtained by averaging the temperatures at the plateau.

The transformation energy was obtained from the time integral of the power absorbed by the specimen during the transformation as defined by the plateau. The instantaneous value of the absorbed power was obtained by subtracting the calculated power loss due

*This work was supported in part by the U.S. Air Force Office of Scientific Research.
**Guest scientist from the Istituto di Metrologia "G. Colonnetti" in Torino, under a fellowship from the Consiglio Nazionale delle Ricerche of Italy.
[1] Figures in brackets indicate the literature references at the end of this paper.

562-903 O - 75 - 6

to thermal radiation from the imparted power (current through the specimen times the potential drop across the specimen). The hemispherical total emittance needed for this computation was obtained from the extrapolation of the measurements above 1500 K reported in an earlier publication [5]. Since the calculated power loss from the specimen due to thermal radiation was not greater than 1 percent of power imparted at the transformation temperature, even a considerable uncertainty (10%) in the emittance does not contribute any significant errors to the absorbed power.

3. Experimental Results

Except where explicitly noted, all temperatures reported in this paper are based on the International Practical Temperature Scale of 1968 [6]. In all computations, the geometrical quantities are based on their room temperature (298 K) dimensions. The experimental results for the temperature and energy of the $\alpha \rightarrow \beta$ phase transformation are presented in table 1.

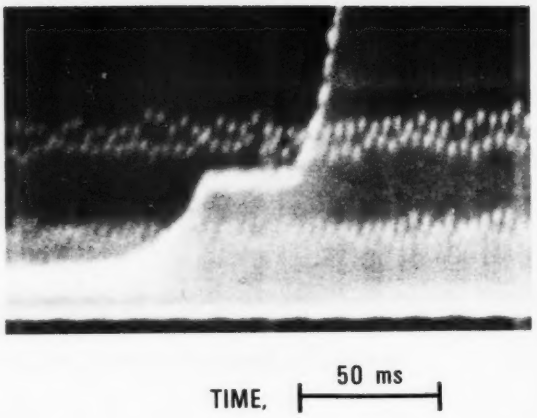

FIGURE 1. *Oscilloscope trace photograph of specimen radiance near and at the transformation point of zirconium as measured with the high-speed pyrometer.*

Dots forming the long horizontal lines correspond to radiances from a reference source.

TABLE 1. *Results for the $\alpha \rightarrow \beta$ transformation temperature and transformation energy of zirconium*

Specimen number	Heating rate [a] ($K \cdot s^{-1}$)	Number of temperatures [b]	Transformation temperature (K)	Standard deviation [c] (K)	Transformation energy ($J \cdot mol^{-1}$)
1	4000	27	1144.9	3.4	3993
2	1800	61	1148.4	3.2	3970
3	3100	47	1146.6	3.4	3968

[a] Evaluated approximately 50 K below the transformation point.
[b] Number of temperatures at the plateau used to obtain the average transformation temperature for a specimen.
[c] Standard deviation of an individual temperature at the plateau from the average transformation temperature for a specimen.

The average value of the transformation temperatures of the three specimens is 1146.6 K with a maximum and average difference of individual specimens from this value of 1.8 K and 1.2 K, respectively. The average value for the transformation energy is 3977 $J \cdot mol^{-1}$ with a maximum and average absolute difference from this value of 0.4 percent and 0.3 percent, respectively. It may be concluded that for $\alpha \rightarrow \beta$ transformation in zirconium, the transformation temperature is 1147 K and the transformation energy is 3980 $J \cdot mol^{-1}$.

As discussed in an earlier publication [5], the measurements of the geometrical quantities of a zirconium specimen after a number of experiments indicated permanent distortions (elongation) due to repeated heating and cooling through the transformation point. The values reported in this paper correspond to the first experiment for a specimen, for which no correction was needed.

Typical experimental results are presented in figures 1, 2, 3, and 4, all referring to specimen 3. Specimen radiance and specimen temperature near and at the transformation point are shown in figures 1 and 2, respectively. Figure 3 shows the variation of electrical resistivity as a function of time, while the variation of resistivity with temperature is shown in

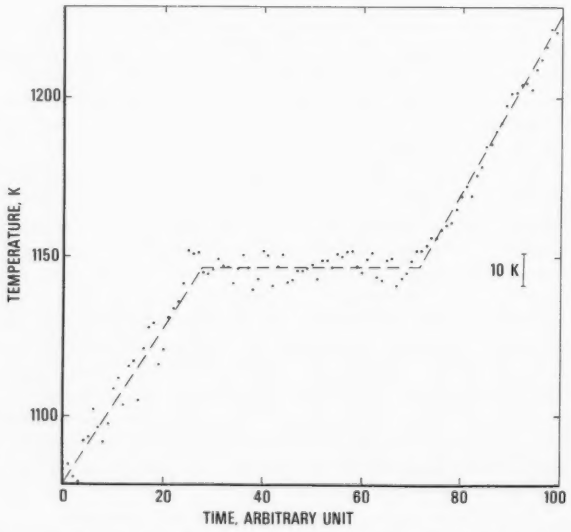

FIGURE 2. *Variation of temperature as a function of time near and at the transformation point of zirconium. The points are the temperatures obtained from individual pyrometer readings.*

The dashed lines represent the linear fits (obtained using the least-squares method) of the data in the three regions (below, during, and above the transformation). (1 time unit = 0.833 ms.)

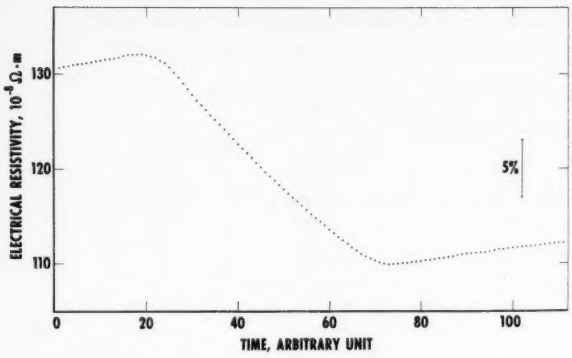

FIGURE 3. *Variation of electrical resistivity as a function of time near and at the transformation point of zirconium. The points are the resistivities obtained from individual data on current and voltage.*

(1 time unit = 0.833 ms.)

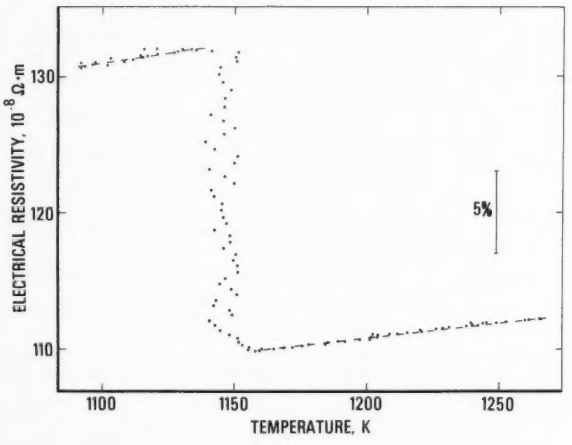

FIGURE 4. *Variation of electrical resistivity as a function of temperature near and at the transformation point of zirconium. The points are resistivities obtained from individual data on current and voltage.*

The two dashed lines represent the linear fits (obtained using the least-squares method) of the data below and above the transformation.

figure 4. It may be seen that the change in the electrical resistivity during the transformation was about 17 percent. Extrapolation of the resistivity values above the transformation to 1500 K is in agreement, within 0.3 percent, with those reported in an earlier publication [5].

The details of methods for estimating errors in measured and computed quantities using the present measurement system are given in an earlier publication [4]. In this paper the specific items were recomputed whenever the present conditions differed from those in the earlier publication.

The results obtained for imprecision [2] and inaccuracy [3] respectively are: 3 and 10 K for the transformation temperature, 1 and 5 percent for the transformation energy, and 0.5 and 2 percent for the electrical resistivity.

In the case of temperature, the standard deviation of an individual point from the average transformation temperature in a given experiment is approximately 3 K. For the three experiments, the average absolute difference of transformation temperatures from their mean is 1.2 K. In the case of energy, the imprecision includes the uncertainty in the computation of the time duration of the transformation plateau.

4. Discussion

The first evidence of a possible solid-solid phase transformation in zirconium was presented by Zwikker in 1926 [7]. Since his experiments were performed on zirconium heated in air, the transformation occurred over an extended temperature range. A sharp transformation was reported by Vogel and Tonn [8] from dilatometric and metallographic measurements and was confirmed by de Boer et al. [9], who noted that the temperature range was extended by small amounts of oxygen and nitrogen in the zirconium. The values for the $\alpha \rightarrow \beta$ transformation temperature for zirconium reported in the literature are given in table 2. Some of the old results could not be corrected to IPTS–68, due to insufficient information in the original papers.

TABLE 2. *Values of the $\alpha \rightarrow \beta$ transformation temperature of zirconium reported in the literature*

Investigator	Reference	Year	Temperature [a] (K)
Vogel and Tonn	8	1931	1135 ± 5
de Boer et al.	9	1936	1138 ± 10
Duwez	10	1951	1123 to 1138
Domagala and McPherson	11	1954	1135
Kneip and Betterton	12	1956	1138 to 1146
Vollmer et al.	13	1967	1155
Present work			1147 ± 10

[a] All temperatures in this table are those reported by the authors of the original papers. No correction to IPTS–68 was possible, due to insufficient information in the original papers.

However, the contribution of the possible differences in the temperature scales may not exceed a few degrees at the transformation temperature.

The present value for the transformation temperature is higher than most of the values given in the literature. This may partly be due to the high heating rates used in this work. A similar effect, though in the opposite direction, was observed by Duwez [10] in experiments on rapid quenching of zirconium specimens (cooling rates from 4 to 10,000 $K \cdot s^{-1}$). The transformation

[2] Imprecision refers to the standard deviation of an individual point as computed from the difference between measured value and either the average or the smooth function obtained by the least-squares method.

[3] Inaccuracy refers to the estimated total error (random and systematic).

TABLE 3. *Change of the electrical resistivity of zirconium during the $\alpha \rightarrow \beta$ transformation reported in the literature*

Investigator	Reference	Year	Temperature [a] of maximum resistivity (K)	Temperature [a] of minimum resistivity (K)	Ratio, $\frac{\rho_{max}}{\rho_{min}}$
Zwikker	7	1926	1150	1430	1.14
de Boer et al.	9	1936	1130	1145	1.19
Squire and Kaufman	17	1941	1067	1142	1.12
Adenstedt	18	1952	1118	1143	1.20
Rogers and Atkins	19	1955	1127	1173	1.19
Powell and Tye	20	1961	1129	1177	1.18
Present work			1134	1158	1.20

[a] All values in this table are based on the results reported by the authors of the original papers. No correction of values to IPTS–68 was possible, due to insufficient information in the original papers.

temperature was found to decrease with increasing cooling rate by as much as 15 K. This behavior was confirmed by Hayes and Kaufman [15]. The result of the energy of transformation of zirconium obtained in this work (3980 $J \cdot mol^{-1}$) is 6 percent higher than the value (3740 $J \cdot mol^{-1}$) of Douglas and Victor [14], 3 percent higher than the value (3850 $J \cdot mol^{-1}$) of Coughlin and King [16], 0.1 percent higher than the most recent value (3975 $J \cdot mol^{-1}$) of Vollmer et al. [13], and 9 percent lower than the value (4350 $J \cdot mol^{-1}$) of Skinner [21].

The values 3980 $J \cdot mol^{-1}$ for the transformation energy and 1147 K for the transformation temperature yield a value of 3.47 $J \cdot mol^{-1} \cdot K^{-1}$ for the entropy of $\alpha \rightarrow \beta$ transformation in zirconium.

Because of the strong dependence of the electrical resistivity on composition for zirconium at the transformation point, it is difficult to compare resistivity values reported in the literature on an absolute basis. However, a meaningful comparison may be made based on the ratio of the maximum to the minimum resistivities for a given specimen. The results of such a comparison are given in table 3. High values for the ratio and small temperature range during which transformation is completed are indications of the high purity of the specimens.

The authors express their gratitude to C. W. Beckett for his encouragement of research in high-speed thermophysical measurements and to M. S. Morse for his help with the electronic instrumentation.

5. References

[1] Cezairliyan, A. and McClure, J. L., A subsecond pulse heating technique for the study of solid-solid phase transformations at high temperatures: application to iron. In preparation.

[2] Foley, G. M., High-speed optical pyrometer. Rev. Sci. Instr., **41**, 827 (1970).

[3] Cezairliyan, A., Design and operational characteristics of a high-speed (millisecond) system for the measurement of thermophysical properties at high temperatures. J. Res. Nat. Bur. Stand. (U.S.), **75C** (Eng. and Instr.), No. 1, 7–18 (Jan.–Mar. 1971).

[4] Cezairliyan, A., Morse, M. S., Berman, H. A., and Beckett, C. W., High-speed (subsecond) measurement of heat capacity, electrical resistivity, and thermal radiation properties of molybdenum in the range 1900 to 2800 K. J. Res. Nat. Bur. Stand. (U.S.), **74A** (Phys. and Chem), No. 1, 65–92 (Jan.–Feb. 1970).

[5] Cezairliyan, A. and Righini, F., Simultaneous measurements of heat capacity, electrical resistivity and hemispherical total emittance by a pulse heating technique: zirconium, 1500 to 2100 K. J. Res. Nat. Bur. Stand. (U.S.), **78A** (Phys. and Chem.), No. 4, 509–514 (July–Aug. 1974).

[6] International Practical Temperature Scale of 1968. Metrologia, **5**, 35 (1969).

[7] Zwikker, C., Modificatieveranderingen bij zirkoon en hafnium. Physica, **6**, 361 (1926).

[8] Vogel, R. and Tonn, W., Über einen umwandlungspunkt des zirkons. Z. anorg. allgem. Chem. **202**, 292 (1931).

[9] de Boer, J. H., Clausing, P. and Fast, J. D., The α-β transition with mechanically treated and with untreated zirconium. Rec. Trav. Chim. **55**, 450 (1936).

[10] Duwez, P., Effect of rate of cooling on the alpha-beta transformation in titanium and titanium-molybdenum alloys. Trans. AIME **191**, 765 (1951).

[11] Domagala, R. F. and McPherson, D. J., System zirconium-oxygen. Trans. AIME **200**, 238 (1954).

[12] Kneip, G. D. and Betterton, Jr., J. O., Floating zone purification of zirconium. J. Electrochem. Soc. **103**, 684 (1956).

[13] Vollmer, O., Braun, M. and Kohlhass, R., Die Atomwärme des Zirkons zwischen 300 und 1700 K. Z. Naturforsch. **22**, 833 (1967).

[14] Douglas, T. B. and Victor A. C., Heat content of zirconium and of five compositions of zirconium hydride from 0 to 900 °C. J. Res. Nat. Bur. Stand. (U.S.), 61, 13–23 (July 1958) RP2878.

[15] Hayes, E. E. and Kaufmann, A. R., "Observations on the alpha-beta transformation in zirconium" in Zirconium and Zirconium Alloys, p. 241 (American Society for Metals, Cleveland, Ohio, 1953).

[16] Coughlin, J. P., and King, E. G., High-temperature heat contents of some zirconium-containing substances. J. Am. Chem. Soc. **72**, 2262 (1950).

[17] Squire, C. F. and Kaufmann, A. R., The magnetic susceptibility of Ti and Zr. J. Chem. Phys. **9**, 673 (1941).

[18] Adenstedt, H. K., Physical, thermal and electrical properties of hafnium and high purity zirconium. Trans. A.S.M. **44**, 949 (1952).

[19] Rogers, B. A. and Atkins, D. F., Zirconium-columbium diagram. Trans. AIME **203**, 1034 (1955).

[20] Powell, R. W. and Tye, R. P., The thermal and electrical conductivities of zirconium and of some zirconium alloys. J. Less-Common Metals **3**, 202 (1961).

[21] Skinner, G. B., Thermodynamic and structural properties of zirconium. Ph.D. Thesis, Ohio State University, 1951.

(Paper 79A1–845)

JOURNAL OF RESEARCH of the National Bureau of Standards — A. Physics and Chemistry
Vol. 79A, No. 1, January-February 1975

Publications of the National Bureau of Standards*

Citations with Selected Abstracts

J. Res. Nat. Bur. Stand. (U.S.), **78A** *(Phys. and Chem.)*, No. 6 (Nov.-Dec. 1974), SD Catalog No. C13.22/sec.A:78/6.

Solubility of β-$Ca_3(PO_4)_2$ in the system $Ca(OH)_2$-H_3PO_4-H_2O at 5, 15, 25, and 37 °C, T. M. Gregory, E. C. Moreno, J. M. Patel, and W. E. Brown.

Solubility of $CaHPO_4 \cdot 2H_2O$ in the quaternary system $Ca(OH)_2$-H_3PO_4-NaCl-H_2O at 25 °C, P. R. Patel, T. M. Gregory, and W. E. Brown.

The enthalpies of combustion and formation of the monochlorobenzoic acids, W. H. Johnson and E. J. Prosen.

J. Res. Nat. Bur. Stand. (U.S.), **78B** *(Math. Sci.)*, No. 4 (Oct.-Dec. 1974), SD Catalog No. C13.22/sec.B:78/4.

Saddlepoints in *P*-pivot classes of skew matrices, M. J. Stein.

Maximizing the number of spanning trees in a graph with *n* nodes and *m* edges, D. R. Shier.

The field of values and spectra of positive definite multiples, C. R. Johnson.

Automatic computing methods for special functions. Part II. The exponential integral $E_n(x)$, I. A. Stegun and R. Zucker.

Monogr. 146 **The theory of the optical wedge beam splitter,** Y. Beers, Nat. Bur. Stand. (U.S.), Monogr. 146, 31 pages (Oct. 1974) SD Catalog No. C13.44:146, 80 cents.

Key words: optical attenuation; optical beam splitter.

An optical wedge beam splitter consists of a prism of transparent material with a very small apex angle, usually about one degree. If a pencil beam of radiation is incident upon it, a portion enters the material and undergoes a series of reflections at the surfaces. At each reflection a refracted beam emerges from the material. This paper gives the basic theory for computing the ratio of the intensity of the incident beam to the intensity of any selected emerging beam and also for computing the direction of the emerging beam, assuming that the wedge angle, index of refraction, angle of incidence, and number of reflections are known.

The paper also gives the results of numerical calculations based upon this theory for sample situations which are of interest. It is shown that polarization effects can be minimized by the use of a small wedge angle and be the proper selection of the angle of incidence. In particular, it is shown that it is possible by the use of four reflections and a wedge angle of one degree to obtain attenuation factors of about 400,000 (56 db), and that the effect of changes in polarization on the attenuation factor can be held down to about one percent.

H115. **Energy Conservation Program Guide for Industry and Commerce (EPIC),** R. R. Gatts, R. G. Massey, and J. C. Robertson, Nat. Bur. Stand. (U.S.), Handb. 115, 212 pages (Sept. 1974) SD Catalog No. C13.11:115, $2.50.

Key words: energy conservation; energy conservation guide; energy conservation opportunities; energy conservation program; industrial energy conservation.

The Energy Conservation Program Guide for Industry and Commerce (EPIC) is a guide to assist business and industry to establish an on-going conservation program. EPIC outlines the steps in an energy conservation program and suggests specific ways to reduce energy use in manufacturing and commercial businesses. EPIC focuses on two aspects of energy conservation: (1) The key steps in an implementation plan for an energy conservation plan; (2) Energy Conservation opportunities which have been identified by industry.

SP305. Supplement 5. **Publications of the National Bureau of Standards 1973 catalog. A compilation of abstracts and key word and author indexes,** B. L. Oberholtzer, Ed., Nat. Bur. Stand. (U.S.), Spec. Publ. 305 Suppl. 5, 349 pages (July 1974) SD Catalog No. C13.10:305, Suppl. 5, $4.15.

Key words: abstracts, NBS publications; key words; publications.

This supplement to Special Publication 305 Supplements 1, 2, 3, and 4 of the National Bureau of Standards lists the publications of the Bureau issued between January 1, 1973 and December 31, 1973. It includes an abstract of each publication (plus some earlier papers omitted from Special Publication 305 Supplement 3), key-word and author indexes; and general information and instructions about NBS publications.

Miscellaneous Publication 240 (covering the period July 1, 1957 through June 30, 1960) and its supplement (covering the period July 1, 1960 through June 30, 1966), Special Publication 305 (covering the period July 1966 through December 1967) and Special Publication 305 Supplement 1 (covering the period 1968-1969), Special Publication 305 Supplement 2 (covering the period 1970), Special Publication 305 Supplement 3 (covering the period 1971), and Special Publication 305 Supplement 4 (covering the period 1972) remain in effect. Two earlier lists, Circular 460 (Publications of the National Bureau of Standards, 1901 to June 1947) and its supplement (Supplementary List of Publications of the National Bureau of Standards, July 1, 1947 to June 30, 1957) are also still in effect. To accompany National Bureau of Standards Special Publication 305; and its Supplements 1, 2, 3, and 4.

SP401. **Computer performance evaluation.** Proceedings of the Eighth Meeting of Computer Performance Evaluation Users Group [CPEUG], held at NBS, Gaithersburg, Md., December 4-7, 1973, H. J. Highland, Ed., Nat. Bur. Stand. (U.S.), Spec. Publ. 401, 155 pages (Sept. 1974) SD Catalog No. C13.10:401, $1.80.

Key words: computer evaluation; computer performance; computer scheduling; hardware monitors; simulation of computer

**Publications with prices and SD Catalog numbers may be purchased directly from the Superintendent of Documents, U.S. Government Printing Office, Washington, D.C. 20402 (foreign: one-fourth additional). Microfiche copies are available from the National Technical Information Service (NTIS), Springfield, Va. 22151. Reprints from outside journals and the NBS Journal of Research may often be obtained directly from the authors.*

systems; software monitors; systems design and evaluation; time-sharing systems evaluation.

The Eighth Meeting of the Computer Performance Evaluation Users Group [CPEUG], sponsored by the United States Army Computer Systems Command and the National Bureau of Standards, was held December 4-7, 1973 at NBS, Gaithersburg. The program chairman for this meeting was Merton J. Batchelder of the U.S. Army Computer Systems Command at Fort Belvoir, Va. 22060 [CSCS-ATA Stop H-14].

About 150 attendees at this meeting heard the 17 papers presented on computer performance, evaluation and measurement. Among the papers presented were those dealing with hardware and software monitors, workload definition and benchmarking, a report of FIPS Task Force 13, computer scheduling and evaluation in time-sharing as well as MVT environment, human factors in performance analysis, dollar effectiveness in evaluation, simulation techniques in hardware allocation, a FEDSIM status report as well as other related topics.

These proceedings represent a major source in the limited literature on computer performance, evaluation and measurement.

BSS54. **Health and medical facilities design.** Proceedings of the First Federal Agency Workshop, held at the National Bureau of Standards Gaithersburg, Md., December 5, 1972, R. J. Kapsch, Ed., Nat. Bur. Stand. (U.S.), Bldg. Sci. Ser. 54, 87 pages (July 1974) SD Catalog No. C13.29/2:54, $1.25.

Key words: architecture; design; hospital design; medical facilities; medical facility research.

The Federal Agencies have a large involvement in this area of Medical Facility Design; both in directly operated Federal facilities and indirectly through grant, loan and funding programs. Because of the impact of technology and because of the very large cost for new medical facilities in the last few years, there has been the rise of a field best described as medical facility research. These papers, presented at a National Bureau of Standard's Federal Agency Workshop, describe the latest medical facility research efforts by the Federal Agencies including, the Department of Defense, Department of Health, Education, and Welfare, the Veterans' Administration and the National Bureau of Standards.

FIPS PUB 31. **Guidelines for automatic data processing physical security and risk management,** S. K. Reed, Ed., Nat. Bur. Stand. (U.S.), Fed. Info. Process. Stand. Publ. (FIPS Pub.) 31, 92 pages (1974) SD Catalog No. C13.52:31, $1.35.

Key words: ADP security; computer reliability; contingency plans; Federal Information Processing Standard; fire safety; natural disasters; physical security; risk analysis; security audit; security awareness; supporting utilities.

This publication provides guidelines to be used by Federal organizations in structuring physical security programs for their ADP facilities. It treats security analysis, natural disasters, supporting utilities, system reliability, procedural measures and controls, off-site facilities, contingency plans, security awareness and security audit. It contains statistics and information relevant to physical security of computer data and facilities and references any applicable publications for a more exhaustive treatment of specific subjects.

FIPS PUB 33. **Character set for handprinting,** R. E. Rountree, Standards Coordinator, Nat. Bur. Stand. (U.S.), Fed. Info. Process. Stand. Publ. (FIPS PUB) 33, 4 pages (1974) SD Catalog No. C13.52:33, 25 cents.

Key words: character sets; character shape; character sizes; Federal Information Processing Standards; handprinting; Optical Character Recognition.

This FIPS PUB announces the adoption of the American National Standard X3.45-1974, Character Set for Handprinting as a Federal Standard. This standard provides the description, scope, and application rules for a character set for handprinting. A major purpose of this standard is to reduce the cost of data input into ADP systems which use Optical Character Recognition (OCR) equipment.

TN361. (Revised). Metric Supplement. **Liquid densities of oxygen, nitrogen, argon and parahydrogen,** H. M. Roder, Nat. Bur. Stand. (U.S.), Tech. Note 361 (Revised), (Metric Supplement), 114 pages (June 1974) SD Catalog No. C13.46:361 (Rev.), Metric Supplement, $1.25.

Key words: argon; compressed liquid; density; density ratios; liquid; nitrogen, oxygen; parahydrogen; pressure; saturated liquid; tables; temperature; uncertainties; volume.

Tables of pressure, volume, density and temperature for the saturated liquid and for compressed liquid states from the triple point to the critical point, of oxygen, nitrogen, argon, and parahydrogen are presented. The table entries of temperature are in Kelvin and degrees Celsius, table entries in pressure are in bars and kp/cm^2. Volumes or densities are given in several different units, and density ratios are tabulated for each entry. Estimates of the uncertainty for the tabulated data are given. The tables were prepared in the style and in the units preferred by the users. They are intended as source for both technician and engineer.

TN646. **Status report on primary frequency standards,** H. Hellwig, Nat. Bur. Stand. (U.S.), Tech. Note 646, 15 pages (Sept. 1973) SD Catalog No. C13.46:646, 30 cents.

Key words: accuracy; atomic frequency standards; cesium beam tubes; clocks; hydrogen masers; lasers; primary frequency standards.

This report surveys the state-of-the-art in atomic frequency standards with exclusive regard to their use as primary frequency reference; i.e., only accuracy is discussed. The report covers operational standards as well as devices which are still in the research or exploratory development phase. It is predicted that accuracies of better than 1×10^{13} will be achieved within a few years, and that, as a consequence of new techniques, accuracy may be treated statistically in the not too distant future. Also, clocks may become available which state accuracy continually.

TN832. **Report on planning session on software engineering handbook,** S. L. Stewart, Ed., Nat. Bur. Stand. (U.S.), Tech. Note 832, 18 pages (Nov. 1974) SD Catalog No. C13.46:832, 70 cents.

Key words: programming; quality software; software engineering.

This report from a planning committee sponsored by the National Bureau of Standards, the National Science Foundation, and the Association for Computing Machinery discusses the need for, coverage of, and audience for a proposed Software Engineering Handbook.

TN838. **The use of weather and climatological data in evaluating the durability of building components and materials,** L. W. Masters and W. C. Wolfe, Nat. Bur. Stand. (U.S.), Tech. Note 838, 101 pages (Aug. 1974) SD Catalog No. C13.46:838, $1.45.

Key words: accelerated aging; building components and materials; climatological data; durability; environmental factors; long-term tests; short-term tests; weathering factors.

The durability of building components and materials is dependent, to a large extent, on the in-service environment to which they are subjected in service. Thus, the prediction of durability requires knowledge of the service environment.

Weathering factors, which comprise one group of environmental factors, are the subject of this report. The objectives of this report are to indicate how, in the present state of knowledge, weather and climate data can be used to aid in quantifying weathering factors so that durability tests for building components and materials may be designed.

TN843. **A technical guide to computer-communications interface standards,** A. J. Neumann, B. G. Lucas, J. C. Walker, and D. W. Fife, Nat. Bur. Stand. (U.S.), Tech. Note 843, 111 pages (Aug. 1974) SD Catalog No. C13.46:843, $1.50.

Key words: ADP standards; communications disciplines; computer networks; data communications.

A technical summary and guide is given for existing and forthcoming Federal and National standards on data communications pertinent to computer networking. Selected international standards and industry practices are included for completeness. Prepared to assist the application of standards within the World Wide Military Command and Control System, this handbook should be useful to all ADP system designers interested in uniform data terminal interfaces, character sets and codes, keyboard arrangements, and communications line disciplines for effective message exchange between computers.

TN845. **Cost analysis for computer communications,** R. P. Blanc, Nat. Bur. Stand. (U.S.), Tech. Note 845, 40 pages (Sept. 1974) SD Catalog No. C13.46:845, 75 cents.

Key words: computer networking; cost study; interactive terminals; value-added networks.

This report summarizes a communication cost study relevant to the needs of the NSF Networking for Science Program. The primary purpose of this report is to provide an approximation to the communications costs of connecting a specified number of host computers in selected locations with a specified number of interactive user terminals. Cost factors from existing, proposed, and modeled value-added networks are applied to hypothetical traffic demands to arrive at cost estimates.

TN848. **A bibliography of the Russian reference data holdings of the library of the Office of Standard Reference Data,** G. B. Sherwood and H. J. White, Jr., Nat. Bur. Stand. (U.S.), Tech. Note 848, 20 pages (Sept. 1974) SD Catalog No. C13.46:848, 55 cents.

Key words: bibliography; reference data; Russian literature.

This text presents a listing of the Russian reference data holdings of the library of the Office of Standard Reference Data of the National Bureau of Standards as of March 1974. In addition to the bibliographic listing, information on the status of translations into English is given where available.

TN849. **A FORTRAN analyzer,** G. Lyon and R. B. Stillman, Nat. Bur. Stand. (U.S.), Tech. Note 849, 28 pages (Oct. 1974) SD Catalog No. C13.46:849, 80 cents.

Key words: computation and flow analysis; FORTRAN language use; programming aids; syntax analysis.

Details of a FORTRAN analysis package are presented. Examples illustrate a current operational level which gathers FORTRAN statement and frequency-of-execution statistics. Arguments support a simple technique for monitoring FORTRAN executions.

TN853. **State building regulatory programs for mobile homes and manufactured buildings—a summary,** P. W. Cooke, H. K. Tejuja, R. D. Dikkers, and L. P. Zelenka, Nat. Bur. Stand. (U.S.), Tech. Note 853, 35 pages (Sept. 1974) SD Catalog No. C13.46:853, 85 cents.

Key words: building regulation; enforcement; evaluation; inspection; legislation; manufactured building; mobile homes; rules and regulations; state-of-the-art study.

Information describing State mobile home and manufactured building regulatory programs are presented in two series of summary tables. The tables provide information on salient elements of the enabling legislation and the administrative rules and regulations promulgated for each State program. Other features of the various enforcement programs, including the status of reciprocity for the interstate acceptance of mobile homes and manufactured buildings are also enumerated.

NBSIR 73-108. **City games—City I operator's manual,** J. E. Moriarty, 24 pages (Oct. 1973). Order from NTIS as COM 74-10701-2.

Key words: city; computer; directors; economic; games; government; metropolitan; players; sectors; simulation; social; urban.

City I is an operational simulation game in which participants make economic, government, and social decisions affecting a hypothetical metropolitan area. The game is run on an IBM 1131 Central Processor with at least 8K and single disc storage.

This manual describes the methods of operating the Central Processor relative to the game along with the special coding required to change and/or update the computer program and core mapping.

It is assumed throughout this manual that the operator knows how to cold start the 1130, change carriage tapes, and load and clear the card reader.

NBSIR 73-109. **City games—City I director's manual,** J. E. Moriarty, 76 pages (Sept. 1973). Order from NTIS as COM 74-10701-1.

Key words: city; computer; director's; economic; games; government; metropolitan players; sectors; simulation; social urban.

City I is an operational simulation game in which participants make economic and government decisions affecting a hypothetical metropolitan area. Through the use of a computer, the simulated urban system responds to the participant's as any real city would. The City I Director instructs the players in procedure and coordinates the overall game play. This manual describes the details of administering the game from the Director's point of view and presents examples of decision codes, formats, and general information necessary to direct the game.

NBSIR 73-110. **City games—City I player's manual,** J. E. Moriarty, Ed., 150 pages (Mar. 1973). Order from NTIS as COM 73-11191.

Key words: city; computer; directors; economic; games; government; metropolitan; players; sectors; simulation; social; urban.

City I is an operational simulation game in which participants make economic, government, and social decisions affecting a hypothetical metropolitan area. Through the use of a computer, the simulated urban system responds to the participant's decisions as any real city would. Each player in City I is assigned to a team which shares an economic and governmental role. This manual describes the player details for the economic and government sectors along with general information required for game play. It is one of three manuals necessary for game play. (Player's Manual, Director's Manual, Computer Operator's Manual). Each of these manuals are designed to be used for reference and by themselves will not describe enough details for a complete game play. The game is run on an IBM 1130 computer with 8K core and single disc.

NBSIR 73-112. **City games—City 4 computer operator's manual,** J. E. Moriarty, 56 pages (Sept. 1973). Order from NTIS as COM 74-10702-3.

Key words: City IV; computer; Fortran; gaming; IBM 360/70; JCL; simulation.

This manual is written for an IBM 360/70 computer. It describes the necessary Fortran & JCL commands required for computer operation of the CITY IV game. Test commands and sequences are presented along with complete computer operating instructions for the Game. It is expected that this manual, along with a Game Director's manual will provide complete instructions for the operation of CITY IV.

NBSIR 73-113. **City games—City 4 director's manual,** J. E. Moriarty, Ed., 286 pages (Mar. 1974). Order from NTIS as COM 74-10702-1.

Key words: city; computer; director's; economic; games; government; metropolitan players; sectors; simulation; social; urban.

City 4 is an operational simulation game in which participants make economic and government decisions affecting a hypothetical metropolitan area. Through the use of a computer, the simulated urban system responds to the participant's as any real city would. The City 4 Director instructs the players in procedure and coordinates the overall game play. This manual describes the details of administering the game from the Director's point of view and presents examples of decision codes, formats, and general information necessary to direct the game.

NBSIR 73-114. **City games—City 4 player's manual,** J. E. Moriarty, Ed., 276 pages (Feb. 1974). Order from NTIS as COM 74-10702-2.

Key words: city; computer; directors; economic; games; government; metropolitan; players; sectors; simulation; social; urban.

City 4 is an operational simulation game in which participants make economic, government, and social decisions affecting a hypothetical metropolitan area. Through the use of a computer, the simulated urban system responds to the participant's decisions as any real city would. Each player in City 4 is assigned to a team which shares an economic and governmental role. This manual describes the player details for the economic and government sectors along with general information required for game play. It is one of three manuals necessary for game play. (Player's Manual, Director's Manual, Computer Operator's Manual). Each of these manuals are designed to be used for reference and by themselves will not describe enough details for a complete game play. The game is run on an IBM O.S./360 computer.

NBSIR 74-485. **Strength of glass—a fracture mechanics approach,** S. M. Wiederhorn, 24 pages (May 1974). Order from NTIS as AD 780704.

Key words: crack growth; fracture; glass; static fatigue; strength.

After a brief review of those factors that determine the strength of glass (brittleness, surface flaws, susceptibility to stress corrosion cracking), a discussion will be given of how fracture mechanics techniques can be used to understand the physics and chemistry of glass strength. In this paper we assume that the strength of glass is limited by the growth of cracks that are always present in normal glass surfaces. Fracture mechanics techniques can be used to characterize the crack growth and to relate the growth to experimental parameters such as temperature, environment, and glass composition. Crack growth data obtained in this manner can be used to develop a deeper understanding of fracture mechanisms, and to develop charts that can be used for the design of glass structural components. Examples of both applications are given in the paper.

NBSIR 74-497. **US/UK joint complementary research program in building, (wind loads, water supply, fire detection), July 1972-June 1973,** C. C. Raley, I. A. Benjamin, R. D. Marshall, and J. E. Snell, 24 pages (Oct. 1973). Order from NTIS as COM 74-11269.

Key words: cooperative programs; fire safety; hydraulics; international building technology; wind loads.

This is a status report of the progress achieved under the "Joint Complementary Research Program" sponsored by the Building Research Establishment (UK) and the Center for Building Technology (US), during the period July 1972 through June 1973. The program includes three projects: Wind Loads on Buildings, Design of Water Supply and Drainage Installations in Buildings, and Fire Detection in Buildings, each of which is discussed in the report.

NBSIR 74-510. **Effect of phase separation on the physical and chemical properties of glasses-density and chemical durability,** J. H. Simmons, S. A. Mills, and B. F. Howell, 33 pages (July 1974). Order from NTIS as AD 782793.

Key words: borosilicate glass; chemical durability; density; immiscibility.

This report covers results from density and chemical durability measurements on a borosilicate glass widely used commercially for chemical glassware while the glass undergoes liquid-liquid immiscibility. A net decrease in density is observed during an isothermal heat-treatment below the transition temperature. This density or molar volume change is related to the effect of pressure on the phase transition temperature by means of equations derived herein. The chemical durability of the material is measured following the ASTM titration technique and shows a large degradation of chemical resistance to attack by water as a result of sub-immiscibility structure development. The effect is analyzed in terms of the change in composition of the phases associated with the immiscibility transition.

NBSIR 74-516. **Chemical kinetics data survey VIII. Rate constants of ClO_x of atmospheric interest,** R. T. Watson, 51 pages (June 1974). Order from NTIS as COM 74-11384.

Key words: absorption cross sections; atmospheric chemistry; chemical kinetics; chlorine; chlorine dioxide; chlorine monoxide; data evaluation; gas phase; optical; rate constants; stratospheric chemistry.

The quantitative data on reactions of chlorine atoms and the chlorine oxides are compiled. Preferred values for rate constants are given where possible. Optical absorption cross sections are given for the species that may photolyze in the atmosphere. The experimental techniques used to obtain the rate data are discussed.

NBSIR 74-539. **Energy conservation at the NBS laboratories,** J. D. Hoffman, 81 pages (July 1974). Order from NTIS as COM 74-11574.

Key words: contingency plans; electricity; energy conservation; heating fuels; humidity control; transportation.

An Energy Task Force was established at NBS to effect energy conservation, to develop contingency plans to keep the Laboratories functioning in the event of reduced energy supply and to assist employees with transportation problems. The NBS Laboratories use a total of ~ 115 million kWh of electricity and ~ 780 billion BTU of heating fuel annually to power equipment and to provide a reliable environment. The Task Force conducted a systems analysis of energy use and found that 85 percent of the energy is used in climate control. A mathematical model for the climate control system was developed that affords an accurate comparison between observed and calculated energy use. As part of the analysis of energy use, conservation measures were identified and implemented. These measures include lighting reductions, building and zone shut-downs, thermostat adjustments, and changes in cooling coil control parameters. The conservation actions resulted in a reduction of ~ 12 percent in electricity and ~ 18 percent in heating fuel. The Task Force formulated contingency plans to reduce energy use on short notice in preparation to respond to area-wide energy problems. These plans provide for a set of priorities to produce a reduction of 2-5 megawatts in electrical demand and for an effective doubling in oil storage capacity. Task Force recommendations address all phases of energy use and implementation of them will increase electricity conservation to ~ 15 percent and heating fuel conservation to ~ 21 percent.

NBSIR 74-554. **City games, disk and tape generation,** J. Moriarty, 12 pages (Sept. 1973). Order from NTIS as COM 74-10703-2.

Key words: city model; computer; computer disks; computer tapes; duplicate tapes and disks.

This document contains the instructions for initializing duplicate disks for the CITY I model and duplicate tapes for the CITY IV model.

NBSIR 74-555. **City games, an executive's overview,** J. E. Moriarty, 50 pages (May 1974). Order from NTIS as COM 74-10704.

Key words: city; computer; computer games; economic; government; metropolitan; simulation; social.

The City Games are realistic gaming simulations of the operation of contemporary cities. They have been in continuous development since the 1960s with their completion by the National Bureau of Standards in 1973-74. In the City Games, participants experience intensive transactions in collaborative planning and in competitive negotiations for the allocation of limited resources. They emulate elements of the government, economic and social sectors of the city system and make planning decisions involving land use, schools, transportation systems, water and sewer facilities, zoning, tax structure, etc. In a 3-hour round of game play, representing a telescoped fiscal year, the decision maker makes quantitative decisions, implements them, and (through the computer aided simulation) sees the consequences of his actions. In successive rounds of play, the participant gains experience in trade-off negotiations, learns systematic approaches to typical problems and acquires new insights into the interdependences of the numerous components of a city system. City Game demonstrations can be conducted over a 2-3 day period and can accommodate between 30 and 60 active participants.

NBSIR 74-556. **City games, mathematical foundations,** J. E. Moriarty, Ed., 92 pages (Nov. 1973). Order from NTIS as COM 74-10703-1.

Key words: computer programs; computers; computer simulation; equations; mathematical foundations; mathematics; simulation; simulation module.

The CITY models are operational simulation games in which the participants make economic, government and social decisions affecting a hypothetical metropolitan area. Through the use of a computer, the simulated urban system responds to the participant's decisions as any real city would. To simplify the description of the theory of the CITY GAMES modules, this manual is written for the four module game. The equations for the other games can easily be obtained by eliminating the descriptors that do not apply to the particular game of intetest. The theoretical structure of all models is consistent and relevant only within the range from a central city area to a regional configuration. The description of the module components and equations are meant to show the scope of decisions including those by the user and by the programs and algorithms of the computer model.

This column lists all outside publications by the NBS staff, as soon after issuance as practical. For completeness, earlier references not previously reported may be included from time to time.

Albares, D. J., **Electron and ion momentum transfer from plasma electrical conductivity in a magnetic field,** *Phys. Fluids* **16,** No. 8, 1252-1258 (Aug. 1973).

Key words: Hall effect; helium; magnetic field; momentum transfer; negative glow plasma.

The electrical conductivity of a partially to strongly (Coulomb collision-dominated) ionized dc plasma in a dc magnetic field was investigated at low frequency by two experimental methods, one utilizing the Hall effect and the other a plasma interaction with an induced solenidal electric field. Electron-ion and electron-atom momentum transfer collision frequencies and ion mobility in the magnetic field (ion slip) were inferred. The helium abnormal negative glow plasma was used at pressures of 0.5 to 2.5 torr, electron densities of 1 to 32×10^{17} m^{-3} and temperature ≈ 600 K; the magnetic field ranged up to 675 G. The data support Shkarofsky's theory of partial ionization. When ion motion becomes dominant, the resulting ion mobility is 75 percent larger than He^+ mobility in helium taken from drift tube measurements. This disagreement suggests that further theoretical work on ion mobility in a plasma is needed.

Alexandropoulos, N. G., Cohen, G. G., Kuriyama, M., **Evidence of optical transitions in x-ray inelastic scattering spectra: Li metal,** *Phys. Rev. Lett.* **33,** No. 12, 699-702 (Sept. 16, 1974).

Key words: Compton scattering; lithium; optical transitions; x-ray inelastic scattering; x-ray Raman scattering.

We report results of x-ray Compton-Raman scattering experiments. In addition to the expected Compton and Raman scattering, there is a prominent feature in the form of a peak near $E/E_c = 1$. The new peak can be explained qualitatively by considering the conduction band of lithium metal to be composed of hybridized orbital electrons, and it furnishes the first evidence of an L-x-ray Raman band.

Ambrose, J. R., Kruger, J., **Tribo-ellipsometry: A new technique to study the relationship repassivation kinetics to stress corrosion,** *Corrosion* **28,** No. 1, 30-35 (Jan. 1972).

Key words: repassivation kinetics; steel; stress corrosion; tribo-ellipsometry.

Since the susceptibility of a material to stress corrosion cracking (SCC) may be related to the rupture of a protective film and the repassivation rate of the material thus exposed, a technique, tribo-ellipsometry, has been developed which simulates film rupture by abrading off the surface oxide. During the subsequent repassivation of the exposed surface, this technique allows simultaneous determination of film growth kinetics by ellipsometry and current transients during that time interval following removal of the oxide film. The major advantage of the technique is that the ellipsometric transient allows one to determine which part of the current transient is responsible for repassivation and which part is involved in metal dissolution. The utility of the technique is demonstrated by comparing repassivation rates for a low carbon steel in a sodium nitrate solution in which the metal is susceptible to SCC to those in a sodium nitrite solution, in which it is not. Results obtained using this method indicate that the repassivation rate is slower at elevated temperatures in the nitrate than it is in the nitrite, and that a larger proportion of the current is involved in metal dissolution in the nitrate. This may offer an insight into the reasons for observed susceptibility of mild steels to SCC in such nitrate environments.

Ausloos, P., Rebbert, R. E., Lias, S. G., **Primary processes in the photolysis of propane: The use of HI as a radical scavenger,** *J. Photochem.* **2,** 267-283 (1973-74).

Key words: equipartition of energy; hydrogen iodide; methylene insertion reaction; propane; radical scavenging; vacuum ultraviolet photolysis.

The photolysis of C_3D_8 has been investigated with 8.4, 10.0 and 11.6-11.8 eV photons, using HI to scavenge the radicals through the reaction: $R_D + HI \rightarrow R_DH + I$ (where R_D is a fully deuterated alkyl or alkenyl radical). Comparison of the results with the results of analogous experiments using H_2S as a scavenger leads to the conclusion that HI is a more efficient radical scavenger than H_2S. The results are discussed with particular emphasis on determining whether the primary processes include direct C–C and C–H bond cleavage. An examination of the effects of HI concentration, conversion, and pressure on the yield of ethyl radicals intercepted indicates that the ethyl radicals are formed in the primary process: $C_3D_8^* \rightarrow C_2D_5 + CD_3$. It is noted that the relative importances of this process and the other primary processes involving breaking of the C–C bond ($C_3D_8^* \rightarrow CD_4 + C_2D_4$ and $C_3D_8^* \rightarrow C_2D_6 + CD_2$) do not change with energy, and it is thus suggested that they all occur from an excitation in the C–C bond, and that RRKM considerations relating to equipartition of energy are not applicable to the dissociations of electroni-

cally excited alkanes. It is pointed out that, as in the photolysis of ethane, the dissociation leading to the formation of a molecule of hydrogen (deuterium) ($C_3D_8^* \rightarrow D_2 + C_3D_6$), which apparently occurs as a result of an excitation in a C–H (C–D) bond, predominates in the 8.4 eV photolysis, but diminishes sharply in importance with respect to the C–C bond cleavage processes when the energy is increased. The insertion of methylene into a primary C–H bond of C_3H_8 to give n-butane is examined, and information concerning the internal energy of the CH_2 species is derived and discussed in terms of the primary dissociation of propane.

Bagg, T. C., Editor, **A report of the micrographic Goodwill People-to-People tour through Europe, including the Soviet Union,** *J. Microgr.* **6,** No. 5, 219-229 (May-June 1973) and **6,** No. 6, 269-279 (July-Aug. 1973).

Key words: microfilm; libraries; microfiche; overseas.

During the fall of 1972 the National Microfilm Association organized and coordinated a delegation of 12 members and 8 of their wives on a visit to Europe and Soviet Union as part of the Goodwill People-to-People Program. The purpose of this trip was to give micrographic leaders in the U.S. an opportunity to meet their overseas counterparts. The major cities visited were, the Hague, Brussels, Paris, Prague, Moscow, Belgrade and London. This report consists of brief discussions by various delegates of the many professional groups visited.

Ballard, D. B., **A low magnification-large sample holder for the SEM,** *Proc. 32d Annual Electron Microscope Society of America Meeting, St. Louis, Mo., Aug. 13-16, 1974,* pp. 446-447 (Aug. 1974).

Key words: large sample; low magnification; scanning electron microscope; stage.

A large specimen stage with low magnification capability was constructed to fit the SEM. The specimen can be rotated for stereo pair photographs. All modes of signal processing and SEM controls that are normally available can be used with this stage.

Bennett, L. H., Cuthill, J. R., McAlister, A. J., Erickson, N. E., Watson, R. E., **Electronic structure and catalytic behavior of tungsten carbide,** *Science* **184,** 563-565 (May 1974).

Key words: catalysis; density of states; magnetic exchange enhancement; Pt; W; WC.

Tungsten carbide has been shown to be an effective catalyst for a number of reactions that are readily catalyzed by platinum, but not at all by tungsten, and it was speculated that this behavior is due to changes in the electron distribution when carbon is added to tungsten. A test of this hypothesis, made by measuring the valence band x-ray photoelectron spectrum of tungsten carbide and comparing it with the spectra of tungsten and platinum, shows that, near the Fermi level, the electronic density of states of tungsten carbide more nearly resembles that of platinum than that of tungsten.

Billingsley, F. P. II, Krauss, M., **Multiconfiguration self-consistent-field calculation of the dipole moment function of CO($X\ ^1\Sigma^+$),** *J. Chem. Phys.* **60,** No. 11, 4130-4144 (June 1, 1974).

Key words: CO; dipole moment; dipole moment functions; infrared intensity; multiconfiguration SCF.

The dipole moment function for the $^1\Sigma^+$ ground state of CO in the vicinity of the equilibrium internuclear distance has been calculated by the optimized valence configurations (OVC) multiconfiguration self-consistent-field method. The results are compared with existing Hartree-Fock and configuration interaction treatments of this molecule at single points and also the dipole moment function deduced from experimental infrared intensities. At the experimental equilibrium separation, the calculated dipole moment is − 0.167 D (C^-O^+) which is in reasonable agreement with the microwave value of − 0.112 D (C^-O^+). The vibrationally averaged expectation value of the dipole moment based on the computed moment function and accurate vibrational wavefunctions is − 0.151 D (C^-O^+) which is in better agreement with the observed microwave quantity and illustrates that the effect of vibrational averaging is not negligible in systems such as CO that possess small permanent dipole moments. A general prescription for constructing OVC wavefunctions for diatomic molecules is also presented.

Billingsley, F. P. II, Krauss, M., **Quadrupole moment of CO, N_2, and NO^+,** *J. Chem. Phys.* **60,** No. 7, 2767-2772 (Apr. 1, 1974).

Key words: CO; hyperpolarizability; multiconfiguration SCF; N_2; NO^+; quadrupole moment.

Quadrupole moments obtained by a variety of experiments exhibit a wide range of values even for molecules such as CO and N_2. Previous theoretical values were obtained with Hartree-Fock single-configuration wavefunctions. This study reports quadrupole moments obtained with multiconfiguration self-consistent-field wavefunctions chosen by the optimized valence configuration approach of Wahl and Das. The theoretical MC-SCF quadrupole moments are compared with both the experimental and Hartree-Fock values. Vibrationally averaged values of the quadrupole moments were obtained for CO and NO^+. The results for the $v=0$, $J=0$ vibrational level are − 2.23 and 0.56×10^{-26} esu cm^2, respectively.

Blair, W., Iverson, W. P., Brinckman, F. E., **Application of a gas chromatograph–atomic absorption detection system to a survey of mercury transformations by Chesapeake Bay microorganisms,** *Chemosphere III,* No. 4, 167-174 (1974).

Key words: anaerobic bacteria; atomic absorption; Chesapeake Bay; dimethylmercury; estuary; faculative bacteria; gas chromatography; mercury; metabolites; methylmercury; sediments.

A flameless atomic absorption spectrophotometer coupled to a vapor phase chromatograph was developed which permits speciation of elemental mercury (Hg^0) methylmercury (CH_3HgCl), and dimethylmercury in gaseous metabolites at environmental concentrations. Through use of this technique, a number of mercury tolerant anaerobic and aerobic bacteria, isolated from Chesapeake Bay sediments, were examined for their ability to produce these compounds in the presence of Hg as $HgCl_2$ (1 ppm). Of the two faculative isolates examined in a N_2 atmosphere, one produced both methylmercury and Hg^0 and the other only Hg^0. In the presence of air only one of these organisms produced slight traces of Hg^0. Of the five anaerobic isolates, one produced Hg^0, methylmercury, and dimethylmercury, two produced only Hg^0, and two evolved only very slight or no detectable traces of Hg^0. These and previous results are consistent with the view that biomethylation of Hg is a more likely process under anoxic conditions.

Boyle, D. R., Clague, F. R., Reeve, G. R., Wait, D. F., Kanda, M., **An automated precision noise figure measurement system at 60 GHz,** *IEEE Trans. Instrum. Meas.* **IM-21,** No. 4, 543-549 (Nov. 1972).

Key words: analysis; automation; noise figure; *Y*-factor.

As part of a millimeter-wave development program at the National Bureau of Standards, a precision measurement method and system was devised to automatically measure the effective input noise temperature of 55-65-GHz receivers.

Salient features of the system include a bolometric *Y*-factor measurement, a working "hot" noise source consisting of a waveguide argon gas tube mount developed at the National Bureau of Standards, and a minicomputer system controller operating in Basic. System design considerations and measurement uncertainties are discussed.

Braun, W., Kurylo, M. J., Kaldor, A., Wayne, R. P., **Infrared laser enhanced reactions: Spectral distribution of the NO_2 chemiluminescence produced in the reaction of vibrationally excited O_3 with NO,** *J. Chem. Phys.* **61,** No. 2, 461-464 (July 15, 1974).

Key words: chemiluminescence reaction; emitting state; enhanced reaction; infrared laser; spectral distribution; vibrationally excited.

Vibrationally excited ozone, produced by CO_2 laser radiation, was found to react significantly faster with NO than does thermal O_3. The emission spectrum of the laser enhanced chemiluminescence from this reaction was measured from 520 to 810 nm. The lowest lying 1^2B_2 statewas identified as the primary source of NO^*_2 emission in the NO $+ O_3$ reaction. One quantum of vibrational excitation in the reactant O_3 was found to introduce one quantum of vibrational energy in the product NO_2 (1^2B_2). The rate enhancement of the reaction channel producing $NO_2(1^2B_2)$ as a result of vibrational excitation of O_3 was 5.6 $\pm$ 1.0. Thus, only about 50 percent of the available vibrational energy is used to enhance this reaction.

Brower, W. S., Minor, D. B., Parker, H. S., Roth, R. S., Waring, J. L., **Flux synthesis of cubic potassium antimonate,** *Mater. Res. Bull.* **9,** No. 8, 1045-1051 (1974).

Key words: cubic potassium antimonate; flux synthesis; impurity stabilization; potassium antimonate; potassium fluoride-antimony oxide; single crystals.

Although the compound $KSbO_3$ has been reported to occur in a high temperature cubic polymorph, only the rhombohedral ilmenite phase was obtained in this study for pure material at ambient pressure and temperatures up to about 1350 °C in open Pt crucibles or sealed Pt tubes. With the addition of about 2 mole percent SiO_2, B_2O_3 or other oxides of small cations a primitive cubic phase was found with a ~9.578 A. Small single crystals of a body centered cubic phase (a=9.605 A) were easily synthesized by a flux evaporation technique at about 1000 °C in an open Pt crucible from a composition of about 5 mole percent Sb_2O_4:95 mole percent KF. The exact composition and structure of this phase (presumably $K_{1-x}SbO_{3-x}F_x$, $0 < \chi \leq 0.5$) is now under investigation.

Brown, D. W., Lowry, R. E., Wall, L. A., **Glass and melting transitions of copolymers of tetrafluoroethylene with propylene and isobutylene,** *J. Polym. Sci. Part A-2* **12,** 1303-1318 (1974).

Key words: copolymer; fluoropolymer; glass temperature; isobutylene; melting temperature; polymer; propylene; tetrafluoroethylene.

Copolymers of tetrafluoroethylene and propylene were prepared that contained 30-65 mole-percent of the former. Reactivity ratios of tetrafluoroethylene- and propylene-ended radicals are 0.008 and 0.06, respectively, resulting in formation of highly alternating copolymers. The glass temperatures, T_g, were determined using a differential scanning calorimeter. Values ranged from 260 to 275 K. A plot of T_g versus composition has a low maximum centered about the equimolar composition. Copolymers of tetrafluoroethylene and isobutylene were prepared that contained 30-56 mole-percent of the former. Reactivity ratios of tetrafluoroethylene- and isobutylene-ended radicals are 0.005 and 0.021, respectively. The glass temperatures of these copolymers range 257 to 313 K. A higher maximum at the equimolar composition is obtained when T_g is plotted versus composition. Isobutylene-containing copolymers having 45-54 mole-percent tetrafluoroethylene are crystalline. Melting temperatures range from 416 to 476 K and have their maximum value at the equimolar composition. It is thought that long sequences of alternating units behave as a third entity in these copolymers, the other two being nonalternating units of the two monomers. Unless inhibited, ionic homopolymerization of isobutylene can be appreciable, sometimes resulting in the polymer having two T_g.

Burke, R. W., Diamondstone, B. I., Velapoldi, R. A., Menis, O., **Mechanisms of the Liebermann-Burchard and Zak color reactions for cholesterol,** *Clin. Chem.* **20,** No. 7, 794-801 (1974).

Key words: carbonium ion formation; cholestapolyenes; cholesterol; enylic cations; Liebermann-Burchard; oxidative reactions; reaction mechanisms; Zak.

Correlation of SO_2 and Fe^{2+} measurements with new spectral data indicates that the Liebermann-Burchard (L-B) and Zak color reactions for cholesterol have similar oxidative mechanisms, each yielding, as oxidation products, a homologous series of conjugated cholestapolyenes. These studies further suggest that the colored species observed in these two systems are enylic carbonium ions formed by protonation of the parent polyenes. Thus, the red (λ_{max}, 563 nm) product typically measured in the Zak reaction is evidently a cholestatetraenylic cation, and the blue-green product in the L-B reaction (λ_{max}, near 620 nm) is evidently the pentaenylic cation. The effects of rate of carbonium ion formation and sulfuric acid concentration on sensitivity and color stability are discussed. A solvent extraction procedure is described for specifically converting cholesterol to 3,5-cholestadiene. Incorporating this step into the typical L-B method can increase the L-B sensitivity for cholesterol by several fold.

Burns, G. W., Hurst, W. S., Scroger, M. G., **High reliability sheathed, beryllia insulated, tungsten-rhenium alloy thermocouple assemblies – their fabrication and EMF stability,** *NASA CR-134549*, pp.1-36 (National Aeronautics and Space Administration, Washington, D.C. June 1974).

Key words: beryllium oxide; emf drift; sheathed thermocouples; tantalum; temperature measurements; tungsten-rhenium alloys.

1.6 mm diameter tantalum sheathed, BeO insulated, W-3 percent Re/W-25 percent Re thermocouple assemblies have been fabricated and their emf drift determined during 2059 hours of exposure at 2073 K in a gaseous helium environment. The sheathed thermocouple assemblies were constructed from aged thermoelements, specially heat-treated BeO insulators, and specially cleaned and etched tantalum sheaths. Their thermal emf drifts ranged from the equivalent of only − 0.3 to − 0.8 K drift per 1000 hours of exposure at 2073 K. No evidence of any gross chemical attack or degradation of the component materials was found. The emf drift and material behavior of some unsheathed, BeO insulated, W-3 percent Re/W-25 percent Re thermocouples at 2250 and 2400 K were also determined. Unsheathed thermocouples tested in an argon environment at 2250 K for 1100 hours and at 2400 K for 307 hours exhibited changes in thermal emf that typically ranged from the equivalent of a few degrees K to as much as +11 K. Post-test examinations of these thermocouples revealed some undesirable material degradation and interaction which included erosion of the BeO insulators and contamination of the thermoelements by tantalum from the tantalum blackbody enclosure in which the thermocouples were contained. Preliminary tests to examine the chemical compatibility of sintered BeO insulators with Ta sheaths in an argon environment at 2073, 2250, and 2400 K were also conducted. They revealed gross erosion of the insulator after only 50 hours exposure at 2400 K. A 50 percent reduction in the insulator diameter at the open end of the sheath was typical. Well inside the sheath, where gaseous reaction products were confined, the erosion was considerably less. Similar behavior occurred with long exposure (1100 hours) at 2250 K. Serious problems with the BeO insulators were not apparent in tests at 2073 K.

Cassidy, E. C., Hebner, R. E., **Experimental study of the behavior of nitrobenzene under varied high voltage conditions,** *Proc. 1972 Annual Report Conf. on Electrical Insulation and Dielectric Phenomena, Buck Hill Falls, Pa., Oct. 23-25, 1972*, pp. 37-44 (National Academy of Sciences, Washington, D.C., 1973).

Key words: dielectric liquid; electrical properties of liquids; electro-optics; high voltage measurements; Kerr effect; laser applications; nitrobenzene; optical properties of liquids.

Recently developed fringe-pattern methods are employed for visualizing time and space variations in electric fields between electrodes immersed in nitrobenzene. Investigations are conducted with operation under high direct, pulsed (μs), and 60 Hz voltage. With minimization of effects resulting from variations in the fringing fields at the electrode ends, the fringe-pattern "mappings" of the field dis-

tribution enable observation of space-charge behavior. Applied voltages are measured simultaneously using calibrated (with state-of-the-art accuracy) devices. Results enable computation and plotting of electric field distribution and intensity, of charge distribution, and of the Kerr constant of nitrobenzene.

Cassidy, E. C., Hebner, R. E., Jr., Zahn, M., Sojka, R. J., **Kerr-effect studies of an insulating liquid under varied high-voltage conditions,** *IEEE Trans. Elec. Insul.* **EI-9,** No. 2, 43-56 (June 1974).

Key words: electric fields; electrical measurements; high voltage measurements; insulating liquids; Kerr effect; nitrobenzene; space charge.

Refined Kerr electrooptial fringe-pattern methods are used to study time and space variations in the electric field between the electrodes of parallel-plate capacitors filled with liquid nitrobenzene. Photographs of fringe-pattern data recorded during application of high direct (both positive and negative) and sinusoidal voltages, ranging in frequency from 40 to 200 Hz, are compiled to enable computation of space-charge distortions of the field bulk of the liquid during the stress of high-field (up to 85-kV/cm) operation. The measurements reveal significant differences between the field and charge behavior under short pulse (microsecond) voltage conditions, during prolonged dc operation, after sudden changes in the dc voltage level and polarity, and, for the first time, at various intervals over the course of entire cycles of sinusoidal voltage. The results show that space-charge distortion in the interelectrode field is influenced by the level, frequency, and duration of applied voltage. Discussions of effects believed due to particulate charge carriers, to electrohydrodynamic motion of the liquid, and to the electrode materials are also included.

Cavallo, L. M., Coursey, B. M., Garfinkel, S. B., Hutchinson, J. M. R., Mann, W. B., **Needs for radioactivity standards and measurements in different fields,** (Proc. First Int. Summer School on Radionuclide Metrology, Herceg Novi, Yugoslavia, Aug. 21-Sept. 1, 1972), *Nucl. Instrum. Methods* **112,** No. 1/2, 5-18 (Sept.-Oct. 1973).

Key words: intercomparisons; radioactivity; standards; traceability.

With the enormous and world-wide increase in the applications of radioactive materials in so many scientific and technological fields, a corresponding need has arisen for increased skill and improved facilities for the assay of such materials. In the U.S.A., the use of radioisotopes, including radiopharmaceuticals is about $80 million annually. The measurements skills and facilities must of necessity tend to lag behind such a rapid growth, and increasingly from many quarters we at the National Bureau of Standards are being requested for help in establishing a consistent measurements system in radioactivity traceable both to us and through us to the international measurements system. This paper will discuss the measures that we are taking in order to achieve such traceability in a consistent measurements system in different fields of radioactivity, with special emphasis on environmental and radiopharmaceutical measurements.

Cezairliyan, A., **Simultaneous measurements of heat capacity, electric resistivity, and hemispherical total emittance of an alloy of niobium, tantalum, and tungsten in the range 1500 to 2800 K,** *J. Chem. Thermodyn.* **6,** 735-742 (1974).

Key words: electrical resistivity; emittance; high-speed measurements; high temperature; refractory alloy; specific heat; thermodynamics.

Simultaneous measurements of the heat capacity, electric resistivity, and hemispherical total emittance of an alloy of niobium, tantalum, and tungsten (nominal composition: 80 mass percent Nb, 10 mass percent Ta, and 10 mass percent W) in the temperature range 1500 to 2800 K by a sub-second-duration transient technique are described. Estimated inaccuracies of measured properties are: 3 percent for heat capacity, 5 percent for hemispherical total emittance, and 0.5 percent for electric resistivity. Properties of the alloy are compared with the properties of the constituent elements. The measured heat capacities are approximately 2.6 percent (on the average) higher than the values computed according to Kopp's additivity law. Although this difference is within the combined estimated inaccuracies, it is higher than the combined estimated imprecision of the measurements. Therefore, the alloy probably departs from Kopp's law. The electric resistivities indicate a significant departure from Matthiessen's law. Like the major constituent niobium, the alloy showed a negative departure from linearity in the plot of electric resistivity against temperature.

Clark, F. O., Johnson, D. R., **Magnetic fields in the Orion molecular cloud from the Zeeman effect in SO,** *Astrophys. J.* **191,** L87-L91 (July 15, 1974).

Key words: dense molecular clouds; magnetic field; Orion A; radio astronomy; sulfur monoxide; Zeeman effect.

Reported line widths of observed emission features from a variety of interstellar molecules are compared for the Orion A molecular cloud. All of the excess width observed for SO in Orion A is assumed to be due to Zeeman splitting of the energy levels in order to obtain an estimate of the upper limit for the ambient magnetic field in this source. From the available data, upper limit estimates yield a most probable value near 6 gauss for the magnetic field in the central feature of Orion A. This estimate can possibly be reduced by a factor of 2 or 3 if other effects such as kinematics are responsible for a portion of the observed widths. The implications of a field of this magnitude in a dense molecular cloud are discussed.

Clark, J. E., **A proposed flammability standard for children's sleepwear,** *Proc. 4th Annual Meeting of the Information Council on Fabric Flammability, New York, N.Y., Dec. 3, 1970,* pp. 142-149 (1970).

Key words: accidents; children; clothing; fabrics; flammability; sleepwear; standards.

Developments toward a flammability standard for children's sleepwear are presented. The basis is reviewed for the legal finding that a standard is needed. The laboratory research studies and the analysis of accident investigation reports are summarized.

The proposed standard provides a vertical test method which uses char length and afterflame time criteria to determine the flammability of children's sleepwear. The procedure, apparatus and care lable requirements are outlined.

Clark, J. E., Tovey, H., **Priorities for fabric flammability investigations,** *Proc. 5th Annual Meeting of the Information Council on Fabric Flammability, New York, N.Y., Dec. 9, 1971,* pp. 208-214 (1972).

Key words: accident data; apparel standard (CS 191-53); fire safety; Flammable Fabrics Act; ignition sources; mandatory standards.

A broad attack is necessary in order to reduce deaths, injuries, and property loss from fabric fires. Standards on the flammability of fabrics are greatly needed and careful study is necessary to ensure that these standards are, as the law requires, reasonable, appropriate, and technologically practicable.

In addition, improvements in standards and engineering design of common heat sources could well contribute to significant reduction of clothing ignitions.

Further study of use and packaging of flammable fluids can be expected to lead to reduced hazard. But much more knowledge is needed in this area before optimum recommendations can be made.

Improved and uniform building fire codes could also contribute to improved occupant safety, through wider use of smoke and fire detectors, audio-visual warning systems, self-closing doors, and automatic sprinklers.

Finally, we must continue and greatly increase our education efforts so that the consumer has an increased awareness of the fabric fire problem, and concomitant knowledge of proper fire prevention and extinguishment procedures.

Cohen, J., Vezzetti, C. F., Edelman, S., **Polymeric pyroelectric detector,** (Proc. of the Special Meeting on the Physics of Detectors U.S. Naval Training Device Center, Orlando, Fla., Mar. 15, 1972), Paper in *Proceedings of the Special Meeting on the Physics of Detectors*, pp. 113-117 (Infrared Information and Analysis Center, Institute of Science and Technology, Willow Run Laboratories, University of Michigan, Ann Arbor, Mich., Aug. 1972).

Key words: detector; infrared; polymer; polyvinyl fluoride; polyvinylidene fluoride; pyroelectric.

Polymers have a number of advantages over conventional pyroelectric materials such as triglycine sulphate crystals; for example, they are not hygroscopic, retain their polarization for long times, and are simple and inexpensive to fabricate into detectors. We have been experimenting mainly with films of polyvinylidene fluoride, and to a lesser extent, polyvinyl fluoride. These experiments will be described.

Collins, R. C., Haller, W., **Protein-sodium dodecyl sulfate complexes: Determination of molecular weight, size and shape by controlled pore glass chromatography,** *Anal. Biochem.* **54,** No. 1, 47-53 (July 1973).

Key words: chromatography; controlled pore glass chromatography; molecular size; porous glass chromatography; protein; protein-sodiumduodecylsulfate complexes; sodiumduodecylsulfate-complexes.

Protein-SDS complexes chromatographed on controlled pore glass elute linearly with log molecular weight over a range from 17,000 to 385,000 daltons. A glass with a pore size of approximately 500 Å allows the inclusion of all complexes in this range.

Exclusion size analysis of the individual complexes gives from 120 to 423 Å as their longest dimension.

Corliss, E. L. R., **Measurement of meter ballistics,** *J. Acoust. Soc. Amer.* **55,** No. 4 (Apr. 1974).

Key words: impact sounds; meter ballistics; sound-level meters.

Measurements of transient phenomena such as impact sounds are influenced by the characteristics of the metering system used. This note describes a method for obtaining the undamped natural frequency and the relative damping of a meter. From this information and the measured electrical impedance of the meter circuit the ballistic behavior of the meter can be predicted.

Cornell, D., Tsang, W., **Pyrolysis generation of dilute concentration of sulfur dioxide,** *Anal. Chem.* **46,** No. 7, 933-935 (June 1974).

Key words: pollution; pyrolysis; SO_2; standards.

SO_2 has been produced in dilute concentrations by pyrolysis of trimethylene sulfone. The decomposition is unimolecular and yields equimolar amounts of SO_2 and C_3 hydrocarbons. Advantages of the method for use in calibration of SO_2 monitors in routine field analytical determinations are discussed.

Crandall, D. H., Kauppila, W. E., Phaneuf, R. A., Taylor, P. O., Dunn, G. H., **Absolute cross sections for electron-impact excitation of N_2^+,** *Phys. Rev. A* **9,** No. 6, 2545-2551 (June 1974).

Key words: cross sections; crossed beams; excitation of N_2^+; 1st negative band.

Crossed beams of N_2^+ and electrons were used to measure the absolute cross sections for the excitation, $N_2^+(X\,^2\Sigma_g^+, v=0)+e \rightarrow N_2^+(B\,^2\Sigma_u^+, v=0)+e$, over an electron energy range from below threshold (3.17 eV) to 91 eV. Absolute emissions of the 391.4-nm band were measured from impact of electrons on N_2^+ ions in various state mixtures. Corrections were made to the data to account for state mixtures and other effects to obtain the cross section for the above process. The cross section falls from its finite threshold value of 3.0×10^{-16} to 0.30×10^{-16} cm^2 at 91 eV. The present values are more than an order of magnitude smaller than either the 1968 values of Lee and Carleton or the 1973 values of Daschenko *et al.* At threshold the Gaunt-factor formula of Seaton predicts a value only 45 percent of that measured, but at the highest energy, the predictions of the Seaton formula have converged to within 20 percent of the present values of the cross section. Rate coefficients calculated from the present measurements are consistent with the recent rate-coefficient measurements of McLean *et al.* Total uncertainty at high confidence is about 18 percent, taken as a quadrature sum of random uncertainty (15% at 98% confidence level) with systematic uncertainties (about 8% at high confidence). The analysis leading to interpretation of the emission cross section in terms of an excitation cross section between specific states is subject to uncertainties which are not well defined, and are not included in the stated uncertainty.

Crandall, D. H., Taylor, P. O., Dunn, G. H., **Electron-impact excitation of the Ba^+ ion,** *Phys. Rev. A* **10,** No. 1, 141-157 (July 1974).

Key words: absolute cross sections; Ba^+ ion; cross beams; electron impact; excitation; polarization.

Crossed beams of Ba^+ and electrons were used to measure the absolute emission cross sections for the Ba^+ lines, 455.4, 493.4, 490.0, and 413.1 + 416.6 nm. Polarization fractions of the light were also measured. The data were analyzed to extract level excitation cross sections. The excitation cross section for the $6\,^2P_{3/2}$ level has a value 34.7×10^{-16} cm^2 at the 2.72-eV threshold, shows marked structure in the 3–10-eV interval, and decreases to 1.71×10^{-16} cm^2 at 747 eV. The polarization fraction for the 455.4-nm light exhibits pronounced oscillatory structure in the interval 3–7 eV. Excitation cross section for the $6\,^2P_{1/2}$, $7\,^2S_{1/2}$, and $6\,^2D_{3/2+5/2}$ levels have values at threshold of 20.0×10^{-16}, 5.4×10^{-16}, and 4.3×10^{-16} cm^2, respectively. Total uncertainties at a "high-confidence level" are about ±10 percent for the $6\,^2P_{1/2}$ and $6\,^2P_{3/2}$ cross sections. Uncertainties range around ±30 percent for the $7\,^2S_{1/2}$ cross section and ±20 percent for the $6\,^2D_{3/2+5/2}$. Measurements for the $6\,^2P$ cross sections agree at high energies with the Coulomb distorted-wave calculation of Sheorey and Burgess. Measurements for the $6\,^2P_{3/2}$ level are in quite good agreement with the measurements of Bacon and Hooper and of Pace and Hooper for energies 6 to 100 eV. However, the Pace and Hooper points at 3 and 4 eV are nearly twice the present values. Signals due to excitation of metastable $5\,^2D$ ions in the ion beam were observed, and estimates could be made of the cross section for excitation from this state to the final states above. Cross sections at threshold were estimated to be 13.4×10^{-16} cm^2 ±34 percent, 9.8×10^{-16} cm^2 ±28 percent, 7.4×10^{-16} cm^2 ±100 percent, 6.9×10^{-16} cm^2 ±27 percent for excitation from the $5\,^2D$ levels to the $6\,^2P_{3/2}$, $6\,^2P_{1/2}$, $7\,^2S_{1/2}$, and $6\,^2D_{5/2+3/2}$ levels, respectively. The rate coefficients for excitation of $6\,^2P_{3/2}$ calculated from the data are in reasonable agreement with the measurements of Hinnov *et al.*

Currie, L. A., Filliben, J. J., DeVoe, J. R., **Statistical and mathematical methods in analytical chemistry,** *Anal. Chem. Ann. Rev.* **44,** 497R-512R (Apr. 1972).

Key words: chemical analysis; curve fitting; distribution functions; experiment planning and optimization; measurement process; on-line computers; recognition techniques; review; statistics; transforms.

The statistical and chemical literature are surveyed for the period October 1967 to October 1971, with emphasis on work related to the application of mathematical statistics to analytical chemistry. Principal categories covered include: Reviews, Conferences, Journal and Books; Method Characterization; Planning and Optimization of Experiments; Curve Fitting; On-line Computers; and Other Topics

(techniques for testing basic statistical assumptions; special distributions; transforms, correlation and signal/noise enhancement; recognition techniques). The bibliography, consisting of somewhat less than 600 references, contains mostly English-language journals and books, but important foreign-language articles – particularly French, German and Russian – also appear.

Cuthill, J. R., **Grating spectrometers and their application in emission spectroscopy,** Chapter 3 in *X-Ray Spectroscopy*, L. V. Azároff, Ed., pp. 133-172 (McGraw-Hill Book Co., New York, N.Y. 1974).

Key words: excitation methods; grating spectrometers; gratings; photon detectors; soft x-rays.

This is a textbook-type chapter on the basic principles and characteristics of grazing incidence grating spectrometers and their components for use in obtaining soft x-ray emission spectra. Correction factors involved in relating the observed soft x-ray emission spectra to the valence band electron density of states is discussed briefly.

Danos, M., Rafelski, J., **Gauge invariance of the vacuum polarization in quantum electrodynamics,** *Lett. Nuovo Cimento Series 2*, **10,** No. 3, 106-110 (May 18, 1974).

Key words: gauge invariance; quantum electrodynamics; renormalization; time-ordering operator; vacuum polarization; weak interactions.

It is shown that the conventional perturbation formalism of field theory treats incorrectly the equal time point in the chronological products of field operators. If this imprecision is rectified the contradictions between the results of the perturbation expansion of the *S*-matrix and of the predictions of axiomatic field theory disappear. In particular, the gauge invariance violating quadratic divergence of the vacuum polarization loop does not arise in the *S*-matrix formulation. This is of particular importance for certain classes of the so-called nonrenormalizable field theories, e.g., the Fermi-type theories of the weak interactions.

Davis, D. D., **Frequency standard hides in every color TV set,** *Electronics* **44,** No. 10, 96-98 (May 10, 1971).

Key words: dissemination frequency; frequency synthesizers; linear phase comparators; television color subcarrier; time.

In color television broadcasting, a color "subcarrier" is transmitted at about 3.58 MHz. It is used as a reference signal in the color television receiver to demodulate the chrominance sidebands. The major U.S. networks use rubidium frequency standards to generate the color subcarrier. This paper describes a method for making use of the color subcarrier as a frequency standard. The output of a 1 MHz local standard synthesized to 3.58 MHz is used as one input to a phase comparator and is adjusted to agree with the received subcarrier signal. Results of actual network measurements are given.

Davis, D. D., Huie, R. E., Herron, J. T., **Direct rate measurements showing negative temperature dependence for reaction of atomic oxygen with *cis*-2-butene and tetramethylethylene,** *J. Chem. Phys.* **59,** No. 2, 628-634 (July 15, 1973).

Key words: atomic oxygen; gas phase kinetics; olefins.

Reported in this paper are the first direct rate measurements showing a negative temperature dependence for the reaction of ground state atomic oxygen with *cis*-2-butene and tetramethylethylene. Wide variations made in the experimental conditions (e.g., total pressure, O atom concentration, and olefin concentration) of these two systems have shown that the measured rate constants were uninfluenced by secondary reactions. The absence of any dependence of the measured rate constants on total pressure at several temperatures indicate that the reactions investigated were bimolecular processes. When expressed in the form of an Arrhenius equation, the observed negative temperature dependence results in an apparent negative activation energy, i.e., $k_{cis\text{-}2\text{-}B} = (9.69 \pm 0.96) \times 10^{-12}$ exp $(319 \pm 63$ cal mol$^{-1}/RT)$ and $k_{TME} = (5.58 \pm 1.07) \times 10^{-12}$ exp $(1570 \pm 120$ cal mol$^{-1}/RT)$. Units are in cubic centimeters per molecule seconds. If a threshold energy of 0.0 cal mole^{-1} is assigned to the reaction of $O(^3P)$ with TME, the temperature dependence of the pre-exponential term for a rate expression of the form $k = A(T)\exp(-E_0/RT), E \geq O)$ is calculated to be T^{-2}. These new results are discussed in terms of both collision and transition state theories.

Decker, G. E., Stiehler, R. D., **Standardization of Mooney viscometer and oscillating-disk cure meter,** *Amer. Soc. Test. Mater. ASTM Spec. Tech. Publ.* **553,** pp. 19-30 (1974).

Key words: cure meter; Mooney viscometer, oscillating-disk cure meter, processability; rubber testing; standardization; vulcanization.

The Mooney viscometer has been the principal instrument used to control the processability of synthetic rubber production for the past 30 years. The oscillating-disk cure meter is now becoming the principal instrument for determining the vulcanization characteristics of standard compounds of raw rubbers and compounding materials and of factory compounds used for rubber products. Therefore, a large amount of effort has been expended in their standardization. Nevertheless, both instruments which have certain similarities are affected by the following factors that still cause variability among instruments: 1. temperature of the rubber in the die cavity; 2. friction between the oscillating or rotating stem and the stationary lower die; 3. slippage at the rubber-metal interfaces; 4. the pressure on the rubber during test; and 5. scale calibration. This paper summarizes past and recent studies on these factors and indicates from recent findings the direction for further standardization.

Measurements of the disk temperature in the oscillating-disk cure meter were made. These measurements indicated that the clearance between the oscillating or rotating stem and the lower die is critical for temperature uniformity. Also, the present design of the upper die in ASTM Measurement of Curing Characteristics with the Oscillating Disk Cure Meter (D 2084-71 T) substantially reduces the rate of heat transfer to the specimen. However, the design is reasonably effective for applying pressure on the specimen which reduces slippage at the rubber-metal interfaces. Other means of applying pressure may be used. Slippage also depends on the torque at the rubber-metal interfaces. In the Mooney viscometer, torque can be reduced by decreasing the speed of the rotor or by increasing the temperature. In the cure meter, torque is most effectively reduced by keeping the amplitude of oscillation as small as practical.

DeVoe, J. R., **A laboratory based multi-instrument computer system,** (Proc. Int. Conf. on Modern Trends in Activation Analysis, Saclay France, Oct. 2-6, 1972), *J. Radioanal. Chem.* **15,** 657-667 (1973).

Key words: computer; digital communication system; laboratory automation; multi-program monitor.

Design of computer system for assistance in the operation of experiments contains certain factors unique to a particular laboratory. Details are given on the procedure that was used to generate design criteria and to implement such a design for a computer system in the Analytical Chemistry Division, NBS. The system is currently servicing ten instruments (ranging from spectrophotometers to mass spectrometers) with a projected capacity exceeding sixty depending upon the type of instruments connected.

DeVoe, J. R., **Automation and computerization of analytical measurements,** *Proc. Seminar Series on Chemistry and Biology of Trace Metals in the Environment, University of Illinois, Urbana, Ill., Spring 1971*, pp. 147-162 (University of Illinois Press, Urbana, Ill., 1972).

Key words: computer; digital communication system; laboratory automation; multi-program monitor.

Design of computer systems for assistance in the operation of experiments contains certain factors unique to a particualr laboratory. Details are given on the procedure used to generate design criteria and to implement such a design for a computer system in the Analytical Chemistry Division, National Bureau of Standards.

Dickens, B., Schroeder, L. W., Brown, W. E., **Crystallographic studies of the role of Mg as a stabilizing impurity in β-$Ca_3(PO_4)_2$. I. The crystal structure of pure β-$Ca_3(PO_4)_2$,** *J. Solid State Chem.* **10,** 232-248 (1974).

Key words: beta tricalcium phosphates; cation vacancies; positional disorder; single crystal; x-ray diffraction.

β-$Ca_3(PO_4)_2$ crystallizes in the rhombohederal space group $R3c$ with unit cell parameters $a = 10.439(1)$, $c = 37.375(6)$ Å (hexagonal setting) and cell contents of 21 [$Ca_3(PO_4)_2$]. The structure was refined to $R_w = 0.026$, $R = 0.030$ using 1143 x-ray intensities collected from a single crystal by counter methods. Corrections were made for absorption, secondary extinction, and anomalous dispersion.

The structure is related to that of $Ba_3(VO_4)_2$, but has lower symmetry because of the widely different ionic sizes of Ca and Ba. Seven [$Ca_3(PO_4)_2$] units occupy a volume corresponding to eight [$Ba_3(PO_4)_2$] units. The requirement of the c glide in β-$Ca_3(PO_4)_2$ has been shown in the least squares refinements to be attained by disorder of one cation over two sites. This disorder has a far-reaching effect on the structure.

Dillon, T. A., Stephenson, J. C., **Calculation of vibrational and rotational energy transfer between HF, DF, HCl, and CO_2,** *J. Chem. Phys.* **58,** No. 5, 2056-2064 (Mar. 1, 1973).

Key words: energy transfer; HF, DF, CO_2; linewidth; unitary.

A theory of vibrational energy transfer which retains the exponential form of the scattering operator is applied to energy transfer between vibrationally excited HF, DF, HCl, and CO_2. The calculations contain several new features, including use of curved classical trajectories and vibrational wavefunctions obtained numerically from RKR potential. Cross sections for multiquantum pure rotational changes caused by the dipole-quadrupole interaction are calculated. These multiquantum rotational transitions play an important role in vibrational energy exchange by allowing large vibrational energy defects to be absorbed by the rotational degrees of freedom. Agreement between theory and experiment is excellent. Cross sections calculated for simultaneous transfer of two vibrational quanta from HF or HCl to CO_2 are very small. However, for DF-CO_2 the calculated two-quantum-transfer cross section is only a factor of 2-6 smaller than that for single-quantum transfer.

Dillon, T. A., Stephenson, J. C., **Energy transfer during "orbiting" collisions,** *J. Chem. Phys.* **60,** No. 11, 4286-4288 (June 1, 1974).

Key words: energy transfer; infrared lasers; molecular collisions; vibrational exchange.

Semiclassical collision theory is used to calculate the temperature dependence of cross sections for exchange of vibrational excitation from HF and DF to CO_2. For collisions with kinetic energy less than four-fifths of the intermolecular potential well depth there exists a narrow range of impact parameter for which the scattering angle exceeds 2π (i.e., more than one revolution). That part of the trajectory in excess of a single revolution can be accurately represented by a simple model of a circular orbit with a constant angular velocity replacing the instantaneous classical turning point. Calculations are compared to experimental data and illustrate the significance of multiple revolution collisions.

Dobbyn, R. C., Calvano, N. J., **Portable ballistic shields,** *NILECJ-STD-0103.00*, 7 pages (U.S. Department of Justice, Law Enforcement Assistance Administration, National Institute of Law Enforcement and Criminal Justice, Washington, D.C., May 1974).

Key words: armor; ballistic shields; standard.

The purpose of this document is to establish performance requirements and a method of test for the ballistic resistance of portable ballistic shields intended to protect against small arms fire.

Dorman, D. E., Torchia, D. A., Bovey, F. A., **Carbon-13 and proton nuclear magnetic resonance observations of the conformation of poly(L-proline) in aqueous salt solutions,** *Macromolecules* **6,** No. 1, 80-82 (Jan.-Feb. 1973).

Key words: carbon-13; nuclear magnetic resonance; poly-L-proline; polypeptides.

Proton nmr at 220 MHz and ^{13}C nmr at 25 and 15.08 MHz have been employed to confirm previous conclusions that the disordering of poly(L-proline) chains in concentrated aqueous salt solutions arises primarily from the formation of random sequences of cis and trans peptide bonds. The effects of KI and $CaCl_2$ are essentially similar. The β- and γ-carbon resonances of the proline ring appear to be the most reliable monitors of this isomerization process, giving distinct and well resolved peaks for the cis and trans conformations.

Durig, J. R., Carreira, L. A., Lafferty, W. J., **Spectra and structure of small ring compounds. Microwave spectrum of cyanocyclobutane,** *J. Mol. Spectrosc.* **46,** No. 2, 187-193 (May 1973).

Key words: cyanocyclobutane; dipole moment; microwave spectrum; molecular structure; ring conformation; rotational constants.

The rotational spectrum of cyanocyclobutane has been investigated in the region 18.0-40.0 GHz. Only A-type transitions were observed. R-branch assignments have been made for the ground state and the first three excited states of the ring puckering mode as well as the first two excited states of the out-of-plane cyano-bending mode. The microwave data are consistent with a bent equilibrium ground state for the ring with the cyano-group in the equatorial position. The dipole moment components were determined to be $\mu_a = 4.04 \pm 0.09$ D and $\mu_c = 0.92 \pm 0.03$ D with the total dipole moment, μ, having a value of 4.14 ± 0.09 D.

Ehrlich, M., **Influence of irradiation on the production of F centers in LiF (TLD grade),** *J. Appl. Phys.* **40,** No. 2, 891-892 (Feb. 1969).

Key words: annealing; F centers; ^{60}Co gamma-ray irradiation; LiF (TLD grade) plaques; readout; thermoluminescence.

Optically polished samples of extruded plaques of LiF (TLD grade) were given ^{60}Co gamma-ray exposures ranging from about 35 000-450 000 R, at exposure rates between about 1.5×10^3 and 5×10^6 R/h. Over this range of exposures and exposure rates, the resulting absorption in the F band was found to be independent of exposure rate, and to increase with exposure, even for exposures for which the thermoluminescence exhibited saturation effects. After thermoluminescence readout at about 235 °C, practically all the absorption in the F band created by the ^{60}Co gamma-ray exposure had disappeared. These results are compatible with the dominant role given F centers in some of the current models for the thermoluminescence process in LiF (TLD grade).

Eliason, L. K., Isler, M. A., Stenbakken, G. N., **Mercury switches for burglar alarm systems,** *NILECJ-STD-0303.00*, 13 pages (U.S. Department of Justice, Law Enforcement Assistance Administration, National Institute of Law Enforcement and Criminal Justice, Washington, D.C., May 1974).

Key words: burglar alarm sensor; burglar alarm system; interior perimeter sensor; mercury; switch.

This standard establishes performance criteria for mercury switches intended for use in protective intrusion alarm circuits to monitor the position of doors, windows, etc. These devices cause the initiation of an alarm signal to a police panel, central station, or local audible alarm device. Included are requirements and test methods

for performance, electrical properties and materials. The characteristics addressed are those which affect the reliability of the device with emphasis on those performance characteristics which affect its false alarm susceptibility. This standard does not provide performance criteria concerning the ability of these devices to resist attempts to defeat them through physical or surreptitious attack.

Ely, J. F., Straty, G. C., **Dielectric constants and molar polarizabilities of saturated and compressed fluid nitrogen,** *J. Chem. Phys.* **61,** No. 4, 1480-1485 (Aug. 15, 1974).

Key words: Clausius-Mossotti function; dielectric constant; dielectric virial coefficients; molar polarizability; nitrogen; saturated liquid densities.

In this paper we present accurate, wide range measurements of the dielectric constant of saturated and compressed fluid nitrogen. Measurements were made from 65 to 125 K along the saturated liquid boundary and along selected liquid and gaseous isotherms ranging from 92 to 300 K at pressures to 34.5 MPa. Densities ranged from the dilute gas to nearly three times the critical density. Molar polarizabilities, thought to be accurate to better than 0.10 percent, were calculated by combining the dielectric constant measurements with densities obtained from least-squares analyses of experimental *pVT* data. A correlation function based on selected experimental data is given for the saturated liquid densities. Dielectric virial coefficients, derived from the calculated molar polarizabilities, are also presented.

Erez, A., **Low-frequency electrical signal measurement by electrooptical methods,** *IEEE Trans. Instrum. Meas.* **IM-21,** No. 4, 358-360 (Nov. 1972).

Key words: electrooptical coupling; feedback amplifiers; light emitting diodes; photodetectors.

An analog system for the optical telemetry of voltage or current information using light-emitting diodes (LED) is described. Errors resulting from variations in the optical coupling efficiency are minimized because the light emitted by LED contains the signal to be measured superimposed on a fixed intensity beam controlled by a reference zener diode. The nonlinearity of the LED is overcome by using part of its emitted light to control the feedback current to an operational amplifier that supplies the signal to the LED. The prototype system developed has a total error of approximately 0.2 percent of the input signal.

Evans, A. G., Wiederhorn, S. M., **Crack propagation and failure prediction in silicon nitride at elevated temperatures,** *J. Mater. Sci.* **9,** 270-278 (1974).

Key words: elevated temperatures; failure prediction; silicon nitride; slow crack growth.

A technique for studying high temperature crack propagation in ceramic materials is developed. The technique is used to obtain relationships between the crack propagation rate and the stress intensity factor for hot-pressed silicon nitride up to 1400 °C. The data are then used to develop proof test diagrams which give values for the safe working stress levels for this material after proof testing (or any other flaw detection procedure).

Evans, B. J., Swartzendruber, L. J., **Supertransferred hyperfine fields and covalency at diamagnetic cations in magnetic insulators,** *Phys. Rev. B* **6,** No. 1, 223-231 (July 1, 1972).

Key words: antimony; ferrites; hyperfine fields; iron; Mössbauer effect; nickel; valency.

The sign and magnitude of the antimony hyperfine fields has been measured in Sb-substituted nickel ferrite using the ^{121}Sb Mössbauer effect. We obtain a value of -311 ± 4 kG for this field at 100 K. This result is compared with results obtained for Sn in yttrium iron garnet and, among the possible mechanisms, 3*d*-5*s* covalent spin transfer appears to make the predominant contribution to the hyperfine field.

Evans, B. J., Swartzendruber, L. J., **Supertransferred hyperfine fields at Sb^{5+} in insulating ferrites: Effects of local order and ion-specific properties,** (Proc. 18th AIP Conf. on Magnetism and Magnetic Materials, (19th Annual Conf.), Boston, Mass., Nov. 13-16, 1973), Paper in *Magnetism and Magnetic Materials*, C. D. Graham, Jr., and J. J. Rhyne, Eds., pp. 518-522 (American Institute of Physics, New York, N.Y., 1974).

Key words: ferrites; hyperfine fields; Mössbauer; Sb; YIG.

The supertransferred hyperfine fields at Sb^{5+} in $LiFe_5O_8$, $CoFe_2O_4$, and YIG have been determined using ^{121}Sb Mössbauer spectroscopy. In contrast to $CoFe_2O_4$, $NiFe_2O_4$, and YIG, the small, average hyperfine field of ~ 100 kOe at Sb^{5+} in $LiFe_5O_8$ requires the existence of significant local order and indicates that the clustering of Li^{1+} about Sb^{5+} is approximately ten times as large as that expected for a random intrasite cation distribution, in agreement with the known strong influence of Sb substitution in destroying the Li:Fe ordering. The decrement in the hyperfine field at Sb^{5+} due to an A-site Co^{2+} is also found to be larger than that due to Ni^{2+}.

Evans, W. H., Grimes, J. J., Jobe, T. L., Henderson, H. A., Beck, D., Beckwith, B., Boyd, R. N., Domalski, E. S., **Bibliography and substance-property index (inorganic), 1968-1973,** *Bull. Thermodyn. Thermochem. Section III. Inorganic Substances* **12,** 267-344, 447-549 (1969); **13,** 226-308, 391-483 (1970); **14,** 183-257, 319-382 (1971); **15,** 211-314, 389-485 (1972); **16,** 261-416, 497-639 (1973).

Key words: inorganic compounds; thermodynamic publications.

Bibliography (authors, title, journal, volume, page, year) and Substance-Property Index of material published from 1968 through 1973. This is a continuation of work done over the past several years and published in earlier editions of the Bulletin.

Evenson, K. M., Wells, J. S., Petersen, F. R., Danielson, B. L., Day, G. W., **Accurate frequencies of molecular transitions used in laser stabilization: The 3.39-μm transition in CH_4 and the 9.33- and 10.18-μm transitions in CO_2,** *Appl. Phys. Lett.* **22,** No. 4, 192-195 (Feb. 15, 1973).

Key words: CO_2 and He-Ne laser frequency; methane; saturated absorption.

The frequencies of three lasers stabilized to molecular absorptions were measured with an infrared-frequency synthesis chain extending upwards from the cesium frequency standard. The measured values are 29.442 483 315(25) THz for the 10.18-μm $R(30)$ transition in CO_2, 32.134 266 891(24) THz for the 9.33-μm $R(10)$ transition in CO_2, and 88.376 181 627(50) THz for the 3.39-μm $P7$) transition in CH_4. The frequency of methane, when multiplied by the measured wavelength reported in the following letter, yields 299 792 456.2 (1.1) m/sec for the speed of light.

Eyler, J. R., Ausloos, P., Lias, S. G., **A novel ion-molecule reaction involving cleavage of the carbonyl bond in ketones and aldehydes,** *J. Amer. Chem. Soc.* **96,** No. 11, 3673-3675 (May 29, 1974).

Key words: aldehyde-chlorocarbon ion; fluorocarbon ion; halocarbon ions; ion-cyclotron resonance; ion-molecule reaction; ketone; mass spectrometer.

The reactions of CF_3^+, CCl_3^+, and $C_2F_5^+$ with aldehydes and ketones have been investigated. Ninety-five percent or more of the reactive encounters between CF_3^+ or CCl_3^+ and CH_3COCH_3, CH_3CHO, $C_2H_5COCH_3$, $C_2H_5COC_2H_5$, and n-$C_4H_9COCH_3$ result in a reaction in which an O atom and a F^+ or CL^+ are exchanged, in what is apparently a concerted mechanism:

$$CX_3^+ + R'COR \rightarrow R'CXR^+ + CX_20$$

(where X is F or Cl, R and R′ are H, CH_3, C_2H_5, or n-C_4H_9 as appropriate). The product $R'CXR^+$ ions have a tendency to dissociate

by losing HX; the stability of the $R'CXR^+$ ions vis-a-vis this dissociation is very sensitive to the exothermicity of the CX_3^+-R'COR reaction, showing a greater tendency to dissociate for larger R'COR reactant molecules. Further, the rate constants of the reactions of CCl_3^+ are slower by 1-2 orders of magnitude (10^{-11}-10^{-10} cm^3/molecule-sec) than the rates of the corresponding reactions of CF_3^+ (10^{-9} cm^3/molecule-sec). The C_2F_3 ion undergoes a reaction analogous to I with these carbonyl compounds, but with ketones larger than acetone an important alternate reaction channel leads to the formation of CF_3CO^+ product ions.

Fanconi, B., **Lattice dynamics of polyglycine I,** *J. Chem. Phys.* **57,** No. 5, 2109-2116 (Sept. 1, 1972).

Key words: frequency distribution; lattice vibrations; normal mode analysis; polyglycine I.

The two-dimensional lattice vibrations of the extended form of polyglycine have been calculated from a five mass model of the glycine chemical repeat unit and with interchain hydrogen bond stretching. The effects of hydrogen bond bending and torsion on the lattice modes are determined using a model in which the entire chemical repeat unit is treated as a single dynamical unit. The valence force field for the latter model is found by fitting the optical frequencies determined from the five mass calculation. The density of phonon states for the two-dimensional lattice is determined for the single mass model.

Fathers, D. J., Jakubovics, J. P., Joy, D. C., Newbury, D. E., Yakowitz, H., **A new method of observing magnetic domains by scanning electron microscopy. II. Experimental confirmation of the theory of image contrast,** *Phys. Status Solidi A*, No. 22, 609-619 (1974).

Key words: contrast measurement; image contrast; iron-silicon alloy; magnetic domains; nickel; scanning electron microscopy.

Experiments have been carried out to test the predictions of the theory of type II magnetic contrast, which is an effect enabling magnetic domains in materials including those with cubic anisotropy to be directly observed by scanning electron microscopy, previously presented in [1]. The experiments include measurements of the contrast as a function of the voltage and angle of incidence of the incident electron beam and of the angle of rotation of the specimen about its surface normal. The results are in good agreement with the theory and confirm beyond doubt that type II contrast arises from the alteration of incident electron trajectories within the solid by the internal magnetic induction. Domain images obtained by the use of type II contrast can be interpreted on the basis of this mechanism.

Fickett, F. R., Sullivan, D. B., **Magnetic studies of oxidized impurities in pure copper using a SQUID system,** *J. Phys. F: Metal Phys.* **4,** No. 6, 900-904 (June 1974).

Key words: copper; impurities; magnetism; quantum interference; susceptibility.

A magnetometer system utilizing a SQUID and a superconducting flux transformer has been used to monitor the internal oxidation process in very pure copper. Both remanent moment and low field susceptibility have been measured for copper containing 0.1-1 at ppm Fe and 70 at ppm Fe in various states of anneal. The results suggest that the oxidation process proceeds quite differently in the previously unobserved situation where very dilute amounts of iron are present than in the case of relatively high impurity concentrations.

Filliben, J. J., **Techniques for tail length analysis,** (Proc. 18th Conf. on the Design of Experiments in Army Research Development and Testing, Aberdeen Proving Ground, Md., Oct. 25-27, 1972), *ARO Report 73-2*, Part 2, 425-450 (Department of Defense, Washington, D.C., 1973).

Key words: correlation coefficient; data analysis; distribution analysis; estimation; Fortran subroutine; Lambda distribution; medians; normality; order statistics; probability plots; probability plot correlation coefficients; statistics.

This paper concerns itself with the problem of estimating from a set of data the tail length of the underlying distribution. A probability plot technique for such distributional analysis is developed which makes use of order statistic medians. The probability plot correlation coefficient r_D for a distribution D is introduced which gives a statistical measure of probability plot linearity. The output from a computerized version (written in machine-independent ANSI Fortran) of the proposed tail length analysis procedure is illustrated. Three examples are discussed.

Finnegan, T. F., Wahlsten, S., **Microwave emission from coupled Josephson junctions,** (Proc. 13th Int. Conf. on Low Temperature Physics-LT 13, Boulder, Colo., Aug. 21-25, 1972), Paper in *Low Temperature Physics-LT 13*, K. D. Timmerhaus, W. J. O'Sullivan, and E. F. Hammel, Eds., **3,** 272-275 (Plenum Publishing Corp., New York, N.Y., 1974).

Key words: ac Josephson effect; frequency-pulling; tunnel-junction array.

Recently, much interest has developed in the possibility of using large arrays of Josephson junctions for various applications. To this end, the properties of the microwave radiation emitted by a pair of coupled Josephson tunnel junctions connected permanently in series but independently current biased have been investigated experimentally. The detected coherent radiation emitted by the individual junctions when biased on the self-resonant voltage steps was between 10^{-13} and 10^{-10} watts. When both junctions were biased to radiate at the same frequency, the radiation from the junctions combined coherently in one of two ways: (1) The total radiation was unusually large as would occur if the oscillations of the two junctions were in phase. When the bias point of one of the junctions was varied slightly, frequency-pulling and phase-locking effects were directly observed. (2) The total radiation was unusually small as would occur if the oscillations of the two junctions were out of phase (with a relative phase difference of π). The details of these results are discussed.

Flynn, J. H., **Thermodynamic properties from differential scanning calorimetry by calorimetric methods,** *Thermochimica Acta* **8,** 69-81 (1974).

Key words: DSC; enthalpy; glass transition; heat capacity; thermal analysis; thermodynamic properties.

Simple theory and techniques are explored and developed to utilize the differential scanning calorimeter for the determination of heat capacities, glass transition and enthalpies of transition between two thermodynamic states of substances. Effects due to the transition kinetics and thermal and electronic lags of the instrument are either corrected for or eliminated.

Fraker, A. C., Ruff, A. W., Green, J. A. S., Bechtoldt, C. J., **Polarization measurements on titanium tube and sheet having preferred orientation textures,** *Corrosion* **30,** No. 6, 203-207 (June 1974).

Key words: corrosion; NaCl solution; passivation; sheet; sulfuric acid; titanium; tubing.

The influence of preferred orientation texture on the anodic polarization behavior of titanium tubing and sheet has been investigated. Potentiostatic polarization measurements were made on specimens in the annealed and deformed conditions during exposure to boiling NaCl solutions (pH = 1) and to 1N H_2SO_4 (pH = 0.3) solutions at 23 °C (73 °F). Results were correlated with single crystal data, and it was found basal (0001) orientation texture has a marked effect on the anodic polarization of titanium, especially in the active region where this texture gives lower current densities. Polarization curves and examples of the microstructures are shown and discussed.

562-903 O - 75 - 7

Franklin, A. D., Crissman, J., Young, K. F., **Point defect interactions in CaF_2:GdF_3,** *J. Phys.* **C9,** C9-179-C9-183 (Nov.-Dec. 1973).

Key words: anelastic relaxation; CaF_2; dielectric relaxation; EPR lifetime broadening; GdF_3; pairs; point defects.

The reorientation of the point-defect pair formed in CaF_2 crystals by substitutional Gd^{3+} and interstitial F^- ions has been studied using EPR lifetime broadening measurements and dielectric and anelastic relaxation studies at temperatures between liquid N_2 and room. The GdF_3 concentration ranged from 0.01 to 0.3 mole percent. The crystals were annealed in an atmosphere of He and HF at temperatures from 600 to 800 °C and quickly cooled. Three major relaxations were observed in the anelastic temperatures corresponding well to two major relaxations observed in the dielectric spectrum. The most important of these correlated both in relaxation parameters and intensity changes upon annealing and/or changing concentration of GdF_3 with the lifetime broadening and intensity of the EPR spectrum from the nearest-neighbor pair. The entire pattern has the proper symmetry for the pair with relaxation modes generated by excursions of the F^- interstitial out to third-neighbor positions, assuming that the most stable positions are closest to the Gd^{+3} ions. However, this model is inconsistent with the relative intensities of the dielectric relaxations, and it is concluded that at least two distinct centers must be present.

Frederikse, H. P. R., Hosler, W. R., **Electrical conductivity of coal slag,** (Proc. 13th Symp. on Engineering Aspects of Magnetohydrodynamics, Stanford University, Standford, Calif., Mar. 26-28, 1973), Paper in *13th Symposium on Engineering Aspects of Magnetohydrodynamics*, pp. IV.4.1-IV.4.3 (Department of Mechanical Engineering, University of Mississippi, University, Miss., 1973).

Key words: coal slag; electrical conductivity; high temperature; magnetohydrodynamics; oxides.

The efficiency of a coal fired MHD-generator will be influenced by the presence of slag layers condensed on the walls of the MHD-channel. Hence, there is a need for physical and chemical characterization of coal slags. As part of such a program, the electrical conductivity of some natural and synthetic slag samples (containing 14-36 wt. % iron) has been measured over the temperature range 1200-1700 K and at oxygen pressures between 1 and 2×10^{-6} atmosphere. The conductivity is relatively high ($\approx 10^{-2}$ ohm^{-1} cm^{-1} at 1700 K) and stems from the transfer of electrons between ferrous and ferric ions. Anomalies in the conductivity around 1600 K are the result of devitrification of the glass samples.

Freeman, D. H., Angeles, R. M., Enagonio, D. P., May, W., **Interactive gel networks. Chromatographic and analytical properties with a pyridine type functional group,** *Anal. Chem.* **45,** 768-774 (Apr. 1973).

Key words: chromatography (liquid); interactive gel; organic separations.

The gel is a copolymer of 2-methyl-5-vinyl pyridine with DVB crosslinking. The composition, infrared absorption, swelling, and gel permeation properties were measured. The pyridine moiety is basic, as indicated by its ability to complex ROH and RCOOH solutes. Chromatographic affinity is directly related to the strength of the solute:gel complex. Solvents mask the pyridine gel in the order EtOH > $CHCl_3$ > CCl_4. The resulting solute affinity varies oppositely with the strength of the solvent:gel complex. ROH affinity correlates systematically with the proton donor strength. Gel capacity is high and several applications are described.

Freeman, D. H., **Interactive gel networks for organic chemical separations,** *Isr. J. Chem.* **10,** 889-891 (1972).

Key words: chromatography; interactive gel; separations.

A comparison is drawn between the fundamental logic of the origin of ion exchange affinity, and that of the newly discovered behavior of interactive gels. The basis for predicting interactive chromatographic affinity is examined.

Freeman, D. H., **The gels for liquid chromatography,** *J. Chromatogr. Sci. II,* 175-179 (Apr. 1973).

Key words: gel; ion exchange; liquid chromatography.

This paper attempts to unify an understanding of various chromatographic gels. First, all gels are reviewed for their common tendency to fractionate on the basis of steric exclusion. The chemical contribution to chromatographic affinity is superimposed. Descriptions of interactive effects and reactive ion exchange processes are referred to their major chemical equilibria. The use of this understanding for solving chemical separation problems is described.

Fromhold, A. T., Jr., Coriell, S. R., Kruger, J., **Transport and thermodynamic analyses of steady-state currents in solids,** *J. Phys. Soc. Japan* **34,** No. 6, 1452-1459 (June 1973).

Key words: electrochemistry; Gibbs-Duhem; local equilibrium; nonequilibrium thermodynamics; oxidation of metals; solid state diffusion; transport in solids.

The usual derivation of the well-known Gibbs-Duhem relation (or its electrochemical analog) from equilibrium thermodynamics is based on certain assumptions which are only approximately met for nonhomogeneous systems; the postulate of local equilibrium generally employed in nonequilibrium thermodynamics is commonly utilized to extend the results to the nonequilibrium domain. The application of the electrochemical Gibbs-Duhem relation to the particular case of several charged diffusing species in a solid is utilized herein to obtain an expression for the local electric field which is then compared with an expression for the field deduced by an ordinary phenomenological transport analysis. The two approaches yield consistent results only in the limit of thermodynamic equilibrium. Implications of the analyses are pointed out for the special problem of the growth of oxides and similar tarnish films on metals.

Frommer, M. A., Lancet, D., **Freezing and nonfreezing water in cellulose acetate membranes,** *J. Appl. Polym. Sci.* **16,** 1295-1303 (1972).

Key words: bound water; cellulose-acetate membranes; differential scanning calorimetry; freezing of water; membranes; nuclear magnetic resonance; reverse osmosis membranes; water in membranes.

The relative amounts of freezing and nonfreezing water in various cellulose acetate (CA) membranes were determined by differential scanning calorimetry. It was found that: (1) A significant fraction (17-40%) of the water (1.0-3.1 g H_2O per gram dry CA) in any membrane does not freeze at temperatures as low as − 60 °C. (2) The amount of nonfreezing bound water (0.4-0.7 g nonfreezing water per gram dry CA) depends upon the nature of the membrane and is significantly higher than the total amount of water (all of which is nonfreezing) absorbed from liquid water by a *dense* film of the same polymer (~ 0.18 g water per gram dry CA). The structures of the membranes were studied by scanning electron microscopy. The results suggest that the amounts of nonfreezing water in cellulose acetate membranes decrease with the increase in the packing density (compactness) of the polymer within the membrane. In dense films, the extent of polymer-polymer interactions within the polymeric matrix is high, and therefore the macro-molecular chains are less accessible to bind water.

Gadzuk, J. W., **Reply to comments on a theory of field-induced tunneling,** *Phys. Rev. B* **3,** No. 5, 1772-1773 (Mar. 1, 1971).

Key words: adsorption; field emission; surface physics; tunneling.

The implication of an observation by Glasser relevant to past theories of field emission are discussed.

Gallagher, A., Lewis, E. L., **Resonance broadening of Hanle-effect signals in rubidium,** *Phys. Rev. A.* **10,** No. 1, 231-241 (July 1974).

Key words: line broadening; rubidium.

We have measured the broadening of Rb^{87} level-crossing signals due to collisions with Rb^{85}. The depolarization or broadening rates for the 5 $^2P_{1/2}$ state orientation, the 5 $^2P_{3/2}$ state orientation and alignment, and the 5 $^2P_{3/2}$ state 58-G crossing were measured. Theoretical resonance-broadening depolarization rates for the electronic angular momentum, due to Carrington, Stacey, and Cooper, have been incorporated into calculations of the Hanle-effect signals in the presence of nuclear-spin coupling. The experimental broadening rates are corrected for a minor amount of coherence narrowing. The measured broadening rate for the three 5 $^2P_{1/2}$ state level-crossing signals are in 20 percent agreement with the theory. The measured 5 $^2P_{1/2}$ state broadening rate exceeds the theoretical by about a factor of 2. This discrepancy may be due to the action of the hyperfine interaction during these unusually long duration collisions. The natural lifetimes of the 5 $^2P_{3/2}$ and 5 $^2P_{1/2}$ states are determined from the low-density linewidth to be 27.0 ± 0.5 and 29.4 ± 0.7 nsec, respectively.

Garfinkel, S. B., Mann, W. B., Pararas, J. L., **The National Bureau of Standard 4π β-γ coincidence-counting and γ-ray intercomparator automatic sample changers,** (Proc. First Int. Summer School on Radionuclide Metrology, Herceg Novi, Yugoslavia, Aug. 21-Sept. 1, 1972), *Nucl. Instrum. Methods* **112,** No. 1/2, 213-217 (Sept.-Oct. 1973).

Key words: 4π β-γ coincidence counting; γ-ray intercomparator automatic sample changers; radioactivity measurements.

Instruments of very simple and somewhat novel design will be described. The 4π β-γ changer holds from 1 to 30 carriers of sources, each of which can be counted for any preset number, up to 10, of counting periods. The γ-ray changer accomodates from 1 to 24 source carriers. In comparing γ-ray source count rates, the detector-to-source distances for individual sources are carefully controlled.

Garfinkel, S. B., Mann, W. B., Schima, F. J., Unterweger, M. P., **Present status in the field of internal gas counting,** (Proc. First Int. Summer School on Radionuclide Metrology, Herceg Novi, Yugoslavia, Aug. 21-Sept. 1, 1972), *Nucl. Instrum. Methods* **112,** No. 1/2, 59-67 (Sept.-Oct. 1973).

Key words: argon-37; carbon-14; internal gas counting; radioactive standardization; tritium; xenon-131m.

The gas-counting equipment at the National Bureau of Standards has been recently modified and reconstructed. The preparation of various radioactivity gaseous standards will be described. In some cases purity is assured by a prior separation in the isotope separator.

Geltman, S., Hidalgo, M. B., **The Coulomb-projected Born approximation. IV. Ionization of hydrogen,** *J. Phys. B: At. Mol. Phys.* **7,** No. 7, 831-839 (1974).

Key words: Born approximation; hydrogen; ionization; triple differential cross section.

The triple differential cross section for the electron impact ionization of hydrogen atoms is calculated in the Coulomb-projected Born approximation, including exchange, and detailed comparison is made with the ordinary Born result. The calculations are done for a variety of energies and angles of the two secondary electrons in coplanar and noncoplanar geometries. Appreciable differences occur in the results predicted by the various approximations.

Gevantman, L. H., Garvin, D., **The compilation and evaluation of chemical kinetics data: A descriptive survey of current efforts,** *Int. J. Chem. Kinet.* **V, 213-230 (1973).**

Key words: chemical kinetics; CODATA kinetics task group; compilation; evaluation; kinetics; national programs; rate constant data.

A description of the current range of activities being pursued in the compilation and evaluation of chemical kinetic data is given. The roles of individual scientists, professional groups, and national and international programs are detailed. The special problems attending on kinetic parameters are enumerated and discussed. An appendix is included which gives a comprehensive list of compilations and evaluations extant in the field of chemical kinetics.

Gevantman, L. H., **Survey of analytical spectral data sources and related data compilation activities,** *Anal. Chem.* **44,** No. 7, 30A-48A (June 1972).

Key words: analytical spectral data; automated spectral data sources; data centers; standard reference data.

A broad survey is made of analytical spectra data sources. The activities described include some description of the operative data systems, their location and the type of data issued. The report describes sources for infrared spectra, mass spectrometric data, atomic absorption data, x-ray diffraction data, NMR spectral data (chemical shift), ultraviolet spectra and others. New initiatives for automation and easy access and retrieval in some spectral areas are mentioned.

Giguere, P. T., Clark, F. O., Snyder, L. E., Buhl, D., Johnson, D. R., Lovas, F. J., **Upper limits for interstellar fulvene and nitric acid,** *Astrophys. J.* **182,** No. 2, 477-479 (June 1, 1973).

Key words: fulvene; interstellar molecules; nitric acid; radio astronomy; rotational transitions; telescope search.

Radio searches for the 1_{01}-0_{00} transition of fulvene (an isomer of benzene) at 6399 MHz and for the 1_{10}-1_{11} transition of nitric acid at 5839 MHz were not successful. Upper limits are reported for fulvene against three galactic sources and for nitric acid against four. Our measurements indicate that nitric acid may be underabundant with respect to cyanoacetylene in the direction of Sgr B2.

Griffin, R. J., Jr., **Pointing the finger at burn safety,** *Ind. Res.* **16,** No. 6, 45 and 47 (June 1974).

Key words: burns; instrumentation; product safety; safety test.

Describes an instrument, developed by NBS, designed to test surfaces for burn hazards. Termed a "thermesthesiometer," the instrument is capable of duplicating the temperature that would be experienced by human contact to heated surfaces.

Halford, D., **Comparing frequencies,** *Phys. Today* **26,** No. 2, 15 (Feb. 1973).

Key words: cesium frequency; frequency multiplication; infrared frequency synthesis; Josephson junction; lasers; methane frequency.

An incorrect and misleading statement was made in a news item in Physics Today, April 1972, page 17, regarding infrared frequency synthesis: "A chain of experiments is needed because two frequencies differing by more than a factor of 12 cannot be compared directly." This Letter to the Editor points out the existence and importance of some previously published papers, including as examples factors of 100 and of 401 obtained in one direct step, respectively, by McDonald and coworkers in 1970 and in 1971.

Haller, W., Blackburn, D. H., Simmons, J. H., **Miscibility gaps in alkali-silicate binaries—data and thermodynamic interpretation,** *J. Amer. Ceram. Soc.* **57,** No. 3, 120-126 (1974).

Key words: alkali-silicates; glass; immiscibility; lithium-silicate binary; melts; miscibility gaps; sodium-silicate binary; thermodynamics.

Measurements of the miscibility gaps in the Li_2O- and Na_2O-SiO_2 binaries are reported and compared to data of other workers. Heat treatments by brief immersion in liquid Sn were used for measuring the properties of glasses with a strong devitrification tendency. The

miscibility-gap boundaries of both systems are successfully described by modified regular-mixing equations based on the concept that the thermodynamic mixing processes are controlled by complex but discrete molecular structures which exist in the melt. The assumptions and implications of the model are discussed.

Hanley, H., Klein, M., Liley, P. E., Saxena, S. C., Sengers, J. V., Thodos, G., White, H. J., Jr., **Recommendations for data compilations and for the reporting of measurements of the thermal conductivity of gases,** *J. Heat Transfer*, pp. 479-480 (Nov. 1971).

Key words: critical evaluation of data; gases; thermal conductivity.

Recommendations are made with respect to what features should be incorporated in compilations of critically evaluated data to provide the greatest reliability and utility. The information required by evaluators for an accurate assessment of the reliability of experimental measurements is also discussed and some recommendations made relating to the presentation of this information.

Harrison, J. O., Jr., **Standards (Computer),** *McGraw-Hill Yearbook of Science and Technology*, pp. 392-396 (McGraw-Hill Book Co., New York, N.Y., 1973).

Key words: American National Standards Institute; ASCII; COBOL; computers; International Standards Organization; standards.

Computer standards are developed at the international level by ISO/TC 97, Computers and Information Processing, at the American national level by American National Standards Committee X3, and at the U.S. Federal Government level by NBS.

Such standards are devoted to many specific purposes, most of them related to the problems of interchanging data and interchanging programs among different computers. The American Standard Code for Information Interchange and the standardization of COBOL are given as examples.

Harrison, J. O., Jr., **The role of standards in data processing,** (Proc. 1969 International Data Processing Conference and Business Exposition, Data Processing Management Association, Montreal, Quebec, Canada, June 16-19, 1969), Paper in *Data Processing*, **XIV,** 451-458 (Data Processing Management Association, Park Ridge, Ill., 1970).

Key words: codes; compatibility; computers; data interchange; information processing; standards.

Federal information processing standards are for use within the data processing installations of the U.S. Government. They are generally, but not always, adopted from approved U.S.A. standards, and they are reflected in U.S. Government ADP procurement specifications. Federal information processing standards are, for the most part, directed to the solution of compatibility problems such as the interchange of data between and among information systems, the interchange of programs among computers of different makes and models, the interchange of devices and components among different product lines and the interchange of computer related ideas among people. The authoritative source of information on Federal information processing standards is the Federal Information Processing Standards Register issued by the National Bureau of Standards and distributed by the U.S. Government Printing Office.

Hastie, J. W., **Mass spectrometric evidence for HO_2 in 1 atm flames,** *Chem. Phys. Lett.* **26,** No. 3, 338-343 (June 1, 1974).

Key words: flame inhibition; flames; HO_2; mass spectrometry.

The perhydroxyl species HO_2 has been observed in 1 atm $H_2 - O_2 - N_2$ flames and its flame concentration determined as a function of flame composition and position. Also the oxidation of small additions of CO to these flames has been observed and the results favor the reaction, $OH + CO \rightarrow CO_2 + H$, rather than the alternative process, $HO_2 + CO \rightarrow CO_2 + OH$.

Hayward, R. W., **Parity,** Paper in *The Encyclopedia of Physics, 2d Edition*, R. M. Besancon, Ed., pp. 671-675 (Van Nostrand Reinhold Co., New York, N.Y., 1974).

Key words: charge conjugation; parity; relativity; space inversion; time reversal.

A short encyclopedic article on the concept of parity and other discontinuous Lorentz transformations and their applications in physics.

Hebner, R. E., Jr., Cassidy, E. C., Zahn, M., Sojka, R., **Electric field distributions and space charge behavior in nitrobenzene under low frequency alternating voltage,** (Proc. 1973 Annual Conference on Electrical Insulation and Dielectric Phenomena, Varennes, Quebec, Canada, Oct. 29-31, 1973), Paper in *1973 Annual Conference on Electrical Insulation and Dielectric Phenomena*, pp. 112-119 (National Academy of Sciences, Washington, D.C., 1974).

Key words: dielectric liquids; electric field mapping; high voltage measurements; Kerr effect; nitrobenzene; space charge.

The measurement of electric field distributions in dielectric liquids during high voltage operation is of interest for applications ranging from high voltage measurements to the physics and chemistry of dielectric fluids to the prediction and control of electrical breakdown in high-voltage apparatus. For this reason, we have used the electro-optic Kerr effect to measure the spatial and temporal variations of electric fields in a nitrobenzene-filled parallel-plate capacitor. Results obtained during operation under low frequency alternating high voltages are emphasized because of the significance of studies in this frequency range for design and testing of high-voltage apparatus. The effects of voltage level and frequency on space charge density and distribution are investigated for voltage up to 20 kV rms and over a frequency range of 0-120 Hz.

The results obtained are compared both with pulses and direct voltage observations in the same system and with some recent discussions of the role of particulate charge carriers in the behavior of insulating liquids.

Heinrich, K. F. J., Barrett, C. S., Newkirk, J. B., Ruud, C. O., Eds., **Advances in x-ray analysis,** *Proc. 20th Annual Conf. on Applications of X-Ray Analysis, Aug. 11-13, 1971*, **15,** 573 pages (Plenum Press, New York, N.Y., 1972).

Key words: automation; defraction; detectors; spectrometry; x-ray analysis; x-ray fluorescence.

The application of solid-state detectors of high energy resolution to x-ray spectrometry, and the increasing use of computers in both measurement and data evaluation, are giving a new stimulus to x-ray techniques in analytical chemistry. The Twentieth Annual Denver X-Ray Conference reflects this renewed interest in several ways.

The invited papers, grouped in Session I, review the characteristics of the detectors used in the measurement of x rays. One paper is dedicated to the detection of single ions. Although such a subject may appear to be marginal to the purposes of the Denver Conference, we must recognize the affinity of techniques applied to similar purposes. Ion probe mass spectrometry is dedicated to tasks similar to those performed by x-ray spectrometry with the electron probe microanalyzer. Scientists and technologists will see these two techniques discussed in the same meetings.

The discussion of automation and programming is not limited to the two invited speakers, but extends to papers presented in more than one session. The matter of fluorescence analysis by isotope- and tube-excitation will also be of great interest to those concerned with the practical applications of x-ray techniques.

The communications contained in this volume, and the lively discussions which frequently followed the presentation of papers, attest to the vitality of the subjects which are the concern of the Annual Denver X-Ray Conference.

Heinrich, K. F. J., **Gegenwärtiger stand der klassischen theorie der quantitativen elektronenstrahl-mikroanalyse,** *Mikrochim. Acta.*, Suppl. IV, pp. 252-262 (1970).

Key words: corrections; electron probe microanalysis; quantitative analysis; x-ray spectroscopy.

Although the foundations for a procedure of data reduction in quantitative electron probe analysis have not been changed for several years, there has been progress in the choice of expressions, parameters, and constants. A brief account of recommended expressions and procedures is given. Reference is made to the Standard Reference Materials of Au-Ag and Au-Cu alloys issued for electron probe microanalysis. These are especially useful for investigating the application of correction procedures.

Heinrich, K. F. J., **Review 3d National Conference on Electron Microprobe Analysis and the 1st Annual Meeting of the Electron Probe Analysis Society of America,** *Applied Optics* **8,** No. 4, 862-863 (1969).

Key words: conference review; electron probe; microanalysis; microscopy; spectroscopy; x rays.

This paper is a review of the Conference mentioned in the title. The review has been requested by the Editorial Consultant of the journal Applied Optics, published by the Optical Society of America.

Hellner, L. Sieck, L. W., **High-pressure photoionization mass spectrometry. Effect of internal energy and density on the ion-molecule reactions occurring in methyl, dimethyl, and trimethylamine,** *Int. J. Chem. Kinet.* **V,** 177-186 (1973).

Key words: amines; collisional stabilization; ionization energy effect; mass spectrometry; photoionization; rate constants.

The ion-molecule reactions of $CH_3NH_2^+$, $(CH_3)_2NH^+$, and $(CH_3)_3N^+$ with the respective amines have been investigated at thermal kinetic energies in a high-pressure photoionization mass spectrometer at several wavelengths (energies) in the vacuum ultraviolet. The absolute rate coefficient for proton transfer from $(CH_3)_3N^+$ to $(CH_3)_3N$ decreases from 8.2×10^{-10} cm^3/molecule·sec at 147.0 nm (8.4 eV) to 4.9×10^{-10} cm^3/molecule·sec at 106.7 – 104.8 nm (11.7 eV). In dimethylamine, the rate coefficient decreases from 11.6×10^{-10} cm^3/molecule·sec at 8.4 eV to 10.2×10^{-10} cm^3/molecule·sec at 11.7 eV, while no significant effect of energy was detected in methylamine. The reactions of several fragment ions are also reported. Experiments were also carried out at pressures up to 0.5 torr in order to investigate the further solvation of $CH_3NH_2^+$, $(CH_3)_2NH_2^+$, and $(CH_3)_3NH^+$. It was found that the maximum proton solvation numbers in methyl-, dimethyl-, and trimethylamine are 4, 3, and 2, respectively, under these conditions.

Herzberg, G., Hugo, T. J., Tilford, S. G., Simmons, J. D., **Rotational analysis of the forbidden $d^3\Delta_i \leftarrow X^1\Sigma^+$ absorption bands of carbon monoxide,** *Can. J. Phys.* **48,** No. 24, 3004-3015 (1970).

Key words: absorption spectrum; carbon monoxide; electronic spectrum; forbidden transition; rotational analysis; rotational perturbations.

The forbidden $d^3\Delta_i - X^1\Sigma^+$ transition of CO has been observed in absorption at high resolution in the vacuum ultraviolet region. The intensity distribution in the rotational structure of the observed bands in conformity with the assumption that the transition occurs on account of the interaction between the $d^3\Delta$ state and a $^1\Pi$ state, presumably the $A^1\Pi$ state. Thirteen bands of the $d - X$ system have been analyzed yielding more extensive rotational data for the $d^3\Delta_i$ state than were previously known. A discussion of the local perturbations in the d state by the $A^1\Pi$ and $a^3\Pi$ states is included.

Heuer, A. H., Cannon, R. M., Tighe, N. J., **Plastic deformation in fine-grain ceramics,** (Proc. 15th Sagamore Army Materials Research Conf., Sagamore Conference Center, Raquette Lake, N.Y., Aug. 20-23, 1968), Chapter 16 in *Ultrafine-Grain Ceramics*, pp. 339-365 (Syracuse University Press, Syracuse, N.Y., 1970).

Key words: fine-grain ceramics; grain boundary; plastic deformation; polycrystalline.

Plastic deformation in fine-grain (i.e., ≤ 10 μ) ceramics is discussed. It is shown that fine-grain polycrystals can be exceptionally ductile, the fine grain size enhancing diffusional deformation and grain boundary sliding processes. The deformation is sensitive to both grain size and temperature.

The influence of grain size (1-10 μ), strain-rate ($2 \times 10^{-6} - 3 \times 10^{-4}$/sec), and temperature (1100-1700 °C) on the deformation of fine-grain alumina has been studied. It is suggested that the predominant deformation mechanism in the larger grained polycrystals is diffusional creep, and that grain boundary sliding makes an increasingly important contribution as the grain size is decreased; in addition, deformation twinning can also be important. These results are shown to be consistent with previous work on deformation in polycrystalline alumina. A brief review of the literature on plastic deformation in fine-grain magnesia, beryllia, thoria, and urania indicates that grain boundary sliding may be important for each of these materials as well.

Heydemann, P. L. M., Houck, J. C., **Bulk modulus and density of polyethylene to 30 kbar,** *J. Polym. Sci.* **10,** Part A-2, 1631-1637 (1972).

Key words: bulk modulus; density; equation of state; glass transition temperature; polyethylene; pressure dependence.

The results of bulk modulus and density measurements on low-density polyethylene to 30 kbar are presented. From these data the pressure coefficient dT_t/dp of the glass transition temperature is obtained, and a comparison is made with data calculated from Pastine's theoretical equation of state for polyethylene.

Hillhouse, D. L., Peterson, A. E., **A 300-kV compressed gas standard capacitor with negligible voltage dependence,** *IEEE Trans. Instrum. Meas.* **IM-22,** No. 4, 408-416 (Dec. 1973).

Key words: capacitor, compressed-gas, negligible voltage dependence; capacitor, high-voltage, negligible voltage dependence; capacitor, negligible voltage dependence; capacitor, standard, negligible voltage dependence; capacitor, 300-kV, negligible voltage dependence; voltage dependence, negligible 300-kV capacitor.

A compressed gas capacitor now in use at the National Bureau of Standards (NBS) changes capacitance by less than 2 parts per million from 0-300 kV. This extremely small variation results primarily from rugged construction, and thus requires only reasonably careful centering of its three cylindrical electrodes. It has a hallow cantilevered high-voltage electrode suspended between an outer 100-pF low-voltage electrode and a segmented inner low-voltage electrode having values of 1, 2, 4, 8, and 10 pF, or any parallel combination thereof. The capacitor's small voltage dependence was inferred from the following independent measurements: 1) comparison with another high-voltage capacitor having a small experimentally determined coefficient; 2) comparison of the inner and outer sections with each other; and 3) measurement of capacitance change resulting from application of known forces on the cantilevered electrodes, and correlating this with calculated high-voltage electrostatic forces. The capacitor is used in determining the voltage coefficients of NBS-owned commercial standard capacitors; in the calibration of customers' standard capacitors, voltage transformers, and dividers to 200 kV and above; and in research on coupling capacitor voltage transformers and other high-voltage devices and materials.

Hockey, B. J., **Use of the hardness test in the study of the plastic deformation of single crystals,** (Proc. ASM-AIME Symp. on the Science of Hardness Testing and its Research Applications, Detroit, Mich., Oct. 18-21, 1971), Chapter 3 in *The Science of Hardness Testing and its Research Applications*, pp. 21-50 (American Society for Metals, Metals Park, Ohio, 1973).

Key words: deformational twinning; dislocations; hardness test; lattice friction; plastic deformation; single crystals.

The use of the hardness test in the study of the plastic deformation of single crystals is reviewed and its applicability to materials of different mechanical behavior discussed. Emphasis is placed on those studies which demonstrate the unique or relative advantages of point loading. It is shown that valuable information on the conditions under which plastic flow occurs, on dislocation slip system identification, on deformational twinning, and on lattice friction effects have been obtained.

Hoer, C. A., **The six-port coupler: A new approach to measuring voltage, current, power, impedance, and phase,** *IEEE Trans. Instrum. Meas.* **IM-21,** No. 4, 466-470 (Nov. 1972).

Key words: admittance; current; directional coupler; hybrid junction; impedance; phase angle; reflection coefficient; six-port coupler; voltage.

A six-port coupler is described having four side arms whose outputs are proportional to the voltage, current, incident voltage wave, and reflected voltage wave at some desired measurement plane in the transmission line. The phase relationship between the outputs is the same as between corresponding quantities at the measurement plane. Complex impedance and phase angle as well as voltage, current, and power can be obtained from simple power or voltage magnitude measurements at the four side arms. A vector voltmeter used with this six-port becomes a direct reading vector impedance meter, admittance meter, or reflection coefficient meter.

Holt, D. R., Nahman, N. S., **Coaxial-line pulse-response error due to a planar skin-effect approximation,** *IEEE Trans. Instrum. Meas.* **IM-21,** No. 4, 515-519 (Nov. 1972).

Key words: asymptotic expansion; characteristic impedance; coaxial line; complimentary error function; conductor; cylindrical; dielectric; error; generator; lossy; microminiature; model; planar; propagation function; pulse; receiving end; skin effect; step response; time domain; voltage divider.

The time-domain error introduced by the planar skin-effect approximation is examined by comparing the approximate response with the cylindrical skin-effect response. Expressions are developed for the cylindrical skin-effect response and applied to line outer conductor ID sizes ranging from a 0.1-mm microminiature size to 10 mm. For 50-Ω air dielectric lines (including 3.5 and 7 mm) curves are given for the cylindrical skin-effect response transition (rise) time (0 to 50 percent and 10 to 90 percent) versus line length (0.01-100 m). Step responses are given for a 1-m length of 0.1-mm 50-Ω microminiature line with relative dielectric constants of 1, 2, and 3.

Holt, H. K., **Theory of gas lasers and its application to an experiment,** *Phys. Rev. A* **2,** No. 1, 233-249 (July 1970).

Key words: collisions; gas laser; line widths; power output; theory; tuning curves.

The semiclassical theory of gas lasers has been reformulated by adding rate terms to the density-matrix component differential equations. The solution to these equations, in the form of a Fourier series, is applicable at high laser intensities. A calculation of the effect of phase-changing collisions is also included so that the results can be compared to experimental data taken with a He-Ne laser operating at a wavelength of 1.15 μm.

Hoover, T. B., **The frequency extrapolation of conductance data for aqueous salt solutions,** *J. Phys. Chem.* **74,** No. 13, 2667-2673 (1970).

Key words: conductance; conductivity; extrapolation; faradaic process; frequency extrapolation; palladium black; platinum, polarization; polarization electrode; Standard Sea Water.

Polarization phenomena in conductivity measurements were investigated in order to reduce systematic error in the standardization of solutions intended for the calibration of conductivity cells and salinometers. Data for demal potassium chloride solutions and for Standard Sea Water were obtained with two cells having constants of 37 and 86, respectively, both with bright platinum and with palladium black-coated electrodes. Four empirical and three theoretical functions of resistance *vs.* frequency were fitted to the data. Correctness of the extrapolation was judged by the agreement of the limiting resistance obtained with bright electrodes with that obtained with coated electrodes. All of the empirical formulas predicted limiting values for the bright electrodes that were lower by 0.02 to 0.15 percent. Equations based on the model of Grahame for the faradaic process, as well as a simplified model, agreed within 0.01 percent while a third theoretical equation was intermediate in accuracy.

Horn, W. A., **Minimizing average flow time with parallel machines,** *Oper. Res.* **21,** No. 3, 846-847 (May-June 1973).

Key words: assignment problems; job scheduling; scheduling.

It is noted that the assignment and sequencing of one-machine jobs in a multimachine environment can be formulated as a linear-programming assignment problem. Means for reducing the size and computational difficulty of this problem are identified.

Horn, W. A., **Some simple scheduling algorithms,** *Nav. Res. Logistics Q.* **21,** No. 1, 177-185 (Mar. 1974).

Key words: job scheduling; minimizing maximum lateness; minimizing total delay; multimachine scheduling; scheduling; scheduling algorithms; single-machine scheduling.

This paper considers situations in which jobs require only one operation on a single machine, or on one of a set of identical machines. Penalty-free interruption is allowed. Some simple algorithms are given for finding optimum schedules to minimize maximum lateness and total delay, for the single-machine case, and maximum lateness for a restricted multimachine case. A simple flow problem formulation permits minimizing maximum lateness for the more general multimachine case.

Hougen, J. T., Bunker, P. R., Johns, J. W. C., **The vibration-rotation problem in triatomic molecules allowing for a large-amplitude bending vibration,** *J. Mol. Spectrosc.* **34,** No. 1, 136-172 (Apr. 1970).

Key words: bending vibration; large amplitude; quasi-linear; theory; triatomic; vibration-rotation.

In this paper we derive an expression for the vibration-rotation Hamiltonian of a triatomic molecule. In the derivation we use a curvilinear bending coordinate and two rectilinear stretching coordinates in such a way that the Hamiltonian obtained is applicable for any triatomic molecule, linear or bent, and allows for large displacements of the bending coordinate (sometimes said to result from the molecule being "quasi-linear" but, in fact, of general occurrence). We derive a zeroth-order Hamiltonian to describe the energy levels associated with the bending vibration, and are able to fit the experimental results on HCN and DCN better than if we had used the standard formalism of rectilinear (and small) displacements. We also use the formalism to describe the dependence of the rotational constant B on the bending vibrational quantum number and apply the results to the microwave data on CsOH and CsOD.

Howard, C. J., Evenson, K. M., **Laser magnetic resonance study of the gas phase reactions of OH with CO, NO, and NO_2,** *J. Chem. Phys.* **61,** No. 5, 1943-1952 (Sept. 1, 1974).

Key words: gas phase reactions of OH with CO, NO, and NO_2; laser magnetic resonance; rate constant.

A laser magnetic resonance spectrometer has been used in combination with a discharge-flow system to measure the gas phase reaction rates of the OH radical with CO, NO, and NO_2 at 296 K and over a pressure range 0.4 – 5 torr. For the bimolecular reaction $OH + CO \rightarrow CO_2 + H$ we measure a rate constant, $k = 1.56 \times 10^{-13}$ cm^3/molecule·sec. For the termolecular reactions $OH + NO + M \rightarrow HNO_2 + M$, $M = He$, $k = 4.0 \times 10^{-31}$ cm^6/molecule^2 · sec; $M = Ar$, $k = 4.4 \times 10^{-31}$ cm^6/molecule^2 · sec; $M = N_2$, $k = 7.8 \times 10^{-31}$ cm^6/molecule^2 · sec. For the reaction $OH + NO_2 + N_2 \rightarrow HNO_3 + N_2$, $k = 2.9 \times 10^{-30}$ cm^6/molecule^2 · sec. Laser magnetic resonance detection of radicals is shown to be extremely sensitive, linear, and versatile. A complete description of this technique is presented with a discussion of its potential in the study of the reactions of free radicals.

Hudson, J., **Programming and control languages for automated laboratory experimentation,** *Astron. Astrophys. Suppl. Ser.* **15,** 487-495 (1974).

Key words: laboratory automation; process control; programming languages.

The problem of coding programs for computers used to control laboratory experiments is discussed. Several compilers which were developed for this purpose are described. The problem of developing "experimenter-proof" control languages is also addressed, and several approaches are mentioned.

Huie, R. E., Herron, J. T., **Kinetics of the reactions of singlet molecular oxygen ($O_2{}^1\Delta_g$) with organic compounds in the gas phase,** *Int. J. Chem. Kinet.* **V,** 197-211 (1973).

Key words: air pollution; kinetics, organic compounds; rate constant; reactions; singlet oxygen.

The reactions of singlet molecular oxygen ($O_2{}^1\Delta_g$) with a series of organic compounds have been studied in the gas phase at 298 K. The concentration of singlet molecular oxygen was determined by titration with 2,5-dimethylfuran. The titration technique was checked using a photoionization technique. Absolute rate constants were measured on the basis of the loss of organic reactant and, in some cases, of singlet molecular oxygen. It was found that the usual method of producing singlet molecular oxygen in the gas phase can also, under some conditions, allow reactive species other than singlet molecular oxygen to enter the reactor, leading to serious errors in the determination of rate constants. This problem was eliminated by carrying out the rate measurements in the presence of a small amount of nitrogen dioxide a radical scavenger.

Huie, R. E., Herron, J. T., **The rate constant for the reaction $O_3 + NO_2 \rightarrow O_2 + NO_3$ over the temperature range 259-362 K,** *Chem. Phys. Lett.* **27,** No. 3, 411-414 (Aug. 1, 1974).

Key words: air pollution; nitrogen dioxide; ozone; rate constant; stratosphere.

The rate constant for the reaction of ozone with nitrogen dioxide has been measured over the temperature range 259 to 362 K, using a stopped-flow system coupled to a beam sampling mass spectrometer. A fit of the data to the Arrhenius equation gave: $k = (9.44 \pm 2.46) \times 10^{10} \exp[(-2509 \pm 76)/T]$ cm^3 mol^{-1} sec^{-1}.

Huntoon, R. D., Lichtenstein, S., **The National Bureau of Standards prepares for the 1970's,** *Science* **165,** 867-874 (Aug. 29, 1969).

Key words: Astin-Branscomb transition; Astin legacy; compatibility and reproducibility of measurements; contributions to basic science; design and performance standards; fundamental constants; international standards; metric system study; National Standard Reference Data System; NBS in the coming decade; public health and safety; self-calibration by users; special NBS facilities.

A retirement story on Allen V. Astin covering his 17 year leadership of the National Bureau of Standards. Discusses Astin's role in acquiring the ultramodern Gaithersburg facility and the nomination of Lewis M. Branscomb as the new director.

Hutchinson, J. M. R., Mann, W. B., Mullen, P. A., **Sum-peak counting with two crystals,** (Proc. First. Int. Summer School on Radionuclide Metrology, Herceg Novi, Yugoslavia, Aug. 21-Sept. 1, 1972), *Nucl. Instrum. Methods* **112,** No. 1/2, 187-196 (Sept.-Oct. 1973).

Key words: aluminum-26; bismuth-207; cobalt-60; niobium-94; radioactivity standardization; sodium-22; sum coincidence counting; yttrium-88.

Very great improvements in accuracy of measurements of radioactivity by the sum-peak technique of coincidence counting have been achieved by the utilization of two NaI(Tl) crystals.

Taking advantage of the coincidence and anticoincidence possibilities in this arrangement, equations and techniques have been developed, so that accuracies obtainable by the sum-peak technique are improved by an order of magnitude, and become comparable to those obtainable by means of conventional β-γ and γ-γ coincidence counting.

Good statistical accuracy can be obtained quickly, and many small but often laboriously determined corrections which appear in β-γ and γ-γ coincidence counting, are important in this new method, which has been applied to the standardization of ^{60}Co, ^{94}Nb, ^{88}Y, ^{22}Na, ^{26}Al and ^{207}Bi.

Hutchinson, J. M. R., Mann, W. B., Perkins, R. W., **Low-level radioactivity measurements,** (Proc. First Int. Summer School on Radionuclide Metrology, Herceg Novi, Yugoslavia, Aug. 21-Sept. 1, 1972), *Nucl. Instrum. Methods* **112,** No. 1/2, 305-318 (Sept.-Oct. 1973).

Key words: aluminum; anticoincidence shielding; bovine liver assay; copper; low-level radioactivity; radioactivity intercomparisons; steel.

Low-level radioactivity measurements are reviewed. Alpha- and β-particle, and γ-ray low-level-radioactivity counting is discussed, and various detector systems are compared for detection sensitivity. Low-level measurements on bovine liver standard reference material, and radioactive contamination in industrial samples of aluminum, copper, and steel are reviewed. The results of low-level radioactivity intercomparisons are discussed.

Isbell, H. S., Pigman, W., **Mutarotation of sugars in solution: Part II,** *Advan. Carbohyd. Chem.* **24,** 14-65 (1969).

Key words: acid and base catalysts; catalysis of mutarotation; deuterium oxide mutarotation of; isotope effects in mutarotations; mechanism of mutarotation reaction; mutarotases; mutarotation of sugars; pseudo-acyclic intermediates in mutarotation; sugars; mutarotation of; thermodynamic data for mutarotations.

The publication is part of a comprehensive review describing and interpreting the changes which occur with reducing sugars in aqueous solutions. It treats, in depth catalysis by acids and bases, isotope effects, equilibrium states, thermodynamic properties, and reaction mechanisms. A new reaction mechanism is proposed in which the sugar ring is opened momentarily, forming a pseudo-acyclic intermediate, having a conformation resembling that of the parent sugar. This intermediate passes through characteristic transition states to the various tautomeric modifications of the sugar.

Isler, M. A., Stenbakken, G., **Magnetic switches for burglar alarm systems,** *NILECJ-STD-0301.00*, 20 pages (U.S. Department of Justice, Law Enforcement Assistance Administration, National Institute of Law Enforcement and Criminal Justice, Washington, D.C., Mar. 1974).

Key words: burglar alarm sensor; burglar alarm system; door switch; magnetically actuated; perimeter sensor; switch.

This standard establishes performance criteria for magnetically-actuated switches intended for use in protective intrusion alarm circuits to monitor the position of doors, windows, etc., and to cause the initiation of a signal sufficient to cause auxiliary equipment to send an alarm to a police panel, central station, or a local audible alarm device. Included are requirements and methods of test for materials, performance, and electrical properties. The performance characteristics selected are those that affect the false alarm susceptibility of the device. This standard does not provide performance criteria for resisting attempts to defeat the device through physical or surreptitious attack. This standard is one of a series establishing standards for intrusion alarm sensors, installation, and operation.

Iverson, W. P., **Biological corrosion,** Chapter in *Advances in Corrosion Science and Technology*, M. G. Fontana and R. W. Staehle, Eds., **2,** 1-42 (Plenum Press, New York, N.Y., 1972).

Key words: algae; bacteria; biological corrosion; fungi; mechanisms; prevention; review.

A review article of biological corrosion. Includes a brief historical outline, a discussion of the organisms involved in, the mechanism of and methods for preventing biological corrosion. The organisms associated with biological corrosion include fungi, bacteria and algae. The bacteria involved in sulfur and iron transformations, the "sulfur" and "iron" bacteria are among the most important organisms involved in biological corrosion. The mechanisms reviewed include the formation of acids, sulfur and sulfur compounds, ammonia and other corrosive compounds by microorganisms, formation of differential oxygen and chemical concentration cells, cathodic depolarization, disruption of protective films and breakdown of corrosion inhibitors. The methods for control and prevention of biological corrosion discussed include proper selection of a suitable environment, modification of a corrosive environment, the use of microbial inhibitors, and the use of protective coatings and cathodic protection separately or jointly.

Iverson, W. P., **Tests in soils,** (Proc. Symp. on State-of-the-Art in Corrosion Testing ASTM Annual Meeting, June 21-26, 1970, Toronto, Canada), Chapter 21 in *Handbook on Corrosion Testing and Evaluation*, W. H. Ailor, Ed., pp. 575-597 (John Wiley & Sons, Inc., New York, N.Y., 1971).

Key words: biological activity; chemical tests; electrochemical tests; pH; polarization measurements; redox-potential; soil corrosivity; soil resistivity.

A review and discussion of various methods used in measuring the corrosivity of soils and thin relative significance.

Methods discussed include soil pH, total ductility redox-potential, redox-capacity, resistivity, chemical tests, biological activity, electrochemical tests, and polarization techniques.

Jackson, R. H. F., Lechner, J. A., Sookne, D. J., **A system for position-location based on ranges,** (Proc. 18th Conf. on the Design of Experiments in Army Research Development and Testing, Aberdeen Proving Ground, Md., Oct. 25-27, 1972), *ARO Report 73-2*, Part 2, 549-577 (Department of Defense, Washington, D.C., 1973).

Key words: algorithms; least-squares; multilateration; position-location; ranges; simulation.

The system in question is intended to employ range-only information, or range-plus-altitude information, to track the positions of up to hundreds of users (only some of which measure ranges to other users) in three dimensions or on the earth's surface. This paper describes the structure, use and results of a simulation study which focused, within a larger analysis, on the absolute and relative adequacies of various mathematical position-estimation algorithms. The discussion will include comparisons among the six different algorithms investigated, considering both accuracy and computer time required.

Jacob, E. J., Lide, D. R., Jr., **Microwave investigation of methyl sulfone and methane sulfonyl fluoride,** *J. Chem. Phys.* **54,** No. 11, 4591-4596 (June 1, 1971).

Key words: dipole moment; internal rotation; methane sulfonyl fluoride; methyl sulfone; microwave spectra; molecular structure.

Rotational constants for the ground state of methyl sulfone and for the ground and first excited torsional state of methane sulfonyl fluoride have been derived from microwave spectra observed in the 18 000 – 37 000-MHz region. Molecular dipole moments of 4.50 ± 0.10 D for $(CH_3)_2SO_2$ and 3.88 ± 0.04 D for CH_3SO_2F were measured. Relative intensity measurements place the barrier to methyl rotation in CH_3SO_2F at 880 ± 120 cm^{-1} (2.52 ± 0.35 kcal/mole). Alternative structures for $(CH_3)_2SO_2$, based on assumption of either the SO or the SC bond length from a recent electron diffraction study, are presented. Both reveal a significant discrepancy between the microwave and diffraction values for the OSO angle.

Jacox, M. E., Milligan, D. E., Guillory, W. A., Smith, J. J., **Matrix-isolation study of the vacuum-ultraviolet photolysis of NF_3. The electronic spectrum of the NF_2 free radical,** *J. Mol. Spectrosc.* **52,** 322-327 (1974).

Key words: infrared spectrum; matrix isolation; NF; NF_2; NF_3; ultraviolet spectrum; vacuum ultraviolet photolysis.

The vacuum-ultraviolet of NF_3 in an argon or a carbon monoxide matrix at 14 K leads to the production of NF_2, identified by its infrared absorption. F-atom photodetachment also leads to the appearance of FCO in the carbon monoxide matrix studies. The photodissociation of NF_2 by 2537 Å radiation has been confirmed. The appearance of a band system near 2600 Å with position and band spacings close to those previously reported for NF_2 in the gas phase demonstrates that the lower state of the gas-phase transition is the ground state of the molecule and confirms the assignment of the observed structure to a progression in the upper-state bending vibration.

Jacox, M. E., Milligan, D. E., **Matrix-isolation study of the vibrational spectrum and structure of the CO_3^- radical anion,** *J. Mol. Spectrosc.* **52,** 363-379 (1974).

Key words: charge transfer; CO_2^-; CO_3^-; CO_3^{-2}; infrared spectrum; K atom reactions; matrix isolation; molecular structure; $N_2O + CO_2^-$ reaction; $O^- + CO_2$ reaction; $O_2^- + CO$ reaction.

Charge-transfer interaction processes which occur upon codeposition at 14 K of an AR:CO_2:N_2O or an Ar:CO:O_2 mixture with an atomic beam of potassium lead to the stabilization of CO_3^- in the solid deposit. Infrared spectroscopic data require a C_{2v} structure for this molecule. Although the deviation of the structure from the expected D_{3h} symmetry may result in part from Jahn-Teller distortion, cation interactions have been found to play a significant role. Evidence is presented for the initial formation of CO_3^- with trigonal symmetry. Upon mercury-arc irradiation of the deposit, absorptions due to CO_3^{-2} grow in importance.

Johnson, C. R., **Hadamard products of matrices,** *Linear and Multilinear Algebra* **1,** 295-307 (1974).

Key words: closure; diagonal matrix; *D*-stability; field of values; Hadamard product; inclusion theorem; Kronecker product; numerical radius; spectrum stable matrix.

The entry-wise product of arbitrary $n \times n$ complex matrices is studied. The principal tools used include the Kronecker product, field of values and diagonal multiplications. Inclusion theorems for the field of values and spectrum are developed in the general case and refined in special cases. These are employed to obain inequalities involving the real parts of the characteristic roots and the numerical radius,

and previously known results are found to be special cases of several of the theorems. In addition, the case of positive stable matrices is considered and a new class of nonnegative stable matrices is introduced, studied and related to *D*-stability.

Johnson, D. R., Powell, F. X., **Microwave spectrum and structure of sulfur difluoride,** *Science* **164,** 950-951 (May 23, 1969).

Key words: microwave spectroscopy; rotational spectrum; sulfur difluoride; molecular structure; dipole moment; electrical discharge.

Sulfur difluoride has been identified and characterized from its microwave spectrum. The analysis of rotational transitions for both sulfur difluoride-32 and sulfur difluoride-34 shows that this molecular species has C_{2v} symmetry with a bond length of 1.589 angstroms, a bond angle of 98°16., and a dipole moment of 1.05 Debye.

Johnson, W. T. K., Dick, C. E., **Half-life measurement of several short-lived nuclear isomers,** *Nucl. Instrum. Methods* **99,** 221-226 (1972).

Key words: bromine; cadmium; erbium; gold; half lives; iridium; measurement; nuclear isomers; solenium; tungsten.

Brehmsstrahlung produced by 3.5 MeV electrons incident on a platinum target was used to populate nuclear isomers in several nuclei through excitation of higher lying states. A shuttle was constructed to transport targets of natural isotopic abundance from an irradiation position to a measuring position. Other than a low background the activity measured was due entirely to the isomeric decay. The measured half-lives in seconds are ^{77m}Se 17.58 ± 0.12, ^{79m}Br: 4.97 ± 0.10, ^{167m}Er: 2.28 ± 0.03, ^{179m}Hf: 18.77 ± 0.07, ^{183m}W: 5.56 ± 0.25, ^{191m}Ir: 4.88 ± 0.03, and ^{197m}Au: 7.86 ± 0.04. The data are presented and the methods of analysis are discussed. The results are compared to recent literature values.

Ju-Te Lin, L., Ausloos, P., **Gas phase photolysis of acetone in the far ultraviolet,** *J. Photochem.* **1,** 453-462 (1972/73).

Key words: acetone; far ultraviolet; photolysis; primary processes; quantum yields.

The photolysis of acetone (pressure: 2 to 25 torr, 7:300 K) was investigated at 147 nm (8.4 eV), 123.6 nm (10 eV) and 106.7 – 104.8 nm (11.6 – 11.8 eV). The quantum yields of the products H_2, CO, CH_4, C_2H_6, C_2H_4, C_2H_2, C_3H_8, C_3H_6, C_3H_4, and $CH_3COC_2H_5$ were measured both in the presence and absence of free radical scavengers (C_2H_4 or NO). These data, in conjunction with the results of deuterium-labelling experiments, demonstrated the occurrence of the following primary processes:

$$CH_3COCH_3 + h\nu \rightarrow 2CH_3 + CO$$

$$\rightarrow CH_3COCH_2 + H$$

$$\rightarrow CH_3COCH + H_2$$

$$\rightarrow CH_4 + CH_2CO$$

It is also suggested that the primary process:

$$CH_3COCH_3 + h\nu \rightarrow C_3H_4 + H_2O \text{ (or } H_2 + O)$$

occurs with a quantum yield of ~0.02. The quantum yield of "molecular" methane (process d) is 0.02 (147 nm), 0.028 (123.6 nm) and 0.043 (104.8 – 106.7 nm). The quantum of "molecular" hydrogen is 0.03 (147 nm) 0.26 (123.6 nm) and 0.28 (104.8 – 106.7 nm). The quantum yield of process (a) is 0.7 ± 0.1 at 147 nm. At shorter wavelengths the quantum yield of the latter process could not be estimated because of the uncertain fate of the cations [$\Phi(CH_3COCH_3^+) = 0.25$ at 123.6 nm and 0.21 at 104.8 – 106.7 nm] and the extensive dissociation of the internally excited species formed in the primary processes.

Kahn, A. H., Candela, G. A., Walatka, V., Jr., Perlstein, J. H., **Magnetic susceptibility of the one-dimensional electron gas; application to BDP(TCNQ)$_2$,** *J. Chem. Phys.* **60,** No. 7, 2664-2669 (Apr. 1, 1974).

Key words: magnetic susceptibility; organic conductors; paramagnetism; TCNQ compounds.

The magnetic susceptibility of the noninteracting electron gas has been studied on the basis of free electrons and the tight-binding model, with application to the properties of organic conducting materials. Theoretical curves of susceptibility versus temperature are presented. The gradual transition from low temperature Pauli paramagnetism to the high temperature Curie law region is shown. In the transition region, the one-dimensional systems show a peak in the susceptibility of the order of 110 percent of the low temperature limit. The magnetic susceptibility of the compound BDP(TCNQ)$_2$ is interpreted in terms of a one-dimensional tight-binding model with an energy bandwidth of 0.07 eV.

Kaldor, A., Hastie, J. W., **Infrared laser modulated molecular beam mass spectrometry,** *Chem. Phys. Lett.* **16,** No. 2, 328-331 (Oct. 1, 1972).

Key words: infrared laser; laser chemistry; mass spectrometry; molecular beam; phase spectroscopy; vibrational energy transfer.

A technique is described whereby a modulated molecular beam can be extracted from gas mixtures which are excited by infrared laser radiation. The method has been applied to time resolved mass spectrometric studies of laser induced molecular processes for systems containing BCl_3 and SF_6 as radiation absorbers, and shows general applicability to studies of laser induced chemical reaction.

Kase, K. R., Domen, S. R., **Calorimetric and ionization measurements of stopping power in carbon for 19.5 GeV electrons,** *Nucl. Instrum. Methods* **118,** 469-475 (1974).

Key words: absorbed dose; calorimeter; carbon; electrons; stopping power.

A portable carbon calorimeter built at the National Bureau of Standards was used in a 19.5 GeV electron beam at the Stanford Linear Accelerator to measure absorbed dose. The dose measurements were normalized to a given number of incident electrons by monitoring the electron intensity with a transmission ion chamber previously calibrated against a quantameter in the same beam. The simultaneous measurements of integrated electron intensity and absorbed dose allowed a direct determination of stopping power in carbon for 19.5 GeV electrons. The measured value of 1.80 MeV cm^2/g is within 6 percent of the calculated value.

Kelley, R. D., Klein, R., **Cross disproportionation of alkyl radicals,** *J. Phys. Chem.* **78,** No. 16, 1586-1595 (1974).

Key words: alkyl radicals; cross disproportionation; steric effects.

The cross disproportionation of several alkyl radicals has been measured using a novel technique that eliminates most of the uncertainties characterizing previous gas-phase results. The radicals are prepared in the condensed phase at 90 K by the H atom addition to a mixture of two olefins. The concentrations are adjusted so that one of the two radicals produced is in great excess. The other radical, then, is involved only in cross and not in autodisproportionation. From the results of a number of measurements, it is shown that alkyl radical disproportionation is governed almost completely by steric factors whereby the hydrogen acceptor-donor characteristics of each radical of the cross-disproportionating pair are independent of the counter radical. The cross disproportionation of an alkyl radical containing a double bond shows that the double bond has an orienting effect on the approach to and reaction with a second radical.

Khoury, F., Fanconi, B., Barnes, J. D., Bolz, L. H., **Effects of polymorphism on the Raman-active longitudinal acoustical mode frequencies of *n*-paraffins,** *J. Chem. Phys.* **59,** No. 11, 5849-5857 (Dec. 1, 1973).

Key words: chain-folded polyethylene crystals; longitudinal acoustical modes; *n*-paraffins; polymorphism; Raman spectroscopy.

Raman spectroscopic measurements on the orthorhombic and monoclinic crystalline forms of n-$C_{36}H_{74}$ and n-$C_{94}H_{190}$ show that the frequencies of the longitudinal acoustical modes depend on the orientation of the chain axis relative to the planes containing the terminal methyl groups as well as the chain length. The frequency differences between the orthorhombic and monoclinic forms of a given *n*-paraffin depend on the magnitude and direction of the regular stagger between neighboring end groups in the monoclinic forms. It is concluded that these frequency differences are most likely associated with variations in end group packing associated with differences in crystalline form. The implications of these observations to the use of Raman spectroscopic data to characterize the morphology of chain-folded polyethylene crystals are discussed.

King, D. A., Madey, T. E., Yates, J. T., Jr., **Interaction of oxygen with polycrystalline tungsten. I. Sticking probabilities and desorption spectra,** *J. Chem. Phys.* **55,** No. 7, 3236-3246 (Oct. 1, 1971).

Key words: adsorption; chemisorption; flash desorption; oxidation; oxygen; tungsten; tungsten oxides.

The interaction of oxygen with a polycrystalline W filament has been studied in the temperature range 300-1200 K and for exposures between 10^{-7} and 1 torr·sec. Both sticking probabilities and desorption spectra have been measured. After low exposures ($< 2 \times 10^{-6}$ torr·sec) the adsorbate is all desorbed as O atoms with first order kinetics. With higher exposures, oxygen is removed as oxides: WO, WO_2, WO_3, W_2O_6. The desorption spectra for each of these species are complex, and nine distinct and reproducible oxide states are identified. Saturation coverages in each of these states are independent of adsorption temperature in the range 300-1200 K. At a total coverage of 8.5×10^{14} O_2 molecules cm^{-2}, 2.2×10^{14} O_2 molecules cm^{-2} are desorbed as oxides; after exposures $> 10^{-2}$ torr·sec at 300 K, the total uptake rises to 15×10^{14} O_2 molecules cm^{-2}. At temperatures between 500 and 1000 K and exposures up to 1 torr·sec, a multilayer oxide film is formed of unlimited thickness. The desorption product from this oxide film is predominantly WO_2, which desorbs in the region of 1200 K. The kinetics of adsorption and desorption are evaluated and discussed.

Kirchhoff, W. H., Lide, D. R., Jr., Powell, F. X., **The microwave spectrum, force field and dipole moment of CF_2,** *J. Mol. Spectrosc.* **47,** No. 3, 491-498 (Sept. 1973).

Key words: CF_2; dipole moment; force field; microwave spectra; structure.

Measurements of the microwave spectrum of CF_2 have been extended to include transitions up to $J = 40$. Using these extended measurements, a centrifugal distortion analysis has been performed and from the distortion constants, the force field, infrared spectrum, average structure, Coriolis coupling constants, and inertial defect have been calculated. The original assignment of the infrared spectrum has been confirmed. An improved value for the dipole moment, 0.469 ± 0.026 D, has been obtained.

Klein, R., **Preparation of contiguous chemisorbed adlayers by sequential deposition and surface migration,** *Surface Sci.* **29,** 309-316 (1972).

Key words: chemisorption; deposition; gas separation; physisorption.

The separation of two sequentially deposited gases on a half shadowed field emission tip by surface migration of the physisorbed layer furnishes a convenient method for the production of distinct, contiguous layers. Oxygen and carbon monoxide on tungsten as well as ruthenium, and oxygen and nitrogen on ruthenium have been separated in this manner.

Kohayakawa, Y., **Contrast-difference thresholds with sinusoidal gratings,** *J. Opt. Soc. Amer.* **62,** No. 4, 584-587 (Apr. 1972).

Key words: vision; visual contrast.

Two halves of a sinusoidally modulated transparency were projected on a diffusing surface. The contrast C of one half of the field was changed by defocusing until a definite difference of contrast, ΔC, was perceived. The contrast of either half of the field could be changed without changing the mean luminance. A plot of $\Delta C/C$ against C declines monotonically with increasing contrast. On the other hand, ΔC against C has a maximum at an intermediate contrast. The contrast difference ΔC can be interpreted as relative luminance difference $\Delta L/L$, to which the Weber law applies. A function relating subjective to objective contrast was obtained. The relation between modulation transfer function (MTF) with constant input and constant output is discussed.

Koonce, C. S., **Peierls transitions in semimetallic one dimensional charge transfer salts,** *Solid State Commun.* **14,** No. 11, 1141-1144 (1974).

Key words: charge transfer salts; electronic energy band structure; electron-phonon coupling; one dimension; Peierls transition; tetrathiofulvalinium-tetracyanoquinodimethan (TTF-TCHNQ).

Peierls transitions in one dimensional charge transfer salts in which both donor and acceptor molecules have even valency such as TTF-TCNQ have been studied. Transitions involving macroscopic occupation of phonon states of wavevector $k_F(\mathrm{TTF}) + k_F(\mathrm{TCNQ}) = 1/2\ G$ and $|k_F(\mathrm{TTF}) - k_F\ (\mathrm{TCNQ})|$ can occur as well as transitions of wavevector $2k_F(\mathrm{TTF})$ [and $2k_F(\mathrm{TCNQ})$].

Kranbuehl, D. E., Verdier, P. H., **Monte Carlo studies of the relaxation of vector end-to-end length in random-coil polymer chains,** *J. Chem. Phys.* **56,** No. 6, 3145-3149 (Mar. 15, 1972).

Key words: end-to-end length; Monte Carlo; polymer chain dynamics; random-coil.

The effects of excluded volume interactions upon the dynamical behavior of random-coil polymer chains are studied by obtaining autocorrelation functions for vector end-to-end length of lattice-model chains of 9, 15, 33, and 63 beads by a Monte Carlo simulation technique. It is found that relaxation of the vector end-to-end length requires from 4 to 7 times as long as relaxation of its square, in contrast to the predictions of simple models without excluded volume effects.

Krell, J. M., Sams, R. L., **Vibration-rotation bands of nitrous oxide: 4.1 micron region,** *J. Mol. Spectrosc.* **51,** No. 3, 492-507 (June 1974).

Key words: Coriolis interaction; Fermi resonance; high resolution; H_2O; infrared; perturbation allowed transitions.

The infrared spectrum of nitrous oxide has been measured and analyzed from 2265 cm^{-1} to 2615 cm^{-1}. Newly refined effective rotational constants for twenty-one vibrational states of $^{14}N_2O$, three vibrational states each of $^{14}N_2{}^{18}O$ and $^{15}N^{14}N^{16}O$, two states of $^{14}N^{15}N^{16}O$ and one state of $^{14}N_2{}^{17}O$ have been calculated.

The most interesting features observed are two Δ-Σ "forbidden" bands, $04^{2e}0$-00^00 and $12^{2e}0$-00^00. These bands occur because of Coriolis interaction between unperturbed vibrational states having $l = 0$ and $l = 2$.

Ku, H. H., **Statistical methods applicable to counting experiments and evaluation of experimental data,** *Nucl. Instrum. Methods* **112,** 377-383 (1973).

Key words: calibration; check standard; control chart on precision measure; data analysis; design of experiments; deporting of results; standards; statistical methods.

In an experiment a sequence of operations is performed that results in the collection, interpretation, and transmission of information on a topic of interest. Statistical methodology may be used to help in increasing the efficiency of collection, in checking the validity of interpretation, and in editing the presentation of results. Some such concepts and methods that are useful to counting experiments, and essential to the operations of standards and calibration laboratories, will be discussed.

Kunasz, P. B., Hummer, D. G., **Radiative transfer in spherically symmetric systems-III. Fundamentals of line formation,** *Mon. Notic. Roy. Astron. Soc.* **166,** No. 1, 19-55 (1974).

Key words: radiative energy loss; radiative transfer; spectral line profiles; spherically symmetric gas clouds; stellar atmospheres.

A generalization of the variable Eddington factor method is presented that makes possible the solution of line formation problems in extended spherical atmospheres whose constitutive properties depend on radius in an arbitrary way. Extensive numerical results for Doppler broadening in models with power law opacities ($n = 0,2,3$) are presented and interpreted. Very substantial deviations are found from the solutions of analogous plane-parallel models. The single-flight escape probability is derived for a general opacity law and is shown to exceed that for an analogous plane-parallel slab by no more than a factor of approximately two for Doppler broadening, or three-halves for Lorentz broadening. However, it is shown that each time a photon is scattered, it has a probability greater than one-half of ending its flight at a radius larger than that at which it was emitted. This effect is peculiar to spherical geometries and may be important in aiding the escape of photons from optically thick systems. Finally the effects of dilution are considered and some properties of the infinite radius, finite optical depth models are inferred. An appendix contains the solution of the line transfer problem for a homogeneous sphere by the kernel-approximation method.

Kunasz, P. B., Hummer, D. G., **Radiative transfer in spherically symmetric systems-IV. Solution of the line transfer problem with radial velocity fields,** *Mon. Notic. Roy. Astron. Soc.* **166,** No. 1, 57-78 (1974).

Key words: gas dynamics; radiative transfer; spectral line profiles; stellar atmospheres.

A numerical procedure is presented for solving the line transfer problem with complete redistribution in spherically symmetric atmospheres in which the radial velocity is an arbitrary function of radius, limited by practical considerations to maximum velocities a few times the mean thermal velocity. In this procedure the transfer equation, written in the observer's frame, is differenced along rays and the resulting very large set of coupled linear equations is cast into the novel form, proposed by Rybicki, that allows for extremely rapid solution of the system. Numerical results are discussed for three sequences of models, two with linear velocity laws and one with constant velocities, in which the effect of the transverse velocity gradient is demonstrated. It is shown that velocities as small as 0.05 of the mean thermal velocity produce observable asymmetries in the flux profile.

Kuriyama, M., Early, J. G., **The dynamical scattering amplitude of an imperfect crystal. III. A dynamical diffraction equation for topography in the spatial coordinate representation,** *Acta Crystallogr.* **A30,** 525-535 (Jan. 1974).

Key words: dynamical diffraction; imperfect crystal; integral equation; topography.

Based on a general dynamical theory of diffraction, an integral equation for dynamical diffraction in imperfect crystals is obtained in the spatial coordinate representation. This equation is derived for diffraction topography in the symmetrical Laue geometry from the basic dynamical equation of diffraction previously derived in the momentum representation. Discussion is presented on an interpretation of this integral equation beyond the given diffraction geometry. This equation can be considered as a basic equation for diffraction topography.

Kurylo, M. J., Braun, W., Kaldor, A., **A laser enhanced reaction technique for the measurement of V → T deactivation rates: Deactivation of vibrationally excited O_3,** *Chem. Phys. Lett.* **27,** No. 2, 249-253 (July 15, 1974).

Key words: apparatus and methods; deactivation; energy transfer; infrared laser; luminescence; ozone.

Rates of V → T transfer for vibrationally excited ozone (O_3) in the (100), (010) and (001) levels have been measured using a laser enhanced chemiluminescent method for the deactivating gases He, Ar, H_2, N_2, O_2, H_2O, CO_2, SO_2, CH_4, and SF_6. The method takes advantage of an enhanced reaction rate between $O_3 + NO$ producing electronically excited NO_2 and uses the NO_2 chemiluminescence as a tracer for the O_3 concentration. Results obtained by this new method are compared with recent results obtained by an IR fluorescence method. Good agreement is obtained for all gases, except methane, and implications of these results on the mechanism for deactivation are described.

Kurylo, M. J., Braun, W., Kaldor, A., Freund, S. M., Wayne, R. P., **Infrared laser enhanced reactions: Chemistry of vibrationally excited O_3 with NO and $O_2(^1\Delta)$,** *J. Photochem.* **3,** 71-87 (1974/75).

Key words: kinetics; laser enhanced reactions; nitric oxide; $O_2(^1\Delta)$; ozone; vibrationally energy.

Vibrationally excited ozone, produced by absorption of CO_2 laser radiation, was found to react significantly faster with NO and $O_2(^1\Delta)$ than thermal ozone. Using a modulation technique, absolute and relative rate constants at 300 K for the following reactions were calculated assuming rapid equilibration between the three closely spaced vibrationally excited levels of O_3, and that only the lowest level of these, the ν_2 bending mode, is active in reaction.

$$O_3 + NO \rightarrow NO_2^*(^2B_1) + O_2 \quad (1)$$
$$O_3\dagger + NO \rightarrow NO_2^*(^2B_1) + O_2 \quad (1')$$
$$O_3 + NO \rightarrow NO_2\dagger(^2A_1) + O_2 \quad (2)$$
$$O_3\dagger + NO \rightarrow NO_2\dagger(^2A_1) + O_2 \quad (2')$$
$$O_3 + O_2(^1\Delta) \rightarrow 2O_2 + O \quad (7)$$
$$O_3\dagger + O_2(^1\Delta) \rightarrow 2O_2 + O \quad (7')$$

$k_1 + k_{2'} = 2.7 \times 10^{-13}$ cm^3 molecule^{-1} s^{-1}; $(k_{1'} + k_{2'})/(k_1 + k_2) = 16.2 \pm 4.0$; $k_{1'}/k_1 = 4.1 \pm 2.0$; $k_{2'}/k_2 = 17.1 \pm 4.3$; $k_{7'}/k_7 = 38 \pm 20$. These rate constants must be modified if a different combination of vibrationally excited levels is involved. The fraction of vibrational energy usable in chemical reaction was found to be about 15, 50 and ~ 100 percent respectively for processes 1', 2' and 7'. Our measurements clearly differentiate between the participation of vibrational energy and thermal energy but do not distinguish differences between the individual vibrationally excited states. Details of the modulation technique, involving chemiluminscence detection of NO_2 and resonance fluorescence detection of oxygen atoms, are described. Comparison of our results with a previous measurement of the summation reaction (1' + 2') shows excellent agreement.

Lafferty, W. J., Ritter, J. J., **Microwave spectrum, structure, and dipole moment of ethynyldifluoroborane, H-C ≡ CBF$_2$,** *Chem. Commun.*, pp. 909-910 (1969).

Key words: dipole moment; ethynyldifluoroborane; microwave spectrum; rotational constant; structure; vibrational frequency.

The microwave spectrum of enthynyldifluoroborane was studied in the 18-33 GHz region. The molecule has been determined to have C_{2v} symmetry and estimates can be made for the C-B bond distance and the FBF angle. The dipole moment of the molecule was found to be 1.93D with a 20-uncertainty of ±0.06D.

Latanision, R. M., Ruff, A. W., Jr., **Extrinsic-intrinsic stacking-fault pairs in an Fe-Cr-Ni alloy,** *J. Appl. Phys.* **40,** No. 7, 2716-2720 (June 1969).

Key words: dislocations; electron microscopy; stacking fault energy; stacking fault pairs; stainless steel.

Transmission electron images of extrinsic-intrinsic fault pairs in a Fe-Cr-Ni alloy are shown to be sensitive to changes in the sign of $(\mathbf{g}\cdot\mathbf{b})s$ for reflections producing either line or stacking-fault contrast. This is interpreted in terms of the overlapping strain fields of the three closely spaced partial dislocations. A differential treatment of the measured widths of the intrinsic and extrinsic faults indicates that the stacking-fault energy ratio $\gamma_e/\gamma_i = 1.6$ in this alloy.

Lauritzen, J. I., Jr., **Effect of a finite substrate length upon polymer crystal lamellar growth rate,** *J. Appl. Phys.* **44,** No. 10, 4353-4359 (Oct. 1973).

Key words: crystallization; growth rate; nucleation substrate; polymer.

The polymer crystal lamellar growth rate G is an often-measured property of semicrystalline polymers. In this paper, we investigate the dependence of G upon the length of the substrate, L, the surface nucleation rate of new growth layers per unit length per unit time, i, the velocity with which the growth layer covers the substrate, g, and the thickness of the growth layer, b. For the purposes of this paper, L is the average length where the polymer segments in the substrate are in crystallographic register. We show that $G = biL/n$, where n is the average number of nuclei that contribute to each growth layer. We show that n depends only on the dimensionless parameter $z = iL^2/4g$. We have not obtained n explicitly, but we can place upper and lower limits on n that closely define G in regime I, where $G \simeq biL$ and into a transition region between regime I and regime II where $G \downarrow bi(g)^{1/2}$. The experimental results for several polymers are analyzed and some are found to be in or near regime I, and others in or near regime II.

Lauritzen, J. I., Jr., Hoffman, J. D., **Extension of theory of growth of chain-folded polymer crystals to large undercoolings,** *J. Appl. Phys.* **44,** No. 10, 4340-4352 (Oct. 1973).

Key words: chain folds; growth rate; isotactic; lamellar thickness; nucleation theory; polyethylene; polymer crystallization; polystyrene; undercooling.

The kinetic theory of the rate of growth G and the initial lamellar thickness l_g^* of chain-folded crystals is extended so that it is applicable at high undercoolings. Attention is centerd on the details of how the first step element and the first fold are put down on the substrate. A parameter ϕ that varies between zero and unity, which apportions the free energy of attachment of the step element between the forward and backward reactions, is used to denote variations in this process. Expressions for G are derived from flux equations for two limiting cases: regime I, single surface nucleation act with rapid substrate completion and regime II, numerous surface nucleation acts with very slow substrate completion. Data from the literature on G for isotactic polystyrene (regime II) and polyethylene single crystals (regime I) are analyzed to obtain surface free energies, and these are used with the revised theory for l_g^* to predict the lamellar thickness of these polymers. Good agreement between l_g^* and published data is found for $1 > \phi > 0$. Values of ϕ below unity imply that the molecules are physically adsorbed onto the substrate prior to actual crystallographic attachment. A discussion is given of the segmental transport effects that dominate the behavior of G at high undercoolings in bulk polymers.

Lauritzen, J. I., Jr., Zwanzig, R., **Exact calculation of the partition function for a generalized model of two-dimensional polymer crystallization by chain folding,** *J. Chem. Phys.* **52,** No. 7, 3740-3751 (Apr. 1, 1970).

Key words: chain-folded crystal; partition function; phase transition; polymer.

A generalized model for two-dimensional polymer crystallization by chain folding is treated by equilibrium statistical mechanics. A generating function for the partition function is obtained in exact analytic form. The model leads to thermodynamically well-defined chain-folded polymer crystals. Under certain circumstances in the limit of an infinitely long polymer chain, the model shows a second-order phase transition from an "extended-chain" crystal to the chain-folded crystal.

LaVilla, R. E., **Semi-Auger electron transitions,** (Proc. Int. Conf. on Inner Shell Ionization Phenomena and Future Applications, Atlanta, Ga., Apr. 17-22, 1972), Paper in *Proceedings of the International Conference on Inner Shell Ionization Phenomena and Future Applications*, R. W. Fink, S. T. Manson, J. M. Palms, and P. V. Rao, Eds., Conf. 720404, 1, 509-522 (U.S. Atomic Energy Commission, Technical Information Center, Oak Ridge, Tenn., Jan. 1973).

Key words: argon, KCl, CH_3Cl, SF_6; L and K x-ray spectra; semi-Auger effect; x-ray photoelectron spectra.

The argon and KCl $L_{2,3}$ x-ray emission spectra excited by direct electron bombardment have been recorded with photon counting on a planar single crystal spectrometer. A prominent feature lying approximately 6, 11, and 14 eV below the parent emission peak in Cl, Ar and K respectively, was observed in the spectra. Comparison with other data on related processes indicates that the low energy features are direct evidence of a "semi-Auger" two electron process, due to configuration interaction in the final state. The initial $L_{2,3}$ single vacancy is filled by an outer shell electron and simultaneously another outer shell electron is excited with the emission of a single photon. The possible identification of this process in other systems will also be discussed.

Lawless, W. N., **Dielectric cooling technology: 15–4.2 K,** (Proc. Cryogenic Cooler Conf., USAF Academy, Colo., Oct. 16-17, 1973), Chapter in *Closed Cycle Cryogenic Cooler Technology and Applications* **1**, 417-440 (AF Flight Dynamics Lab., (FEC), Wright-Patterson AFB, Ohio, Dec. 1973).

Key words: adiabatic polarization; cooling technology; dielectric cooling; glass-ceramics; magnetic thermal valve; mechanical thermal valve; refrigeration, solid-state; $SrTiO_3$.

A comprehensive analysis of a proposed dielectric refrigerator operating in a closed cycle between a load at 4.2 K and a reservoir at 15 K is presented. The working dielectric material is a $SrTiO_3$ glass-ceramic, for which the dielectric equation of state is experimentally determined. Hysteretic phenomena, breakdown strength, and phonon-polarization data are presented and discussed. A realistic engineering model for the refrigerator is described and analyzed, including parasitic thermal loads and losses. Some of the dimensional parameters of the model maximize the performance, and these optimal dimensions are physically reasonable. Computer analyses are made of these models, which are right circular cylinders of diameter D and height D. The results are that the net powers absorbed from the load at 4.2 K vary from 1 to 50 W for D-values between 5 and 20 cm and for cycle times ~ second. These results are shown to be relatively insensitive to the choice of metals used for the electrodes and heat conductors in the model (Rh, Pt, W, Cr, Cu) or to the approximations employed. A joint development program between the National Bureau of Standards and Corning Glass Works is underway to develop a prototype dielectric refrigerator along the lines discussed in this paper.

Layer, H. P., **Circuit design for an electronic self-nulling ellipsometer,** *Surface Sci.* **16,** 177-192 (1969).

Key words: corrosion; electronic ellipsometer; Faraday cells; self-nulling ellipsometer; thin films.

The importance of automating the ellipsometer has been recognized by researchers active in the field and considerable attention has been given to the development of a practical instrument. The present work was motivated by the belief that a more satisfactory automatic ellipsometer could be developed if the all-electronic approach suggested by Winterbottom was used. This approach has resulted in the design and construction of an instrument that is sensitive, stable, relatively inexpensive and which has a response time that is of the order of milliseconds. The electronic circuits will easily lend themselves to duplication by investigators interested in such a device and are of such a configuration that existing instruments need only minor modifications. An automatic gain stage circuit is included to maintain maximum sensitivity where spectral emission and sensitivity variations are encountered, as in continuous wavelength scanning ellipsometric measurements.

Lesclaux, R., Searles, S., Sieck, L. W., Ausloos, P., **Modes and rates of reaction of cyclopentene and methylcyclopentene ions with their parent molecules,** *J. Chem. Phys.* **54,** No. 8, 3411-3418 (Apr. 15, 1971).

Key words: cyclopentene; ion-molecule reactions; mass spectrometry; methyl cyclopentene; photoionization; vacuum ultraviolet.

Cyclopentene and methylcyclopentene ions were generated by irradiating the respective parent compounds with 10.0-eV photons; cyclopentene was also irradiated with 11.6–11.8-eV photons. The ionic products of ion-molecule reactions were observed in the NBS high-pressure photoionization mass spectrometer, while the neutral products of these reactions were determined by chemical analysis of products formed in photolytic experiments in a closed system. The cyclopentene ion, which at 10.0 eV retains its cyclic structure, undergoes an H_2 transfer reaction ($c\text{-}C_5H_8^+ + c\text{-}C_6H_8 \rightarrow c\text{-}C_5H_{10} + c\text{-}C_5H_6^+$, $k = 3.3 \times 10^{-10}$ cm³/molecule·sec) and a condensation reaction ($c\text{-}C_5H_8^+ + c\text{-}C_5H_8 \rightarrow C_{10}H_{16}$, $k = 2.7 \times 10^{-10}$ cm³/molecule·sec) with the parent molecule. The same reactions are observed for ions formed at 11.6-11.8 eV, but at the higher energy, approximately 20 percent of the ions are observed to undergo ring opening to form 1,3-$C_5H_8^+$ ions; the latter ions undergo an H_2 transfer reaction with the cyclopentene molecule ($1,3\text{-}C_5H_8^+ + c\text{-}C_5H_8 \rightarrow 2\text{-}C_5H_{10} + C_5H_6^+$, $k = 1 \times 10^{-10}$ cm³/molecule·sec). The three methylcylopentene ions also undergo H_2 transfer reactions with the corresponding parent molecules [$C_6H_{10}^+ + C_6H_{10} \rightarrow (CH_3)C_5H_9 + C_6H_8^+$, $k = 4.6$, 1.8, and 2.9×10^{-10} cm³/molecule·sec for 1-, 3-, and 4-methylcylopentene, respectively]. Condensation reactions between these ions and their parent molecules are observed to only a minor extent, but a second major mode of reaction, namely H transfer, is observed ($C_6H_{10}^+ + C_6H_{10} \rightarrow C_6H_{11} + C_6H_9^+$, $k = 0.6$, 2.8, and 1.2×10^{-10} cm³/molecule·sec for 1-, 3-, and 4-methylcyclopentene, respectively). Structural reasons for these rate variations are discussed.

Levin, E. M., **System Y_2O_3-GeO_2 below 1700 °C,** *J. Amer. Ceram. Soc.* **57,** No. 4, 189-190 (Apr. 1974).

Key words: germania-yttria system; immiscibility; phase equilibrium; yttria-germania system.

The phase diagram for the system has been determined up to 1700 °C using the quenching technique. Phases were identified with the aid of the polarizing microscope and by x-ray powder diffraction. The system contains three compounds, Y_4GeO_8, Y_2GeO_5, and $Y_2Ge_2O_7$. A region of liquid immiscibility extends from 83.5 to 96.5 mol. percent GeO_2 at 1593 ± 5°.

Lias, S. G., Viscomi, A., Field, F. H., **Chemical ionization mass spectra. XXI. Reactions in $t\text{-}C_5H_{11}Cl$, $t\text{-}C_5H_{11}Br$, $t\text{-}C_5H_{11}OH$, and $t\text{-}C_5H_{11}SH$,** *J. Amer. Chem. Soc.* **96,** No. 2, 359-364 (Jan. 23, 1974).

Key words: alcohols; alkyl halides; chemical ionization; ion-molecule reactions; mass spectrometry; mercaptans.

Mixtures of isobutane with small amounts (0.01-1%) of added $t\text{-}C_5H_{11}Cl$, $t\text{-}C_5H_{11}Br$, $t\text{-}C_5H_{11}OH$, and $t\text{-}C_5H_{11}SH$ have been studied in a high-pressure mass spectrometer as a function of total pressure, temperature, and concentration of additive. It is seen that proton transfer occurs only to $t\text{-}C_5H_{11}SH$, and even in this case, proton transfer is a minor process. The major reaction observed with each of the four molecules is the formation of a condensation ion which dissociates rapidly to give ($C_9H_{19}^+ + HX$) or ($C_5H_{11}^+ +$ neutral products) where X is Cl, Br, OH, or SH. The formation of $C_5H_{11}^+$ is favored under all conditions, but the formation of $C_9H_{19}^+$ becomes more important as the pressure is raised or the temperature is lowered. When $i\text{-}C_4D_{10}$ is substituted for $i\text{-}C_4H_{10}$, it is seen that in the mercaptan, where proton transfer may be slightly exothermic, the departing hydrogen sulfide molecule carries away a D species from the reacting *tert*-butyl ion with a high probability; conversely, in $t\text{-}C_5H_{11}Br$, the departing hydrogen bromide molecule has a low probability of containing a hydrogen species from the reacting *tert*-butyl ion. This result suggests that when proton transfer competes with the displacement reaction, the two reactions proceed through the same intermediate ion, a $C_9H_{20}X^+$ species, in which "internal" proton transfer has occurred. The product $C_5H_{11}^+$ ion undergoes an analogous displacement reaction with all of these molecules to form the following as products: ($C_{10}H_{21}^+ + HX$) and ($C_6H_{13}^+ +$ neutral products). The $C_6H_{13}^+$ product ion also undergoes a displacement reaction with all of these molecules to form as products ($C_{11}H_{23}^+ + HX$).

Lieblein, J., **Generalized propagation of error using a new approach,** *Proc. 11th Annual Meeting of the Institute of Nuclear Materials Management, Gatlinburg, Tenn., May 25-27, 1970,* pp. 190-211 (1970).

Key words: coefficients subject to error; determinant; error propagation; implicit functions; linear equations; matrix; propagation of error; variance.

Propagation of error formulas for the case of one function of several variables or several explicitly known functions have been studied. The only untreated case remaining is the one where the "dependent" variable is an implicit function and cannot readily (or at all) be solved in terms of the independent variables. This case is treated in the present paper which takes the general matrix viewpoint and thereby obtains results in concise form. A special case is application to linear (algebraic) system, arising in an idealization of a nuclear process flow, without the necessity for obtaining the explicit solution.

Lilly, R. L., Rebbert, R. E., Ausloos, P., **Far ultra-violet photolysis of ammonia quantum yield determination for the primary process: $NH_3(ND_3) + h\nu \rightarrow NH(ND) + H_2(D_2)$,** *J. Photochem.* **2,** 49-61 (1973/74).

Key words: ammonia; extinction coefficients; far ultraviolet photochemistry; free radicals; primary processes; quantum yields.

The gas phase photolysis of NH_3-C_2D_4 and ND_3-C_2H_4 mixtures has been investigated at 147 nm (8.4 eV), 123.6 nm (10eV) and 104.8-106.7 nm (11.6-11.8 eV). The quantum yield of D_2 in the irradiation of ND_3-C_2H_4 mixtures is independent of the concentration of C_2H_4 and of the pressure of ND_3 (10 to 180 torr). It is concluded that in these mixtures D_2 is entirely formed by molecular elimination from excited ND_3. The quantum yields of such a process are as follows at these energies: 147 nm, 0.032 ± 0.005; 123.6 nm, 0.244 ± 0.01; and 104.8 – 106.7 nm, 0.306 ± 0.007 ($M/N_{ex} = 0.52 \pm 0.02$). Although the $NH_3 - C_2D_4$ photolysis data exhibit less reliability, it can be concluded that the quantum yield of molecular H_2 at 147 nm is twice that of molecular D_2. Isotope effects are much less pronounced at higher photon energies.

562-903 O - 75 - 8

Little, J. L., **ASCII code applications to alphanumeric display terminals,** *Proc. Society for Information Display Terminals, Gaithersburg, Md., Nov. 30-Dec. 1, 1971, 14,* No. 2, Second Quarter, 67-72 (1973).

Key words: alphanumeric displays; ASCII code; cathode-ray-tube displays; control functions; display terminals; interactive terminals; remote computer terminals; soft copy; text-editing displays; visual displays.

This paper reviews briefly the evolution of the American Standard Code for Information Interchange (ASCII) and its international version (ISO R-646). It also reviews the evolutionary impact of typewriters, teletypewriters and the ASCII code on conventions now employed in alphanumeric display terminals. It shows a proposed keyboard layout, some approved graphic subsets of ASCII, and some codes used in computers. Current developments in the representation of extended versions of ASCII in 7 and 8 bits are given. Proposed standards for control functions for alphanumeric display terminals are also included, with a warning that their standardization is under the jurisdiction of the American National Standards Institute's Technical Committee X3L2 on Character Codes.

Lloyd, A. C., **A critical review of kinetics of the dissociation-recombination reactions of fluorine and chlorine,** *Int. J. Chem. Kinet.* **III,** 39-68 (1971).

Key words: bimolecular; chlorine; dissociation; evaluation; fluorine; gas; recombination; review; termolecular; third body.

A critical evaluation of the rates of the dissociation and recombination reactions of fluorine and chlorine is given. Data are presented graphically and in tabular form. The effect of various third bodies is discussed. Rate expressions for specified temperature ranges are recommended, while comparison with theoretical values obtained from the Benson and Fueno theory is made where applicable.

Lovas, F. J., Johnson, D. R., **Microwave spectrum of BF,** *J. Chem. Phys.* **55,** No. 1, 41-44 (July 1, 1971).

Key words: boron monofluoride; dipole moment; discharge; microwave spectrum; quadrupole structure; rotational transitions; transient species.

Direct rotational transitions have been observed in the ground vibrational state of $^{10}B^{19}F$ and $^{11}B^{19}F$ produced in the gas phase by a discharge in flowing BF_3. Measurements on the $J=1 \leftarrow 0$ transitions yield $B_0(^{10}BF) = 48\,022.63 \pm 0.08$ MHz, $eq_0Q(^{10}B) = -9.5 \pm 0.8$ MHz, $B_0(^{11}BF) = 45\,185.77 \pm 0.06$ MHz, and $eq_0Q(^{11}B) = -4.5 \pm 0.4$ MHz. New molecular parameters are derived for ^{11}BF including $B_e = 45\,481$ MHz, and $r_e = 1.2625$ Å. The electric dipole moment of BF is determined to be 0.5 ± 0.2 D.

Lovas, F. J., Tiemann, E., Johnson, D. R., **Spectroscopic studies of the SO_2 discharge system. II. Microwave spectrum of the SO dimer,** *J. Chem. Phys.* **60,** No. 12, 5005-5010 (June 15, 1974).

Key words: centrifugal distortion; dipole moment; microwave spectrum; molecular structure; sulfur monoxide dimer; rotational spectrum.

Microwave spectra assignable to a dimer of SO have been detected in an electric discharge of SO_2. A centrifugal distortion analysis has been carried out on the spectra from the ground state and the lowest excited vibrational state of $^{16}O^{32}S^{32}S^{16}O$ and the ground vibrational state of $^{16}O^{32}S^{34}S^{16}O$. The molecule was found to have a planar *cis* configuration with the following geometry: $r(SO) = 1.458(2)$ Å, $r_s(SS) = 2.0245(6)$ Å, and $\angle SSO = 112.7(5)°$. The observed dipole moment of OSSO is $\mu = 3.17(10)$ D.

Mackay, D. R., **NBS information services on engineering standards,** *Stand. Eng.*, pp. 17-19 (June 1971).

Key words: information services; standards.

This paper covers the history of the information services provided by the National Bureau of Standards on published standards and standardization activities and describes the current activities of the Information Section of the Bureau's Office of Engineering Standards Services.

Madey, T. E., **Adsorption of oxygen on W(100): Adsorption kinetics and electron stimulated desorption,** *Surface Sci.* **33,** 355-376 (1972).

Key words: adsorption; chemisorption; desorption; electron reflection; electron stimulated desorption; oxygen; single crystal W(100); surface; tungsten; work function.

The interaction of O_2 with a single crystal W(100) surface at ~ 300 K has been examined using a combination of techniques. A precision gas dosing system was used to deposit O_2 onto the crystal; the absolute accuracy in the average flux F (molecules cm^{-2} s^1) is ± 6 percent. The initial sticking probability for 0_2 on W(100) is effectively unity; $\mathscr{S}_0 - 0.98 \pm 0.03$. The accuracy of this measurement arises from the fact that a known large fraction of the O_2 molecules entering the experimental chamber strike the crystal before reaching the mass spectrometer detector. The Electron Stimulated Desorption (ESD) measurements of absolute O^+ ion yields and energy distributions as a function of oxygen exposure were made during bombardment by 100 eV electrons. A measurable ion yield is detectable at the earliest stages of adsorption; a slight maximum in the ion yield of $\sim 5 \times 10^{-9}$ ions/electron occurs at about one half monolayer coverage. Evidence of reconstruction of the substrate at this coverage follows from this and other work. At oxygen coverages $\gtrsim 4 \times 10^{14}$ molecules cm^{-2}, a high-ion yield ESD state appears ($\sim 10^{-6}$ O^+ ions/electron). An estimate of the angular distribution of ESD-liberated O^+ ions was made using a primitive two-segment collector. The ion angular distribution is strongly peaked in the direction normal to the surface. The functional form of this distribution is not known, but if the distribution were of the form $\cos^n\theta$, the results are consistent with $n \gtrsim 14$. Implications of this observation for the possible identification of chemisorption sites are discussed. Work function changes and elastic electron reflection characteristics have been measured for the oxygen-covered and clean W(100) surface.

Madey, T. E., **Chemisorption of H_2 on W(100): Absolute sticking probability, coverage, and electron stimulated desorption,** *Surface Sci.* **36,** 281-294 (1973).

Key words: deuterium; electron stimulated desorption; hydrogen; isotope effect; probability; tungsten.

Measurements of both the absolute sticking probability near normal incidence and the coverage of H_2 adsorbed on W(100) at ~ 300 K have been made using a precision gas dosing system; a known fraction of the molecules entering the vacuum chamber struck the sample crystal before reaching a mass spectrometer detector. The initial sticking probability $\mathscr{S}_0$ for H_2/W(100) is 0.51 ± 0.03; the hydrogen coverage extrapolated to $\mathscr{S}_0 = 0$ is 2.0×10^{15} atoms cm^{-2}. The initial sticking probability $\mathscr{S}_0$ for D_2/W(100) is 0.57 ± 0.03; the isotope effect for sticking probability is smaller than previously reported. Electron stimulated desorption (ESD) studies reveal that the low coverage β_2 hydrogen state on W(100) yields H^+ ions upon bombardment by 100 eV electrons; the ion desorption cross section is $\sim 1.8 \times 10^{-23}$ cm^2. The H^+ ion cross section at saturation hydrogen coverage when the β_1 state is fully populated is $\ll 10^{-25}$ cm^2. An isotope effect in electron stimulated desorption of H^+ and D^+ has been found. The H^+ ion yield is $\gtrsim 100 \times$ greater than the D^+ ion yield, in agreement with theory.

Madey, T. E., Yates, J. T., Jr., Erickson, N. E., **Use of x-ray photoelectron spectroscopy for studies of gases chemisorbed on metals,** *Electron. Fisc. Apl.* **17,** Nos. 1-2, 190-192 (1974).

Key words: carbon monoxide; chemical shifts; chemisorption; ESCA; nitric oxide; oxygen; photoelectron spectroscopy.

X-ray photoelectron spectroscopy (ESCA) has been used in a study of O_2, NO and CO adsorbed on polycrystalline tungsten. The adsorption and oxidation studies were carried out under ultrahigh vacuum conditions. Chemical shifts of several eV in the O(ls) spectra for each of these adsorbates were found to be correlated with different modes of bonding between adsorbate and substrate. In general, the core level binding energies associated with adsorbed species are smaller than the binding energies for the same atoms in small gaseous molecules.

Mahoney, R., Srinivasan, G. R., Macedo, P. B., Napolitano, A., Simmons, J. H., **Effect of subcritical microstructure on the viscosity of a sodium borosilicate glass,** *Phys. Chem. Glasses* **15,** No. 1, 24-31 (Feb. 1974).

Key words: borosilicate; environmental-relaxation model; glass; microstructure; phase-separation; viscosity.

Viscosity and electron microscopy measurements were made on a phase separating glass as a function of time, at various temperatures. The viscosity changed by five orders of magnitude during the phase separation in a time period identified to be solely in the coarsening stage by electron microscopy. The stage during which composition changes are dominant occurs very quickly despite the high starting viscosity (10^{11} P) and, therefore, is nearly complete before reliable viscosity data can be obtained (2 min). Analysis of the rate of increase of the average particle size identified a rearrangement stage proceeding by bulk diffusion through the fluid phase with an apparent activation energy of 98 kcal × mole (4.1×10^5 J/mole). Superposition of the viscosity-microstructure size curves for various temperatures demonstrated that the change in viscosity was totally controlled by the growth of the viscous phase whose activation energy for viscosity is 132 kcal/mole (5.52×10^5 J/mole). The change of viscosity with time is explained in terms of changes in the size of the microstructure by applying an environmental relaxation model proposed by two of the authors. The significance of the good quantitative fit of the data by the model and the physical significance of the parameters are discussed.

Maki, A. G., Sams, R. L., **Infrared spectrum of CS_2: "Hot" bands associated with the 2185 cm^{-1} band and evidence for the CS_2 laser assignment,** *J. Mol. Spectrosc.* **52,** 233-243 (1974).

Key words: absorption spectra; carbon disulfide; energy levels; infrared; lasers; molecular spectra.

The $10^01 - 00^00$ band of CS_2 has been measured with a resolution of 0.030 cm^{-1}. The following "hot" bands associated with this transition were also measured and analyzed: $11^11 - 01^10$, $12^01 - 02^00$, $12^21 - 02^20$, $13^31 - 03^30$, $20^01 - 10^00$, $30^01 - 20^00$, $21^11 - 11^10$, and $22^01 - 12^00$. In addition, the $10^01 - 00^00$ bands of the isotopic species $^{13}C^{32}S_2$, $^{12}C^{32}S^{33}S$, and $^{12}C^{32}S^{34}S$ were measured in natural abundance. With the results of these measurements it is shown that the $0201 - 12^00$ transitions do indeed coincide with the CS_2 laser transitions, as do the $00^01 - 10^00$ transitions. New arguments are given favoring the latter assignment.

Malmberg, M. S., Kryder, S. J., Maryott, A. A., **Vapor phase dielectric relaxation spectra and dipole moments of paraldehyde and *cis*-1,3,5-trimethylcyclohexane,** *J. Chem. Phys. Letters to Editor* **61,** No. 6, 2476-2477 (Sept. 15, 1974).

Key words: *cis*-1,3,5-trimethylcyclohexane; dielectric; dipole moment, gas; microwave absorption; paraldehyde; relaxation.

Vapor phase dielectric relaxation spectra are obtained from measurements of microwave nonresonant absorption for paraldehyde and *cis*-1,3,5-trimethylcyclohexane. Gas dipole moments are found to be 1.43 ± .02 D and 0.25 ± .01 D respectively.

Malmberg, M. S., Maryott, A. A., **Dipole moments of $ClSF_5$ and CF_3SF_5 from the dielectric relaxation spectra of the vapors,** *J. Chem. Phys.* **53,** No. 4, 1614-1615 (Aug. 15, 1970).

Key words: CF_3SF_5; ClSF; dielectric relaxation time; dipole moment; microwave absorption; vapor phase.

The microwave absorption associated with the dielectric relaxation spectra of the symmetric-top gases, $ClSF_5$ and CF_3SF_5, was measured at various pressures up to two atmospheres at a frequency of 1216 MHz at 298 K. Values of the electric dipole moments derived from these data are 0.51_1 D for $ClSF_5$ and 0.38_4 D for CF_3SF_5.

Mandel, J., **The evaluation of standard test methods,** *Stand. News* **2,** No. 4, 17-20 (Apr. 1974).

Key words: interlaboratory studies; measurement; precision accuracy; test methods.

Test methods can be classified into two types: those for which the quantity to be measured is defined independently of the test method and those for which it is defined in terms of the test method. In either case, the evaluation of the precision and accuracy of single measurements can be made only in terms of the characteristics of the method itself. The study of a test method requires the postulation of a mathematical model which in turn determines the proper statistical method of data analysis. The interpretation of the results must be made in terms of the requirements imposed on the method by its practical applications.

Mangum, B. W., **Standard Reference Materials 933 and 934: The National Bureau of Standards' precision thermometers for the clinical laboratory,** *Clin. Chem.* **20,** No. 6, 670-672 (1974).

Key words: clinical laboratory; enzymology; health care; standard reference material; SRM 933; SRM 934; thermometers.

Because many facets of clinical laboratory work, such as enzymatic reactions, pH measurements, and blood-gas analysis, are highly sensitive to temperature, there is a need to measure temperature accurately and closely control it. To help satisfy these needs and to aid in getting a usable temperature scale into the clinical laboratory, the National Bureau of Standards has developed SRM 933 and SRM 934. These precision thermometers are calibrated at 0, 25, 30, and 37 °C. Their value to the clinical laboratory is described.

Mann, D. B., **ASRDI oxygen technology survey. Volume VI: Flow measurement instrumentation,** *NASA Spec. Publ.* **3084,** 104 pages (National Aeronautics and Space Administration, Washington, D.C. 1974).

Key words: argon; calibration; cryogenic; flowmeter, measurement; nitrogen; oxygen.

A survey of the literature combined with the results of a joint government-industry cooperative program on cryogenic flowmetering is presented. The objective was to establish the state of the technology and art of oxygen flowmetering in liquid and gaseous states.

Only those meters with demonstrated performance are considered. These were classified as quantity, head, momentum and velocity types. A comparison of the performance of these devices and a discussion of future requirements for flow reference systems and metering are given.

Mann, W. B., **Radioactive calorimetry—a review of the work at The National Bureau of Standards,** (Proc. First Int. Summer School on Radionuclide Metrology, Herceg Novi, Yugoslavia, Aug. 21-Sept. 1, 1972), *Nucl. Instrum. Methods* **112,** No. 1/2, 273-277 (Sept.-Oct. 1973).

Key words: intercomparative measurements; nickel-63; radioactive calorimetry; radioactive standardization.

Calorimetric measurements in the field of radioactivity will be reviewed with special reference to the standardization of ^{63}Ni. Intercomparative measurements with the National Research Council of Canada and Atomic Energy of Canada Limited will be discussed.

Marezio, M., Dernier, P. D., Santoro, A., **Twinning in Cr-doped VO_2,** *Crystallogr.* **A29,** 618-621 (1973).

Key words: chromium doping; metal-insulator transitions; twinning; vanadium oxide; x rays.

Twinning has been studied in several samples of VO_2 containing substitution solid solution 0.5 and 2.5 at.% Cr. The twinning is by reticular pseudo-merohedry and it is controlled by the tetragonal pseudo-symmetry of a superlattice obtained from the original monoclinic cell ($a \simeq 9.1$, $b \simeq 5.8$, $c \simeq 4.55$ Å, $\beta \simeq 90$) by means of the transformation 100/002/010. More than one twin law is found in every sample studied. All the theoretically possible twin laws, except one, have been observed. The possibility of twinning simulating a lattice and a space group different from the true ones has been pointed out and methods for detecting twins in these cases are given.

Marlowe, D. E., Sushinsky, G. F., Dexter, H. B., **Elastic torsional buckling of thin-walled composite cylinders,** *Amer. Soc. Test. Mater. Spec. Tech. Publ.* **546,** pp. 84-108 (1974).

Key words: composite materials; elastic buckling; reinforced aluminum; stability; thin shells; torsional buckling.

The elastic torsional buckling strength has been determined experimentally for thin-walled cylinders fabricated with glass/epoxy, boron/epoxy, and graphite/epoxy composite materials and composite-reinforced aluminum and titanium. Cylinders have been tested with several unidirectional-ply orientations and several cross-ply layups. Specimens were designed with diameter-to-thickness (D/t) ratios of approximately 150 and 300 and in two lengths (L), 10 in. (25.4 cm) and 20 in. (50.8 cm).

The results of these tests were compared with the buckling strengths predicted by the torsional buckling analysis of Chao. In this analysis, the instability loads of heterogeneous anisotropic cylinders are calculated with Timoshenko's equilibrium equations. The computer program associated with the analysis seeks the solution with the lowest buckling strength by iterating on the number of circumferential buckling waves. For the cylinders considered ($L/r = 3.3$ and $L/r = 6.7$), the experimental buckling torques were approximately 85 percent of the torques predicted by the Chao analysis. In the cross-ply laminate cylinders, the stacking sequence of the plies was found to have a marked effect on the elastic buckling torque.

Reversal of the stacking sequence of the cross-plied cylinders resulted in buckling torques which differed by a factor of 2. Similar results were obtained by reversal of the direction of twist on the original stacking sequence. This observation may be important in applications where reversal of loading can occur. The size effect of linear scaling was investigated for cylinders whose dimensions were different but whose L/r and D/t ratios were the same. As expected from the analysis, the experimental buckling stress remained constant.

Marsden, C. P., **The formation and growth of Committee F-1,** *ASTM Stand. News* **1,** No. 4, 24-28 and 54 (Apr. 1973).

Key words: ASTM; history; semiconductors; vacuum tubes.

The organization of Committee F-1, an outgrowth of Committee B-4, was formalized on June 27, 1955. Since that time, the committee has tripled its membership and increased the number of documents under its jurisdiction by a factor of six to a total of 122 documents. While retaining the original number of ten subcommittees, it has reorganized these subcommittees away from the vacuum tube industry towards the semiconductor technology. It has assumed projects on lasers and memory cores and plans to assume other aspects of the electronic technology.

Marshall, R. D., Hsi, G., **Techniques for measuring wind loads on full-scale buildings,** (Proc. U.S.-Japan Research Seminar on Wind Loads on Structures, Honolulu, Hawaii, Oct. 19-24, 1970), Paper in *Proc. of Seminar Wind Loads on Structures*, pp. 133-148 (University of Hawaii, Honolulu, Hawaii, 1970).

Key words: buildings; full-scale tests; instrumentation; pressure fluctuations; statistical analysis; wind loads.

Wind pressure measurements are being made on a four-story building on the National Bureau of Standards campus at Gaithersburg, Md. Field data will be used to develop new design criteria and to improve wind tunnel modeling techniques. Simultaneous wind velocity measurements from six meteorological towers make it possible to relate pressure distributions and fluctuations on the building to the undisturbed wind field.

Marshall, R. D., **Surface pressure fluctuations near an axisymmetric stagnation point,** *Fluid Dyn. Trans.* **5,** Part II, 135-163 (1970).

Key words: disk; pressure fluctuations; turbulence.

Surface pressure fluctuations on a circular disk placed normal to a turbulent air stream have been investigated. Turbulence intensities of approximately 10 percent were produced by a coarse grid installed at the test-section entrance. The turbulent field in the neighborhood of the disk was homogeneous and nearly isotropic.

Experimental results indicate that existing linear theories which do not consider distortion of the flow fail to predict the nature of surface pressure fluctuations on a bluff body. Only for wavelengths which are large compared to the body do these theories yield satisfactory results. A strong attentuation of the high frequency components occurs as the flow stagnates. This is accompanied by a transfer of energy from short to long wavelengths. The opposite effect is observed as the flow attains a radial direction and approaches the edge of the disk. A neutral wavelength which undergoes little change in energy was observed. Integral scales of pressure fluctuations are much larger than the lateral integral scale of the free-stream turbulence.

Pressure-velocity correlations indicate the existance of two distinct regions, an inner region in which correlations and optimum delay times exhibit considerable change along the radius of the disk, and an outer region where there is little dependence on radial distance. Maximum values of the optimum correlations are found in the outer region. There is qualitative agreement between the experimental results and theoretical predictions which consider the effect of vortex stretching.

Martin, W. C., **Low-energy level structure of neutral cerium (Ce I),** *Phys. Rev. A* **3,** No. 6, 1810-1815 (June 1971).

Key words: atomic energy levels; atomic spectra; electron configurations; neutral cerium; Zeeman effect.

The low portion of an extensive level structure derived from analysis of the optical spectrum is reported. Positions, J values, and g_J factors are given for 98 levels, including all 91 levels expected below 10 000 cm^{-1}. A previous report on this analysis showed the ground level to be $4f5d6s^2\ {}^1G_4^\circ$, and gave the lowest levels of $^4f5d^26s$. Comparison of the observed odd-parity levels with calculations by Goldschmidt and Salomon shows that all 86 of the odd levels tabulated here belong to these configurations. All but seven of these odd levels are assigned LS names, although the calculations show that many of them have low LS purities, and a few have strong mixtures of the two configurations. The much simpler system of even levels below 10 000 cm^{-1} includes only the six levels of $4f^26s^2\ {}^3H$ and ^3F, beginning with $^3H_4$ at 4762.718 cm^{-1} above the ground-state level. The table of even levels also includes $4f^26s^2\ {}^1G_4$ and the lowest two levels of each of the lowest two terms of $4f^25d6s$, $^5I_{4,5}$, and $^5K_{5,6}$.

Maryott, A. A., Farrar, T. C., Malmberg, M. S., **^{35}Cl and ^{19}F NMR spin-lattice relaxation time measurements and rotational diffusion in liquid ClO_3F,** *J. Chem. Phys.* **54,** No. 1, 64-71 (Jan. 1, 1971).

Key words: angular-momentum; correlation-times; molecular-reorientation; NMR-relaxation-times; ^{19}F; ^{35}Cl.

The NMR spin-lattice relaxation times of ^{35}Cl and been ^{19}F have measured by pulse techniques over the entire liquid range of ClO_3F (130-368 K). The chlorine relaxation which is due solely to the nuclear quadrupole interaction can be used together with the known quadrupole coupling constant to determine the correlation time for molecular orientation, $\tau_{\theta,2}$. The fluorine relaxation is dominated by the spin-rotation interaction with only a small intermolecular dipole contribution at the lowest temperatures. In order to obtain the angular momentum correlation time, τ_J, an independent estimate of the spin-rotation tensor was made by combining gas-phase measurements of $T_1(^{19}F)$ with previous data on the chemical shift and gas-phase dielectric relaxation. The results for this quasispherical molecule are in accord with rotational diffusion theory and Hubbard's relation, $\tau_{\theta,2}\tau_J = I/6kT$, at the lowest temperatures and agree over the entire range with the extended treatment of McClung.

Mayer, I., Roth, R. S., Brown, W. E., **Rare earth substituted fluoride-phosphate apatites,** *J. Solid State Chem.* **11,** 33-37 (1974).

Key words: crystal structure; $Ln_xM_{10-2x}Na_x(PO_4)_6F_2$; rare earth apatites.

Compositions with the general formula $Ln_xM_{10-2x}Na_x(PO_4)_6F_2$ (Ln = La, Pr, Nd, Sm, Eu, Dy, Er, Lu, and Y; M = Ca, Sr, and Ba) have been prepared and studied by x-ray diffraction methods. The hexagonal apatite like structure was indicated by the powder patterns of all the compounds (with Ba compounds only when Ln = La through Sm). Single crystal precession data reveal that the crystal lattice of all the compositions in the Ca and Sr system have space group $P6_3/m$, the $Ln_2Ba_6Na_2(PO_4)_6F_2$ compounds crystallize in space group $P6$ and the $Ln_3Ba_4Na_3(PO_4)_6F_2$ compounds in the trigonal space group $P3$. Order and disorder mechanisms of the substitution and its dependence on size and polarization effects are discussed.

McClendon, L. T., DeVoe, J. R., **Substoichiometric radioisotope dilution analysis of tungsten as a major constituent in molybdenum containing materials using toluene-3,4-dithiol,** *Anal. Chem.* **41,** No. 11, 1454-1456 (Sept. 1969).

Key words: molybdenum; radioisotope dilution; substoichiometric; toluene-3,4-dithiol; tungsten.

A radioisotope dilution procedure was developed for tungsten determination in molybdenum containing materials using a substoichiometric amount of the complexing reagent, toluene-3,4-dithiol. Using this approach, an equal amount of tungsten is isolated before and after dilution of the radioisotope, thus avoiding serious interferences by eliminating the need for quantitative separation. This technique was used for tungsten determination in NBS tungsten-molybdenum alloy (SRM-480) indicate composition of alloy found by standard method where the average concentration found was 79.32 percent with a pooled estimate of the standard deviation (for a single determination) of ±0.43 percent. The precision obtained is very good for this type of technique.

McLaughlin, W. L., Kosanić, M., **The gamma-ray response of pararosaniline cyanide dosimeter solutions,** *Int. J. Appl. Radiat. Isotop.* **25,** No. 6, 249-262 (June 1974).

Key words: dosimetry; dyes; dye yield; gamma rays; pararosaniline cyanide; 4,4′,4″-triaminotriphenylacetonitrile; triphenyl-methane dyes.

Triphenylmethane dye derivatives, especially the colorless nitriles in organic or aqueous solution, serve as convenient radiation dosimeters. With large absorbed doses (10^3-10^6 rads), permanent ionized dye is produced with sufficient color for routine photometric measurement. If a polar solvent is used and the solution is oxygenated and stabilized by weak acid, the optical density measured at the absorption maximum of dye is a linear function of dose. Dye yield varies with the type of solvent, concentration of the dye precursor, temperature during irradiation, acid and oxygen content and batch of dye precursor used. Additions of small amounts of acid to solutions prevent back reactions. Dissolved oxygen or a weak oxidizing agent helps extend the dose range of response by scavenging free-radical agents formed in the solvent during irradiation. Suitable plastic containers may be used, without the need for ultraclean handling procedures or superdistilled solvents. Since the main sources of systematic error are easily controlled and since the new dosimeter solutions may be used over a wide dose range, they show advantages over other chemical dosimeters for many applications.

McNesby, J. R., **Standard reference materials for air pollution,** *Proc. Tech. Conf. on the Observation and Measurement of Atmospheric Pollution (TECOMAP), Helsinki, Finland, July 30-Aug. 4, 1973,* Special Environmental Report No. 3, 595-603 (World Meteorological Organization, Geneva, Switzerland, 1974).

Key words: air pollution; Standard Reference Materials.

The compatibility and accuracy of air pollution measurements depends strongly upon the integrity of the measurement standards to which calibration gases are referred. For this reason it is essential that great care be exercised in establishing scientifically their integrity. The emphasis at the U.S. National Bureau of Standards is being placed upon the development of Standard Reference Materials for those air contaminants designated by the U.S. Environmental Protection Agency as ambient air pollutants, i.e., particulate matter, SO_2, NO_x, CO, hydrocarbons, and photochemical oxidants. Standard Reference Materials must be developed also in different concentration ranges for automobile exhaust and for point source effluents. All of these categories are under development at the National Bureau of Standards.

Mebs, R. W., Carter, G. C., Evans, B. J., Bennett, L. H., **NMR chemical shifts in cuprous salts: The magnetic moment of Cu,** *Solid State Commun.* **10,** No. 9, 769-774 (1972).

Key words: chemical shifts; copper (I) compounds; copper salts; Knight shift; magnetic moment; nuclear magnetic resonance.

An extensive study has been made of chemical shifts of the ^{63}Cu resonance in a number of cuprous salts. The observed trend in chemical shifts for the cuprous halides is in disagreement with theoretical ionicity estimates of either Pauling or Phillips. This trend has been explained by taking into account the relative importance of π bonding for the different halides. On the basis of the present data, CuBr is the most suitable Knight shift reference compound. The measurements indicate $\mu = 2.2206$ nm for ^{63}Cu and $\mu = 2.3791$ nm for ^{63}Cu for reference moment, without diamagnetic correction.

Meijer, P. H. E., Scherer, W. D., **Phonons and lambda temperature in liquid ^{4}He as obtained by the lattice model,** (Proc. 13th Int. Conf. on Low Temperature Physics, Boulder, Colo., Aug. 21-25, 1972), Paper in *Low Temperature Physics-LT 13,* K. D. Timmerhaus, W. J. O'Sullivan and E. F. Hammel, Eds., 1, 84-86 (Plenum Publ. Corp., New York, N.Y., 1974).

Key words: helium four; lambda temperature; lattice model; phonons.

This paper describes the density of the condensate in helium four from $T = 0$ to the lambda temperature using an extension of the Matsubara Matsuda Lattice model.

Meinke, W. W., **The ultimate contribution of nuclear activation to analysis,** *J. Radioanal. Chem.* **15,** 419-433 (1973).

Key words: accuracy limits; activation analysis; activation spectrometry; analytical chemistry; measurement biases; ppb; ppm; real samples; Standard Reference Materials; trace element analysis.

This paper challenges the implied accuracy of many of the analytical results below the ppm level reported in the literature. The present status of trace element techniques including activation analysis is evaluated. Practical experiences at NBS in the use of clean facilities, ultrapure reagents and special clean containers for obtaining trace composition values with known accuracy for the certification of Standard Reference Materials are described. The use of recently certified NBS Standard Reference Materials to aid the trace analyst in the biological and geochemical areas in understanding the biases of their methods is also described.

Activation spectrometry (i.e., nondestructive analysis) as opposed to activation analysis involving radiochemical separations, has the limitations of other spectrometries. However, nuclear activation analysis with careful attention to the principles of accurate measurement should be able to lower the limits of meaningful measurement of many inorganic elements several orders of magnitude during the next decade.

Melmed, A. J., Carroll, J. J., **Oxidation of (011) iron at room temperature: Mainly LEED aspects,** *J. Vac. Sci. Technol.* **10,** No. 1, 164-169 (Jan.-Feb. 1973).

Key words: ellipsometry; low energy electron diffraction; metal oxidation; oxidation kinetics; oxide structure; surface potential.

The interaction of oxygen with (011) Fe at room temperature has been investigated using simultaneous combinations of LEED, ellipsometry, and surface potential measurements. This paper is concerned mainly with the LEED aspects. The sequence of LEED patterns found was either similar to that previously found or slightly different, depending on experimental conditions. In most experiments a new LEED pattern, $p(2\times1)$, was observed instead of the $c(3\times1)$ pattern previously reported. Direct keying of the LEED patterns to the ellipsometry-derived growth kinetics leads to further understanding of the oxidation mechanism. The occurrence of heterogeneous oxide nucleation is supported, and it is shown that an oxide consistent with the expected diffraction properties of FeO grows to a "limiting" thickness of about 25-30 Å in oxygen. The terminal oxide in the air is concluded to have about the same thickness but a significantly different structure.

Merris, R. L., Pierce, S., **The Bell numbers and *r*-fold transitivity,** *J. Combinatorial Theory* **12,** No. 1, 155-157 (Jan. 1972).

Key words: Bell numbers; permutation group; *r*-fold transitivity; Stirling numbers.

Let G be a permutation group of order $|G|$ acting on a set of n elements. For $g \in G$, let $\theta(g)$ be the number of elements left fixed by g. Then, for $1 \leq r \leq n$,

$$\sum_{g\in G} (\theta(g))^r \geq X_r|G|$$

with equality if and only if G is r-fold transitive. Here, X_r is the r-th Bell number.

Merris, R., Pierce, S., **Monotonicity of positive semidefinite hermitian matrices,** *Proc. Amer. Math. Soc.* **31,** No. 2, 437-440 (Feb. 1972).

Key words: character; Kronecker power; symmetric group; tensor power.

Inequalities which compare elements of the convex cone of positive semidefinite hermitian matrices with products of roots of elements are proved. They yield inequalities for Schur functions (generalized matrix functions) which, when specialized to the determinant, give a result of R. Bellman and L. Mirsky.

Meshkov, S., **How good are symmetry predictions?** (Proc. Int. Conf. on Symmetries and Quark Models, Wayne State University, Detroit, Mich., June 18-20, 1969), Paper in *Proceedings of the International Conference on Symmetries and Quark Models*, R. Chand, Ed., pp. 199-209 (Gordon and Breach, New York, N.Y., 1970).

Key words: exotic; mesons; reactions; structure; $SU(6)_W$; symmetry.

A summary discussion of the comparison of experiment and $SU(6)_W$ reaction predictions is presented.

Meyerson, M. R., **International voluntary standards,** *Food Technol.*, pp. 58 and 62 (Nov. 1972).

Key words: consumer standards; DoC-NBS voluntary product standards; international standardization; international trade; national standards.

Various aspects of the activities of the National Bureau of Standards in national programs of voluntary consensus standards writing are discussed, and the operation of the DoC-NBS Voluntary Product Standards Program described. This is followed by observations and a discussion of the role of standardization in international trade.

Mies, F. H., **Ultraviolet fluorescent pumping of OH 18-centimeter radiation in comets,** *Astrophys. J.* **191,** L145-L148 (Aug. 1, 1974).

Key words: comet; fluorescence; OH; optical pumping; radiowave spectrum.

In the absence of collisions, optical pumping of cometary OH by solar ultraviolet radiation determines the relative population of OH molecules in the Λ-doubled levels of the $^2\Pi_{3/2}$ ground state. The distribution is extremely sensitive to the heliocentric radial velocity of the comet, and at appropriate velocities the level populations will be either inverted or anti-inverted. Thus the OH 18-cm spectrum of a comet, measured with respect to the 10 K galactic background at 1665 and 1667 MHz, may be observed either in *emission* or in *absorption* at different periods during the trajectory. Optical pumping also will produce an alignment of the magnetic sublevels along the axis of the incident solar radiation, and variable degrees of linear polarization are expected.

Miller, E. F., Jr., Lindamood, G. E., **Structured programming: Top-down approach,** *Datamation* **19,** No. 12, 55-57 (Dec. 1973).

Key words: GOTO statements; hierarchical design; programming; structured programming; top-down design.

Structured programming is the topic of considerable current interest and discussion in computing circles. This informal, tutorial article explains the basic concepts of structured programming—GOTO-less programming, top-down design, and abstract resources—and traces their origins.

Miller, L. D., Schima, F. J., **The half-life of ^{129m}Xe,** *Int. J. Appl. Radiat. Isotop.* **24,** 353 (1973).

Key words: gamma-ray energy; half-life; isomeric ^{129}Xe; radioactivity; transition probability.

The decay of the isomeric level in ^{129}Xe has been studied by means of Ge(Li) and Si(Li) detectors. Sources of the isomeric activity were prepared by (n,γ) reaction on isotopically enhanced ^{128}Xe ion implanted in Al foil. Two γ-rays have been observed. The energies and estimated standard errors were found to be $39.50 \pm .17$ and $196.46 \pm .02$ keV. The isomeric half-life and estimated standard error have been determined to be $8.89 \pm .02$ days. The reduced transition probabilities of the four M4 isomers of Xe are compared to the quasiparticle theory.

Moldover, M. R., **Visual observation of the critical temperature and density: CO_2 and C_2H_4,** *J. Chem. Phys.* **61,** No. 5, 1766-1778 (Sept. 1, 1974).

Key words: C_2H_4; carbon dioxide; CO_2; critical density; critical point; critical temperature; ethylene; temperature reference point.

The critical temperature (T_c) and density (ρ_c) of carbon dioxide (CO_2) and ethylene (C_2H_4) have been determined by a modern version of the classical technique of visual observation of the disappearance of the meniscus. We discuss in some detail what a "visual observation of the disappearance of the meniscus" is, a subject that is relevant to the possible use of critical temperatures as secondary temperature reference points. For CO_2 we find $T_c = 30.977 \pm 0.004$ °C and $\rho_c = 0.4678 \pm 0.0022$ g/cm³. For C_2H_4 we find $T_c = 9.194 \pm 0.004$ °C and $\rho_c = 0.2146 \pm 0.0006$ g/cm³. The errors quoted for ρ_c are two standard deviations from a fit to an assumed symmetrical scaling equation of state. The errors quoted for T_c are an "estimated" limit of error. A comparison of the values of T_c which we have measured with recent *PVT* data yields new values for the critical pressures (P_c). We find that $P_c = 73.753$ bar (72.789 atm) for CO_2 and $P_c = 50.390$ bar (49.731 atm) for C_2H_4.

Molino, J. A., **Equal aversion levels for pure tones and 1/3-octave bands of noise,** *J. Acoust. Soc. Amer.* **55,** No. 6, 1285-1289 (June 1974).

Key words: audition; aversion for sound; escape and avoidance; loudness; noisiness; psychophysics; schedules of reinforcement.

College students tapped rapidly on a telegraph key to reduce the intensity of a continuous acoustic stimulus presented through earphones. Failure to respond resulted in an intensity of 1 dB every 4 sec. A group of 14 students responded during 10-min sessions to eight pure tones and eight 1/3-octave bands of noise at octave frequencies from 63 Hz to 8 kHz. The average SPL maintained by the subjects became stable after about 5 min. The different asymptotic levels observed from 5-10 min were taken as a measure of equal aversion levels for the stimuli. Equal aversion levels were compared with other subjective weighting contours: equal loudness level, *A*-weighted sound level, perceived noise level, etc. They were closest to an *A*-weighted sound level of 80-85 dB.

Molino, J. A., **Odor pollution detection and measurement,** *ASTM Stand. News Letter to Editor* **1,** No. 3, 47 (Mar. 1973).

Key words: pollution; psychophysics.

This paragraph proposes the organization of a committee, task force, or working group to study psychophysical measurement techniques and data concerning human tolerance to and permissible standards for various sorts of pollution, e.g., odor, noise, glare, vibration, etc.

Mopsik, F. I., **Dielectric constant and loss,** Chapter 3 in *Digest of Literature on Dielectrics* **32,** 76-99 (National Academy of Sciences, Washington, D.C. 1970).

Key words: dielectric constant; dielectric literature; dielectric loss; dielectric theory; digest of literature; ionic processes.

The coverage of this chapter is a direct continuation of last year's chapter. The papers included are those abstracted during 1968 by *Chemical Abstracts* and *Physics Abstracts* and are those that are concerned with dielectric theory, either theoretical or experimental. No attempt has been made to include papers that would adequately be covered by the preceding chapter.

Mopsik, F. I., **High pressure dielectric measurements and the theories for the dielectric constant of a liquid,** *Proc. Conf. Electrical Insulation and Dielectric Phenomena, Buck Hill Falls, Pa., Oct. 20-22, 1969,* pp. 64-68 (National Academy of Sciences, Washington, D.C., 1970).

Key words: density; dielectric constant; dielectric theory; dipole moment; high pressure; liquids; polarizability.

The conventional approach to the examination of the validity of the theories for the dielectric constant of the liquid state is to use dielectric measurements over a range of temperature and perhaps, also refractive index measurements. However, density is one of the most important variables in these theories and the molecular parameters involved could be mildly density dependent. Therefore a more valid approach is to combine high pressure dilatometry with dielectric measurements so that temperature and density dependencies of the dielectric constant can be separated.

Results of measurements to 2 kbar over a moderate range of temperature for several liquids will be presented and examined in order to establish the validity of dielectric theory.

Morrissey, B. W., Stromberg, R. R., **The conformation of adsorbed blood proteins by infrared bound fraction measurements,** *J. Colloid Interface Sci.* **46,** No. 1, 152-164 (Jan. 1974).

Key words: blood proteins; infrared bound fraction; protein adsorption; protein conformation.

The likelihood that surface-induced blood coagulation results from specific protein-material interactions has led to a study of the conformation of adsorbed blood proteins. Infrared difference spectroscopy was used to determine the bound fraction, i.e., the fraction of carbonyl groups of an adsorbed molecule directly interacting with the surface, of serum albumin, prothrombin, and fibrinogen *in situ*. Measurements were carried out on individual proteins as a function of the amount adsorbed, time of absorption, pD, and ionic strength using a silica surface.

The results obtained for serum albumin and prothrombin indicate that the internal bonding of these globular proteins is sufficient to prevent changes in the structure while adsorbed, even at low surface population. The bound fraction of fibrinogen increases with increasing adsorbance, suggesting possible interfacial aggregation. The conformation of all three proteins was found to be independent of the time of adsorption, although major differences in the rates of adsorption were observed.

Studies of cross-linked and denatured serum albumin have provided information on the conformational changes concomitant with adsorption of the native protein. Qualitatively, such changes, if they occur, are small. This conclusion is supported by computer simulation studies of lysozyme adsorption. Studies of the effect of pD and ionic strength on the adsorbance and bound fraction of serum albumin show that caution must be exercised when identifying the plateau adsorbance of a protein isotherm with a close-packed monolayer.

Mount, G. H., Linsky, J. L., **One- and multicomponent models of the upper photosphere based on molecular spectra. II: CN(1,1) of the CN violet system,** *Solar Phys.* **35,** 259-276 (1974).

Key words: best-fit model; carbon abundance; molecular spectra; upper photosphere.

We have obtained center-to-limb photoelectric spectra of the CN(1,1) B-X bandhead region λ3868-3872 Å at Kitt Peak National Observatory. From these spectra and a detailed analysis of the formation of the CN(1,1) spectrum we derive a best-fit upper photospheric model differing from the HSRA which is consistent with our previous CN(0,0) λ3883 spectra. We derive a solar carbon abundance of $\log A_c = 8.30 \pm 0.10$ compared to the HSRA value of $\log A_c = 8.55 \pm 0.10$. In addition we specify the regions of formation for the CN(0,0) λ3883.35 and CN(1,1) λ3871.38 bandheads at disc center and limb.

Mount, G. H., Linsky, J. L., **One- and multi-component models of the upper photosphere based on molecular spectra. III: CH(O,O) λ3144 of the CH C-X system,** *Solar Phys.* **36,** No. 2, 287-298 (June 1974).

Key words: best-fit model; carbon abundance; molecular spectra; upper photosphere.

We have obtained accurate center-to-limb photoelectric spectra of the CH(0,0) C-X bandhead region λ3143-3148 Å at Kitt Peak National Observatory. From these spectra and a detailed analysis of the formation of the CH(0,0) spectrum we demonstrate that the best-fit upper photospheric model derived from our previous analyses of CN(0,0) and CN(1,1) spectra adequately explains the CH C-X observations. In addition we derive a solar carbon abundance of log $A_c = 8.30 \pm 0.20$ compared to the HSRA value of log $A_c = 8.55$. This confirms our previous CN analyses which demonstrated that if the HSRA nitrogen abundance of log $A_N = 7.93 \pm 0.10$ is assumed, then log $A_c = 8.20 \pm 0.10$. We also specify the regions of formation for the CH(0,0) λ3143.47 Å bandhead at disc center and limb.

Natrella, M. G., **Design and analysis of experiments,** Section 27 in *Quality Control Handbook, Third Edition*, J. M. Juran, F. M. Gryna, Jr., and R. S. Bingham, Jr., Eds., pp. 27-1—27-49 (McGraw Hill Book Co., New York, N.Y., 1974).

Key words: analysis of variance; block designs; design of experiments; factorial designs; interlaboratory tests; mixture designs.

This chapter provides an introduction to the design and analysis of experiments, including a classification of designs and a summary of important recent developments. Detailed designs and methods of analysis are given for factorial and fractional factorial designs, for completely randomized designs, and for the more common types of block designs (e.g., randomized blocks, balanced incomplete blocks, Latin Squares). Descriptions are given of some special-purpose designs, such as mixture designs, group screening designs and crossover designs. Some simple techniques that are useful in planning and analyzing the results of interlaboratory tests are included.

Newbury, D. E., Christ, B. W., Joy, D. C., **Relevance of electron channeling patterns to embrittlement studies,** *Met. Trans.* **5,** 1505-1508 (June 1974).

Key words: cleavage surfaces; electron channeling contrast; embrittled iron; grain surfaces; scanning electron microscopy.

The new technique of scanning electron microscopy utilizing electron channeling contrast has been applied to the study of fracture surfaces of embrittled iron. The degradation of electron channeling patterns with increasing amounts of surface layer (11 mn deep) deformation is an ideal tool for qualitatively measuring plastic flow in small areas (10 μm diameter) of fracture surfaces. Electron channeling patterns were obtained from grain surfaces and cleavage surfaces. It was always possible to obtain channeling patterns from grain surfaces, but there were many regions on cleavage surfaces where electron channeling contrast was completely eliminated. Variations in the amount of plastic flow were evident from point to point on both grain surfaces and cleavage surfaces.

Newbury, D. E., Yakowitz, H., **Magnetic domain studies in iron-3 1/4 weight percent silicon transformer sheet using the scanning electron microscope,** (Proc. 18th AIP Conf. on Magnetism and Magnetic Materials, (19th Annual Conf.), Boston, Mass., Nov. 13-16, 1973), Paper in *Magnetism and Magnetic Materials*, C. D. Graham, Jr., and J. J. Rhyne, Eds., pp. 1372-1376 (American Institute of Physics, New York, N.Y., 1974).

Key words: iron-silicon transformer alloy; magnetic contrast; magnetic domains; scanning electron microscope.

The form of the magnetic domain configuration of oriented transformer sheet plays an important role in determining the magnitude of power losses during use of the sheet. In the present work, a recently developed technique for observation of magnetic domains in iron in the scanning electron microscope (SEM) has been employed. The mechanism by which this magnetic contrast arises, and the electron-optical and signal processing requirements to obtain the contrast are described. The maximum value of the contrast is about 0.3 percent with an accelerating potential of 30kV. Changes in the domain configuration due to residual strain gradients, inclusions, and applied magnetic fields have been studied in the SEM using this contrast.

Nicholson, W. L., **Some revised approaches to x-ray crystal structure analysis calculations,** Paper in *Critical Evaluation of Chemical and Physical Structural Information*, D. R. Lide, Jr., and M. A. Paul, Eds., pp. 45-47 (National Academy of Sciences, Washington, D.C., 1974).

Key words: least squares; robust techniques; statistics.

This note is a progress report on a reanalysis of the International Union of Crystallography (IUCr) Single-Crystal Intensity Measurement Project on d(+)—tartaric acid. X-ray structure factor data are currently being analyzed by classic least squares procedures with complex pseudo-theoretical model components to account for observed inadequacies of the classic model, a linear combination of Gaussian characteristic functions. The purpose of the present reanalysis is to illustrate that introduction of terms for systematic error into the classic model and use of fitting techniques not crucially dependent on the Gaussian error assumption may bring the results of supposedly discrepant collaborative studies into agreement.

Nyyssonen, D., **Partial coherence in imaging systems,** *Opt. Eng.* **13,** No. 4, 362-367 (July-Aug. 1974).

Key words: coherence measurement; microdensitometry; optical imaging; partial coherence.

An improved method of measuring spatial coherence is described and some sources of measurement errors are discussed. Partial coherence in the image plane of an optical system is discussed and results of coherence measurements are given that demonstrate the scaling of the coherence function for coherence intervals large compared to the diameter of the Airy disk and the limiting value for the coherence interval equal to the diameter of the Airy disk. The application of these results to microdensitometry is discussed and results of coherence measurements in the source plane of currently-used classical microdensitometers are given.

Orvini, E., Gills, T. E., LaFleur, P. D., **Method for determination of selenium, arsenic, zinc, cadmium, and mercury in environmental matrices by neutron activation analysis,** *Anal. Chem.* **46,** No. 9, 1294-1297 (Aug. 1974).

Key words: activation analysis; arsenic; cadmium; environmbnt; mercury; pollution; radiochemical separations; selenium.

A procedure has been developed for the simultaneous determination of selenium, arsenic, zinc, cadmium, and mercury in different environmental matrices. The radiochemical separation method involves the combustion of the samples, followed by reduction with carbon monoxide and volatilization of the metals at high temperature. The method was initially tested with radiotracer experiments; then by analyzing some NBS Standard Reference Materials. The procedure has been used to determine the Se, As, Zn, Cd and Hg concentration of some new Standard Reference Materials being prepared by the National Bureau of Standards.

Paffenbarger, G. C., Rupp, N. W., **Composite restorative materials in dental practice: A review,** *Int. Dent. J.* **24,** No. 1, 1-11 (Mar. 1974).

Key words: abrasion resistance; BIS-GMA; coefficient of thermal expansion; composite resin; compressive strength; silane coupling agent; silicate filler.

This review of the literature concerning composite resins discusses the composition, physical properties, uses and the manipulation techniques for some current, 1973, commercial products. These restorative materials are based upon the BIS-GMA resin reinforced with inorganic silicious fillers bonded to the resin matrix with a silane

coupling agent. Their use is limited to the restoration of non-load bearing surfaces of the teeth.

Pardoe, G. W. F., Larson, S. J., Gebbie, H. A., Strickler, S. J., Ingham, K. D., Johnson, D. G., **Far-infrared spectrum of** *ortho*-xylene, *J. Chem. Phys. Letters to Editor* **52,** 6426-6427 (1970).

Key words: far infrared; *ortho*-xylene; torsional vibration.

Far infrared measurements have been made on *ortho*-xylene in the liquid and vapor phases. A band in the region of 180 cm^{-1} is plausibly assigned to a torsional vibration of methyl groups.

Peterson, R. L., Day, G. W., Gruzensky, P. M., Phelan, R. J., Jr., **Analysis of response of pyroelectric optical detectors,** *J. Appl. Phys.* **45,** No. 8, 3296-3303 (Aug. 1974).

Key words: detectors; gold-blacks; optical radiation detectors; optics; polymers; pyroelectric detectors; pyroelectricity; self-calibrated detectors.

Several configurations of pyroelectric optical-radiation detectors are mathematically modeled to determine their frequency response and current response to step-function heat inputs. Included in the analysis are heat losses by conduction and reradiation, effects of absorptive coatings, and an experimentally observed nonuniformity of polarization through the thickness of polymer pyroelectric films. Roll-off of the frequency response at both low and high frequencies is carefully examined. Curve fitting to response data allows a quantitative determination of the pyroelectric coefficient and the degree of nonuniformity of the polarization. The thermal conductivities of gold blacks used as absorbers are determined from the high-frequency data together with independent measurements of the black thicknesses and densities. The total emissivity of evaporated nickel films sometimes used as absorbers can be estimated from the low-frequency data. The difference in response to optical and electrical heat inputs is examined as a part of our effort in fabricating electrically self-calibrating optical detectors.

Phelan, R. J., Peterson, R. L., Klein, G. P., Hamilton, C. A., Day, G. W., **Absolute, pyroelectric radiometers and two dimensional arrays,** *Proc. American Electro-Optical Systems Design Conference, New York, N.Y., Sept. 18-20, 1973,* pp. 117-123 (1973).

Key words: IR detectors; polyvinylfluoride; pyroelectrics; radiometers.

In pursuit of useful techniques for measurements of laser power and beam profiles, we have been developing some pyroelectric detector devices and systems. The power measurements are based on electrical substitution techniques and thus do not require standard optical sources. The beam profiles have been measured using two axis mirror scanners with a single detector, single axis scanners with linear arrays, and two dimensional arrays of pyroelectrics. We will briefly discuss the general calibration scheme to indicate why we are using pyroelectrics, give some of the properties of pyroelectrics, give some of the details of device construction, describe a few systems and give some experimental results.

Powell, C. J., **Attenuation lengths of low-energy electrons in solids,** *Surface Sci.* **44,** 29-46 (1974).

Key words: attenuation lengths; Auger-electron spectroscopy; inelastic cross sections; inelastic electron scattering at low energies; solids; x-ray photoelectron spectroscopy.

A compilation is presented of measured attenuation lengths of low-energy electrons in solids in the energy range (40 to 2000 eV) normally employed in x-ray photoelectron and Auger-electron spectroscopy. The techniques used to obtain electron attenuation lengths are summarized, and it is pointed out that the accuracy of measurement needs both to be defined adequately and to be improved for more meaningful intercomparisons of data and theory. An approximate expression is derived to predict attenuation lengths using either dielectric data (derived from optical or electron-energy-loss data) or average excitation energies estimated from electron binding energies for given materials at electron energies greater than about 500 eV. Good agreement is found between the predictions of this formula and some measured attenuation lengths (e.g., for Al, C, Mo, W) but further work is required to validate the formula and to extend it to lower electron energies.

Powell, C. J., **Internal x-ray photoemission in aluminum: Excitation of electrons from the valence band,** *Solid State Commun.* **10,** No. 12, 1161-1164 (1972).

Key words: aluminum; density of states; photoelectron energy distribution; x-ray photoemission.

Measurements are reported of Al valence-electron excitation by $K\alpha_{1,2}$ x-rays internally generated in evaporated specimens by electron bombardment. The x-ray photoelectron energy distribution is consistent with the u.v. distributions of Huen and Wooten. Weak structures are found in the energy distribution at positions corresponding to those in the calculated density of states.

Powell, C. J., **Structure on the high-energy side of the $KL_{23}M$ Auger peak from solid aluminum: Internal photoemission,** *Appl. Phys. Lett.* **20,** No. 9, 335-337 (May 1, 1972).

Key words: aluminum; Auger-peak; secondary-electron energy distribution; x-ray photoemission.

Some weak structure on the high-energy side of the $L_{23}MM$ Auger peaks for Al and Si has been recently interpreted as being possibly due to the simultaneous decay of an inner-shell vacancy and a volume plasmon. It is shown here that similar structure due to multiple ionization is to be expected and that photoemission caused by internally generated x rays can be observed if the fluorescent yield is not too small. Relatively strong structure of the latter type has been observed in the secondary-electron energy distribution of evaporated Al on the high-energy side of the $KL_{23}M$ Auger peak.

Pruitt, J. S., **Correction to electron beam monitor papers,** *Nucl. Instrum. Methods* **109,** 393-395 (1973).

Key words: beam; calibration electron; Faraday-cup; ferrite; monitor.

Two mistakes have been found in previously published papers about the electron beam monitor system of the NBS Linac. They invalidate the previously proposed explanation of the change in the measured Faraday cup error when vacuum foils are introduced into the beam line. When these mistakes are corrected, it is found that the generation of secondary electron by Møller scatter in the vacuum foils accounts for only about one third of the observed change, rather than all of it, as originally claimed. Additional experiments at 50 MeV have shown that the observed change is a non-linear function of foil thickness, and that the beam transmitted by the foils includes electrons with energies as small as 0.3 MeV. Electrons with this low an energy could not have been generated by Møller scattering and must be the product of multiple processes in the foils.

Pruitt, J. S., **Electron beam current monitoring system,** *Nucl. Instrum. Methods* **92,** 285-297 (1971).

Key words: electron beam; errors; Faraday cup; ferrite; linac; monitor.

A beam current monitoring system used with the NBS electron linac is described in detail. The system consists of a water-cooled Faraday cup designed to dissipate the energy in a 1 cm diameter, 100 kW beam of 100 MeV electrons, and a non-intercepting ferrite loaded toroidal coil. The ferrite is used for continuous-duty monitoring and can be calibrated in absolute units with the Faraday cup. The Faraday cup errors have been measured with an absolute accuracy of better than 0.1 percent by bucking the Faraday cup current against the beam current, using the ferrite monitor as a null detector. The

Faraday cup losses are about 0.5 percent at 30 MeV and decrease to less than 0.1 percent at 120 MeV. These losses are attributed to backscatter of high energy electrons from the front face of the cup. In addition, it is shown that secondary electrons produced by Møller scattering in the Faraday cup entrance foils may lead to spurious measurements of beam current, and a correction for this effect is derived.

Pyke, T. N., Jr., **Terminal requirements for interactive bibliographic retrieval,** *Proc. Forum on Interactive Bibliographic Retrieval, Oct. 4-5, 1971*, pp. 9-12 (U.S. Atomic Energy Commission, Technical Information Center, Oak Ridge, Tenn., 1973).

Key words: bibliographic retrieval; computer terminals; remote computer systems.

General requirements placed on interactive terminals used for bibliographic retrieval are identified. These requirements include not only those for input/output and hard copy but also those resulting from constraints placed on the terminal by the attached communication line and computer system. The implications of these requirements on terminal design are then described, with emphasis on ideas for new, potentially useful terminal features.

Quintiere, J., **Radioactive characteristics of fire fighter's coat fabrics,** *Fire Technol.* **10,** No. 2, 153-161 (May 1974).

Key words: firefighters; protective clothing; reflectance; spectral radiation; transmittance.

The results of spectral reflectance measurements are reported for a number of typical and proposed fabrics for the outer shell of firemen's turnout coats. The spectral range of measurement was from 0.35 to 22 μm. Spectral transmittance values are also presented for some samples. From these data total reflectance values were calculated for blackbody source distributions over a range of temperature from 300 to 6000 K and for a solar spectral distribution. The implications of these results are considered for thermal protection and comfort of clothing worn by firefighters.

Rains, T. C., Menis, O., **Determination of submicrogram amounts of mercury in standard reference materials by flameless atomic absorption spectrometry,** *J. Ass. Offic. Anal. Chem.* **55,** No. 6, 1339-1344 (1972).

Key words: flameless atomic absorption; liver and coal; loss of mercury; mercury in orchard leaves; standard reference materials.

In a study of the flameless atomic absorption method for the determination of nanogram amounts of mercury in organic materials, the technique was improved to provide greater precision and accuracy. The loss of mercury during the digestion of organic materials with nitric, sulfuric, and perchloric acids is prevented by controlled heating and a packed refluxing column. The reduction and absorption system was simplified by using a heated absorption cell which alleviates the interference of volatile vapors. This method has been applied to the determination of mercury in NBS standard reference materials of orchard leaves, liver, and coal, and the results were compared with results obtained with two other analytical methods.

Reader, J., **Position of the sp^6 configuration in the neutral halogens,** *J. Opt. Soc. Amer. Letters to Editor* **64,** No. 7, 1017-1018 (July 1974).

Key words: bromine; chlorine; electronic configuration; halogen; iodine; spectra.

An extrapolation of the unperturbed position of the $4s4p^6\ ^2S_{1/2}$ level in the Br I isoelectronic sequence shows that this level will most likely lie above the ionization limit in neutral Br. It is concluded that the sp^6 configuration cannot be identified in the neutral halogen atoms by isoelectronic extrapolation of observed level positions, thus calling into question the identification of this configuration in neutral chlorine, bromine, and iodine.

Rebbert, R. E., Lias, S. G., Ausloos, P., **Photolysis of alkyl iodides at 147.0 nm. The reaction $H + C_nH_{2n+1}I \rightarrow HI + C_nH_{2n+1}$,** *Int. J. Chem. Kinet.* **V,** 893-908 (1973).

Key words: alkylhalides; far ultraviolet photochemistry; free radicals; hydrogen atoms; photochemical dissociation; rate constants.

The 147 nm (8.4 eV) photolysis of gaseous C_2H_5I, n-C_3H_7I, and sec-C_3H_7I was investigated in the presence of and absence of HI. The main overall processes are:

$$C_2H_5I + h\nu \rightarrow \quad C_2H_4 + H + I \quad \Phi = 0.75$$

$$\text{n-}C_3H_7I + h\nu \rightarrow \quad C_3H_6 + H + I \quad \Phi = 0.38$$

$$\rightarrow CH_3 + C_2H_4 + I \quad \Phi = 0.47$$

$$\text{sec-}C_3H_7I + h\nu \rightarrow \quad C_3H_6 + H + I \quad \Phi = 0.80$$

$$\rightarrow CH_3 + C_2H_4 + I \quad \Phi = 0.07$$

These dissociative processes occur mainly as a result of initial cleavage of the weak C – I bond, followed by decomposition of the internally excited alkyl radicals. In all cases, approximately 5-10 percent of the alkyl radicals thus formed do not undergo dissociation at pressures around 3-7 torr. There is also evidence for the elimination of HI as well as C – C cleavage in the primary dissociation. The former is indicated by deuterium labeling experiments and the formation of cyclopropane ($\Phi = 0.04$) as a product in the photolysis of n-C_3H_7I. Because the processes listed above provide a constant source of H atoms whose quantum yield can be exactly determined, it was feasible to obtain accurate values for k_a/k_b:

$$H + C_nH_{2n+1}I \xrightarrow{a} C_nH_{2n+1} + HI$$

$$H + HI \xrightarrow{b} H_2 + I$$

For thermally equilibrated H atoms (300 K), k_a/k_b is 0.44 ± 0.04, 0.57 ± 0.06, 0.95 ± 0.1, and 0.024 ± 0.01 for C_2H_5I, n-C_3H_7I, sec-C_3H_7I, and C_2H_5Br, respectively.

Rice, J. R., Thomson, R., **Ductile versus brittle behaviour of crystals,** *Phil. Mag.* **29,** No. 1, 73-97 (Jan. 1974).

Key words: dislocation nucleation; ductile vs. brittle; fracture; theoretical strength.

A necessary criterion for brittle fracture in crystals is established in terms of the spontaneous emission of dislocations from an atomically sharp cleavage crack. We have calculated the stability of a sharp crack against emission of a blunting dislocation for a number of crystals and crystal types in two dimensions and the energy to form a stable loop of dislocation from the crack tip in three dimensions. We find that contrary to previous expectations, an atomically sharp cleavage crack is stable in a wide range of crystal types, but that in the face centered cubic metals investigated, blunting reactions occur spontaneously. Of the body centred metals investigated, iron is an intermediate case between the brittle and ductile cases, and the ionic and covalent crystals investigated are all stable against dislocation emission. Qualitatively, we find that crystals whose dislocations have wide cores, and small values of the parameter $\mu b/\gamma$ ($\mu b/\gamma < 7.5$ to 10) are ductile while crystals with narrow cores and large values of $\mu b/\gamma$ are brittle.

Richmond, J. C., **Test procedures for night vision devices,** *LESP-RPT-0302.00*, 21 pages (U.S. Department of Justice, Law Enforcement Assistance Administration, National Institute of Law Enforcement and Criminal Justice, Washington, D.C., July 1974).

Key words: contrast transfer function; distortion; flare; light equivalent background; light induced background; night vision devices; optical gain; test methods.

This report includes descriptions of the test procedures that will be used for testing image intensifier night vision devices of the passive type, in a project sponsored by the Law Enforcement Standards Laboratory at NBS. These same procedures, modified, if necessary, in the light of experience gained in testing a number of the night vision devices, will be incorporated in a Standard for such devices.

Rossmassler, S. A., **Public/private cooperation in planning and developing reference data programs,** *J. Chem. Doc.* **13,** No. 2, 65-68 (1973).

Key words: advisory services; consultation; cooperative programs, NSRDS; reference data.

The National Standard Reference Data System relies heavily on the advice of experts in special subject-areas of science and technology to plan and develop programs for compilation and evaluation of quantitative data. Advisory panels provide a means of bringing together generators and evaluators of data to define needs, recommend specific projects, determine priorities, and coordinate new activities with those already in process. Such advisory panels are the natural basis for the development of cooperative programs, not only for data compilation and evaluation, but also for improvement in the quality of original experimental work, standardization of techniques, and agreement on formats for the presentation of, e.g., spectroscopic data. While such panels are sponsored by the Federal Government, the panel membership includes people from universities, private industry, professional societies, and consultant organizations. The cooperative nature of the undertakings fosters attention to user needs and public benefits.

Roszman, L. J., Hooper, C. F., Jr., **Time-dependent plasma microfield distribution,** *Physica* **73,** 259-286 (1974).

Key words: cluster expansion; collective-coordinates; distribution; ion correlations; microfield; plasma; time-dependent microfield.

The theory of the distribution of the finite-interval time average of the time-dependent low-frequency microfield (ion produced) in a plasma containing ion-ion correlations is developed The plasma model contains ion-ion interactions in the appropriate statistical ensemble (statistical ion correlations), but does not contain ion interactions in its dynamics (free-streaming dynamics). The theory allows inclusion of statistical ion correlations to any order. A discussion of all approximations is included.

Rowe, J. M., Nicklow, R. M., Price, D. L., Zanio, K., **Lattice dynamics of cadmium telluride,** *Phys. Rev. B* **10,** No. 2, 671-675 (July 15, 1974).

Key words: cadmium telluride; frequency dispersion; lattice dynamics; neutron inelastic scattering; phonon dispersion relation; semiconductors.

The phonon dispersion relation of CdTe at 300 K has been measured for the [100], [111], and [110] directions of propagation using neutron inelastic scattering. The CdTe single crystal was grown from the melt with Cd present as ^{114}Cd to reduce the neutron absorption of the specimen. The results have been fitted to a 14-parameter shell model that represents both the neutron data and other measured properties well when the non-neutron data are included in the fit. The present results, along with earlier measurements on α-Sn and InSb, complete the isoelectronic sequence α-Sn $\rightarrow$ InSb $\rightarrow$ CdTe. The systematic trends in the lattice dynamics of this series of semiconductors (which is characterized by increasing band gap and ionicity) are brought out by comparison of frequency distributions calculated from the shell-model fits.

Rowe, J. M., Rush, J. J., Flotow, H. E., **Neutron-quasielastic-scattering study of hydrogen diffusion in a single crystal of tantalum,** *Phys. Rev. B* **9,** No. 12, 5039-5045 (June 15, 1974).

Key words: hydrogen diffusion; hydrogen in tantalum; interstitial sites; neutron scattering; quasielastic scattering; residence time; single crystal; vibration amplitudes.

The diffusion of hydrogen in a single crystal of bcc tantalum ($TaH_{0.02}$) at 584 K has been investigated by neutron-quasielastic scattering at a variety of crystal orientations, and over a range of wavevector transfer $|Q|$, from 0.8 to 2.5 $Å^{-1}$. A detailed analysis of the observed quasielastic line shapes and widths shows that the results cannot be fitted by any simple jump-diffusion model involving instantaneous jumps between octahedral and tetrahedral interstitial sites. The quasielastic width curves (full width at half-maximum versus Q) are much more isotropic than those predicted by any of the hydrogen-jump models, although the general shape of the widths at large Q is closer to that predicted by a tetrahedral-site model. These results are in distinct contrast to a recent neutron study of hydrogen diffusion in single-crystal (fcc) palladium, where the details of the quasielastic scattering were fitted well by a model assuming instantaneous jumps between octahedral sites. The $TaH_{0.02}$ quasielastic peaks suggest a diffusion "relaxation time" between 1 and 2 ps at 584 K. Analysis of the data also provides an average "mean-square hydrogen vibration amplitude" of 0.040 $Å^2$. The present single-crystal results are in reasonable agreement with the results of a previous neutron study of polycrystalline (α-phase) TaH_x. In addition, a value for the macroscopic diffusion constant at 584 K of $2.8 \times 10^{-5} cm^2 s^{-1}$ is derived from the low-Q results, which is in excellent agreement with the value predicted from Gorsky-effect measurement.

Sakuma, E., Evenson, K. M., **Characteristics of tungsten-nickel point contact diodes used as laser harmonic-generator mixers,** *IEEE J. Quantum Electron.* **QE-10,** No. 8, 599-603 (Aug. 1974).

Key words: laser harmonic generator-mixer; tungsten-nickel point contact diodes.

Properties of tungsten-nickel point contact diodes, when used as harmonic-generator mixers, were measured. The measured properties are those which will be useful to workers wishing to use these high-speed devices (faster than 10^{-14} s). Some of the properties measured were: the decrease in signal with mixing order; the detected signal as a function of laser frequency; and the power required to optimize the harmonic beat notes.

Santoro, A., **Characterization of twinning,** *Acta Crystallogr.* **A30,** Part 2, 224-231 (Mar. 1974).

Key words: coincidence-site lattices; determination of twin laws; equivalence of twin laws; lattices; oriented crystal growths; twin obliquity and twinning.

A new twinning condition is derived. It is more general than Friedel's ratios [Friedel, G. (1964). *Leçons de Cristallographie*, p. 249, Paris: Blanchard], and it allows one to predict not only the twin laws of a crystalline species, but also the regular associations of crystals mutually oriented according to noncrystallographic rotations. The deviation suffered by the twin lattice at the composition surface is better described in terms of the new twinning condition than in terms of the twin obliquity.

Saunders, J. B., **A simple interferometric method for workshop testing of optics,** *Appl. Opt.* **9,** No. 7, 1623-1629 (July 1970).

Key words: interferometry; optical shop testing; shearing interferometer; testing of optics.

A simple step-by-step method is given for deriving the shapes of wavefronts from data obtained with a wavefront shearing interferometer. No mathematics, other than arithmetic, is used. The result is the accurate deviation of the wavefront from a reference sphere

that coincides with it at three chosen reference points. The method is intended primarily for the use of opticians in optical workshops, but is also quite practical for the final testing of optics for performance rating. A method is given by which an optician can evaluate an optical surface by comparing the interferogram produced by it and a known prism interferometer, with a drawing of the desired interferogram. This procedure is analogous to using test plates for visual inspection of optical surfaces.

Saunders, J. B., **Reflection, transmission and phase shift of light at imbedded optical films,** *J. Opt. Soc. Amer.* **62,** No. 1, 6-9 (Jan. 1972).

Key words: interferometry; Kösters prism; optical films; phase shift; polarized light; reflection; thin films; transmission.

Reflectance and transmittance of polarized light at imbedded optical films are measured for films of different compositions and thicknesses. The reflectance/transmittance ratio of plane-polarized light from such films, whose reflectance equals the transmittance at normal incidence, can be varied from approximately 1/3 to 4 by rotating the plane of polarization. A method is described that permits measurement of differences of phase shift, between reflected and transmitted light, for optical films imbedded in dielectric media that are approximately homogeneous. Phase-shift differences were obtained for two different aluminum films. Whereas values approximately $\pi/2$ rad were expected, values of 106 and 74°, respectively, were found for light polarized parallel and perpendicular to the plane of incidence. The two interferograms, produced by light of these two polarizations, appear to be complementary. However, the two interferograms produced by either polarization and observed from opposite sides of the film are not complementary—thus indicating a variation of absorption of the film with optical-path difference.

Sawyer, D. E., **Prevalent error sources in transistor delay-time measurements,** (Proc. Annual Conf. on Nuclear and Space Radiation Effects, Seattle, Wash., July 24-27, 1972), *IEEE Trans. Nucl. Sci.* **NS-19,** No. 6, 121-124 (Dec. 1972).

Key words: delay time; measurement errors; radiation effects; transistors.

Measurements of bipolar transistor delay times are extensively employed to predict neutron vulnerability. Of the various possible delay times, phase delay is most commonly measured. Although this is the simplest delay measurement to implement, the measurement circuit may be quite susceptible to extraneous signal coupling at the measurement frequency and this can cause the accuracy to be severely degraded. A technique for minimizing this delay-time error has been developed. It employs simple, preferably nonreactive, but at least known, networks in place of the transistor. From the differences between the "delay times" measured on these known networks, the location and magnitude of the error sources in the circuit are found. This allows one to reduce greatly the effects of the error sources on all subsequent measurements.

To confirm the theory of the error-correcting technique, RC networks with known delay times were assembled on transistor headers. For a particular bridge configuration, the uncorrected delay times measured were quite frequency dependent, but this dependence was removed by adding a correction term to the delay times. The correction term is obtained from measurements on the nonreactive networks and does not at all depend on the measured RC network delay times.

The effects of error-sources are particularly severe when transistors with low or moderate h_{fe} values are measured, as when measurements are made on transistors that have been degraded by subjecting them to neutron radiation. The delay time then observed may show significant frequency-dependence, but, as for the measurement described on the RC networks, this dependence is the signature of the measurement system rather than the transistor, and may be removed by adding an independently-obtained correction term. In the absence of this correction, erroneous conclusions may be reached as to the effects of the radiation on the devices under test.

Schaefer, A. R., Mohan, K., **A new gonioradiometer for total flux measurements,** *J. Illum. Eng. Soc.* **3,** No. 4, 349-353 (July 1974).

Key words: geometrically total luminous; gonioradiometer; spectral radiant flux.

This paper describes the design, construction, and characterization of a new instrument for the measurement of geometrically total flux. This is done by measuring the flux emanating from a source in different directions and integrating it over an entire imaginary surface surrounding the source. A new approach is suggested for the realization of the scales of total luminous flux and geometrically total spectral flux. In this approach, these scales would be derived from standards of irradiance and illuminance.

Schafft, H. A., **Failure analysis of wire bonds,** *Proc. 11th Annual IEEE Reliability Physics Symp., Las Vegas, Nev., April 3-5, 1973, IEEE Catalog No. 73CHO 755-9PHY,* pp. 98-104 (1973).

Key words: electrical connection; failure analysis; intermetallic compounds; Kirkendall voids; microelectronics; reliability; semiconductor devices; wire bond.

Failure analysis of wire bonds has an important part to play in determining the causes of microelectronic device failure and ways for making and using devices to achieve greater reliability. Several tests and procedures used in the failure analysis of wire bonds are reviewed. Some of the inferences about possible causes of permanent or intermittent failure that can be drawn from such tests, particularly those involving inspection with an optical microscope and with a scanning electron microscope, are discussed. Some attention is paid to the effects on the reliability of the wire bond of the growth of gold-aluminum intermetallic compounds, of Kirkendall voids, and of the use of poor materials, poor processes in making the wire bond, and poor control over the processes used. Also reviewed are some metallurgical sectioning techniques and a variety of methods used in opening the commonly used packages and in exposing wire bonds that are encapsulated in epoxy, phenolic resin, or silicone materials.

Schneider, S. J., McDaniel, C. L., **The BaO-Pt system in air,** *J. Amer. Ceram. Soc. Discussions and Notes* **52,** No. 9, 518-519 (Sept. 21, 1969).

Key words: BaO-Pt system; BaO-PtO_2 system; dissociation; phase equilibria.

The phase relations between BaO and Pt in air were studied by x-ray diffraction, differential thermal analysis, and quenching techniques. At lower temperatures the system can be represented by the BaO-PtO_2 pseudobinary. Prominent features of the system include a hexagonal $4BaO \cdot PtO_2$ compound, a phase of unknown composition and symmetry and a solid solution (orthorhombic) existing approximately between 33 and 50 mole % PtO_2 at 1025 °C. At higher temperatures all intermediate phases eventually dissociate to BaO and Pt. The dissociation temperature of PtO_2 in air was determined as 585 °C.

Schooley, J. F., **Superconductive transition in cadmium,** *J. Low Temp. Phys.* **12,** Nos. 5/6, 421-437 (1973).

Key words: cryogenics; pure cadmium; reproducibility; superconductivity; thermometric fixed point; transition temperature; transition widths.

Mutual inductance measurements of the superconductive transitions occurring in single-crystal and polycrystalline cadmium samples in magnetic fields of $0-10^{-4}T$ (0–1 G) are presented. The tem-

perature at which the zero-field superconductive transition midpoints occur appears to be constant within ±0.2 mK for transitions narrower than 2 mK, but T_c increases for broader transitions. The transitions exhibited both narrowing and hysteresis, the latter perhaps due to supercooling, in fields of a few tenths of a gauss. T_c has been measured as $0.515 \pm 0.002_5$ K on the T_{62} temperature scale.

Schwartz, R. B., Schrack, R. A., Heaton, H. T. II, **Total neutron cross sections of uranium-235, uranium-238, and plutonium-239 from 0.5 to 15 MeV,** *Nucl. Sci. Eng.* **54,** 322-326 (1974).

Key words: MeV neutrons; time-of-flight; total neutron cross sections; ^{239}Pu; ^{235}U; ^{238}U.

The total neutron cross sections of ^{235}U, ^{238}U, and ^{239}Pu were measured over the energy range 0.5 to 15 MeV, using the U.S. National Bureau of Standards electron linear accelerator as a pulsed neutron source. Neutron energies were measured by the time-of-flight method, with a resolution of 0.1 nsec/m. The measurement accuracy is estimated to be ±1 percent. The cross-section curve is smooth, with no observable fine structure. The data are in excellent agreement with recent results from the Rensselaer Polytechnic Institute, and in satisfactory agreement with the ENDF/B-III data file, except at the high and low energy ends of our energy range.

Schwarz, F. P., Okabe, H., Whittaker, J. K., **Fluorescence detection of sulfur dioxide in air at the parts per billion level,** *Anal. Chem.* **46,** No. 8, 1024-1028 (July 1974).

Key words: detection; fluorescence; H_2O; SO_2; Zn lamp.

A previously reported detector capable of rapid and continuous measurement of SO_2 in air has been modified to extend the detection limit to the low ppb range. The principle of detection is based on photon counting of the SO_2 fluorescence excited by the Zn 2138-Å line. Fluctuation of the lamp intensity was accounted for by measuring the ratio of the fluorescence photon counts to that of the excitation source. At 8.6 ppb, the standard deviation is 29 percent for a counting time of about 1 minute. The detector response is linear from at least 8.6 ppb to 1.8 ppm. The major source of measurement error at low ppb concentrations is the statistical fluctuation of the low scattered light and signal counts, whereas at high SO_2 levels, it is due to fluctuations in the sample preparation. The cell design was modified to reduce the scattered light. The inside of the cell was coated with a non-water-absorbing black Teflon to reduce possible H_2O-SO_2-wall interactions. With the Zn lamp as an excitation source, the quenching effect of water vapor on the SO_2 fluorescence signal previously observed with Cd 2288-Å excitation was found negligible. The result can be reasonably explained by the shorter life time of the SO_2 fluorescence.

Sebastian, K. J., Nelson, C. A., **$|\Delta I| = 1/2$ rule from the symmetric quark model,** *Phys. Rev. D* **8,** No. 9, 3144-3161 (Nov. 1, 1973).

Key words: color-quark model; current algebra and pcac; nonleptonic Ω^- decays; paraquark model; symmetric quark model; three-triplet quark model.

Two topics are treated in this paper: the explanation of the $|\Delta I| = 1/2$ rule based on the symmetric quark model and the tests for this explanation in Ω^- nonleptonic decays. From the "color-quark," the three-triplet, and the paraquark models, the $|\Delta I| = 1/2$ rule follows for the octet-hyperon, the Ω^-, and the kaon weak nonleptonic decays as a consequence of current algebra, pion PCAC (partially conserved axial-vector current), and dispersion relations. Gronau's successful numerical results for the octet-hyperon decay amplitudes also follow in these alternatives to the Bose-quark model. However, though the origin of both explanations is the Fierz reshuffling property of the $V \pm A$ interactions, the explanations of the $|\Delta I| = 1/2$ rule are quite distinct, e.g., in the Bose-quark model this rule is *exact* whereas in the other versions it is only *approximate*, being violated by continuum contributions to the absorptive parts. Because $\langle 0|\mathscr{H}_w|K\rangle$ and $\langle \pi|\mathscr{H}_w|K\rangle$ vanish in the symmetric quark model, the usual current-algebra soft-pion argument for $|\Delta I| = 1/2$ rule and the K^*-pole-dominance assumption (as a Feynman diagram) for $K_1^0 \to 2\pi$ are *not* convincing. On the other hand, the ordinary Fermi-quark model supplemented with octet dominance can be excluded, as it predicts $D/F = 3$ in the SU(3) limit for the matrix element of the parity-conserving Hamiltonian for two baryons in the nucleon octet ($D/F \simeq -0.85$ from P-wave fits). The ΛK^- decay mode of the Ω^- should be *predominantly* P wave (parity-conserving), whereas the $\Xi\,\pi$ mode should have the P wave strongly *suppressed* and comparable to the D wave (parity-violating). This implies $\Gamma(\Omega^- \to \Xi\,\pi)/\Gamma(\Omega^- \to \Lambda K^-) << 1$. The estimated total Ω^- decay rate is consistent with the present experimental number.

Selig, H., Sarig, S., Abramowitz, S., **Alkali fluorotellurates (VI),** *Inorg. Chem.* **13,** 1508-1511 (1974).

Key words: alkali hexafluorotellurates; inorganic complex; intermediate phases; structure; thermodynamic analysis.

The reactions of tellurium hexafluoride with cesium fluoride or rubidium fluoride go nearly to completion if the alkali fluorides are suspended in the inert solvent, C_6F_6. With cesium fluoride a limiting composition of $CsF \cdot TeF_6$ is approached, while rubidium fluoride gives compounds of composition $2RbF \cdot TeF_6$. Thermogravimetric analyses of the products show various inflection points indicating the existence of intermediate products stable at higher temperatures. Complete decomposition of the complexes is not achieved up to the melting points of the alkali fluorides, except in some cases under prolonged pumping. The infrared and Raman spectra of the materials have been tentatively interpreted in terms of D_{3h} and D_{4d} structures for the TeF_7^- and TeF_8^{2-} anions, respectively.

Seltzer, S. M., Berger, M. J., **Bremsstrahlung in the atmosphere at satellite altitudes,** *J. Atmos. Terr. Phys.* **36,** 1283-1287 (1974).

Key words: atmosphere; auroral electrons; bremsstrahlung; energy spectra; Monte Carlo calculation; satellite altitudes.

Transport calculations have been made to determine the emission of bremsstrahlung by electrons in the atmosphere and the penetration of this radiation to high altitudes where it can be detected by satellite-borne instruments. The calculations were done assuming uniform wide-area precipitation into the atmosphere of an electron flux isotropic over the downward hemisphere. The intensity and energy spectrum of the bremsstrahlung have been obtained for the case of incident monoenergetic electron beams at energies between 20 keV and 2 MeV, for incident electron beams witn exponential spectra with e-folding energies between 5 and 200 keV.

Seltzer, S. M., Berger, M. J., **Transmission and reflection of electrons by foils,** *Nucl. Instrum. Methods* **119,** 157-176 (May 1974).

Key words: angular distribution; electrons; energy spectra; reflection; transmission; transport calculation.

This paper describes Monte Carlo calculations pertaining to the penetration of electron beams through foils. The method of calculation is validated by comparisons with experimental transport data at energies between 50 keV and 1 MeV. New data are presented on the transmission and reflection of electrons through beryllium, mylar, aluminum, and titanium foils, for incident beam energies between 100 and 400 keV. The results given include transmission and reflection coefficients and the energy spectra and angular distributions of transmitted electron beams.

Sengers, J. M. H. L., **Compressibility, gas,** *Encycl. Phys. 2d Edition*, pp. 149-151 (1974).

Key words: adiabatic compressibility; density fluctuations; equation of state; isothermal compressibility; speed of sound.

This is an entry for the Encyclopedia of Physics. Isothermal and adiabatic compressibilities are defined. Their experimental behavior is discussed and an explanation of this behavior in terms of molecular theory is given. The most important experimental technique for obtaining these compressibilities are discussed. Some of the newer developments using the theory of the radial distribution functions are indicated. References to general material for further study are given.

Sengers, J. M. H. L., **From Van der Waals' equation to the scaling laws,** *Physica* **73,** 73-106 (1974).

Key words: coexistence curve; corresponding states; critical exponents; critical isotherm; rectilinear diameter; scaling laws; scaling symmetry; universality; Van der Waals' equation; vapor pressure curve.

From our present-day perspective, the most important results obtained by Van der Waals for thermodynamic behavior in the critical region of gases are: the cubic critical isotherm and quadratic coexistence curve; the continuity of slope of the vapor-pressure curve; the law of the rectilinear diameter and the law of corresponding state. The critical behavior of Van der Waals' equation is typical for equations of state that are regular at the critical point in a sense to be discussed; those equations are presently called "classical." The confrontation with experiment took place before 1900. At that time, the first power-law analyses of data were made and their results disproved classical theory convincingly. It took, however, another 65 years before classical theory was replaced by the scaling laws. The very limited validity of the law of corresponding states, however, never posed a serious threat to the classical equation. On the contrary, by generalizing this law in various ways, our insight into the relation between molecular interaction and thermodynamic behaviour has been deepened considerably. In a sense, the principle of universality may be considered the latest generalization of the law of corresponding states. The principle of continuity of slope of the vapor-pressure curve has been preserved; the direction of the vapor-pressure curve at the critical point is a very special one according to the thermodynamic theory of Wheeler and Griffiths and also in the theories of "extended scaling." The law of the rectilinear diameter, now under siege by theory, has not yet failed us experimentally.

The lines from the past to the present are sketched in this contribution, and the modern concepts of scaling will be developed from the classical equation of state. The consequences of the scaling laws for the description of thermodynamic data of fluids in the critical region will be discussed and illustrated with experimental material. Universality of critical behavior in fluids will be demonstrated.

Siddiqi, A. A., Chen, C. T., Meisels, G. G., Gorden, R., Jr., **On the ionization efficiencies of C_4H_8 isomers at 123.6 nm,** *J. Chem. Phys. Letters to Editor* **57,** No. 10, 4506-4507 (Nov. 15, 1972).

Key words: butene; ionization efficiency; isomers; krypton resonance line; quantum yield; ultraviolet.

The ionization efficiencies of the C_4H_8 isomers were determined at the krypton resonance line at 123.6 nm using total absorption and attenuation techniques. Average ionization efficiencies (ionization quantum yields) obtained independently in both laboratories are: isobutene, 0.206, 1-butene, 0.201, *cis*-2-butene, 0.201, *trans*-2-butene, 0.268, methylcyclopropane, 0.136, and cyclobutane, 0.0022.

Sieck, L. W., Gorden, R., Jr., Ausloos, P., **Effects of low concentrations of O_2 and CO on the ion-clustering reactions in the lower ionosphere of Mars,** *Planet. Space Sci. Research Notes* **21,** 2039-2041 (1973).

Key words: ion clusters; ion-molecule reactions; ionosphere; Martian atmosphere; mass spectrometry; photoionization.

It is demonstrated that under conditions which approximate those of the Martian ionosphere traces of CO and O_2 can be effectively incorporated in ion clusters via ion-molecule reaction schemes initiated by the CO_2^+ ion. For example, when 0.3 percent CO is added to CO_2, $(CO)_2^+$ and $[(CO)_2CO_2]^+$ appear as the major cations (584 Å radiation, 300 K). In mixtures containing O_2 in addition to CO, $(CO_2{\cdot}O_2)^+$ and $[(CO_2)_2O_2]^+$ are important species. A recently proposed mechanism to account for the low abundance of CO and O_2 in the Martian atmosphere is discussed in the light of these observations.

Sieck, L. W., Gorden, R., Jr., Ausloos, R., Lias, S. G., Field, F., **Ion-clustering of the cations in the high energy irradiation of nitrous oxide,** *Radiat. Res.* **56,** No. 3, 441-459 (Dec. 1973).

Key words: ion clustering; ion-molecule reactions; mass spectrometry; nitrous oxide; photoionization radiolysis.

The reactions of the positive ions in N_2O have been studied mass spectrometrically at pressures up to approximately 2 torr and at temperatures in the vicinity of 300 K, that is, under conditions similar to those which prevail in a gas phase radiolysis experiment.

The N_2O^+ parent ion associates with a N_2O molecule to form a $(N_2O)_2^+$ dimer, with a termolecular rate constant of $4.8 \pm 0.5 \times 10^{-28}$ cm^6/molecule^2-sec at 300 K. The ratio $(N_2O)_2^+/N_2O^+$ shows a sharp decrease with an increase in temperature. The NO^+ fragment ion also associates with a N_2O molecule to form the $NO^+{\cdot}N_2O$ association ion. At pressures greater than 1 torr, this ion associates with a second molecule of N_2O to form $NO^+{\cdot}(N_2O)_2$.

In order to investigate the effects of accumulated radiolytic products on the ionic mechanisms in N_2O, experiments were performed in which small amounts ($\sim 0.1\%$) of O_2, NO, and N_2 were added to N_2O. In the presence of 0.1 percent O_2, $O_2^+{\cdot}N_2O$ is formed. In the presence of 0.1 percent NO, $NO^+{\cdot}N_2O$ and $(N_2O)_2NO^+$ were observed in much greater abundance than in pure N_2O, presumably from a reaction of N_2O^+ or $(N_2O)_2^+$ with NO molecules. The $(NO)_2^+$ dimer ion was also observed in these experiments. No reactions of the positive ions in N_2O with N_2 were observed.

The results obtained in earlier pulse radiolysis and conventional low dose rate radiolysis experiments are reevaluated in order to take into account the formation of association ions. If one assumes that no dissociation occurs in the N_2O species formed by neutralization of $(N_2O)_n^+$ ions by SF_6^-, it can be shown that observed pulse radiolysis results are consistent with the electron neutralization of $(N_2O)_n^+$ to give only one excited N_2O^* species which dissociates; an alternate assumption about the neutralization mechanism involving SF_6^- leads to the conclusion that, on the average, 1.8 N_2O species dissociate for each $(N_2O)_n^+$ ion neutralized by an electron. In the low dose rate radiolysis, accumulated products may be expected to modify the ionic mechanism, so that radiolytic product yields will be dependent on dose.

Sieck, L. W., Gorden, R., Jr., **Formation of association ions in the photoionization of alkyl halides,** *Int. J. Chem. Kinet.* **5,** No. 3, 445-454 (May 1973).

Key words: alkyl halides; ion-molecule reactions; mass spectrometry; photoionization; radiolysis; rate constants.

The methyl and ethyl chlorides and bromides, as well as methyl iodide, were photoionized in the vacuum ultraviolet at 300 K in a mass spectrometer over the pressure range 0.5 to approximately 100 millitorr. Under these conditions, stabilized parent ion dimers are found in CH_3Br, CH_3I, and C_2H_5Br, but not in the chlorides. Lower limits for the dissociative lifetimes of the ion-molecule collision complexes were estimated and are as follows: $(CH_3Br)_2^+$, 1.6 μs; $(CH_3I)_2^+$, 1.9 μs; and $(C_2H_5Br)_2^+$, 5.4 μs. An increase in photon energy (internal energy content of the reactant ion) decreases the dissociative lifetime of the collision complex in CH_3I.

Sieck, L. W., Gorden, R., Jr., **Photoionization of N_2O at 73.6 – 74.4 and 58.4 nm. Evidence for collision-induced dis-**

sociation at thermal kinetic energies, *J. Chem. Phys.* **58,** No. 6, 2653-2654 (Mar. 15, 1973).

Key words: ion-molecule reaction; mass spectrometry; N_2O; rate constant; vapor phase.

The photoionization of N_2O at 73.6-74.4 and 58.4 nm has been investigated in the NBS high pressure mass spectrometer up to approximately 0.1 torr. Evidence has been found for the collision-induced dissociation

$$N_2O^+ + M \rightarrow NO^+ + N + M$$

which occurs at thermal kinetic energies and involves excited levels with lifetimes $>> 10^{-5}$ s. Experiments with various additive gases have revealed that initial population of the $A^2\Sigma$ level (certainty), and $B^2\pi$ and $C^2\Sigma$ (possibly) results in formation of the N_2O^+ states responsible for the dissociation. No evidence was found for participation of vibrationally excited ground state $X^2\pi$ states in this reaction.

Sieck, L. W., Gorden, R., Jr., **Photoionization of simple hydrocarbons at 73.6-74.4 and 58.4 nm. Comparison with Penning ionization,** *Chem. Phys. Lett.* **19,** No. 4, 509-512 (Apr. 15, 1973).

Key words: energy transfer; hydrocarbons; ionic fragmentation; mass spectra; photoionization; unimolecular reactions.

Ionic fragmentation patterns have been determined for CH_4, CD_4, C_2H_2, C_2H_6, and C_3H_8 following photoabsorption at 73.6-74.4 (16.7-16.9 eV) and 58.4 nm (21.2 eV). These mass spectra have been compared with previous spectra obtained via Penning ionization processes involving collisions of these same molecules with metastable Ne (16.6-16.7 eV) and He (19.8-20.6 eV). On the basis of this comparison it is concluded that the molecular ions produced in Penning ionization have a higher internal energy content than is produced by photoionization at the same energy.

Simiu, W., **Wind spectra and dynamic alongwind response,** *J. Struct. Div. Proc. Amer. Soc. Civil Eng.* **100,** No. ST9 1897-1910 (Sept. 1974).

Key words: acceleration; aerodynamics; building (codes); deflection; dynamic structural analysis; pressure; spectra; structural engineering; tall buildings; turbulence; wind (meteorology).

Current methods for determining dynamic alongwind response are based on the assumption that turbulence spectra are independent of height. The adequacy of this assumption is assessed in the light of recent theoretical and experimental results of boundary layer meteorology. Expressions for the alongwind response, including deflections and accelerations, are proposed. It is shown that, in the case of tall, flexible, lightly damped structures (i.e., of structures for which the resonant response, as defined by Davenport and Vickery, is high), expressions of the spectrum which reflect its dependence upon height yield lower values of the alongwind fluctuating response than the expression currently used in building codes and standards, in which this dependence is ignored. Results of numerical calculations show that the values of the fluctuating deflections and of the gust factors obtained if the latter expression is used may be higher by as much as 50 and 25 percent, respectively, than those obtained if the variation of spectra with height is taken into account.

Simmons, J. H., Mills, S. A., Napolitano, A., **Interaction of microstrucure development with viscous flow processes in glass,** *J. Non-Cryst. Solids* **14,** 302-309 (Jan. 1974).

Key words: microstructure; phase separation; viscosity.

Measurements in glasses undergoing phase separation showed a large increase of viscosity with heat-treatment time. A correlation of this effect with electron micrographs of the structure indicated that the change in viscosity was related to an increase in size of the microstructure. A theoretical analysis is presented which is based on a model relating point-to-point variations in molecular environments to viscous flow processes in glass.

Simmons, J. H., Mills, S. A., Napolitano, A., **Viscous flow in glass during phase separation,** *J. Amer. Ceram. Soc.* **57,** No. 3, 109-117 (Mar. 1974).

Key words: glass; microstructure; phase separation; viscosity.

The isothermal viscosities of two borosilicate glasses, one a commercial glass widely used for chemical glassware, increase by 4 to 5 orders of magnitude with heat-treatment time near the annealing point. The glasses are basically sodium borosilicates but differ greatly in phase-separation characteristics. Electron micrographs were used to analyze the development of microstructure during the suspected phase separation. In both glasses, structure development is primarily responsible for the viscosity increase. An analysis of the data and a theoretical interpretation of the effect are presented.

Simmons, J. H., **Miscibility gap in the system PbO-B_2O_3,** *J. Amer. Ceram. Soc.* **56,** No. 5, 284-285 (May 1973).

Key words: glass; lead-borate; immiscibility temperatures.

The immiscibility temperatures of lead-borate glasses are reported. The data indicate the existence of a $PbO{\cdot}4B_2O_3$ structure in the melt. A fit of the data by a regular mixing equation leads to the calculation of miscibility gap and spinodal boundaries.

Siu, M. C. I., **Equations for thermal transpiration,** *J. Vac. Sci. Technol.* **10,** No. 2, 368-372 (Mar.-Apr. 1973).

Key words: anomalous Knudsen limit; de Broglie wavelength; diffuse scattering; distribution function; free-molecular flow; irreversible thermodynamics; specular reflection.

A formalism for analytically obtaining an expression for the thermal transpiration pressure ratio R is presented. An experimental parameter σ, which is associated with the type of molecule-solid surface collisions, is introduced. A completely diffuse scattering and a completely specular scattering from a solid surface correspond to $\sigma = 0$ and $\sigma = 1$, respectively. A known distribution function is used to derive a practical formula for R in the case of long tubes and very low pressures. Quantitative results obtained from this formula indicate that deviations from completely diffuse scattering of molecules from solid surfaces give rise to an anomalous Knudsen limit.

Snyder, W. F., **Lord Kelvin on atoms as fundamental natural standards (for base units),** *IEEE Trans. Instrum. Meas.* **IM-22,** No. 1, 99, (Mar. 1973).

Key words: atomic frequency standards; fundamental standards; Lord Kelvin; Maxwell; natural standards; wavelength standards.

In the 1879 edition of *Elements of Natural Philosophy*, Lord Kelvin stated, at the suggestion of Maxwell, that atoms of hydrogen and sodium could serve as natural standards of time (frequency) and length. This was a far-sighted view in terms of recent developments of atomic frequency standards and the use of wavelengths of light as length standards.

Sparks, L. L., **ASRDI oxygen technology survey. Volume IV: Low temperature measurement,** *NASA Spec. Publ. 3073,* 153 pages (National Aeronautics and Space Administration, Washington, D.C., 1974).

Key words: calibration; cryogenics; liquid helium; liquid hydrogen; liquid neon; liquid nitrogen; liquid oxygen; reference data; resistance thermometers; thermocouples; thermometry; vapor pressure.

The specific goal of this review is to present up-to-date information on temperature measurement between the triple and critical point of oxygen. Temperature transducers which can be used in this range are treated over their entire range of usefulness. Three broad types of

thermometer are considered—resistance thermometers, thermocouples, and filled systems. In particular, platinum, indium, copper, germanium, carbon, and thermistor resistance thermometers are considered; thermocouple standard types E, K, T, and J plus various combinations utilizing *Au*-Co and *Au*-Fe alloys are considered; vapor pressure systems utilizing He, H_2, Ne, N_2, and O_2 as fill substances are discussed. Methods of low temperature thermometry are presented along with methods of calibration and analytical representation. Reference data are given in terms of Cragoe Z functions for indium and copper resistance thermometers and resistance ratios for carbon. Reference tables are included for each thermocouple type along with the power series coefficients necessary to generate the tabular data. Tabular vapor pressure data and analytical functions for each fill gas are also included. The relationship of the IPTS-68 temperature scale to previously used scales is discussed.

Spiegel, V., **Age of californium-252 fission neutrons to indium resonance energy in water,** *Nucl. Sci. Eng.* **54,** 28-34 (1974).

Key words: age; ^{252}Cf; fission spectrum; neutron; neutron age.

The age of ^{252}Cf fission neutrons to indium resonance energy (1.44 eV) was measured in water using a source encapsulated in a 7.6-mm-diam by 7.6-mm-high cylinder. The correction for the displacement of the moderator by the source was experimentally determined to be -0.13 cm^2 or about -0.5 percent in approximate agreement with calculation. The distribution of indium resonance energy neutrons close to the source was measured to be Gaussian. The age measured for this experiment was 28.69 ± 0.39 cm^2. An average energy for the ^{252}Cf neutron spectrum of 2.21 ± 0.05 MeV is inferred from this age.

Steiner, B., **Conference on photometry and colorimetry,** *Zlatni Piasatsi, 27-30 June 1973, Appl. Opt. Meeting Reports* **12,** No. 12, 2992-2993 (Dec. 1973).

Key words: colorimetry; photometry; review.

A personal view of the International Conference on Photometry and Colorimetry in Varna is given for inclusion in the meeting report column of Applied Optics.

Straty, G. C., **Velocity of sound in dense fluid methane,** *Cryogenics* **14,** No. 7, 367-370 (July 1974).

Key words: compressibility; methane; sound velocity; specific heat ratio.

Measurements of the velocity of sound in saturated and compressed fluid methane are reported. Measurements were made on the saturated liquid from 91 K to 186 K and on the compressed fluid along selected isotherms from 100 K to 300 K at pressures to about 35 MN m^{-2}. Data were combined with newly available $P\rho T$ data to obtain the isentropic compressibility and the ratio of the specific heats. Measurements along the higher temperature isotherm were limited to densities greater than about 10 mole l^{-1} at 300 K increasing to about 14 mole l^{-1} at 210 K due to the large low pressure sound attenuation in methane.

Sullivan, D. B., Dziuba, R. F., **Low temperature direct current comparators,** *Rev. Sci. Instrum.* **45,** No. 4, 517-519 (Apr. 1974).

Key words: current comparator; current ratio; shielding; superconductivity; transformer.

This paper presents an improved version of the low temperature direct current comparator described originally by Harvey. The comparator described herein exhibits a resolution of 1.5 nA · turn and provides ratios which have uncertainties of less than 4 parts in 10^{10}. An alternate approach to the shielding of the windings is discussed and a preliminary comparator based on this concept is shown to have equally good performance. The latter comparator is probably better suited to the attainment of large current ratios.

Swartzendruber, L. J., Bennett, L. H., **Retained austenite developed during surface grinding of a carbon steel,** *Scr. Met.* **6,** No. 8, 737-741 (1972).

Key words: electron conversion; Mössbauer; retained austenite; standard sample; steel.

Light surface grinding on a spheroidized Fe-C alloy of the eutectoid composition raises the surface layer to a temperature sufficient to dissolve the carbide particles. The rapid quenching provided by the sample substrate and the cutting fluid retains a surface layer of austenite approximately 0.01 μm thick. Mössbauer scattering experiments, using electron conversion, can detect the retained austenite.

Swartzendruber, L. J., **Localized moments on Fe impurities in Nb-Mo alloys: Mössbauer effect absorber study,** *Int. J. Magn.* **2,** 129-138 (1972).

Key words: alloys; iron; magnetic moments; molybdenum; Mössbauer effect; niobium.

Mössbauer effect spectra for absorbers of Mo and $Mo_{0.8}$ $Nb_{0.2}$ alloys containing ^{57}Fe impurities have been obtained in an external field as a function of temperature. The spectra for the Mo-Fe alloys are in close agreement with the results of Kitchens *et al.* for (^{57}Co)Mo sources. The $Mo_{0.8}Nb_{0.2}$ spectra show the presence of two distinct moment values for the Fe impurities, one with a moment of 1.9 μ_B and one with a moment of zero (with experimental upper limit of 0.6 μ_B). The two moment species are present in nearly equal proportions. This result gives direct support for a discontinuous moment formation model of the *type* proposed by Jaccarino and Walker. The saturation hyperfine field of 115 kG for Fe in Mo is apparently reduced to 90 kG for moment bearing Fe in $Mo_{0.8}Nb_{0.2}$. There appears to be no quenching of the Fe moment for Fe-Fe pairs such as that observed for Co-Co pairs in Mo-Nb alloys.

Swartzendruber, L. J., Siegel, E., **The effect of cobalt on the formation of a non-magnetic surface developed in grinding carbon steel,** (Proc. 18th AIP Conf. on Magnetism and Magnetic Materials, (19th Annual Conf.), Boston, Mass., Nov. 13-16, 1973), Paper in *Magnetism and Magnetic Materials*, C. D. Graham, Jr., and J. J. Rhyne, Eds., pp. 735-739 (American Institute of Physics, New York, N.Y., 1974).

Key words: cobalt; grinding; Mössbauer effect; scattering; steel; surfaces.

The effect of grinding on the metallurgical and magnetic structure of the surface of carbon steels containing cobalt has been investigated using ^{57}Fe Mössbauer scattering. Differences between the surface and the bulk are revealed by comparing scattering spectra obtained by counting 14 keV gamma rays with those obtained by counting conversion electrons. Light grinding produces a thin nonmagnetic layer (< 0.05 μm) of austenite (i.e., γ Fe) on the surface of a carbon steel. This layer is too thin to be observed by conventional techniques, including glancing angle x-ray diffraction and 14 keV γ-ray of 6 keV x-ray detected Mössbauer scattering. A series of steels containing 3.6 a/o carbon and from 0 to 12 a/o cobalt were given identical heat treatments followed by identical grinding treatments. The cobalt is found to have considerable influence on the composition of the surface layer.

Swing, R. E., **The optics of microdensitometry,** *Opt. Eng.* **12,** No. 6, 185-198 (Nov.-Dec. 1973).

Key words: linear optical systems; microdensitometry; optics; partial coherence.

A review of the current developments in microdensitometry is made, with emphasis on the investigations leading to the current level of understanding of optical performance. The classical microdensitometer is then analyzed according to the principles of the theory of partial coherence. Conditions for the insuring of linear operation are derived, and the idea of effective incoherence at the source aperture

is presented with a discussion of the implications. The various microdensitometer configurations are subjected to analysis, and the four possible variations (viz., overfilling, underfilling, with two possible locations for the sampling aperture) are thoroughly evaluated. The new concept of linear microdensitometry is discussed and summarized briefly. The current concerns of microdensitometry are then presented and considered. The restrictions on maximum sample frequency as a result of the partial coherence in the illumination is a major concern of this paper, and tables are presented for typical microdensitometer configurations that delineate the kinds of limitations that can be expected.

Sze, W. C., Kotter, F. R., **The design of near-perfect instrument transformers of simple and inexpensive construction,** *J. Appl. Meas.* **2,** No. 1, 22-27 (Jan.-Feb. 1974).

Key words: current ratio; leakage impedance; magnetizing impedance; ratio error; single-stage transformer; two-stage transformer; voltage ratio.

A brief discussion of the causes of ratio errors in single- and two-stage transformers is presented. The design and construction of two simple two-stage transformers, which can be used in either the voltage or current mode with an accuracy better than 10 ppm in ratios over the frequency band of 50 to 2000 Hz are described. Multiple ratios are obtained by series-parallel interconnections of windings.

Tetelman, A. S., Evans, A. G., **Failure prediction in brittle materials using fracture mechanics and acoustic emission,** Chapter in *Fracture Mechanics of Ceramics*, R. C. Bradt, D. P. H. Hasselman, and F. F. Lange, Eds. **2,** 895-924 (Plenum Publ. Corp., New York, N.Y., 1974).

Key words: acoustic emission; failure prediction; fast crack propagation; fracture mechanics; slow crack growth.

Acoustic emission testing has found many uses in recent years and new applications are constantly being uncovered. The interesting areas for application lie in failure prediction and the characterization of the microscopic processes of yielding and fracture, and the macroscopic processes of slow crack growth and onset of fast crack propagation. This paper has described these applications and emphasized that the total counts and count rate depend on the energy released per event and the density of events per unit of deformation. Where models are presented, they should be regarded as first order approximations which await confirmation.

Thomson, R. M., **The fracture crack as an imperfection in a nearly perfect solid,** *Annu. Rev. Mater. Sci.* **3,** 31-51 (1973).

Key words: brittle material; cleavage; deformation; fracture; hydrogen embrittlement; mechanical properties; stress corrosion; ultimate strength.

The field of fracture is reviewed from the standpoint of physical models which are used and appraisal is attempted of the major areas where new theoretical physical progress is required. Topics include fracture vs. ductility, Griffith criterion, nonlinear theories, atomic theories and effects of atmospheres.

Tiemann, E., Hoeft, J., Lovas, F. J., Johnson, D. R., **Spectroscopic studies of the SO_2 discharge system. I. The microwave spectrum and structure of S_2O,** *J. Chem. Phys.* **60,** No. 12, 5000-5004 (June 15, 1974).

Key words: chemistry; centrifugal distortion; disulfur monoxide; microwave spectra; structure; vibrational state.

The microwave spectrum of S_2O has been reexamined in order to obtain reliable predictions of all rotational transitions up to $J = 50$ in the frequency region 10-130 GHz and to determine the structure of the molecule. A centrifugal distortion analysis has been carried out on the ground state and lowest bending vibrational state of $^{32}S^{32}S^{16}O$. Centrifugal distortion corrected rotational constants have also been obtained for $^{34}S^{32}S^{16}O$ and $^{32}S^{34}S^{16}O$. These observations allowed the determination of the structure: $r_s(S - S) = 1.88248(10)$ Å, $r(S - O) = 1.4637(5)$ Å, $\angle SSO = 118.26(7)°$.

Tiemann, E., **Isotope dependence of the rotational constant of sulfur monoxide in the $^3\Sigma$-ground state,** *J. Mol. Spectrosc.* **51,** 316-320 (1974).

Key words: Born-Oppenheimer approximation; isotopic effects; microwave spectra; molecular parameters; rotational transitions; sulfur monoxide.

The rotational spectra of $^{32}S^{16}O$, $^{34}S^{16}O$ and $^{32}S^{18}O$ were measured. The rotational constant B_0 was accurately determined for all three isotopes whereas the spin-spin coupling λ_0 and the spin-rotation coupling γ_0 have less accuracy due to the strong correlation of these constants for the observed transitions. The evaluated breakdown of the Born-Oppenheimer approximation can primarily be attributed to the nonadiabatic correction term found for $^1\Sigma$-diatomic molecules. The small adiabatic correction for SO is obtained with the opposite sign as usually derived in $^1\Sigma$-molecules.

Torchia, D. A., Lyerla, J. R., Jr., **Molecular mobility of polypeptides containing proline as determined by ^{13}C magnetic resonance,** *Biopolymers* **13,** 97-114 (1974).

Key words: biopolymers; carbon-13 magnetic resonance; polypeptides; relaxation times.

The molecular conformations and dynamics of poly(L-prolyl), poly(hydroxyl-L-prolyl), poly(L-prolyl-glycyl), poly(hydroxyl-L-prolyl), and poly(glycyl-glycyl-L-prolyl-glycyl), in aqueous solution, have been studied using ^{13}C pulse Fourier transform nmr spectroscopy. From a measurement of the intensities of major and minor resonances in the spectra of the copolypeptides, it was determined that 15-20 percent of the glycyl-prolyl and glycyl-hydroxyprolyl peptide bonds are *cis*. Effective rotational correlation times (τ_{rgg}), obtained from measurements of spin-lattice relaxation times (T_1) of individual backbone and side-chain carbons, demonstrated that backbone reorientation is approximately isotropic for the five polypeptides and is characterized by correlation times of ca. 0.3-0.6 nanoseconds as a result of rapid segmental motion. In a given polypeptide glycyl and pyrrolidine residues were found to have the same backbone correlation times, but backbone carbon τ_{eff} values did decrease as the glycyl content of the peptides increased. A semi-quantitative analysis of C^b, C^g, and C^d correlation times suggests that rapid ring motion in both prolyl and hydroxyprolyl involves primarily C^g and C^b, with the prolyl ring being more mobile than the hydroxyprolyl ring.

Torchia, D. A., Piez, K. A., **Mobility of elastin chains as determined by ^{13}C nuclear magnetic resonance,** *J. Mol. Biol. Letters to Editor* **76,** 419-424 (1973).

Key words: carbon-13 relaxation times; collagen; configurational entropy; correlation times; elastic properties; elastin; ligamentum nuchea; rotational correlation times.

Relaxation times and integrated intensities of ^{13}C have been obtained from nuclear magnetic resonance spectra of elastin in unstretched calf ligamentum nuchae and indicate that about 80 percent of the backbone carbonyl carbons have short rotational correlation times, $\tau_R \sim 40$ nanoseconds. τ_R is reduced by only a factor of two when the ligament is in contact with 2M-KCNS, a strong denaturant. By contrast, the highly ordered chains of collagen in insoluble calf achilles tendon give no spectrum until denatured in 2 M-KCNS, when τ_R decreases by many orders of magnitude. These results show that elastin is composed largely of highly mobile chains under physiological conditions, suggesting that configurational entropy has an important role in its elastic properties.

Treado, M. J., Taggart, H. E., Nelson, R. E., Workman, J. L., **Mobile antennas,** *NILECJ-STD-0205.00*, 9 pages (U.S. Department of Justice, Law Enforcement Assistance Administration, National In-

stitute of Law Enforcement and Criminal Justice, Washington, D.C., May 1974).

Key words: antenna; communications; law enforcement; mobile; standard; transceiver.

This standard establishes minimum performance requirements and methods of test for mobile antennas mounted in vehicles which are used by law enforcement agencies.

Van Brunt, R. J., Lawrence, G. M., Kieffer, L. J., Slater, J. M., **Electron energy dependence of the kinetic energy and angular distributions of O^+ from dissociative ionization of O_2,** *J. Chem. Phys.* **61,** No. 5, 2032-2037 (Sept. 1, 1974).

Key words: dissociation; electron impact; ionization; oxygen.

The electron energy dependence of the kinetic energy and angular distributions of O^+ have been measured for the process of dissociative ionization of O_2. The kinetic energy distributions for energies above 0.5 eV are compared with other dissociative ionization measurements as well as results of dissociative photoionization and dissociative excitation by electrons leading to production of Rydberg excited neutral fragments. Angular distributions are interpreted in terms of symmetries of possible molecular ion states contributing to dissociation, and the results near threshold are compared with recent measurements of O^- from dissociative ion pair formation in O_2. Information about the states of excitation of the dissociation fragments as a function of ion energy is obtained from appearance potential measurements. The results indicate that predissociation may be important and that dissociative ionization of O_2 is in general a complicated process involving many O_2^+ states.

Vomhof, D. W., Thomas, J. H., **Determination of moisture in starch hydrolyzates by near-infrared and infrared spectrophotometry,** *Anal. Chem.* **42,** No. 11, 1230-1233 (Sept. 1970).

Key words: hydrolyzates; infrared; moisture; near-infrared; spectrophotometry; starch.

Evidence is presented that the near-infrared method, employing either DMF or Me_2SO as the solvent, and the infrared method, with Me_2SO as the solvent, are quite applicable to the determination of the moisture content of starch hydrolyzates. The near-infrared method is superior in terms of both accuracy and precision to both the present vacuum-oven method and the infrared method. These methods do not seem to be influenced by the method of manufacture, the saccharide distribution, or the ash content. They are sufficiently rapid that they could be used for quality control both by manufacturers and users of corn syrups and solid sugars.

Voth, R. O., Petropoulos, S. K., **Cryogenic refrigerators for shipboard forward looking infrared applications,** (Proc. Cryogenic Cooler Conf., USAF Academy, Colo., Oct. 16-17, 1973). Chapter in *Closed Cycle Cryogenic Cooler Technology and Applications* **1,** 27-33 (AF Flight Dynamics Lab., (FEC), Wright-Patterson AFB, Ohio, Dec. 1973).

Key words: cryogenics; infrared detector; 77 K refrigerator; low capacity; reliability; shipboard.

The Naval Ordnance Laboratory (NOL) has asked the Cryogenics Division of the National Bureau of Standards to investigate and evaluate 1) commercially available refrigerators, 2) refrigerators under development, and 3) new or novel ideas applicable to a refrigerator to cool infrared detectors in a shipboard Forward Looking Infrared (FLIR) system. The FLIR requires a refrigerator capacity of approximately 2 watts at 77 K and a physical configuration allowing for an interface to the FLIR unit. Information was collected by interviewing FLIR manufacturers, surveying refrigerator manufacturers and by contacting users of similar systems. Correlation of this information with the NOL requirements is presented herein. The primary difference between airborne/spaceborne refrigerators and a shipborne refrigerator is the accessibility for minor repairs on-board ship although major repairs may be deferred for extended periods of time. It is anticipated that the shipboard units will operate away from major maintenance facilities, for periods as long as 6 months, with the refrigerator operating at least half of this time. Thus, reliability and ease of maintenance are emphasized when evaluating the various systems.

Wall, L. A., Straus, S., Florin, R. E., Fetters, L. J., **Pyrolysis of anionic and thermally prepared polystyrenes,** (Paper presented at American Chemical Society Meeting, New York, N.Y., Aug. 28-31, 1972), *Polym. Prepr. Amer. Chem. Soc. Div. Polym. Chem.* **13,** No. 2, 1044-1045 (Aug. 1972).

Key words: anionic polystyrene; molecular weight distributions; polymers; polystyrene degradation; pyrolysis.

The changes in molecular weights and their distributions during pyrolysis have been examined for a series of polystyrenes prepared by thermal and anionic procedures. The initial rates of weight loss for the thermal polymer showed a 0.25 power dependence on the reciprocal of the number average molecular weight, while the anionic polymer showed zero dependence. The information obtained and previous results can be explained to a very large extent by a kinetic chain decomposition comprised of competing end and random initiation, depropagation, intra- and inter-molecular transfer and termination by combination.

For thermal polystyrenes the ratio of rate constants for random to end initiation has a value of 3×10^{-4} initially. The present treatment assumes this value is constant with conversion. On the other hand the anionic polymers initiate at random in the limit of zero time, after which end-initiation begins to occur, as the number of ends increases. The inter-molecular transfer constant, zip length and kinetic chain length are dependent on the steady state radical concentration and are functions of the molecular weight. Their values, at the molecular weights present when the pyrolytic weight loss exceeds 5 percent, agree well with earlier estimates.

Walls, F. L., Dunn, G. H., **Storing ions for collision studies,** *Phys. Today* **27,** No. 8, 30-35 (Aug. 1974).

Key words: dissociative recombination; electron collisions; ion trap.

Overcoming the limitations of plasma and colliding beam techniques, the new ion storage methods have proved their effectiveness in ion recombination studies.

Weisman, H. M., **A survey on the use of National Standard Reference Data System publications,** *J. Chem. Doc.* **12,** No. 4, 211-216 (1972).

Key words: National Standard Reference Data System; properties data; survey; users.

The purpose of this mail survey to purchasers of National Standard Reference Data System publications was to assess what benefits the publications provided its users and to obtain feedback on user experience, requirements, and problems of use. Survey returns gave evidence that NSRDS publications were helpful to users in meeting their data requirements. Specific uses and benefits were identified. The greatest use of NSRDS publications was in connection with basic research. Because NSRDS compilations have utility in the applied areas as well, their usefulness needs to be promoted among applied workers and engineers.

Weiss, A. W., **Series perturbations in atomic spectra: Superposition-of-configurations calculations on Al I and Al II,** *Phys. Rev. A* **9,** No. 4, 1524-1536 (Apr. 1974).

Key words: atomic spectra; atomic wave functions; oscillator strengths; series perturbations.

Configuration-interaction calculations, using only Hartree-Fock discrete-state configurations, are reported for the two perturbed se-

ries, $3snf\,^3F$ of Al II and $3s^2nd\,^2D$ of Al I. While good results are obtained for term values and oscillator strengths in Al II, this is not the case for Al I, where the calculations predict the $3s3p^2$ perturber to be expelled into the continuum. To study this case more closely, superposition of configurations (SOC) calculations, which include all correlation effects, were carried out on the five lowest ^2D states of Al I. These results indicate that the perturber actually remains in the discrete spectrum, but loses its identity and is smeared out over the entire series. New Rydberg orbitals are extracted from the SOC wave functions which are quite different from the Hartree-Fock but very similar to those of the Coulomb approximation. Various truncations of the SOC functions are also analyzed and the implications for the correlation problem discussed.

Wiederhorn, S. M., Evans, A. G., Roberts, D. E., **A fracture mechanics study of the Skylab windows,** Chapter in *Fracture Mechanics of Ceramics*, R. C. Bradt, D. P. H. Hasselman, and F. F. Lange, Eds., **2,** 829-841 (Plenum Publ. Corp., New York, N.Y., 1974).

Key words: crack growth; fracture mechanics; glass; static fatique; structural design; windows.

Design criteria based on fracture mechanics concepts are developed for spacecraft windows. Critical stress intensity factor data and crack velocity data are used for lifetime predictions and for the development of acceptance tests for the eight candidate glass compositions for the Skylab. Design charts are presented which give the minimum time to failure of the Skylab windows as a function of service stress and proof test stress. Surface adsorbed water is shown to be detrimental to the strength of spacecraft windows, even after the spacecraft has left the earth's atmosphere, because of the slow rate of evaporation of water from surface cracks.

Wiederhorn, S. M., **Subcritical crack growth in ceramics,** Chapter in *Fracture Mechanics of Ceramics*, R. C. Bradt, D. P. H. Hasselman, and F. F. Lange, Eds. **2,** 613-646 (Plenum Publ. Corp., New York, N.Y., 1974).

Key words: ceramics; crack growth; delayed failure; fracture; proof testing.

Subcritical crack growth that causes delayed failure is discussed in terms of fracture mechanics concepts. Techniques of characterizing subcritical crack growth are presented and the available crack growth data are discussed with particular emphasis on fracture mechanisms. Finally a design technique is presented to predict useful component lifetime from crack growth data after proof testing.

Wilson, W., Swartzendruber, L. J., **A flexible least squares routine for general Mössbauer effect spectra fitting,** *Computer Phys. Commun.* **7,** 151-162 (1974).

Key words: FORTRAN; least squares fitting; Mössbauer effect; numerical analysis.

A FORTRAN version of a versatile and flexible least squares fitting routine for Mössbauer effect data is described.

Winzer, G. E., **National Bureau of Standards mobile acoustical laboratory,** *Sound Vib.* **4,** No. 5, 12-15 (May 1970).

Key words: acoustical instrumentation; architectural acoustics; building research; field measurements; noise control; sound measurements; sound transmission.

A mobile laboratory has been designed for research and measurement of the acoustical performance of buildings and for the study of environmental noise. The measurement capabilities are of the quality usually associated only with fixed acoustical laboratories. Data may be collected, reduced and analyzed in the field, or stored on magnetic tape for future reduction.

Wright, J. R., **Building research in the National Bureau of Standards (U.S.A.): How it relates to other Federal agencies and to industry,** *Proc. 2d South African Building Research Congress, Johannesburg, South Africa, May 5-8, 1969*, Paper No. S4/2, 1-23 (May 1969).

Key words: building research; building standards; measurement techniques; performance requirements.

The National Bureau of Standards (NBS) is the central measurement laboratory for the USA, covering the entire spectrum of the physical sciences and many fields of engineering. NBS serves as the focal point in the Federal Government for assuring maximum application of the physical sciences and engineering to the advancement of technology in industry and commerce. Building research constitutes a major activity and is carried out primarily in the Building Research Division of the Institute for Applied Technology, NBS. The Division conducts scientific and technical investigations of the chemical, physical, and engineering properties of building materials, components and systems, and their interaction with the building occupants, as a basis for defining the performance requirements and the measurement techniques required to better adapt the physical and functional characteristics of buildings to user needs. The Division provides laboratory and field support to: Federal agencies concerned with building construction and technology; public and private organizations that draft, promulgate and distribute building standards and codes; and the building industry, primarily to stimulate industrial innovation in building systems. The building research program is sufficiently basic to maintain a resource capability yet flexible enough to assist with the practical problems of 35 Federal agencies that construct buildings. The building industry is supported in a major way through technical-committee activities (285 separate memberships), consultation, publication, and direct laboratory research (Industry Associates program). The relationship of the NBS building research program to industry and to other Federal agencies is presented, covering problem selection, research programs and results, implementation of output, and effectiveness feedback.

Wright, J. R., **Performance criteria in building, Sci. Amer. 224,** No. 3, 16-25 (Mar. 1971).

Key words: agrément system; building code of New York State; building codes; human requirements; National Conference of States; performance approach; performance criteria; performance methodology; regulatory system.

The performance approach seeks the solution to building problems in terms of human requirement satisfaction, irrespective of the methods or materials employed. The approach has application both to the regulatory (building codes) system and to the full range of concerns in building, from research to design. The performance-oriented National Conference of States on Building Codes and Standards is expected to be instrumental in modernizing the regulatory system.

Wright, R. N., Kramer, S., **Buildings in the 1972 Managua earthquake,** *Mil. Eng.* **65,** No. 428. 382-388 (Nov.-Dec. 1973).

Key words: building; building codes; earthquakes; hazards; natural disasters; structures.

Following the Managua, Nicaragua earthquake of December 23, 1972, a team of engineers representing the U.S. Department of Commerce's National Bureau of Standards and the National Academy of Engineering performed field investigations in Managua, Nicaragua, from December 26, 1972 to January 4, 1973. The objectives were to assist the Nicaraguan government in surveying major buildings to determine whether each was suitable for emergency use, repairable, or appropriate for clearance. The team also viewed the patterns of successful performance and damage to identify needs for improvements in building practices for mitigation of earthquake hazards and opportunities for more detailed investigations which could provide information for future improvements in practices.

The Managua earthquake, estimated at Richter magnitude 6.25, was not a great earthquake, but the loss of life approached 10,000, approximately 75 percent of Managua's 450,000 occupants were

rendered homeless, and property damages are estimated to approach $1 billion. In general, these damages cannot be attributed to unusual intensities of ground shaking or severity of surface faulting. Most damages appeared to result from deficiencies in building practices; deficiencies which had been exhibited many times before in previous earthquakes, deficiencies which would be avoided by implementation of up-to-date provisions for earthquake resistant design and construction. However, Managua did not employ a building code with seismic design requirements appropriate to its earthquake risk, and furthermore, did not have a building regulatory system capable of effective implementation of its building code provisions.

The Managuan experience may serve as an incentive to improvement of building practices in many other areas which are subject to substantial earthquake risks and have not consistently accounted for these risks in their building codes and building regulatory system.

Wu, Yung-Chi, **Material properties criteria for thermal safety,** *J. Mater.* **7,** No. 4, 573-579 (1972).

Key words: heat conduction; thermal inertia; thermal injury; thermal safety; thermal tissue damage.

The purpose of this study is to establish the relationship between the thermal properties of materials and thermal injury to human tissue. The interdependency of temperature and time to the conditions required for thermal safety is based on the physiological process of thermal injury. By the application of Fourier's heat equation, the relationship between the permissible temperature and time of contact of a heated body and its thermal properties is determined.

Wu, Yung-Chi, **Young's mixture rule and its significance,** *J. Phys. Chem.* **74,** No. 21, 3781-3786 (1970).

Key words: electrolytes; excess thermodynamic properties of mixtures; mixture; ternary solutions; thermodynamics; Young's mixture rule.

Young's general mixing rule postulates that in the mixing of two binary solutions of the same ionic strength to produce a ternary solution an excess thermodynamic quantity of the ternary solution may be expressed accurately as the sum of the corresponding excess thermodynamic quantities of the pure binary solutions. Young's corollary to the general rule postulates further that deviations from the rule are a function both of the ionic strength and of the respective solute fractions of the mixture. In terms of Young's two postulates any mixing process at constant ionic strength may be treated as one of four special cases. Young's postulates may also be applied to ternary mixtures of different ionic strength in which the mixing ratio of the constituents is constant.

Yap, W., **Binding of ions to oligopeptides,** *Biophys. J.* **13,** 1160-1165 (1973).

Key words: ion binding; nearest-neighbor interaction; oligopeptide; titration curve.

A model for the binding of ions to oligopeptides, in which nearest neighbor interactions are considered is developed. Equations for the titration curves are derived. The apparent association constants are determined as a function of the degree of polymerization and of the interactions between nearest neighbors.

Yates, J. T., Jr., King, D. A., **Chemisorption of carbon monoxide on tungsten: Correlation of reflection-absorption infrared spectra with CO binding state population,** *Surface Sci.* **30,** 601-616 (1972).

Key words: carbon monoxide; chemisorption; flash desorption; infrared spectroscopy; molecular vibration; tungsten.

The vibrational frequency of carbon monoxide chemisorbed on an atomically clean polycrystalline tungsten ribbon has been studied using reflectance-infrared spectroscopy and ultrahigh vacuum techniques. The initial appearance of an infrared absorption band at 2093 cm^{-1} is unequivocally associated with the onset of adsorption of the weakly-bound α-CO state, which occurs at coverages where the more strongly-bound β-CO species are already extensively populated. As the α-CO coverage is increased to its maximum value, the infrared band shifts to 2117 cm^{-1}. Partial thermal desorption of the α-CO by pumping at 295 K for $\sim$2000 sec causes the band to reversibly shift back to $\sim$2093 cm^{-1}. The band disappears rapidly and completely upon thermal desorption of CO at 403 K, confirming that the absorption band observed in this region of the spectrum is due to α-CO. The spectral frequency indicates that the α-CO species on tungsten are closely analogous to the linear CO moieties found in transition metal carbonyls. The vibrational frequency observed is in close agreement with low energy electron energy-loss measurements made for CO on W(100). A model is proposed for the slight strengthening of the carbon-oxygen bond in α-CO as the CO coverage increases. The model involves coverage-dependent electronic back-donation from surface W atoms into Π-antibonding orbitals as originally proposed by Blyholder for adsorbed CO, and by Jones for certain transition metal hexacarbonyls.

Yolken, H. T., **Standard reference materials and meaningful x-ray measurements,** (Proc. Denver X-Ray Conference, Denver, Colo., Aug. 21-23, 1973), Paper in *Advances in X-Ray Analysis*, C. L. Grant, C. S. Barrett, J. B. Newkirk, and C. O. Ruud, Eds., **17,** 1-15 (1974).

Key words: standard reference materials; x-ray calibration; x-ray measurements.

A review of the procedures and efforts at the National Bureau of Standards (NBS) to provide for meaningful measurements through the use of Standard Reference Materials (SRM's) is presented.

The examples of NBS standardization efforts for x-ray analysis range from basic metrology to applied environmental measurements. These examples include a determination of x-ray wavelength by a method which in part utilizes simultaneous x-ray and optical interferometry measurements of the atomic planes of near perfect silicon. In addition, Standard Reference Materials (SRM's) are being developed and applied to trace element analysis using x-ray fluorescence techniques. These efforts include development of SRM's for trace element analysis of air particulates. In another area, work is proceeding on the development of a silicon powder Standard Reference Material intended for x-ray diffractometer calibration. An effort to develop a suitable x-ray diffraction technique to determine the amount of quartz in mine dust is also underway. NBS efforts to provide SRM's for the calibration of electron microprobes and the validating of correction factor calculations are also described.

Young, R. D., **Surface microtopography,** *Phys. Today* **24,** No. 11, 42-49 (Nov. 1971).

Key words: microscope; microtopography; single-crystal surface; surface; surface finish; surface profile.

The growing field of surface science would benefit considerably from measurements of surface microtopography down to the atomic level. A brief review is presented of several instruments used to quantitatively characterize the surface microtopography of metallic surfaces. Techniques are discussed for employing the transmission electron microscope, the scanning electron microscope, the optical interference microscope and an engineering profile measuring instrument to measure surfaces suitable for surface science experiments. In addition a new noncontacting instrument which is presently under development will be described. It is concluded that several techniques are presently available for detecting single atom steps on single-crystal surfaces.

Zapas, L. J., **Non-linear behavior of concentrated polymer solutions,** (Paper presented at American Chemical Society Meeting, Atlantic City, N. J., Sept. 1974), *Polym. Prepr. Amer. Chem. Soc. Div. Polym. Chem.* **15,** No. 2, 131-136 (Sept. 1974).

Key words: BKZ theory; concentrated solutions; nonlinear behavior; polyisobutylene; polystyrene; superposition.

A phenomenological approach based on the elastic fluid theory of Bernstein, Kearsley and Zapas is discussed, with respect to the shear behavior of concentrated solutions. For certain systems a concentration superposition scheme can be found which covers the linear and nonlinear region. This is true only when the nonlinear stress relaxation modulus can be represented as a product of a function of time and a function of strain.

Zapas, L. J., **Nonlinear behavior of polyisobutylene solutions,** (Proc. Battelle Colloquium on Deformation and Fracture of High Polymers, Kronberg, Germany, Sept. 11-16, 1972), Paper in *Deformation and Fracture of High Polymers*, H. H. Kausch, J. A. Hassell and R. I. Jaffee, Eds., pp. 381-395 (Plenum Press, New York, N.Y., 1974).

Key words: BKZ; nonlinear shear behavior; polyisobutylene.

Experiments on various histories of simple shear were obtained with a polyisobutylene solution. A possible inadequacy of the BKZ theory is presented, together with a modified theory whose predictions are in agreement with the experimental data.

Zief, M., Barnard, A. J., Jr., Rains, T. C., **Magnesium gluconate as a standard for the determination of serum magnesium,** *Clin. Chem.* **19,** No. 11, 1303-1304 (1973).

Key words: atomic absorption spectrometry; magnesium gluconate; serum magnesium; standard material.

Magnesium gluconate dihydrate has been prepared and tested as a source of material for a magnesium standard in atomic absorption spectrometry. This material meets the criteria for purity (99.9%), stability, weighing factor and flame characteristics and would serve as an ideal standard for serum magnesium. Magnesium gluconate dihydrate has a solubility of 16g/100 ml of water at 25 °C and can be acidified with a mineral acid to insure a long shelf life as a magnesium standard stock solution.

U.S. GOVERNMENT PRINTING OFFICE : 1975 OL - 562-903

UNITED STATES
GOVERNMENT PRINTING OFFICE
PUBLIC DOCUMENTS DEPARTMENT
WASHINGTON, D.C. 20402

OFFICIAL BUSINESS
PENALTY FOR PRIVATE USE, $300

U.S. DEPARTMENT OF COMMERCE
POSTAGE AND FEES PAID
COM-215

U.S.MAIL

JOURNAL OF RESEARCH o
A. Physics and Chemistry

A, No. 1 Jan.–Feb. 1975

SJRA UNIVE300UA R 1
UNIVERSITY MICROFILMS INC
ATTN SERIALS SECTION
300 NORTH ZEEB RD
ANN ARBOR MI 48106

Page

Polarization effects on fluorescence measurements. E. D. Cehelnik, K. D. Mielenz, and R. A. Velapoldi. 1

The iron-neon hollow-cathode spectrum. H. M. Crosswhite. 17

Equation of state for thermodynamic properties of fluids. Robert D. Goodwin. 69

Thermodynamic studies of the $\alpha \rightarrow \beta$ phase transformation in zirconium using a subsecond pulse heating technique. A. Cezairliyan and F. Righini. 79

Publications of the National Bureau of Standards 83

Library of Congress Catalog Card Number: 62-37059

For sale by the Superintendent of Documents, U.S. Government Printing Office, Washington, D.C. 20402. (Order by SD Catalog No. C 13.22/sec.A:79/1). Single copy price varies. Subscription price: $17.00 a year; $4.25 additional for foreign mailing.

UNITED STATES GOVERNMENT PRINTING OFFICE, WASHINGTON : 1975